SOLID STATE SPECTROSCOPY:

LASER SELECTIVE EXCITATION OF

ERBIUM IONS IN CRYSTALLINE SOLIDS

A thesis submitted in partial fulfilment
of the requirements for the Degree
of Doctor of Philosophy in Physics
in the University of Canterbury

by

Nigel J. Cockroft

University of Canterbury
1987

ABSTRACT

Optical absorption and laser selective excitation (l.s.e.) spectroscopy have been used to study Er^{3+} ions in the $CsCdBr_3$ and hydrogenated CaF_2 and SrF_2 crystalline lattices. Sixteen hydrogenic charge compensation sites for both the H^- and D^- isotopes were found in CaF_2:0.05%Er^{3+}, and nine new D^- ion sites in SrF_2:0.05%Er^{3+}. The relative occurrence of these sites can be controlled by variation of the duration of hydrogenation. For $SrF_2:Er^{3+}$, this results in a change of the principal D^- ion charge compensation arrangement. Classification of local-mode vibronic fluorescence transitions and consideration of isotope shifts of electronic transitions enabled the assignment of model configurations to several sites. Most hydrogenic sites were classified into one of two distinct families. A new effect, reversible polarised bleaching was observed, whereby hydrogenic ion migration in Er^{3+} ion site configurations can be controlled by l.s.e. with polarised light in oriented crystals. One hydrogenic site was found to consist of two photo-induced interconvertible components. Five new fluoride ion sites in $CaF_2:Er^{3+}$ and nine in $SrF_2:Er^{3+}$ were also determined. For <100> and <111> oriented crystals, the fluorescence spectra of several sites exhibited well defined polarisation which may be used to determine the Er^{3+} ion symmetry. Trigonal symmetry of the F^- B site of $CaF_2:Er^{3+}$ was confirmed by this means. Crystal field analysis of tetragonal and

trigonal symmetry sites is also reported. An infra-red study revealed local mode lines of seven new sites in hydrogenated $CaF_2:Er^{3+}$ and enabled correlation of some sites to those observed in the optical spectra. Reduction of Er^{3+} ions by the short range beta decay of tritium in the lattice was identified by local mode absorption. Erbium ions in $CsCdBr_3$ exhibited efficient upconverted fluorescence consistent with the formation of a dominant dimer site. Detailed spectroscopy resulted in the assignment of energy levels from twelve groups of transitions. Several of these transitions, studied by absorption and l.s.e., were found to consist of two components.

ACKNOWLEDGEMENTS

This thesis is dedicated to my wife, Jane, without whose encouragement, support and tolerance of long absences the work reported, and the thesis writing, would have taken a considerably longer period of time to complete.

I should also especially like to thank my supervisors, Drs. Glynn Jones and Rod Syme for their guidance, and interest during this project. Particularly for Glynn's willingness to put in many hours of personal time to help with problems as they arose, and for Rod's help with the polarisation dependence calculation.

The early assistance from, and regular discussions with, fellow research students Roger Reeves and Thomas Han are also appreciated.

Technical assistance from departmental staff, Terry Rowe, Wayne Smith, Ross Ritchie and Clive Rowe prevented any major delays, and their willingness to tackle problems immediately as they arose is gratefully recognised. Tom Walker ensured that a constant liquid Helium supply was available, as and when required during the early part of this study.

A number of individuals and institutions deserve particular thanks. The Physics and Engineering Laboratory of the DSIR generously offered the use of their Bomem FTIR spectrometer for infra-red studies, and Dr. Bob Buckley willingly showed me its operation. Dr. Andy Edgar of the Victoria University of Wellington provided a $CsCdBr_3:Er^{3+}$ crystal, and on occasions provided enthusiastic and useful dialogue on several aspects of the systems studied.

Dr.Roger M. Macfarlane, IBM Almaden Research Centre and Harold K. Welsh, Division of Applied Physics, CSIRO, both provided interesting interaction and results prior to publication.

The drafting of this thesis was signficantly aided by several individuals. I should like to thank Mrs Beverley Bristowe for her tireless typing and tolerance of several revisions; Dr. Paul Goodson, for his invaluable proofreading and advice; Paul Rodley for many hours of assistance with the drafting of figures and for the loan of equipment; and Jeff and Kathleen Mcdonnell for their assistance with computer generated graphs.

This Ph.D course was supported by a Postgraduate Scholarship provided by the New Zealand Grants Committee.

Finally, I should like to thank my parents for their many years of support and encouragement.

CONTENTS

LIST OF FIGURES

LIST OF TABLES

CHAPTER ONE

INTRODUCTION

Upon application of an electric field, the energy levels of trivalent rare-earth ions, RE^{3+}, are split into components which can be determined by examination of optical transitions. Such an electric field of well defined symmetry can be conveniently supplied by the charges of the ions in an ionic solid at low temperature. The optical properties of the erbium ion, Er^{3+}, make it useful for spectroscopic study since transitions between several multiplets are observed in the visible region of the spectrum.

This thesis reports the results of an investigation into the influence of various crystallographic environments, or sites, on the spectroscopic properties of the Er^{3+} ion in each of the ionic hosts CaF_2, SrF_2 and $CsCdBr_3$. An emphasis is placed on the study of sites in CaF_2:Er^{3+} involving nearby hydrogenic ions, with the aim of providing a comprehensive base of information to improve the understanding of such systems in the general case.

A review of any previous work of interest is given at the beginning of each section of the study, but certain aspects common to both the CaF_2 and SrF_2 systems are briefly outlined here.

1.1 The Fluorite Structure, MeF_2

CaF_2 and SrF_2 have the crystal structure commonly known as the fluorite structure which is shown in Figure 1.1.

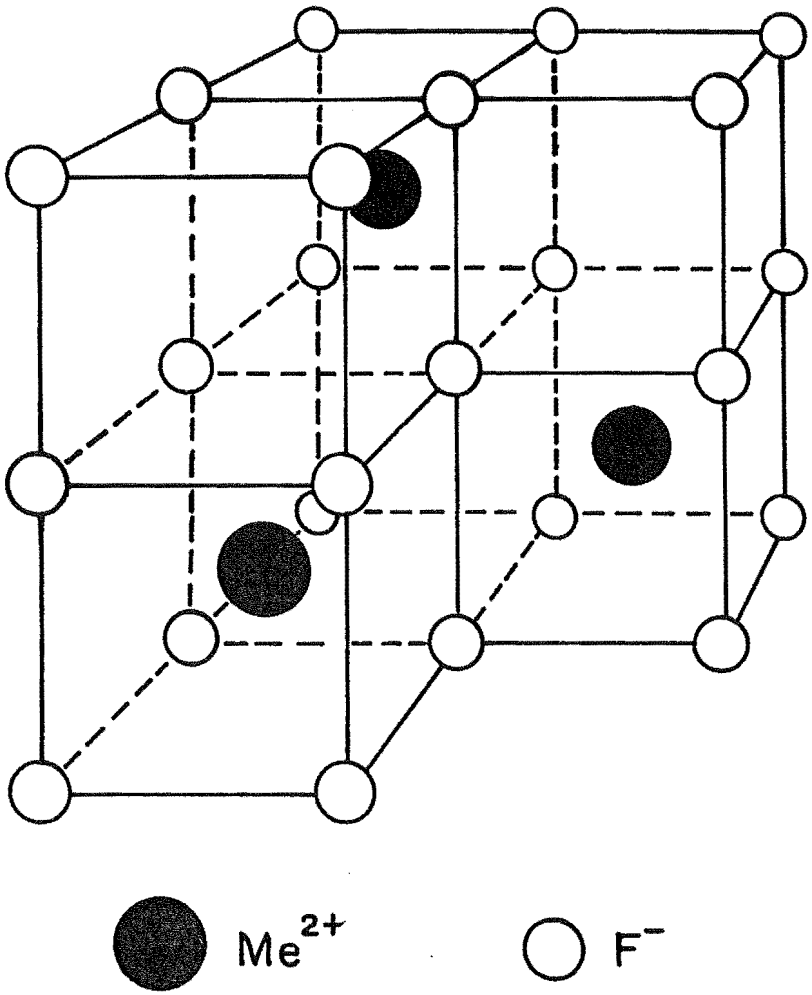

Figure 1.1 : The structure of the MeF_2, alkaline earth fluoride, crystal lattice.

This consists of a cubic lattice of F^- ions, with an Me^{2+} (=Ca^{2+}, Sr^{2+}) ion at the centre of alternate cubes of F^- ions, with Ca^{2+} separations of 5.45Å, and Sr^{2+} separations of 5.78Å.

The space group symmetry of the crystal is O_h^5 with point group symmetries of Td for the F^- ions and O_h for both the Me^{2+} ions and the vacant interstitial (empty F^- ion cube) sites.

The fluorite lattices are ideal for optical studies since they are transparent over a very large spectral range, and absorption in the visible region is negligible.

1.2 Rare-earth Doped MeF_2 Crystals

It is well established that rare-earth ions are very soluble in fluorite lattice structure. They are normally added as a small percentage of the total crystal mass in the form of powdered trifluorides before crystal growth. These RE^{3+} ions substitute for Me^{2+} ions in the lattice, thereby requiring some form of charge compensation for the crystal to maintain neutrality.

At low RE^{3+} concentrations and for the case of MeF_2:RE^{3+} with no other impurity ions present, the charge compensation is normally provided by additional fluoride ions in interstitial positions (F_I^-) close to the RE^{3+} ion. At higher concentrations more complex combinations involving several rare-earth ions and several fluoride ions can occur.

Figure 1.2a shows the simplest charge compensation mechanism possible which has an F_I^- ion in the nearest neighbour (NN) interstitial position. The RE^{3+} ion in this site has a point group symmetry of C_{4V} (tetragonal symmetry)

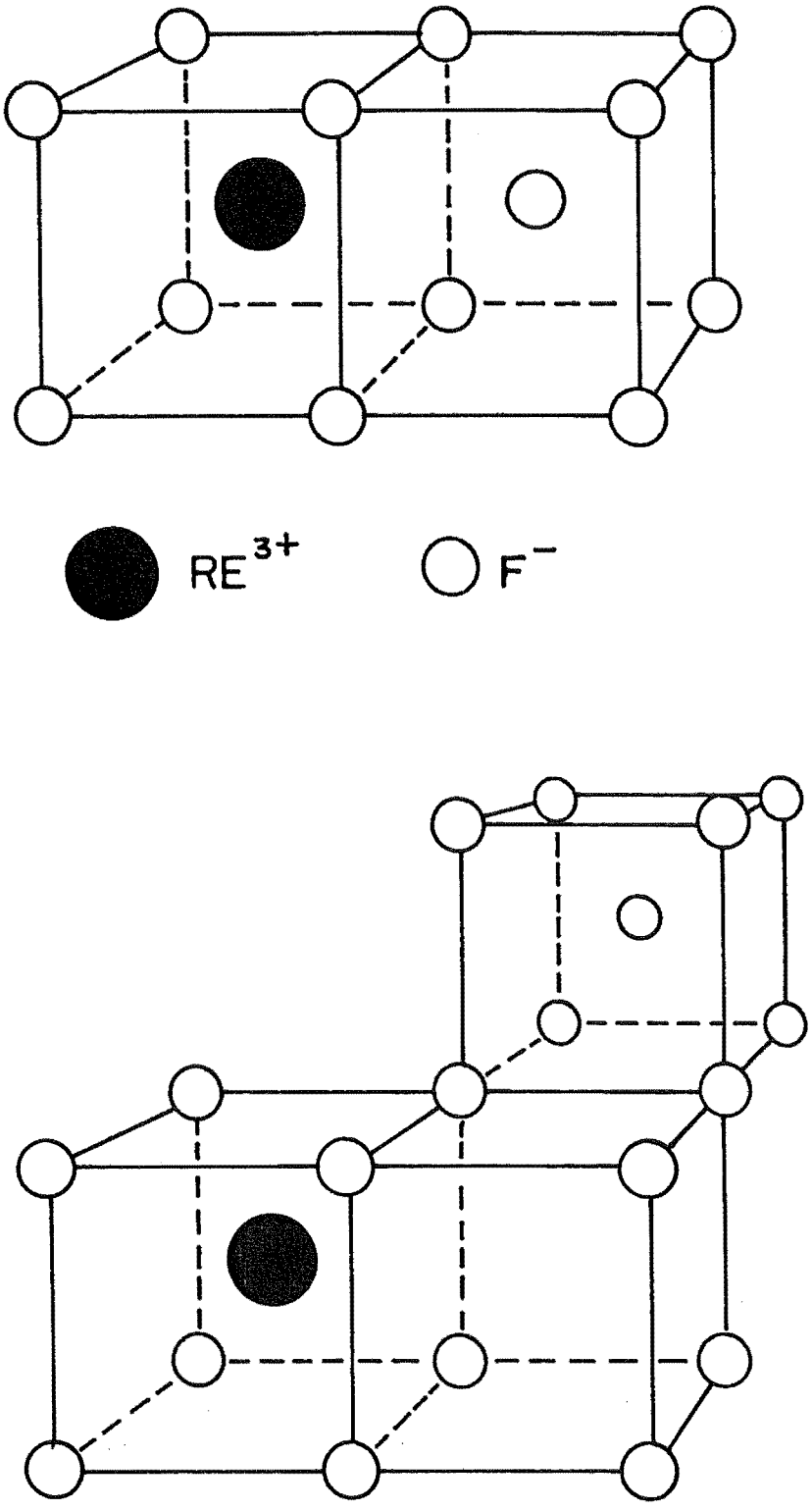

Figure 1.2 : Possible charge compensation configurations for trivalent rare-earth ions in the MeF_2 lattice : (a) C_{4V} (tetragonal) symmetry site involving nearest neighbour compensation. (b) C_{3V} (trigonal) symmetry site involving next nearest neighbour compensation.

with an axis of four-fold rotational symmetry in the direction of the F_I^- ion. This site is the dominant one for CaF_2 doped with RE^{3+} concentrations of 0.05% or less and for SrF_2 doped with the RE^{3+} ions of the early part of the rare-earth series (Corish *et al.*1982 and references therein).

An alternative site with a charge compensating F_I^- ion in the next nearest neighbour (NNN) interstitial position is shown in Figure 1.2b. This site has C_{3V} point group symmetry (trigonal) and is generally expected for the RE^{3+} of the latter part of rare-earth series when doped in SrF_2.

The crystal field for each different site configuration splits the RE^{3+} energy levels into different patterns that can be determined by optical techniques. Sites of both C_{4V} and C_{3V} symmetries are encountered in this investigation.

1.3 Hydrogenated $MeF_2:RE^{3+}$ Crystals

Hall and Schumacher (1962) established a technique for adding hydrogen in the form of H^- ions (or isotopes D^-, or T^-) into CaF_2 crystals. This has the effect of creating new sites, analogous to those in Figures 1.2 involving charge compensation by interstitial H^- ions. The most direct means of detecting H^- ions uses infra-red absorption by their local modes of vibration. Such studies have shown that in addition to the interstitial positions, the H^- ions can also replace lattice F^- ions to form a site with T_d symmetry (Elliott *et al.* 1965).

The hydrogenic charge compensated sites are of particular interest in this study and are investigated primarily by optical techniques. Crystals containing

rare-earth ions in sites involving any of the isotopic hydride ions H^-, D^- or T^- have several features not shared with the non-hydrogenated crystals :

(a) **Richer spectra** due to a substantial number of lower symmetry hydrogenic sites arising from modification of the original F^- ion sites. In addition to interstitial H^- ion sites, it is found that sites with hydrogenic ions substituting for regular lattice F^- ions near to the RE^{3+} ion are spectroscopically inequivalent to sites with F^- lattice ions only.

(b) **Variable site distributions.** The high mobility of hydride ions compared to fluoride ions results in an evolution of some sites with time, due to migration of ions in the lattice.

(c) **Local modes.** These modes of vibration are observed either by infra-red absorption or as vibronics associated with electronic transitions. Laser excitation is particularly useful for measuring vibronics.

(d) **Electron-phonon effects.** Substitution of a D^-, T^- ion for an H^- ion will slightly alter the electronic energy levels of the RE^{3+} ion.

All of these features are important in this study, and (c) and (d) are used to help assign specific model configurations to sites by identifying the position of H^- ions relative to the Er^{3+} ion.

1.4 Laser Selective Excitation

The work on both hydrogenated systems and on the $CsCdBr_3$ system used the very powerful technique of laser selective excitation (l.s.e.). This technique was first reported in 1975 by Tallant and Wright (henceforth [TW75]) where it was used to determine the F^- ion sites present in $CaF_2:Er^{3+}$.

The frequency of a narrowband tunable dye laser is set to that of an absorption feature corresponding to a transition between levels of an Er^{3+} ion for a particular site configuration. Many resonant photons of the laser light are absorbed, and a high proportion of Er^{3+} ions in the laser path can be excited to an upper multiplet level. If the absorption line pumped is well resolved from absorption due to sites of other symmetry, then the subset of ions excited will be exclusively those present in a single crystallographic environment. The subsequent radiative decay of the ions enables identification of other crystal field levels associated with that particular site. Traditional optical absorption techniques, on the other hand, have the disadvantage that transitions due to all sites are superposed. For the hydrogenic systems investigated here with many sites present, complete classification by traditional techniques would not be possible. Other advantages of l.s.e. over optical absorption include :

(a) **Advantage of fluoresence.** Absorption transitions occur from the few thermally populated ground state levels, whereas transitions from laser

excited upper levels are normally observed to all ground state multiplet levels.

(b) **Increased ease of study of energy transfer phenomena.** Luminescence from one ion observed after excitation of another ion gives information on mechanisms such as upconversion and cross-relaxation. Excitation by upconversion can give access to multiplets not accessible by direct laser excitation. For example, additional spectroscopic information was obtained by upconversion in the $CsCdBr_3:Er^{3+}$ system.

(c) **Improved sensitivity for small size crystals.** Optical absorption studies require long slabs of single crystal to measure weak features. L.s.e. requires only very small samples.

(d) **Relatively easy identification of local mode phonon frequencies.** For the hydrogenated system for instance, transitions involving simultaneous emission of a photon and a hydride ion local mode vibration phonon occur, giving rise to vibronic transitions.

(e) **Polarisation information.** Absorption transitions of the sites in cubic symmetry crystals are not polarised. In this study it is shown that polarisation of emission, for oriented samples, can identify site symmetries.

1.5 Structure of this Thesis

Chapter Two outlines some of the basic principles such as crystal field theory, localised modes of vibration and

energy transfer phenomena that are encountered during the study, while Chapter Three describes the experimental techniques used for crystal preparation and spectroscopic study.

It is shown in Chapter Four that emission for C_{3V} and C_{4V} symmetry sites in the fluorite crystals is expected to be polarised, and polarisation ratios for the <100> and <111> crystal geometries are calculated. Previous studies have neither reported nor used this effect.

The major emphasis of this investigation is on the spectroscopic study of the hydrogenated $CaF_2:Er^{3+}$ system described in Chapter Five. Optical absorption, laser selective excitation and infra-red spectroscopy are used to determine and classify sixteen hydrogenic sites and five new fluoride ion sites. Isotope studies using deuterium and tritium are also described, together with crystal field computer fitting of tetragonal symmetry sites. C_{3V} symmetry for the F^-B site is confirmed using polarisation dependence of emission.

Chapter Six describes the spectroscopy of the deuterated $SrF_2:Er^{3+}$ system. No optical spectroscopic studies of this system have previously been reported, and nine new D^- ion sites are classified together with nine new F^- ion sites additional to previous studies (Kurz and Wright 1977). The dominant charge compensation mechanism is found to involve nearest neighbour D^- ions in contrast to the next nearest neighbour F^- ions for the non-deuterated system. Trigonal crystal field Hamiltonian computer programs were written and the results of fitting the trigonal symmetry Er^{3+} sites in SrF_2 and CaF_2 are presented and discussed.

A new phenomenon named 'reversible polarised bleaching' was discovered for sites in hydrogenated $CaF_2:Er^{3+}$. Two sites in <100> oriented $CaF_2:Er^{3+}$ and one in $SrF_2:Er^{3+}$ crystals exhibit this effect which is reported in Chapter Seven and attributed to a photo-induced reorientation of tetragonal $Er^{3+} - H^-$ dipoles. Several other hydrogenic sites exhibit a non-reversible bleaching effect which is also discussed.

Chapter Eight outlines the results of the first optical study of the Er^{3+} ion pair site in $CsCdBr_3:Er^{3+}$ crystals. This work utilises the efficient upconversion process that results from laser selective excitation of the site to obtain extensive crystal field level information. Polarised absorption and lifetime measurements are also reported.

Finally, Chapter Nine summarises the thesis and presents several suggestions for further work that arise as a result of this investigation.

CHAPTER TWO

BACKGROUND

2.1 Electronic Spectra of Rare-earth Ions

It was observed as early as 1908 (Becquerel 1908) that the absorption and emission spectra of rare-earth ions in ionic crystals had the rather exceptional property that the linewidths of spectral lines in ionic crystals could be almost as narrow as free ion transitions if measured at low temperatures. Typically the rare-earth ion spectra for crystalline hosts consists of several groups of such narrow transitions with lines within a group being separated by a few hundred cm^{-1} at most, and groups being separated by a few thousand cm^{-1}.

The spectral lines observed arise from transitions within $4f^{11}$ configurations of the typically trivalent rare-earth ions. As the spatial extension of the 4f wavefunction decreases substantially at the commencement of the rare-earth series (Mayer 1941, Latter 1955, Coulson and Sharma 1962) and the binding energy of a 4f electron increases, the trivalent ions are formed by ionisation of the 5d and 6s electrons and, at most, one 4f electron (Wybourne 1965, hereinafter called Wy65). A consequence of this is a decrease in ionic radius as the nuclear charge is increased along the rare-earth series.

The unusually narrow linewidth of the transitions observed for rare-earth ions in ionic crystals is due to shielding of the valence electrons. Since the maximum electron density of the 4f wavefunctions is within the closed shell $5s^2 5p^6$ orbitals, the interaction between the

lattice ionic charges and the 4f electrons is reduced to the extent that the rare-earth ion wavefunctions can often be treated as a perturbation of the free ion states (Wy65 and references therein).

Electric dipole transitions between levels of a pure $4f^N$ configuration are forbidden by the parity selection rule, making the free ion spectra of such transitions very difficult to resolve from allowed transitions between configurations of opposite parity (van Vleck 1937). When the ion is added to a crystalline host, however, the interaction with the crystal field or with lattice vibrations can mix states of different parity into the 4f wavefunctions. The resultant wavefunction admixtures can give rise to readily measurable transitions except for sites, such as the cubic centre in CaF_2, which has a centre of inversion symmetry.

The dominant structure of the spectra of rare-earth ions in solids is the spacing between LSJ multiplets which is determined by interactions within the ion, and approximated closely by that of the free ion. The finer structure is generally caused by the crystal field interaction. An appropriate Hamiltonian for the electronic system is as follows :

$$H = H_F + V_{CF} \tag{2.1}$$

where

$$H_F = -\frac{\hbar^2}{2m_e}\sum_{i=1}^{N}\nabla_i^2 - \sum_{i=1}^{N}\frac{Ze^2}{r_i} + \sum_{i<j}^{N}\frac{e^2}{r_{ij}} + \sum_{i}^{N}\zeta_i(\underline{r}_i)\underline{\ell}_i\underline{s}_i \tag{2.2}$$

H_F is the free ion Hamiltonian and V_{CF} is the crystal field Hamiltonian appropriate for the particular crystal system. Each of the symbols in eqn. (2.2) has its normal meaning, as defined, for instance, by Wybourne (1965), the first term being the sum of electron kinetic energies, the second the nucleus-electron potential energy, the third the inter-electron coulombic repulsion potential, and the final term the relativistic electron spin-orbit interaction. Since the first three terms of eqn.(2.2) commute with $\underline{L}$, the total orbital angular momentum operator, and $\underline{S}$, the total spin angular momentum operator, the basis states often used for the eigenfunctions of the total Hamiltonian are those formed by LS (Russell-Saunders) coupling. However, the spin orbit term, which commutes with neither $\underline{L}$ nor $\underline{S}$, (but does commute with $\underline{J} = \underline{L} + \underline{S}$), splits the ^{2S+1}L terms of LS coupling into $^{2S+1}L_J$ levels distinguished by the J label. As rare-earth ions have a spin orbit interaction of moderate strength compared to the other terms of the Hamiltonian, the intermediate coupling scheme is appropriate. The wavefunctions in this scheme consist of linear combinations of $^{2S+1}L_J$ functions of the same J value but are conventionally labelled by the dominant basis state in each case. In many cases spectroscopists have arbitrarily labelled the terms by an alphabetic character of no particular physical significance. In this study both $^{2S+1}L_J$ labels and single letter labels are used where convenient.

Each of the $^{2S+1}L_J$ terms of the free ion system is (2S+1)-fold degenerate, and much of this degeneracy may be removed by the influence of the crystal field exerted by the surrounding ions in a host lattice. For ions with an odd

number of electrons (Kramers' ions), however, the terms can be split into a maximum of J+½ levels by the electric field (Kramers 1930). Application of an external magnetic field or a magnetic exchange interaction is required to lift the degeneracy totally.

The nature of the crystal field splitting is the primary concern of this study, and the modern theories build on the contribution of many workers on crystal field theory over the last six decades. The original theory was developed by Bethe (1929, 1930) who considered perturbations on the ion wavefunctions by electrostatic fields of neighbouring ions (taken as point charges), and showed that the splittings observed were related to the symmetry of the ion site in the host crystal.

A signficant development in 1952 was the introduction of Stevens' theory of operator equivalents (Stevens 1952) to treat crystal field perturbation using an appropriate linear combination of angular momentum operators as a potential.

Subsequently, the more powerful and elegant Racah tensor operator techniques have been developed, and their application to rare-earth spectroscopy has been summarised by Judd (1963) and Wybourne (1965). This technique involves expressing the crystal field potential V_{CF}, as an expansion of Racah tensor operators :

$$V_{CF} = \sum_{k,q,i} B_q^k \, (C_q^{(k)})_i \qquad (2.3)$$

where B_q^k are the coefficients of the expansion and the Racah spherical tensors are related to the spherical harmonics Y_k^q in the following way :

$$C_q^{(k)} = \left[\frac{4\pi}{2k+1}\right]^{\frac{1}{2}} Y_k^q \quad . \qquad (2.4)$$

The first term of the expansion with $k = q = 0$ is spherically symmetric and is ignored for crystal field splitting since it shifts all levels uniformly. For f electrons with orbital angular momentum $\ell = 3$, only terms with $k \leq 6$ may be non zero and the $k = 1, 3, 5$ terms vanish for interaction within a configuration of equivalent electrons. These rules leave a maximum of eleven non zero components of the expansion, namely : B_0^2, B_2^2, B_0^4, B_2^4, B_3^4, B_4^4, B_0^6, B_2^6, B_3^6, B_4^6 and B_6^6. The relationship of these parameters to the Stevens operator equivalents has been previously summarised (Wy65, Dieke 1968 and others).

The important application of the technique is that the required values of k are further restricted by the point group symmetry of the site of the ion. For instance, the forms of the potential for the C_{4V} and C_{3V} point group symmetries are presented and used in Chapters Five and Six of this study. The Racah tensors used are those which transform according to the identity representation under the symmetry operations of the point group. The form of the potential can thus be generalised for a wide variety of crystal systems with the same point group symmetry, despite different lattice constants or ions involved.

Wybourne (1965) and Judd (1963) have provided convenient summaries of the method of determination of the matrix elements of the crystal field potential and this is outlined below.

The f^N wavefunctions of levels split by the crystal field may be expressed as linear combinations of basis functions characterised by the L, S, J and J_z quantum

numbers. The matrix elements required for the crystal field expansion are given by :

$$\langle SLJJ_z|V_{CF}|SL'J'J'_z\rangle = \sum_{kq} B^k_q \langle SLJJ_z|U^{(k)}_q|SL'J'J'_z\rangle \times \langle \ell \|C^{(k)}\| \ell \rangle \qquad (2.5)$$

where $$\langle \ell \|C^{(k)}\| \ell \rangle = (-1)^{\ell}(2\ell+1)\begin{pmatrix} \ell & k & \ell \\ 0 & 0 & 0 \end{pmatrix} \qquad (2.6)$$

Here the last term is the 3j symbol, $\ell = 3$ for the f electrons of rare-earth ions, and $U^{(k)}_q$ is the unit tensor operator which is diagonal in S.

Application of the Wigner-Erkart theorem gives the J_z dependence in the form of a 3j symbol :

$$\langle SLJJ_Z|U^{(k)}_q|SL'J'J'_Z\rangle = (-1)^{J-J_z}\begin{bmatrix} J & k & J' \\ -J_z & q & J'_z \end{bmatrix} \times \langle SLJ\|U^{(k)}\|SL'J'\rangle \qquad (2.7)$$

The J dependence can be decoupled using a 6j symbol (in curved brackets), since

$$\langle SLJ\|U^{(k)}\|SL'J'\rangle = (-1)^{L'+S'J+k}\sqrt{(2J+1)(2J'+1)}\begin{Bmatrix} J & J' & k \\ L' & L & S \end{Bmatrix} \times \langle SL\|U^{(k)}\|SL'\rangle \qquad (2.8)$$

The appropriate doubly reduced unit tensor operator matrix elements can be obtained from Nielson and Koster (1964), and 3j and 6j symbols are tabulated by Rotenberg *et al.* (1959).

The matrix elements for the various k, q values allowed for the particular point group symmetry can then be

calculated and expressed as separate matrices. If each of these matrices is multiplied by the appropriate B_q^k parameter and all are then summed, diagonalisation of the final matrix should yield eigenvalues corresponding to the observed energy levels and eigenfunctions specifying the appropriate wavefunctions in the $|LSJJ_z>$ basis.

2.2 Energy Levels of the Er^{3+} Ion

The rare-earth ion studied in this work is trivalent erbium. Erbium has an atomic number of 68 and has the following electron configurations in addition to the closed shell structure of the xenon atom :

Er	Er^+	Er^{2+}	Er^{3+}
$4f^{12}6s^2(^3H_6)$	$4f^{12}6s(^4H_{13/2})$	$4f^{12}(^3H_6)$	$4f^{11}(^4I_{15/2})$

The ground state multiplet for each configuration is in brackets.

The ionic radius of Er^{3+} is 0.88Å which is relatively small compared with the extreme values for the rare-earth series of 1.03Å(Ce^{3+}) and 0.85Å(Lu^{3+}) (*CRC*, 1982).

Figure 2.1 shows the $^{2S+1}L_J$ multiplets for the $4f^{11}Er^{3+}$ ion, and it is apparent that transitions between several multiplets in the optical region are convenient for optical spectroscopy. The f^{11} system of Er^{3+} has three 'holes' in the 4f shell and can be treated as equivalent to the f^3 system of Nd^{3+} except that the sign of the charge is opposite in the coulombic terms, giving rise to a reversal of the order of J components for a given LS term. The odd number of electrons gives Kramers degeneracy for each of the crystal-field split levels.

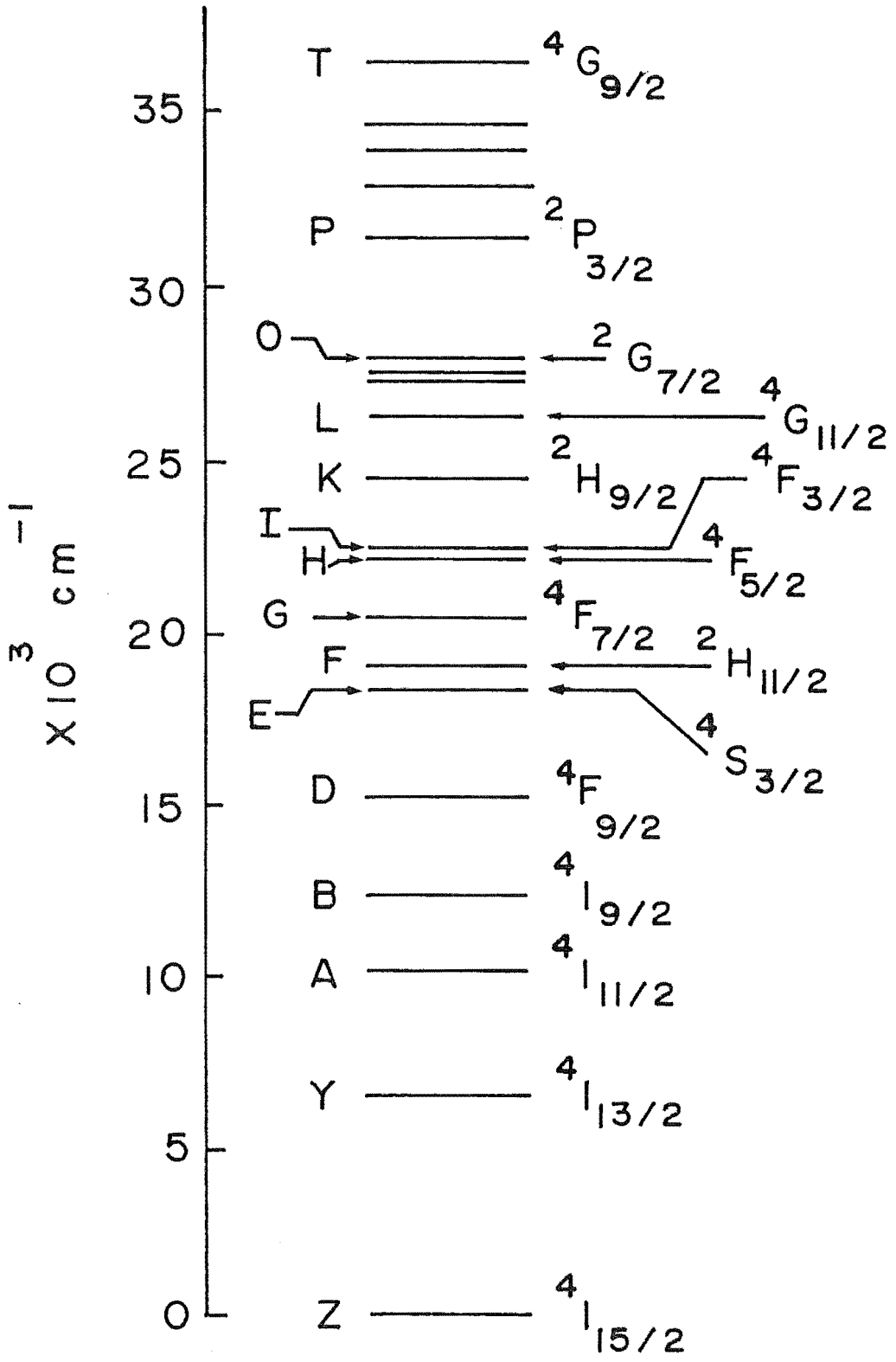

Figure 2.1 : Free ion Er^{3+} energy levels of the $4f^{11}$ configuration.

2.3 Energy Transfer Between Ions in Pair Sites

The doped CaF_2 (Tallant and Wright 1975), SrF_2 (Kurz and Wright 1977) and $CsCdBr_3$ (Barthem *et al.*1985) hosts all have stable, and in the latter case dominant, crystallographic sites involving two or more RE^{3+} ions in close proximity. Although the $4f^{11}$ electrons are well shielded from neighbouring influences, certain processes rely on the small interactions that do occur. If the inter-ionic spacing becomes small enough there can be sufficient overlap of the wavefunctions to affect efficient transfer of energy between rare-earth ions (Wright 1976, hereinafter called Wr76, and references therein). The development over the last two decades of intense, narrowband tunable lasers able to generate high excitation densities of such centres has made the study of such energy transfer both possible and necessary.

These processes account for many of the practical applications to which rare-earth ions have been applied. For instance, many phosphors use rare-earth ion activators including infra-red to visible phosphors (Auzel 1973). The use of rare-earth ions as infra-red quantum counters (IRQC) (Brown and Shand 1970 and references therein) is also well documented, and certain solid state laser processes are enhanced by energy transfer between rare-earth ions (Johnson and Guggenheim 1971).

Two review articles on energy transfer in rare-earth doped materials provide a thorough discussion about the two main classes of energy transfer, ion pair relaxation and upconversion outlined here (Wr76, Riesberg and Weber 1976). The energy transfer processes of sites in $CaF_2:Er^{3+}$ are

specifically discussed by Tallant *et al.* (1976).

Non-resonant ion pair relaxation may occur when one ion in the pair is excited by a laser pulse and the other is in a low energy state. The excited ion can decay radiatively, non-radiatively by creation of lattice phonons, or alternatively, the energy can be transferred to the other ion by ion pair relaxation with energy conservation by creation or annihilation of phonons. It was shown by Miyakawa and Dexter (1970) that the energy transfer rate between ions is proportional to $e^{-\alpha\Delta E}$ where ΔE is the energy mismatch involved in the non-resonant energy transfer. In general, low temperature measurements such as those used in this study preclude the observation of pair relaxation processes involving the annihilation of lattice phonons. Tallant *et al* (1976) have shown that in some cases the pair relaxation mechanism can compete effectively with the rapid single ion multiphonon decay process for the excited ion. Evidence for such mechanisms is provided by studying the time dependence of the fluorescence transients for such centres, and somewhat complex mechanisms can be deduced with careful scrutiny. Figure 2.2 shows an example of a succession of relaxations proposed by Tallant *et al.* to account for the decay, after laser excitation, of the dimer sites of $CaF_2:Er^{3+}$.

Upconversion provides an alternative process of energy transfer between ions. One mechanism for this process, known as co-operative upconversion, requires two ions in a pair to be simultaneously excited. Subsequent transfer of energy between these ions results in one of them being excited to an energy greater than that of excitation. Bloembergen (1959) first proposed an alternative "stepwise"

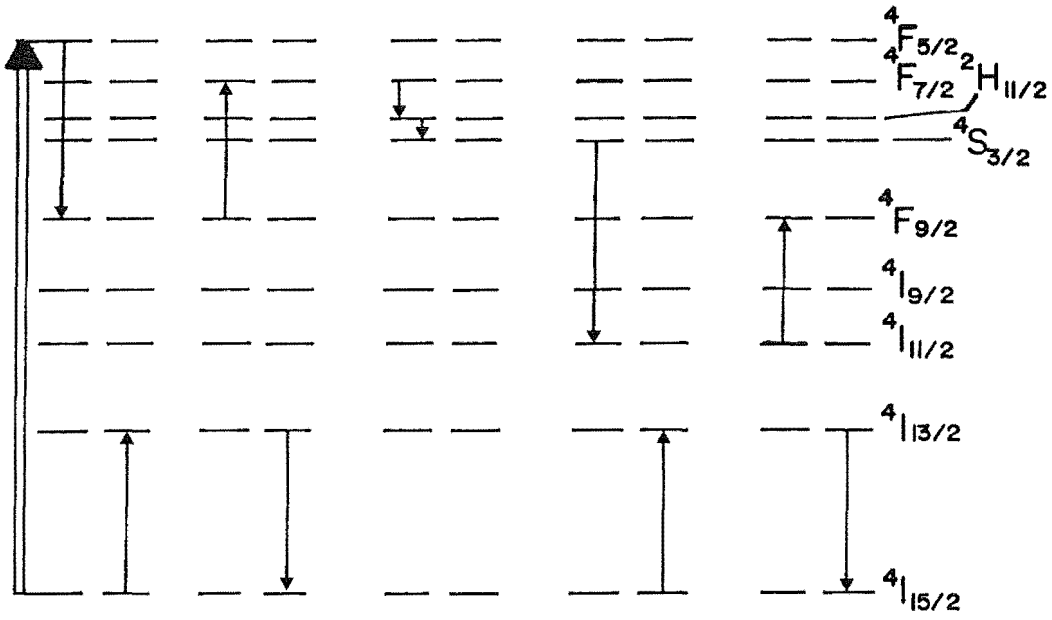

Figure 2.2 : An example of relaxation processes between ions in a pair site upon laser excitation of $^4I_{15/2} \rightarrow {}^4F_{5/2}$ transitions. This scheme was proposed by Tallant *et al.* (1976) for dimer sites in $CaF_2:Er^{3+}$.

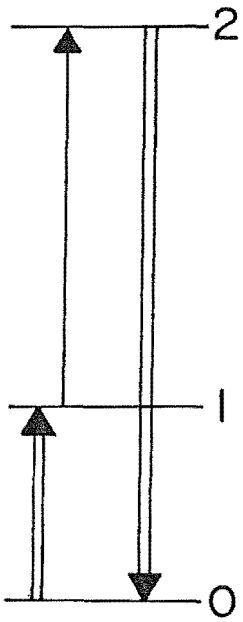

Figure 2.3 : Stepwise upconversion process as applied to infra-red quantum counters. An optical source is tuned to the transition energy gap 1-2. Absorption of incident infra-red radiation of energy 0-1 results in optical emission between levels 2 and 0.

upconversion process, illustrated in Figure 2.3, which was absorption from an already excited state rather than from the ground state. This involved providing an excitation source tuned to the energy gap between levels 1 and 2 (Figure 2.3), such that if infra-red radiation is subsequently absorbed between 0 and 1 then the visible fluorescence between 2 and 0 can be observed. It was then shown by Esterowitz *et al.* (1967) that the energy gap between 1 and 2 can be best provided by energy transfer from an excited donor ion added to the sample. Schemes of this nature are the basis of infra-red quantum counters.

A three-body co-operative upconversion process has also been observed for systems double doped with Tb^{3+} and Yb^{3}, where two excited Yb^{3+} ions simultaneously transfer their energy almost resonantly to a Tb^{3+} ion in the trimer site (Feofilov and Ovsyankin 1967).

The most studied upconversion process involving Er^{3+} ions is the double doped system involving Er^{3}-Yb^{3+} clusters, and much of this work has been summarised by Wright (1976). The Yb^{3+} ion has a single 4f manifold, $^{2}F_{5/2}$, around 10500 cm^{-1}, which can decay to give excitation of the Er^{3+} ion initially to its $^{4}I_{11/2}$ manifold and subsequently to the $^{4}F_{7/2}$ multiplet. Non-radiative decay to the $^{4}S_{3/2}$ or $^{4}F_{9/2}$ multiplets is followed by visible emission from the Er^{3+} ion as it relaxes to its $^{4}I_{15/2}$ ground state. A practical application of this is to a phosphor recently developed using CdF_2:Er^{3}/Yb^{3+}. The Yb^{3+} excitation to the $^{2}F_{5/2}$ level can be conveniently supplied by the 0.93 μm infra-red emission of a Si:GaAs diode. By variation of the concentration of Yb^{3+} the combined system can be made to emit either red ($^{4}F_{9/2} \rightarrow {}^{4}I_{15/2}$) or green ($^{4}S_{3/2} \rightarrow {}^{4}I_{15/2}$)

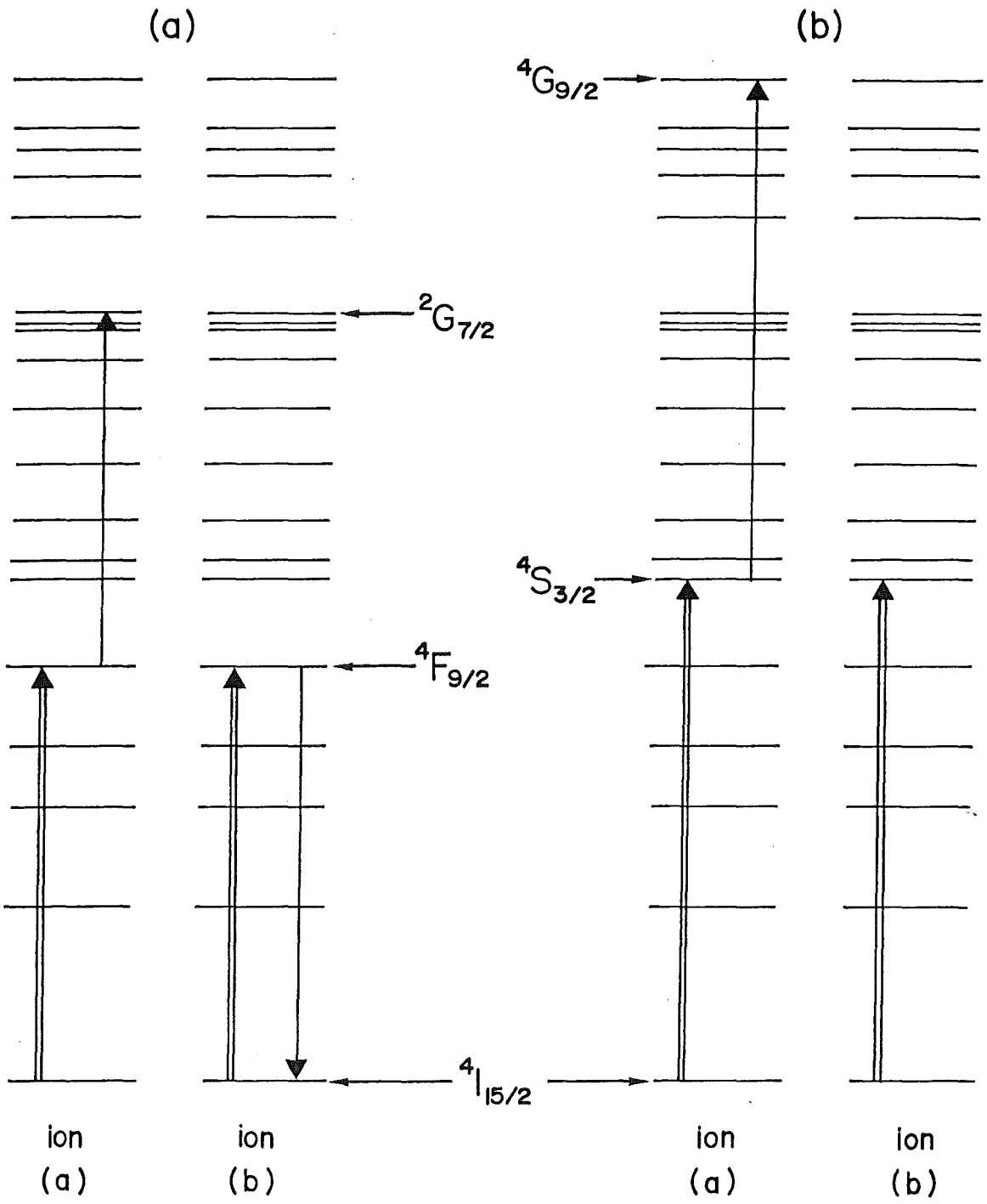

Figure 2.4 : Upconversion mechanism proposed by Tallant *et al.* (1976) for dimer sites in $CaF_2:Er^{3+}$ (a) for $^4I_{15/2} \rightarrow {}^4F_{9/2}$ excitation, and (b) for $^4I_{15/2} \rightarrow {}^4S_{3/2}$ excitation.

light (Greenblatt and Banks 1977).

Tallant and Wright (1975) investigated upconversion for the C, C', and D sites of $CaF_2:Er^{3+}$ and observed $^4S_{3/2} \rightarrow {}^4I_{15/2}$ emission for $^4I_{15/2} \rightarrow {}^4F_{9/2}$ excitation. They subsequently proposed (Tallant *et al.*1976) the two schemes of Figure 2.4 for upconversion upon $^4F_{9/2}$ or $^4S_{3/2}$ excitation.

2.4 Lattice Vibrations in Fluorite Crystals

The generalised theory of lattice vibrations in perfect lattices is outlined in several standard references (for example, Ziman 1972), and is not detailed here. The solution of the lattice dynamics of a crystal makes use of the translational symmetry of the lattice to reduce the problem to a finite number of equations of motion. An expression for the potential energy is expanded in a Taylor series of the powers of atomic displacements, and the harmonic approximation is usually assumed. The equations of motion can be expressed concisely using a force constant tensor, and if plane wave solutions for the form of the displacement are chosen, then an expression involving the associated dynamical matrix is obtained which can be solved to give the frequencies of vibration, ω, as a function of wavevector, $\underline{k}$.

Solution of the phonon dispersion relations $\omega(\underline{k})$ for a system with three atoms per unit cell, such as CaF_2, gives nine lattice phonon branches with six optical, and three acoustical, modes. The interaction of light with a mode depends on the nature of the vibrational motion for that mode. Three of the optical modes, involving relative motions of ions with identical charges, are Raman active,

whereas the other three optical modes change the electric dipole moment of the unit cell by relative motion of ions with different charges and are infra-red active.

2.5 Localised Modes of Vibration

The main interest in vibrational dynamics in this study is the behaviour of hydride ions in the fluorite lattices. Introduction of such defects destroys the translational periodicity of the lattice, and the normal vibrational modes are modified. The solution to the problem of point defects in three dimensions is difficult but can be solved exactly in some cases using Green's functions (Maradudin *et al*.1963). The principal qualitative features of the vibration of an atom of different mass to its neighbours can be determined by considering the one dimensional case of a linear diatomic chain (Newman 1973, hereinafter called Ne73).

An infinite chain of atoms separated by distance 'a' with alternate atoms having mass m and M and effective spring force constants equal to 'f' have the following equations of motion if nearest neighbour harmonic forces only are considered :

$$M\ddot{x}_{2n} = f(x_{2n-1} + x_{2n+1} - 2x_{2n}) \qquad (2.9)$$

$$m\ddot{x}_{2n+1} = f(x_{2n} + x_{2n+2} - 2x_{2n+1}) \qquad (2.10)$$

where x_{2n} is the longitudinal displacement of the 2nth atom from its equilibrium position.

These equations have travelling wave solutions, using the notation of Newman (1973), of the form :

$$x_{2n} = A\exp[-i(\omega t-2nqa)] \qquad (2.11)$$

and $$x_{2n+1} = B\exp[-i(\omega t-(2n+1)qa] \qquad (2.12)$$

where q is the wavevector of a mode and A and B are amplitudes of vibration for atoms of mass M and m respectively.

For non-vanishing values of A and B, the solution for ω has the form

$$\omega^2 = f(\frac{1}{m}+\frac{1}{M}) \pm f\left[(\frac{1}{m}+\frac{1}{M})^2 - \frac{4\sin^2 qa}{Mm}\right]^{\frac{1}{2}} \qquad (2.13)$$

These two solutions labelled "+" and "-" are plotted against wavevector in Figure 2.5 with the upper branch being the optic mode, with neighbouring atoms oscillating in opposite directions, and the lower branch, the acoustic mode, having A and B of the same sign. This lattice will not propagate vibrations with frequencies either higher than ω_{max} or in the band gap between the two modes

where $$\omega^2_{max} = 2f(\frac{1}{m}+\frac{1}{M}) \qquad (2.14)$$

and the band gap lies between

$$\omega = (2f/M)^{\frac{1}{2}} \quad \text{and} \quad \omega = (2f/m)^{\frac{1}{2}} \qquad (2.15)$$

In the case of a lighter atom of mass m' being substituted for an atom of mass m, a high frequency mode for q=0 occurs with frequency

$$\omega = \left[2f\left(\frac{1}{m'} + \frac{1}{\alpha M}\right)\right]^{\frac{1}{2}} \qquad (2.16)$$

where α is a modifying parameter such that $\alpha \rightarrow 1$ as $m' \rightarrow m$ and $\alpha \rightarrow 2$ as $m' \rightarrow 0$; or, alternatively, if the heavier atom with mass M is replaced by a ligher atom of mass M', then

$$\omega = \left[2f\left(\frac{1}{M'} + \frac{1}{\alpha m}\right)\right]^{\frac{1}{2}} . \qquad (2.17)$$

Both of these frequencies are greater than the value of ω_{max} and are increased as the mass ratio of the substitutional light atom to the original lattice atom is increased. For very light atoms, this results in a highly localised mode of vibration that cannot be propagated by the lattice. It can be shown (Montroll and Potts 1955) that for the case of a monatomic chain (with m = M) the amplitude of vibration, x_r, of the rth neighbour of the impurity atom (mass = m') is :

$$x_r = (-1)^r \left(\frac{1 - \epsilon}{1 + \epsilon}\right)^{|r|} x_o \qquad (2.18)$$

where x_o is the amplitude of the impurity atom

and $\epsilon = \left(\frac{M - m'}{M}\right)$.

Thus as $\frac{m'}{M}$ is decreased, the amplitudes decrease rapidly with r. A similar localised mode can be verified for a diatomic chain (Ne73) system.

The case considered in this study is the substitution of H^- ions and D^- ions in the fluorite lattice. Since the ions are charged, the localised modes are infra-red active

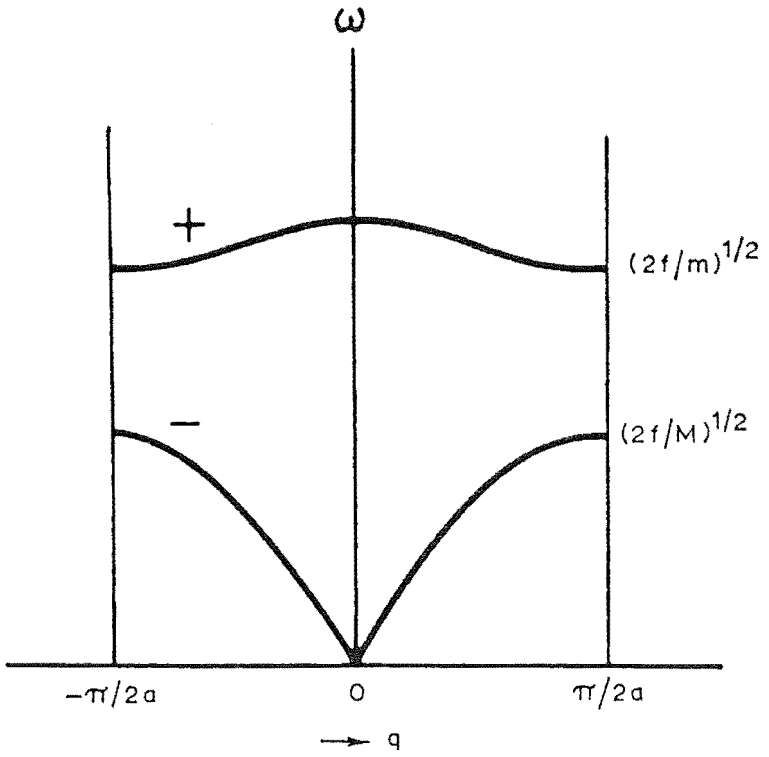

Figure 2.5 : Normal mode frequencies of a diatomic linear chain as a function of the wavevector, q (after Newman (1973)).

and can be observed as sharp absorption lines around 1000 cm^{-1} for H^- ions. This frequency is more than twice the highest lattice vibrational frequency (463 cm^{-1}), and it has been shown (Elliott *et al.* 1965) that the H^- ion can be treated in the static potential well approximation, since the motion from equilibrium of neighbouring lattice ions that determines the potential can be regarded as negligible. This approximation was justified since the ratio of H^-/D^- local mode frequencies was found to be 1.39 in close agreement with the expected ratio of $\sqrt{2}$ with ω proportional to $m^{-½}$ and m doubled for D^- ions.

An estimate of the mean square displacement of the H^- ion can be made. For $\omega = 1000\ cm^{-1}$ this is given by $\langle\Delta x\rangle^2 = \hbar/2m\omega = 1.74\times10^{-22}m^2$. This corresponds to an amplitude of approximately 5% of the $F^- - F^-$ separation in CaF_2.

2.6 The Vibrational Hamiltonian

An H^- ion in CaF_2 or SrF_2 can be treated as a single particle anharmonic oscillator in a three dimensional potential well that must be invariant under the symmetry operators of the appropriate point group of the H^- ion for that particular site.

The forms of the potential energy for four site symmetries of H^- ions in MeF_2 lattices have been considered (Ne73 and references therein). These have point group symmetries of cubic (O_h) for an isolated interstitial H^- ion, tetrahedral (T_d) for a substitutional H^- ion in the centre of a tetrahedron of Me^{2+} ions, tetragonal (C_{4V}) for an interstitial H^- ion next to a trivalent rare-earth ion

(Figure 1.2a), and trigonal (C_{3V}) for an interstitial H^- ion in a next nearest neighbour position to the rare-earth ion (Figure 1.2b).

An example of the vibrational Hamiltonian with modes observed in this study is that of C_{4V} point symmetry which has a potential of the form :

$$V = a(x^2+y^2) + bz^2 + cz^3 + dz(x+y) + f(x^4+y^4) + gz^4 + hz^2(x^2+y^2) + kx^2y^2 + \ldots \text{higher order terms.} \quad (2.19)$$

In the harmonic approximation using the first two terms only, two fundamental frequencies for the first excited state are obtained with :

$$\omega_x = \omega_y = \sqrt{\frac{2a}{m}} \quad \text{and} \quad \omega_z = \sqrt{\frac{2b}{m}} \quad (2.20)$$

where m is the H^- ion mass.

If n_1, n_2 and n_3 are the phonon occupation numbers for three dimensional harmonic oscillators in the x,y and z directions, then the wavefunctions can be denoted by $|n_1n_2n_3\rangle$ and the energies of the levels given by :

$$E_{n_1n_2n_3} = (n_1+\tfrac{1}{2})\hbar\omega_x + (n_2+\tfrac{1}{2})\hbar\omega_y + (n_3+\tfrac{1}{2})\hbar\omega_z \quad . \quad (2.21)$$

Thus the two energies of the first excited state are :

$$E_{100} = E_{010} = 2\hbar\omega_x + \tfrac{1}{2}\hbar\omega_z \quad \text{and} \quad E_{001} = \hbar\omega_x + \tfrac{3}{2}\hbar\omega_z \quad . \quad (2.22)$$

The effect of the anharmonic terms can be evaluated using perturbation theory in the creation and annihilation operator formalism and results in a shift of all energy

levels and allows the appearance of certain harmonics.

A solution of the C_{4V} symmetry problem has been obtained by Maradudin and Peretti (1967). The application of group theory is useful for this problem since the wavefunctions for each of the levels decompose into irreducible representations of the C_{4V} group. It was shown that the first excited level decomposes to $^1\Gamma_1 + {}^2\Gamma_5$ and the second excited level can be reduced to $2{}^1\Gamma_1 + {}^1\Gamma_3 + {}^1\Gamma_4 + {}^2\Gamma_5$. Infra-red active transitions are those between two levels with wavefunctions having irreps Γ_a and Γ_b where Γ_a x Γ_b contains an irrep of the electric dipole operator which transforms as $^1\Gamma_1 + {}^2\Gamma_5$. In this case the ground state $|000\rangle$ is of Γ_1 symmetry, so that two transitions occur between the ground state and first excited state ($^1\Gamma_1$ and $^2\Gamma_5$), and three infra-red active transitions occur between the ground and second excited states ($^1\Gamma_1$, $^1\Gamma_1$ and $^2\Gamma_5$).

For the H^- C_{4V} site in $CaF_2:Er^{3+}$ the two first excited state modes have energies of $\omega_z = 1081$ cm^{-1} and $\omega_{xy} = 1037$ cm^{-1} (Elliott *et al.*1965) corresponding physically to a vibration of the H^- ion in the direction of the axis of symmetry (z), and vibration on the xy plane, respectively.

2.7 Electron-phonon Interaction

The electron-phonon interaction is the coupling between the electronic states of the rare-earth ion and the local mode vibrational states of the hydride ion. It is responsible for several phenomena observed in studies such as this, including :

(a) a shift in the electronic levels of the rare-earth ion if different isotopes of hydrogen are used,

(b) related isotope shifts of g values,

(c) splitting of some vibrational modes,

and (d) the occurrence of vibronic transitions involving local mode phonons.

The interaction arises because of a change in the crystal field seen by the rare-earth ion as the neighbouring H^- ion is displaced from equilibrium during vibration. If the static crystal field is V^o_{CF} and the new field for a displacement from equilibrium is V'_{CF}, then the electron phonon interaction potential is :

$$V_{ev} = V'_{CF} - V^o_{CF} \quad . \tag{2.23}$$

The interaction can be expressed as a general power series expansion in the normal co-ordinates Q_i, such that:

$$V_{ev} = \sum_i f_i Q_i + \sum_{i,j} g_{i,j} Q_i Q_j + ... \tag{2.24}$$

This is simplified for the H^- ion vibration case since the normal co-ordinates are simply X,Y and Z, the displacements of the ion from equilibrium in the cartesian co-ordinate system, so that :

$$V_{ev} = f_z Z + f_x X + f_y Y + g_{zz} Z^2 + g_{xx} X^2 + g_{yy} Y^2 + g_{xy} XY + g_{xz} XZ + g_{yz} YZ + \ldots \tag{2.25}$$

The effects of the electron phonon interaction have been outlined by Jacobs *et al.* (1971) for the case of Ce^{3+}, where relatively large effects were observed associated with the 4f → 5d electronic transitions around 30,000 cm^{-1}. These effects are enhanced compared to those of 4f → 4f

transitions, since the 5d orbitals are not shielded. H^-/D^- isotope shifts of the order of 15 times those of Er^{3+} sites were observed. The interaction is treated as a perturbation of the electronic Hamiltonian (eqn 2.1), and the combined system has for a basis the product states of the electronic and vibrational wavefunctions :

$$|\phi> = |JJ_z>|n_1n_2n_3> \qquad (2.26)$$

It has been shown for the C_{4V} site that the electronic level isotope shift between H^- and D^- ion sites is due to three terms (Edgar *et al.*1979 and references therein). The first is the first order, second degree term involving g_{zz}, the second is due to mixing of the vibrational states by the anharmonic terms of the vibrational Hamiltonian, and the third is a term involving an interaction between two closely spaced electronic levels of energy E_i and E_j. The net energy level shift δ_i^{H-D}, of the ith level is the difference for H^- and D^- of :

$$\delta_i = \beta<\phi_i|Z'|\phi_i> + \alpha<\phi_i|X'|\phi_i>$$

$$-\Sigma_k\left(\frac{\hbar}{2m\omega}\right)_k \Sigma_{i\neq j} \left(|<\phi_i|f_k|\phi_j>|^2\right)/(E_j-E_i+\hbar\omega_k) \qquad (2.27)$$

$$\text{where} \quad k = x,y,z \quad , \quad \alpha = \frac{\hbar}{2m\omega_x} \quad , \quad \beta = \frac{\hbar}{2m\omega_z} \qquad (2.28)$$

$$<\phi_i|Z'|\phi_i> = <\phi_i|g_{zz}|\phi_i> - [(3c<\phi_i|f_z|\phi_i>)/2m\omega_z^2]$$
$$\text{and} \quad <|\phi_i|X'|\phi_i> = <\phi_i|g_{xx} + g_{yy}|\phi_i> - [(2d<\phi_i|f_z|\phi_i>/2m\omega_z^2] \qquad (2.29)$$

The labels c and d are the coefficients used in equation 2.19. The contribution from the interaction with

the nearby states ϕ_j (the third term in equation 2.27) is small in most cases, and isotope shifts for 4f-4f transitions are typically of the order of 1 cm^{-1}.

Another important consequence of the electron-phonon interaction that is utilised in this study is the occurrence of vibronic fluorescence transitions at frequencies reduced from the electronic transitions by approximately the local mode phonon energies of the H^- ion. Edgar *et al.* (1979) have summarised the local mode vibronic shifts expected and compared the local mode intervals from vibronic transitions in the optical absorption spectra to those measured directly in the infra-red spectra for six transitions in the $CaF_2:Er^{3+}$ system.

The treatment of the electron-phonon interaction outlined above assumes a point charge for each of the ions involved. Jacobs *et al.*(1971) extended the 'model to account for a nonlinear polarisation of the H^- ion by the nearby rare-earth ion. It was shown that the H^- ion can then be represented by a dipole moment directed towards the rare-earth ion with the dipole assumed to have constant magnitude independent of instantaneous position. This model accounted for the lowering of frequency from the cubic value for both the (X,Y) and Z vibrational modes of all C_{4V} centres and also for the reduction of intensity of the (X,Y) mode compared to the Z mode for the infra-red spectrum of the Ce^{3+} site.

2.8 Covalency Effects

In all previously reported cases the centre of gravity of electronic levels of H^- ion charge compensated sites is reduced from that of the equivalent F^- ion sites for all

excited state multiplets. It has been shown by Jones and Satten (1966) that this effect is primarily due to a change in the covalent bonding of the rare-earth ion with its neighbours and in particular with the H^- ion. The effect due to the change of crystal field was shown to account for only a small component of the overall decrease.

The effect is significant in this study as transitions of sites involving two H^- ions were found to be reduced further in energy compared to similar sites involving a single ion.

CHAPTER THREE

EXPERIMENTAL TECHNIQUES

3.1 Crystal Preparation

3.1.1 $CaF_2:Er^{3+}$ and $SrF_2:Er^{3+}$

Most of the erbium doped CaF_2 crystals and all of the SrF_2 crystals used in this study were grown in this department using an Arthur D.Little 38 kW radio frequency induction furnace. The remainder of the $CaF_2:Er^{3+}$ crystals used were purchased from Optovac Inc. (U.S.A.). Rare-earth concentrations of 0.05mol% were typically used although some 0.01mol%Er^{3+} crystals were grown. These concentrations are small enough to ensure cluster sites do not dominate the system.

The crystals were grown from alkaline earth fluoride starting material purchased in the form of pre-grown crystal fragments from Optovac Inc. This material was crushed and a measured weight of ErF_3 (99.9%, Alpha Inorganics Inc., U.S.A.) added to a graphite crucible with inside diameter of typically 10 mm. On some occasions a small amount (less than 2% by weight) of lead fluoride was added to act as an oxygen scavenger. This procedure was not widely adopted as the oxygen content was found to be sufficiently low without it.

The crystals were grown using the Bridgman-Stockbarger technique of lowering the crucible containing the crystal material slowly through a temperature gradient. In most cases a lowering speed of 3.5 mm/hr was used giving a growth time of about 18 hours. The crystal was then annealed by

decreasing the temperature slowly over a period of twenty-four hours before being removed. It was found that this improved the durability of the crystals and prevented cracking during hydrogenation. A vacuum of approximately $4x10^{-6}$ torr was maintained in the furnace during crystal growth by an oil diffusion pump.

Some crystals oriented in either a <100> or <111> direction were used in this study for polarisation work. These crystals were cut from unoriented stock grown here. The principal plane of cleavage in CaF_2 and SrF_2 is the (1,1,1) plane and crystals with two parallel cleaved surfaces are oriented in the <111> direction. Alignment in the <100> direction was more difficult and required the following procedure. The intersection of two (111) cleavage planes forms a line in the <110> axis direction with an angle between the two planes of $\theta \simeq 109.5^{o}$. A wedge of this angle was cut from the end of a brass rod and the crystal was glued onto it. This rod was then fastened to a diamond saw bench and the crystal was aligned with the <110> axis direction vertical and parallel with the blade surface. A swivel joint on the saw bench enabled the long axis of the rod to be set at 45^{o} with respect to the line normal to the plane of the blade surface while maintaining a vertical <110> axis, and cuts at this angle were made part way through the crystal boule. The brass rod was then rotated by 90^{o} about the <110> crystal axis again to form a 45^{o} angled with the line normal to the blade. Slices of the crystal cut at this angle then had three well-defined <100> surfaces.

3.1.2 Hydrogenation

Hydrogen or its isotopes were introduced into the crystals in the form of H^-, D^- or T^- ions by the method of Hall and Schumacher (1962). Flat aluminium coils of the same diameter of the crystals were wound from 99.99% pure aluminium wire. These coils and the crystal were then carefully cleaned with acetone and the crystal was placed between two coils in an alumina crucible. The crucible was then placed in a quartz tube and evacuated to a vacuum of better than 10^{-4} torr using a rotary backed mercury diffusion pump, and the tube was placed in a thermostatically controlled electric furnace. It was then gradually heated to 180°C and allowed to bake under vacuum for approximately five hours in an attempt to remove moisture. Dry hydrogen or deuterium gas was then flushed through the system two or three times and the tube was sealed with a gas pressure of about 70kPa. The system was then normally heated to 860°C and held at this temperature for a period of time (hereinafter referred to as the "duration of hydrogenation") before being cooled.

Three methods of cooling were used :

(i) Leaving the tube in the furnace to cool after switching off the power. This typically cooled exponentially and reached room temperature after three hours;

(ii) the quartz tube is removed while at 860°C and plunged into liquid nitrogen; or

(iii) the tube is removed while at 860°C and allowed to cool to room temperature.

The last cooling method was used for most crystals since

method (ii) tended to crack the crystals and method (i) left a greater concentration of cluster sites than desired.

The duration of hydrogenation used in other studies (Thompson 1983, Edgar *et al.* 1979 and references therein) has been typically four to sixteen hours. It was found in this study that the site distribution was much richer when longer durations in the range sixteen to 144 hours were used.

The system temperature was determined using a thermocouple in the space between the tube and the heating coil. For this reason, coupled with the relatively high thermal conductivity of hydrogen (since some of the volume of the tube was outside the hottest part of the furnace), the sample temperature may be slightly lower than indicated. The critical factor for successful hydrogenation is that the aluminium coil is melted onto the surface.

Crystals after hydrogenation often had fragments of aluminium attached to the surface and this was removed by etching in dilute hydrochloric acid. This treatment did not affect the spectroscopic properties of the crystal in any way.

Before experimental use, all crystals were polished either by hand using various grades of carborundum grit on a glass or plastic surface, or alternatively, using tin oxide on a felt covered polishing wheel. In all cases it was found that the hydrogen content was approximately uniform throughout the crystals and such grinding or polishing did not remove a noticeable quantity of hydrogen compensated rare-earth ion sites.

Tritium gas was purchased in small capsules containing

4 cc at S.T.P. and 10 ci from Amersham International. A smaller volume quartz tube was constructed to increase the gas pressure attainable, and into it was placed the capsule together with the crystals in a crucible. The tritium capsule was then broken with a rod and the system heated for 65 hours and cooled to room temperature. The gas pressure by this method was about ten per cent of that for normal hydrogenation.

3.1.3 $CsCdBr_3:Er^{3+}$

Some of the results reported were obtained using a crystal (0.7mol%Er^{3+}) supplied by Dr A. Edgar, Victoria University of Wellington, that was grown at the Australian National University. Other crystals used were grown in this department.

These crystals were prepared using stoichiometric quantities of the powdered starting materials $CdBr_3$ (99%, Hopkins and Williams), $CsBr_3$ (99.9% Aldrich Chemical Co.Ltd.) and Er_2O_3 (99.9%, Semi-elements Inc.). The last-named is used since $ErBr_3$ is not readily available.

The preparation technique used is one that was developed by Mr R. Ritchie in this department. First the materials are added to a quartz tube of diameter 8 mm having a small bulb with pointed tip at the end formed by a constriction of the inside tube diameter to about 2 mm at a position 15 mm from the end of the tube. This constriction increases the likelihood of formation of a single well defined crystal growth axis. A quartz sieve prevents the material from filling the tube until melted, as shown in Figure 3.1. Dry hydrogen bromide gas was then passed

through the powdered mixture as the temperature was raised from room temperature to 700°C over a period of three hours. This had the effect of excluding air and water vapour while melting the material. The direction of gas flow was then reversed and the melted material was forced through the sieve to the bottom of the tube which was then sealed off.

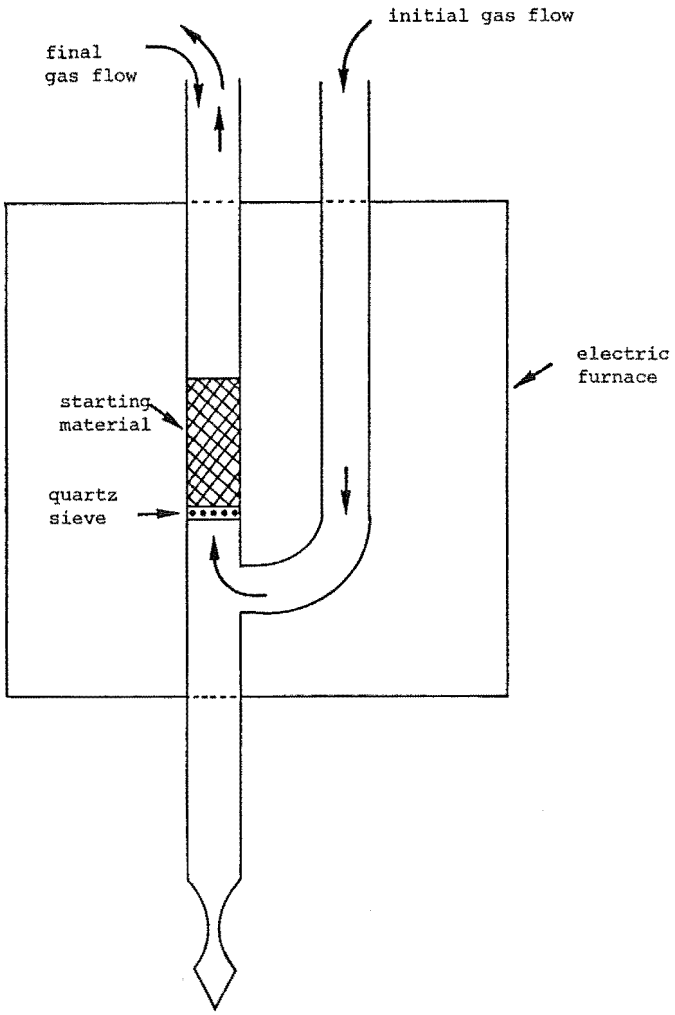

Figure 3.1 : Tube used for growth of $CsCdBr_3:Er^{3+}$ crystals.

The crystals could be grown in these capsules by lowering them through the well defined temperature gradient of a department-built Bridgman furnace at a rate of 0.42 mm/hour. The furnace temperature gradient was established

by two separate thermostatically controlled heating coils set to 560°C and 330°C. After five to seven days the full length of crystal had been grown and then it was annealed by decreasing the temperature at a constant rate for eighteen hours until at room temperature.

Although the resultant crystals were not uniform throughout, sufficient good quality material from each crystal boule was obtained to be used for fluorescence experiments. Starting material erbium concentrations of 0.3mol% and 0.7mol% were used, but it is probable that some of the erbium was not dissolved in the system since there seemed to be a lower concentration in this department's crystals than the A.N.U. crystal.

Since $CsCdBr_3$ is hygroscopic, all samples were stored and mounted on sample holders in a dry box with humidity of approximately 12%. The crystals have a crystallographic c axis along the line of two intersecting cleavage planes, and this axis, where possible, was aligned parallel to one possible polarisation direction of the incoming light for both absorption and excitation experiments.

3.2 Cryogenics

All spectroscopic measurements were recorded at low temperature, cooled by one of four cryogenic systems.

The early part of this study used an Andonian Associates variable temperature dewar with quartz windows. Samples were clamped in a vertical plane, to one of a variety of indium foil wrapped copper holders fastened to the base of an exchange gas column that was coupled to the liquid refrigerant. This dewar was used with a liquid

helium refrigerant to achieve sample temperatures around 15K suitable for laser selective excitation and optical absorption measurements.

Lower temperature optical absorption spectra were recorded using a British Oxygen Company liquid Helium emersion dewar. The samples were fastened to a rod that could be moved vertically and the dewar was filled with liquid helium. Sample temperatures of slightly less than 2K were achieved by pumping the helium to a superfluid state with a 450 ℓ/min pump. Since the dewar used 35-60 ℓ of liquid helium per experiment, these temperatures were not available for all measurements.

The greater part of the experimental work presented here was on crystals cooled using a CTI Cryogenics Model 21C Cryodyne closed cycle conducting type cryostat with a base temperature, measured by a thermocouple mounted at the cold head, of 9.5K. The temperature of the sample could be varied using a Palm Beach Cryophysics Inc. temperature controller model 4025. Optical absorption measurements were generally made at a variety of temperatures between 10K and 80K, with laser selective excitation spectra normally recorded at 10-12K. Indium foil was used between samples and the cold finger for maximum thermal contact.

The fourth system of cooling was a department-built, liquid nitrogen cooled, cold finger conduction dewar that was used for the infra-red absorption measurements reported in Chapter Five. This consisted of an outer vacuum jacket with an inside liquid nitrogen can that was attached to a conducting copper cold finger. The crystals were mounted vertically on copper holders having a 4 mm hole drilled

through the centre so that light could pass through the faces of the crystal. The windows used were 1.5 mm thick BaF_2 crystals.

3.3 Optical Absorption

The optical absorption spectra were recorded photoelectrically on a Spex 1700 Czerny-Turner configuration single monochromator with a $\frac{3}{4}$ metre focal length and an effective aperture of ~ f/7. The plane grating with 1200 grooves/mm, blazed for 7500Å gave a dispersion of 10.6Å/mm in first order.

Most of the measurements used an EMI 9558 photomultiplier tube with S20 response, although other measurements were made using an RCA 31034 tube with an extended S20 response. Both tubes were cooled thermoelectrically to $-25^{o}C$. The output of the photomultiplier tube was fed to a Keithley 610B electrometer and then to either a Bristol or, for later measurements, a Sekonic chart recorder.

A 100W quartz-iodine lamp powered by a 12V voltage regulated power supply was used as an optical source, and in some cases Corning filters were used to provide the bandpass required for the particular region to be scanned. The light was focussed on the crystal then collected and collomated with a short focal length lens and focussed onto the spectrometer slits with another lens. In most cases the optical pathlength of the crystals was 10 mm and the typical slit width of the spectrometer was 50 μm.

The $CsCdBr_3:Er^{3+}$ absorption spectra were recorded for both polarisations by placing a polarising sheet in the

light path, either parallel or orthogonal to the c axis of the crystal.

Except for the $^4I_{15/2} \rightarrow {}^2H_{9/2}$ and $^4I_{15/2} \rightarrow {}^4G_{11/2}$ first order spectra of $CsCdBr_3:Er^{3+}$, all absorption spectra were recorded in second order.

All energy levels derived from optical spectroscopy measurements are presented in units of cm^{-1} measured in air.

3.4 Laser Selective Excitation

The experimental configuration used for this study is shown in Figure 3.2. A dye laser is used to excite an electronic transition of the Er^{3+} ions in the crystal and the resultant fluorescence focussed onto the slits of the double monochromator. The laser frequency is finely tuned manually until the fluorescence intensity for a desired transition (monitored with the spectrometer) is optimised. The spectrometer is then scanned in frequency over the fluorescence region. The spectrometer, photon counting and data acquisition are computer controlled and output is recorded on a plotter.

3.4.1 Dye Laser

The excitation source used was a Spectra Physics Model 375 tumble dye laser pumped by a Spectra Physics Model 171 18W argon-ion laser.

Coumarin 6 dye (Exciton Chemical Company Ltd.) was the most useful dye available for pumping the Er^{3+} transitions. This dye had a lasing range of 18100-19200 cm^{-1} when pumped by the 4880Å line of the argon ion laser and typical powers of 20-40 mW were used. Cyclo-octatetraene (COT) (Exciton)

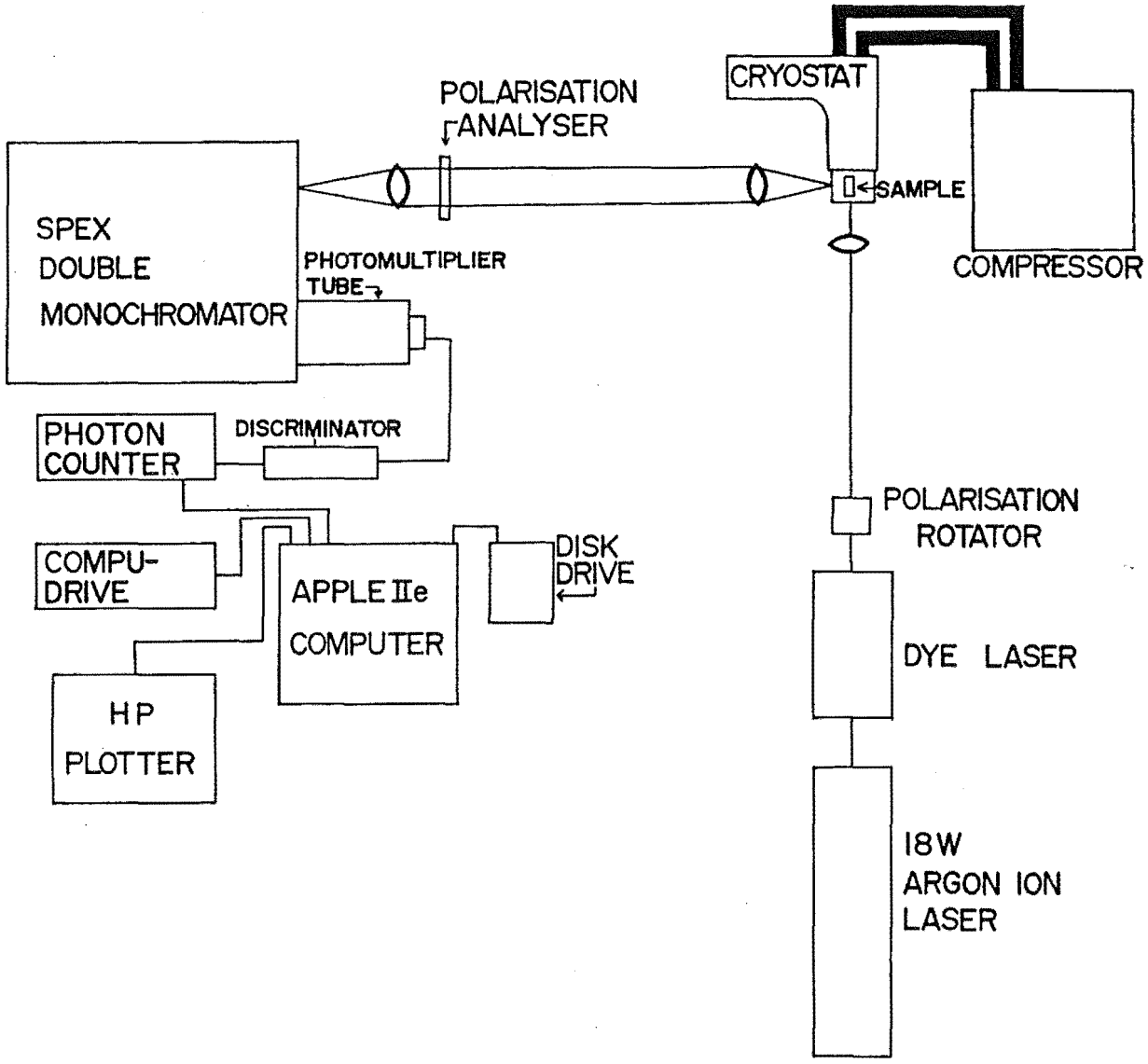

Figure 3.2 : Schematic diagram of the experimental apparatus used for the laser selective excitation spectroscopy.

was used to inhibit the lower frequency fluorescence of the dye and to increase the laser power in the region desired. Rhodamine 6G dye (Exciton) was used to excite the $^4I_{15/2} \rightarrow {}^4F_{9/2}$ transitions of the F^- ion charge compensated sites in $CaF_2:Er^{3+}$ but did not lase at the slightly lower frequencies required for sites in $SrF_2:Er^{3+}$, $CsCdBr_3:Er^{3+}$ or any of the hydrogenic sites in $CaF_2:Er^{3+}$.

For the first half of the period taken for this study the laser was fitted with the standard Spectra Physics wedge and etalon tuning elements. This method of tuning was somewhat cumbersome and the laser output tended to jump in frequency by 30 cm^{-1} during scans. The installation of a 3-plate birefringent tuning element improved the stability of the laser and tuning was achieved by rotation of a micrometer screw. The dye laser output had a linewidth of about 0.8 cm^{-1} and was linearly polarised. Several experiments required rotation of the laser polarisation and this was achieved using a Spectra Physics 310 polarisation rotator.

3.4.2 Detection

The fluorescence was detected photoelectrically using a Spex model 1403 double monochromator in the Czerny-Turner configuration with a focal length of 0.85 m, an effective aperture of ~ f/7.8, and equipped with holographic gratings with 1800 groves/mm.

An RCA 31034 photomultiplier tube with thermoelectrical cooling was used as the detector and connected to a Princeton Applied Research Model 1112 photon counter via a Model 1121 amplifier/discriminator. The tube had a dark

current of 10-20 counts/sec. and a maximum usable countrate of 10^6 counts/sec. A photon counting integration time of 1 second was typically used although some of the weak features were scanned using a 3 second time constant.

Manual control of the spectrometer was through a Spex Compudrive CD2 microprocessor unit, and spectra were recorded using an Apple IIe microcomputer control system designed and built by Mr T. Han and Mr R. Ritchie. This system, which is shown in block form in Figure 3.3, drives the spectrometer and stores data on floppy disks while plotting the output on a Hewlett Packard HP7475A graphics plotter.

Most spectra were recorded with slitwidths between 10 μm and 100 μm, depending on the intensity of the fluorescence.

For the polarisation dependence studies, a sheet of polaroid (Spex Inc.) was used as an analyser and placed in the collimated beam between the sample and spectrometer. A Hanle quartz wedge was used directly in front of the spectrometer slits to eliminate the effects of the grating response to polarised light.

For all of the bleaching experiments, with the spectrometer monitoring a single transition (Chapter Seven), the output from the photomultiplier tube was connected to a Keithley 610B electrometer and recorded directly with a Sekonic chart recorder. This system had the advantage of faster response to transients than photon counting.

3.4.3 Excitation

The excitation spectra presented in Chapter Seven were

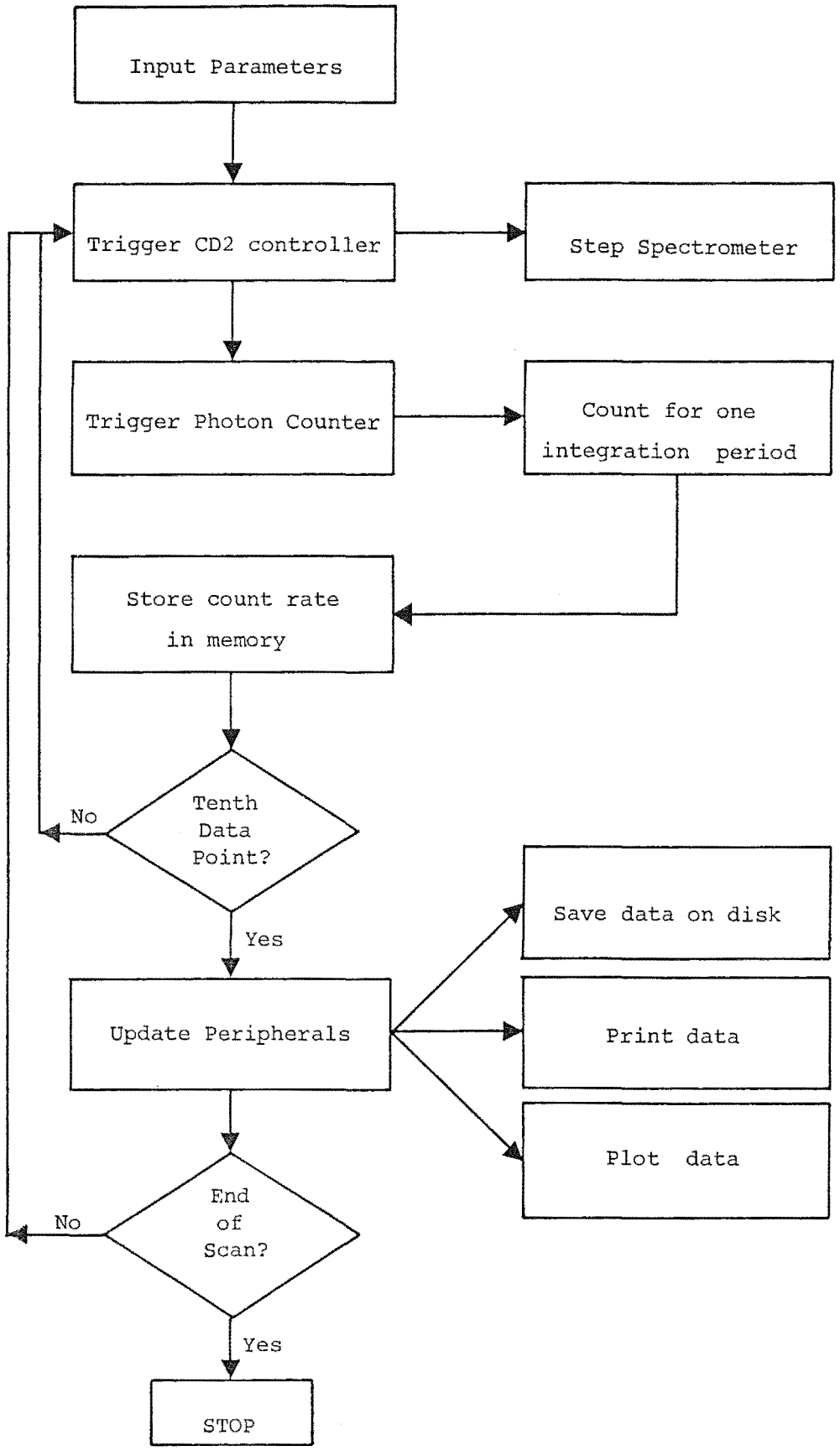

Figure 3.3 : Schematic diagram of the computer program used to control the laser selective excitation detection electronics.

recorded using an RCA31034 tube connected to a $\frac{1}{4}$ m focal length monochromator (Bausch and Lomb Inc.) with a 1350 groove/mm grating. Output from this tube was converted using an electrometer and plotted directly with the chart recorder while a Phillips stepping meter was used to drive the dye laser tuning micrometer screw through the useful absorption region.

Laser transmission through the crystals was also recorded in some instances using either an RCA 931A photomultiplier tube, with appropriate filters to attenuate the beam, or an FPT100 transistor as a photodiode.

3.5 Fluorescence Lifetime Measurements

The fluorescence lifetimes for transitions in $CsCdBr_3:Er^{3+}$ were determined using a Photochemical Research Associates Inc. PRA LN107 dye laser pumped by an PRA LN1000 nitrogen pulsed laser. The latter had a specified maximum energy per pulse of 1.1 mJ and pulse duration of 800 psec. No calibrated meter was available to confirm this.

Coumarin 540A (Exciton) and Coumarin 481 (Exciton) dyes were used in the dye laser to excite the $^4I_{15/2} \rightarrow {}^4S_{3/2}$ and $^4I_{15/2} \rightarrow {}^4F_{7/2}$ transitions in $CsCdBr^{3+}:Er^{3+}$ respectively. Extensive attempts made to pump hydrogenic sites in $CaF_2:Er^{3+}$ were not successful and this is interpreted as being due to either insufficient pulse energy for the weak fluorescence or to lifetimes being too fast to detect with the available equipment.

The closed cycled refrigerator and the Spex 1700 monochromator were used for these measurements with the direction of incidence of the laser on the crystal being

parallel to the slits of the spectrometer. The thermoelectrically cooled RCA 31034 photomultiplier tube was used since it has a relatively fast response time of less than 3 nsec.

The spectrometer PM tube anode was connected directly to a Stanford Research Systems Inc. Boxcar Integrator SR280 system and an Iwatsu SS5711 100 MHz oscilloscope. A trigger pulse for both the boxcar and oscilloscope was provided by an RCA 931A PM tube monitoring part of the nitrogen laser pulse.

For some of the measurements an ORTEC 9305 Fast preamp was used. In most cases, however, the signal was measured directly from the PM tube by the SR250 boxcar integrator.

The data acquisition and experiment control for lifetime measurements was computerised and used the SR265 (Stanford Research Systems Inc.) program with an IBM PC microcomputer. The oscilloscope signal was used to determine the appropriate time duration of the boxcar scan and the boxcar gate delay was scanned over this range by the computer. Most of the curves used were the average of thirty separate scans with typically 200 steps of the boxcar gate delay per scan; that is, 6000 laser pulses per measurement with a laser repetition rate of approximately 10 Hz. A boxcar width of 1-10 μsec was used for most of the measurements. The fitting of exponential decay curves to the data to determine lifetimes was also incorporated in the SR265 software.

The results of lifetime measurements, using this system, for the F^- anion compensation sites in $CaF_2:Er^{3+}$

were found to be very consistent with those obtained by Tallant *et al.* (1976), indicating that the methods of triggering and curve fitting used were reliable.

3.6 Infra-red Absorption

These measurements on hydrogenated $CaF_2:Er^{3+}$ were made during a short visit to the Physics and Engineering Laboratory of the Department of Scientific and Industrial Research in Wellington, New Zealand. The machine used was a Bomem DA3.02 Fourier Transform Interferometer with crystals mounted in the liquid nitrogen dewar previously described and the entire system purged continuously with oxygen free nitrogen to reduce the presence of water vapour. Crystal holders were built to hold three samples at once and a specially constructed stand moved the dewar vertically to enable beam access to all crystals.

A glowbar source was used and the beam aperture set to 3 mm so that the light could be directed through the centre of the sample without striking the crystal holder. A KBr beamsplitter and liquid nitrogen cooled mercury cadmium telluride detector were used.

The spectrometer had wavelength accuracy of ± 0.001 cm^{-1} at 2000 cm^{-1} with calibration by a stabilized He-Ne laser. A resolution of 0.15 cm^{-1} was chosen as adequate since some broadening and line overlap occurs at liquid nitrogen temperatures and higher resolution scans take considerably more time.

The entire system was controlled by a Digital Equipment Corporation LSI-11 minicomputer using Bomem software. Typically 100 scans were coadded to give the final

interferogram for which a Fourier transformation using Hamming apodization was carried out on a Bomem High Speed Vector Coprocessor. The transmittance spectra presented were obtained by normalisation against the background scan made through the dewar windows and vacuum space. In some cases water lines were not completely cancelled in the spectra due to variability of the purging process.

CHAPTER FOUR

PREDICTION OF POLARISATION DEPENDENCE

Previous studies have not reported polarisation dependence of the emission of rare-earth ion sites in the fluorite crystals. It was found in this study that for certain high symmetry sites in specially oriented crystals with the polarised laser light incident along a crystal symmetry direction, some orientations of the sites were preferentially excited giving rise to a polarised fluorescence spectrum.

This polarisation dependence gives information on site symmetry and crystal field energy levels. Polarisation ratios for the C_{4V} (tetragonal) symmetry sites and C_{3V} (trigonal) symmetry sites are predicted here, and the technique is shown to be particularly powerful for verifying trigonal symmetry of unknown sites.

4.1 Symmetry Reduction due to the Crystal Field

If an Er^{3+} ion in an Me^{2+} ion position in MeF_2 has remote charge compensation, then the crystal field due to the remaining Me^{2+} and F^- ions has a cubic point group symmetry. The free ion $^{2S+1}L_J$ terms are therefore split into levels with wavefunctions characterised by the double valued $\Gamma_6^{(2)}$, $\Gamma_7^{(2)}$ and $\Gamma_8^{(4)}$ irreducible representation, irreps, of the O_h double group.

Many of the Er^{3+} ions in the crystal have nearby charge compensation with negative ions in NN or NNN positions as shown in Figure 1.2. Such a negative ion exerts an axial force on the Er^{3+} ion, thereby reducing the point group

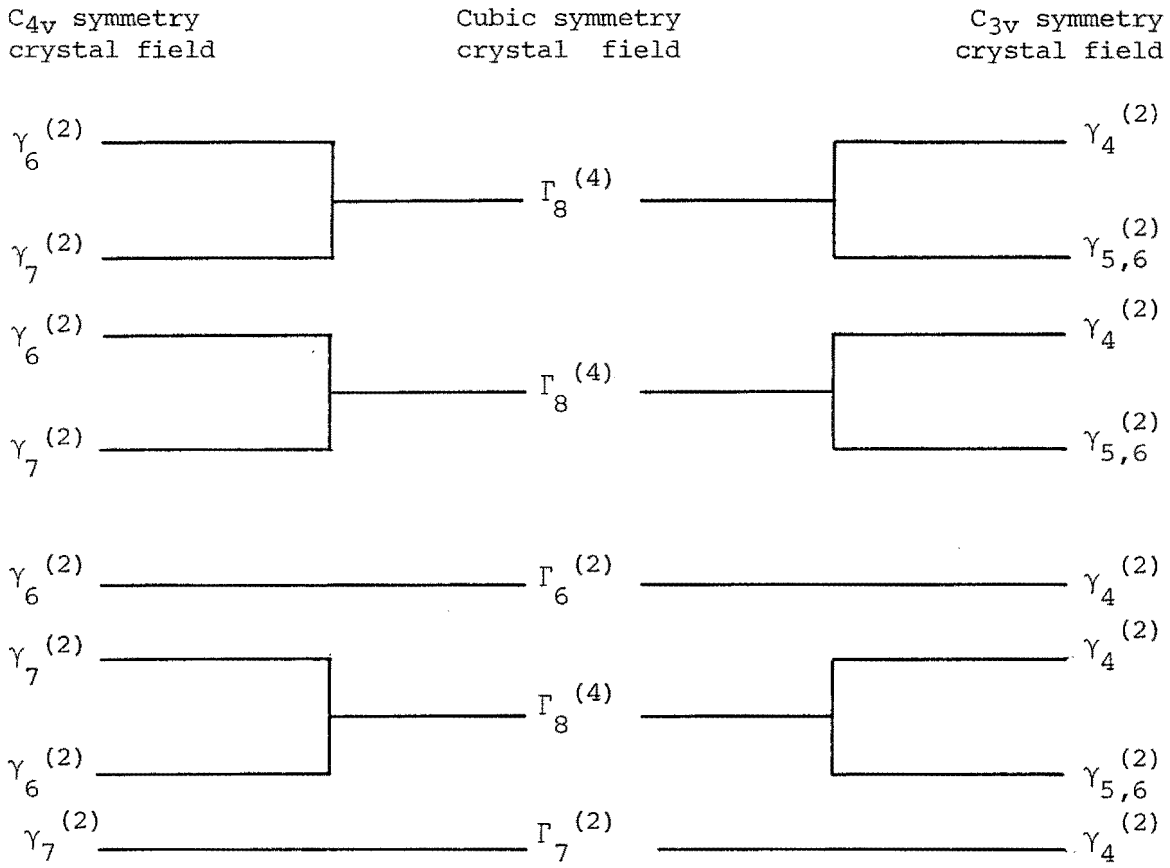

Figure 4.1 : Schematic indication of the reduction of symmetry from cubic to C_{4V} or C_{3V} by an axial crystal field.

symmetry of the Er^{3+} ion. The decomposition from cubic to C_{4V} or C_{3V} symmetry shown in Figure 4.1 demonstrates that degeneracy of the cubic $\Gamma_8^{(4)}$ wavefunctions is reduced by the axial field. The wavefunctions represented by the cubic irreps Γ_6, Γ_7 and Γ_8 decompose to the C_{4V} double group irreps τ_6, τ_7 and $\tau_6 + \tau_7$ or to the C_{3V} double group irreps τ_4, τ_4 and $\tau_4 + \tau_{5,6}$. The $\tau_{5,6}$ and τ_4 wavefunctions of C_{4V} and C_{3V} respectively consist of linear combinations of $|JJ_z>$ functions involving $J_z = \frac{1}{2}$ and coupled values, while the τ_7 and $\tau_{5,6}$ wavefunctions for C_{4V} and C_{3V} respectively, have linear combinations of $|JJ_z>$ functions involving $J_z = \frac{3}{2}$ and coupled values. Each of the relevant C_{4V} and C_{3V} irreps has double degeneracy (Kramers degeneracy) which may be lifted by a magnetic field.

4.2 Electric Dipole Selection Rules

The electric dipole operator for the C_{4V} group transforms as the τ_1 (z polarisation) and τ_5 (x,y polarisation) irreps of C_{4V}.

An electric dipole transition can occur between states of symmetry τ_a and τ_b if :

$$\tau_a \times \tau_{light} \rightarrow \tau_b \quad .$$

Therefore the electric dipole selection rules for transitions between levels with various symmetries can be determined from the group multiplication table which has :

$$\gamma_6 \times \gamma_1 \rightarrow \gamma_6 \qquad \gamma_6 \times \gamma_5 \rightarrow \gamma_6 + \gamma_7$$

$$\gamma_7 \times \gamma_1 \rightarrow \gamma_7 \qquad \gamma_7 \times \gamma_5 \rightarrow \gamma_6 + \gamma_7$$

Thus polarised light with the $\underline{E}$ vector perpendicular to the four-fold symmetry axis can excite any lower level state to any upper level state, while light with the $\underline{E}$ vector parallel to the symmetry axis can couple only states of the same symmetry.

These selection rules can be summarised as follows :

Table 4.1 Electric dipole selection rules for the C_{4V} group

C_{4V}	γ_6	γ_7
γ_6	$\sigma\pi$	σ
γ_7	σ	$\sigma\pi$

where σ or π polarisations correspond to the $\underline{E}$ vector of light perpendicular or parallel respectively to the four-fold symmetry axis (z) of the C_{4V} group.

Similarly the C_{3V} group multiplication table can be used to show that the following electric dipole section rules for Er^{3+} ions in trigonal symmetry sites apply :

Table 4.2 Electric dipole selection rules for the C_{3V} group

C_{3V}	γ_4	$\gamma_{5,6}$
γ_4	$\sigma\pi$	σ
$\gamma_{5,6}$	σ	π

where σ and π are now defined with respect to the three-fold

symmetry axis (z') of the C_{3V} group.

4.3 Polarisation Geometry

The polarisation geometry used is that shown in Figure 4.2 and specified as x(ab)z where x is the direction of propagation of the incident laser, z the direction of propagation of fluorescence, a(=y or z) the plane of polarisation (E vector) of the laser, and b(=x or y) the polarisation of the fluorescence.

4.4 The <100> Crystal Orientation

For crystals prepared in such a way that the crystal surfaces are the (100), (010) and (001) planes (Chapter Three), the direction of laser incidence and monitored fluorescence propagation can be made parallel to the dipoles formed by RE^{3+} ions and NN charge compensating ions.

The four-fold symmetry axis of each C_{4V} site can be aligned along the [100], [010] or [001] crystal axes. For transitions between levels of τ_6 and τ_7 (or τ_7 and τ_6) symmetry, only light polarised perpendicularly to the dipole can be absorbed (Table 4.1). Therefore, only two of the three sets of C_{4V} site orientations are excited. For example, with laser polarised in the y direction, only the [100] and [001] aligned centres are excited (Figure 4.2). For transitions between levels of different symmetry labels, the emission is also σ only. With the analyser aligned in the x direction, only emission from the [001] centres is detected while the emission from both [100] and [001] centres is detected for the analyser in the y direction.

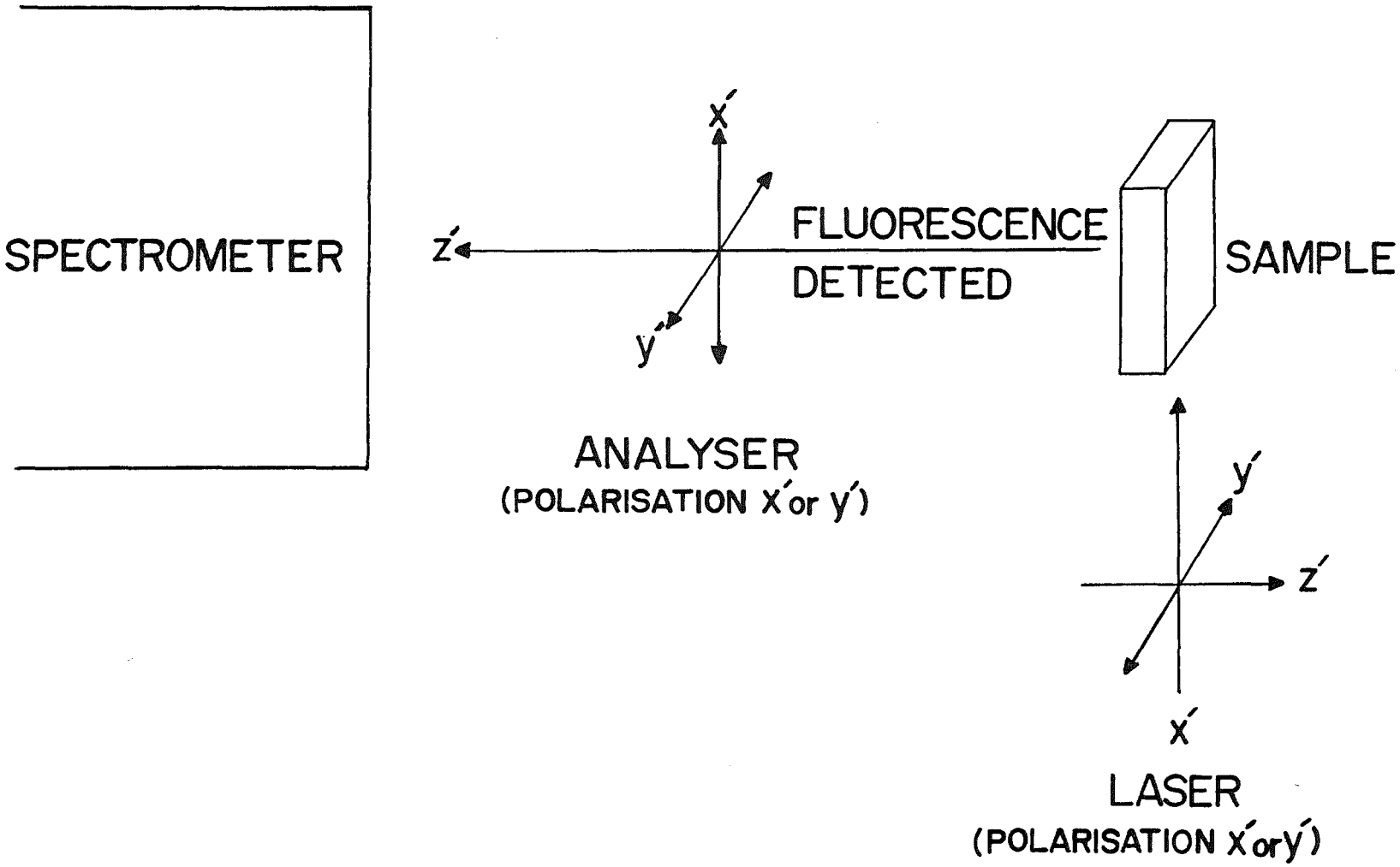

Figure 4.2 : Experimental geometry used for the study of polarisation dependence of emission for $CaF_2:Er^{3+}$ and $SrF_2:Er^{3+}$ crystals.

If the laser is polarised in the z direction, the emission detected (for the same transitions) is identical for both analyser positions.

When either the absorption or emission transition is between levels of the same symmetry, any observed polarisation dependence is a consequence of the absorption and emission probabilities for the different polarisation geometries of the centres and no specific ratios can be predicted.

Thus, any departure from a 2:1 intensity ratio for the x(yy)z:x(yx)z polarisation confirms the involvement of a $\tau_6 \rightarrow \tau_6$ or $\tau_7 \rightarrow \tau_7$ transition, whereas the x(zx)z and x(zy)z intensities are identical for all transitions.

C_{3V} symmetry sites can also be studied in the <100> oriented crystals. These sites have four axes (z') of three-fold symmetry ([1,1,1], [1,-1,1], [-1,1,1] and [11,-1]) that are all equally inclined to each <100> direction in the experiment geometry. The fluorescence intensities for any transitions in such crystals are therefore independent of the polarisation used.

4.5 The <111> Crystal Orientation

4.5.1 Trigonal Symmetry Geometry

The usual cleavage plane of CaF_2 and SrF_2 is the (111) plane and crystals with two parallel faces of this type can be used to study both C_{4V} and C_{3V} symmetry sites. This geometry is particularly useful for confirming trigonal symmetry and is investigated experimentally in Chapters Five and Six.

Since the four trigonal axes, z', are not orthogonal,

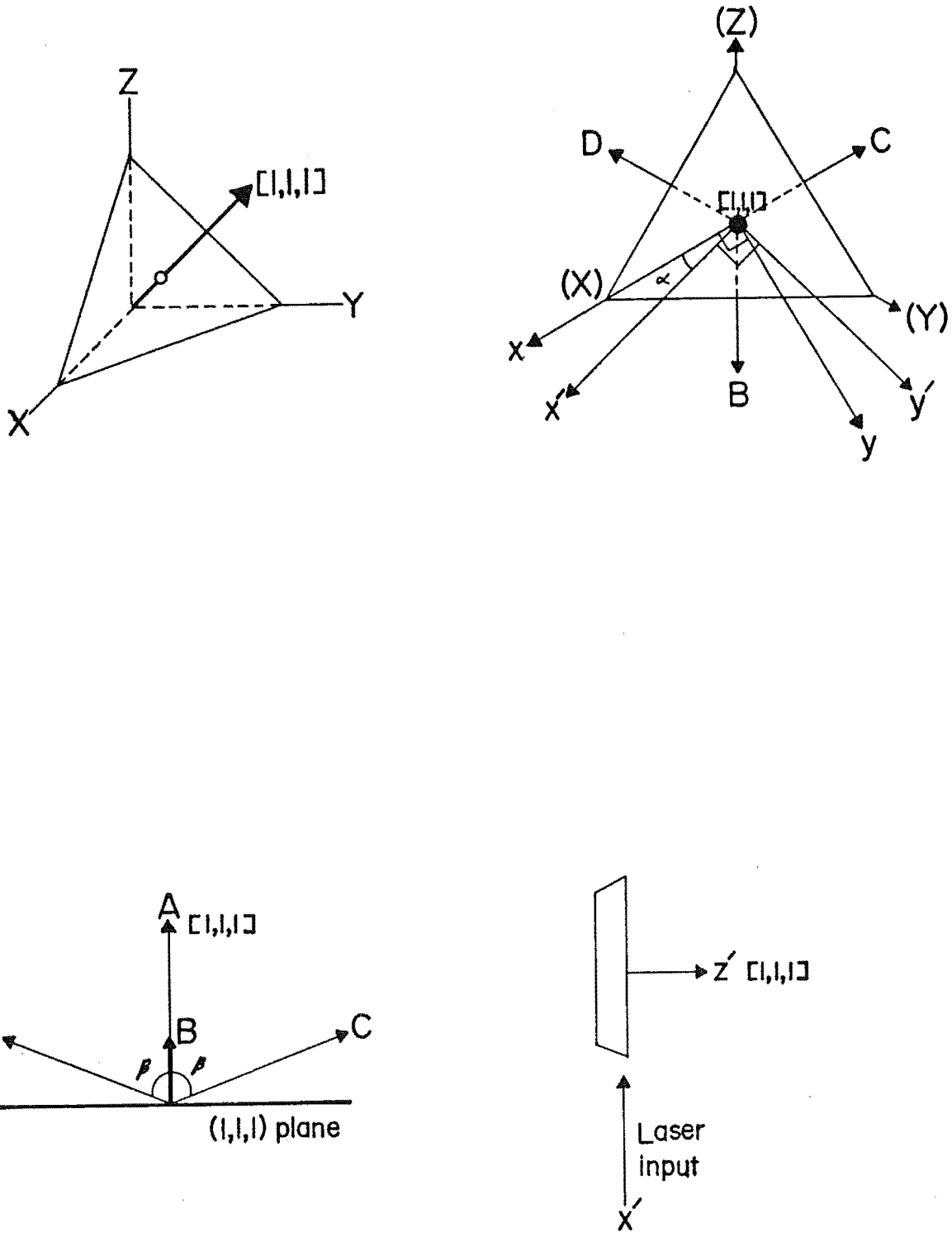

Figure 4.3 : Co-ordinate system used for calculation of polarisation dependence of C_{3V} symmetry sites in <111> oriented crystals: (a) the (1,1,1) plane. X,Y and Z are the cubic crystal axis directions. (b) [1,1,1] direction, z', is pointed directly out of the page. B, C and D are other <1,1,1> directions, (c) and (d) are different perspectives of the axis system.

the σ and π components of absorption and emission are not clearly separated for all trigonal sites simultaneously, making analysis more complicated than for C_{4V} sites in the <100> geometry.

The four z' axes and the co-ordinate system used to consider this problem are shown from several perspectives in Figure 4.3. The z' axis that is normal to the (1,1,1) crystal surface is pointed in the direction of propagation of detected fluorescence and the laser is incident parallel to the crystal surface in the experimental geometry co-ordinate direction x'. The two polarisations of the laser can have the $\underline{E}$ vector either parallel to the z' direction or in the orthogonal y' direction on the (1,1,1) plane.

Each of the three C_{3V} axes in the [1,1,-1], [1,-1,1] and [-1,1,1] directions is at angle $\beta = \cos^{-1}(\frac{1}{3})$ to the [1,1,1] centre. The components of the $\underline{E}$ vector both parallel and perpendicular to each of these centres must be calculated and the total σ and π absorption/emission components from all centres in the crystal determined. Intensity ratios can then be predicted for the x'(ab)z' polarisations (a,b=x',y') using the electric dipole selection rules (Table 4.2) appropriate to each transition.

4.5.2 Predictions

4.5.2(a) C_{3V} *Symmetry Sites*

It was found that for laser incidence parallel to a (1,1,1) plane, the polarisation ratios do not depend on the direction of the laser beam (x') relative to the orientation of the other three trigonal axes. This is proved in

Appendix I, and a consequence of this is that crystals may be prepared simply by cleaving two parallel faces and grinding flat surfaces for laser beam entrance and exit anywhere perpendicular to the (1,1,1) faces.

The totals of the contributions from all four alignments of the C_{3V} centres to the x'(ab)z' polarisations of all possible absorption/emission combinations ($(\sigma\sigma)$, $(\sigma\pi)$, $(\pi\sigma)$ and $(\pi\pi)$) are derived in Appendix I and summarised in Table 4.3(a). The polarisation intensity ratios for C_{3V} site transitions can be predicted by considering each type of transition separately.

As a specific example, if the absorption transition is $\gamma_4 \rightarrow \gamma_{5,6}$, then only σ absorption occurs. If the excited state decays by $\gamma_{5,6} \rightarrow \gamma_{5,6}$, then only π emission is possible. Thus the only component valid for this process is $(\sigma\pi)$ which has the relative values (Table 4.3(a)) $\frac{12}{27}$, $\frac{28}{27}$, $\frac{32}{27}$ and $\frac{32}{27}$ for x'(y'y')z', x'(y'x')z', x'(z'x')z' and x'(z'y')z' respectively. The other possible emission for the $\gamma_{5,6}$ excited state is $\gamma_{5,6} \rightarrow \gamma_4$ in which case the component $(\sigma\sigma)$ is appropriate, giving $\frac{60}{27}$, $\frac{44}{27}$, $\frac{40}{27}$ and $\frac{40}{27}$ for the four corresponding polarisations. It can therefore be concluded that if a $\gamma_4 \rightarrow \gamma_{5,6}$ transition is pumped by the laser, then the x'(y'y')z':x'(y'x')z' polarisation ratio will be $\frac{12}{28} = \frac{3}{7}$ or $\frac{60}{44} = \frac{15}{11}$ for the $\gamma_{5,6} \rightarrow \gamma_{5,6}$ and $\gamma_{5,6} \rightarrow \gamma_4$ emission transitions respectively. Similarly, the x'(y'x')z':x'(z'x')z' ratios will be $\frac{7}{8}$ and $\frac{11}{10}$ for $\gamma_{5,6} \rightarrow \gamma_{5,6}$ and $\gamma_{5,6} \rightarrow \gamma_4$ emission respectively.

All possible combinations of transitions may be determined by this method and are summarised in Table 4.4. Certain polarisation ratios have a range of possible values,

Table 4.3 : Components of polarisation intensity for combinations of absorption and emission of axial symmetry centres in <111> oriented crystals The first term in parentheses represents the polarisation of the absorption, while the second represents the polarisation of the emission.

(a) C_{3V} symmetry centres

C_{3V}	$(\sigma\sigma)$	$(\sigma\pi)$	$(\pi\sigma)$	$(\pi\pi)$
x'(y'y')z'	$\frac{20}{9}$	$\frac{4}{9}$	$\frac{4}{9}$	$\frac{8}{9}$
x'(y'x')z'	$\frac{44}{27}$	$\frac{28}{27}$	$\frac{28}{27}$	$\frac{8}{27}$
x'(z'x')z'	$\frac{40}{27}$	$\frac{32}{27}$	$\frac{32}{27}$	$\frac{4}{27}$
x'(z'y')z'	$\frac{40}{27}$	$\frac{32}{27}$	$\frac{32}{27}$	$\frac{4}{27}$

(b) C_{4V} symmetry centres

C_{4V}	$(\sigma\sigma)$	$(\sigma\pi)$	$(\pi\sigma)$	$(\pi\pi)$
x'(y'y')z'	$\frac{3}{2}$	$\frac{1}{2}$	$\frac{1}{2}$	$\frac{1}{2}$
x'(y'x')z'	$\frac{7}{6}$	$\frac{5}{6}$	$\frac{5}{6}$	$\frac{1}{6}$
x'(z'x')z'	$\frac{4}{3}$	$\frac{2}{3}$	$\frac{2}{3}$	$\frac{1}{3}$
x'(z'y')z'	$\frac{4}{3}$	$\frac{2}{3}$	$\frac{2}{3}$	$\frac{1}{3}$

TABLE 4.4: Predicted polarization intensity ratios for trigonal (C_{3v}) and tetragonal (C_{4v}) sites in a <111>-oriented crystal.

Pump Transition	Decay Transition	Polarization Ratios $\frac{x'(y'y')z'}{x'(y'x')z'}$	Polarization Ratios $\frac{x'(y'x')z'}{x'(z'x')z'}$
C_{3v} sites			
$\Gamma_4 \rightarrow \Gamma_4$	$\Gamma_4 \rightarrow \Gamma_4$	Arbitrary	Arbitrary
	$\Gamma_4 \leftrightarrow \Gamma_{5,6}$	$\frac{3}{7} \rightarrow \frac{15}{11}$	$\frac{7}{8} \rightarrow \frac{11}{10}$
	$\Gamma_{5,6} \rightarrow \Gamma_{5,6}$	$\frac{3}{7} \rightarrow 3$	$\frac{7}{8} \rightarrow 2$
$\Gamma_4 \leftrightarrow \Gamma_{5,6}$	$\Gamma_4 \rightarrow \Gamma_4$	$\frac{3}{7} \rightarrow \frac{15}{11}$	$\frac{7}{8} \rightarrow \frac{11}{10}$
	$\Gamma_4 \leftrightarrow \Gamma_{5,6}$	$\frac{15}{11}$	$\frac{11}{10}$
	$\Gamma_{5,6} \rightarrow \Gamma_{5,6}$	$\frac{3}{7}$	$\frac{7}{8}$
$\Gamma_{5,6} \rightarrow \Gamma_{5,6}$	$\Gamma_4 \rightarrow \Gamma_4$	$\frac{3}{7} \rightarrow 3$	$\frac{7}{8} \rightarrow 2$
	$\Gamma_4 \leftrightarrow \Gamma_{5,6}$	$\frac{3}{7}$	$\frac{7}{8}$
	$\Gamma_{5,6} \rightarrow \Gamma_{5,6}$	3	2
C_{4v} sites			
$\Gamma_6 \rightarrow \Gamma_6$, $\Gamma_7 \rightarrow \Gamma_7$	$\Gamma_6 \rightarrow \Gamma_6$, $\Gamma_7 \rightarrow \Gamma_7$	Arbitrary	Arbitrary
	$\Gamma_6 \leftrightarrow \Gamma_7$	$\frac{3}{5} \rightarrow \frac{9}{7}$	$\frac{5}{4} \rightarrow \frac{7}{8}$
$\Gamma_6 \leftrightarrow \Gamma_7$	$\Gamma_6 \rightarrow \Gamma_6$, $\Gamma_7 \rightarrow \Gamma_7$	$\frac{9}{7}$	$\frac{7}{8}$
	$\Gamma_6 \leftrightarrow \Gamma_7$	$\frac{3}{5} \rightarrow \frac{9}{7}$	$\frac{5}{4} \rightarrow \frac{7}{8}$

with the actual value depending on the relative intensity of the σ and π components of absorption or emission for the particular transitions involved.

4.5.2(b) C_{4V} *Symmetry Sites*

The C_{4V} sites in the <111> oriented crystals have only three principal axes of (four-fold) symmetry with none aligned in the [1,1,1] fluorescence propagation direction and each having an angular separation of $\beta' = \cos^{-1}\left(\frac{1}{\sqrt{3}}\right)$ from this direction. Table 4.3(b) includes the appropriate contributions to the polarisation intensities of each of the combinations of absorption and emission as derived in Appendix I . Polarisation ratios for specific transitions deduced from these are included in Table 4.4.

4.6 Summary

These calculations have illustrated that information on overall site symmetry and symmetry of the wavefunction point group irrep labels can be gained by studying the polarisation ratios of sites in <100> and <111> oriented fluorite crystals.

Trigonal (C_{3V}) site symmetry can be conclusively identified if all transitions have polarised emission consistent with the predicted ratios of Table 4.4 for the <111> oriented crystals and no polarisation dependence in the <100> geometry.

Sites with tetragonal (C_{4V}) symmetry should have transitions polarised in both geometries with identification of wavefunction symmetry being clearest for the <100> geometry.

The use of polarised emission for determining site symmetries has obvious experimental advantages over traditional techniques such as Zeeman spectroscopy, since it requires less equipment. It is used in this study to identify trigonal symmetry for the F^-B site in $CaF_2:Er^{3+}$, a proposal which has not previously been unambiguously proven.

CHAPTER FIVE

SPECTROSCOPY OF HYDROGENATED $CaF_2:Er^{3+}$

5.1 Introduction

5.1.1 Previous Studies of the Parent System

The parent $CaF_2:Er^{3+}$ system is probably the most comprehensively studied system of the $MeF_2:RE^{3+}$ type. Tallant and Wright (1975) (hereinafter [TW75]) first applied the technique of laser selective excitation (l.s.e) to the system, providing a good summary of the spectroscopy of the sites involving Er^{3+} ions charge compensated by F^- ions. This work consolidated several years of investigation by other workers using more traditional optical techniques (Rector, Pandey and Moos 1966 [RPM66]) (see also references in [TW75]).

The features of the optical absorption [RPM66] and l.s.e. [TW75] spectra of $CaF_2:Er^{3+}$ crystals have been assigned to the following sites involving F^- ion compensation.

(a) a site having cubic Er^{3+} ion symmetry, (Moore 1980, Aizenberg *et al.* 1972 [Ai72]) ;

(b) a tetragonal (C_{4v}) symmetry site, (the A site) in which the charge compensating F^- ion is in the nearest-neighbour interstitial position, i.e. in a <100> direction from the Er^{3+} ion; the symmetry was confirmed by Zeeman studies ([RPM66], Freeth *et al.* 1982 [Fr82]) ;

(c) a trigonal (C_{3v}) symmetry site (the B site) in which the charge compensating ion is in the next-nearest-neighbour interstitial position, i.e., in a <111> direction from the Er^{3+} ion; two optical absorption lines have been shown by Zeeman splitting to exhibit trigonal symmetry [RPM66] ;

(d) two sites (C and C') involving two Er^{3+} ions, and

(e) fifteen other sites divisible into two families of eleven (D_{1a}-D^1_{1k}) and four (D_{2a}-D_{2d}) sites involving clusters of Er^{3+} ions.

This summary formed the basis for a wide range of subsequent studies of the properties of the sites and processes occurring in the system.

Pulsed selective excitation techniques have been used to measure energy transfer between individual ions within given multiple Er^{3+} ion sites and extended to demonstrate energy transfer in mixed rare-earth doped CaF_2 (Tallant *et al.* 1976). Simultaneous monitoring of absorption and emission of Er^{3+} transitions using pulsed laser excitation was incorporated into an EXABS system by Miller *et al.*(1977) to determine radiative quantum efficiences, radiative and non-radiative relaxation rates, absorption coefficients and hence absolute concentrations of the various centres. Using this technique, the defect centre population equilibria for CaF_2:Er^{3+} F^- ion sites could be studied as a function of dopant concentration (Tallant *et al.* 1977) and sample annealing temperature (Moore and Wright 1981) It was

found that annealing the crystal at high temperatures (T>1000K) markedly increased the concentration of single ion erbium sites compared to cluster sites.

In addition to fluoride ions, other ions may provide charge compensation. Aizenberg *et al* (1969) showed that Na^+, K^+ or Li^+ could replace Ca^{2+} ions to provide charge compensation about an Er^{3+} ion. The absorption lines in $CaF_2:Er^{3+}$ crystals fired in oxygen were classified by laser selective excitation into five principal sites involving oxygen charge compensations (Gustafson 1978, Gustafson and Wright 1977 [GW77]. The dominant site (recently labelled 'G1' but previously known as 'T2') is formed when an O^{2-} ion replaces an F^- ion in the nearest shell about the Er^{3+} ion forming a site of trigonal symmetry, determined by ENDOR and EPR (Reddy *et al*. 1971).

The spectroscopy of fluoride and oxygen ion compensation sites of the $CaF_2:Er^{3+}$ system is sufficiently well known that it was used as an analytical tool in the SEPIL (selectively excited probe ion luminescence) technique([GW77], Johnston and Wright 1979). The trace concentrations of non-resonant rare earths in unknown solutions are determined to high precision by adding a known concentration calcium and erbium solution and precipitating $CaF_2:Er^{3+}$ by adding fluoride. The presence of non fluorescent rare-earth ions near Er^{3+} ions is detected by selectively exciting the Er^{3+} ions in the modified sites.

The laser spectroscopy of the F^- C_{4v} site in single crystals was extended by Freeth *et al* (1982) in a laser selective excitation transverse Zeeman effect study. This provided positive confirmation of the site symmetry and, by

successful crystal field fitting calculations, group labelling of the wavefunctions for many crystal-field levels of the A site.

In parallel with these laser studies, other techniques have been applied to study this crystal system. If an electric field or stress is applied to dipolar centres, reorientation of the dipole can occur. This motion can be detected by either ionic thermocurrent (I.T.C.) or dielectric loss measurements. Such studies, summarized by Andeen *et al.*(1981), reveal five principal relaxation peaks labelled R_I-R_V. The effect of quenching on the distribution of peaks has enabled the following correlation of the various relaxation peaks to the specific optical sites to be made : A → R_I, B → R_{II}, C → R_{IV} and D(2a) → R_{III} (Andeen *et al.* 1981, Fontanella *et al.* 1980). Welsh (1985) has subsequently suggested that the correlation of R_{II} to the optical B site does not, however, conclusively support a simple NNN model for the site.

Recent work (Catlow 1976, Corish *et al.* 1982) has used computer simulation techniques to calculate stabilities and reorientation activation energies of various fluoride ion compensation sites. This confirmed that both nearest-neighbour (NN) and next nearest-neighbour (NNN) compensation sites should be stable for CaF_2:Er^{3+} with other single Er^{3+} sites involving additional F^- ions being possible. These calculations emphasise that the defect centre's stability is predominantly determined by the large reduction in lattice strain energy due to relaxation of lattice ions from equilibrium around the defect rather than by the Coulomb term associated with the charge compensation.

Neutron diffraction (Cheetham *et al.* 1971, Catlow *et al.* 1983a) and extended X-ray absorption fine structure (EXAFS) (Catlow *et al.* 1983b, 1983c, 1984) studies have investigated erbium clustering and longer range structure for crystals of 5-30% dopant levels. Such studies demonstrated that effects of temperature and dopant radius are considerable for cluster structures, although these techniques are less sensitive at the lower concentrations used for most optical techniques.

5.1.2 Previous Studies of Hydrogenated CaF_2 and $CaF_2:Er^{3+}$

In an ENDOR study of hydrogenated CaF_2, Hall and Schumacher (1962) investigated neutral hydrogen atoms. They established the presence of interstitial hydrogen or deuterium atoms in samples prepared by heating CaF_2 single crystals with aluminium in an H_2 or D_2 atmosphere and subsequently x-irradiating.

The initial effect of hydrogenation before irradiation is to add H^- ions to the crystal, and the most convenient technique for study of the hydride ions in fluorite lattices is infra-red absorption spectroscopy.

Schaefer (1960) was the first to report the infra-red absorption due to an H^- ion substituting for an anion in alkali halides. This centre, known as the U centre, had previously been identified by a strong absorption in the ultra-violet region due to the $^1S \rightarrow {}^1P$ electronic transition of the H^- ion.

The first infra-red study of hydrogenated CaF_2 revealed a site exhibiting fundamental, second and third harmonic

transitions of a line at 965 cm^{-1} (Elliott *et al.* 1965). This site was shown to be one of T_d symmetry resulting from an H^- ion replacing a lattice F^- ion. The H^- ion is surrounded by four Ca^{2+} ions located at the vertices of a tetrahedron. The principal additional feature was the occurrence of broad bands at frequencies correlated to the sum (or difference) of the local mode and the various peaks in the one-phonon density of states.

An alternative technique for the study of local modes is Raman scattering. Harrington *et al.* (1970) used this method to determine the fundamental and second harmonic localised modes of H^- and D^- ions in the T_d site of CaF_2, SrF_2 and BaF_2.

Hydrogenation of CaF_2 crystals containing trivalent rare earth ions, RE^{3+}, results in additional sites involving interstitial H^- ions providing the required charge compensation. The most simple site, involving an H^- ion in the nearest-neighbour (NN) interstitial position has a C_{4V} point group symmetry. Jones (1964) observed two local modes in the infra-red region for the site. One mode, labelled Z, corresponds to a vibration parallel to the RE^{3+} - H^- axis while a doubly degenerate mode, labelled (X,Y), is due to vibrations perpendicular to this axis. Absorption lines due to an additional site were shown to be independent of the rare-earth ion present (Yatsiv *et al.* 1967). This site, having cubic symmetry, has been proposed to have an interstitial H^- ion remote from the RE^{3+} ion.

The hydrogenated CaF_2:Er^{3+} system provided an unusual four-line infra-red spectrum in which both modes were slightly split (Jones *et al.* 1968). This effect was

subsequently attributed (Chambers and Newman 1969) to the presence of a low-lying excited electronic level having vibronic lines different from those associated with the ground state crystal field level.

An infra-red absorption study (Robson 1969) of CaF_2 crystals containing a variety of rare-earth ions revealed additional absorption lines in Er^{3+} doped crystals. Most of these lines were found to be independent of the dopant ion but one set of two lines at 1071 cm^{-1} and 1150 cm^{-1} (at 83K) were found to grow together with time after hydrogenation. A subsequent study by Thompson (1983) verified this site assignment, arbitrarily labelling it the B site, and assigned three further sets of infra-red transitions to sites labelled A, C and D.

Another method of investigating these sites involves the use of optical spectroscopy techniques to observe the electronic transitions between crystal field levels of Er^{3+} ions in hydrogenated CaF_2:Er^{3+}. Hydride ions replacing fluoride ions in CaF_2 have two principal effects on the levels of the Er^{3+} ion. Firstly, the crystal field on the Er^{3+} ion is changed due to the resultant lattice distortion in the vicinity of the hydride ion, and secondly, the degree of covalency between the Er^{3+} ion and its hydride ion neighbour is greater than between the Er^{3+} ion and fluoride ions.

Optical absorption transitions between crystal field energy levels for the Er^{3+} - H^- C_{4V} site in CaF_2 were first reported by Edgar *et al.* (1979). Using absorption spectroscopy at 15K and 85K, this study determined levels at 0, 4.5 cm^{-1} and 26.3 cm^{-1} for the $^4I_{15/2}$ ground state

multiplet in the H^- C_{4V} site. This technique, however, limits the identification of ground state multiplet levels to those which are thermally occupied.

Additional information, unavailable for fluoride ion compensation sites, can be obtained by optical absorption measurements of the electronic transition shifts resulting from charge compensation by deuteride (D^-) or tritide (T^-) ions rather than hydride ions. Edgar *et al.* (1979) interpreted the resultant shifts in electronic and vibronic lines for the C_{4V} site in terms of a point-charge model of the electron-phonon interaction between the various erbium electronic states and hydride ion local modes. This study also verified the tetragonal symmetry of this centre by EPR spectroscopy. One further site, with four electronic energy levels correctly identified, was reported and assigned rhombic symmetry by EPR. The site, whose population was observed to grow with time, was arbitrarily labelled the R site. A subsequent study (Cockroft 1983) confirmed the correlation of the R site to the infra-red B site.

In the most recent optical study of the hydrogenated $CaF_2:Er^{3+}$ system, Thompson (1983) assigned levels in several upper multiplets to the C_{4V} and R sites and to two new sites labelled J and L. The 11.3 cm^{-1} Z_2 ground state level of the J site had previously been observed by far infra-red absorption spectroscopy (Campbell, Private Com.). A tentative assignment of two $^4S_{3/2}$ levels for two additional sites, T and H, was made although no ground state levels could be identified. Laser selective excitation was used to determine two additional Z levels and three Y levels for

the hydrogenic C_{4V} site, although fluorescence spectra in many cases were swamped by the much stronger emission of underlying fluoride ion sites also present. In addition to the transitions due to Er^{3+} ions an emission around 14100 cm^{-1} was observed while pumping the Z → E transitions. This has been assigned to 4f-5d transitions of Sm^{2+} ions present in trace quantities.

All previous work summarised here used crystals hydrogenated by the method of Hall and Schumacher. During my honours project (Cockroft 1983) an optical and infra-red study of crystals hydrogenated by a two-stage process involving calcium rather than aluminium metal was performed. In the first stage chips of calcium were heated at 850°C with the crystal in an argon atmosphere. This resulted in a darkened crystal proposed to be due to absorption by colour centres formed. (For a review of colour centres, see Hayes 1974.) After cleaning, the crystals were heated at 850°C for 20-70 hours in hydrogen gas. The hydrogen content by this method (as measured by infra-red absorption of the T_d site line) was increased by a factor of 3.9 ± 0.8 relative to a usual hydrogenation, using aluminium, of comparable heating duration. The method was not, however, adopted in the present study since such crystals were more brittle, gave no significantly different site distribution, and crystal darkening caused absorption too excessive for optical studies.

The other technique that has been applied to the $CaF_2:Er^{3+}:H^-$ system is that of infra-red laser excitation of the local mode vibration frequencies of the C_{4V} site (Campbell *et al.* 1982). Using a CO_2 laser the (X,Y) modes

of the H^-C_{4V} site in CaF_2 were selectively pumped for Dy^{3+}, Ho^{3+}, Er^{3+}, Tm^{3+} and Lu^{3+} dopants and the Z vibrational mode for Er^{3+}, Lu^{3+} and Y^{3+} dopants. Of these systems the Er^{3+} site was the only one which exhibited a saturation effect with transmission through the sample increasing as laser power is increased. A possible explanation for this involved the low lying electronic levels of the Er^{3+} ion. Determination of electronic levels of other sites in CaF_2:Er^{3+} is of relevance for further studies of this nature.

5.1.3 Aim of this Study

Thompson's work showed that hydrogenated CaF_2:Er^{3+} had many more optical absorption lines than the parent system. Results for the D^-C_{4V} site showed that sites in the system could be separately studied using laser selective excitation although swamping of fluorescence by F^- sites was found to restrict the technique to certain sites.

Most spectroscopy previously reported has been on crystals hydrogenated for a brief period, typically less than 24 hours. My previous report (1983) showed that hydrogenations of longer periods of up to three days produced many more lines. Although no attempt was made at that time to assign any of the new lines, it was apparent that site populations might be controlled by varying the length of time the crystal is maintained at high temperature in hydrogen atmosphere during the hydrogenation process.

The aim of this study was to establish an extensive information base for this particular hydrogenated system and to study the phenomena associated with hydride ion compensation. The usefulness of such study on a control system is illustrated by the extent of subsequent work using the $CaF_2:Er^{3+}$ summary of Tallant and Wright (1975). Specific aims were as follows :

- Assignment of all optical and infra-red absorption lines to sites.
- Investigate the dependence of site distributions on the thermal history.
- Control site populations to obtain desired site distributions.
- Determine crystal field levels of as many sites as possible.
- Check site symmetries by their emission polarisation dependence.
- Determine local mode frequencies from vibronic intervals for as many sites as possible.
- Find any new fluoride ion sites that may have been missed in earlier studies.
- Perform crystal field fits for the H^- and D^- C_{4V} sites analogous to that done for the F^-C_{4V} site (Freeth *et al.* 1982).
- Make model proposals for all of the hydrogenic sites observed.

Erbium is of particular interest for study since both tetragonal and trigonal symmetry sites are known to exist in $CaF_2:Er^{3+}$ [RPM66], whereas many rare-earth ions have a stable tetragonal site only.

This work was principally aimed at investigating sites involving a single Er^{3+} ion only, so dopant levels were kept to an appropriately low level ($\lesssim$ 0.1%) to minimise the variety and concentration of cluster sites.

Knowledge of the spectroscopy and behaviour of this hydrogenated system will assist related study of other problems such as the effect of high pressure hydrogenations and thermal treatment. Correlations between optical spectroscopy and other techniques such as dielectric loss, I.T.C., neutron scattering, EXAFS, Zeeman spectroscopy or CO_2 laser excitation of local modes should be possible subjects of further study.

5.2 Optical Absorption Spectroscopy

5.2.1 Spectroscopic Results

5.2.1(a) *Outline*

The optical absorption spectra of representative crystals of CaF_2 doped with 0.01, 0.05 and 0.1 molar% weight of Er^{3+} were examined before hydrogenation. Only lines of the A, B and, to a lesser extent, C sites due to F^- ion charge compensation were apparent [TW75].

The absorption spectra of the hydrogenated samples varied markedly with the duration of the hydrogenation treatment. For hydrogenation periods of up to sixteen hours, several new lines appeared, in addition to those of the F^- sites already present. After longer hydrogenation periods, the spectra became more complex with many new hydrogenic site lines appearing while the original F^- site lines had vanishing intensity.

The assignment of absorption lines to a specific site

was done by comparing the spectra of many crystals of different site distribution and determining which sets of lines maintained constant relative intensity at a given crystal temperature. Measurements at 2K provided the simplest spectrum. The energies of thermally populated crystal field ground state levels (either Z_2 or Z_2 and Z_3) for a given site at temperatures between 10K and 100K were used to identify other lines of the site, since these must occur in groups with characteristic Z_1, Z_2, Z_3 spacing for appropriate transitions to different upper multiplet levels,with the lines originating from the Z_2 and Z_3 levels having vanishing intensity at the lowest temperatures.

As the absorption intensities and line positions of corresponding transitions of the H^- sites are very similar to those of the D^- case, only absorption spectra for the latter case, for which extensive laser selective excitation was measured, are reproduced here. Absorption transitions observed for both the hydride and deuteride systems are included in all tables.

A total of sixteen hydrogenic sites for the hydrogenated CaF_2:0.05% Er^{3+} were found, which can be conveniently divided into two classes : thirteen sites involving nearby hydride ion charge compensation, and three sites of near cubic Er^{3+} ion site symmetry involving more remote charge compensation.

5.2.1(b) *Hydrogenic Sites Involving Nearby H^- ion Charge Compensation*

These sites account for most lines of the optical absorption spectra and have transitions of narrow linewidth,

typically 2-3 cm^{-1}.

The absorption transitions to the $^4S_{3/2}$ multiplet are the simplest to analyse as only two upper crystal field levels (E_1 and E_2) occur for each site present. As it is possible to excite to this multiplet using the dye laser with coumarin 6 dye, a detailed study of the $^4I_{15/2} \rightarrow {}^4S_{3/2}$ absorption spectra was performed. Levels of the previously reported (Edgar *et al.* 1979, Thompson 1983) H^-C_{4V}, R, J and L sites were measured and all remaining narrow linewidth transitions were assigned to ten additional sites arbitrarily labelled K, M, W, X, P, L, T, N, S and V. The 2K spectra of two crystals of different hydrogenation duration with sites labelled are given in Figure 5.1. Identification of site lines was confirmed for all sites except W, by the observation of transitions arising from the thermally occupied ground state multiplet level, Z_2, as the temperature was raised. In addition, transitions from Z_3 were identified for the C_{4V}, R, J, K and M sites.

Corresponding lines for all of these sites, except M, were assigned as $^4I_{15/2} \rightarrow {}^4F_{9/2}$ transitions in the 15000 - 16000 cm^{-1} spectral region. Spectra for these transitions are reproduced in Figure 5.2. The crystal field levels determined by absorption for all hydride ion sites are given in Table 5.1 with corresponding deuteride ion values in parentheses. The standard notation of a letter with a numerical subscript is used to label the levels of the various multiplets.

In addition to the new sites identified, several modifications of the results of previous workers have been made as follows :

Reference Number	Original Assignment	New Assignment
Edgar *et al.*1979	Z_1-E_2 C_{4V} site	Z_1-E_1 W site
	Z_2-E_2 C_{4V} site	Z_1-E_2 X site
	Z_1-E_2 R site	Z_1-E_2 P site
	Z_2-E_2 R site	Z_1-E_1 X site
Thompson 1983	L site (Z_3=35.9cm^{-1})	Z_3=284cm^{-1}(by emission)

To avoid confusion with hydrogenic labelling, the 'H' site of Thompson has been renamed the 'P' site. Identification of the weak Z_1-D_1 transitions of the C_{4V}, R and J sites has shown that the only previously identified $^4F_{9/2}$ level is actually the D_2 level. A search for the C_{4V}, R and J site E_2 levels to replace the previous incorrect assignments was not successful since, as is shown by laser selective excitation in the next section, the levels are coincident with more intense transitions of other sites.

The narrow linewidth of site transitions and the observation of isotope shifts (see §5.2.2) confirms the hydrogenic nature of those sites with the magnitude of shift, typically comparable to those of the C_{4V} site, indicating nearby hydrogenic charge compensation.

5.2.1(c) *Hydrogenic Sites of Near Cubic Symmetry*

In addition to the new sites classified in the previous section, several additional absorption features appear for both the $^4S_{3/2}$ and $^4F_{9/2}$ multiplets. After deuteration duration of at least 40 hours the 2K $^4I_{15/2} \rightarrow {}^4S_{3/2}$ multiplet absorption spectrum has a broad line at 18607.4

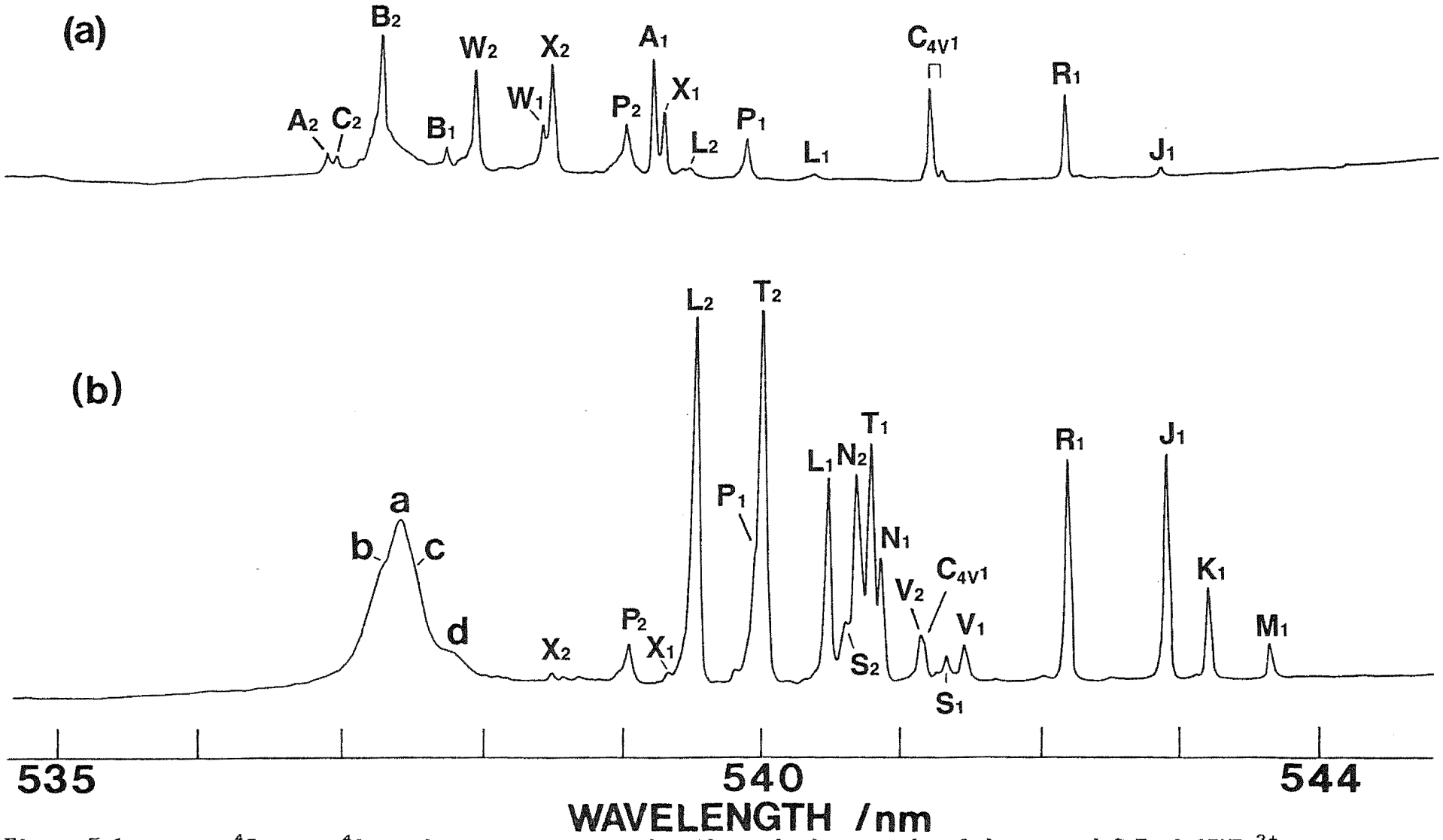

Figure 5.1 : $^4I_{15/2} \rightarrow {}^4S_{3/2}$ absorption spectra for 10 mm thick crystals of deuterated CaF_2:0.05%Er^{3+} at 2K: (a) 16 hour deuteration, and (b) 68 hour deuteration. Transitions are identified by a site label and the upper multiplet crystal field level involved. Lines a, b, c and d are due to near cubic symmetry site.

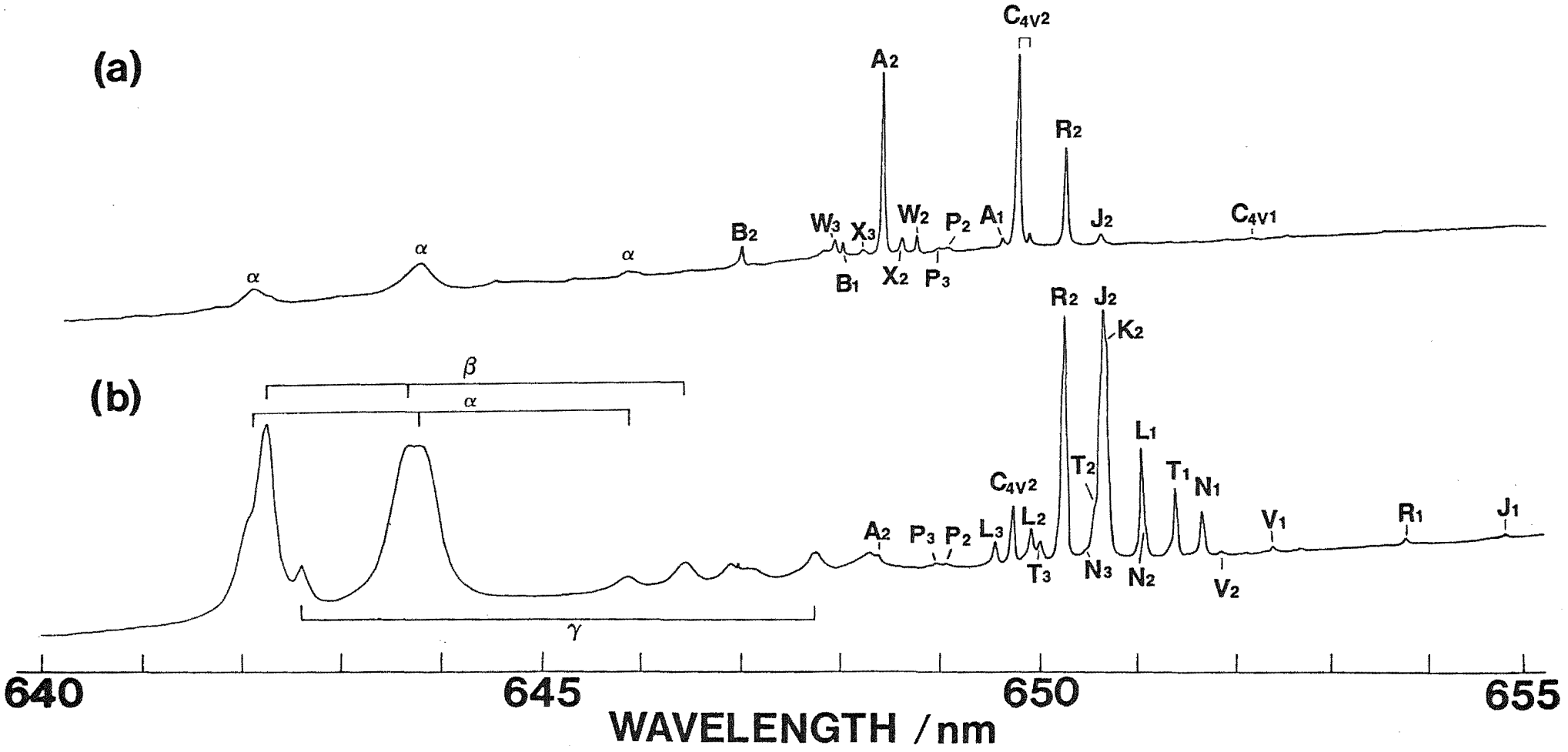

Figure 5.2 : $^4I_{15/2} \rightarrow {}^4F_{9/2}$ absorption spectra for 10 mm thick crystals of deuterated CaF_2:0.05%Er^{3+} at 2K : (a) 16 hour deuteration, and (b) 68 hour deuteration. Transitions are identified by a site label and the associated upper multiplet level involved.

Table 5.1 : Energy levels (in cm^{-1}±0.4 unless otherwise indicated) of three Er^{3+} ion multiplets for thirteen hydrogenic sites as derived from the 10K absorption spectra of hydrogenated or deuterated CaF_2:0.05%Er^{3+} crystals. The D^- site energies are in parentheses.

		C_{4V}	R	J	K	M	W	X	P	L	T	N	S	V
$^4S_{3/2}$	E_2	-	-	-	-	-	18589.5 (90.2)	18568.5 (70.2)	18548.8 (51.3)	18532.0 (5.0)	18515.0 (8.2)	18491.0 (5.3)	18493.5 (8.1)	18475.2 (9.7)
	E_1	18480.5 (78.7)	18444.2 (44.2)	18418.4 (9.8)	18407.2 (9.3)	18391.2 (4.2)	18572.9 (2.7)	18541.1 (1.5)	18518.4 (20.1)	18499.1 (502.3)	18488.9 (92.0)	18485.8 (9.5)	18469.6 (73.4)	18464.0 (9.2)
	D_3	-	-	-	-	-	15436.6±0.6 (7.1)	15428.3±0.8 (9.7)	15409.4 (10.4)	15395.3 (6.3)	15383.6 (5.7)	15372.4±0.8 (4.8)	-	-
$^4F_{9/2}$	D_2	15393.1 (2.4)	15379.2 (80.0)	15369.7 (70.7)	15368.5 (70.0)	-	15415.7±0.6 (15.7)	15418.6 (9.7)	15405.9 (7.9)	15385.0 (7.5)	15371.0±0.8 (2.9)	15356.6 (60.0)	15333.9±0.8 (6.5)	15338.4 (42.5)
	D_1	15333.9±0.8 (1.8)	15297.5±0.8 (97.5)	15271.5±0.8 (2.0)	15260.3±0.6 (1.0)		-	-	-	15358.8 (60.8)	15350.7 (3.1)	15343.9 (6.8)	15320.1±0.8 (2.8)	15326.5 (30.5)
	Z_3	25.8 (.0)	35.4 (.7)	44.0 (.9)	55.8 (57.0)	60.3 (60.6)	-	-	-	-	-	-	-	-
$^4I_{15/2}$	Z_2	4.5±0.3 (2.9)	8.6±0.3 (9.1)	11.3±0.3 (12.1)	20.0±0.3 (20.9)	33.0±0.3 (32.1)	-	29.8 (29.3)	21.7±0.3 (20.8)	23.5±0.3 (22.5)	24.5 (25.5)	27.2±0.3 (26.2)	-	29.7 (30.6)
	Z_1	0	0	0	0	0	0	0	0	0	0	0	0	0

cm^{-1} with side structure at 18611.5, 18603.9 and 18595.3 cm^{-1} (identified by labels a, b, c and d respectively in Figure 5.1). Similarly, the 2K $^4I_{15/2} \rightarrow {}^4F_{9/2}$ spectrum has three sets of lines labelled α(15576.6, 15534.8 and 15485.1 cm^{-1}), β(15572.9, 15538.1 and 15471.4 cm^{-1}) and γ(15563.8 and 15439.9 cm^{-1}) in Figure 5.2. The linewidth of these transitions is typically 6-8 cm^{-1}. Small frequency differences, typically 1-2 cm^{-1}, between corresponding transitions in hydrogenated and deuterated crystals confirmed the hydrogenic nature of these sites.

The principal peak in the $^4S_{3/2}$ multiplet spectrum is proposed to be a hydrogenic equivalent of the transition previously identified (Moore 1980) for an Er^{3+} ion site of cubic symmetry in $CaF_2:Er^{3+}$ involving remote charge compensation. Energy levels of the cubic site as determined from pure $CaF_2:Er^{3+}$ crystals are reproduced in Table 5.2 from Moore.

Transitions for purely cubic sites are expected to be very weak because electric dipole transitions are forbidden for sites having inversion symmetry. The observations of lines of such sites with enhanced intensity after hydrogenation is attributed to the effect of substitutional H^- (or D^-) ions in the lattice sufficiently close to the erbium ion to reduce the inversion symmetry significantly. The lowering of the Er^{3+} ion site symmetry from exact cubic symmetry gives non-zero electric dipole transition intensities, and through the random distribution amongst many possible positions of the extra hydride ions, broad lines.

The separate sites α, β and γ of Figure 5.2(b) were

Table 5.2 : Previously determined energy levels (in cm^{-1}, vacuum) of the Er^{3+} ion in a site of cubic symmetry in CaF_2. Column (a) are the values from Moore (1980) and column (b) from Aizenberg *et al.* (1972).

Manifold	Energy (a)	Energy (b)
$^4F_{5/2}$	22462	
	22420	
$^4S_{3/2}$	18607	18608
$^4I_{13/2}$	6645	
	6635	
$^4I_{15/2}$	632	626
	564	558
	104	91
	92	91
	0	0
Phonon frequencies	358 (broad)	375
	225 (broad)	228
	134 (narrow)	135

classified by their change of relative occurrence with increased duration of the hydrogenation treatment. Similar correlations could not be confirmed for the $^4S_{3/2}$ multiplet spectra because of the overlap in this region with the A, B and C sites due to F^- ion compensation. Three further weak peaks in Figure 5.2(b) have not been assigned.

Since the epr results (Edgar *et al.*1979) show that a significant proportion of cubic symmetry Er^{3+} sites are present in such crystals, the appearance of associated lines in the optical spectrum through perturbations is reasonable. The infra-red D site in $CaF_2:Er^{3+}$ with broad lines near the known cubic site line has been proposed to be the same type of centre (Cockroft *et al.* 1987a).

As the transitions observed are too broad to unambiguously assign any excited ground state multiplet transitions for higher temperature spectra, a definite correspondence to the cubic site of $CaF_2:Er^{3+}$ could not be confirmed.

5.2.1(d) *Hydrogenic Site Distribution*

(i) Effect of Duration of Hydrogenation

This parameter played a key role in determining site distributions, and it was possible to produce any desired distribution solely through control of the period of hydrogenation. Most of the crystals were hydrogenated for periods of 16, 36 or 68 hours at a temperature of 860°C, then cooled rapidly to room temperature. Variation of hydrogenation temperature between 800°C and 900°C had only a slight effect on the total amount of hydrogen introduced and resulted in essentially the same site distributions. More

rapid quenching of the crystal after heating with hydrogen by immediately plunging the hydrogenation tube into liquid nitrogen produced very similar spectra, but often caused cracking of the crystal, so was not adopted.

Figures 5.1 and 5.2 illustrate the difference between a 16-hour and a 68-hour deuteration. After 16-hour deuteration the spectrum reveals lines of the fluoride A and B sites, the lines of deuteride C_{4V}, P, W and X sites, weaker lines of the R and L sites and very weak lines of the J site. After 68-hour deuteration the spectrum shows strong lines due to the deuteride T, L, J and R sites, less intense lines of the K, N, S and V sites, weak lines of the deuteride P, M and C_{4V} sites, but only traces of lines of the fluoride A, B and C sites and the deuteride X and W sites. Intermediate deuteration periods of 30 and 50 hours produced intermediate site distributions. Broken 68-hour deuteration treatments of three successive 20-hour deuterations separated by 4-hour cooling periods produced superposed lines of both 16 and 50 hour deuterations. Figure 5.3 shows the spectrum at 12K for such a crystal with transitions of both F^- and D^- sites present.

As a qualitative example of the effect of hydrogenation time on site population, the absorption intensity for the R site increased in the approximate ratio 1:1.5:2.5 for 15, 40 and 68-hour hydrogenations respectively. The L site increased by the ratio 1:12:35 for the same durations.

(ii) <u>Time Evolution of the Site Distribution</u>

It was observed that a steady state site distribution for hydrogenic sites was not reached until several weeks

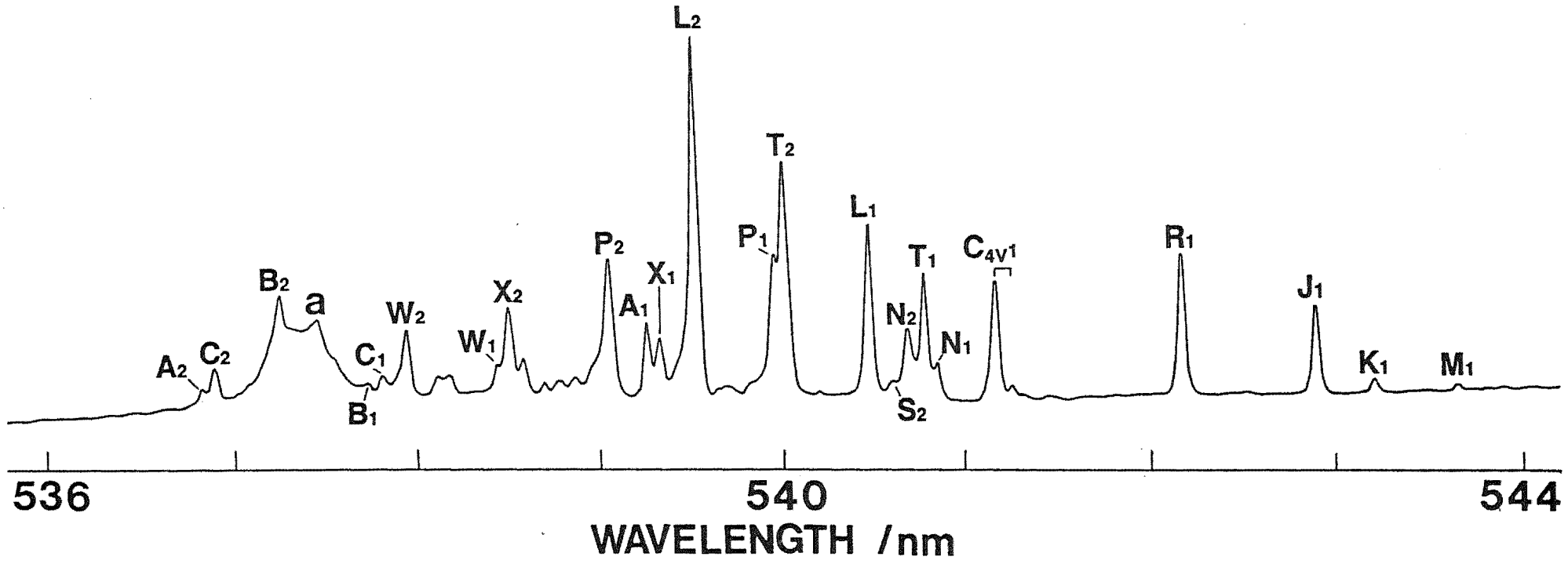

Figure 5.3 : $^4I_{15/2} \rightarrow {}^4S_{3/2}$ absorption spectrum for a 10 mm thick crystal of $CaF_2 0.05\% Er^{3+}$ at 2K that was deuterated for 3 periods of 20 hours separated by 4 hour cooling periods.

after hydrogenation with some sites observed to grow at the expense of others. Such effects indicate appreciable preferential migration of hydride ions between sites in the crystals, even at room temperature. The most dramatic time dependence is for the R site which builds up to double its original intensity within the first eight weeks, thereafter increasing only slowly. Other sites that increase significantly with a time scale of weeks are the P and X sites, whereas the W site decreases.

In addition to these rapid changes, other site populations change at a slower rate. The absorption spectra of a crystal which was hydrogenated for a twenty-hour period and quenched in liquid nitrogen was recorded two weeks after hydrogenation and again thirty-three months later. The key features of the spectra were the increase of the R and J sites accompanied by a substantial decrease in the H^-C_{4V} site and a factor of two decrease in the F^-A site. The W site had decreased by a factor of ten, whereas the L, T and P sites increased. Also of interest was the decrease by a factor of at least two of the F^- B site until it was unresolved from the near cubic centre structure which had increased slightly in intensity. It was observed that the X site, after its initial growth over the first few months, actually began to decrease as other sites grew at its expense over a longer scale of years. After two years the X site intensity in one crystal had decreased by an approximate factor of 2.5.

The observed migration is temperature dependent and storage of crystals at elevated temperatures accelerates these site distribution changes. After a week, crystals

maintained at 500K attained site distributions typical of approximately six-month-old crystals. In particular, the R, P, X and L site lines increased while the C_{4V}, and W site lines decreased. The J site lines stayed approximately constant.

The ageing process is the most significant factor, after that of the duration of hydrogenation, that must be considered for preparation of a desired site distribution.

(iii) Effect of Er^{3+} ion Concentrations

CaF_2 crystals of 0.01% Er^{3+} and 0.05% Er^{3+} concentration that were deuterated under identical conditions had very similar optical absorption spectra apart from the expected overall increase in absorption with Er^{3+} concentration.

(iv) Effect of Oxygen Treatment

A crystal of CaF_2:0.05% Er^{3+} was heated in oxygen in the presence of aluminium to assess the effect of possible trace oxygen entering the crystals. This crystal was found to contain principally the G1 site (Gustafson 1978) due to oxygen ion charge compensation. This crystal, together with another crystal cleaved from the same boule, was then hydrogenated in the usual way for 40 hours. The two crystals were found to have indistinguishable spectra, apart from the G1 site present in the previously oxygenated crystal. It is concluded that none of the reported hydrogenic sites are due to inadvertent oxygen contamination or to combined oxygen-hydrogen compensation sites.

(v) Effect of Traces of Moisture

The efficiency of the hydrogenation process was illustrated by the result of heating a CaF_2:0.05% Er^{3+} crystal in contact with aluminium at a temperature of 860°C in a nominal vacuum ($P \leq 2$ μm Hg) without first baking the system at 150°C to remove all moisture. A crystal treated in this way for 68 hours and quenched to room temperature had an absorption spectrum typical of that for a crystal hydrogenated at normal pressure (500 mm Hg) for approximately 10 hours. The presence of hydrogenic sites is attributed to a trace quantity of moisture that is hydrolysed at the aluminium/crystal interface. The relative pressure of hydrogen gas to other gases present governed the extent of hydrogenation. When the process was repeated using either helium or dry argon gas as a buffer, the number of Er^{3+} ions in hydrogenic sites decreased considerably.

5.2.1(e) *The Titrated System*

An attempt was made to apply the Hall and Schumacher method using small quantities available of tritium gas. The main problem encountered was the low vapour pressure of tritium in the hydrogenation chamber, typically 10% of the normal hydrogen pressure used. Hydrogen was present both in the isotopic mixture used and could also be hydrolysed from trace moisture in the system. The result was a site distribution for a 65-hour duration that at normal pressure would be typical of a 20-hour hydrogenation. The best T^-/H^- ratio obtained for the $Z_1 \rightarrow E_1$ transition of the C_{4V} site was approximately one third, making identification of

T^- ion site transitions difficult to resolve from H^- sites. Figure 5.4 is the absorption spectrum for a crystal after a 65 hour tritiation. The presence of F^- ion sites in the spectra is characteristic of crystals having a shorter effective hydrogenation period at the usual pressure.

5.2.2 Isotope Shifts

There are two principal methods of determining the isotope shifts of electronic transitions for analogous sites involving H^-, D^- or T^- isotopes :

(a) A double crystal method using an hydrogenated crystal in series with a deuterated one. The shifts, if resolvable, can be measured directly from the spectrum.

(b) A single crystal may be hydrogenated in a mixture of hydrogen and deuterium gas. Transitions from each of the isotopic versions of a site should be observed.

Most of the measurements made were for pairs of similar H^- and D^- crystals placed in series. Figure 5.5 shows part of a spectrum illustrating this shift for some of the $^4I_{15/2}$ $^4S_{3/2}$ transitions for comparable hydrogenated and deuterated crystals. Table 5.3 gives the H^-/D^- isotope shifts measured by this technique for the Z_1-E_1 and Z_1-E_2 transitions at 1.8K. These shifts are determined to greater precision than those obtainable by the differences of H^- and D^- frequencies determined separately. This is due to difficulty of both spectrometer and chart recorder reproducibility between consequent scans.

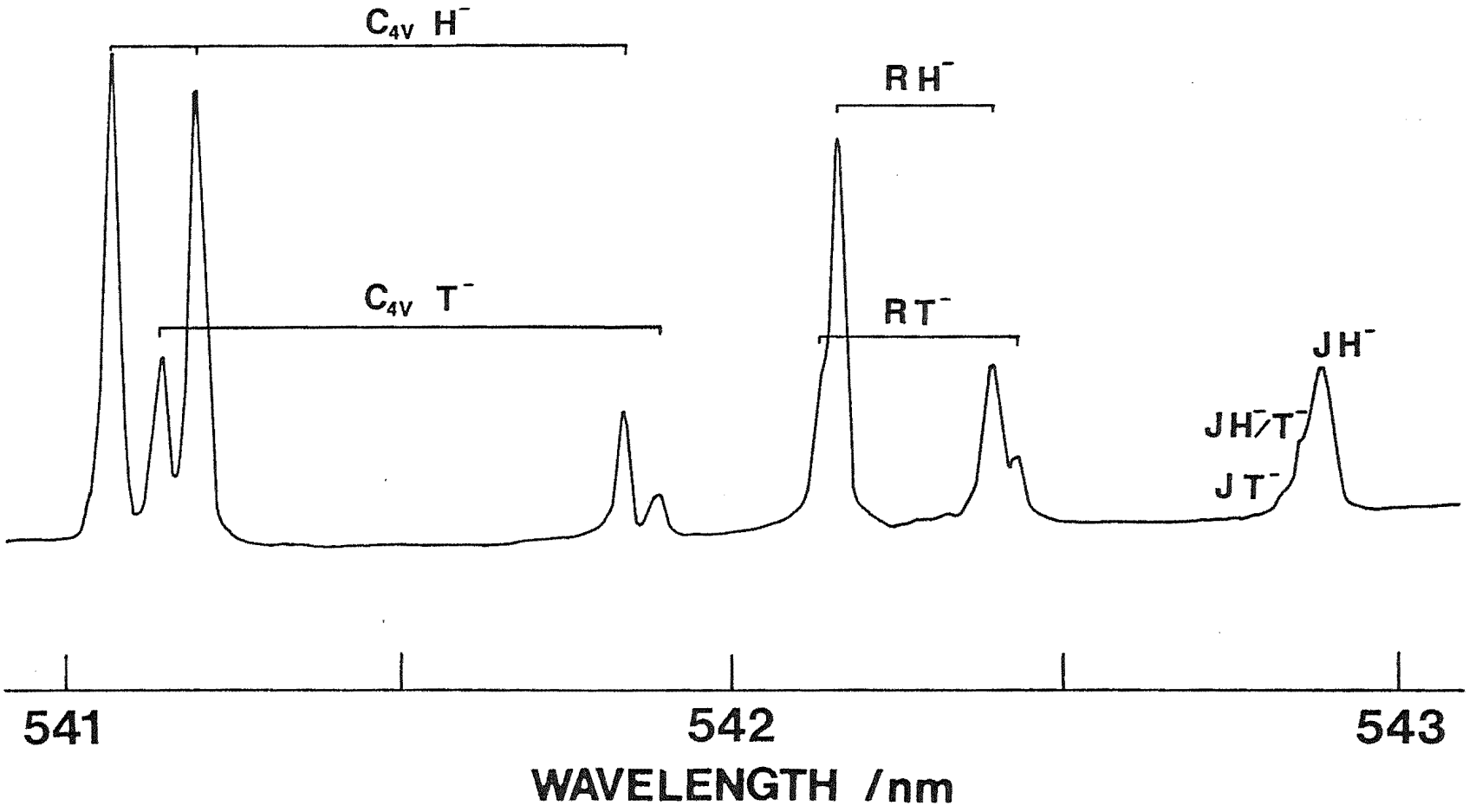

Figure 5.4 : $^4I_{15/2} \rightarrow {}^4S_{3/2}$ absorption transitions, recorded at 20K, of a CaF_2:0.05%Er^{3+} crystal tritiated for 65 hours. Transitions indicated are from various Z levels to the E_1 level of each site.

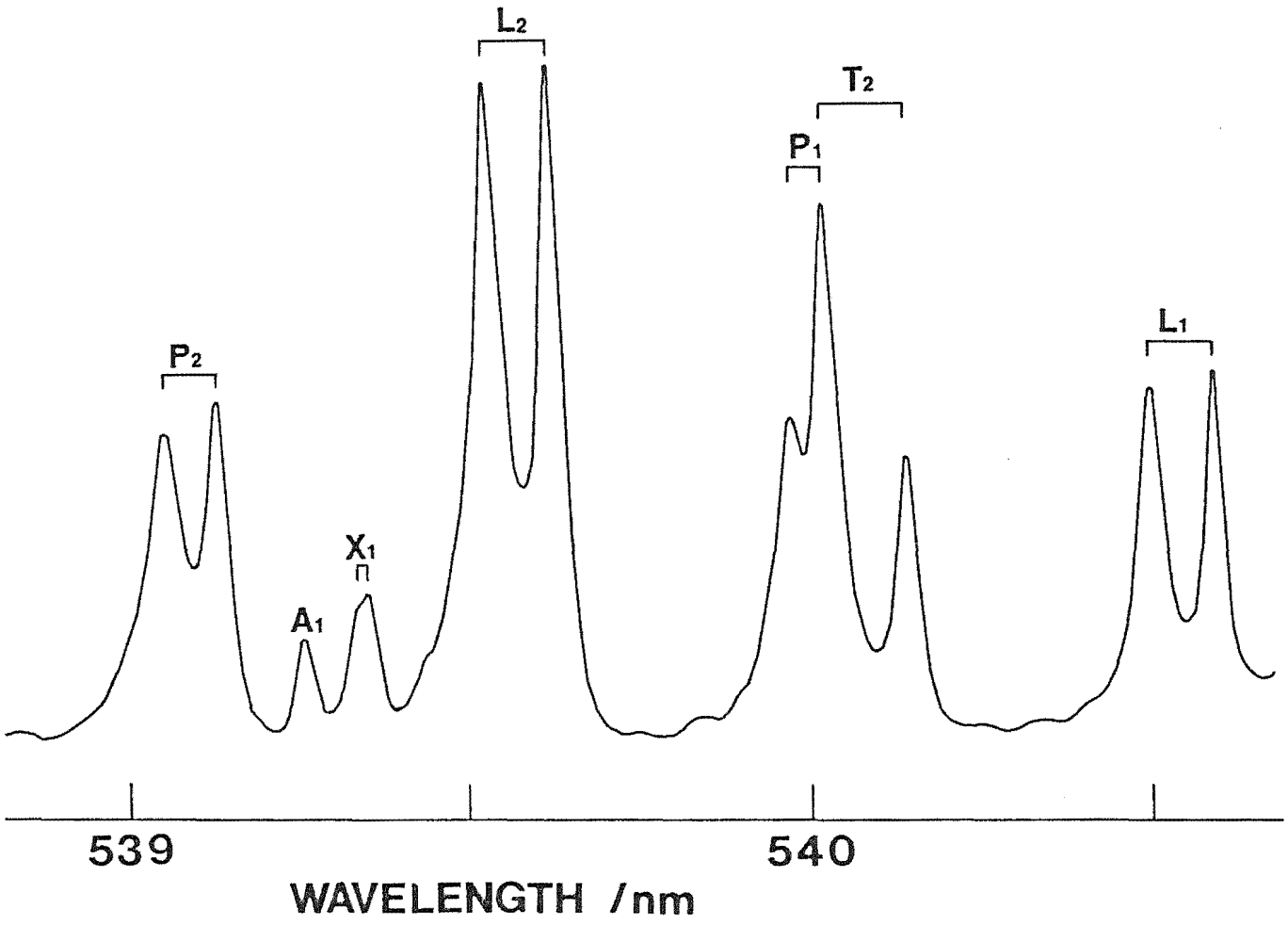

Figure 5.5 : Some $^4I_{15/2} \rightarrow {}^4S_{3/2}$ absorption transitions illustrating H^-/D^- isotope shifts using the two crystal method at 2K. The absorption of light through a deuterated and hydrogenated $CaF_2:Er^{3+}$ crystal mounted together is shown. In all cases the lower wavelength line is due to the D^- ion site.

TABLE 5.3 : Electronic line isotope shifts (in cm^{-1}, ± 0.3) of D^- sites relative to H^- sites determined from the 10K absorption spectrum of hydrogenated and deuterated CaF_2: 0.05% Er^{3+} crystals placed in series.

	P	L	T	N	S	V	W	X	C_{4v}	R	J	K	M
E_2	2.5	3.1	3.7	3.9	4.2	4.7	0.7	1.8	*	*	-	-	-
E_1	1.8	3.0	3.0	4.3	4.5	5.4	-0.2	0.5	-1.8	0	1.4	2.1	3.0

* obscured by F^- site lines

The isotope shift results from the modulation by vibrational motion of the hydrogenic ion of the crystal field at the erbium ion. Such vibrational frequencies are mass dependent so differ for various isotopes. The sign of the isotope shift from D^- to H^- is usually found to be positive, but may be negative as is the case for the Z_1-E_1 transition of the C_{4V} site. The dominant, second degree contribution to the magnitude of the isotope shift is proportional to $1/R^2$ where R is the separation of the rare earth ion and the hydride ion (Jones 1979). The observation of H^-/D^- shifts greater than that of the C_{4V} site is consistent with the possibility of sites involving hydride ions in lattice positions about the Er^{3+} ion.

Crystals that have been treated in a 1:1 mixture of hydrogen and deuterium are expected to show two sets of absorption lines : one from the H^- sites and the other from the corresponding D^- sites. This was found for the hydrogenic C_{4V} site. Crystals hydrogenated in a 1:1 mixture of hydrogen and deuterium for 68 hours have broader absorption lines for the L, T, N, S, V, J and K sites indicative of the presence of mixed H^-/D^- varieties of these sites.

The linewidths of these transitions were broader than either of the H^- and D^- centres separately, although no distinct structure could be resolved even using spectrometer slitwidths of 15 microns. Figure 5.6 compares the spectra of the $Z_1 \rightarrow E_2$ transitions for the L and T sites of a pure H^- ion crystal with those of the mixed H^-/D^- crystal. Figure 5.7 shows the configuration of crystals used to ensure both spectra were recorded on the same day at the

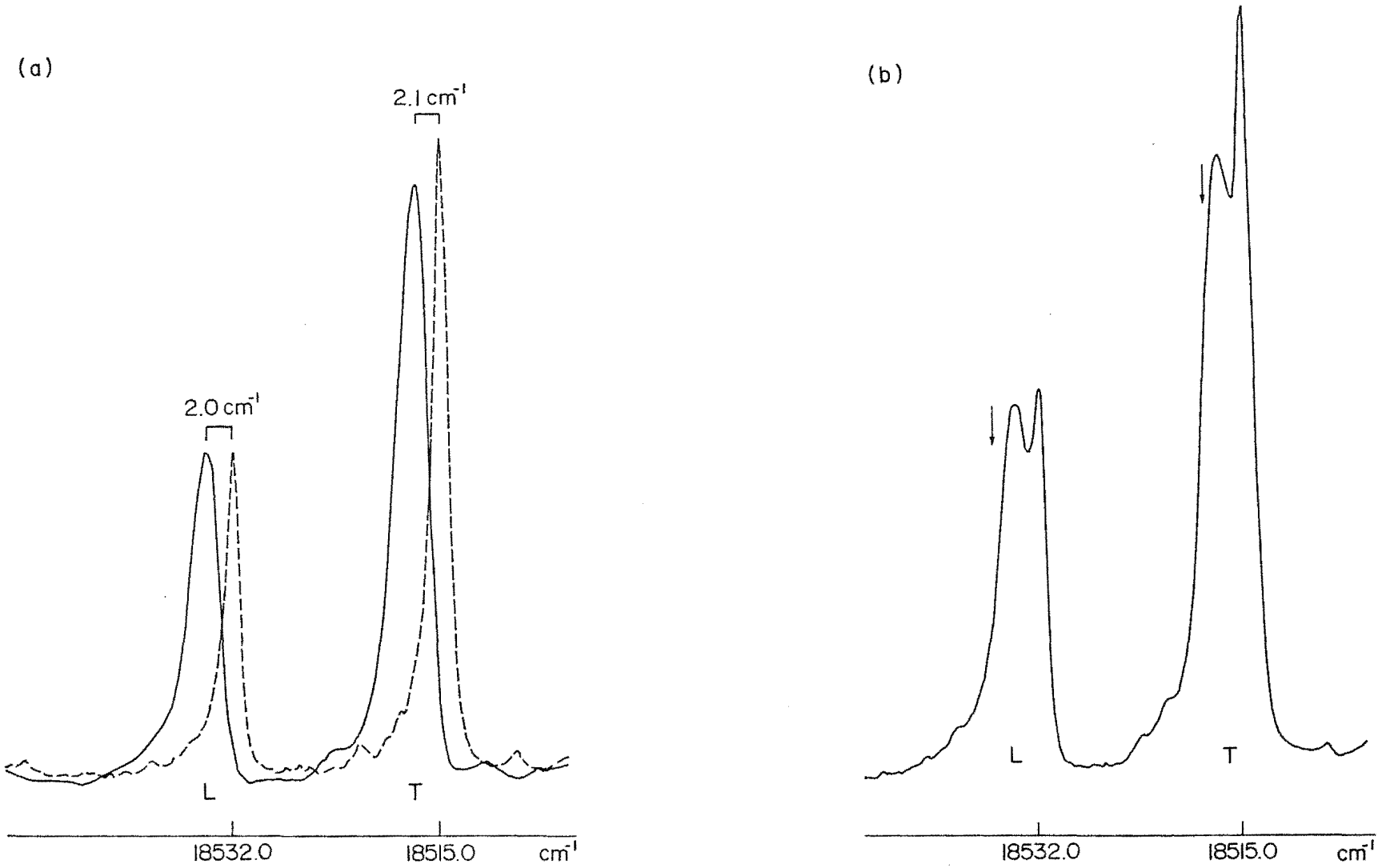

Figure 5.6 : Optical absorption of the $Z_1 \rightarrow E_2$ transitions of the L and T site in $CaF_2:Er^{3+}$ crystals at 10K : (a) solid line-mixed H^-/D^- crystal. Dotted line - H^- crystal alone. (b) Mixed H^-/D^- crystal in series with the H^- crystal. The arrows indicate the expected pure D^- ion site transition position.

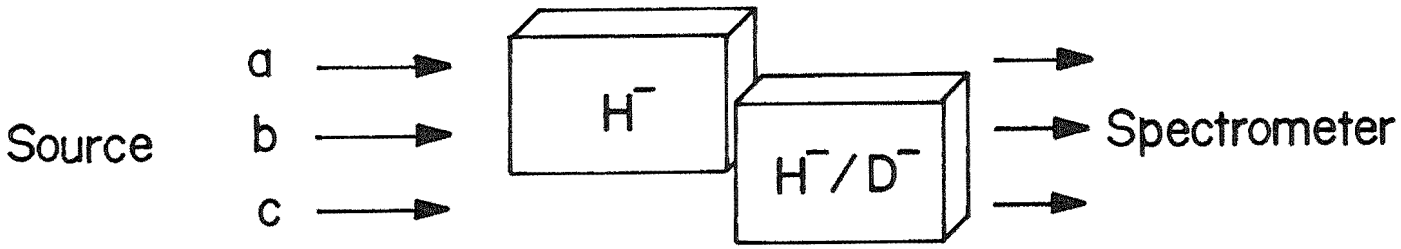

Figure 5.7 : Configuration of crystals used for optical absorption to compare transitions for (a) pure H^- site, (b) H^-/D^- crystals in series (see Figure 5.6b), and (c) H^-/D^- crystal alone. This configuration ensured identical measurement conditions for all spectra.

same temperature. Figure 5.6(b) shows the absorption of light through the path labelled b in Figure 5.7. This shows that the centre of the new peaks does not coincide with the pure H^- centres nor with the expected position of the D^- ion sites which are marked with arrows. The mixed crystal transitions shown for the L and T sites are increased in frequency from the H^- transitions by (2.0 ± 0.2) cm^{-1} and (2.1 ± 0.2) cm^{-1} respectively compared to the H^- to D^- site shifts of (3.1 ± 0.3) cm^{-1} and (3.7 ± 0.3) cm^{-1}. The existence of these additional absorptions suggests that all of these sites involve two hydrogenic ions in their configurations. This hypothesis is confirmed by an analysis of the vibronic spectra of these sites by laser selective excitation presented in Section 5.3.

The best tritiated sample still contained a mixture of H^- ions and T^- ions. The isotope shifts between the H^- and T^- sites were investigated for the sample and additional structure was resolved between the peaks for most sites except for the C_{4V} and the W sites. This is interpreted to be due to varieties of each site involving a combination of H^- and T^- ions in a similar fashion to the mixed H^-/D^- sites. The results confirm that the X, P, L and J sites each involve two hydrogenic ions described above. The structure was resolved in this case, however, where the isotope shifts tended to be larger. The isotope shifts, including those of the intermediate frequency features, are given in Table 5.4, and the $^4I_{15/2} \rightarrow {}^4S_{3/2}$ absorption spectrum is shown in Figure 5.4. The sites T, N, S, V, K and M were not measured since tritiated analogues could not be formed for the effective hydrogenation period used.

Table 5.4 : Isotope shifts for some sites as determined from 10K absorption spectra of tritiated CaF_2:0.05%Er^{3+} crystals. $\delta(H^- - T^-)$ is the difference between the pure T^- site and pure H^- site while $\delta(H^- - T^-/H^-)$ is the shift between the pure H^- site and a hybrid site involving both H^- and T^- ions. Uncertainty is $\pm$ 0.3 cm^{-1}.

Site	Transition	$\delta(H^- - T^-)$ (cm^{-1})	$\delta(H^- - H^-/T^-)$ (cm^{-1})
W	$Z_1 \rightarrow E_2$	0.7	-
W	$Z_1 \rightarrow E_1$	0.8	-
X	$Z_1 \rightarrow E_2$	2.5	1.2
X	$Z_1 \rightarrow E_1$	2.1	0.9
P	$Z_1 \rightarrow E_2$	3.2	1.4
P	$Z_1 \rightarrow E_1$	2.1	1.0
L	$Z_1 \rightarrow E_2$	2.6	1.3
C_{4V}	$Z_1 \rightarrow E_1$	-2.5	-
C_{4V}	$Z_3 \rightarrow E_1$	-1.7	-
R	$Z_1 \rightarrow E_1$	0.6	obscured
R	$Z_2 \rightarrow E_1$	-1.1	obscured
J	$Z_1 \rightarrow E_1$	1.8	0.9

5.2.3 Discussion: Site Classification

The optical absorption measurements showed the wide variety of charge compensation sites available for the hydrogenated system. Some ions are present in near cubic symmetry sites, while the presence of thirteen distinctly different hydrogenic sites (Table 5.1) of nearby charge compensation contrasts with the existence of only two main F^- ion sites in the parent crystals. Three main factors concur in showing that these sites involve a single Er^{3+} ion only :

(a) Lack of dependence of the site distribution on erbium concentration between 0.05% and 0.01% Er^{3+} dopant levels. In particular the ratio of all sites to the known single Er^{3+} ion site, H^- C_{4V}, remained constant. A cluster site involving two Er^{3+} ions would be expected to have a relative reduction by a factor of five between these two concentrations.

(b) During the hydrogenation process the crystals are heated to temperatures (1130K) known to be sufficient to dissociate almost all Er^{3+} ion cluster sites (Moore and Wright 1979, 1981).

(c) No evidence of electronic energy level splitting due to Er^{3+}-Er^{3+} ion pair interaction was found for these sites, in contrast to the case observed for the Z_2 level of the F^- C site [TW75].

It is proposed that the large number of observed single Er^{3+} ion hydrogenic sites arises from the many inequivalent positions any additional H^- ion can occupy relative to an

Er^{3+}-charge compensation ion pair. The F^-A and B sites of the parent crystals are two simple Er^{3+}-F^- charge compensation arrangements, and the primary effect of any hydrogenation treatment is to produce hydrogenic analogues of these arrangements. From the results it is apparent that the thirteen sites of Table 5.1 may be categorised into two sets or 'families' indicative of modifications of the two basic sites.

5.2.3(a) *Family A*

This set, resembling the F^-A site, comprises the hydrogenic C_{4V} site and also the R, J, K and M sites. The reasons for such a classification are as follows :

(a) The sites all have $^4S_{3/2}$ and $^4F_{9/2}$ levels grouped at energies slightly lower than the F^-A site with descending order C_{4V}, R, J, K and M for both multiplets.

(b) The energy level schemes have consistent similarities. The Z_1-E_1, D_2-D_1, Z_1-Z_2 and Z_2-Z_3 energy level separations show systematic trends along the ordered series.

(c) There are similar intensity patterns for corresponding absorption transitions for different member sites (Figures 5.1 and 5.2). The clearest examples, for all of these sites, are the weak $Z_1 \rightarrow D_1$ line compared to the $Z_1 \rightarrow D_2$ transition, and the weak $Z_1 \rightarrow E_2$ line compared to the $Z_1 \rightarrow E_1$ transition. This behaviour closely follows that of the F^-A site.

It is therefore proposed that the R, J, K and M sites are modifications of the hydrogenic C_{4V} site. The isotope shifts and mixed crystal line broadening suggest the involvement of addditional hydrogenic ions. Laser selective excitation studies described in the next section are needed to propose specific configurations.

5.2.3(b) *Family B*

The set of sites W, X, P, L, T, N, S and V bear a marked resemblance to each other and also to the F^- B site, so are classified together as a family. Common features include :

(a) Absorption transitions occurring at higher frequencies than those of the Family A sites (Figures 5.1, 5.2).

(b) Similar energy level patterns that differ significantly from those of the Family A sites. Transitions from the Z_3 level are not observed for these sites because they all lie at sufficiently high energy above the Z_1 level to be depopulated even at 100K.

(c) Similar absorption line intensity patterns. For example, both $Z_1 \rightarrow E_1$ and $Z_1 \rightarrow E_2$ transitions are apparent, with the latter more intense, in contrast to the Family A sites where the Z_1-E_2 transition is not observed.

The W site was included in this family on the basis of its known $^4S_{3/2}$ and $^4F_{9/2}$ levels, although the Z_2 level of the site has not been determined. Transitions from this

level are probably obscured by transitions of other sites in the spectra examined.

It is proposed that this family contains the hydrogenic analogue of the F^-B site, that is, a site with a <111> orientated Er^{3+}-H^- ion pair. Other family members are expected to be hydrogenic modifications of this. The broadened absorption lines for most of these sites in mixed H^-/D^- crystals is indicative of the modifications being caused by additional hydrogenic ions.

The two families of sites exhibited similar behaviour in the variation of individual site concentrations with duration of hydrogenation treatment. For Family A, the F^-A site was first replaced by the hydrogenic C_{4V} site, followed by the sequential growth of the R, J, K and M sites.

Likewise, for the other family, the W, X and P sites appeared first at the expense of the F^-B site, followed by successive appearance of lines of the L, T, N, S and V sites. After 68 hours hydrogenation, the dominant sites for each set were the J and T sites respectively.

5.3 Laser Selective Excitation

5.3.1 Outline

While optical absorption spectroscopy is useful for determining hydrogenic site distribution in the crystals as a whole and for studying the effect of various treatments on

these site distributions, it has the disadvantage that transitions due to all sites appear simultaneously and are difficult to correlate with particular sites.

The transitions between the $^4I_{15/2}$ and $^4S_{3/2}$ multiplets for most sites identified by optical absorption were excited using a tunable dye laser. Several of the sites could be pumped cleanly using the $Z_1 \rightarrow E_1$ transition. For some sites the fluorescence spectra produced were confirmed by pumping the $Z_1 \rightarrow E_2$ transition, while other sites, less cleanly resolved for such absorption transitions, were also pumped using the $Z_2 \rightarrow E_1$ transition since the Z_2 level was partially populated at 10K. The remainder of sites had either insufficient absorption, very weak emission, or their fluorescence could not be discriminated from the more intense fluorescence of fluoride ion sites having sufficient absorption at the same laser wavelength to be simultaneously excited.

As a consequence of non-radiative processes involving hydrogenic ions, the H^- and D^- ion sites have weaker fluorescence than the F^- ion sites, by factors of typically 10^4 and 10^3 respectively. The weakness of fluorescence of H^- sites relative to D^- sites is a result of higher corresponding local mode frequencies for the H^- site giving additional, more probable, non-radiative decay channels involving fewer phonons than for the analogous D^- centres. Generally the proximity of the H^- ion also resulted in a decrease, relative to the fluoride ion centres, of multiplet barycentres due to greater covalency for the Er^{3+}-H^- site.

Because of the strong influence of local mode phonon decay channels on the fluorescence intensities of hydrogenic

sites, the deuterated crystals were preferentially studied. For some sites the H^- ion site emission was undetectable, while for the corresponding D^- ion site, emission was readily observed.

For the spectrometer sensitivity used, the first order Raman scattering line of the CaF_2 host lattice (Denham *et al.* 1970) frequently appeared as a single sharp line located 327 cm^{-1} below the laser pump frequency. This has been labelled 'R' in the spectra while the position of the laser frequency is labelled with an 'L'.

Although the absorption lines of the F^- sites in 68-hour hydrogenated crystals have become too weak to be observed, laser selective excitation still yields F^- site emission lines at about 1% of parent crystal intensity; sufficient to cause discrimination difficulties between D^- and F^- sites having coincident energy levels at the laser pump wavelength. Laser excitation studies pumping transitions to the $^4F_{9/2}$ multiplet were hampered by such underlying excitation of F^- sites present. The $Z_1 \rightarrow D_1$ transitions for the hydrogenic sites have energies below the range of the red dye available, while interfering F^- sites precluded clean pumping of $Z_1 \rightarrow D_2$ transitions. The emission from this multiplet was, therefore, also obtained by exciting to the $^4S_{3/2}$ multiplet.

Five new F^- fluoride ion sites labelled F1-F5 were also observed while pumping to the $^4S_{3/2}$ manifold, and energy levels were determined and assigned. These sites are discussed in Section 5.5.

Table 5.5 gives the energy levels determined for eight D^- ion sites by laser selective excitation. The results for these sites will now be discussed in turn.

TABLE 5.5 : Energy levels (in cm^{-1}) of eight D^- sites derived from the 10K fluorescence spectra of deuterated CaF_2: 0.05% Er^{3+} crystals.

	C_{4v}	R	J	K	L	T	N	V
E_2	18613.6±0.8	18590.9±1.0	-	-	18535.0±0.4	18518.2±0.4	18495.3±0.4	18479.7±0.8
E_1	18478.7±0.4	18444.2±0.4	18419.8±0.4	18409.3±0.4	18502.3 "	18492.0 "	18489.5 "	18469.2±0.8
D_3	-	-	-	-	15396.3 "	15385.7 "	15374.8 "	15362.0±0.4
D_2	15392.4 "	15380.0 "	15370.7 "	15370.0±0.8	15387.5 "	15372.9 "	15360.0 "	15342.5 "
D_1	15331.8 "	15297.5 "	15272.0 "	15261.0±1.0	15360.8 "	15353.1 "	15346.8 "	15330.5 "
Y_7	6894.8±1.2	6935.3±1.2	6965.3±1.2	-	6837.5±1.2	6851.1±1.2	6850.5±1.2	6844.5±1.2
Y_6	6824.0±1.0	6849.0 "	6861.8 "	-	6817.1 "	6818.1 "	6817.0 "	6813.5 "
Y_5	6800.6±1.2	6806.7±1.0	6826.3±1.0	-	6797.8±1.0	6802.6±1.0	6810.8±1.0	6807.5±1.0
Y_4	6795.8±1.0	6795.9 "	6798.3 "	-	6794.3±0.8	6792.1±0.8	6788.3±0.8	6776.5±0.8
Y_3	6709.4±0.8	6723.3±0.8	6731.3±0.8	-	6727.0±1.2	6730.6±1.2	6733.7±1.2	6730.5±1.2
Y_2	6596.6 "	6605.1 "	6611.8 "	-	6701.5±0.8	6709.6 0.8	6708.9±0.8	6701.5±0.8
Y_1	6561.2 "	6563.4 "	6566.3 "	-	6634.3 "	6635.1 "	6635.8 "	6633.5 "
Z_8	583.5±2.0	642.0±2.0	678.0±2.0	-	516.2±1.5	510.5±1.5	509.3±1.5	503.0±1.5
Z_7	424.1±0.7	454.9±0.8	466.0±1.2	471.0±1.2	467.3±1.0	464.5±1.0	462.5±1.0	469.0±1.0
Z_6	422.0±1.0	426.3 "	449.5±0.8	461.5±0.8	437.2±0.8	436.4±0.8	439.4±0.8	434.0±0.8
Z_5	374.4±0.7	373.4 "	377.5 "	401.0 "	305.1 "	306.0 "	301.7 "	307.5 "
Z_4	281.4±1.0	308.8 "	326.0 "	342.0±1.0	290.1 "	298.0 "	289.6 "	289.0 "
Z_3	25.0±0.3	35.7±0.4	44.9±0.4	57.0±0.5	283.8±0.5	278.6±0.5	272.7±0.5	258.0±0.5
Z_2	2.9 "	9.1±0.3	12.1±0.3	20.9±0.3	22.5±0.3	25.5±0.4	26.2±0.3	30.6±0.3
Z_1	0	0	0	0	0	0	0	0

5.3.2 The C_{4V} Symmetry Site

5.3.2(a) *Identification of Energy Levels*

This centre is the most spectroscopically useful one since it has well-defined configuration and symmetry. The compensation mechanism involving a single nearest neighbour interstitial hydride ion was established by the infra-red local mode vibrations and absorption vibronics (Edgar *et al.* 1979). A reason for investigation of the site is that it can be compared to its fluoride ion analogue, the A site, and equivalent F^- C_{4V} sites known for several other rare earth ions in CaF_2 (for summary see Baker 1974). Spectroscopic information can be used for crystal field analysis and models to calculate both distortion of the lattice caused by ligands (Reid and Butler 1982) and Er^{3+}-hydride ion covalency.

Laser selective excitation was used to study the H^-, D^- and T^- C_{4V} centres at 10K, the lowest temperature available. The relative intensity ratios of transitions of the H^- and D^- centres to the corresponding F^- C_{4V} transitions were found to be approximately 1:8000 and 1:2000 respectively.

Laser excitation of the $Z_1 \rightarrow E_1$ transition resulted in fluorescence for $^4S_{3/2} \rightarrow {}^4I_{15/2}$, $^4S_{3/2} \rightarrow {}^4I_{13/2}$ and $^4F_{9/2} \rightarrow {}^4I_{15/2}$ transitions in descending order of intensity. Typical spectra for the D^- C_{4V} site are given in Figure 5.8. A close correspondence to the F^- C_{4V} site spectra [TW75] was found and the energies of crystal field levels of the $^4I_{15/2}$ manifold are compared in Figure 5.9. For $Z_1 \rightarrow E_1$ excitation, transitions were observed from the E_1 level to

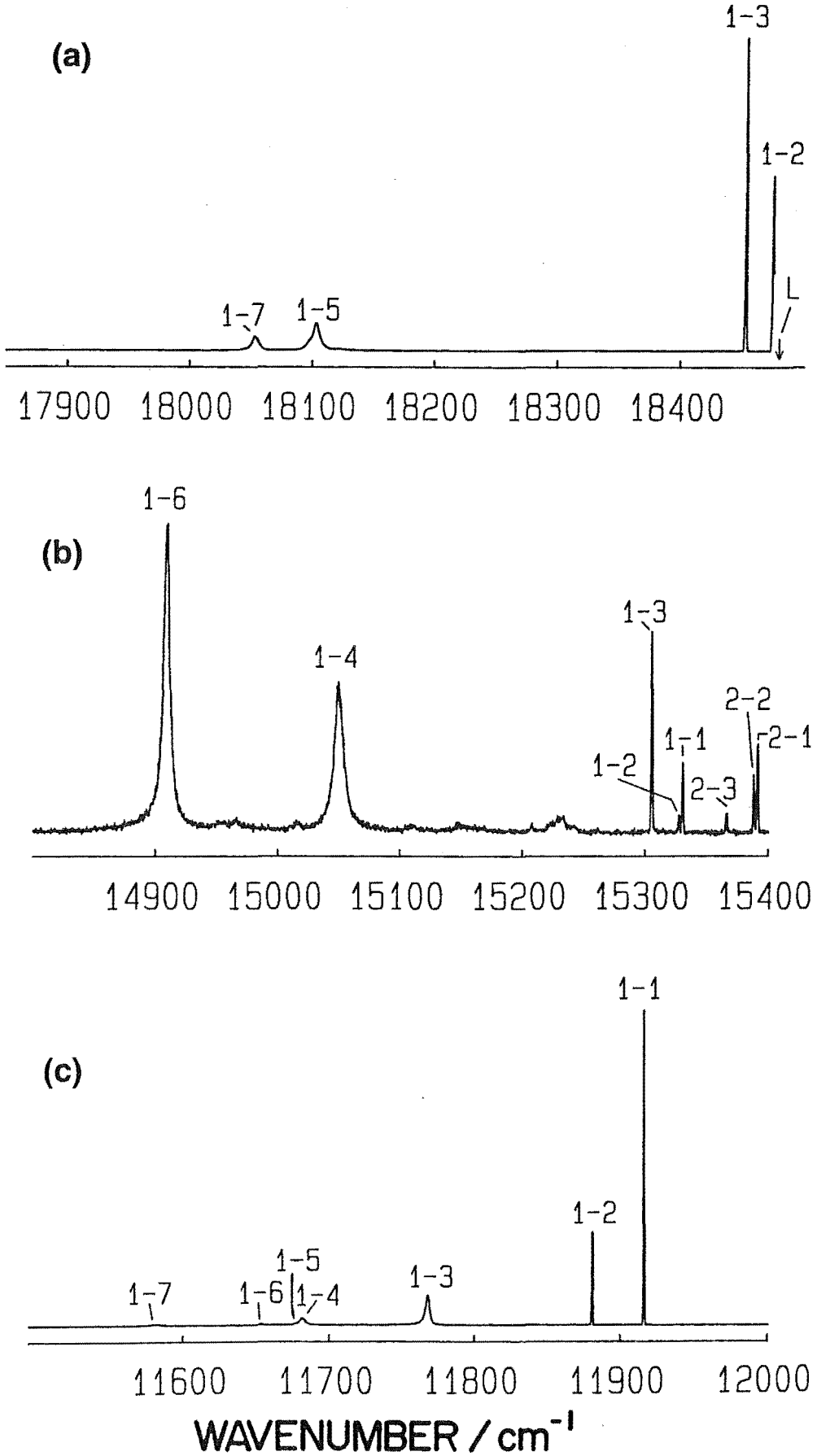

Figure 5.8 : 10K fluorescence for laser excitation of the $Z_1 \rightarrow E_1$ transition of the D^- C_{4V} site of $CaF_2:Er^{3+}$: (a) $^4S_{3/2} \rightarrow {}^4I_{15/2}$, (b) $^4F_{9/2} \rightarrow {}^4I_{15/2}$, and (c) $^4S_{3/2} \rightarrow {}^4I_{13/2}$. "L" identifies the laser position. Transition labels represent the upper and lower multiplet levels involved.

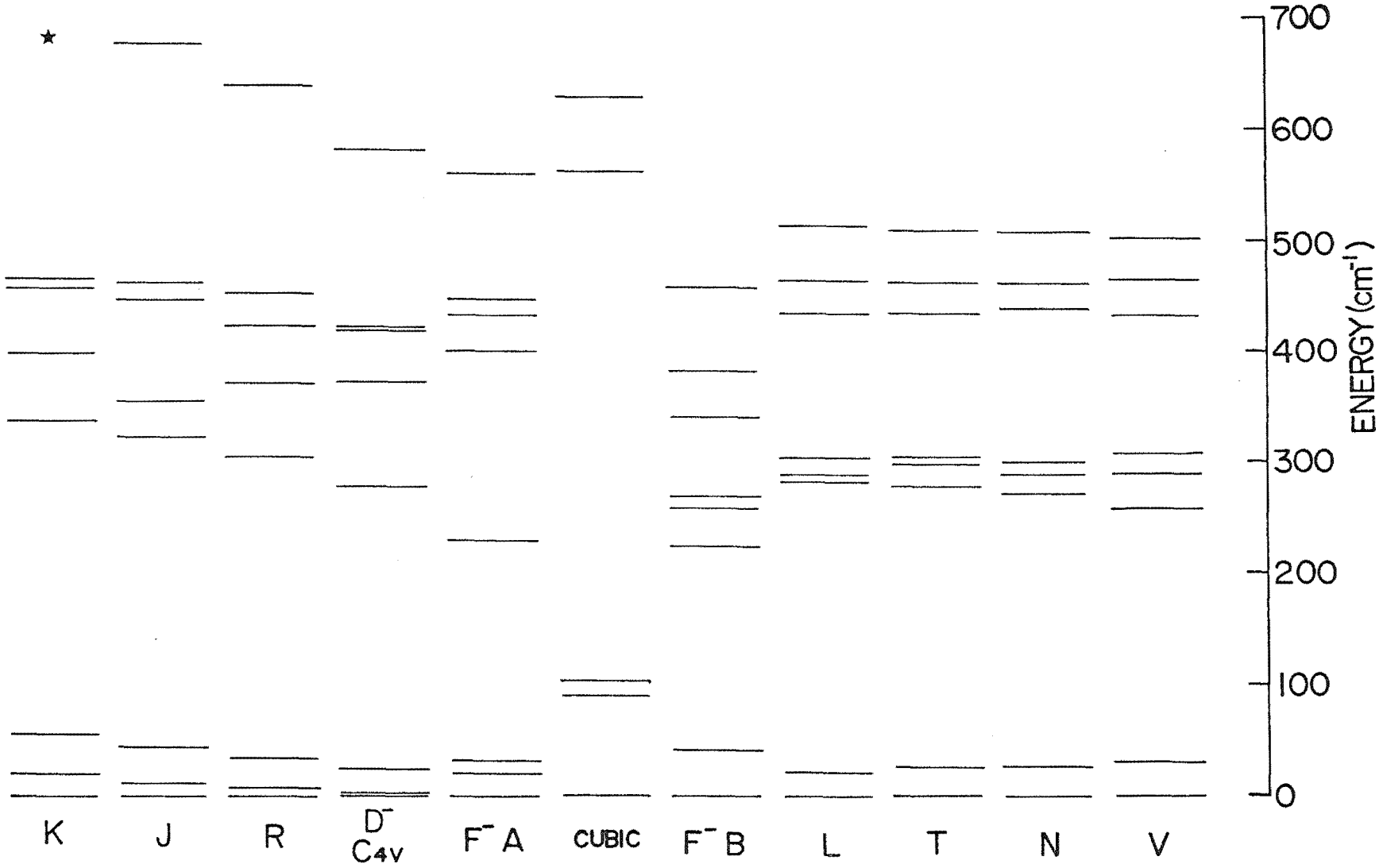

Figure 5.9 : Schematic comparison of the $^4I_{15/2}$ multiplet energy levels of several new D^- ion sites and F^- ion A and B sites with the cubic site energy levels (Moore 1980) from which they are derived.

the Z_2, Z_3, Z_5 and Z_7 levels, with careful examination revealing an additional very weak transition from which was assigned the Z_8 level. The dominant lines of the $^4F_{9/2} \rightarrow {}^4I_{15/2}$ spectrum were the $D_1 \rightarrow Z_4$ and $D_1 \rightarrow Z_6$ transitions. It was found that there was a small but definite difference between the levels assigned to be Z_7 (from the E_1 level) and Z_6 (from the D_1 level) of 3.5, 2.1 and 1.4 cm^{-1} for the H^-, D^- and T^- sites respectively.

It is clearly apparent from Figure 5.8(b) that the D^- C_{4V} site transition at 15392.4 cm^{-1} which is dominant in the absorption spectrum (Figure 5.2) is the $D_2 \rightarrow Z_1$ transition, whereas the D_1 level assigned to be 15331.8 cm^{-1} corresponds to an extremely weak absorption line in Figure 5.2(a). This intensity ratio is consistent with that observed for the F^- A site.

The E_2 level of the D^- C_{4V} site was found, by excitation spectroscopy monitoring the $E_1 \rightarrow Z_1$, Z_2 and Z_3 transitions, to be coincident with the $Z_1 \rightarrow E_2$ transition of the F^- B site at 18613.6 cm^{-1}, and amends the previously incorrectly assigned level (Edgar *et al.* 1979). Figure 5.10 shows the resultant fluorescence from the site when the $Z_1 \rightarrow E_2$ transition is pumped. Attempts to determine the E_2 level of the analogous H^- ion C_{4V} site were unsuccessful due to the weaker emission for this site.

All eight levels of the $^4I_{15/2}$ manifold and all seven for the $^4I_{13/2}$ manifold were identified for the $H^-$and D^- C_{4V} sites, and all except Z_8 and Y_5 were determined for the T^- C_{4V} site.

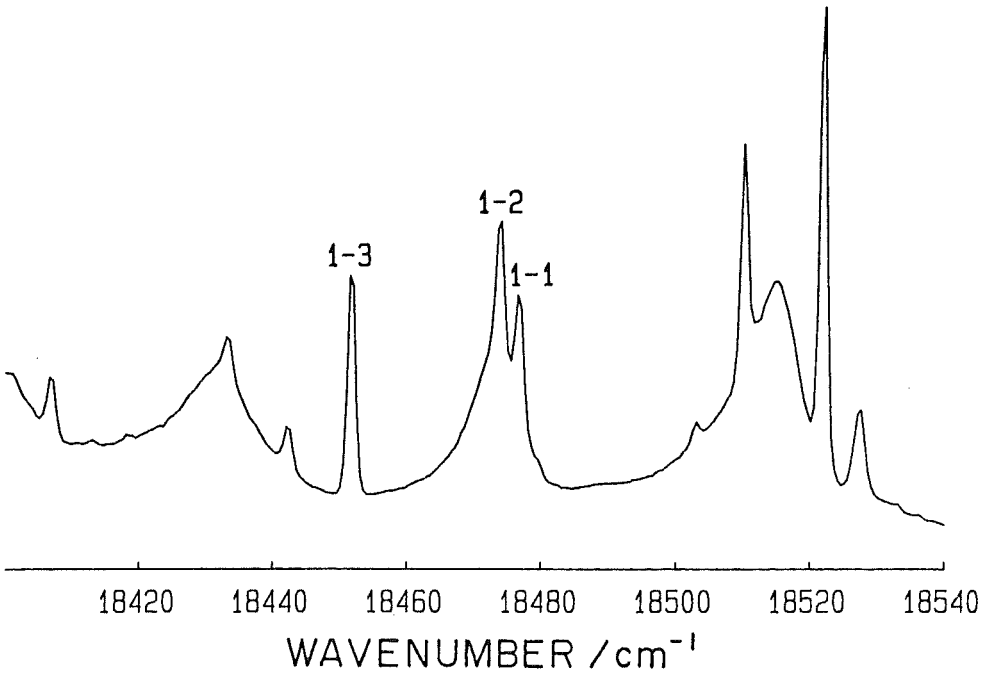

Figure 5.10 : 10K fluorescence of the D^- C_{4V} site (transitions labelled) for laser excitation of the $Z_1 \rightarrow E_2$ transition.

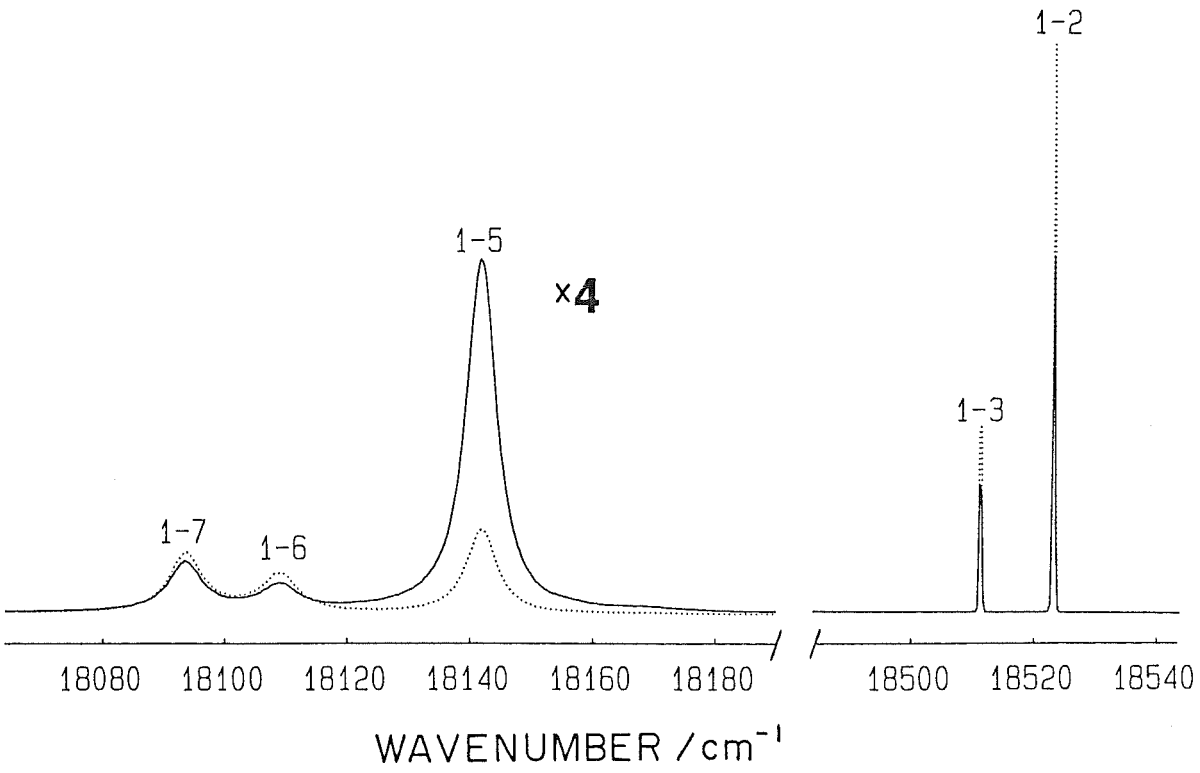

Figure 5.11 : 10K polarised (x(yx)z_____, x(yy)z...) $^4S_{3/2} \rightarrow {}^4I_{15/2}$ fluorescence for laser excitation of the $Z_1 \rightarrow E_1$ transition of the F^- C_{4V} site of $CaF_2:Er^{3+}$.

5.3.2(b) *Polarisation of C_{4V} Site Emission*

The description in Chapter Four of the dependence of emission intensities on the polarisation of incident and emitted light in oriented crystals can be applied to the C_{4V} site.

For plane polarised light incident in a given <100> direction the fluorescence monitored in an orthogonal direction was found to be partially polarised for the H^- and D^- C_{4V} sites, consistent with the expected tetragonal symmetry. The tritium site intensities were sufficiently low, due to low site concentration in the crystals, that any polarisation information obtained was unreliable. The F^- C_{4V} site lines were also found to be polarised, and polarisation information obtained for this site is included in this section as polarisation dependence has not previously been reported for the site. As expected, it was found that the ratio x(zx)z:x(zy)z was unity for all transitions of the H^-, D^- or F^- C_{4V} sites.

Several problems were encountered when measuring polarised spectra due to both power and frequency instability of the dye laser used, as the dyes available for coverage of this spectral region, such as coumarin 6, have particularly low output power and stability. Scans taking the periods of time needed, typically 30-45 minutes, to give the required resolution for narrow linewidth transitions over a whole multiplet spectrum, were found to have laser power changes of up to 10%. Subsequent recording of another long scan of different polarisation was found to give unreliable intensity ratios. For this reason most spectra presented in this study are unpolarised and recorded

TABLE 5.6 : Wavenumbers, linewidths and relative intensities within each multiplet (± 10% between the two polarisations for a given transition) of 10K fluorescence transitions of the F^-, H^- and D^- C_{4V} sites measured in <100> oriented CaF_2: 0.05% Er^{3+} crystals.

Excitation	Transition	Wavenumber (cm^{-1})	Linewidth (cm^{-1}) (±10%)	Relative Intensity (± 15%) x(yx)z	x(yy)z
Laser tuned to F^- C_{4V} site $Z_1\gamma_7 \rightarrow E_1\gamma_7$ at 18544.3 cm^{-1}	$E_1 \rightarrow Z_2\gamma_6$	18523.3 ±0.4	1.0	0.40	0.65
	$\rightarrow Z_3\gamma_7$	18511.6 "	1.0	0.15	0.23
	$\rightarrow Z_4\gamma_6$	-			
	$\rightarrow Z_5\gamma_7$	18140.5 ±0.7	6.0	1.00	0.16
	$\rightarrow Z_6\gamma_6$	18107.8 "	7.0	0.090	0.14
	$\rightarrow Z_7\gamma_7$	18092.5 "	6.5	0.14	0.19
	$\rightarrow Z_8\gamma_6$	-			
	$D_2\gamma_7 \rightarrow Z_1$	15424.5±0.4	0.8	0.0006	0.0005
	$\rightarrow Z_2$	15403.5 "	0.8	0.0012	0.0021
	$\rightarrow Z_3$	15391.3 "	0.6	0.0004	0.0006
	$D_1\gamma_6 \rightarrow Z_1$	15396.0 "	0.8	0.0039	0.0063
	$\rightarrow Z_2$	15375.0 "	0.6	0.025	0.0073
	$\rightarrow Z_3$	15363.5 "	0.6	0.017	0.029
	$\rightarrow Z_4$	15165.0±0.8	10.0	0.12	0.19
	$\rightarrow Z_5$	14991.0 "	obscured	-	-
	$\rightarrow Z_6$	14959.5±1.0	8.0	1.00	0.18
	$\rightarrow Z_7$	-			
	$\rightarrow Z_8$	-			
	$E_1 \rightarrow Y_1\gamma_6$	11970.6±0.6	0.4	0.61	1.00
	$\rightarrow Y_2\gamma_7$	11940.8 "	0.4	0.23	0.18
	$\rightarrow Y_3\gamma_7$	11845.5 "	1.7	0.23	0.28
	$\rightarrow Y_4\gamma_7$ / $\rightarrow Y_5\gamma_6$	11727.8±0.7	5.4	0.80	0.22
	$\rightarrow Y_6\gamma_6$	11701.3±0.8	8.5	0.085	0.064
	$\rightarrow Y_7\gamma_7$	11665.6 "	7.0	0.18	0.14
Laser tuned to F^- C_{4V} site $Z_1 \rightarrow D_2$ at 15424.5 cm^{-1}	$D_2 \rightarrow Z_2$	15403.5±0.4	0.8	0.0046	0.0032
	$\rightarrow Z_3$	15391.3 "	0.6	0.0012	0.00083
	$D_1 \rightarrow Z_1$	15396.0 "	0.8	0.0077	0.0054
	$\rightarrow Z_2$	15375.0 "	0.6	0.022	0.033
	$\rightarrow Z_3$	15363.5 "	0.6	0.028	0.019
	$\rightarrow Z_4$	15165.0±0.8	10.0	0.18	0.13
	$\rightarrow Z_5$	14991.0 "	obscured	-	-
	$\rightarrow Z_6$	14959.5±1.0	8.0	0.55	1.00
	$\rightarrow Z_7$	-			
	$\rightarrow Z_8$	-			
	$E_1 \rightarrow Z_1$	18544.3±0.4	0.8	0.59	0.47
	$\rightarrow Z_2$	18523.3 "	1.0	1.00	0.79
	$\rightarrow Z_3$	18511.6 "	1.0	0.40	0.33
	$\rightarrow Z_4$	-			
	$\rightarrow Z_5$	18140.5±0.7	6.0	0.27	0.45
	$\rightarrow Z_6$	18107.8 "	7.0	0.047	0.039
	$\rightarrow Z_7$	18092.5 "	6.5	0.076	0.07
	$\rightarrow Z_8$	-			
Laser tuned to F^- C_{4V} site $Z_1 \rightarrow E_2\gamma_6$ at 18628.9 cm^{-1}	$E_1 \rightarrow Z_1$	18544.3±0.4	1.0	0.17	0.26
	$\rightarrow Z_2$	18523.3 "	1.0	0.32	0.59
	$\rightarrow Z_3$	18511.6 "	1.0	0.13	0.22
	$\rightarrow Z_4$	-			
	$\rightarrow Z_5$	18140.5±0.7	6.0	1.00	0.11
	$\rightarrow Z_6$	18107.8 "	7.0	0.091	0.15
	$\rightarrow Z_7$	18092.5 "	6.5	0.14	0.20
	$\rightarrow Z_8$	-			

Continued next page

TABLE 5.6 : continued

Excitation	Transition	Wavenumber (cm^{-1})	Linewidth (cm^{-1}) (±10%)	Relative Intensity (±15%) x(yx)z	x(yy)z
Laser tuned to H^- C_{4v} site $Z_1\gamma_7 \rightarrow E_1\gamma_7$ at 18480.2 cm^{-1}	$E_1 \rightarrow Z_2\gamma_6$	18476.0±0.4	0.8	0.38	0.55
	$\rightarrow Z_3\gamma_7$	18454.7 "	0.8	0.90	0.63
	$\rightarrow Z_4\gamma_6$	-			
	$\rightarrow Z_5\gamma_7$	18104.0±0.7	7.5±1.0	1.00	0.45
	$\rightarrow Z_6\gamma_6$	-			
	$\rightarrow Z_7\gamma_7$	18054.5 "	7.0	0.30	0.40
	$\rightarrow Z_8\gamma_6$	-			
Laser tuned to D^- C_{4v} site $Z_1 \rightarrow E_1$ at 18478.7 cm^{-1}	$E_1 \rightarrow Z_2$	18475.8±0.4	1.2	0.39	0.53
	$\rightarrow Z_3$	18453.7 "	1.2	1.00	0.60
	$\rightarrow Z_4$	-			
	$\rightarrow Z_5$	18104.3±0.7	7.5±1.0	0.64	0.34
	$\rightarrow Z_6$	-			
	$\rightarrow Z_7$	18054.6 "	6.0	0.18	0.27
	$\rightarrow Z_8$	17895.7±1.0	10.0±2.0	very weak	
	$D_2\gamma_7 \rightarrow Z_1$	15392.4±0.4	2.4	0.053	0.033
	$\rightarrow Z_2$	15389.3 "	1.8	0.017	0.024
	$\rightarrow Z_3$	15367.4 "	1.2	0.0075	0.0072
	$D_1\gamma_6 \rightarrow Z_1$	15331.8 "	1.8	0.023	0.028
	$\rightarrow Z_2$	15329.0 "	1.8	0.011	0.011
	$\rightarrow Z_3$	15306.7 "	2.9	0.11	0.14
	$\rightarrow Z_4$	15050.4±0.8	9.4	0.43	0.57
	$\rightarrow Z_5$	-			
	$\rightarrow Z_6$	14909.8 "	6.5	1.00	0.45
	$\rightarrow Z_7$	-			
	$\rightarrow Z_8$	-			
	$E_1 \rightarrow Y_1\gamma_6$	11917.5±0.6	0.8	0.74	1.00
	$\rightarrow Y_2\gamma_7$	11882.1 "	1.2	0.51	0.31
	$\rightarrow Y_3\gamma_7$	11769.3 "	2.0	0.22	0.24
	$\rightarrow Y_4\gamma_7$	11682.9±0.8	2.8	0.14	0.078
	$\rightarrow Y_5\gamma_6$	11678.1±1.0	2.0	very weak	
	$\rightarrow Y_6\gamma_6$	11654.7 "	2.0	0.01	0.01
	$\rightarrow Y_7\gamma_7$	11583.9 "	6.0	0.045	0.045
Laser tuned to D^- C_{4v} site $Z_2 \rightarrow E_1$ at 18475.8 cm^{-1}	$E_1 \rightarrow Z_1$	18478.7±0.4	1.0	0.37	0.51
	$\rightarrow Z_2$	laser			
	$\rightarrow Z_3$	18453.7 "	1.0	1.00	0.35
	$\rightarrow Z_4$	-			
	$\rightarrow Z_5$	18104.3±0.7	7.0	0.66	0.042
	$\rightarrow Z_6$	-			
	$\rightarrow Z_7$	18054.6 "	6.0	0.14	0.23
	$\rightarrow Z_8$	-			
	$E_1 \rightarrow Y_1$	11917.5±0.6	0.8	0.59	1.00
	$\rightarrow Y_2$	11882.1 "	1.2	0.51	0.15
	$\rightarrow Y_3$	11769.3 "	2.2	0.15	0.26
	$\rightarrow Y_4$	11682.9±0.8	3.0	0.12	0.022
	$\rightarrow Y_5$	11678.1±1.0	2.2	very weak	
	$\rightarrow Y_6$	11654.7 "	2.2	0.011	0.0083
	$\rightarrow Y_7$	11583.9 "	6.0	0.060	0.045

using a scrambler placed before the spectrometer slits. To determine polarisation intensities more reliably, short scans over the relevant sections of a spectral region were recorded such as those given in Figure 5.11.

Table 5.6 summarises a variety of intensity ratios and linewidths determined in the <100> geometry for transitions of the F^-, D^- and H^- C_{4V} sites. Intensities are normalised to unity for the largest peak in each multiplet and the geometric labels, x(ab)z, used are those defined in Chapter Four. Each of the predicted 2:1 x(yy)z:x(yx)z ratios of transition intensities was observed within uncertainty.

It can be seen from the table that the H^- and D^- site intensity patterns follow those of the F^- site. These observations provide the basis for modified Judd-Ofelt intensity calculations similar to those attempted for the unpolarised F^- A site results by Reid (1981).

5.3.2(c) *Vibronic Measurements*

In addition to the emission due to pure electronic transition emission described, laser excitation of the H^-,D^- and T^-C_{4V} sites resulted in an emission region of lines associated with vibronic transitions. These transitions have energies shifted from the zero phonon electronic lines by the magnitude of a local mode vibration phonon of the hydrogenic ion. For the C_{4V} site there are up to two vibronics (one for each of the transverse and longitudinal H^- ion modes) associated with each parent electronic transition.

The vibronics are factors of 10^2-10^3 weaker than the parent transition and are shown for all three cases in

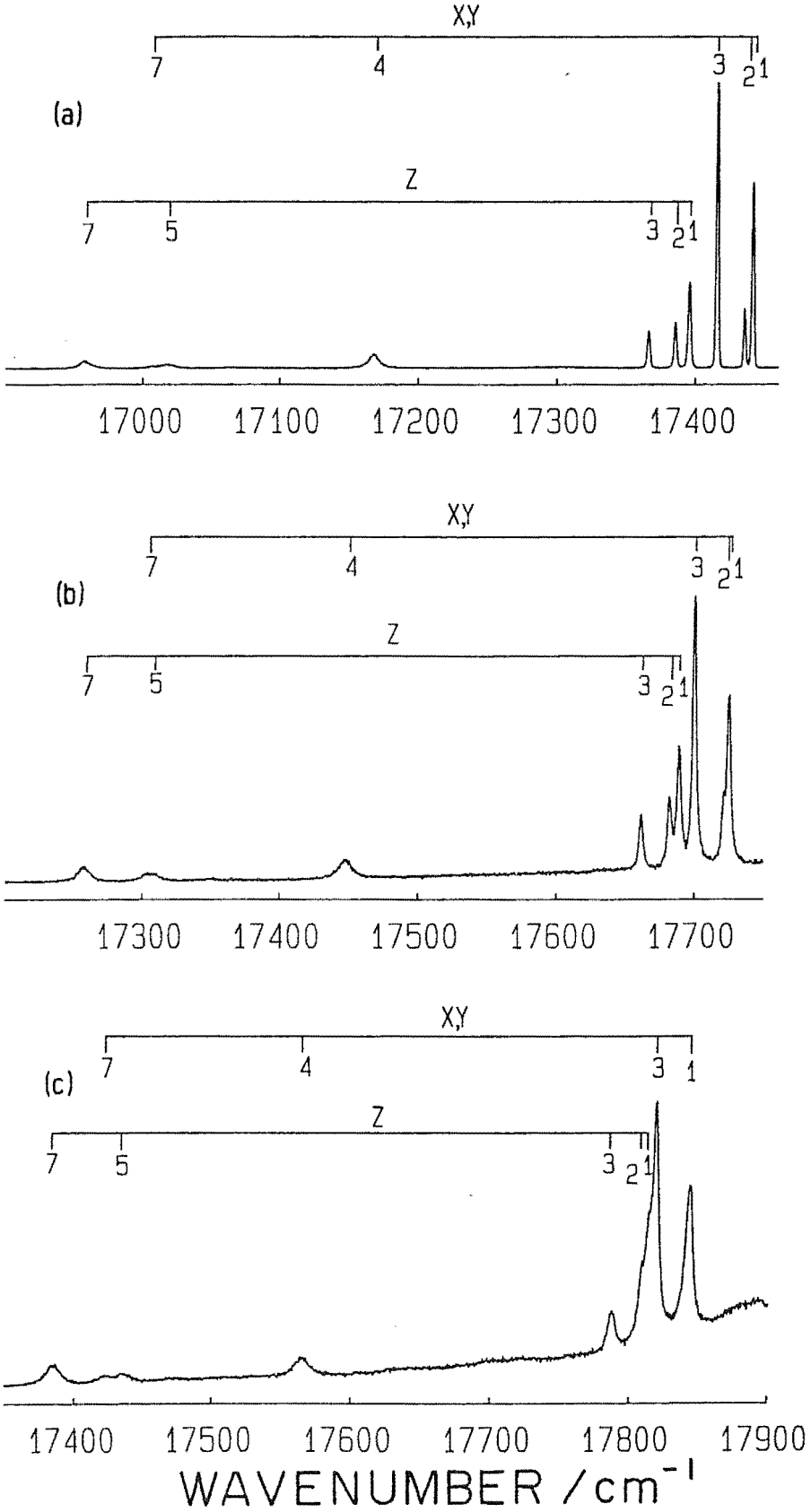

Figure 5.12 : 10K fluorescence ($^4S_{3/2} \rightarrow {}^4I_{15/2}$) vibronics for $Z_1 \rightarrow E_1$ excitation : (a) the H^- C_{4V} site, (b) the D^- C_{4V} site and (c) the T^- C_{4V} site. All transitions are from E_1 and are labelled by the terminal Z level and the particular local mode ("X,Y" or "Z") involved.

TABLE 5.7 : Spectral data for the local mode vibronic fluorescence transitions of the H^- and D^- C_{4V} sites in CaF_2:0.05%Er^{3+} crystals at 10K.

Parent electronic transition	Associated local mode	Deuterium Local Mode Vibronics						Hydrogen Local mode vibronics					
		Wavenumber (cm^{-1})	Vibronic interval (cm^{-1})	Linewidth (cm^{-1}) (±10%)	Relative intensity (±15%)† x(yx)z	x(yy)z	Intensity ratio* ($x10^{-3}$) (±20%)	Wavenumber (cm^{-1})	Vibronic interval (cm^{-1})	Linewidth (cm^{-1}) (±10%)	Relative intensity (±15%)† x(yx)z	x(yy)z	Intensity ratio* ($x10^{-3}$) (±20%)
$E_1 \rightarrow Z_1$	X,Y	17728.1±0.4	750.6±0.5	2.1	0.73	0.52	Laser	17443.2±0.4	1037.3 ±0.5	1.8	0.77	0.44	Laser
	Z	17692.3 "	786.4 "	2.6	0.52	0.71	Laser	17397.7 "	1082.8 "	2.4	0.36	0.37	Laser
$\rightarrow Z_2$	X,Y	17724.5 "	751.3 "	2.2	0.40	0.28	5.5	17437.2 "	1038.8 "	1.2	0.17	0.074	7.1
	Z	17685.4 "	790.4 "	3.0	0.43	0.48	5.5	17387.5 "	1088.5 "	2.4	0.20	0.22	6.7
$\rightarrow Z_3$	X,Y	17703.1 "	750.6 "	2.1	0.93	1.00	9.1	17417.6 "	1037.1 "	1.8	1.00	0.97	14.3
	Z	17664.5 "	789.2 "	2.6	0.30	0.32	3.0	17368.2 "	1086.5 "	2.4	0.19	0.15	3.0
$\rightarrow Z_4$	X,Y	17451.3±0.5	746.0±0.8	9.4	0.23	0.32	-	17170.1±0.6	1031.3±0.9	8.8	0.18	0.26	-
$\rightarrow Z_5$	Z	17311.0±0.8	793.3±1.1	10.0±2.0	0.17±0.06	0.11±0.04	1.2±0.3	17018.6±0.8	1085.4±1.1	12.0±2.0	0.10±0.03	0.073±0.02	1.4±0.4
$\rightarrow Z_7$	X,Y	17306.0 "	748.6 "	10.0 "	0.14±0.05	0.095±0.03	3.3±0.8	17010.1 "	1044.4 "	9.6 "	0.069±0.02	0.053 "	2.9±1.0
	Z	17260.1±0.5	794.5±0.8	7.7	0.15	0.023	4.0	16959.1±0.6	1095.4±0.9	9.6±1.5	0.10±0.03	0.14±0.04	5.8

* Relative to the corresponding parent electronic line.

† (±10%) between each polarization for a given transition.

Table 5.8 : Spectral data for the local mode vibronic fluorescence transitions of the T^- C_{4V} site. Uncertainties are ± 0.5 cm^{-1}. The ratios of the individual T^- vibronic intervals to the corresponding H^- and D^- vibronic intervals are also included.

Parent electronic transition	Associated Local mode	Wavenumber (cm^{-1})	Vibronic Interval (cm^{-1})	Ratio H^-/T^-	Ratio D^-/T^-
$E_1 \rightarrow Z_1$	XY	17848.5	629.5	1.65	1.19
	Z	17818.5	659.5	1.64	1.19
$\rightarrow Z_2$	XY	obscured	-		
	Z	17813.5	662.0	1.64	1.19
$\rightarrow Z_3$	XY	17824.0	629.0	1.65	1.19
	Z	17792.0	661.0	1.64	1.19
$\rightarrow Z_4$	XY	17569.5	626.5	1.65	1.19
$\rightarrow Z_5$	Z	17439.5	664.5	1.63	1.19
$\rightarrow Z_7$	XY	17426.5	628.0	1.66	1.19
	Z	17389.5	665.0	1.65	1.19

Figure 5.12. Tritium vibronics were less easily resolved due to lower T^- ion site concentration obtained in crystals, and the broader linewidths. The observed vibronic lines are identified by both the terminating electronic level and the (X,Y) or Z local mode phonon involved in the transition from the E_1 upper level. Table 5.7 summarises the complete vibronic data including intensities relative to parent lines for the H^- and D^- sites. The derived vibronic intervals agree closely with the local mode frequencies previously determined by infra-red absorption (Edgar *et al.* 1979). The average ratio of corresponding H^- to D^- vibronic intervals for transitions from E_1 is 1.380 ± 0.007 in excellent agreement with the expected reduced mass ratio (Elliott *et al.* 1965).

Tritium local modes have not been reported for the Er^{3+} C_{4V} site by any technique and would be difficult to observe directly in the infra-red absorption spectrum because of lattice mode absorption at this frequency. A summary of vibronic intervals for the T^- site is therefore given in Table 5.8. The averaged ratio of corresponding H^-/T^- local mode energies is 1.645 ± 0.015.

5.3.2(d) *Crystal Field Analysis*

The energy levels of the T^-, D^- and H^- C_{4V} sites were analysed using the following Racah tensor operator expansion of the crystal field Hamiltonian:

$$H_{CF} = B_0^2 C_0^{(2)} + B_0^4 C_0^{(4)} + B_0^6 C_0^{(6)}$$

$$+ B^4\left[C_0^{(4)} + (C_4^{(4)} + C_{-4}^{(4)})\sqrt{\frac{5}{14}}\right]$$

$$+ B^6\left[C_0^{(6)} - (C_4^{(6)} + C_{-4}^{(6)})\sqrt{\frac{7}{2}}\right] \qquad (5.1)$$

where B_m^n are the crystal field parameters
and $C_m^{(n)}$ are Racah tensor operators.

This form of the expansion was previously used by Freeth *et al.*(1982) to analyse the F^- C_{4V} site levels, and by Edgar *et al.* (1979) to fit the known levels of the H^- centre. This parameterisation is preferable to the traditional form $H_{CF} = B_0^2 C_0^{(2)} + B_0^4 C_0^{(4)} + B_4^4 C_4^{(4)} + B_0^6 C_0^{(6)} + B_4^6 C_4^{(6)}$ since it distinguishes an axial part from an octahedral part.

The magnetic field effect can be included using a Zeeman Hamiltonian term. Two splitting factors, $S_{\|}$ and $S_{\perp}$ are calculated from the components :

$$H_z = \beta B_z (k_z L_z + g_s S_z)$$

$$\text{and} \quad H_x = \beta B_x (k_x L_x + g_s S_x) \qquad (5.2)$$

where $g_s = 2.00232$

$\beta = \frac{e\hbar}{2m}$, the Bohr magneton

k_x and k_z are the orbital angular momentum reduction factors.

The intermediate coupling wavefunctions used in this study were those fitted to the $^4I_{15/2}$, $^4I_{13/2}$, $^4F_{9/2}$, $^4S_{3/2}$, $^4F_{3/2}$, and $^2P_{3/2}$ barycentres for the F^- C_{4V} site (Freeth *et al.* 1982). At this stage an insufficient number of H^- C_{4V} site barycentres are known to perform a similar fit to the electrostatic (E^1, E^2, E^3) and spin-orbit (ζ) parameters for this site.

The present study used the computer routines of C.A. Freeth (1980) to diagonalise the crystal field and Zeeman terms of the Hamiltonian simultaneously, and to perform a least squares fit on the energies of the $^4I_{15/2}$ and $^4I_{13/2}$ crystal field level and $g_{\parallel}$ and $g_{\perp}$ values for the Z_1 and Z_2 levels, whilst varying B_0^2 , B_0^4 , B_0^6, B^4 , B^6 , k_x and k_z.

The best parameter values and calculated energy levels from a fit having a standard deviation of 1.9 cm^{-1} are included in Table 5.9 for both the H^- and D^- C_{4V} sites. The predicted Z_1 and Z_2 g values are in close agreement with those observed by Edgar *et al.* (1979).

A least squares fit of the T^- centre was attempted although the Z_8 and Y_5 electronic levels and g values were not known for the site. The resultant best fit parameters with a best fit standard deviation of 1.7 cm^{-1} are included in Table 5.10.

The observation of many additional crystal field levels, since the previous attempt (Edgar *et al.* 1979) at the crystal field fit of the hydrogenic C_{4V} sites, has substantially improved the accuracy of the resultant parameters. An additional uncertainty had been introduced into the previous result by using the intermediate coupling wavefunctions given by Weber (1967) for Er^{3+} in LaF, since

TABLE 5.9 : Calculated and experimentally determined energy levels of the $^4I_{13/2}(Y)$ and $^4I_{15/2}(Z)$ multiplets of the H^- and D^- C_{4v} sites in CaF_2: 0.05% Er^{3+} crystals at 10K. The g-values for the two lowest crystal-field levels and the crystal-field Hamiltonian parameters (in cm^{-1}) are included.

State	H^- C_{4v} Site Energy (cm^{-1})		D^- C_{4v} Site Energy (cm^{-1})	
	Calculated	Observed	Calculated	Observed
Y_7	6896.1	6893.3±1.5	6897.3	6894.8±1.2
Y_6	6824.7	6823.3±1.2	6824.2	6824.0±1.0
Y_5	6799.3	6802.1±1.5	6798.8	6800.6±1.2
Y_4	6798.8	6796.1±1.0	6798.5	6795.8±1.0
Y_3	6709.9	6708.9±0.8	6710.3	6709.4±0.8
Y_2	6593.7	6596.9±0.8	6593.6	6596.6±0.8
Y_1	6560.2	6562.1±0.8	6559.7	6561.2±0.8
Z_8	590.1	-	590.0	583.5±2.0
Z_7	426.3	426.5±0.8	424.9	424.1±0.7
Z_6	426.0	423.0±1.5	423.9	422.0±1.0
Z_5	373.9	376.5±0.8	372.2	374.4±0.7
Z_4	277.2	279.1±1.0	281.4	281.4±1.0
Z_3	26.0	25.8±0.3	25.1	25.0±0.3
Z_2	4.4	4.5±0.3	2.8	2.9±0.3
Z_1	0	0	0	0
$Z_1 g_{\parallel}$	7.469	7.465±0.005	7.339	7.335±0.005
$Z_2 g_{\parallel}$	1.682	1.683±0.001	1.682	1.683±0.001
$Z_1 g_{\perp}$	6.30	6.10±0.05	6.34	6.10±0.05
$Z_2 g_{\perp}$	9.08	9.09±0.01	9.08	9.09±0.01
ζ	2363.0		2363.3	
k_x	0.9778		0.9859	
k_z	0.9850		0.9876	
B_0^2	834.9		847.5	
B_0^4	1180.0		1189.6	
B_0^6	623.7		628.2	
B^4	-1663.0		-1663.4	
B^6	416.0		413.7	

Table 5.10 : Calculated and experimental energy levels (in cm^{-1}) of the T^- C_{4V} site in CaF_2:0.05%Er^{3+}. No g values are known for the site. The crystal field parameters (in cm^{-1}) are included.

State	Energy (cm^{-1}) Calculated	Observed
Y_7	6896.9	6894.4 ± 1.5
Y_6	6822.1	6821.1 ± 1.2
Y_5	6796.6	-
Y_4	6796.1	6793.6 ± 1.0
Y_3	6709.3	6708.0 ± 0.8
Y_2	9592.0	6594.4 ± 0.8
Y_1	6557.9	6559.0 ± 0.8
Z_8	591.8	-
Z_7	424.9	423.4 ± 0.7
Z_6	423.4	422.0 ± 1.0
Z_5	371.2	373.9 ± 0.8
Z_4	280.3	282.0 ± 1.0
Z_3	25.0	25.0 ± 0.3
Z_2	2.6	2.5 ± 0.3
Z_1	0	0
B_0^2	853.7	
B_0^4	1201.1	
B_0^6	636.6	
B^4	-1660.8	
B^6	412.6	

this included misassignment of a $^2K_{11/2}$ level to $^4G_{5/2}$. The previously reported conclusion that the cubic field is substantially smaller for the H^- C_{4V} site than for the F^- C_{4V} site is no longer supported by the present data, with the cubic field parameters being similar for both C_{4V} sites.

5.3.3 Other Family A Sites

5.3.3(a) *Spectroscopy of Sites*

Laser selective excitation was used to verify the assignment of absorption lines and to obtain additional energy levels for the R, J and K sites. Attempts to detect fluorescence from the M site were unsuccessful. These results, tabulated in Table 5.5, support the classification of the sites as a related family.

Fluorescence was recorded for the H^-, D^- and T^- varieties of the R site at 10K for excitation of the $Z_1 \rightarrow E_1$ transition. Spectra for the E → Z, D → Z and E → Y transitions of the D^- R site are reproduced in Figure 5.13. The H^- site emission was weaker and mixed with fluoride ion site emission from overlapping sites. Similarly, because of the low site concentration, the T^-R site lines were less clearly discriminated from lines of other sites than for the D^-R site. However, all T^-R site levels of the $^4I_{15/2}$ and $^4I_{13/2}$ multiplets were identified except Y_7, and are presented in Table 5.11.

Typical spectra for the same three multiplets of the D^-J site with $Z_1 \rightarrow E_1$ excitation are shown in Figure 5.14. The assignment by absorption of the Z_2 and Z_3 levels of the H^- J site was also verified by laser excitation in an

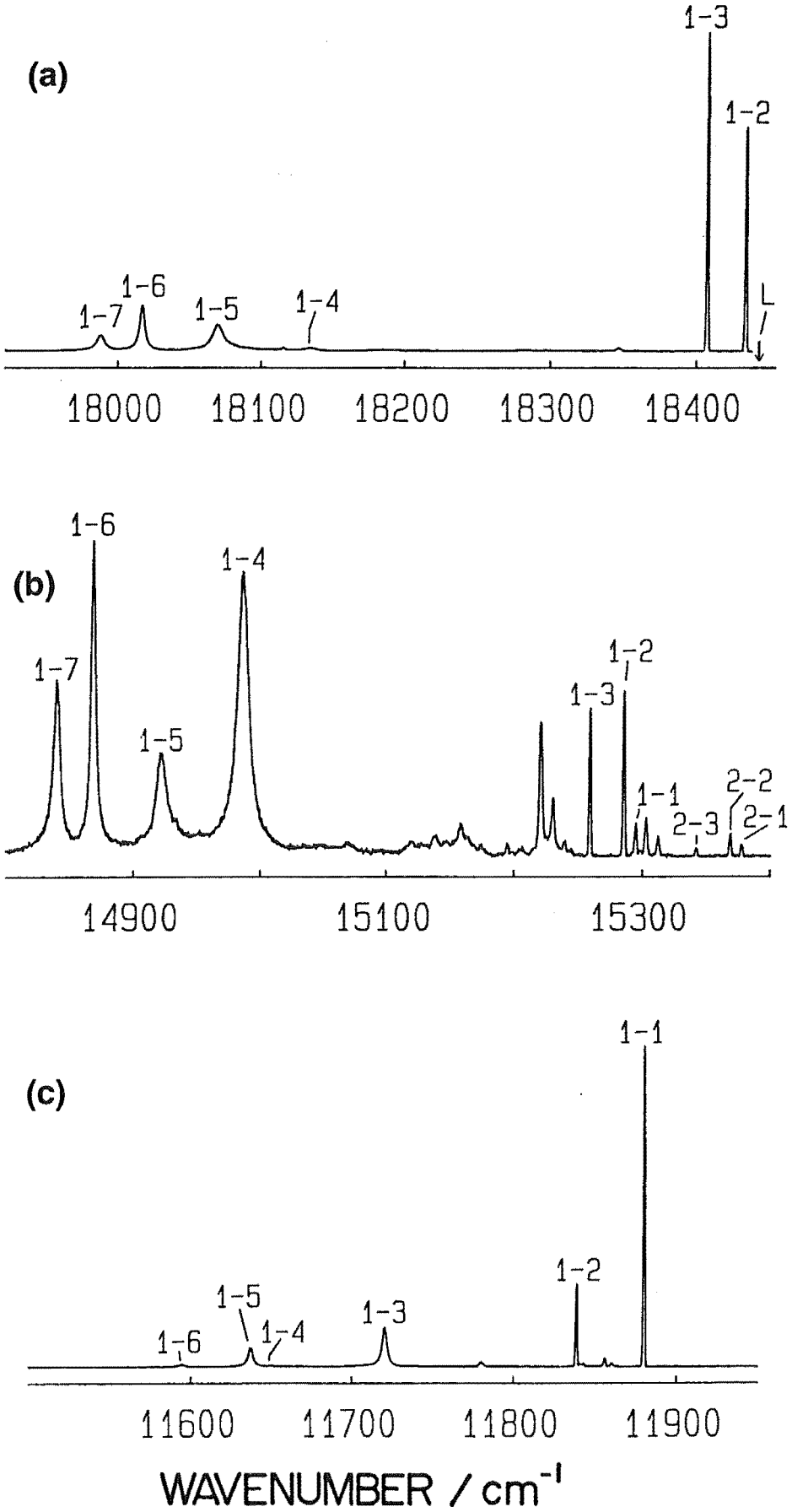

Figure 5.13 : 10K fluorescence of the D^-R site for $Z_1 \rightarrow E_1$ excitation : (a) $^4S_{3/2} \rightarrow {}^4I_{15/2}$, (b) $^4F_{9/2} \rightarrow {}^4I_{15/2}$, and (c) $^4S_{3/2} \rightarrow {}^4I_{13/2}$. "L" indicates the laser position.

Table 5.11 : Energy levels (in cm^{-1}) of the T^-R site determined from the 10K laser selective excitation spectra of tritiated CaF_2:0.05%Er^{3+} crystals.

Multiplet	State	Energy
$^4S_{3/2}$	E_1	18444.6 ± 0.4
$^4F_{9/2}$	D_2	15379.8 ± 0.4
	D_1	15297.5 ± 0.4
$^4I_{13/2}$	Y_6	6847.8 ± 1.2
	Y_5	6804.6 ± 1.2
	Y_4	6791.9 ± 1.2
	Y_3	6721.8 ± 1.0
	Y_2	6603.4 ± 1.0
	Y_1	6561.5 ± 1.0
$^4I_{15/2}$	Z_8	639.0 ± 2.0
	Z_7	454.7 ± 1.0
	Z_6	425.6 ± 1.0
	Z_5	373.7 ± 0.8
	Z_4	310.0 ± 1.0
	Z_3	36.0 ± 0.4
	Z_2	9.6 ± 0.3
	Z_1	0

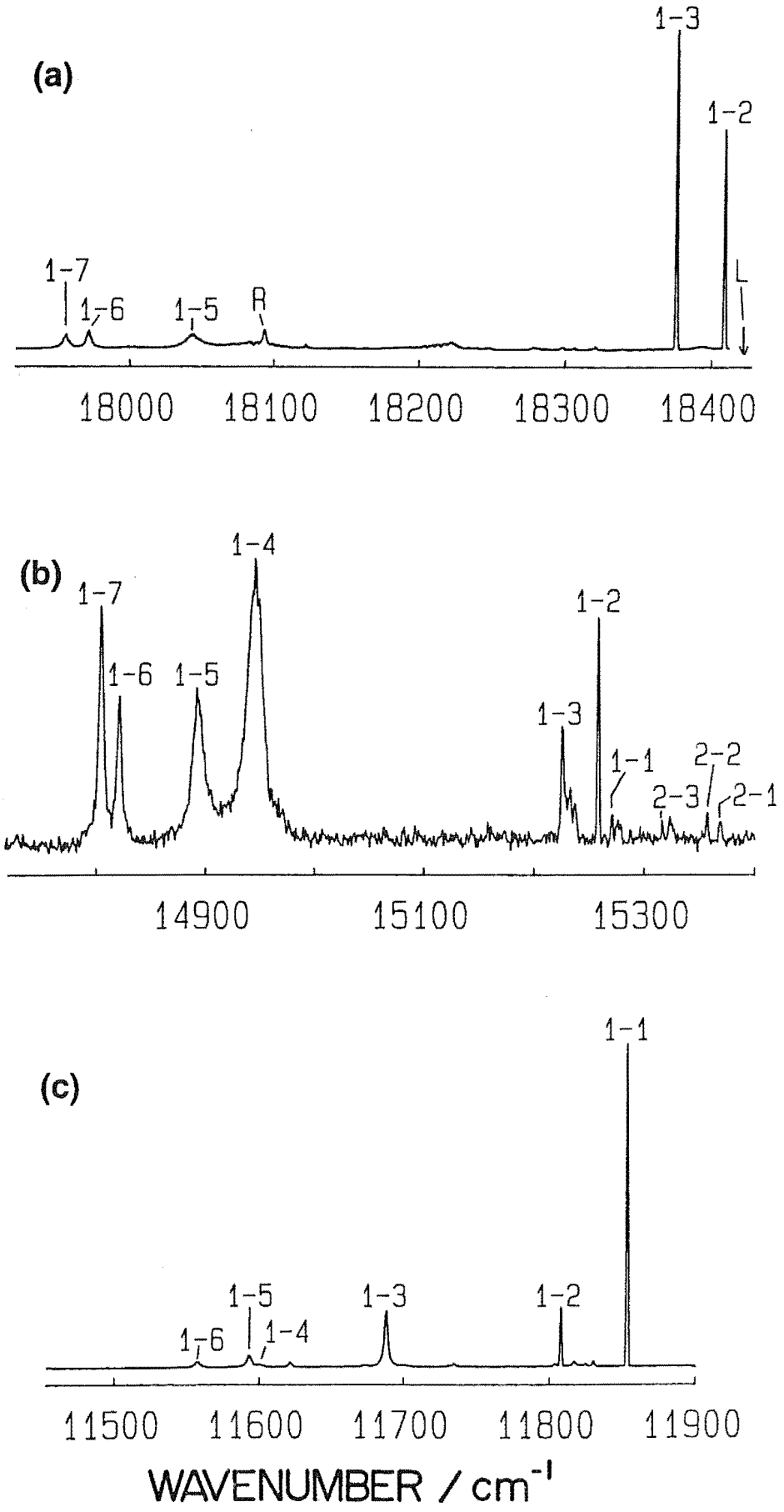

Figure 5.14 : 10K fluorescence of the D^-J site for $Z_1 \rightarrow E_1$ excitation : (a) $^4S_{3/2} \rightarrow {}^4I_{15/2}$, (b) $^4F_{9/2} \rightarrow {}^4I_{15/2}$, and (c) $^4S_{3/2} \rightarrow {}^4I_{13/2}$. "L" identifies the laser position and "R" the first order "Raman" scattering line.

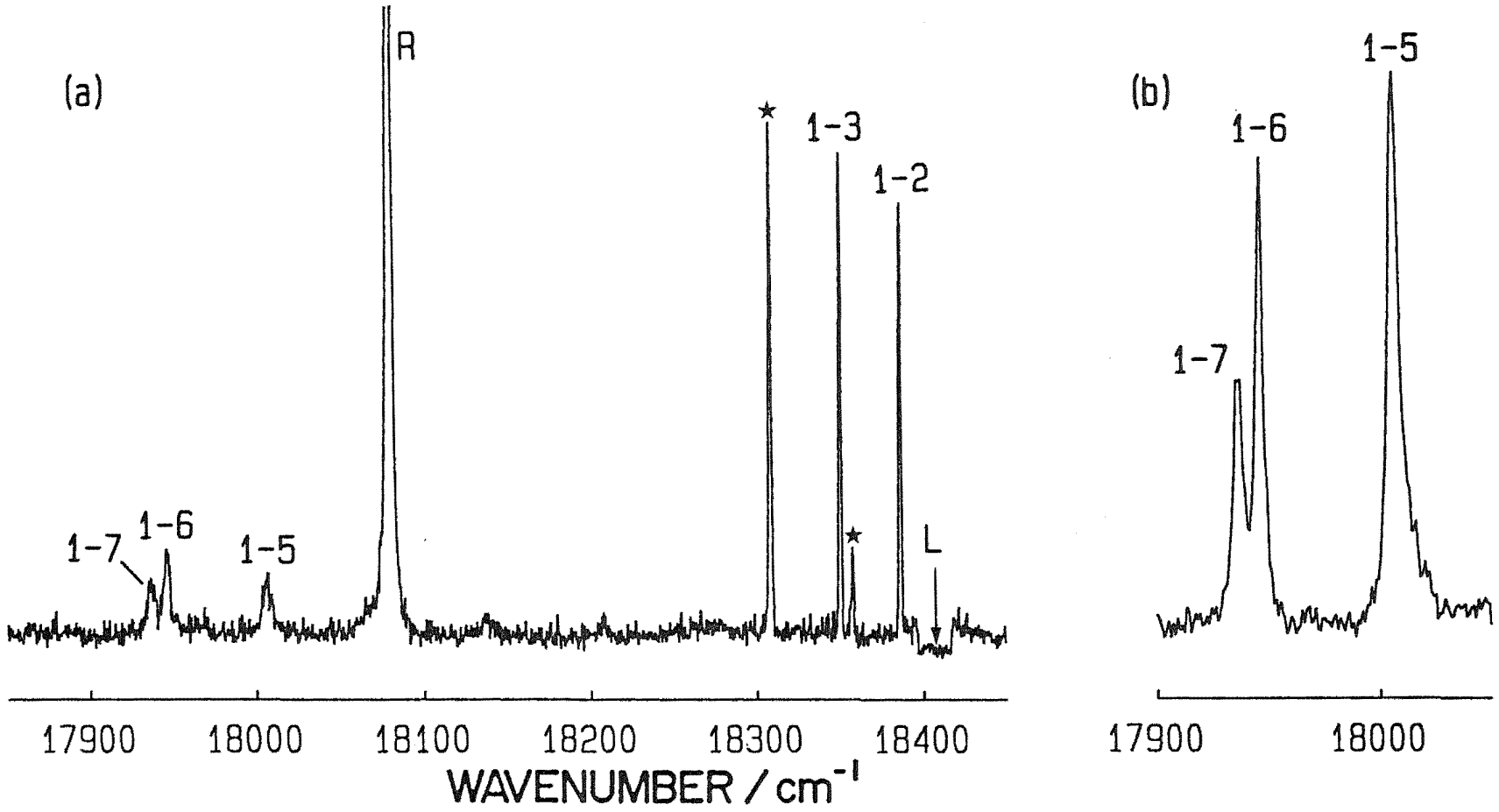

Figure 5.15 : 10K fluorescence of the D^-K site for laser excitation of the $Z_1 \rightarrow E_1$ transition : (a) $^4S_{3/2} \rightarrow {}^4I_{15/2}$ transitions recorded after the site has bleached to a stable fluorescence level, and (b) $E_1 \rightarrow Z_5$, Z_6 and Z_7 transitions (same scale as (a)) recorded while bleaching a new position of crystal. Stars indicate positions of G1 site transitions.

hydrogenated crystal, but other H^- site transitions were too weak to resolve.

Additional levels of the D^- K site were identified for the $^4I_{15/2}$ multiplet by excitation of the $Z_1 \rightarrow E_1$ transition and observation of E → Z and D → Z fluorescence. The E → Z spectrum of Figure 5.15 illustrates the problem caused by the G1 oxygen compensated site $Z_1 \rightarrow E_1$ transition at 18408.6 cm^{-1}. Emission from the two centres was always mixed due to overlap of transitions at the laser frequency. The oxygen site fluorescence is a factor of at least 10^3 more intense than the K site when the laser is tuned on each site separately.

A new and important effect discovered, common to the R, J and K site, is that they all exhibit a bleaching effect. Upon resonant laser excitation at constant power and frequency of any of these centres, the fluorescence level detected with the spectrometer at the constant frequency of another transition for the site is observed to decrease with time. This effect will be discussed in more detail in Chapter Seven and it is sufficient at this point to say that net decreases by factors of up to 5, 10 and 15 occurred for the D^- R, J and K sites respectively after 3-5 minutes. The corresponding H^- sites bleach even more quickly. These decreases in intensity caused difficulties with the spectroscopy as most scans took 30-45 minutes. Generally, spectra were recorded after the bleached site had reduced to a steady level, but this gave low site discrimination against non-bleaching sites that were simultaneously present. This made weak features such as vibronics extremely difficult to determine. In some cases, however,

the bleaching could also be used as a method of site identification, since the fluorescence level of an unknown line increased when the sample was moved to a non-bleached section, if the line was due to the bleaching site. Each of the transitions of the R, J and K sites was checked separately for such behaviour before the energy levels were assigned. Figure 5.15 demonstrates the use of this technique.

In addition to the bleaching effects, the spectra of the R, J and K sites have the following common features :

(a) Very similar intensity ratios of emission transitions within a multiplet. These patterns have a marked resemblance to those of the C_{4V} sites. For example, the $E_1 \rightarrow Z_4$ transition is weak, while the $D_1 \rightarrow Z_4$ transition is dominant.

(b) The additional energy level patterns determined by emission also show the systematic trends along the series C_{4V}, R, J and K (Figure 5.9) that were noted by absorption.

The transitions of the J and K sites show sufficient polarisation in the <100> geometry to suggest an approximately tetragonal symmetry derived from the C_{4V} site.

For example, with $Z_1 \rightarrow E_1$ excitation the ratios of x(yy)z:x(yx)z polarisations were :

D^-J site E_1	$\rightarrow Z_2$	1.00 ± 0.05
	$\rightarrow Z_3$	0.90 ± 0.05
D^-K site E_1	$\rightarrow Z_2$	0.85 ± 0.06
	$\rightarrow Z_3$	0.90 ± 0.06

There was no detectable polarisation dependence for the <111> oriented crystals or for the R site in either

orientation. These dependences could only be checked after bleaching to a relatively stable level of fluorescence.

Local mode vibronic spectra were recorded for the R and J sites and representative D^- site spectra are presented in Figure 5.16. The vibronic analysis is included in Table 5.12. An attempt to resolve the R site tritium vibronics revealed values of 472 ± 2 cm^{-1} and 519 ± 2 cm^{-1} for R_a and R_b respectively. These intervals have H^-/T^- ratios of 1.61 and 1.63 consistent with the C_{4V} site ratio. No values for R_c or R_d were obtained due to the weakness of the fluorescence.

The vibronic spectra for the H^- and D^- R sites and the D^- J site have lines corresponding to more than three distinct local mode intervals, indicating that more than one H^- or D^- ion is present in these sites. Two of the R site vibronic intervals (R_c and R_d) correspond to the two lines of the infra-red B site (Thompson 1983), which is consistent with the correlation of the two sites (Cockroft 1983). A remaining line in the R site vibronic spectra at 17814 cm^{-1} for H^-, 17802 cm^{-1} for D^- (labelled 'x' in Figure 5.16) and 17798 cm^{-1} for T^-, was assigned to be the $E_1 \rightarrow Z_8$ electronic transition. The J site has the corresponding $E_1 \rightarrow Z_8$ transition at 17744 cm^{-1} for H^- and 17742 cm^{-1} for the D^- centre. In the latter case the transition has superposed on it the Z_1, Z_2, Z_3 structure of a local mode interval, J_d, at 678.0 cm^{-1}. This structure was more clearly apparent when several plots of the region were superposed. An attempt was made to find more D^- J site vibronic intervals of magnitude greater than 700 cm^{-1}. Two extremely weak transitions were observed that suggest an additional

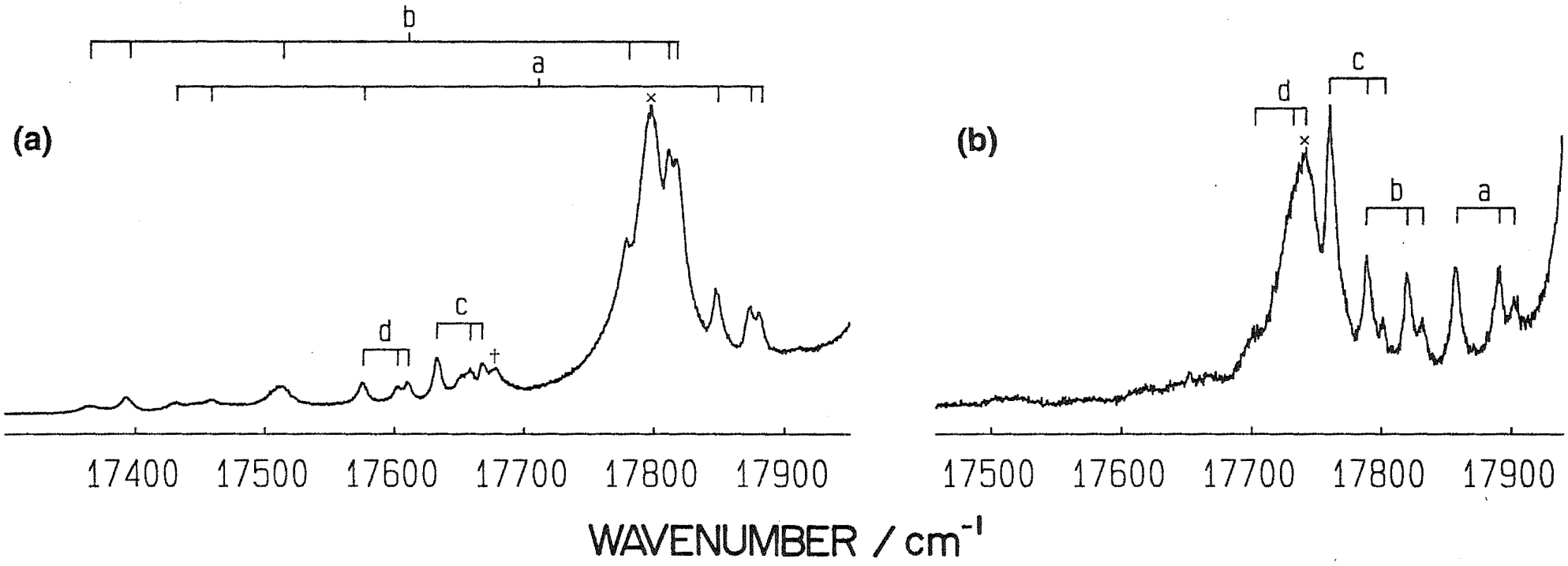

Figure 5.16 : 10K fluorescence ($^4S_{3/2} \rightarrow {}^4I_{15/2}$) vibronics for $Z_1 \rightarrow E_1$ excitation of (a) the D^-R site, and (b) the D^-J site. In each case the labels a, b, c, and d identify groups of transitions from E_1 with the same vibronic interval and x indicates the $E_1 \rightarrow Z_8$ electronic transition. † identifies a possible additional vibronic position.

TABLE 5.12 : Wavenumbers and vibronic transitions of the R and J sites as measured in the 10K fluorescence spectra of hydrogenated CaF_2: 0.05% Er^{3+} crystals.

Parent Electronic Transition	Local Mode	D^- R site		H^- R site		Local Mode	D^- J site	
		Wavenumber ($\pm 0.5\ cm^{-1}$)	Vibronic interval ($\pm 1.0\ cm^{-1}$)	Wavenumber ($\pm 0.5\ cm^{-1}$)	Vibronic interval ($\pm 1.0\ cm^{-1}$)		Wavenumber ($\pm 0.5\ cm^{-1}$)	Vibronic interval ($\pm 1.0\ cm^{-1}$)
$E_1 \rightarrow Z_1$	R_a	17884.0	560.0	17681.0	763.0	J_a	17902.5	517.5
$\rightarrow Z_2$		17876.5	558.5	17673.0	762.5		17890.5	517.0
$\rightarrow Z_3$		17850.0	558.5	17648.0	761.0		17858.5	516.5
$\rightarrow Z_6$		17462.0	556.0					
$\rightarrow Z_7$		17434.0	555.5					
$E_1 \rightarrow Z_1$	R_b	17821.0	623.0	17598.5	845.5	J_b	17832.0	588.0
$\rightarrow Z_2$		17815.0	620.0	17591.0	844.5		17821.0	586.5
$\rightarrow Z_3$		17783.0	625.5	17565.0	844.0		17791.0	584.0
$\rightarrow Z_4$		17514.5	621.0					
$\rightarrow Z_6$		17396.0	622.0					
$\rightarrow Z_7$		17367.5	622.0					
$E_1 \rightarrow Z_1$	R_c	17671.0	773.0	17374.0	1070.0	J_c	17801.5	618.5
$\rightarrow Z_2$		17661.5	773.5	17365.0	1070.5		17790.5	617.0
$\rightarrow Z_3$		17636.0	772.5	17338.0	1071.0		17762.0	613.0
$E_1 \rightarrow Z_1$	R_d	17613.5	830.5	17298.0	1146.0	J_d	17742.0±1.5	678.0±2.0
$\rightarrow Z_2$		17605.5	829.5	17290.0	1145.5		17732.0±1.0	675.5±1.5
$\rightarrow Z_3$		17578.0	830.5	17260.0	1149.0		17700.0±1.0	675.0±1.5

vibronic interval at 755 ± 2 cm^{-1}. Due to poor reproducibility of relative intensities, accentuated by bleaching of the site, a definite assignment could not be made.

5.3.3(b) *Configuration of Sites*

A tentative assignment of the Family A sites can be attempted on the present data. From the crystal field levels obtained (Figure 5.9 and Table 5.5), it is apparent that the sites are similar to the C_{4V} symmetry centre, with the remnant C_{4V} polarisation dependence suggesting they are lower symmetry modifications of it.

The R site is believed to be one of the several rhombic symmetry sites observed by epr spectroscopy (Edgar *et al.* 1979). Figure 5.17(a) shows such a possible site for $CaF_2:Er^{3+}$ with the perturbation from tetragonal symmetry being provided by a second hydrogenic ion substituting for a fluoride ion in the lattice. The substitutional H^- ion is expected to have up to three local mode vibration frequencies derived from the well-established T_d site line at 965 $cm^{-1}(H^-)$ or 694 $cm^{-1}(D^-)$ (Elliott *et al.* 1965). A second set of up to three vibronic intervals similar to the hydrogenic C_{4V} site modes is expected due to vibrations of the charge compensating interstitial hydride ion. This model of two hydride ions is therefore expected to have between four and six vibronic intervals, with those corresponding to the hydride ion closer to the Er^{3+} giving the more intense vibronic transitions. The main features of this model account qualitatively for the observed features of the R site vibronic spectra.

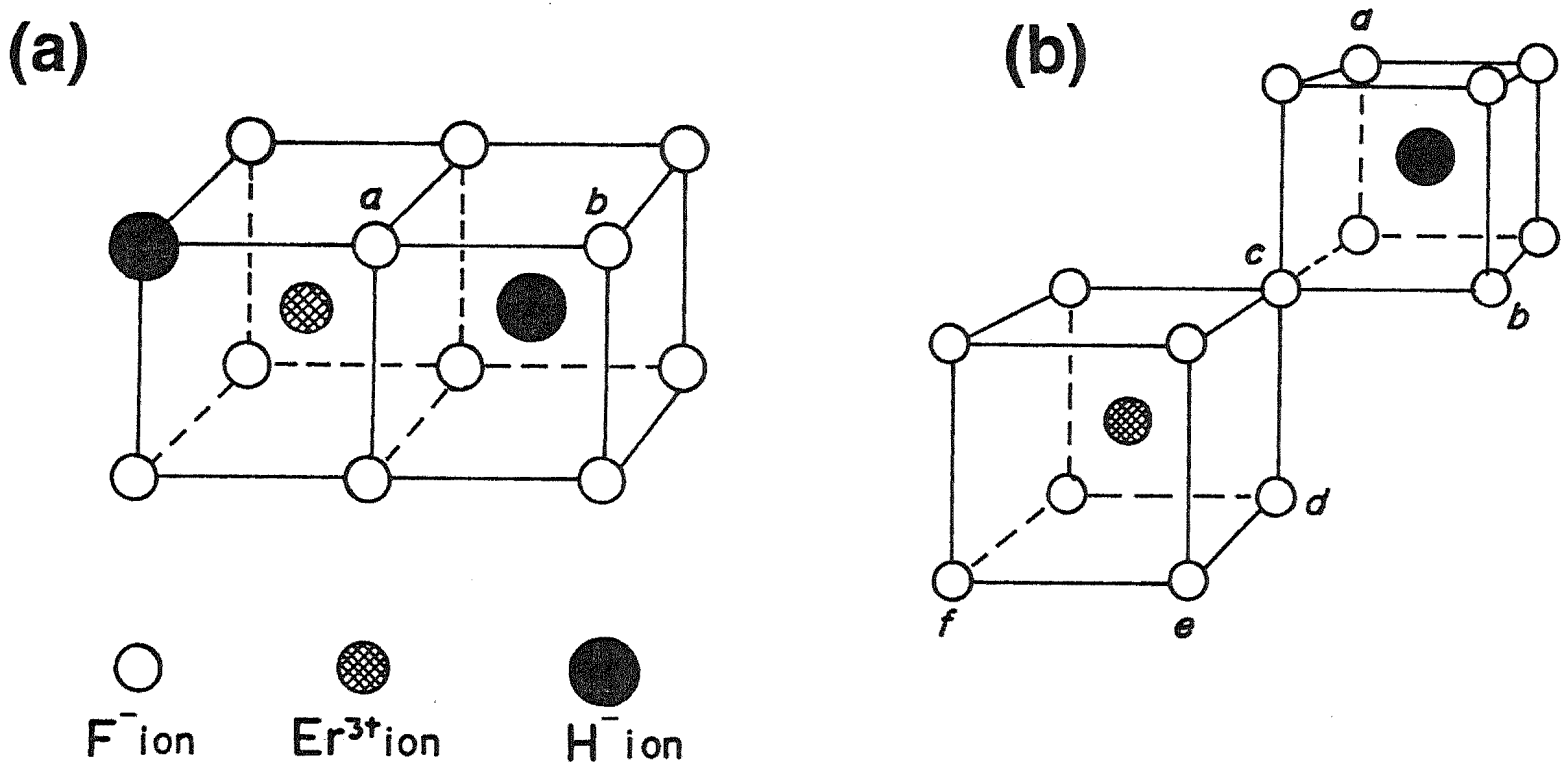

Figure 5.17 : (a) Model for the R site. A proposed model for the J site has the substitutional H^- ion in position a
(b) Model for the W site. Possible models for the X, P, L, T and N sites have an additional substitutional H^- ion in positions a,b,d,c (or f) and e respectively.

The four local mode vibronic intervals are assigned as follows :

The two lower energy vibronic intervals, R_a and R_b, are attributed to a substitutional hydrogenic ion replacing one of the eight F^- ions around an Er^{3+} ion and having approximate trigonal (C_{3V}) symmetry; the other two vibronic intervals R_c and R_d are attributed to the nearest-neighbour interstitial hydrogenic ion. There is evidence that the lower vibronic interval for the interstitial hydrogenic ion corresponds to the doubly-degenerate vibrational mode, as there is a possible additional vibronic interval (with lines marked by † in Figure 5.16(a)) of 1057 cm^{-1} for H^- and 763 cm^{-1} for D^-, indicating a small splitting of this mode.

For the D^- J site the three well-defined local mode vibronic intervals J_a, J_b and J_c are assigned to a substitutional D^- ion adjacent to the Er^{3+} ion, since the average value of 573 cm^{-1} is likely to be derived from the T_d line at 694 cm^{-1} rather than the averaged C_{4V} D^- interstitial ion local mode value of 763 cm^{-1}. The lifting of degeneracy for the substitutional ion modes for this site is the result of perturbation by the nearby charge of the interstitial hydride ion. A model consistent with these results is one with a hydride ion in position 'a' of Figure 5.17(a) between the Er^{3+} and D^- ions of the tetragonal site configuration. It is proposed that the vibronic interval J_d and the tentative weak mode observed are two of the modes of the interstitial ion.

Crystal field level patterns and bleaching characteristics suggest that the K and M sites are also derived from the tetragonal centre. The downward frequency

shift of the $^4S_{3/2}$ and $^4F_{9/2}$ levels suggests either a greater crystal field perturbation from C_{4V} symmetry (compared to the C_{4V}, R or J sites), or further H^- ions present giving increased covalency with the Er^{3+} ion. The greater splitting of the $^4I_{15/2}$ levels is also consistent with increased perturbation from the C_{4V} site. These observations suggest that configurations involving a single substitutional hydride ion at positions further from the Er^{3+} than that proposed for the R and J sites (for instance, in position 'b' of Figure 5.17(a)), are unlikely. The most likely configurations for the K and M sites are those involving a third hydride ion in a second substitutional position in the lattice about the Er^{3+} ion. The increasing isotope shift for the progression J, K and M (Table 5.3) is consistent with such a model. Due to insufficient vibronic data, however, no site configuration for the K or M sites can be made.

5.3.4 Family B Sites

5.3.4(a) *Spectroscopy of Sites*

The laser selective excitation results for the X, P, L, T, N and V sites support the classification of these sites as a related family. Attempts to pump the W and S sites selectively were unsuccessful. Family B sites have $Z_1 \rightarrow E_1$ and $Z_1 \rightarrow E_2$ transitions at frequencies higher than Family A sites and located in the same spectral region as most fluoride ion sites, so less discrimination between lines of these sites could be achieved.

The D^- varieties of the L, T and N sites provided the cleanest emission spectra and were recorded for the

$^4F_{9/2} \rightarrow {}^4I_{15/2}$, $^4S_{3/2} \rightarrow {}^4I_{15/2}$ and $^4S_{3/2} \rightarrow {}^4I_{13/2}$ transitions. Fluorescence spectra for the three sites are given in Figures 5.18, 5.19 and 5.20, and the inferred energy levels are summarised in Table 5.5. In contrast to the Family A sites, the $Z_1 \rightarrow E_2$ absorption intensity was generally greater than for $Z_1 \rightarrow E_1$, so excitation to both E levels was possible to provide verification of the assignment of transitions to a given site. The N site spectra were notable, in that pumping the $Z_1 \rightarrow E_2$ level produced an increased fluorescence intensity from E_2 relative to E_1 compared to that for $Z_1 \rightarrow E_1$ excitation. This is attributed to the minimal nonradiative decay from the E_2 level to the E_1 level because of the small energy gap of 5.8 cm^{-1} between the two levels.

Attempts to pump the H^- varieties of these sites were less successful since the fluorescence was very weak, with discrimination from fluoride ion sites being impossible for most transitions. The frequencies of the $E_2 \rightarrow Z_1$, $E_1 \rightarrow Z_1$ and $E_1 \rightarrow Z_2$ transitions for the H^- L, T and N sites were, however, confirmed as those determined by optical absorption.

The D^- P and X sites were excited by the $Z_1 \rightarrow E_2$ transition resulting in emission of the $E_1 \rightarrow Z_1$ and $E_1 \rightarrow Z_2$ transitions (Figure 5.21) consistent with the assignment from the absorption spectra. These fluorescence measurements also determined the D_1 level of the D^- X site to be at 15391 ± 1 cm^{-1}. This transition is swamped in the absorption spectrum by the D^- C_{4V} site transitions. Fluorescence for the P and X sites was found to bleach in a manner similar to the Family A sites but with no

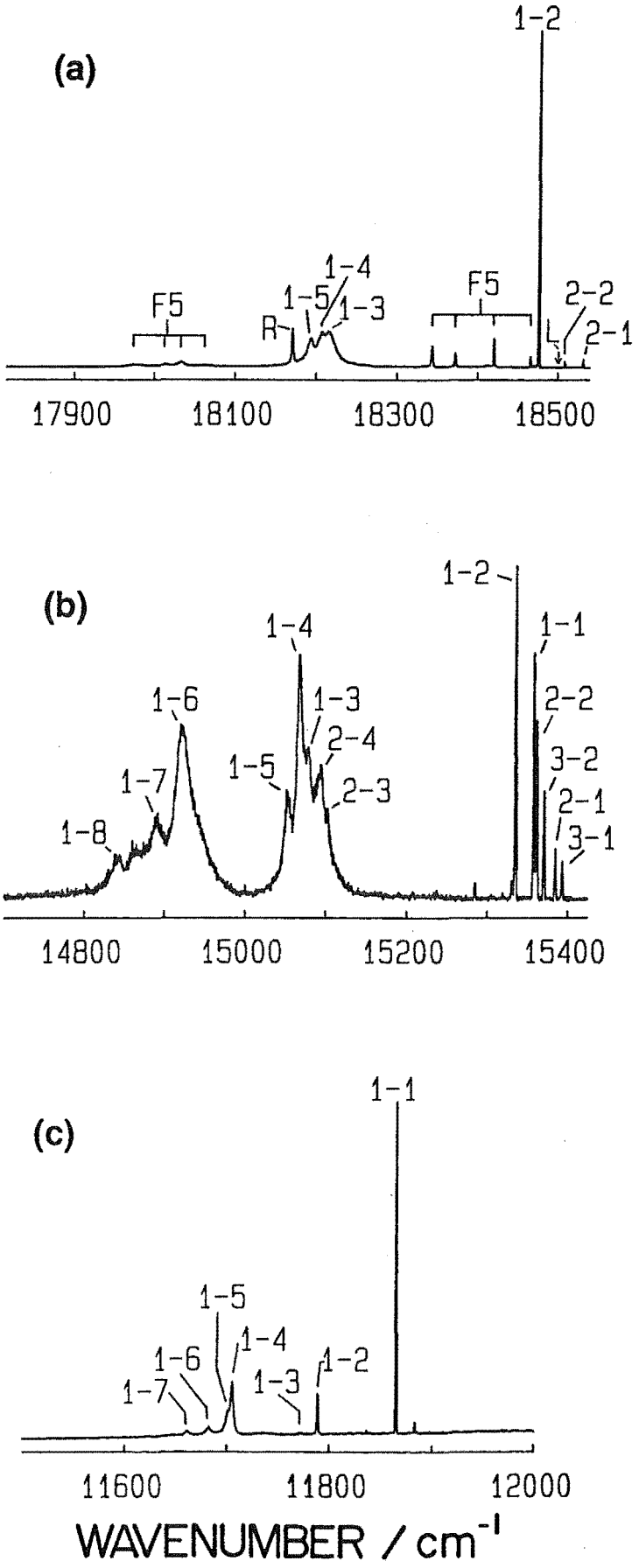

Figure 5.18 : 10K fluorescence of the D^-L site for $Z_1 \rightarrow E_1$ excitation : (a) $^4S_{3/2} \rightarrow {}^4I_{15/2}$, (b) $^4F_{9/2} \rightarrow {}^4I_{15/2}$, and (c) $^4S_{3/2} \rightarrow {}^4I_{13/2}$. Transitions of the F5 site that were simultaneously present are indicated.

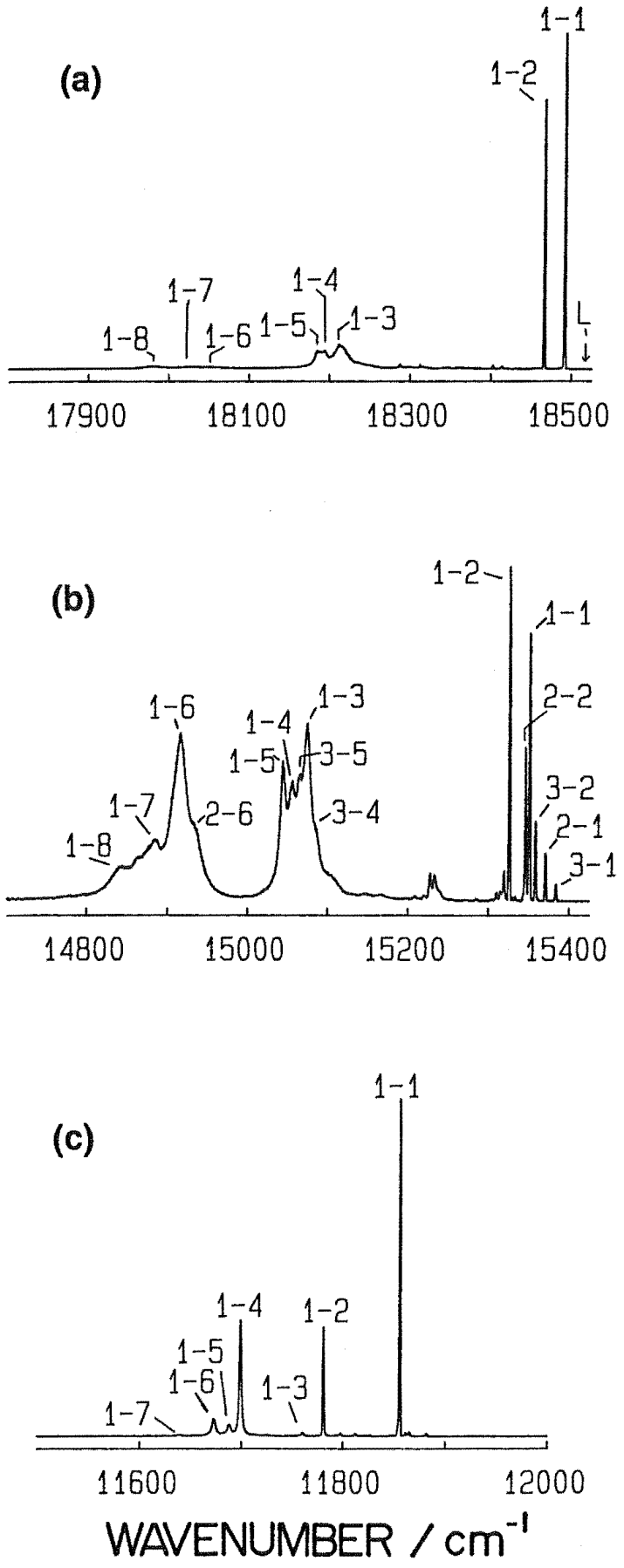

Figure 5.19 : 10K fluorescence of the D^-T site for $Z_1 \rightarrow E_2$ excitation : (a) $^4S_{3/2} \rightarrow {}^4I_{15/2}$, (b) $^4F_{9/2} \rightarrow {}^4I_{15/2}$, and (c) $^4S_{3/2} \rightarrow {}^4I_{13/2}$.

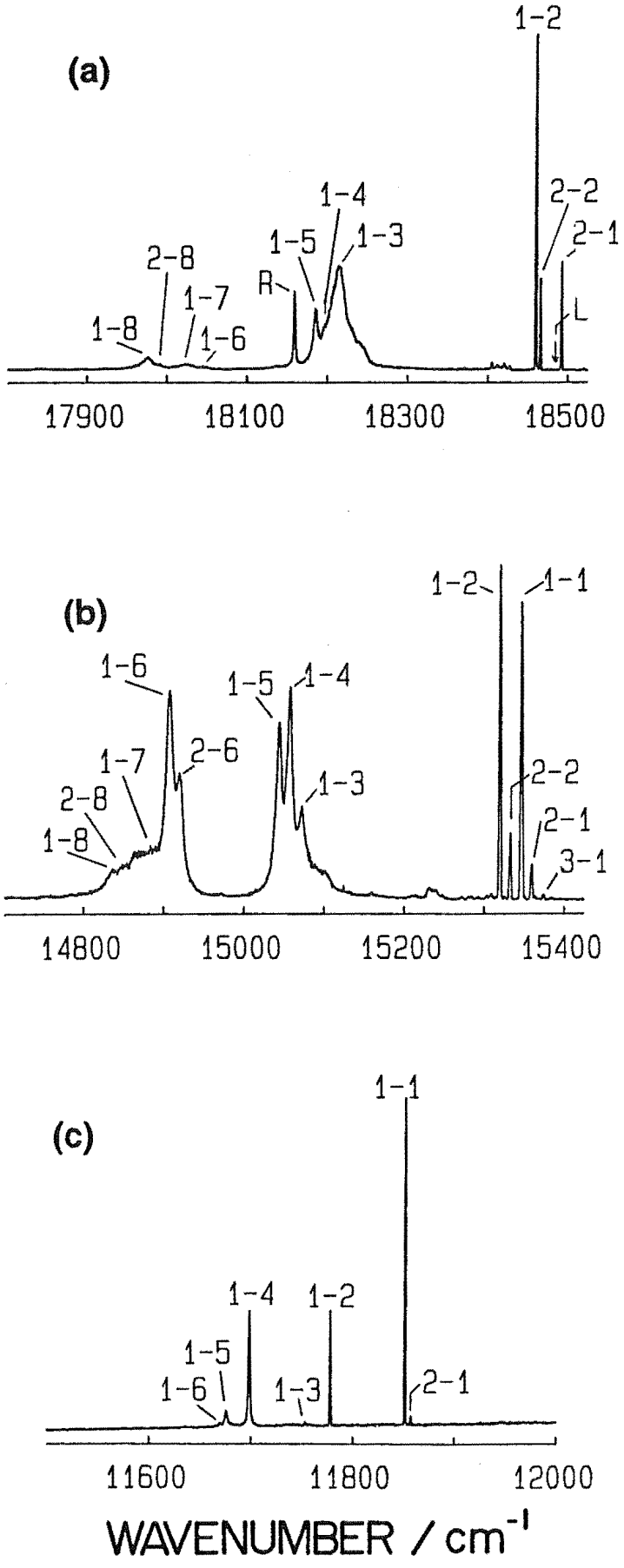

Figure 5.20 : 10K fluorescence of the D⁻N site for $Z_1 \rightarrow E_2$ excitation : (a) $^4S_{3/2} \rightarrow {}^4I_{15/2}$, (b) $^4F_{9/2} \rightarrow {}^4I_{15/2}$, and (c) $^4S_{3/2} \rightarrow {}^4I_{13/2}$.

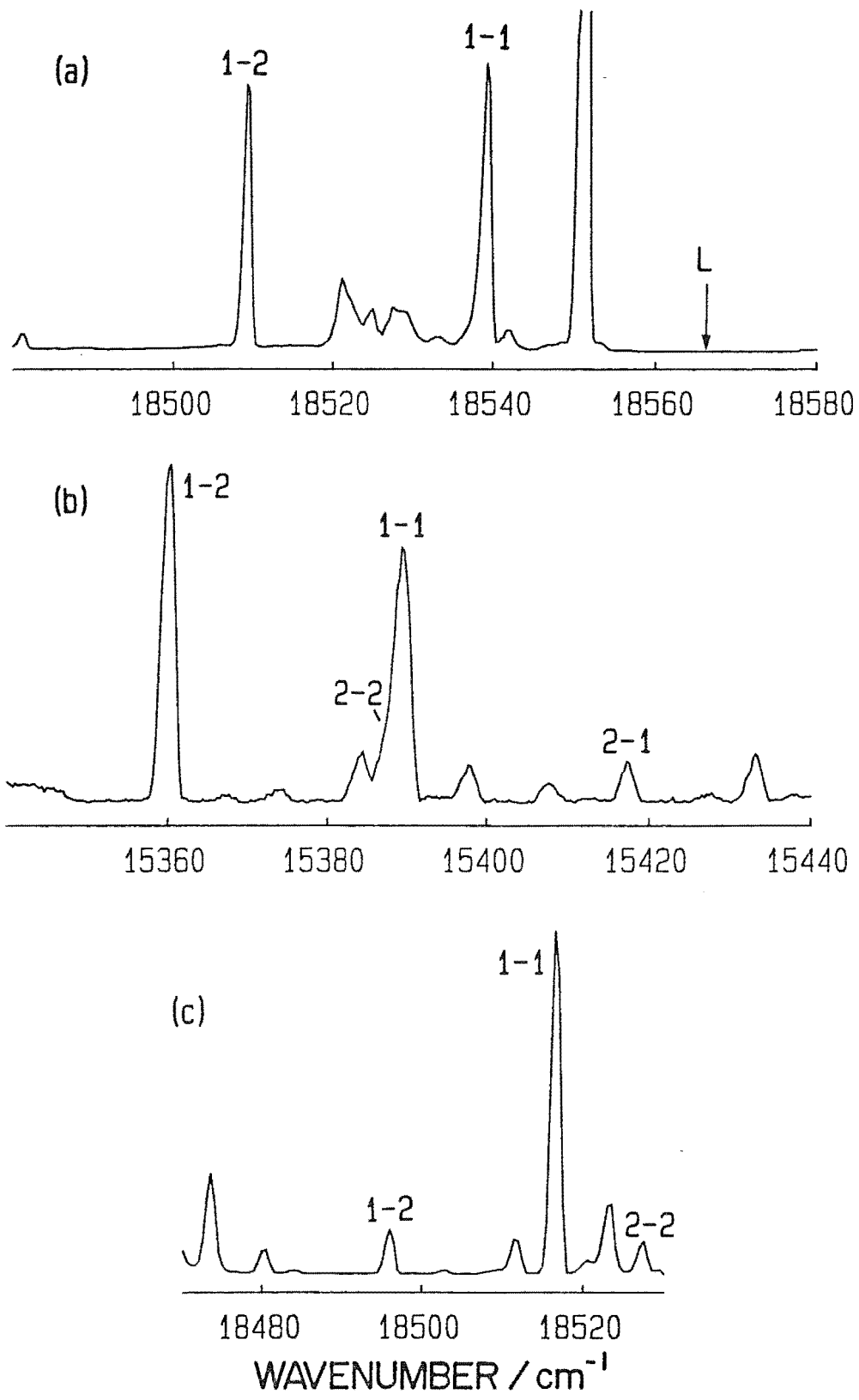

Figure 5.21 : 10K fluorescence spectra for $Z_1 \rightarrow E_2$ excitation of the D^- X site ((a) $^4S_{3/2} \rightarrow {}^4I_{15/2}$, and (b) $^4F_{9/2} \rightarrow {}^4I_{15/2}$) and the D^-P site ((c) $^4S_{3/2} \rightarrow {}^4I_{15/2}$).

polarisation reversibility apparent for the oriented crystals. Underlying fluoride ion sites caused a particular problem for these centres, as the transitions pumped overlap absorption bands of the cluster D sites [TW75]. These cluster sites have strong emission over a broad spectral range completely obscuring any lower frequency transitions and vibronics of the X and P sites. Discrimination was further hampered by the necessary preparation method for the crystals since the X and P sites are maximised by short duration hydrogenations. The brief period of heating, typically 10 hours at 860°C for such an hydrogenation is insufficient to cause the extensive dissociation of cluster sites observed for 68-hour heating periods.

Emission spectra for the D^- V site were also recorded, and derived energy levels included in Table 5.5. Lines of the V site were mixed with those of other sites. Pumping the $Z_1 \rightarrow E_2$ transition resulted in simultaneous emission from the D^- C_{4V} site, while Z_1-E_1 excitation gave mixed fluorescence with the lines due to the F5 site (see next section). Spectra for excitation of the $Z_1 \rightarrow E_2$ transition are shown in Figure 5.22.

Attempts to resolve spectral lines for excitation of the W or S sites were unsuccessful due to the lack of a pumping transition at 12K that was isolated from underlying transitions of other sites.

Several similarities between the spectra of Family B sites were apparent. All sites show a marked resemblance both in intensities and energy levels (Table 5.5, Figure 5.9) to the F^- B site. The family have intense $E_1 \rightarrow Z_1$ and $E_1 \rightarrow Z_2$ transitions, smaller but broader $E_1 \rightarrow Z_3$ and $E_1 \rightarrow Z_5$

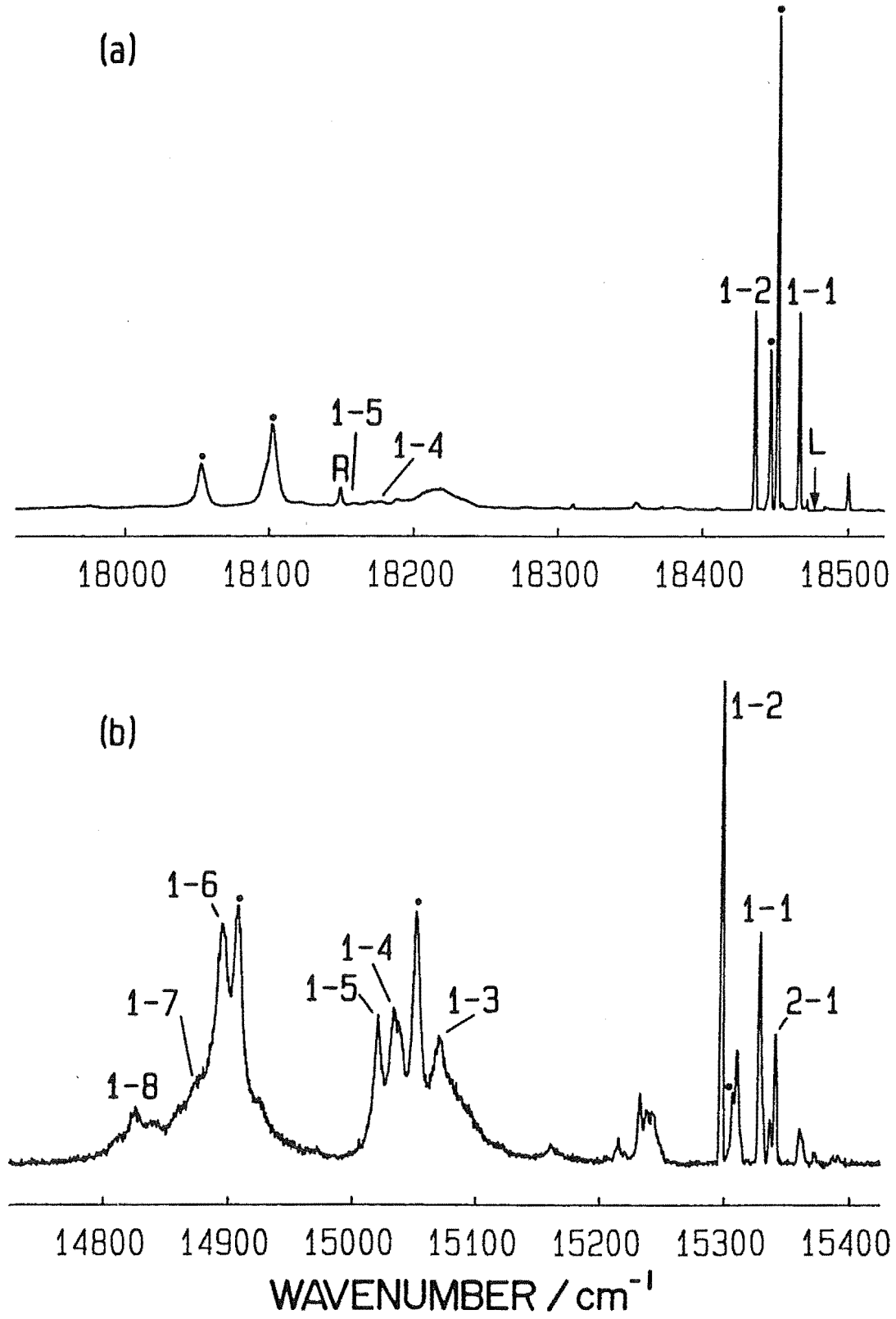

Figure 5.22 : 10K fluorescence of the D^-V site for laser excitation of the $Z_1 \rightarrow E_2$ transition : (a) $^4S_{3/2} \rightarrow {}^4I_{15/2}$, and (b) $^4F_{9/2} \rightarrow {}^4I_{15/2}$. Transitions of the D^- C_{4V} site that were simultaneously present are marked with a dot.

transitions and very weak $E_1 \rightarrow Z_4$, Z_6, Z_7, Z_8 transitions. Most of the Z levels were identified in the $^4F_{9/2} \rightarrow {}^4I_{15/2}$ spectrum which had transitions to higher energy ground state levels of relatively greater intensity. The notable feature of the $^4S_{3/2} \rightarrow {}^4I_{13/2}$ spectra was the very weak $E_1 \rightarrow Y_3$ transition compared to the $E_1 \rightarrow Y_4$ transition.

The L, T and N sites have two features additional to electronic transitions that were reproduced by pumping both the $Z_1 \rightarrow E_1$ or $Z_1 \rightarrow E_2$ transitions:

(a) An emission feature between the Z_7 and Z_8 levels at 495.0, 487.5 and 481.5 cm^{-1} for the L, T and N sites respectively that is of comparable intensity, in the $D \rightarrow Z$ spectrum, to the $D_1 \rightarrow Z_7$ and $D_1 \rightarrow Z_8$ transitions, but which is very weak in the $E \rightarrow Z$ spectrum (Figures 5.18, 5.19, 5.20).

(b) A weak but broad structure close to the $E_1 \rightarrow Z_3$ and $D_1 \rightarrow Z_3$ transitions, around 250 cm^{-1} for all sites. This structure is obscured by the nearby electronic transitions, making exact central location and shape of the feature uncertain.

These features are attributed to vibronic transitions involving lattice phonons with peaks correlating to the known longitudinal and transverse optical phonon frequencies (for k=0) of the CaF_2 host (Elcombe and Pryor 1970, Ward and Whippey 1974, Schlesinger and Drake 1976). Other peaks in the phonon density of states should be present but would be obscured by the electronic emission.

5.3.4(b) *Local Mode Vibronics*

Local mode vibronic spectra were recorded for the D^-L, T and N sites with spectra given in Figure 5.23. The spectra were closely examined for spacings between transitions corresponding to the known Z_1-Z_2 splitting for the site. Such assignment was more difficult than for the Family A sites which have three low-lying ground state levels reducing the likelihood of coincidental separation of unrelated lines. Family B sites, however, have the advantage that both the $Z_1 \rightarrow E_1$ and $Z_1 \rightarrow E_2$ transitions could be pumped enabling confirmation of all vibronics. Table 5.13 summarises the vibronic analysis for these sites and includes vibronic intervals for the N site measured both for transitions from the E_2 and E_1 levels.

The three sites show six distinct local mode vibronic intervals indicating that at least two D^- ions are present for each site, which is consistent with the broadened linewidth of transitions observed in mixed crystal absorption spectra. Several broad lines present in the vibronic spectra have not been assigned. Some of the vibronics associated with higher electronic Z levels are expected to occur in the region of these lines but could not be conclusively assigned.

5.3.4(c) *Polarisation Dependence*

Polarisation of emission was checked for the P, L, T, N and V sites in both <100> and <111> geometries. The P, T and N sites had a complete lack of emission polarisation for the <100> geometry, while all sites showed partial polarisation dependence for the <111> geometry, consistent

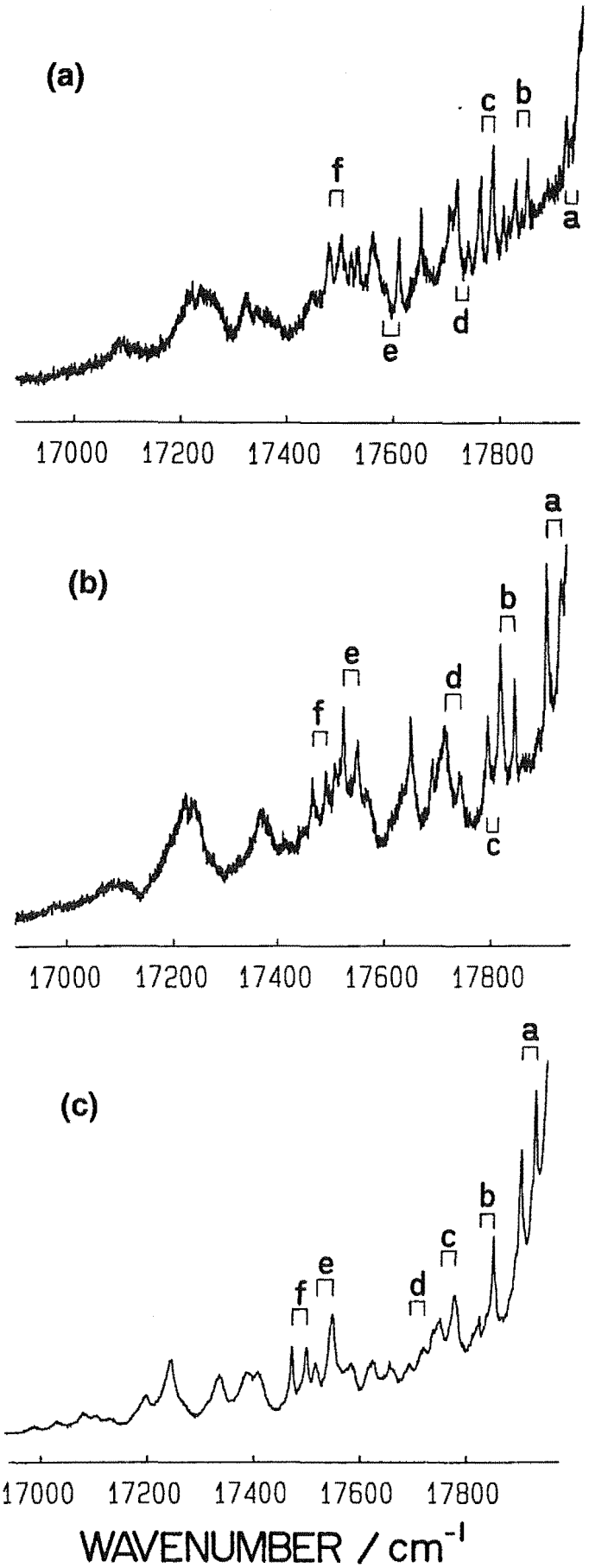

Figure 5.23 : 10K fluorescence ($^4S_{3/2} \rightarrow {}^4I_{15/2}$) vibronics : (a) for $Z_1 \rightarrow E_1$ excitation of the L site, (b) for $Z_1 \rightarrow E_1$ excitation of the T site, and (c) for $Z_1 \rightarrow E_2$ excitation of the N site. In each case, labels a-f identify groups of transitions with the same vibronic interval.

TABLE 5.13 : Wavenumbers and vibronic intervals of local mode vibronic transitions of the D^- L, T and N sites as measured in the 10K fluorescence spectrum of deuterated CaF_2: 0.05% Er^{3+} crystals.

Local Mode	Terminating Level	L Site		T Site		N Site		N Site	
		Wavenumber from E_1 level (± 0.5 cm^{-1})	Vibronic interval (± 1.0 cm^{-1})	Wavenumber from E_1 level (± 0.5 cm^{-1})	Vibronic interval (± 1.0 cm^{-1})	Wavenumber from E_1 level (± 0.5 cm^{-1})	Vibronic interval (± 1.0 cm^{-1})	Wavenumber from E_2 level (± 0.5 cm^{-1})	Vibronic interval (± 1.0 cm^{-1})
a	Z_1	17947.0	555.5	17936.5	555.5	17925.5	564.5	17933.0	562.5
	Z_2	17925.0	555.0	17910.5	556.0	17897.5	564.5	17906.5	563.0
b	Z_1	17852.0	650.5	17848.0	644.0	17844.5±1.0	645.0±1.5	17856.0	639.5
	Z_2	17830.0	650.0	17822.5	644.0	17818.5	645.0	17830.0	639.5
c	Z_1	17787.5	715.0	17822.5	669.5	17777.0±1.0	712.5±1.5	17782.0±1.0	713.5±1.5
	Z_2	17764.5	715.5	17796.0	670.0	17749.0±1.0	714.5±1.5	17755.0	714.5
d	Z_1	17741.5	761.0	17745.0	747.0	17721.0	768.5	17727.0±1.0	768.5±1.5
	Z_2	17719.0	761.0	17718.0±1.0	748.5±1.5	obscured	-	17698.5±1.0	771.0±1.5
e	Z_1	17613.0	889.5	17553.5	938.5	17547.5±1.0	942.0±1.5	17553.5	942.0
	Z_2	17589.5±1.0	890.5±1.5	17527.5	939.0	17519.5	944.0	17533.5±1.0	946.0±1.5
f	Z_1	17505.5	997.0	17494.5	997.5	17500.0	988.5	17506.5	989.0
	Z_2	17483.0	997.0	17469.0	997.5	17471.5	992.0	17479.5	990.0

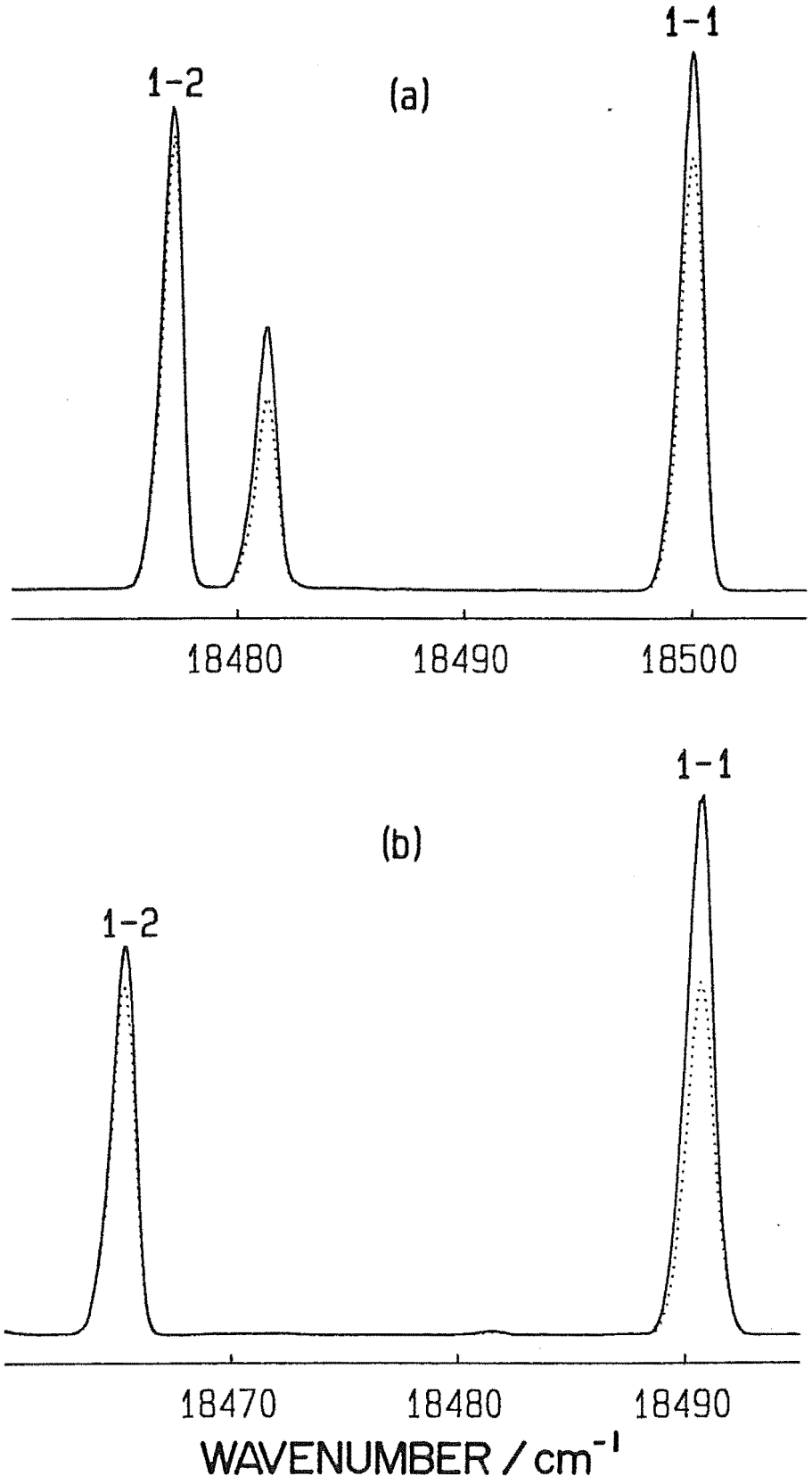

Figure 5.24 : 10K polarised (x(yx)z_____,x(yy)z...) $^4S_{3/2} \rightarrow {}^4I_{15/2}$ fluorescence for $Z_1 \rightarrow E_2$ excitation of : (a) the D^-L site, and (b) the D^-T site. The unlabelled feature in (a) is the $E_1 \rightarrow Z_1$ transition of the F3 site.

Table 5.14 : **Intensity ratios observed for the polarised emission transitions of Family B sites in <111> oriented deuterated CaF_2:0.05%Er^{3+} crystals for $Z_1 \rightarrow E_2$ excitation**

Site	Fluorescence transition		
	$E_1 \rightarrow Z_2$	$E_1 \rightarrow Z_1$	$E_1 \rightarrow Z_2$
P	0.72 ± 0.05	1.14 ± 0.07	1.22 ± 0.08
L	*	1.20 ± 0.06	1.08 ± 0.04
T	*	1.53 ± 0.08	1.12 ± 0.06
N	1.00 ± 0.02	1.06 ± 0.04	obscured
V	1.08 ± 0.04	1.10 ± 0.06	0.90 ± 0.03

with a basic trigonal symmetry structure. Measured polarisation ratios for the <111> geometry for transitions to the Z_1 and Z_2 levels are included in Table 5.14. Figure 5.24 illustrates such <111> polarisation dependence for the D^- L and T sites. For reasons previously outlined, only short scans over well-resolved lines give accurate ratios. The additional polarised line in the L site spectrum is the $E_1 \rightarrow Z_1$ transition of the F3 site.

The x(yx)z and x(yy)z emission levels had a slight difference, typically around 4%, for transitions of the V site in a <100> geometry. The only other site of the family with a definite <100> dependence for some transitions was the L site. For example, with $Z_1 \rightarrow E_2$ excitation, the ratio x(yx)z:x(yy)z was 1.38 ± 0.08 for the $E_1 \rightarrow Z_1$ transition and 1.02 ± 0.02 for the $E_1 \rightarrow Z_2$ transition.

5.3.4(d) *Mixed H^-/D^- Sites*

The broadened absorption lines for Family B sites in a 1:1 mixed H^-/D^- crystal were pumped by the laser in an attempt to resolve structure for the centres. The transitions that had least overlap with other sites were the $Z_1 \rightarrow E_2$ transitions of the L and T sites. Figure 5.25 has superposed fluorescence spectra for three laser frequencies within the inhomogeneous linewidth of this transition for the T site in both a mixed crystal and one containing deuterium only. The solid line is the spectrum after maximising tuning on the site in the pure D^- crystal. It was found that the fluorescence transition frequencies for the series of laser frequencies were within the inhomogeneous line profile of the D^- centre for the

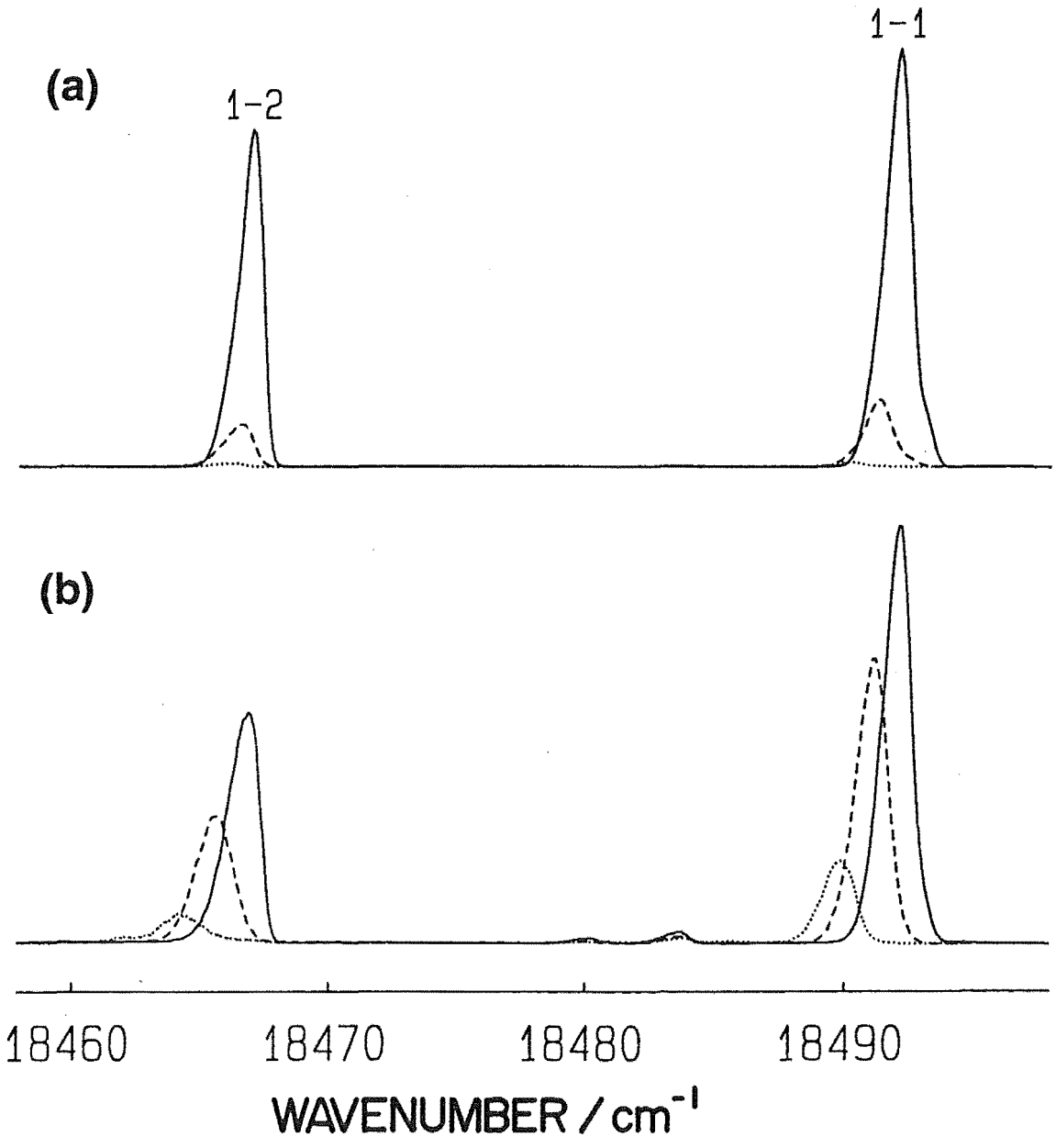

Figure 5.25 : Comparison of 10K fluorescence ($^4S_{3/2} \rightarrow {}^4I_{15/2}$) of the T site for three closely spaced laser frequencies within the $Z_1 \rightarrow E_1$ absorption profile in a CaF_2:0.05%Er^{3+} crystal. (a) deuterated for 68 hours, and (b) treated identically but in a 1:1 mixture of hydrogen and deuterium.

deuterated crystal, but transition frequencies for the mixed crystal changed markedly for laser excitation between the pure D^- ion site and pure H^- ion site frequencies known by absorption.

These intermediate frequency fluorescent transitions are due to the excitation of T site configurations of mixed H^- and D^- ion composition, confirming the involvement of more than one hydrogenic ion. The decrease in intensity with decreasing transition frequency is attributed to the previously discussed weaker fluorescence of the H^- sites,since D^- ion are replaced by H^- ions, rather than to decreased population of that particular centre. Similar results were obtained for the L site, but transitions for other sites could not be adequately isolated to confirm similar effects.

5.3.4(e) *Configurations of Sites*

The similarity of emission for these sites to the F^- B site suggests correspondingly similar site configurations. The observation of an EPR site of trigonal symmetry in 12-hour hydrogenated crystals with no detectable isotope shift for deuterated crystals implies that an H^- analogue of the F^- B site is present (Edgar *et al.* 1979). According to the accepted model for the B site, this would be a site with an Er^{3+} ion having charge compensation by an H^- ion located in a next nearest interstitial position in a <111> direction from the Er^{3+} ion. Such a site would have two local mode vibration frequencies expected for axial symmetry and would have a small isotope shift, since the hydride ion is further removed than for the C_{4V} site.

The L, T and N sites are not possibilities for the site because of the known number of vibronic intervals, large isotope shifts and mixed H^-/D^- crystal behaviour, all indicative of involvement of more than one hydrogenic ion. The extent of crystal field perturbation from the B site, as indicated by all known crystal field levels, also eliminates the V or S site from being the simple site, as the perturbation resulting from simply replacing the interstitial F^- ion with a D^- or H^- ion should be relatively small.

The lack of vibronic information for the remaining sites W, X and P makes positive assignment of the configuration difficult. The most likely candidate for the simple trigonal hydrogenic centre is the W site for the following reasons :

(a) This site has very small isotope shifts (Table 5.3) consistent with EPR results, and that expected for a single, remote ion.

(b) Its known crystal field levels are the closest to those of the B site (see Figure 5.1).

(c) It is the first site to form after brief hydrogenation duration treatment and is simultaneously present with the other simple sites: F^-A, F^-B and H^-C_{4V}.

(d) Its concentration decreases as the crystals age, whereas others such as X and P increase. This is consistent with modification of the simple site to other sites by the substitution of additional migrating hydride ions - similar to the growth of the R site.

It is proposed that other members of the family are modifications of the W site. The progression of increasing isotope shifts has the same site order as the decreasing trend in the $^4S_{3/2}$ multiplet barycentres. This trend is both the result of decreasing the distance between the Er^{3+} ions and the neighbouring hydrogenic ions, and/or of having an increasing number of hydrogenic ions associated with the Er^{3+} centre.

Figure 5.17(b) shows a simple model configuration for the trigonal centre with various lattice F^- ion positions labelled as possible positions for H^- ions to substitute and form various Family B sites. Tentative models for most sites can be prepared using the known information as follows :

(a) The X and P sites with relatively small isotope shifts probably have a single additional hydride ion remote from the erbium ion in positions 'a' and 'b' respectively. Slight lattice deformation due to this hydride ion would cause a small crystal field perturbation but would be predominantly trigonal symmetry as observed for the <111> polarisation dependence of the P site.

(b) The L, T and N sites have similar vibronic spectra with differing polarisation dependence. An increased isotope shift suggests a substitutional hydride ion in various positions of the nearest neighbour cage about the erbium ion. The observation of six vibronic intervals for the deuteride ion sites (Table 5.13) supports this model. The lower three vibronic intervals

centred around 640 cm^{-1} are attributed to the substitutional ion and derived from the 694 cm^{-1} T_d site line. The other three D^- ion vibronics centred at 883 cm^{-1}, 895 cm^{-1} and 901 cm^{-1} for L, T and N respectively are derived from the cubic site line at 950 cm^{-1} and assigned to the interstitial D^- ion in the <111> direction from the erbium ion. As the T site has the most well defined <111> polarisation dependence with negligible <100> dependence, it is a good candidate for a trigonal centre with the substitutional H^- ion at position 'c' or 'f' in Figure 5.17(b). The existence of three vibronics for each hydride ion would require a net displacement of one of the ions off axis. It is not obvious, however, why this would occur. The L site has similar vibronics to the N site but has a <100> as well as a <111> polarisation dependence indicative of an H^- ion in position 'd', such that any net deformation caused by the two H^- ions would have a significant <100> component with respect to the erbium ion. The N site has virtually no polarisation symmetry for any orientation consistent with a deformation from both the interstitial hydride ion and another ion in position 'e'.

(c) The increased isotope shift and overall crystal field level shifts for the S and V sites could result from a second substitutional hydride ion in the nearest neighbour cage about the Er^{3+} ion.

There are several possible configurations of this type but no evidence for any particular combinations.

5.3.5 'Near Cubic' Hydrogenic Sites.

These sites, identified by optical absorption, had weak fluorescence that could not be clearly distinguished from swamping F^- site fluorescence simultaneously excited when the laser was tuned to pump the absorption transitions. All fluoride ion sites A, B, C, present in the absorption spectrum caused interference problems.

5.4 Infra-Red Absorption Spectroscopy of Hydrogenated Crystals

5.4.1 Outline

A study was made of the infra-red absorption spectra of hydrogenated $CaF_2:Er^{3+}$ in the region 800 cm^{-1} to 1500 cm^{-1} to classify the various local mode vibration frequencies into sites for a variety of crystals of different thermal treatments. Such frequencies are slightly temperature dependent and increase with decreasing temperature, due to the contraction of the lattice (Newman 1973 and references therein) and the consequent increase in force constants. These measurements were made at 83 K.

The main motivations for this study were firstly to attempt to accurately calibrate and classify local mode lines for future CO_2 laser excitation studies similar to those previously reported (Campbell *et al.* 1982), and secondly, to check for correlation with sites determined in the optical absorption spectra and local mode vibronic

intervals determined by laser selective excitation.

The number of lines associated with a hydride ion in a particular centre depends on the point group symmetry of the H^- ion site in the centre. A site of cubic symmetry has a single triply degenerate fundamental line. Sites of axial symmetry have two lines, one twofold degenerate and one nondegenerate, while sites of lower symmetry have three lines.

The lines belonging to a specific centre have constant relative intensity in all crystals, although this was difficult to determine in some instances due to the large variation in background level caused by the overlap by absorption lines of other sites. For crystal thicknesses used in this study the CaF_2 lattice transmits down to 800 cm^{-1} and has a reasonably steep decrease in transmission below this frequency.

Hydride ion local modes conveniently occur within the 8-13 μm atmospheric window. It is anticipated, however,that some local modes exist at frequencies below the 800 cm^{-1} limit set by the crystal thicknesses used. The onset of significant lattice absorption also made measurements of the fundamental frequencies of D^- or T^- ion local modes impracticable although second harmonics of the D^- and T^- T_d site lines were identified.

Crystal thicknesses used varied from 1.3 mm to 2.5 mm with a typical thickness of 2.0 mm. Due to the variability of the humidity between scans, the 6 μm band of water lines still appeared in most spectra. These lines are very sharp and the thickness of plotting pens used exceeded their true linewidth, resulting in the water lines appearing more

intense in the spectra presented, than they actually were.

5.4.2 Results

Transmission spectra for ten CaF_2:0.05%Er^{3+}:H^- crystals of various hydrogenation treatments were recorded as well as one mixed H^-/D^- crystal and one tritiated crystal. Sixty-four principal absorption lines were determined altogether for the CaF_2:Er^{3+}:H^- spectra, including those of the sites already known, with each of these lines being numbered in a frequency sequential pattern, for easy identification in tables and spectra.

The frequencies of lines for sites previously known were also determined in this study since the FTIR spectrometer calibration by HeNe laser is more accurate than that for the grating spectrometers previously used. A summary is provided of all known lines since this has not been presented elsewhere. Table 5.15 compares the previously reported values of the A,B,C,D,C_{4V},T_d and cubic site lines with those obtained in this study. Several other lines were assigned to seven new sites E,F,G,H,I,Q and Y by intensity correlation between spectra of different crystals. The local mode frequencies for these sites are included in Table 5.16. In several cases a third line is expected for these sites but was not identified and is probably obscured either by other lines in the spectrum or by the lattice absorption below 800 cm^{-1}. The remaining thirteen lines reported here were found not to correlate with others, and related site lines are expected to be

Table 5.15 Local mode energies of H^- ion sites in $CaF_2:Er^{3+}$ determined in this study compared to previous studies. Energies are in cm^{-1}, uncertainty is ± 0.3 cm^{-1}, and measurments were made at 83K.

Site	Reference	Previous study	Present study	Label in spectra
T_d	a	965.1 ± 0.3	965.1	22
C_{4V}	b*	1036.2 ± 0.1	1037.4	36
		1037.4 ± 0.1	1038.8	37
		1081.2 ± 0.1	1082.5	44
		1085.8 ± 0.1**	1086.6	45
		1086.7 ± 0.1	1087.8	46
Cubic	c	1312	1310.5	57
A	d	991 ± 3	991.5	28
		1050 ± 3	1051.8	39
B	d	1069 ± 3	1070.0	42
		1149 ± 3	1148.2	48
C	d	843 ± 3	844.3	4
		1316 ± 3	1315.1	58
		-	1242.0	53
D	d	1208 ± 3	1213.4	52
		1331 ± 3	1335.1	60
		1390 ± 3	1391.1	64

References:

a Elliott *et al.* (1965)
b Edgar *et al.* (1979)
c Jones *et al.* (1968)
d Thompson (1980) (See Cockroft *et al.* 1987a).

* Measured at 15K
** Measured at 30K

Table 5.16 : Local mode energies (in cm^{-1}) assigned to seven new infra-red sites in hydrogenated CaF_2:0.05%Er^{3+} crystals at 83K. Uncertainty is ± 0.3 cm^{-1} and the labels used to represent each mode in the spectra is given in parentheses.

E	F	G	H	I	Q	Y
1267.9 (54)	1125.0 (47)	919.7 (11)	835.4 (3)	819.5 (2)	1360.4 (61)	998.0 (29)
1378.4 (63)	1192.7 (50)	921.0 (12)	1170.3 (49)	871.3 (6)	1370.2 (62)	1001.4 (31)
		1202.0 (51)				

present but obscured by other features.

All infra-red sites and unassigned lines are discussed in more detail below.

5.4.2(a) *The T_d, Cubic and C_{4V} Symmetry Sites*

Figure 5.26 shows the spectrum of a 1.47 mm thick crystal hydrogenated at 860°C for 12 hours and quenched rapidly to room temperature. The main absorption lines are the large T_d site line at 965.1 cm^{-1}, the C_{4V} site lines and the cubic symmetry site line at 1310.5 cm^{-1} (see references in Table 5.15). These site lines are the same, within experimental uncertainty, as those determined previously.

The structure of the C_{4V} site spectrum was particularly well resolved in this study as shown in Figure 5.27. Edgar *et al.* (1979) assigned (using temperature dependence) each of the peaks to particular local mode phonons associated with particular thermally populated electronic levels Z_1, Z_2 and Z_3 as follows :

Line label	Local mode phonon	Electronic state
36	X,Y	Z_1
37	X,Y	Z_2
44	Z	Z_1
45	Z	Z_3
46	Z	Z_2

Electron-phonon effects are responsible for the energy differences between the various local mode lines associated with the different electronic states. The frequencies of these lines at 83 K are included in Table 5.15 since the

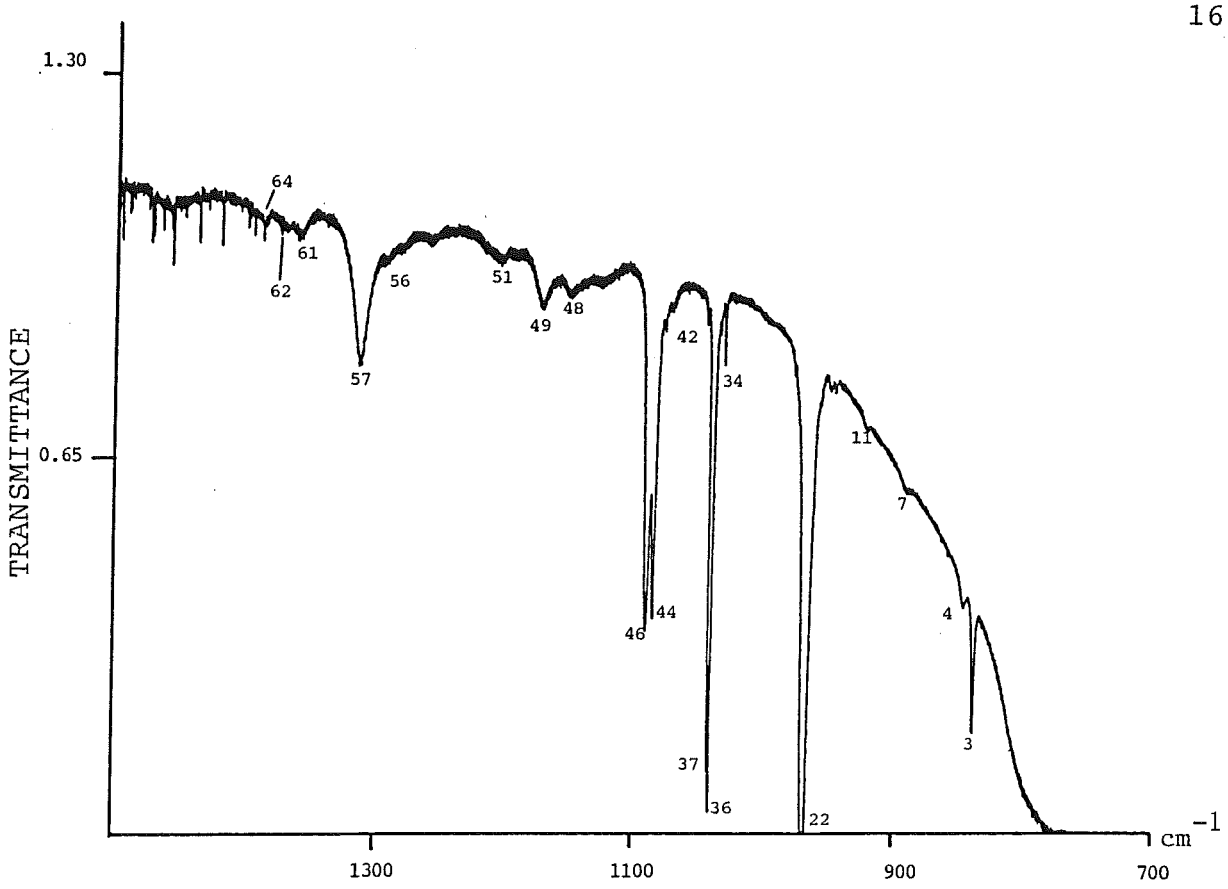

Figure 5.26 : 83K infra-red transmittance spectrum for a 1.47 mm thick CaF_2:0.05%Er^{3+} crystal hydrogenated for twelve hours. H^- ion local modes are identified by the numerical labels used in this study.

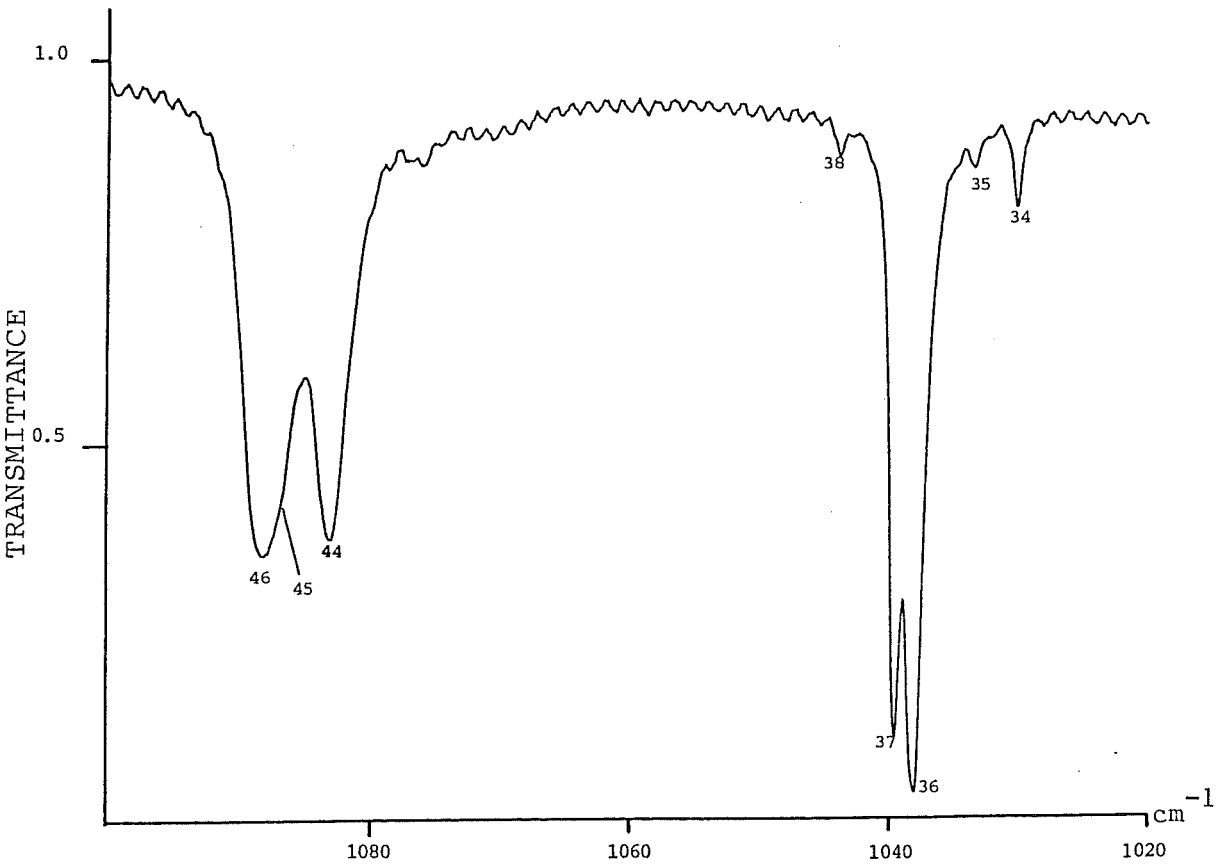

Figure 5.27 : 83K infra-red spectrum illustrating structure on the C_{4V} local mode lines (for the crystal used in Figure 5.26).

values for this temperature have not previously been reported.

As observed in the optical absorption spectra (Section 5.2), the C_{4V} site lines decreased substantially with increasing duration of hydrogenation until, after 68 hours, they were barely distinguishable from the background profile.

The intensity of the T_d site line fundamental could not be determined directly since in all crystals it had 100% absorption, but intensities could be determined using the second harmonic line which is a factor of 23 weaker at 20 K (Elliott *et al.*1965). The absorption coefficient for this line was determined for crystals of six different hydrogenation periods and is plotted in Figure 5.28. Since the T_d site is independent of the rare-earth ion charge compensation mechanism, its absorption is indicative of overall hydrogen content in the crystal and was found to increase approximately linearly as a function of the duration of hydrogenation.

Another interesting observation was a ratio of 2.1 ± 0.3 for the second harmonic lines of two 2.5 mm thick crystals hydrogenated simultaneously in the same crucible for 61 hours, with one crystal having aluminium coils on both surfaces and the other (with lower resultant hydrogen content) having a coil on one surface only. This result shows that the introduction of hydrogen to the crystal results from a surface reaction with the aluminium, and that the hydrogen diffusion from each of the two surfaces into the crystal acts almost independently. The single coil crystal had a second harmonic T_d site line absorption

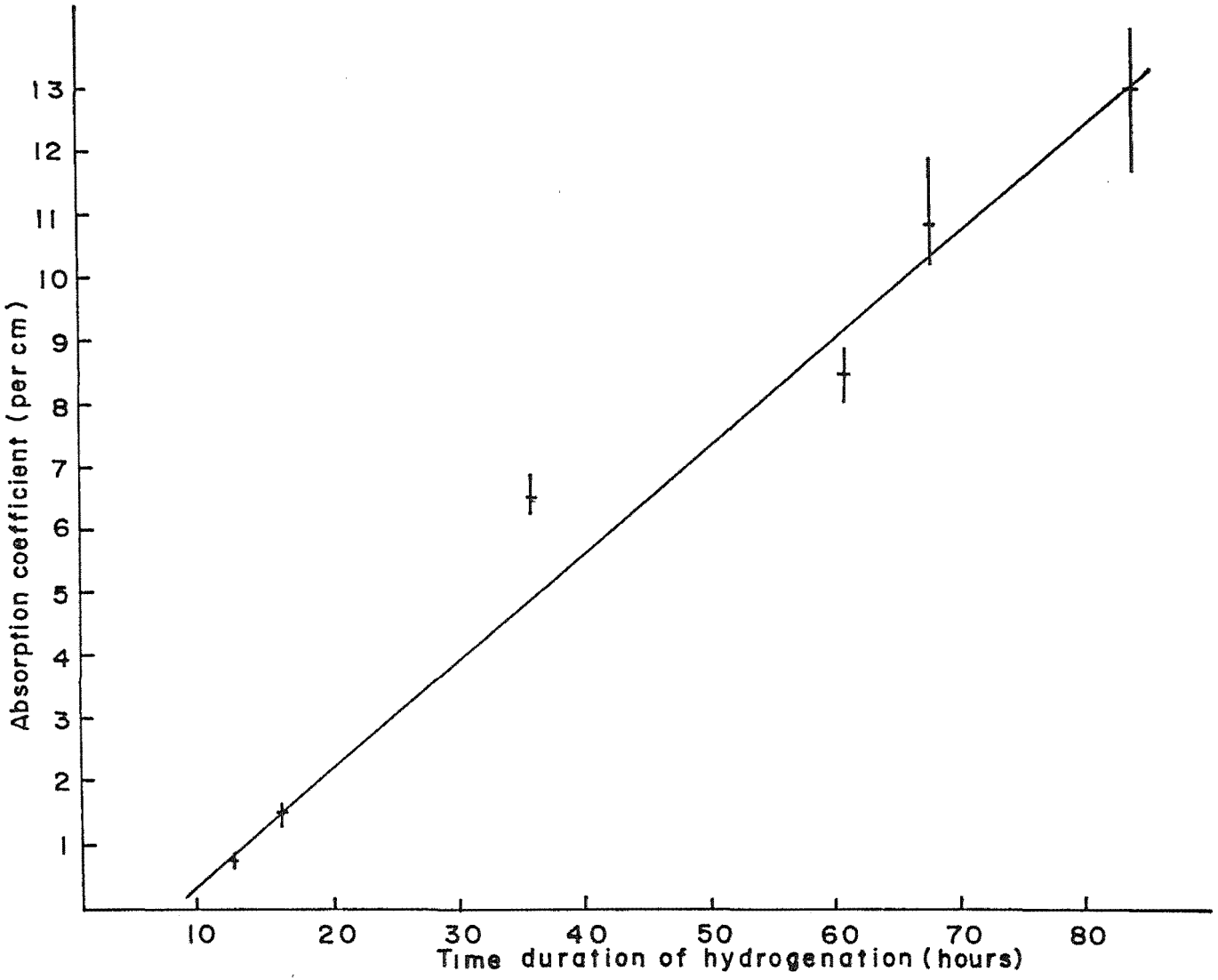

Figure 5.28 : Variation of the absorption coefficient of the second harmonic line of the $H^- T_d$ site with the period of heating during the hydrogenation process.

coefficient (per cm) of 3.95 ± 0.30 . The equivalent hydrogenation duration (from Figure 5.28) for a double coiled crystal is about thirty hours. Crystals of such hydrogenation duration were found to have site distributions very close to that observed for this single coil crystal. This suggests that the site distribution is a function of total hydrogen content regardless of the hydrogenation duration used to obtain it. Hydrogenation duration is still, however, the most convenient means of controlling total content and therefore site distribution.

The three-fold degenerate cubic site line corresponding to an interstitial hydride ion remote from a rare-earth ion was found to be well resolved only for crystals hydrogenated for fewer than 16 hours. For crystals hydrogenated for longer times, many other local modes with similar frequencies that are apparently derived from this site become dominant. The line in most crystals (labelled "58" in Figure 5.29) that may be mistaken for the cubic site line using less well calibrated spectrometers, is actually (4.6 ± 0.8) cm^{-1} higher in frequency and assigned to the C site.

5.4.2(b) *Site A*

It was found that these measurements did not support the previous report (Thompson 1983) that the lines of the A site are only present in crystals hydrogenated several years earlier. Absorption lines for the site were found with varying intensity in all freshly hydrogenated crystals except for those hydrogenated for fewer than sixteen hours.

By comparing the optical and infra-red absorption spectra for all ten crystals, these local modes were

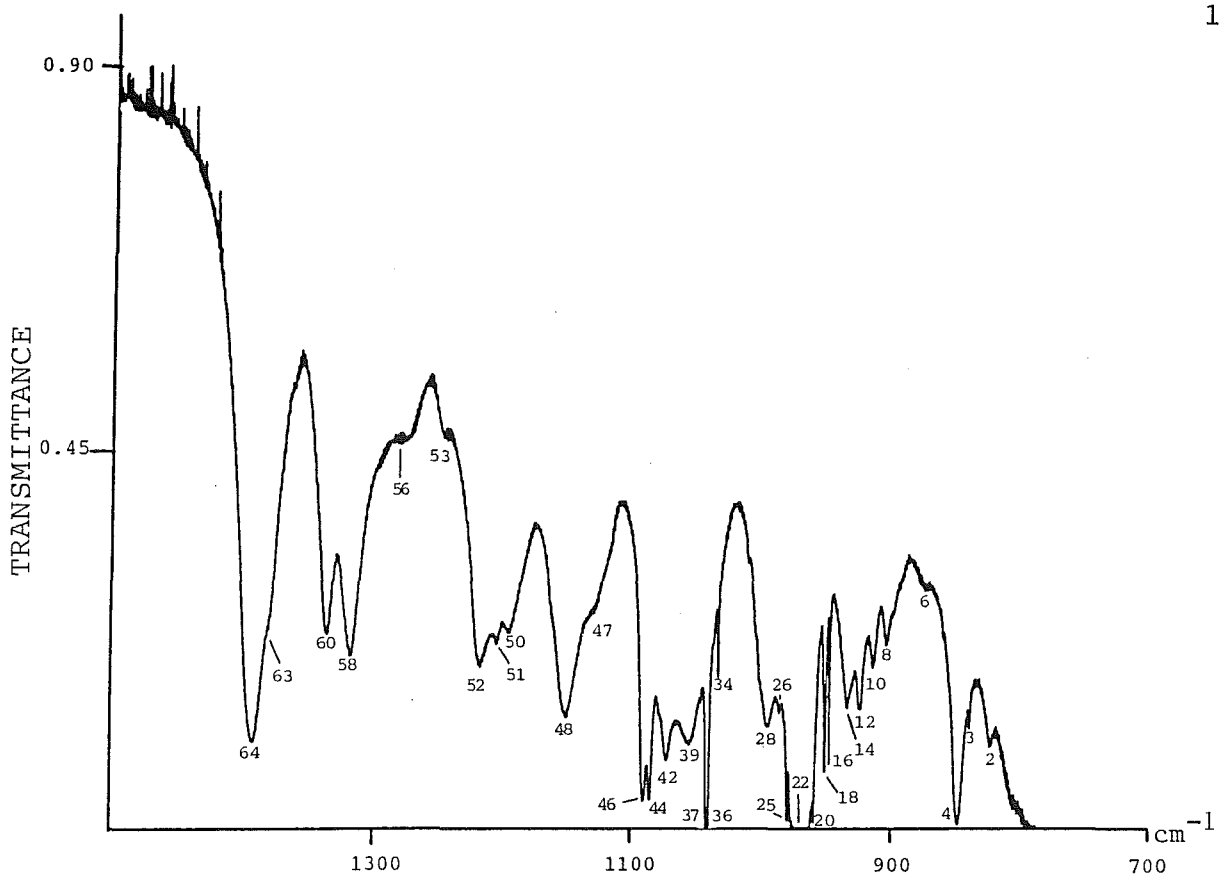

Figure 5.29 (a): Local mode spectrum of a 1.84 mm thick CaF_2:0.05%Er^{3+} crystal hydrogenated for 36 hours.

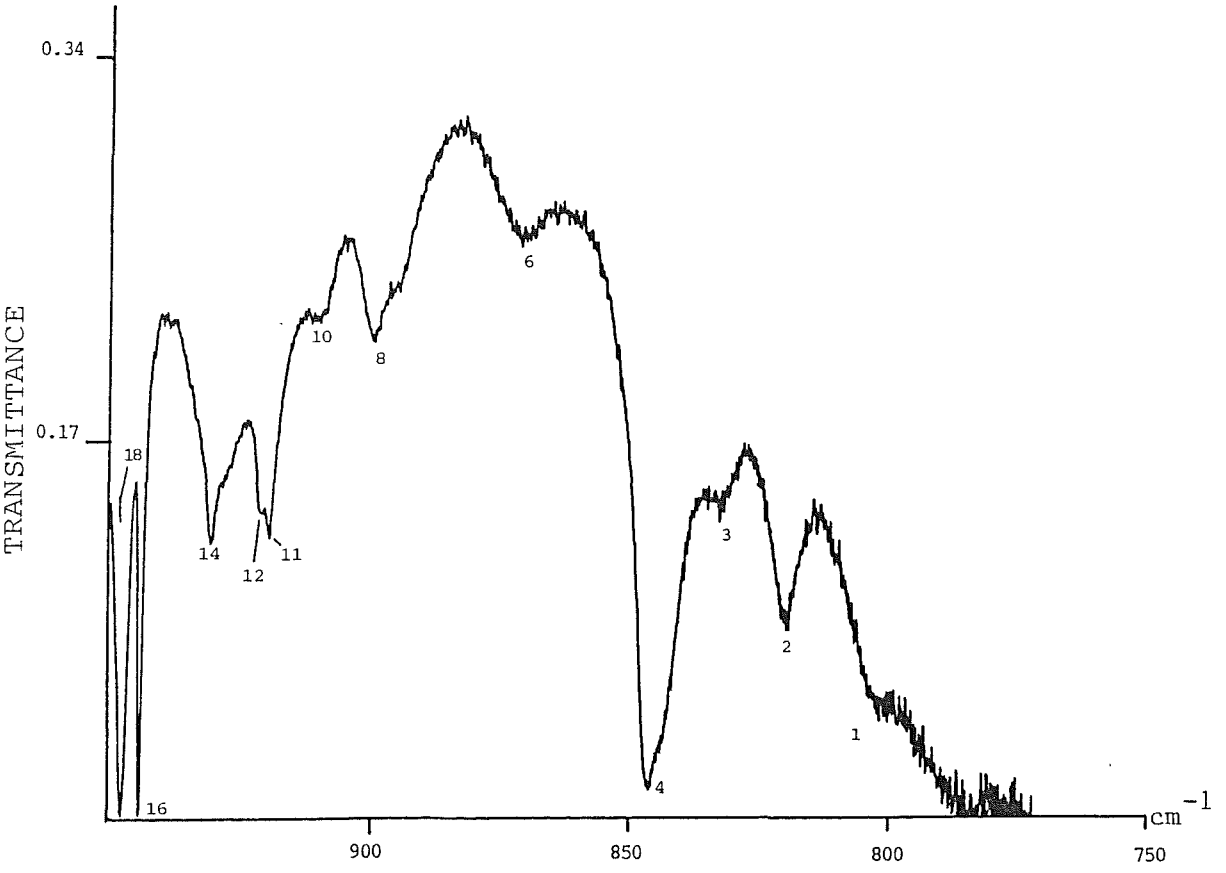

(b): Low frequency region local mode spectrum of a 1.42 mm thick CaF_2:0.05%Er^{3+} crystal hydrogenated for 84 hours.

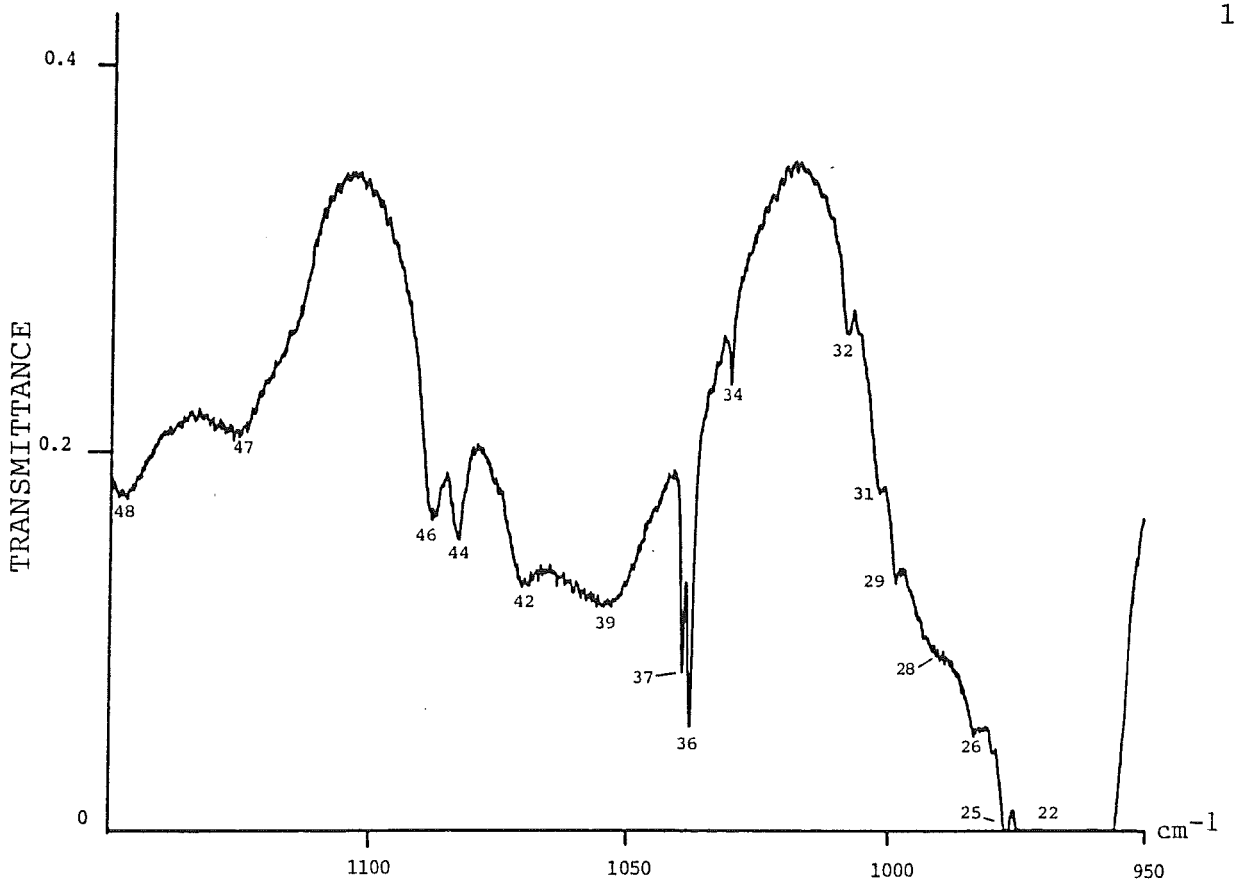

Figure 5.29 (c) Mid frequency region spectrum of crystal used in (b).

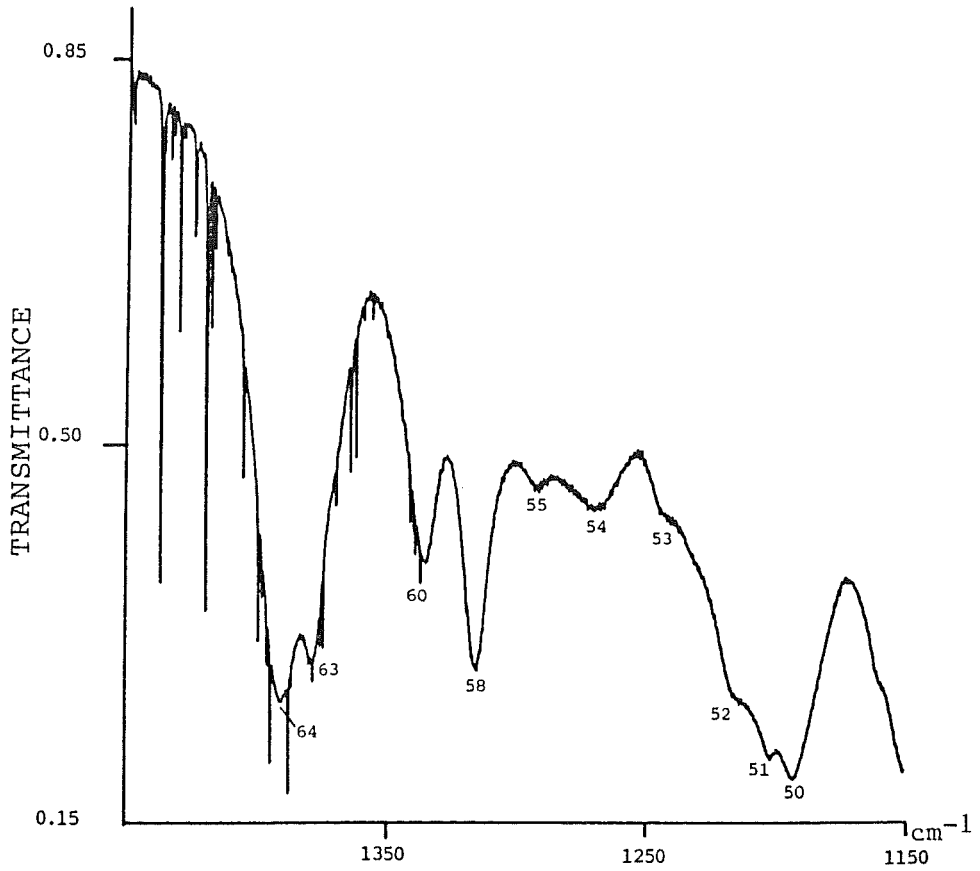

(d) Higher frequency region local mode spectrum of crystal used in (b) and (c).

correlated to the optical J site. A particularly useful comparison was provided by the neighbouring lines at 1051.8 cm^{-1} and 1070.0 cm^{-1} (labelled 39 and 42 respectively) of the A and B sites respectively, and the neighbouring $Z_1 \rightarrow E_1$ electronic transitions of the optical R and J sites. The absence of significant A site mode absorption in new crystals for previous studies (Robson 1969, Thompson 1983) is attributed to the short duration hydrogenations always used.

Attempts to assign a third line to the site were unsuccessful. It is proposed that these modes are those of the interstitial hydride ion of the J site (Figure 5.17(a)). The previous section reported a vibronic interval for this ion, determined by laser selective excitation, to be at 678 cm^{-1} for the D^- analogue. This would correspond to an H^- ion mode around 936 cm^{-1}. Although several lines exist in this region, no definite correlation could be established. The weak vibronic proposed at (755 ± 2) cm^{-1} for the D^- ion in the site is confirmed here as it corresponds, by reduction by the mass factor of 1.39, to the 1051.8 cm^{-1} line observed for this site.

The three local modes of the substitutional ion of the D^-J site were also established by l.s.e. (Table 5.12). The hydrogenic analogues of these modes would be expected to be in the ranges :

$$J_a = (701 - 719)\ cm^{-1}$$
$$J_b = (795 - 815)\ cm^{-1}$$
$$J_c = (837 - 857)\ cm^{-1}$$

Of these modes only the J_c mode is in a spectral region

accessible for study and an appropriate local mode was not identified. In any case, features in this region may be obscured by the intense absorption of the C site line at 844.3 cm^{-1} which varies in a similar manner to the intensity of the A site lines; that is, increasing with hydrogenation duration up to the limit tested of an 84-hour period.

5.4.2(c) *Site B*

The previous correlation of the optical R and infra-red B sites by spectra comparison (Cockroft 1983) and by vibronic intervals of the l.s.e. spectra (Section 5.3.3) was confirmed by comparison of the spectra of these ten crystals. The two local modes listed in Table 5.12 are those of the interstitial H^- ion. The l.s.e. vibronic spectra showed some evidence of a slight splitting of the lower frequency mode around 1060 cm^{-1}. Such a mode was not resolved in the infra-red spectrum, probably due to the overlap of the broad A and B site lines in this spectral region.

Associated with this site should also be the two substitutional H^- ion modes (Table 5.12 R_a (762.5 cm^{-1}) and R_b (844.5 cm^{-1})). R_a is swamped by lattice absorption for the crystal thicknesses used, and R_b has a closely similar frequency to a line of the C site. The absorption of the latter is more intense than would be expected for the B site, although the line was found to vary under similar conditions to the B site and no evidence of distinctly different behaviour was established. It is possible that this feature at 844.3 cm^{-1} is the sum of a line for both the B and C sites.

Consistent with the proposed model for the site (Figure 5.17(a)), no further local modes were expected or found.

5.4.2(d) *Site C*

The C site lines increased markedly with the duration of hydrogenation and are distinct in all crystals, but occurred only weakly in the crystal hydrogenated for twelve hours only. The lowest frequency line showed an additional shoulder structure at 846.0 cm^{-1} in crystals hydrogenated for periods longer than 36 hours. Structure is also present, in some instances, on the higher frequency line although this was not clearly resolved. Such structure suggests that further perturbations of the site are being formed. An additional weaker absorption line at 1242.0 cm^{-1} is tentatively assigned to the site as it has similar thermal history dependence.

Thompson (1983) proposed, by analogy to SrF_2 work by Edgar *et al.*(1977), that the C site consisted of the trigonal F^- B site modified by a hydride ion substituted in the lattice cage surrounding the F^- interstitial ion and furtherest from the Er^{3+} ion. This analogy predicted, however, that the missing local mode line should have a frequency less than the 965 cm^{-1} T_d site line rather than the higher frequency line proposed in this study. No definite correlation was established with the sites of the optical absorption spectra, so no definite site proposal can be made.

5.4.2(e) *Site D*

This site was not found in crystals hydrogenated for

twelve hours or fewer but increased markedly with the duration of hydrogenation. The three vibrational frequencies have an average of 1313.2 cm^{-1} compared to the single line, at 1310.5 cm^{-1}, of the isolated hydride ion site. This site is assigned to be due to a remote interstitial ion providing charge compensation for an Er^{3+} ion which has almost cubic symmetry. On the basis of the behaviour of such 'near cubic' symmetry Er^{3+} ion sites in the optical spectrum, it is possible that the D site may have additional substitutional H^- ions associated with it. Such ions would probably have local modes below the 965 cm^{-1} T_d site line with some modes below the lattice transmission limit for the crystal thicknesses used. In crystals where the D site absorption is large, other local mode lines exist below 965 cm^{-1} but none were correlated to this site.

The previously reported (Thompson) increase in intensity of the D site along the rare-earth series is consistent with the pattern of abundance of cubic centres in CaF_2 (Hayes 1974) determined by EPR measurement.

5.4.2(f) *Sites E and F*

The lines of these new sites are important features in crystals hydrogenated for longer than 60 hours. Reliable correlation of each of the sets of two lines was established despite some overlap with other absorption lines. It is proposed that these sites are modifications of the cubic site and are similar to the D site. There are no sites of this nature expected with axial symmetry, so it is expected that there is a third local mode line for each of the sites that is completely obscured by other lines in the spectrum.

Each of the new unassigned lines was discounted as a candidate for such a third line by comparison of intensities in different crystals.

Any component of the line of the E site at 1267.9 cm^{-1} was obscured in crystals of fewer than 60 hours hydrogenation by a slightly shifted broad line centred at 1274.1 cm^{-1} (labelled 56) which decreased in intensity after this duration of hydrogenation. As with the D site, an unsuccessful attempt was made to correlate lower frequency lines of substitutional ion modes to these sites. The intensity of the D, E and F sites as a function of hydrogenation duration resembled the pattern of growth of the α, β and γ sites from the optical absorption spectra (Figure 5.2). These sites are tentatively assigned, by such comparison, as follows :

$$D \rightarrow \alpha$$

$$E \rightarrow \beta$$

$$F \rightarrow \gamma$$

5.4.2(g) ***Sites G, H, I, Q and Y***

These sets of lines were established by intensity correlations, but the nature of the sites is not known and they appear under a variety of conditions.

The G site, with an almost degenerate mode split by only 1.3 cm^{-1}, and one higher frequency line, was present in all crystals. It had only a very weak intensity for the 12-hour hydrogenated crystal and increased for 16-36 hour hydrogenation durations, but had no substantial increase in intensity for hydrogenations of duration greater than 36 hours.

Site H had two lines similar in frequency to site C. This site has greatest relative intensity for very short duration hydrogenations of twelve hours or less with both lines being clearly resolved. As the duration is increased, the lower frequency line intensity is observed to decrease significantly, and the higher one becomes swamped by nearby stronger absorption lines.

Site I consists of two lines that increase in intensity with hydrogenation duration. The line at 819.5 cm^{-1} is the more easily resolved and appeared weakly in a crystal hydrogenated for 36 hours. Its intensity increased almost linearly as hydrogenation duration was increased. The lattice absorption edge prevented any transmission measurement for the line in thicker crystals. The low frequency of the two known modes suggests the H^- ion may be in a substitutional position for this site.

Site Q consists of two lines that appear together for intermediate period hydrogenations of between 16 and 36 hours duration. The site was not observed for hydrogenations greater than this period. As no third line was found for this site, no configuration can be proposed.

Two weak lines on the side of the 965 cm^{-1} line were classified by intensity comparison and labelled site Y. These lines were present in most crystals and were enhanced by increasing the hydrogenation duration. It is likely, by analogy with nearby satellite structure discussed in the next section, that a third line may exist below the T_d site line and that the site is due to a substitutional H^- ion located about an unexpected trace impurity ion. Alternatively, since the intensity increases in a similar

manner as a function of hydrogenation duration, the site may be the vibrational modes of a second hydride ion in either the D, E or F centres.

5.4.2.(h) *Satellite Lines about the T_d Site Line*

The sites reported above account for the vast majority of the overall absorption due to hydride ion local modes. Several weaker lines were observed, however, and these were carefully checked for correlation with other lines in the spectrum and with literature reports. Such a summary is important for future infra-red laser excitation work.

Satellite structure around the 965 cm^{-1} T_d site line was observed and categorised. A variety of these sites has been previously reported in different references. Newman (1973) has reviewed several of the lines due to compensation by other rare-earth ions and trace impurities. The most common contaminant in CaF_2 is yttrium and evidence of such contamination was found here. Another useful summary of sites due to centres involving traces of Sr^{2+} or Ba^{2+} ions replacing a Ca^{2+} ion was provided by Chambers (1971). Sites of C_{3V} symmetry were found for nearest neighbour Sr^{2+} - H^- pairs and of C_s symmetry for second neighbour Sr^{2+} - H^- pairs (and the equivalent Ba^{2+} - H^- pairs).

Table 5.17 compares the frequencies of lines observed in this study with the values of those previously reported, and accounts for seventeen additional lines. The site configurations proposed by previous authors were not tested.

It was noted that although all crystals exhibited slight strontium contamination, the site lines due to barium contamination, particularly those of 927.4, 935.7 and 1022.0

Table 5.17: Summary of 'satellite structure' local mode lines observed about the T_d site line in the 83K infra-red spectra of hydrogenated CaF_2:0.05%Er^{3+} crystals. The line number used in this study is included and the energy determined (±0.3 cm^{-1}) is compared to previous reports.

Line number	Energy Present	Energy Previous	Reference†	Previous Site Label	Proposed site configuration
34	1030.0	1028.9	a	A1	Y^{3+}-H^-(C_{4V})
43	1075.2	1074.8	"	"	"
38	1043.5	1044.2	a	A2	O_4^{2-} -- -Y^{3+}-H^-(s)(C_{3V})
16	944.0	943.8	a	A3	O^--H^-(s) (C_{2V})
18	947.5	947.2	"	"	"
25	975.7*	976.0	"	"	"
5	846.0	847.0	a	A4	[v]-H^-(s)
20	955.7	955.4	"	"	"
21	956.8	956.4	"	"	"
23	971.7	971.8	"	"	"
24	973.0*	973.0	"	"	"
19	948.3	948.6	b	α	Sr^{2+}-H^-(C_{3V})
32	1007.8	1007.6	"	"	"
24	973.0*	973.0	b	β	Sr^{2+}-H^-(C_s)
25	975.7*	976.0	"	"	"
15	935.7	935.6	b	α	Ba^{2+}-H^-(C_{3V})
33	1022.0	1021.9	"	"	"
13	927.4	927.1	b	β	Ba^{2+}-H^-(C_s)
27	989.0	989.0	"	"	"

* Assignment of these lines is ambiguous with both references attributing it to different origins.

† References a Newman (1973)
b Chambers (1971)

cm^{-1}, were present only in those crystals obtained from Optovac Inc. and not in those grown at Canterbury. The crystal in which this site was most intense also had a broad feature centred at 1056.4 cm^{-1} which is therefore tentatively assigned to be due to barium ions present in another site.

Of the sites in Table 5.17, the most intense lines present in all crystals were those due to the site labelled A_3 by Newman. Some evidence of Sr^{2+} contamination was found in all crystals, although, again, the Canterbury crystals tended to have slightly less contamination. The relative intensity of all lines in the table confirmed the assignments made, except for the higher frequency lines of the A_1 and A_2 sites due to Y^{3+} contamination that were obscured in some instances by modes of the A and B site,while the line at 1030.0 cm^{-1} was often pronounced. This made correlation difficult for this particular site and the remaining A_2 site line at 1030.9 cm^{-1} was not resolved.

5.4.2.(i) *Additional Lines*

Several additional lines observed were each compared with all other lines in the spectrum and found not to correlate with any of the categorised lines or with any previously reported rare-earth ion impurity sites. It is expected that other lines of the sites to which these local modes belong are either obscured by other site lines or by the CaF_2 lattice absorption.

These remaining lines are tabulated in Table 5.18 together with observations of the intensity variation of the lines.

Table 5.18: **Summary of observations related to the unassigned lines in the infra-red absorption spectra of hydrogenated CaF:0.05%Er^{3+} crystals. Energies are in cm^{-1} and "H.D." is used as an abbreviation for duration of hydrogenation.**

Line number	Energy	Comments
1	802.0	Increases with H.D. Appears after 24 hours H.D.
7	890.0	Optomised for H.D. of 16-24 hours.
8	899.0	Relatively intense after 68 hours H.D.
9	900.2	Overlaps with line 8 but is less intense
10	910.0	Possible doublet. Optimised for 36 hours H.D.
14	930.7	Inconsistent H.D. dependence.
17	946.9	Suspected satellite line of T_d site involving trace impurity.
26	982.6	Weak intensity. Present most crystals.
35	1033.1	Small feature with narrow linewidth. No obvious H.D. dependence.
41	1061.2	Broad feature. Present in one crystal only.
55	1270.5	Weak feature. Apparent only after H.D. of at least 60 hours
56	1274.1	Broad feature. Optimised for 16-36 hours H.D.
59	1318.8	Structure on C site line. Appears after 24 hours H.D.

5.4.3 Comparison with the Results of the Optical Study

A considerable amount of the absorption intensity of a crystal hydrogenated for more than 24 hours is due to the lines of the D, E and F sites. This observation is consistent with the large optical absorption by Er^{3+} ions in such corresponding sites of 'near cubic' symmetry (see Figure 5.2).

The H^- ion T_d symmetry site does not involve an Er^{3+} ion and hence has no optical region transitions.

Correlation of the infra-red and optical C_{4V} site is well established (Edgar *et al.* 1979) and was consistent with the observations in this study.

The infra-red B and A sites which are correlated to the optical R and J sites respectively, correspond to the vibrational modes of the interstitial hydride ion rather than to the substitutional hydride ion. The latter modes were well established by laser excitation but have frequencies in regions obscured by lines of site C and site H.

The remaining principal features of the optical absorption spectra are the sites of Family B. The local modes of these sites are known for D^- ions by vibronics (Table 5.13) but are not known directly for H^- ion equivalents. Using an expected reduced mass factor of 1.38, these modes would be expected (within 1% variation) to have the following sets of local mode frequencies :

(766, 897, 987, 1050, 1228 and 1375) cm^{-1} for the L site,
(767, 889, 925, 1032, 1295 and 1376) cm^{-1} for the T site, and
(778, 886, 985, 1062, 1302 and 1366) cm^{-1} for the N site.

Only the second lowest frequency mode for each site and the third lowest for the T site are in a region not swamped by the intense, known absorption lines. These frequencies are very close to those of several unassigned lines described in Table 5.18. On the basis of frequency matching and approximate intensity dependence on the duration of hydrogenation treatment, three lines are tentatively assigned :

Number 10	910.0 cm^{-1}	(L site)
8	899.0 cm^{-1}	(T site)
14	930.7 cm^{-1}	(T site)

Absorption intensities for lines in other regions were difficult to compare.

5.4.4 Deuterium/Hydrogen Mixed Crystals

In the $CaF_2:Er^{3+}$ crystal hydrogenated in a 1:1 mixture of hydrogen and deuterium gas, the second harmonic of the D^- ion T_d site line was observed at 1384.0 cm^{-1} with an intensity ratio to the equivalent H^- site line of 1.17 ± 0.8. A fundamental frequency vibration for the D^- R site was observed at 830.0 ± 0.5 cm^{-1} corresponding to the H^-B site line at 1148.2 cm^{-1} together with some structure around 862 cm^{-1} and 870 cm^{-1} that is also attributed to the

presence of D^- ion modes. These were insufficiently resolved to assign their hydrogenic equivalents.

An interesting feature noted for the mixed crystal was the observation of shifts in energy of the hydrogenic local mode frequencies of the infra-red B site. The B site local mode frequencies determined in the crystal were (1065.8 ± 0.4) cm^{-1} and (1145.8 ± 0.4) cm^{-1}, a shift with respect to the pure H^- ion site of 4.2 cm^{-1} and 2.4 cm^{-1} respectively. Such a shift is consistent with the R site model proposed in Section 5.3.3(b), with the new absorption features in the spectrum being the superposition of the lines of the standard H^- variety of the site and the lines of a new centre involving a substitutional D^- ion about the interstitial H^- ion -Er^{3+} ion pair.

5.4.5 Tritium/Hydrogen Mixed Crystal

None of the fundamental frequency local modes could be observed for the case of tritium because the host lattice has strong absorption in the expected spectral region.

A new line observed at 1211.4 ± 0.7 cm^{-1} was assigned to the second harmonic of the T^- analogue of the T_d site line. In addition, four new lines were observed in the tritiated crystal spectrum that were not in the H^- ion system. These were at frequencies 846.8, 856.4, 938.9 and 999.2 cm^{-1} and Figure 5.30 shows the low frequency modes of the tritiated crystal.

The intense lines at 938.9 cm^{-1} and 999.2 cm^{-1} correspond to a site of C_{3V} symmetry involving an Er^{2+} - H^- ion pair which has previously been found only after x or γ

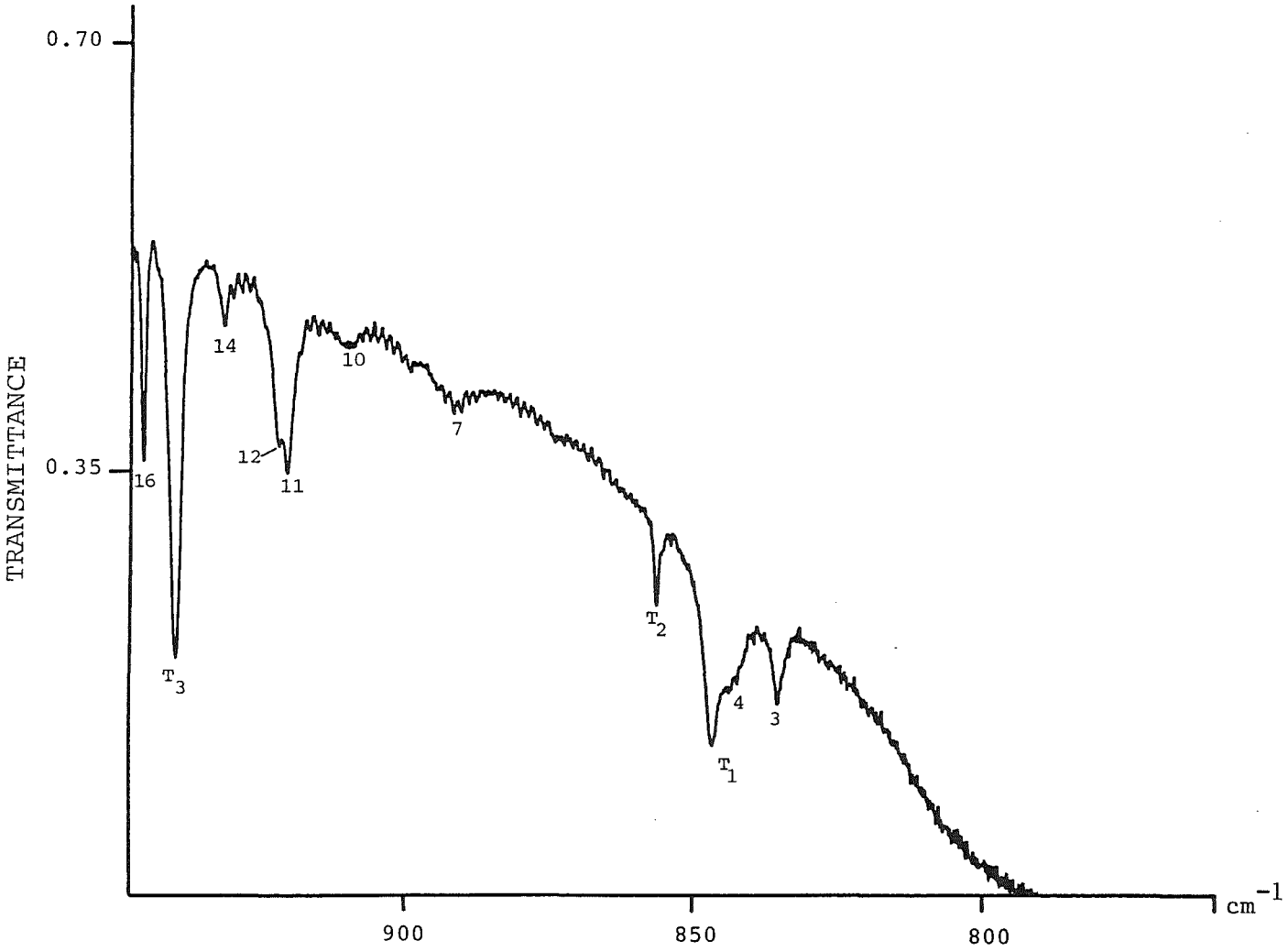

Figure 5.30 : Low frequency region of the local mode spectrum of a 2.08 mm thick tritiated CaF:0.05%Er^{3+} crystal. The modes labelled T_1, T_2 and T_3 were not observed in hydrogenated crystals. T_3 is a local mode of an H^- ion in an Er^{3+} ion site produced by beta irradiation by the tritium in the crystal.

irradiation of the sample by an external source (Chambers and Newman 1971). Such irradiation results in reduction of the rare-earth ion from the trivalent to divalent state (Merz and Pershan 1967). It is proposed that the site is formed in this case by the radioactive beta decay of the tritium ions in the crystal irradiating and reducing the Er^{3+} ions present. Such implantation of a radioactive source may have application to other crystal systems.

5.5 Spectroscopy of Fluoride Ion Sites

During the course of this study measurements on both new and previously known fluoride ion compensation sites were undertaken for three reasons:

(a) In the determination of the spectroscopy of any new sites in the hydrogenic crystals it was necessary to categorise all of these F^- ion site transitions before assigning some of the hydrogenic site transitions.

(b) As polarisation dependence has not yet been reported for any of the F^- sites, this was investigated for the F^-A and B sites in light of the predictions of Chapter Four.

(c) Basic spectroscopy of all F^- sites was needed for any investigation of unreported upconversion of the single ion Er^{3+} sites using the c.w. dye laser.

Each of these features is now discussed in turn.

5.5.1 New Fluoride Ion Charge Compensated Sites

Five further sites additional to those of Tallant and Wright (1975) were identified in the laser excitation study, with maximum fluorescence intensities of between 1% and 10% of the well-established F^-A and B sites, but showing no distinct lines in the absorption spectra.

The sites have been labelled F1-F5 and are attributed to F^- ion charge compensation, since two (F1 and F2) appear in the parent crystals (as obtained from Optovac), and the other three appear in crystals thermally cycled to 860°C with aluminium either in vacuum or as part of the hydrogenation treatment. The site distribution, emission intensity and frequencies of transitions were identical for hydrogenated and deuterated crystals. As expected, no vibronic transitions were found in any spectral region and no correlation with oxygen content, monitored by the intensity of the $Z_1 \rightarrow E_1$ transition of the G1 site (Gustafson 1978), was established.

Table 5.19 summarises the energy levels determined for these sites.

5.5.1(a) *The F1 and F2 Sites*

These sites were found to be 4.5 times more intense for 0.1%Er^{3+} crystals than for 0.05%Er^{3+} crystals and were not observed at all in 0.01%Er^{3+} samples. Typical spectra for the 0.05%Er^{3+} crystals are shown in Figure 5.31.

The two sites were found to show coupled behaviour in

TABLE 5.19: Energy levels (in cm^{-1}) of the F1 to F5 sites as derived from the 10K fluorescence spectra of CaF_2: 0.05% Er^{3+} crystals.

	F1	F2	F3	F4	F5
E_2	18604.0±0.5	18605.5±0.5	18537.6±0.5	18528.9±0.5	18503.3±0.5
E_1	18585.1 "	18579.5 "	18484.2 "	18487.5 "	18469.8 "
D_3	15455.0 "	-	-	-	-
D_2	15441.0 "	15463.5 "	15397.2 "	15389.5 "	-
D_1	15431.4 "	15432.0 "	15373.2 "	15362.5 "	15334.5 "
Y_7	6840.0±1.5	-	6920.5±1.5	6891.9±1.5	6842.0±1.5
Y_6	6806.0 "	6891.0 1.5	6870.5 "	6874.7 "	6821.0 "
Y_5	6777.0±1.0	6880.0±1.0	6861.0±1.0	6833.2±1.0	6804.0±1.2
Y_4	6734.5 "	6867.0 "	6849.0 "	6820.9 "	6784.5±1.0
Y_3	6695.5 "	6674.5 "	6627.5 "	6631.7 "	6629.5 "
Y_2	6677.5 "	6626.0 "	6614.2 "	6608.8 "	6600.0 "
Y_1	6624.0 "	6621.5 "	6612.0 "	6596.8 "	6582.5 "
Z_8	438.5 "	618.0 "	617.2 "	554.5 "	492.0 "
Z_7	409.0 "	560.0 "	530.0 "	524.7 "	452.5 "
Z_6	379.0 "	521.2 "	501.2 "	476.0 "	432.0 "
Z_5	258.5 "	499.5 "	489.0 "	453.3 "	405.0 "
Z_4	243.0 "	115.5 "	111.0 "	116.7 "	122.5 "
Z_3	201.5 "	92.0±0.8	81.2±0.8	82.1±0.8	94.0±0.8
Z_2	38.0±0.4	69.2±0.4	69.5±0.4	59.0±0.4	45.5±0.5
Z_1	0	0	0	0	0

that excitation of transitions to one site always revealed some fluorescence from the other, even though their energy levels are distinct. In particular, the sites exhibited efficient upconversion; pumping either site gives a strong upconversion spectrum containing both sites in constant proportion.

The assignment of energy levels (Table 5.19) was unambiguous for the $^4S_{3/2}$, $^4F_{9/2}$ and $^4I_{15/2}$ manifolds. However the E → Y transitions were difficult to assign, since the F2 lines are weak compared to F1 with the fluorescence always being mixed.

The emission lines of the F1 site showed no distinct polarisation dependence for either <111> or <100> geometry, whereas the F2 site fluorescence had marked <100> but no <111> polarisation. As an example, for $Z_1 \rightarrow E_1$ excitation the ratios x(yx)z:x(yy)z for transitions from E_1 to Z_2, Z_3 and Z_4 were 0.57, 0.57 and 6.2 respectively.

The energy levels of the F1 site bear a close resemblance to the F^- B site, while those of the F2 site resemble those of the F^- J and L sites in SrF_2 and BaF_2 respectively (Aizenberg *et al.* 1973a) (See Chapter Six),whose levels are similar to those of the cubic site (Table 5.2).

It appears that the F1 and F2 sites form a neighbouring pair of weakly coupled Er^{3+}-F^- dipoles. Each Er^{3+} ion has a different site symmetry with distinctly different crystal field levels but the Er^{3+} -Er^{3+} separation is sufficiently small to give efficient upconversion. The crystal field at each Er^{3+} site in the centre is modified by the presence of the other Er^{3+} ion, thereby accounting for the simultaneous

Figure 5.31 : 10K fluorescence spectra of the F1 and F2 sites :

(a) $^4F_{9/2} \rightarrow {}^4I_{15/2}$, for $Z_1 \rightarrow D_1$ excitation of F1 site.

(b) $^4F_{9/2} \rightarrow {}^4I_{15/2}$, for $Z_1 \rightarrow D_1$ excitation of F2 site.

(c) $^4S_{3/2} \rightarrow {}^4I_{15/2}$ upconversion, for $Z_1 \rightarrow D_1$ excitation of F1 site.

(d) $^4S_{3/2} \rightarrow {}^4I_{13/2}$, for $Z_1 \rightarrow E_2$ excitation of F1 site.

In (c) and (d), transitions from $^4S_{3/2}$ are labelled by F1 and F2 as appropriate.

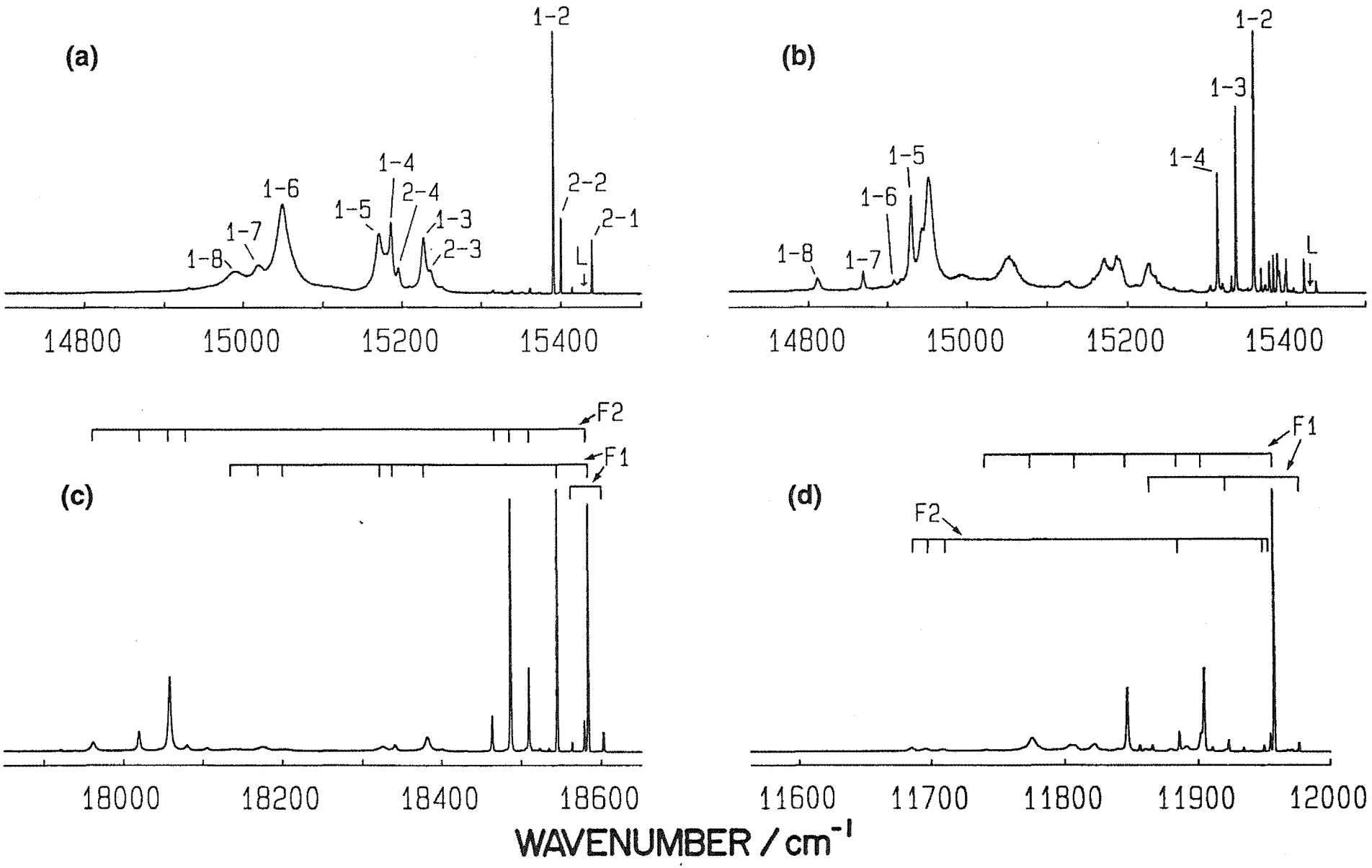
(a)
1-2
1-6
1-4
2-4
1-5
1-3
2-2
1-7
2-1
1-8
2-3
L
14800
15000
15200
15400
(b)
1-2
1-3
1-5
1-4
1-6
1-8
1-7
L
14800
15000
15200
15400
(c)
F2
F1
18000
18200
18400
18600
(d)
F1
F2
11600
11700
11800
11900
12000
WAVENUMBER / cm-1

presence of the two sites and the observed concentration dependence.

A possible pair of Er^{3+} ions in such a centre is shown in Figure 5.32. The Er^{3+} ion labelled (a) has charge compensation more remote than the next nearest neighbour interstitial position but experiences a weak axial field from ion (b) in the <100> direction. This ion therefore has crystal field levels split only slightly from the cubic site levels, since the immediate cage of fluoride ions is not significantly perturbed from cubic symmetry, but transitions may exhibit some tetragonal symmetry polarisation dependence caused by the axial field. This site corresponds to the behaviour of the F2 site. The F1 site has energy levels similar to the F^-B site consistent with an ion in position (b). The reduction of <111> polarisation dependence for the site may be the result of the weak axial field exerted by the other Er^{3+} ion, (a).

5.5.1(b) *The F3, F4 and F5 Sites*

These sites are enhanced by the hydrogenation process and can also be selectively pumped with no other site lines appearing in a vacuum cycled crystal. Typical spectra for $Z_1 \rightarrow E_1$ or $Z_1 \rightarrow E_2$ excitation are shown in Figure 5.33. It is clear that the sites have similar spectra and energy levels, suggesting similar site configuration. There is sufficient evidence to conclude that these sites involve a single Er^{3+} ion, viz :

(a) They have J+½ energy levels for each multiplet.

(b) They exist at low Er^{3+} concentration (0.01%).

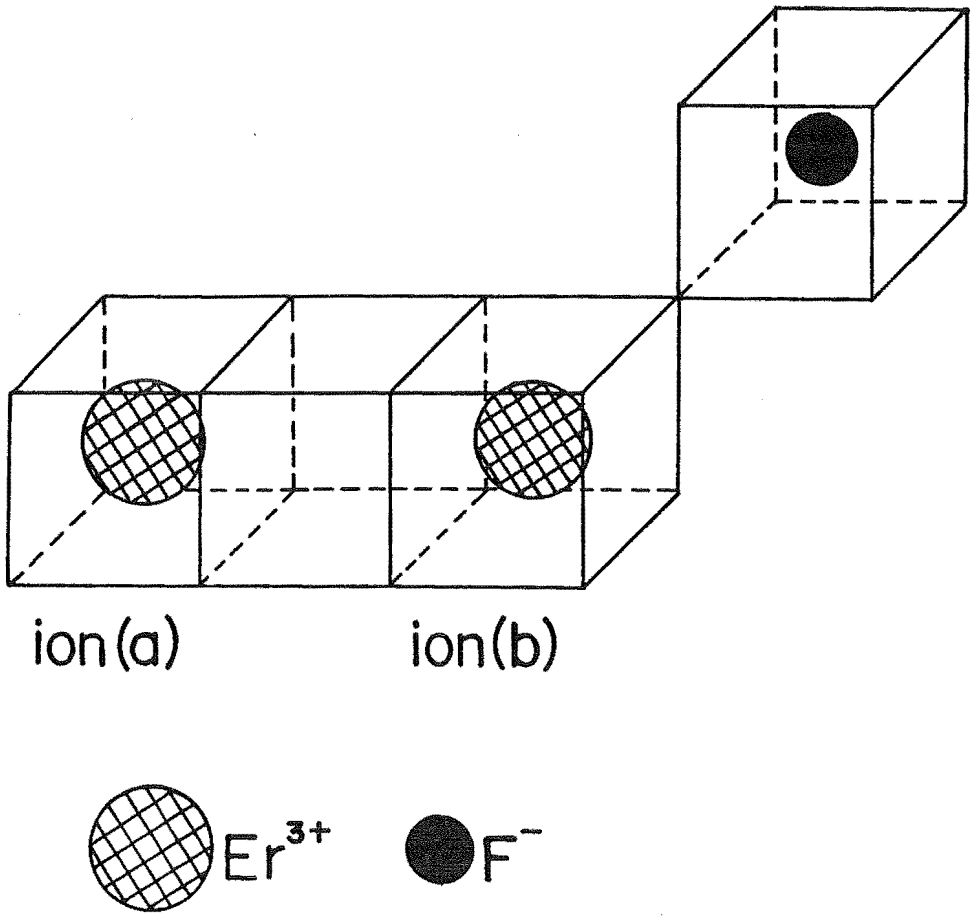

Figure 5.32 : Possible configuration for the coupled F1 (ion (b)) and F2 (ion (a)) fluoride ion sites. Ion (a) has remote charge compensation.

(c) They are enhanced rather than diminished by vacuum cycling of the crystal.

(d) No evidence of upconversion was found.

These sites all exhibit <111> geometry polarisation dependence with varying degrees of <100> dependence.

The site with the most distinct trigonal symmetry is the F3 site and the polarisation ratios for the <111> geometry of the site are summarised in Table 5.20. Ratios are not included for the $E_1 \rightarrow Y_4$, Y_5, Y_6 or Y_7 transitions since these were too weak to be reliably measured. Included in the table is the assignment of wavefunction symmetry labels that best fits the predicted ratios of Table 4.4. This assignment is consistent with γ_4 symmetry for the E_1 level and $\gamma_{5,6}$ for the E_2 level. Since the values are not precisely those expected in all cases, some degree of mixing of the wavefunctions must be occurring, indicating that the site may have a slight deviation from exact trigonal symmetry.

It was found that the F3 site had no <100> polarisation dependence, whereas the F4 and F5 sites have less distinct <111> ratios but also some <100> variation.

There are two main possibilities for additional F^- ion sites involving a single Er^{3+} ion:

(a) *Sites formed by the F^-A or B sites trapping an additional F^- interstitial ion.* These have been predicted, by computer simulation of energies of formation, to be at least marginally stable in CaF_2:Er^{3+} (Corish *et al.* 1982). The site

Figure 5.33 : 10K fluorescence spectra of the F3 site ((a) - (c)), the F4 site ((d) - (f)), and the F5 site ((g) - (i)) :

(a), (d), (g) $^4S_{3/2} \rightarrow {}^4I_{15/2}$, for $Z_1 \rightarrow E_1$ excitation.

(b), (e), (h) $^4F_{9/2} \rightarrow {}^4I_{15/2}$, for $Z_1 \rightarrow E_1$ excitation.

(c), (f), (i) $^4S_{3/2} \rightarrow {}^4I_{13/2}$, for $Z_1 \rightarrow E_2$ excitation.

L identifies the laser excitation position.

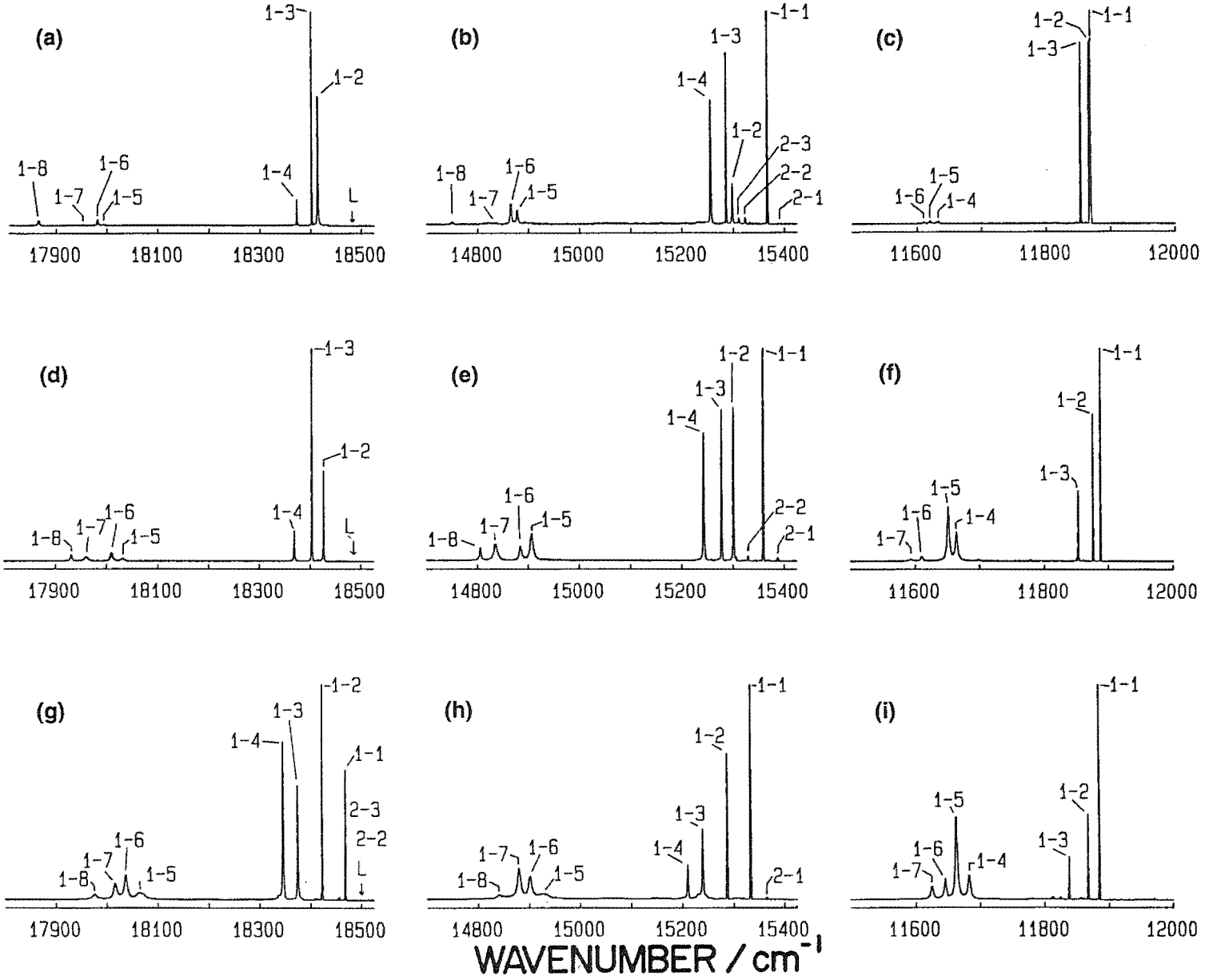
(a)
(b)
(c)
(d)
(e)
(f)
(g)
(h)
(i)
1-1
1-2
1-3
1-4
1-5
1-6
1-7
1-8
2-1
2-2
2-3
L
17900
18100
18300
18500
14800
15000
15200
15400
11600
11800
12000
WAVENUMBER / cm-1

TABLE 5.20 : Intensity ratios of the polarised emission transitions from the E_1 level of the F3 site in <111> oriented CaF_2 :0.05%Er^{3+} crystals. The predicted ratios are those assuming $\gamma_{5,6}$ and γ_4 symmetry for the E_1 and E_2 levels respectively. Uncertainties are ±10% except where indicated.

Lower State	Proposed irrep label	Pump $Z_1\gamma_4 \rightarrow E_1\gamma_{5,6}$ Observed	Pump $Z_1\gamma_4 \rightarrow E_1\gamma_{5,6}$ Expected	Pump $Z_1\gamma_4 \rightarrow E_2\gamma_4$ Observed	Pump $Z_1\gamma_4 \rightarrow E_2\gamma_4$ Expected
Z_1	γ_4	-	$\frac{15}{11}$	0.70	0.43 → 1.36
Z_2	$\gamma_{5,6}$	$\frac{4.6}{7}$	$\frac{3}{7}$	1.72	0.43 → 3.0
Z_3	γ_4	$\frac{14.5}{11}$	$\frac{15}{11}$	0.69	0.43 → 1.36
Z_4	γ_4	$\frac{14.9}{11}$	$\frac{15}{11}$	0.68	0.43 → 1.36
Z_5	γ_4	$\frac{(12.7\pm1.9)}{11}$	$\frac{15}{11}$	0.91	0.43 → 1.36
Z_6	$\gamma_{5,6}$	$\frac{4.6}{7}$	$\frac{3}{7}$	1.62	0.43 → 3.0
Z_7	γ_4	$\frac{13.1}{11}$	$\frac{15}{11}$	0.81	0.43 → 1.36
Z_8	$\gamma_{5,6}$	$\frac{4.4}{7}$	$\frac{3}{7}$	1.70	0.43 → 3.0
Y_1	$\gamma_{5,6}$	$\frac{4.3}{7}$	$\frac{3}{7}$	1.71	0.43 → 3.0
Y_2	γ_4	$\frac{13.0}{15}$	$\frac{15}{11}$	0.78	0.43 → 1.36
Y_3	γ_4	$\frac{13.0}{15}$	$\frac{15}{11}$	1.24	0.43 → 1.36

predicted to be the most stable is shown in Figure 5.34.

(b) *Sites involving lattice vacancies.* The effect of aluminium during the hydrogenation process is to scavenge F^- ions from the crystal to form AlF_3 at the surface. This may enhance the formation of vacancy sites.

Techniques revealing site symmetries such as EPR or ENDOR would be needed for more definite site configurations to be assigned.

5.5.2 Polarisation Dependence of Previously Known Sites in the <111> Geometry

As described in Chapter Four, the polarisation of emission measured for the <111> crystal geometry of the erbium sites can give useful information about the site symmetry. The positive identification of trigonal site symmetries is made simply by observation of the presence of <111> geometry dependence and the simultaneous absence of <100> dependence. In addition, the predicted intensity ratios summarised in Table 4.4 can be used to identify the group symmetry irrep label of wavefunctions for the various energy level of sites with exact trigonal or tetragonal symmetry.

C_{3V} symmetry had been previously experimentally determined for the F^- B site by an optical Zeeman study of two absorption lines (Rector *et al.* 1966), that were subsequently assigned to the site (Tallant and Wright 1975),

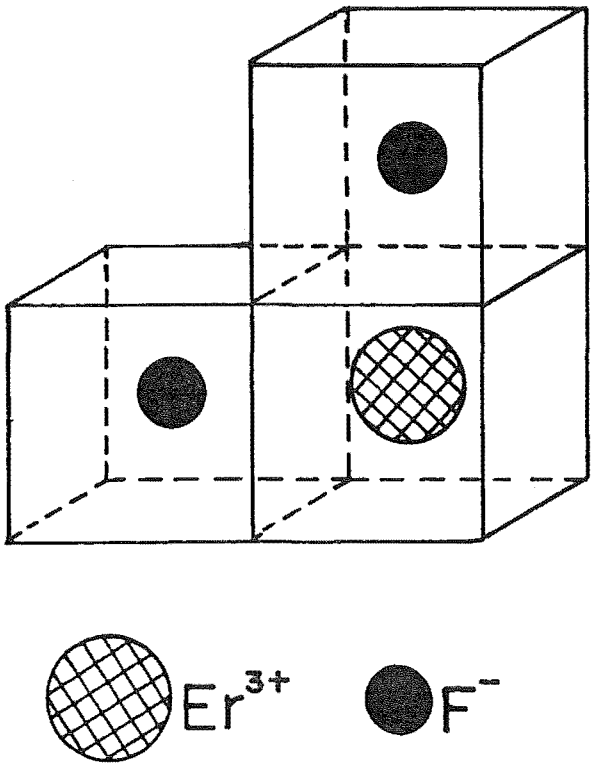

Figure 5.34 : A double interstitial ion charge compensation site predicted by Corish *et al.* (1982) to be stable in CaF_2:Er^{3+}. The site has not previously been experimentally observed.

and for the O^{2-} compensation site G1 (Gustafson 1978) by an EPR study (Reddy *et al.* 1971). In this study transitions for both sites were found to have distinct polarisation dependence for the <111> geometry and the required null dependence on the <100> geometry. The polarisation data for the G1 oxygen site was recorded and is included in Table 5.21. The B site was studied in more detail.

5.5.2(a) *The B Site*

The F^-B site is of particular interest as the assignment of an exact symmetry to the centre has been the subject of recent literature discussion (Welsh 1985 and references therein). The crystal field levels are apparently distinctly different from those of the trigonal sites in BaF_2 and SrF_2, and a comprehensive Zeeman study has not been performed since the energy levels of the site were fully classified (Tallant and Wright 1975). For this reason the various transitions of this site were studied in detail.

For C_{3V} symmetry sites the wavefunctions have either τ_4 or $\tau_{5,6}$ symmetry. The $^4S_{3/2}$ multiplet is split into two energy levels by the trigonal crystal field, with one level being of τ_4 type and one of $\tau_{5,6}$ type. Both the $Z_1 \rightarrow E_2$ transitions could be pumped for the B site, and the most accurately measured fluorescence transitions, since they have no overlap with other transitions, are $E_1 \rightarrow Z_1$, $E_1 \rightarrow Z_2$ and $E_2 \rightarrow Z_2$. The latter transition only appears at a useful intensity if the $Z_1 - E_2$ transition is pumped, and the observed polarisation ratios for such excitation are listed in Table 5.22.

Table 5.21 : Intensity ratios observed for the polarised emission transitions of the G1, oxygen compensated, site in <111> oriented CaF_2:0.05%Er^{3+}.

Uncertainties are ±10%.

Transition	Observed ratio ($Z_1 \rightarrow E_1$ excitation)	Observed ratio ($Z_1 \rightarrow E_2$ excitation)
$E_1 \rightarrow Z_1$	-	1.00
Z_2	0.59	0.93
Z_3	1.23	1.00
Z_4	1.16	obscured
Z_5	0.84	obscured
Z_6	0.62	0.83
Z_7	0.90	obscured
Z_8	0.64	0.89
Y_1	1.19	1.06
Y_2	0.59	0.95
Y_3	1.20	0.89
Y_4	0.60	1.00

Table 5.22 : Predicted and experimentally determined polarisation dependence of the $F^{-}B$ site emission transitions in a <111> geometry for the ratio x'(y'y')z :x'(y'x')z'. Uncertainty is ±10% except where indicated

Laser Pumping transitions	Upper state	Proposed irrep label	Fluorescence transition: Lower state	Fluorescence transition: Proposed irrep label	Polarisation Ratio: Observed	Polarisation Ratio: Expected
$Z_1 \rightarrow E_1$	E_2	γ_4	Z_1	γ_4	0.60	0.43→1.36
($\gamma_4 \rightarrow \gamma_{5,6}$)			Z_2	$\gamma_{5,6}$	$\frac{15.0}{11}$	$\frac{15}{11}$
	E_1	$\gamma_{5,6}$	Z_2	$\gamma_{5,6}$	$\frac{3.2}{7}$	$\frac{3}{7}$
			Z_3	γ_4	$\frac{14.7}{11}$	$\frac{15}{11}$
			Z_4	γ_4	$\frac{(15.5\pm2.3)}{11}$	$\frac{15}{11}$
			Z_5	$\gamma_{5,6}$	$\frac{(2.8\pm0.4)}{7}$	$\frac{3}{7}$
			Z_6	γ_4	$\frac{(14.8\pm2.2)}{11}$	$\frac{15}{11}$
			Z_7	γ_4	$\frac{(14.7\pm2.2)}{11}$	$\frac{15}{11}$
			Z_8	$\gamma_{5,6}$	$\frac{(3.7\pm0.7)}{7}$	$\frac{3}{7}$

Continued next page

Table 5.22 continued

Laser Pumping transitions	Upper state	Proposed irrep label	Fluorescence transition: Lower state	Fluorescence transition: Proposed irrep label	Polarisation Ratio: Observed	Polarisation Ratio: Expected
	D_2	$\tau_{5,6}$	Z_1	τ_4	$\frac{15.0}{11}$	$\frac{15}{11}$
	D_1	$\tau_{5,6}$	Z_1	τ_4	$\frac{15.0}{11}$	$\frac{15}{11}$
			Z_2	$\tau_{5,6}$	$\frac{3.2}{7}$	$\frac{3}{7}$
	E_1	$\tau_{5,6}$	Y_1	τ_4	$\frac{14.7}{11}$	$\frac{15}{11}$
			Y_2	$\tau_{5,6}$	$\frac{3.0}{7}$	$\frac{3}{7}$
			Y_3	τ_4	$\frac{14.6}{11}$	$\frac{15}{11}$
			Y_4	τ_4	$\frac{14.6}{11}$	$\frac{15}{11}$
			Y_5	τ_4	$\frac{(14.9\pm2.2)}{11}$	$\frac{15}{11}$
			Y_6	$\tau_{5,6}$	$\frac{(3.5\pm0.6)}{7}$	$\frac{3}{7}$
			Y_7	τ_4	$\frac{(15.0\pm2.3)}{11}$	$\frac{15}{11}$

Continued next page

Table 5.22 continued

Laser Pumping transitions	Upper state	Proposed irrep label	Fluorescence transition: Lower state	Fluorescence transition: Proposed irrep label	Polarisation Ratio: Observed	Polarisation Ratio: Expected
$Z_1 \rightarrow E_2$	E_2	γ_4	Z_2	$\gamma_{5,6}$	0.89	0.43→1.36
($\gamma_4 \rightarrow \gamma_4$)						
	E_1	$\gamma_{5,6}$	Z_1	γ_4	0.74	0.43→1.36
			Z_2	$\gamma_{5,6}$	1.67	0.43→3.0
			Z_3	γ_4	0.71	0.43→1.36
			Z_4	γ_4	0.70±0.10	0.43→1.36
			Z_5	$\gamma_{5,6}$	1.20±0.20	0.43→3.0
			Z_6	γ_4	0.67±0.10	0.43→1.36
			Z_7	γ_4	0.74±0.11	0.43→1.36
			Z_8	$\gamma_{5,6}$	1.38±0.21	0.43→3.0

The unique assignment from the information obtained for such excitation when compared to the ratios predicted in Chapter Four is the following :

Z_1	γ_4
Z_2	$\gamma_{5,6}$
Z_8	$\gamma_{5,6}$
E_1	$\gamma_{5,6}$
E_2	γ_4

This combination of levels is particularly useful since it is predicted that for $Z_1 \rightarrow E_1$ (i.e. $\gamma_4 \rightarrow \gamma_{5,6}$) excitation, all transitions from E_1 to γ_4 lower levels must have an intensity ratio $x(yy)z : x(yx)z$ equal to $\frac{15}{11}$, while those from E_1 to $\gamma_{5,6}$ lower states will have a corresponding ratio of $\frac{3}{7}$. The results for such excitations are included in Table 5.22 and the ratios for all transitions were in excellent agreement with those predicted. From these results the proposed C_{3V} symmetry of the B site is conclusively verified and the following unambiguous assignment of wavefunction type can be made :

	$^4I_{15/2}$	$^4I_{13/2}$	$^4F_{9/2}$	$^4S_{3/2}$
γ_4 type:	Z_1, Z_3, Z_4, Z_6, Z_7	Y_1, Y_3, Y_4, Y_5, Y_7		E_2
$\gamma_{5,6}$ type:	Z_2, Z_5, Z_8	Y_2, Y_6	D_1, D_2	E_1

This agrees with the number of τ_4 and $\tau_{5,6}$ levels expected for each of the multiplets. As the $^4F_{9/2}$ multiplet is expected to have only two levels of type $\tau_{5,6}$, it follows that the D_3, D_4 and D_5 levels identified by Tallant and Wright must be of type τ_4.

The ratio x(yx)z:x(zx)z for $Z_1 \rightarrow E_1$ excitation is also restricted for all transitions from E_1, to being either $\frac{11}{10}$ or $\frac{7}{8}$. This was found to be the case, within experimental uncertainty, for every transition listed in Table 5.22. However, as these ratios are predicted to be so close to unity, level assignments based on these values are less convincing than those based on the distinctly different x(yy)z:x(yx)z values tabulated.

A hitherto unreported feature of the B site fluorescence is an additional transition located (419.5 ± 0.5) cm^{-1} below the $E_1 \rightarrow Z_1$ transition. This line falls between the $E_1 \rightarrow Z_7$ and $E_1 \rightarrow Z_8$ transitions, similar to that observed for the hydrogenic Family B sites. It also exhibited distinct trigonal polarisation dependence with x(yy)z:x(yz)z ratios of 0.79 ± 0.15 and 1.24 ± 0.15 for $Z_1 \rightarrow E_2$ and $Z_1 \rightarrow E_1$ excitation respectively, and therefore appears to have a τ_4 symmetry. This is consistent with a symmetric lattice vibration phonon coupled to the Z_1 level.

5.5.2(b) *The A Site*

Confirmation of some of the wavefunction labels of the F^-A site of C_{4V} symmetry could also be obtained by examining <111> polarisation ratios for various transitions. Freeth *et al.* (1982) established the wavefunction irrep labels of

the Z_1, Z_2, Z_3, E_1 and E_2 levels by Zeeman spectroscopy and those of the other $^4I_{15/2}$ levels. The eigenfunctions of a computer crystal field fit, and the labels obtained are included in Table 5.6. Well-defined ratios, summarised in Table 4.4 are expected for $\tau_6 \rightarrow \tau_6$, or $\tau_7 \rightarrow \tau_7$ transition emission after $\tau_7 \rightarrow \tau_6$ excitation in a <111> orientation sample.

The only $^4I_{15/2} \rightarrow {}^4S_{3/2}$ F^-C_{4V} site transition of type $\tau_7 \rightarrow \tau_6$ that could be pumped is the $Z_1 \rightarrow E_2$ transition. Ratios could not be obtained for such excitation of the H^- or D^- C_{4V} sites due to unavoidable mixing with B site fluorescence.

The F^-A site $^4S_{3/2} \rightarrow {}^4I_{15/2}$ transition polarisation ratios are given in Table 5.23 and compared to those expected from the irrep labelling of levels by Freeth *et al.* The ratios of x(yy)z:x(yx)z for the $E_1 \rightarrow Z_1$, $E_1 \rightarrow Z_3$ and $E_1 \rightarrow Z_7$ transitions are in good agreement with the expected value of $\frac{9}{7}$, giving verification of τ_7 symmetry for the Z_1, Z_3 and Z_7 levels. Similarly, the $E_1 \rightarrow Z_2$ transition ratios are within the allowed range for τ_6 assignment to the Z_2 level. The $E_1 \rightarrow Z_6$ transition is weaker and has greater uncertainty in polarisation ratios due to partial overlap with other transitions and, within uncertainty, could be assigned to either τ_6 or τ_7 symmetry.

It is apparent from the table that the assignment of τ_7 symmetry to the Z_5 level is inconsistent with the polarisation information obtained for both ratios. The ratios obtained are, however, within the allowed limits for assignments of τ_6 symmetry, so it is probable that the symmetries of the Z_5 and Z_6 wavefunctions are actually

Table 5.23 : Intensity ratios of polarised emission transitions of the F^-A site in <111> oriented CaF_2:0.05%Er^{3+} crystals for laser excitation of the $Z_1 \rightarrow E_2$ ($\gamma_7 \rightarrow \gamma_6$) transition.

Uncertainty is ± 10% except where indicated.

Upper state	Lower state	Proposed* irrep label	x(yy)z:x(yx)z Observed	x(yy)z:x(yx)z Expected	x(yx)z:x(zx)z Observed	x(yx)z:x(zx)z Expected
$E_1\gamma_7$	Z_1	γ_7	$\frac{8.6}{7}$	$\frac{9}{7}$	$\frac{7.3}{8}$	$\frac{7}{8}$
	Z_2	γ_6	1.24	0.6→1.29	0.97	0.875→1.25
	Z_3	γ_7	$\frac{8.8}{7}$	$\frac{9}{7}$	$\frac{7.4}{8}$	$\frac{7}{8}$
	Z_4	γ_6	not observed	0.6→1.29	not observed	0.875→1.25
	Z_5	γ_7	$\frac{4.3}{7}$	$\frac{9}{7}$	$\frac{8.5}{8}$	$\frac{7}{8}$
	Z_6	γ_6	1.33±0.20	0.6→1.29	0.96	0.875→1.25
	Z_7	γ_7	$\frac{8.4}{7}$	$\frac{9}{7}$	$\frac{7.7}{8}$	$\frac{7}{8}$
	Z_8	γ_6	not observed	0.6→1.29	not observed	0.875→1.25

* From Freeth *et al.* (1982)

reversed from that previously reported. This observation may account for the problems encountered during a previous attempt at calculating the unpolarised intensity ratios for E → Z transitions of the site (Reid 1981). In particular, the $E_1 \rightarrow Z_6$ transition was predicted to be much larger than was observed. Such calculations, if attempted in the future, should use the polarised data determined here and should utilise a crystal field fit routine which assigns the experimental transitions to levels of definite symmetry in order to ensure the Z_5 level is fixed at τ_6 symmetry.

5.5.2(c) *The F^- C Site*

It is well established that the F^-C site consists of a pair of Er^{3+} ions with associated F^- interstitial compensation ions (Tallant and Wright 1975). Although the exact configuration is not proved, it is expected to be a site of low symmetry. The polarisation dependence of C site emission was found to be only very slight for both the <100> and <111> geometries, and determination of reproducible ratios was beyond the limits of the experimental apparatus available. Such slight dependence is consistent with proposed low symmetry configurations but does not give a clear confirmation of a particular model.

5.5.3 Upconversion of Single Er^{3+} Ion F^- Compensated Sites

The F^-C and F^-D sites involving multiple Er^{3+} ions in close proximity exhibit strong upconversion due to energy transfer from one excited ion to the other excited ion upon laser excitation (Tallant and Wright 1975, Tallant *et al.*

1975). Tallant and Wright also searched for F^-A and B site upconversion but found no evidence for this.

In this study, however, the spectrometer sensitivity used was such that fluorescence was observed from the F^-C_{4V} site $^4S_{3/2}$ multiplet for excitation of transitions to the $^4F_{9/2}$ multiplet. The intensities of upconversion transitions were a factor of 10^5 less than those obtained by direct excitation of the $^4S_{3/2}$ multiplet. Laser absorption and therefore intensity of upconverted emission was greatest for the $Z_1 \rightarrow D_2$ pumping transition which is of type $\tau_7 \rightarrow \tau_7$. Another $\tau_7 \rightarrow \tau_7$ transition is $Z_1 \rightarrow E_1$. For the <100> geometry the polarisation ratio x(yy)z:x(yx)z for the upconverted transitions $E_1 \rightarrow Z_2$, $E_1 \rightarrow Z_3$ and $E_1 \rightarrow Z_5$ were 0.79, 0.80 and 1.7 respectively, while the polarisation data of Table 5.6 yielded corresponding ratios of 1.6, 1.5 and 0.16 for direct excitation of the $Z_1 \rightarrow E_1$ transition.

Since the F^- C_{4V} site is believed to be a single Er^{3+} ion site, the upconversion mechanism involved is postulated to be the successive absorption of two photons by a single Er^{3+} ion, rather than the co-operative two Er^{3+} ion excitation process proposed for the C and D site upconversion. Such a single ion stepwise excitation process would require an appreciable lifetime for the intermediate state (Bloembergen 1959, Jouant *et al.* 1984). An alternative process is the intercluster mechanism reported for $CaF_2:Pr^{3+}$ (Lezama *et al.* 1986). This work reported upconversion for the Pr^{3+} ion C_{4V} site independently of the observations made here. A measurement of the upconversion lifetimes would be helpful but could not be achieved in this study. This may be due to either

insufficient power of the PRA pulsed laser available, or to the mechanism for upconversion if it involves the sequential absorption of two photons.

Upconversion for excitation of the $^4F_{9/2}$ multiplet of the B site was searched for but not found. The upper limit of upconversion intensity efficiency for the site, if it occurs at all, was determined to be 10^{-7}.

5.5.4 $^4I_{9/2}$ Level of the F^-B Site

A search was made of the spectral region 12000-13000 cm^{-1} whilst pumping the $^4I_{15/2} \rightarrow {}^4S_{3/2}$ transitions for evidence of emission from $^4I_{9/2} \rightarrow {}^4I_{15/2}$ for the H^-, D^-, T^- and F^- sites of C_{4V} symmetry. The F^- A site was the only one that showed lines due to such emission and results in the reassignment of the B_1 level. Rector *et al.* (1966) have made the only previous assignment for the level. Using optical absorption they assigned a level at 12801.2 cm^{-1} (converted to air cm^{-1}) which has subsequently been quoted by other workers (Freeth *et al.* 1982, Dieke 1968).

Three weak lines of the required spacing 0,21.4 and 32.9 cm^{-1} to be transitions from B_1 to Z_1, Z_2 and Z_3 respectively gave a value of (12385.9 ± 0.5) cm^{-1} for the B_1level. Other crystal hosts such as $LaCl_3$ (Dieke 1968) and $CsCdBr_3$ (see Chapter Eight) have strong Er^{3+} emission from the $^4I_{9/2}$ multiplet. The new value for B_1 compares more favourably with other hosts such as LaF_3 (12419.7 cm^{-1}), $LaCl_3$ (12392.7 cm^{-1}) and $LaBr_3$ (12375.4 cm^{-1}) that are summarised by Dieke.

5.5.5 New Lines of the F^-C Site

It was reported by Tallant and Wright (1975) that the F^-C site exhibited more than the J + ½ levels expected for the $^4I_{15/2}$ ground state multiplet. Detailed scans of $^4S_{3/2} \rightarrow {}^4I_{15/2}$ fluorescence were carried out in this study in an attempt to ensure that all levels of the site had been identified. Close examination of the $E_1 \rightarrow Z_2$, $D_1 \rightarrow Z_2$ and $K_1 \rightarrow Z_2$ transitions revealed structure due to five lines as shown in Figure 5.35. Tallant and Wright commented that if the average frequency of this structure is considered to be a single level, and if the levels of 53, 64, and 106 cm^{-1} are ignored, then the crystal field levels and transitions are remarkably similar to the B site.

The spectral region of frequency immediately below the reported $^4S_{3/2} \rightarrow {}^4I_{15/2}$ transitions was scanned to check for fluorescence to additional Z levels. Figure 5.36 shows the spectrum of new transtions found and correlated to the C site for excitation of both $Z_1 \rightarrow E_1$ and $Z_1 \rightarrow E_2$. The peak of the most intense transition was thirty per cent of the height of the transition from the E level to the Z level located at 429.5 cm^{-1}. Comparison of these new lines with the spectrum of $^4S_{3/2} \rightarrow {}^4I_{13/2}$ emission (Figure 5.37) shows that the transitions were from an unreported upper multiplet level at (24622.5 ± 1.0) cm^{-1} to the $^4I_{13/2}$ multiplet. Such emission is the result of upconversion to the K_1 level of the $^2H_{9/2}$ multiplet.

This spectrum is particularly useful since it is the only verification available for the previously reported $^4I_{13/2}$ levels determined by E → Y emission, and close examination verified additional structure for the multiplet.

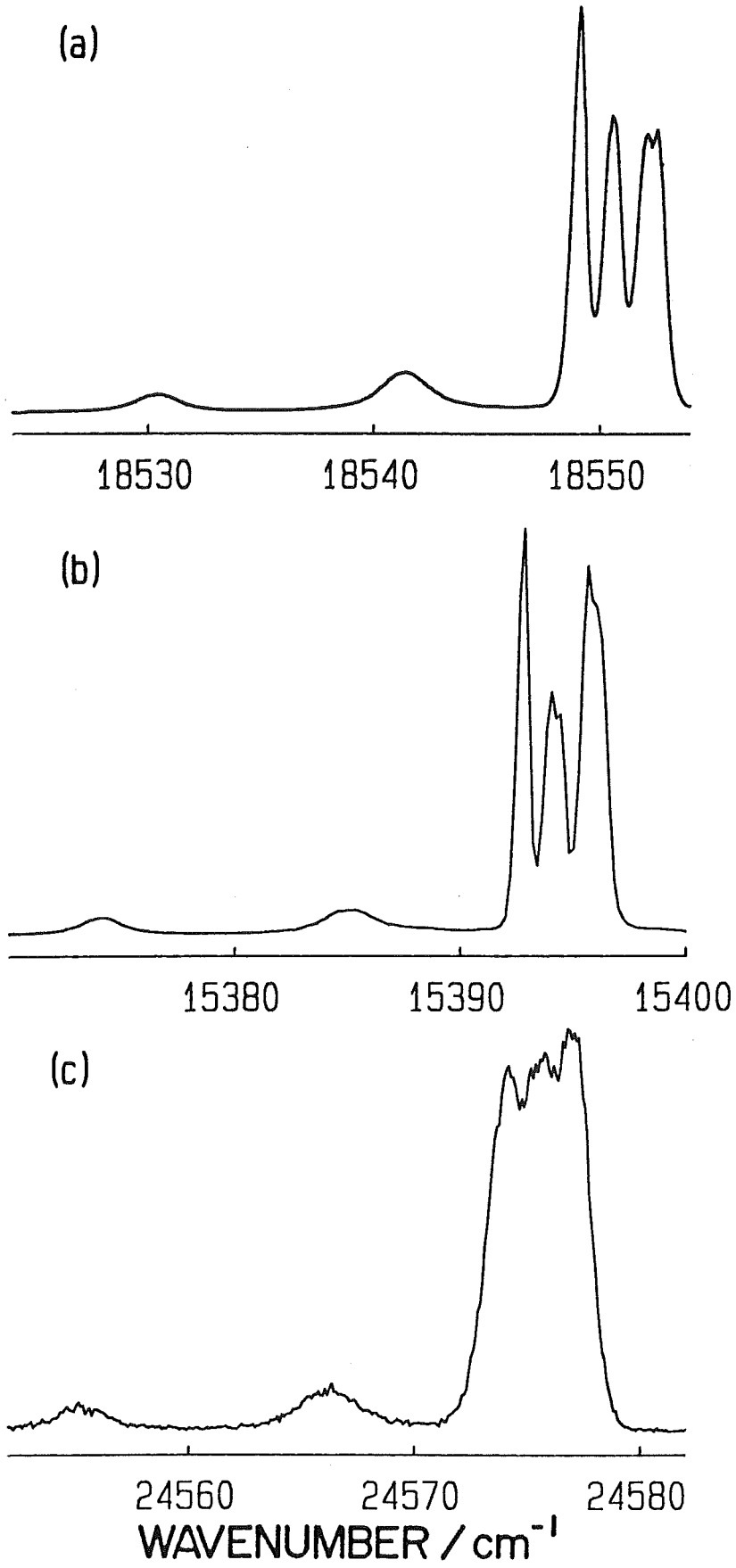

Figure 5.35 : 10K fluorescence spectra for $Z_1 \rightarrow E_2$ excitation of the F^-C site in CaF_2:0.05%Er^{3+} crystals. The higher frequency transitions in each are to the lowest levels above the ground state and are from the : (a) E_1 level, (b) D_1 level, and (c) K_1 level.

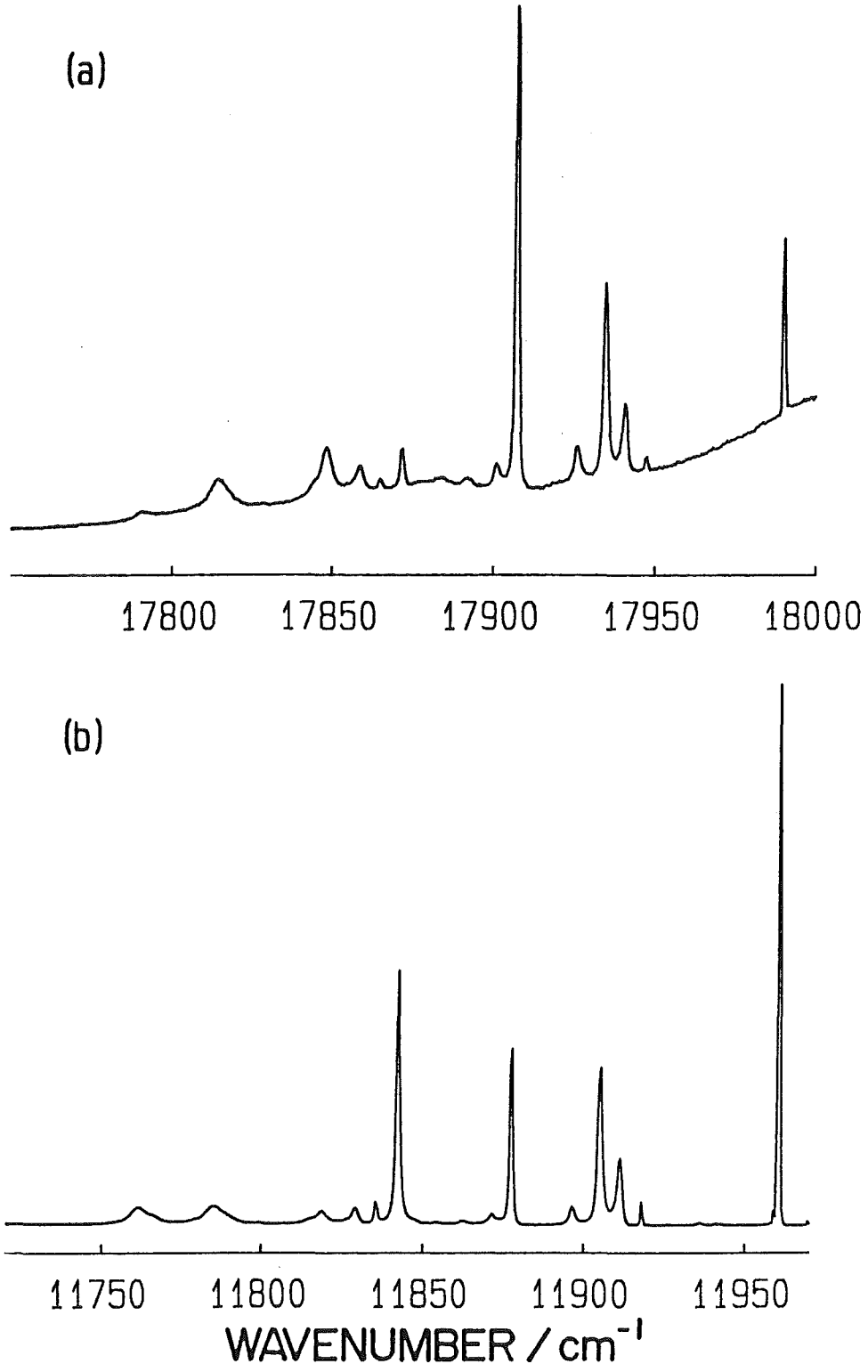

Figure 5.36 : 10K fluorescence for $Z_1 \rightarrow E_2$ excitation of the F^-C site in CaF_2:0.05%Er^{3+} : (a) the newly identified $^2H_{9/2} \rightarrow {}^4I_{13/2}$ transitions, and (b) (for comparison) the $^4S_{3/2} \rightarrow {}^4I_{13/2}$ transitions.

Table 5.24: Energy levels (in cm^{-1}) for the $^4I_{13/2}$ (Y) and $^4I_{15/2}$ (Z) multiplets of the F^-C site determined by comparison of fluorescence from the $^2H_{9/2}$, $^4S_{3/2}$ and $^4F_{9/2}$ multiplets in $CaF_2:Er^{3+}$. Uncertainty is ± 0.5 cm^{-1} for Z levels and ± 1.0 cm^{-1} for Y levels except where indicated.

$^4I_{13/2}$	$^4I_{15/2}$
6830.0	475.5
6807.0	429.5
6792.0*	396.5
6676.0*	282.5
6773.0	248.0
6762.5	215.5
6756.0	106.0
6749.5	63.6
6745.0*	52.9
6738.0*	45.1
6729.5*	43.8
6720.0	43.5
6714.0	42.0
6695.0	41.7
6686.5	0.0
6680.5	
6673.5	
6631.0	

* extremely weak structure

The energy levels determined in this study for the $^4I_{13/2}$ and $^4I_{15/2}$ multiplets are included in Table 5.24.

CHAPTER SIX

SPECTROSCOPY OF DEUTERATED $SrF_2:Er^{3+}$

6.1 Introduction

6.1.1 Previous Studies of the Parent System

Although some EPR, optical and ITC work has been reported, the $SrF_2:Er^{3+}$ system has had considerably less previous attention than the $CaF_2:Er^{3+}$ system.

Brown *et al.* (1969a) (hereinafter [Br69a]) reported the first optical study on the system with broad band fluorescence and absorption measurements of SrF_2 doped with 1% to 10% of Er^{3+} showing evidence for seven sites. Lifetimes were measured for transitions from the $^4S_{3/2}$, $^4F_{9/2}$, $^4I_{13/2}$ and $^4I_{11/2}$ multiplets to the $^4I_{15/2}$ multiplet. From the fact that lifetimes are fast for four of these sites, they deduced that the bulk of Er^{3+} ions in this concentration range were in sites involving clusters of more than one Er^{3+} ion.

In a consecutive paper Brown *et al.* (1969b) (hereinafter [Br69b]) reported an EPR study of the various site symmetries present in crystals with erbium concentrations in the range 0.002 mol% to 0.7 mol%. They found in agreement with a previous report (Antipin *et al.* 1967), that a site of tetragonal symmetry (with $g_{\parallel} = 10.04 \pm 0.005$ and $g_{\perp} = 4.632 \pm 0.005$), a site of trigonal symmetry (with $g_{\parallel} = 6.163 \pm 0.005$ and $g_{\perp} = 7.038 \pm 0.007$) and a cubic symmetry site ($g = 6.775 \pm 0.006$) existed in this concentration range. Furthermore, the occurrence of the tetragonal site was found to be a factor of one hundred

weaker than the trigonal site, and both the trigonal and cubic site intensities were maximum around 0.4 mol%Er^{3+}. This paper also proposed, using the EPR data that was available at that time, that the symmetry of the dominant centre formed in SrF_2 depended on the rare-earth ion dopant radius, and changes from tetragonal to trigonal symmetry as the radius decreases across the rare-earth ion series. This was justified on the basis of a calculation of the energy of formation of tetragonal symmetry nearest neighbour (NN) and trigonal symmetry next nearest neighbour (NNN) fluoride ion compensated sites. It was proposed that the most important effect involved is the lattice contraction about the smaller RE^{3+} ion when it replaces the larger Sr^{2+} ion. No change of dominant site symmetry with rare-earth ion radius was found in the CaF_2 case.

A higher resolution optical study by Aizenberg *et al.*(1969) (hereinafter [Ai69]) of the trigonal symmetry site in $SrF_2:Er^{3+}$ and $BaF_2:Er^{3+}$ was published at the same time as Brown's papers and determined several of the $^4I_{15/2}$ and $^4S_{3/2}$ crystal field levels of the site. The lifetime of the $^4S_{3/2}$ manifold at 77K was found to be 12.1 ms. compared to 2.1 ms. for the trigonal $CaF_2:Er^{3+}$ centre. Such a variation was considered consistent with the decrease in coupling to lattice vibrations for the increased lattice constant of SrF_2. Electron-vibrational (vibronic) transitions were also observed for the trigonal site with a vibrational frequency interval of 223 cm^{-1} for the SrF_2 host and 189 cm^{-1} for the BaF_2 host, with the vibronics being strongest in the latter.

A subsequent study (Aizenberg *et al.* 1973a [Ai73a]) determined crystal field levels for the $^4I_{13/2}$, $^4I_{11/2}$, $^4G_{11/2}$, $^4F_{9/2}$, $^4F_{7/2}$, $^2P_{3/2}$ and $^2H_{11/2}$ multiplets of the trigonal erbium site by both luminescence and absorption. The resultant data was used in an attempt to calculate the lattice deformation for the Er^{3+} site using a model of electrostatic point charges.

Aizenberg and co-workers also investigated the $SrF_2:Er^{3+}$ sites of rhombic symmetry involving the charge compensation by Na^+ and K^+ ions replacing Sr^{2+} ions close to the Er^{3+} ion (Aizenberg *et al.* 1973b), and in a separate study determined the cubic symmetry site crystal field levels for Er^{3+} ions in SrF_2, CaF_2, BaF_2 and PbF_2 (Aizenberg *et al.*1972). The cubic levels were partially inferred from the presence of vibronic lines at appropriate intervals, as the electronic transitions are weak because electric dipole transitions are forbidden for sites with inversion symmetry.

$SrF_2:Er^{3+}$ crystals grown in an oxygen atmosphere were subsequently shown by EPR (Newman and Woodward 1974) to contain an $Er^{3+} - O^{2-}$ defect of trigonal symmetry, but no evidence of sites of the type $Er^{3+} - O_4^2 - F^-$, that exist in $CaF_2:Er^{3+}$, was found.

The application of the laser selective excitation technique to the $SrF_2:Er^{3+}$ system by Kurz and Wright (1977) (hereinafter [KW77]) forms the most useful summary of the sites to date. Their optical study reported nine crystallographically inequivalent sites in crystals with erbium concentrations in the range 0.001% to 0.2%. At the lower concentrations, four sites labelled J, N1, N2, and N3 are present, while at higher concentrations the sites M1,

M2, K, L1 and L2 are strongest. The site labelled J is that previously assigned ([Ai69],[Ai73a]) to the principal Er^{3+} site of trigonal symmetry. Emission spectra of the N1, N2 and N3 sites were found to be closely similar, and the sites were dominant in the 0.0001% crystals but barely observable for concentrations greater than 0.05%. The N3 site was weaker than the other N sites and all three were attributed to configurations involving a single Er^{3+} ion.

The $^4F_{5/2}$ broadband excitation spectrum for the 0.2% crystal was characterised by broadbands between 448.0 nm and 449.5 nm. The M1 and M2 sites have lines within these bands, and were assumed to be representative of other sites apparently located within the bands. For Er^{3+} concentrations decreasing between 0.05% and 0.01%, the M1 site disappeared while the M2 site remained. The short lifetimes, occurrence of upconversion and excess of crystal field levels are all indicative of clustering of Er^{3+} ions to form these sites. The behaviour of the M1 and M2 sites was paralleled to that of the D1 and D2 sites respectively for the CaF_2 case [TW75]. The L1 and L2 sites showed weaker emission than the M sites, and generally L site lines appeared as shoulders on more intense lines. From the lifetime and concentration dependence Kurz and Wright suggested that these sites were also associated with Er^{3+} clusters.

The remaining site, K, was proposed to be a pair of Er^{3+} ions which had the interesting feature that the spectral lines of each Er^{3+} ion in the pair could be distinguished, but not isolated, by changing the laser pumping transition. The lifetime dependence differs for

two sets of lines in each multiplet associated with the site. A recent study of the K site (Wietfeldt *et al.* 1986) reported the temperature and magnetic field dependence of the non-resonant energy transfer rate between the two ions of the site.

Additional information on sites in $SrF_2:Er^{3+}$ has been obtained by dipolar reorientation techniques. (Techniques are outlined in Chapter Seven.) The ionic thermocurrent (ITC) technique revealed that for most rare-earth ions in SrF_2 two peaks occurred, corresponding to a tetragonal and a trigonal site (Lenting *et al.* 1976). However, the ratio of concentrations of tetragonal to trigonal complexes decreased markedly with decreasing RE^{3+} radius; for example, it was 6.0, 0.5 and 0.07 for Gd^{3+}, Tb^{3+} and Dy^{3+} respectively. This trend is in accordance with the predictions of the model proposed by Brown *et al.* (1969b). No peak for tetragonal centres was detected for the $SrF_2:Er^{3+}$ case and the large peak located at 214.4K was attributed to reorientation of a NNN F^- interstitial charge compensating ion in a trigonal site. In a later paper (Dorenbos and den Hartog 1985) the trigonal centre was found to occur with the greatest intensity for an Er^{3+} concentration of 0.44%, in good agreement with that previously reported by EPR measurements [Br69b].

Results of the related technique of dielectric loss were described for $SrF_2:Er^{3+}$ by Andeen *et al.* (1981), Fontanella *et al.* (1978) and references therein. Again, the dominant feature at 0.1% Er^{3+} was the trigonal peak which they correlated to the optical J site. Weak dielectric loss peaks were assigned to the M site cluster,

and the optical K site was correlated to a relaxation labelled R_{IV} for which the corresponding peak in $CaF_2:Er^{3+}$ had been assigned to the C site (Fontanella *et al.* 1980). Additional weak relaxations at 0.15eV and 0.3eV were tentatively assigned to the N sites.

The simple dielectric loss peak for the $SrF_2:Er^{3+}$ system was used for the first study of the effect of pressure on the dipole reorientation peak (Andeen *et al.* 1980) and it was found that the trigonal site peak shifted to a higher temperature with the application of pressure.

The principal theoretical investigation of the stability of sites in $SrF_2:Er^{3+}$ was reported, together with corresponding predictions for CaF_2 and BaF_2 (Corish *et al.* 1982). With a more sophisticated simulation than that of Brown *et al.* (1969b), the same expected dominance of tetragonal centres for large radius RE^{3+} ions in SrF_2 was confirmed and comparable stabilities of the tetragonal and trigonal centres for smaller radius RE^{3+} ions were predicted. For the case of $SrF_2:Er^{3+}$, the experimentally observed ratio of trigonal to tetragonal sites is actually greater than predicted.

6.1.2 Previous Studies of Hydrogenated SrF_2 and $SrF_2:Er^{3+}$

The optical spectroscopy of hydrogenated SrF_2 crystals containing RE^{3+} ions has been little studied compared to the CaF_2 case.

Infra-red absorption of the undoped hydrogenated SrF_2 system has been investigated (Elliott *et al.* 1965), and revealed the frequencies of the Td symmetry site local mode

fundamental and second harmonics together with lattice phonon sidebands. These modes were subsequently confirmed by Raman scattering (Harrington *et al.* 1970) which located additional second harmonic transitions. The local mode frequencies determined were found to be reduced from those of CaF_2 due to the weaker force constant associated with the increased lattice size.

For the case of the hydrogenated $SrF_2:Er^{3+}$ system, no optical absorption or emission spectroscopy has been previously reported, while only two papers have investigated the infra-red local mode of the system as part of a study of the series of RE^{3+} ions in SrF_2 (Edgar *et al.* 1977 (hereinafter [EFJ77]), Timans and den Hartog 1976).

The two infra-red papers both reported the formation of an H^- C_{4V} symmetry site for the large radius dopant ions of La^{3+}, Ce^{3+}, Pr^{3+}, Nd^{3+} Sm^{3+}, Tb^{3+} and Dy^{3+}. Edgar *et al.* also found evidence for the Gd^{3+} and Ho^{3+} C_{4V} sites and conducted a detailed EPR study of the $SrF_2:Gd^{3+}:H^-$ system revealing three additional hydrogenic sites of rhombic symmetry. One of these, the R_1 site, was attributed to a site configuration identical to that assigned in Chapter Five to the R site in $CaF_2:Er^{3+}$. A C_s symmetry site consisting of three local modes was also found in the infra-red spectrum of $SrF_2:RE^{3+}:H^-$ (for RE = La...Ho), and was correlated for the Gd^{3+} case to the EPR R_1 site [EFJ77]. These sites were found to increase in intensity with time after hydrogenation.

For rare-earth ions of smaller radius than that of the Ho^{3+}, the C_{4V} site was not found by either group. Edgar *et al.* reported, for rare-earth dopant ions from Dy^{3+} to Lu^{3+}

and for Y^{3+}, a new low symmetry site consisting of two low frequency lines (811.3 cm^{-1} and 831.8 cm^{-1} for Er^{3+}) and one higher frequency line (1275.6 cm^{-1} for Er^{3+}). The exact symmetry of this site is not yet known. It was proposed that since the fluoride ion charge compensation mechanism was known to change from NN (tetragonal) to NNN (trigonal) between gadolinium and erbium in the rare-earth series, the site was probably related to the trigonal site configuration.

A possible site configuration to account for the three lines had an Er^{3+} - F^- dipole in a <111> configuration, with a substitutional hydride replacing a fluoride ion in the shell around the interstitial fluoride ion.

Also reported was a low intensity site that can be induced by subjecting the crystals to ultraviolet irradiation for a period of two hours [EFJ77]. The frequencies of the two lines induced in this way were (749.7 ± 0.8)cm^{-1} and (1242.5 ± 1.6)cm^{-1}. No site configuration was advanced for this centre.

6.1.3 Aim of this Study

The principal aim of this study was to characterise the hydrogenic ion sites in $SrF_2:Er^{3+}$ for erbium concentrations $\leq$ 0.05 mol%, by optical technqiues. The heavy isotope deuterium was used since hydride ion site emission intensities were too weak to be distinguished using the available experimental apparatus and techniques.

The erbium ion in SrF_2 is of particular interest for study for several reasons. The size of the ion is such that it is just beyond the cross-over point in the

rare-earth series where trigonal centres are preferentially formed over tetragonal sites involving compensation by fluoride ions. This contrasts the case of $CaF_2:Er^{3+}$ where the most readily formed site has tetragonal symmetry [RPM66].

The aim of this section was threefold. The first aim was to investigate the nature of the sites due to deuteride ion compensation to determine whether variation of the charge compensating ligand, normally a fluoride ion, affected the formation stability of the sites of various symmetries. No optical study has been previously attempted, and the application of laser selective excitaton is a powerful method for determining the energy levels and nature of the sites present. Previous infra-red reports were restricted to crystals hydrogenated for a maximum period of eighteen hours. From the large variation of site distribution observed with the increase in hydrogenation duration for the $CaF_2:Er^{3+}$ study, it was evident that crystals hydrogenated for much longer periods should also be examined for the $SrF_2:Er^{3+}$ system.

The second aim of this study was to improve the quality of information available for the previously reported fluoride ion compensation centres. The most comprehensive study to date by Kurz and Wright (1977) gave little spectroscopic data with only a few crystal field levels being reported; insufficient to allow a crystal field analysis by other workers. No satisfactory crystal field fitting of the C_{3V} symmetry centre in $SrF_2:Er^{3+}$ has been previously achieved. An early attempt by Aizenberg *et al.* (1973a) was based on less data than laser excitation can

reveal. Using the laser selective excitation data and a revised crystal field Hamiltonian, a more reliable crystal field fit was desired.

The final aim of the study was to summarise and report the spectroscopic observations of additional sites formed during the hydrogenation process that are not due to hydrogenic ion compensation. This is necessary to enable investigation of these sites by future workers, since several of the sites have interesting features in themselves. It is also necessary since accurate classification will prevent their misinterpretation by future investigators of hydrogenic sites.

6.2 Results

6.2.1 Outline

Optical absorption measurements of the $SrF_2:Er^{3+}$ system were considerably more difficult than the corresponding measurements for the $CaF_2:Er^{3+}$ case, as it was found that the absorption strengths for comparable crystal thicknesses were factors of up to twenty less. As a result the absorption spectra had to be expanded to obtain useful peak heights, and the adverse effects of increased spectral noise and accentuated sloping backgrounds due to photomultiplier tube response then became apparent.

The enhancement of the absorption peaks by amplification also enhanced the fluctuations due to experimental apparatus. The instability of the available quartz halogen light sources proved to be the greatest problem, with intensity variations sometimes of the order of the smaller absorption peaks being measured. All

absorption peaks were conclusively determined as real by comparison of several scans of each spectral region for all crystals.

In the laser selective excitation part of this study the discrimination of emission of H^- ion sites from background F^- ion sites proved to be particularly poor. As a consequence both the absorption and emission results reported are for the sites observed in the deuterated system.

As the $SrF_2:Er^{3+}$ absorption was much weaker, coupled with the absence of thermally populated Z_2 and Z_3 levels for some sites even at 70 K, it was not possible to do as much preliminary site classification by absorption alone as was possible for hydrogenated $CaF_2:Er^{3+}$ crystals, and the l.s.e. techniques were necessary almost at the outset of the study. The information from each technique complemented the other, as some transitions were not easily resolved by absorption, while others could not be pumped cleanly by the laser but were correlated by absorption.

A total of eight sites, labelled D1 to D8 involving D^- ion charge compensation nearby to the Er^{3+} ion were classified by both absorption and emission, and the energy levels determined are included in Table 6.1. An additional site involving remote charge compensation was also observed.

Detailed spectroscopic studies of the four known F^- ion compensation sites involving a single Er^{3+} ion were carried out in which energy levels for each were determined.

Furthermore, nine additional sites arbitrarily labelled S1 to S9 were found and are discussed since many of them caused discrimination difficulties with the D^- ion sites.

TABLE 6.1 : Energy levels (in cm^{-1}) of the new D^- ion sites, D1 to D8, as derived from absorption and fluorescence spectra of deuterated SrF_2 :0.035%Er^{3+} crystals. Uncertainties are ±0.5 cm^{-1} for the Z, D and E levels and ±1.0 cm^{-1} for the Y levels except where indicated.

	D1	D2	D3	D4	D5	D6	D7	D8
E_2	18580.3					18470.0	18489.0	18589.5
E_1	18564.3	18426.5±0.4	18415.3±0.4	18400.0±0.4	18453.5	18457.9	18463.8	18565.8
D_4	15479.0							
D_3	15475.7	15408.3*	15391.6*	15401.8*				
D_2	15442.1	15352.5	15342.1	15347.0	15362.0	15343.2	15360.0	15443.0
D_1	15435.8	15278.0	15265.5	15249.0	15309.5	15327.2	15329.3	15436.6
Y_7		6878.0	6831.0	6824.0		6806.5		
Y_6		6805.0	6809.0	6806.5		6752.5		
Y_5		6773.0	6786.5	6793.0		6740.0		
Y_4		6746.5	6770.5	6786.5		6729.0		
Y_3		6691.0	6704.5	6712.0	6609.7	6673.0		
Y_2		6589.5	6600.0	6603.0	6573.0	6661.5		
Y_1		6553.4±0.8	6557.4±0.8	6561.0±0.8	6554.9±0.8	6606.5		
Z_8						407.0	407.0	
Z_7		394.5	400.5	439.0	384.5	382.0	379.0	
Z_6		380.0	390.5	399.5	362.5	365.0	364.5	
Z_5		318.5	342.0	352.0	318.5	243.0	245.0	
Z_4		265.5	283.5	297.5	247.5	219.0	239.0	
Z_3	86.9±0.4	33.1±0.4	44.8±0.4	50.5±0.4	25.6±0.4	205.0	222.0	
Z_2	80.8±0.3	10.1±0.3	20.3±0.3	16.5±0.4	9.7±0.3	11.1±0.3	10.7±0.3	
Z_1	0	0	0	0	0	0	0	0

* tentative assignment by absorption only

The optical absorption spectroscopy and laser excitation results of the D^- ion sites and F^- ion sites are now discussed in more detail.

6.2.2 Optical Absorption

Optical absorption spectra of the $SrF_2:Er^{3+}$ crystals before and after deuteration were examined at 10 K, to determine the excited state multiplet levels of sites and at 20 and 70 K to determine Z_2 and Z_3 levels of the sites. Deuterated crystals showed no marked change in site distribution for the 0.035 mol% and 0.05 mol% Er^{3+} dopant levels used.

The spectra of the $SrF_2:Er^{3+}$ crystals before hydrogenation are shown in Figures 6.1(a) and 6.2(a) and for both the $^4I_{15/2} \rightarrow {}^4S_{3/2}$ spectrum and the $^4I_{15/2} \rightarrow {}^4F_{9/2}$ spectrum the dominant lines are those of the (NNN) F^- ion J site. In addition, the latter spectrum has three weak, previously unreported, absorption transitions and two weak emission peaks. The highest frequency absorption peak is attributed to the $Z_1 \rightarrow D_3$ absorption of the J site, while the other two marked U1 (at 15405.9 ± 0.5 cm^{-1}) and U2 (at 15413.3 ± 0.5 cm^{-1}) are of uncertain origin because it was not possible to gain further information from l.s.e. as the transitions were out of range of the dyes available. It is likely that they may be the $Z_1 \rightarrow D_1$ and $Z_1 \rightarrow D_2$ transitions of a previously unreported F^- ion site, with additional ground state levels at (65.2 ± 0.4) cm^{-1} and (68.1 0.4) cm^{-1} determined from the positions of the U3 and U4 emission peaks. Alternatively, the U1 and U2 peaks may be the $Z_1 \rightarrow D_1$ transitions of the N2 and N1 F^- ion sites respectively

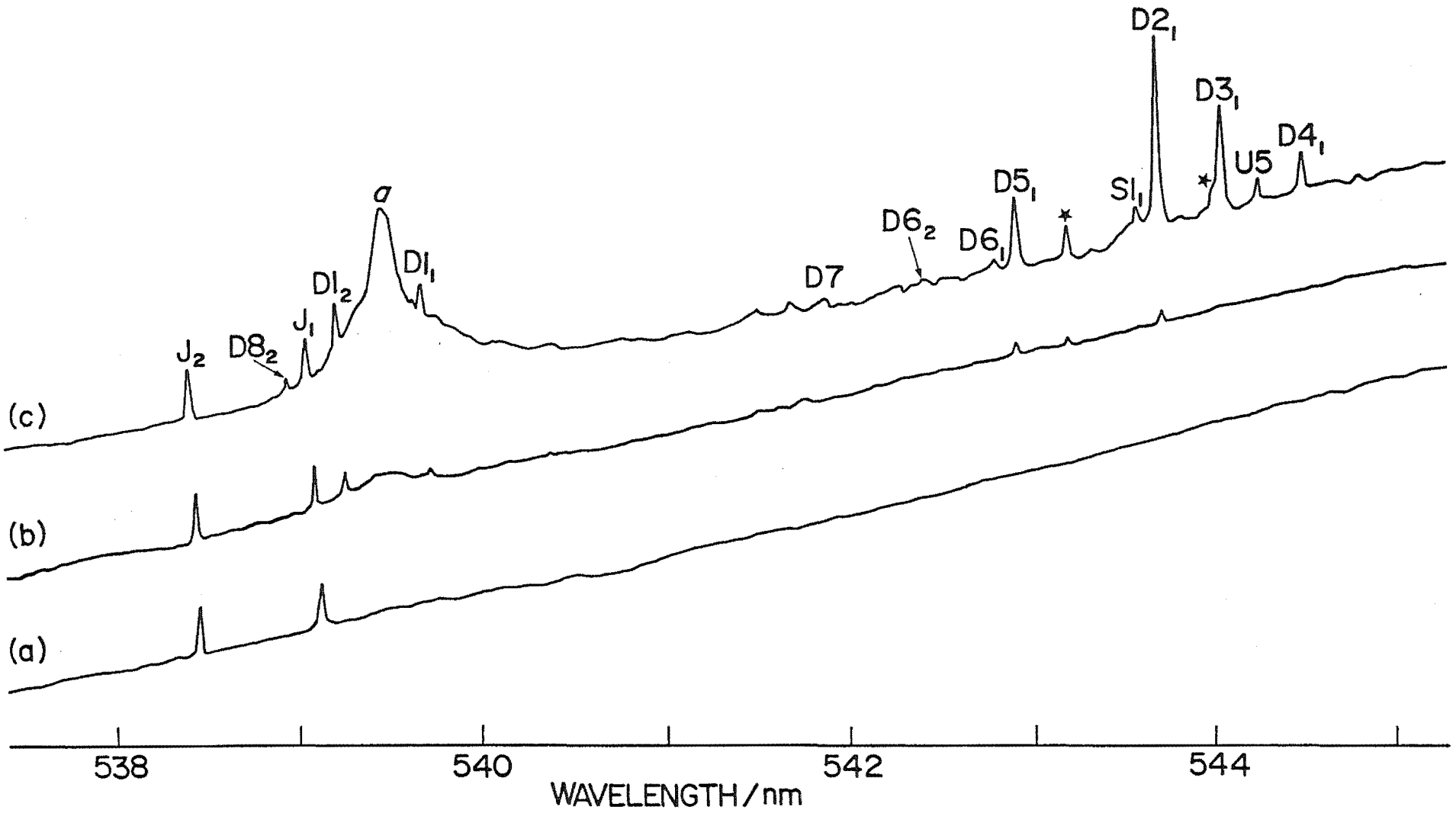

Figure 6.1 : $^4I_{15/2} \rightarrow {}^4S_{3/2}$ absorption spectra for 10 mm thick crystals of deuterated SrF_2:0.035%Er^{3+} crystals at 10K : (a) Before deuteration, (b) 16 hour deuteration, and (c) 68 hour deuteration. Transitions from Z_1 are identified by a site label and subscript representing the upper multiplet level. Stars mark transitions from Z_2 levels of sites and the transition 'a' is due to the near cubic symmetry site.

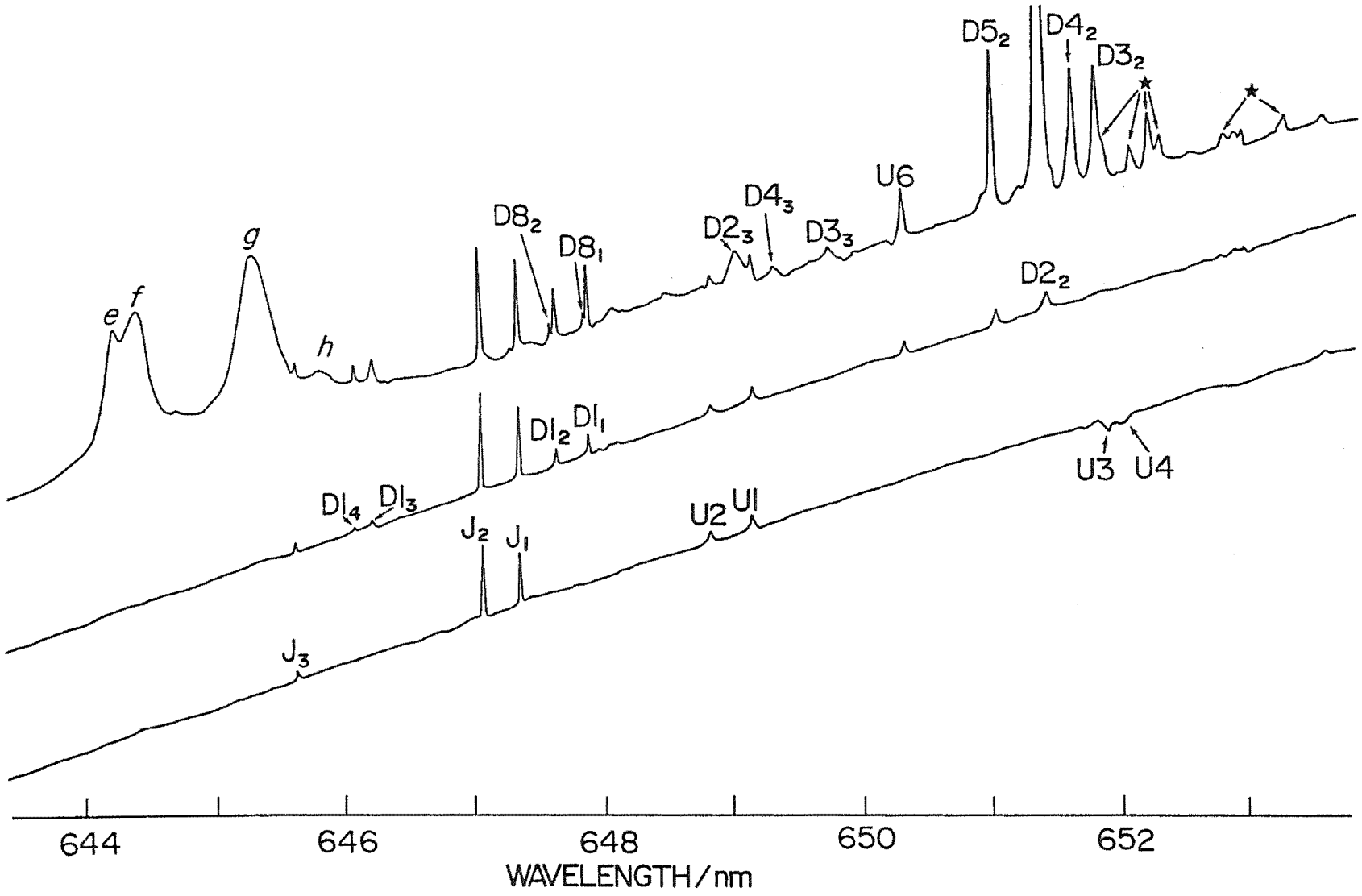

Figure 6.2 : $^4I_{15/2} \rightarrow {}^4F_{9/2}$ absorption spectra for 10 mm thick crystals of deuterated SrF_2:0.035%Er^{3+} crystals : (a) Before deuteration, (b) 16 hour deuteration, and (c) 68 hour deuteration.

that were determined, in the l.s.e. part of the study, to be of very similar frequency. This seems less likely, however, since these sites would be expected (by analogy to the F^- A site that they closely resemble) to have corresponding transitions in the $^4I_{15/2} \rightarrow {}^4S_{3/2}$ spectrum and to have a very weak $Z_1 \rightarrow D_1$ transition but more intense $Z_1 \rightarrow D_2$ transition.

Absorption spectra of the deuterated SrF_2:0.035%Er^{3+} crystals are given in Figures 6.1 and 6.2 and show the changes in both multiplets between crystals deuterated for 16 hours and 68 hours. Figures 6.3 and 6.4 are spectra for a crystal deuterated for 144 hours and confirm that, as for the CaF_2:Er^{3+} system, the duration of deuteration plays a significant role in determining the site distribution of both the D^- ion and F^- ion sites.

The transitions marked in the spectra presented here are labelled with both the site name and a subscript corresponding to the numerical label of the upper multiplet state. For simplicity, only transitions from the Z_1 ground state are labelled, as transitions from the Z_2 and Z_3 levels of most sites are frozen out at 10 K. The weak transitions from Z_2 levels of the few remaining sites that do appear are marked with a star. Spectra for higher temperatures,not shown here, were used to confirm the origin of these lines.

The $^4S_{3/2}$ multiplet spectra of Figure 6.1 are the simplest to analyse, and as transitions to the multiplet can also be pumped by the dye laser, a detailed study was made of the $^4I_{15/2} \rightarrow {}^4S_{3/2}$ transitions.

A short deuteration of sixteen hours results in the appearance of additional transitions due to deuteride ion sites. The $Z_1 \rightarrow E_1$ and $Z_1 \rightarrow E_2$ transitions of the D1 site occur together with a weak broad feature between these two transitions. The $Z_1 \rightarrow E_1$ and $Z_2 \rightarrow E_1$ transitions of the D5 site are evident for such short hydrogenations, and the $Z_1 \rightarrow E_1$ transition of the D2 site is also present. Assignment of the Z_2 and Z_3 levels of the D1 site was achieved by the observation of very weak transitions in the 70K spectrum of such a crystal.

On increasing the duration of deuteration to 68 hours, additional sites are evident. Figure 6.1(c) illustrates that the D2 site transition is dominant over the J, D1 and D5 site transitions, while three new sites D3, D4 and D8 and a weak transition of a new F^- ion site, S1, appear. A weak unassigned transition, labelled U5, appears as 18406.3 cm^{-1} and a large increase in intensity of the broad feature 'a' is apparent.

Deuteration for 144 hours (Figure 6.3) dramatically increases the intensity of the D2, D3 and D4 sites while producing the new sites D6 and D7. The broad feature 'a' increases further and shows shoulder structure (b, c and d) at 18576.0, 18572.9 and 18559.2 cm^{-1} respectively.

In contrast to the $CaF_2:Er^{3+}$ case where the F^-A and B sites typically decrease by a factor of 100 after a 68-hour deuteration, the intensity of the F^-J site decreased only slightly as the duration of deuteration was increased.

Although they were less simple to analyse, the transitions of the new sites to the $^4F_{9/2}$ multiplet were also examined. Figure 6.2 shows the same dependence of

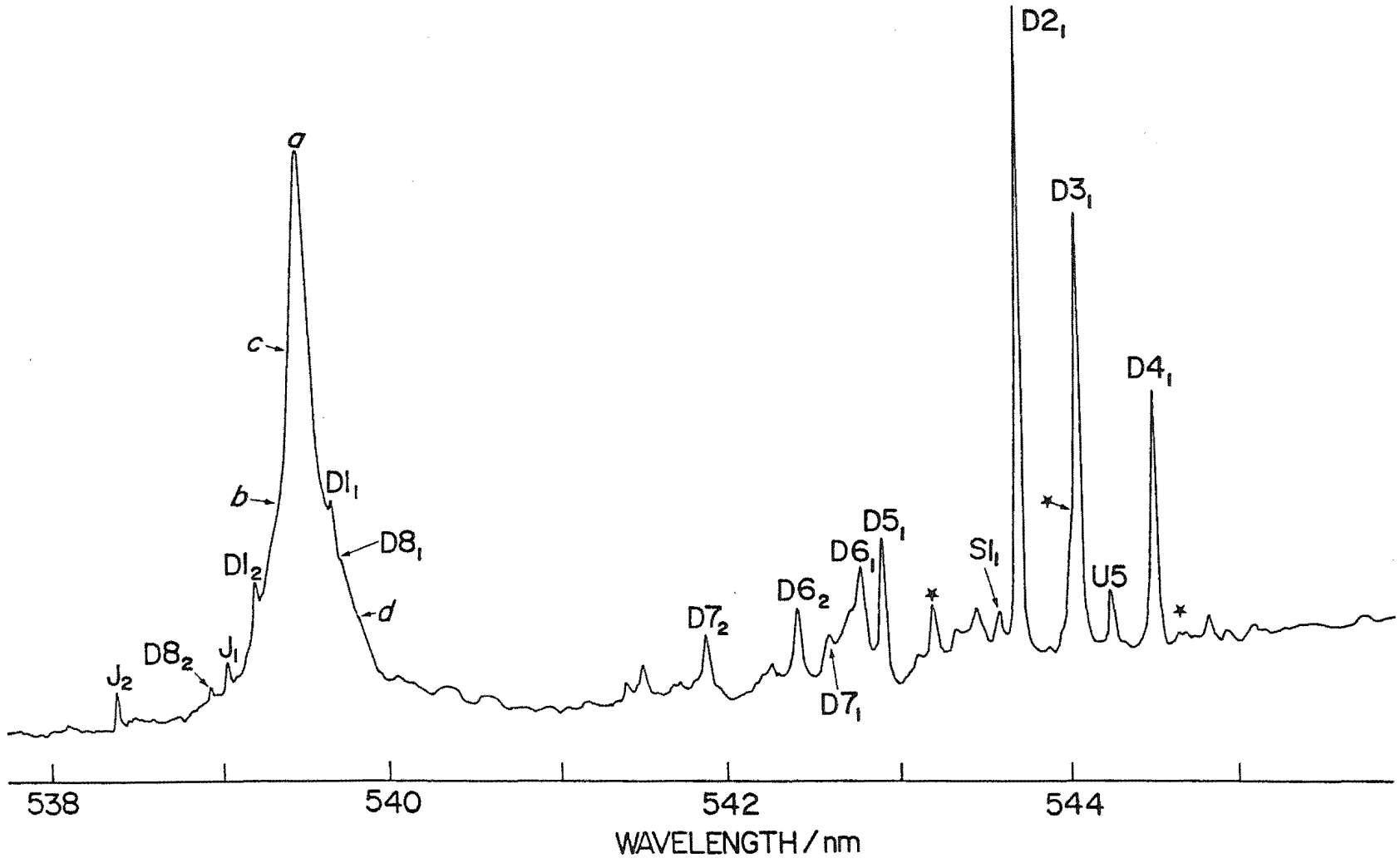

Figure 6.3 : The 10K $^4I_{15/2} \rightarrow {}^4S_{3/2}$ absorption spectrum of a 10 mm thick SrF_2:0.05%Er^{3+} crystal deuterated for 144 hours.

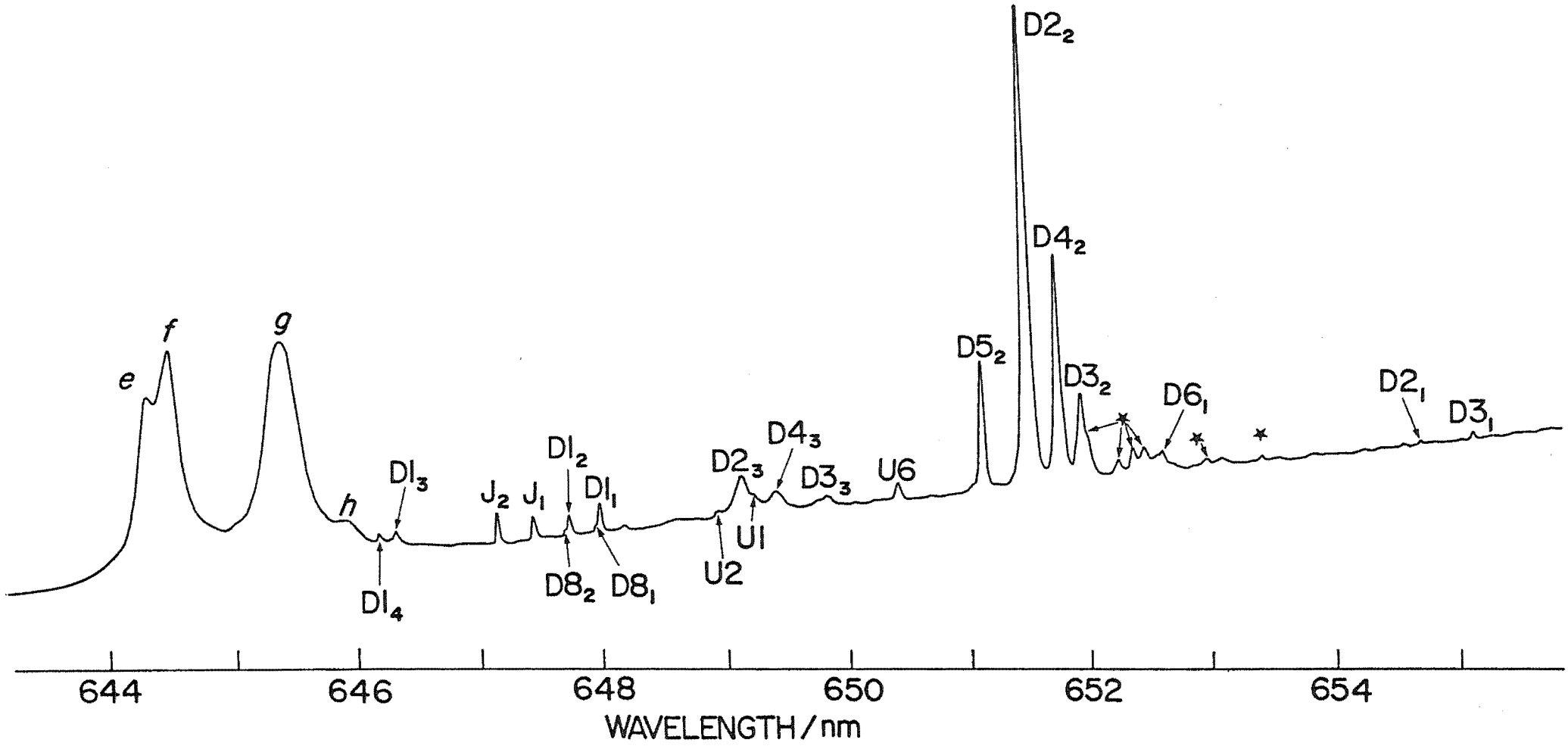

Figure 6.4 : The 10K $^4I_{15/2} \rightarrow {}^4F_{9/2}$ absorption spectra of a 10 mm thick SrF_2:0.05%Er^{3+} crystal deuterated for 144 hours.

site distribution on deuteration duration for transitions between the $^4I_{15/2}$ and $^4F_{9/2}$ multiplets.

Four $^4F_{9/2}$ levels are identified in Figure 6.2(b) for the D1 site in the 16-hour deuterated crystal together with the $Z_1 \rightarrow D_2$ transitions of the D2 and D5 sites. One further product of deuteration is the unassigned line labelled U6 at (15378.8 ± 0.5) cm^{-1}. The origin of this line is not obvious but it may be a D^- ion analogue of the site with transitions U1 and U2, since no corresponding line appears in the $^4S_{3/2}$ multiplet. Increasing the deuteration duration did not substantially increase the intensity of this line.

An increase of deuteration duration to 68 hours caused several new $^4F_{9/2}$ transitions to appear. A notable feature of Figure 6.2(c) is the broad lines labelled e(15523.7 ± 0.8) cm^{-1} , f(15519.3 ± 1.0) cm^{-1}, g(15497.5 ± 1.5) cm^{-1} and h(15485 ± 1.5) cm^{-1}. Lines e, f and g were found to remain at constant relative intensity to each other as a function of both the duration of deuteration and the crystal temperature, and correlated with the feature 'a' of the $^4S_{3/2}$ absorption spectrum. These features are therefore attributed to transitions from the Z_1 level of the same site. The transitions of the D1 to D5 sites are also identified in the spectrum.

The 144-hour deuteration duration (Figure 6.4) enhanced the intensity of the broad lines 'e' - 'h' and the transitions of the D2 to D5 sites, enabling tentative assignment of the $Z_1 \rightarrow D_3$ transitions of the D2, D3 and D4 sites to be made. One new site, D8, was assigned with $Z_1 \rightarrow D_1$ and $Z_1 \rightarrow D_2$ transitions at slightly higher energies

than the corresponding transitions for the D1 site. $Z_1 \rightarrow E_1$ and $Z_1 \rightarrow {}_2$ transitions are also assigned and shown in Figure 6.3.

A rather obvious overall trend in the spectra is the rapid growth of certain lines compared to others as the deuteration duration is increased. This is reflected, for example, in the intensity ratio of the $Z_1 \rightarrow D_2$ transition of the D2 site to the $Z_1 \rightarrow D_1$ transition of the D1 site which was 0.69 for a 16-hour deuteration and 17.1 for a 144-hour deuteration.

6.2.3 Laser Selective Excitation

The optical absorption studies provided the upper multiplet energy levels of the different sites required for the laser selective excitation study. L.s.e. proved invaluable for the assignment of $^4I_{13/2}$ and $^4I_{15/2}$ multiplet levels.

The immediately obvious feature of the l.s.e. study of the hydrogenated $SrF_2:Er^{3+}$ system was the diversity of fluoride ion sites present compared to the $CaF_2:Er^{3+}$ system for the same dopant level. Attempts to selectively pump several of the D^- ion sites were partially successful, while none of the corresponding H^- ion sites was able to be discriminated from the background fluoride ion site emission. The sites were excited by pumping the $^4I_{15/2} \rightarrow {}^4S_{3/2}$ transitions and fluorescence was recorded for the $^4S_{3/2} \rightarrow {}^4I_{15/2}$, $^4F_{9/2} \rightarrow {}^4I_{15/2}$ and $^4S_{3/2} \rightarrow {}^4I_{13/2}$ transitions.

The D2 to D5 sites all exhibited fluorescence bleaching upon laser excitation analogous to that observed for the

tetragonal sites of $CaF_2:Er^{3+}$. Such phenomena are discussed in more detail later (Chapter Seven). This bleaching had the undesirable effect of reducing site fluorescence intensity and causing additional difficulties in discrimination against other interfering non-bleaching sites. This bleaching effect was, however, also used to advantage by doing repeated short scans over a small spectral range with the crystal moved to unbleached portions at the beginning of each scan. Those features that increased with respect to the background fluorescence could be attributed to the bleaching centre. In this way most of the energy levels of the D2 to D5 sites could be confirmed and are included in Table 6.1.

The discrimination of the D1 to D5 sites from the underlying F^- ion sites was found to be better for the $^4F_{9/2} \rightarrow {}^4I_{15/2}$ spectra than for the $^4S_{3/2} \rightarrow {}^4I_{13/2}$ or $^4S_{3/2} \rightarrow {}^4I_{15/2}$ spectra. This is consistent with a greater rate of non-radiative decay from the $^4S_{3/2}$ level to the $^4F_{9/2}$ level for the D^- ion sites, which is probably due to additional decay processes available involving local mode phonons. Identification of $^4I_{13/2}$ levels proved particularly difficult in many cases.

The D3 and D4 sites were the most clearly resolved from other sites. Fluorescence was measured for excitation of the $Z_1 \rightarrow E_1$ transitions and comparison of the E → Z and D → Z emission spectra enabled the classification of seven of the eight ground state multiplet levels. The emission from $^4S_{3/2} \rightarrow {}^4I_{13/2}$ gave the seven Y levels for D3 and six for D4. Figure 6.5 includes the emission spectra for the D3 site with transitions marked corresponding to the site.

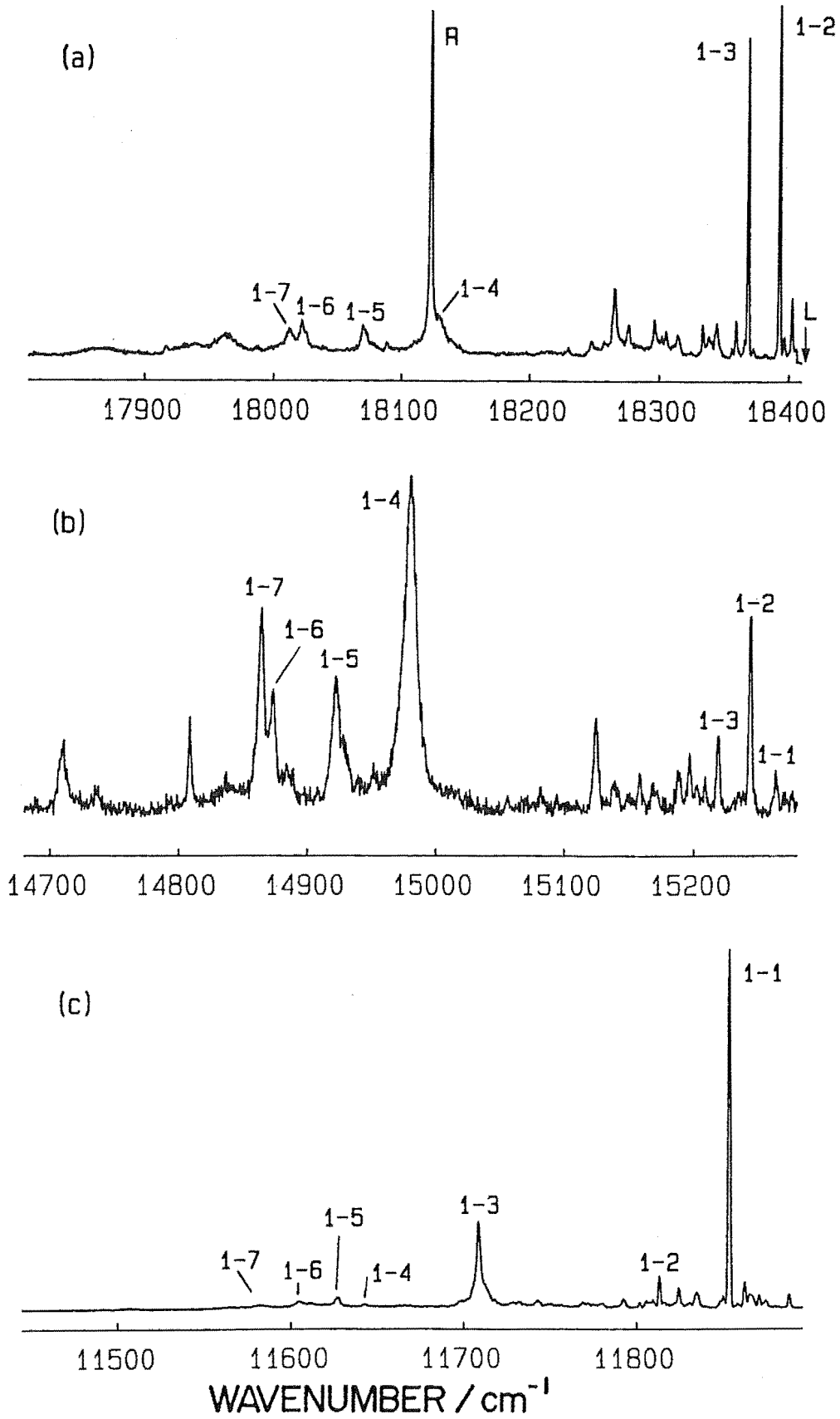

Figure 6.5 : 10K fluorescence for laser excitation of the $Z_1 \rightarrow E_1$ transition of the D3 site : (a) $^4S_{3/2} \rightarrow {}^4I_{15/2}$, (b) $^4F_{9/2} \rightarrow {}^4I_{15/2}$, and (c) $^4S_{3/2} \rightarrow {}^4I_{13/2}$. Transition labels represent the upper and lower multiplet crystal field levels involved. "L" identifies the laser position and "R" the first order Raman scattering line.

The first order Raman scattering line at 290 cm^{-1} is marked with an 'R' and other lines present are mostly due to the S5 and S6 fluoride ion sites. The D4 site could also be pumped reasonably cleanly and its spectra are included in Figure 6.6. The pattern of intensity of the $D_1 \rightarrow Z_4$ and $D_1 \rightarrow Z_6$ transitions show marked similarity to the Family A sites of CaF_2.

Two other sites, D2 and D5, have closely similar energy levels and spectra to the D3 and D4 sites. The best spectra that could be obtained for these sites were still mixed with emission from other sites, with the S5 and S6 sites interfering with the D2 site and the S7 site interfering with the D5 site. This prevented identification of any more than three of the seven Y levels of the D5 site.

The improved site discrimination for the D → Z transitions compared to the E → Z transitions, resulted in identification of most of the Z levels from the former. This is illustrated by the fluorescence of the D5 site for which only the Z_1, Z_2 and Z_3 levels could be identified from $^4S_{3/2}$ emission (Figure 6.6(a)), while the remainder were determined by $^4F_{9/2}$ emission. The D2 site spectra are given in Figure 6.7 and the Z_4, Z_5, Z_6 and Z_7 levels are also readily identified from the $^4F_{9/2} \rightarrow {}^4I_{15/2}$ spectra.

Laser selective excitation of the D6 site revealed a very different pattern of energy levels and transition intensities to the D2, D3, D4, or D5 sites, and no fluorescence bleaching was observed. The spectra for the site are given in Figure 6.8. This site could be pumped by both the $Z_1 \rightarrow E_1$ and $Z_1 \rightarrow E_2$ transitions and the energy

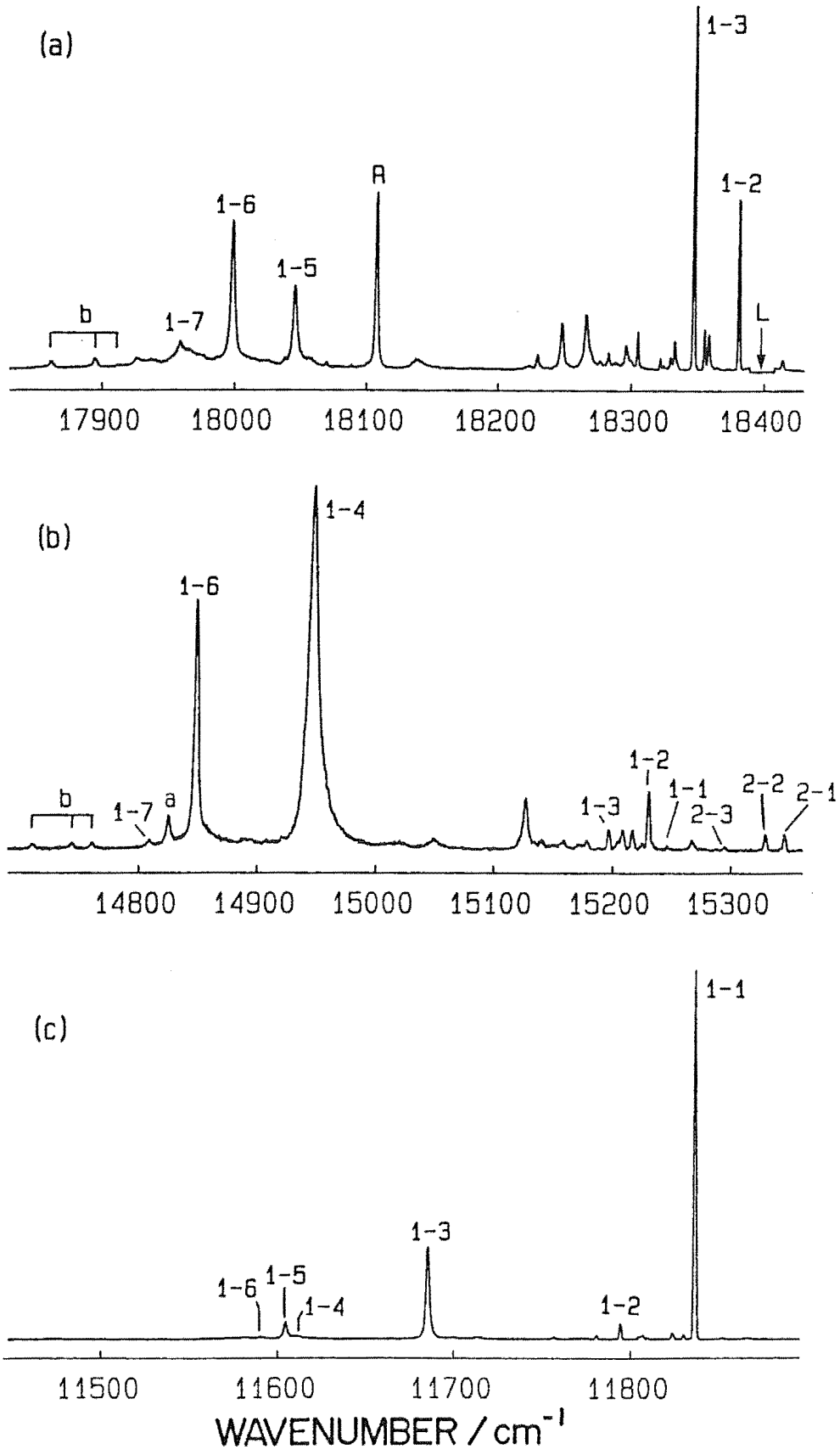

Figure 6.6 : 10K fluorescence for laser excitation of the $Z_1 \rightarrow E_1$ transition of the D4 site : (a) $^4S_{3/2} \rightarrow {}^4I_{15/2}$, (b) $^4F_{9/2} \rightarrow {}^4I_{15/2}$, and (c) $^4S_{3/2} \rightarrow {}^4I_{13/2}$. Vibronics are identified by "a" and "b".

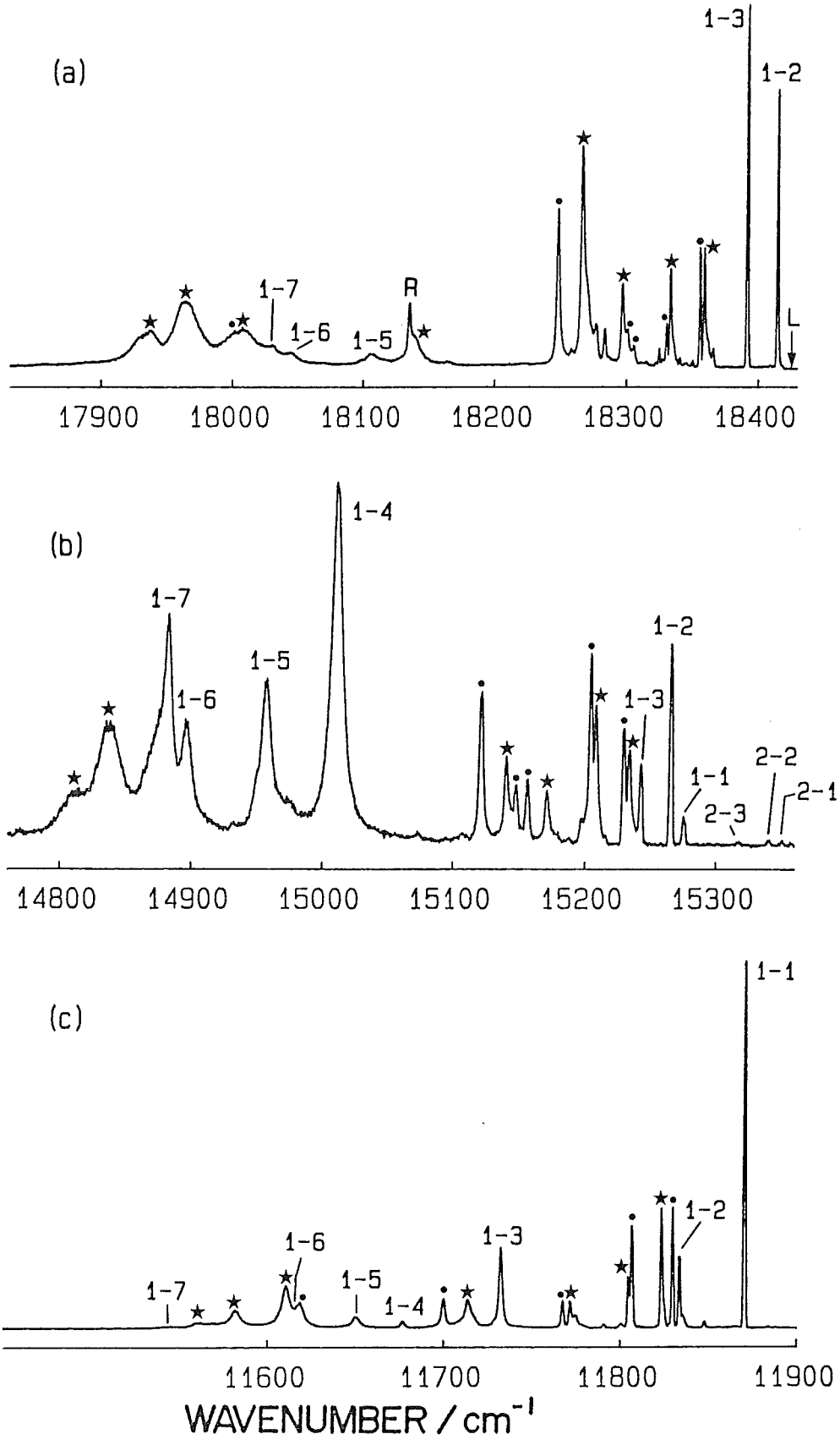

Figure 6.7 : 10K fluorescence for laser excitation of the $Z_1 \rightarrow E_1$ transition of the D2 site : (a) $^4S_{3/2} \rightarrow {}^4I_{15/2}$, (b) $^4F_{9/2} \rightarrow {}^4I_{15/2}$, and (c) $^4S_{3/2} \rightarrow {}^4I_{13/2}$. Transitions of the simultaneously excited S5 and S6 sites are identified by stars and dots respectively.

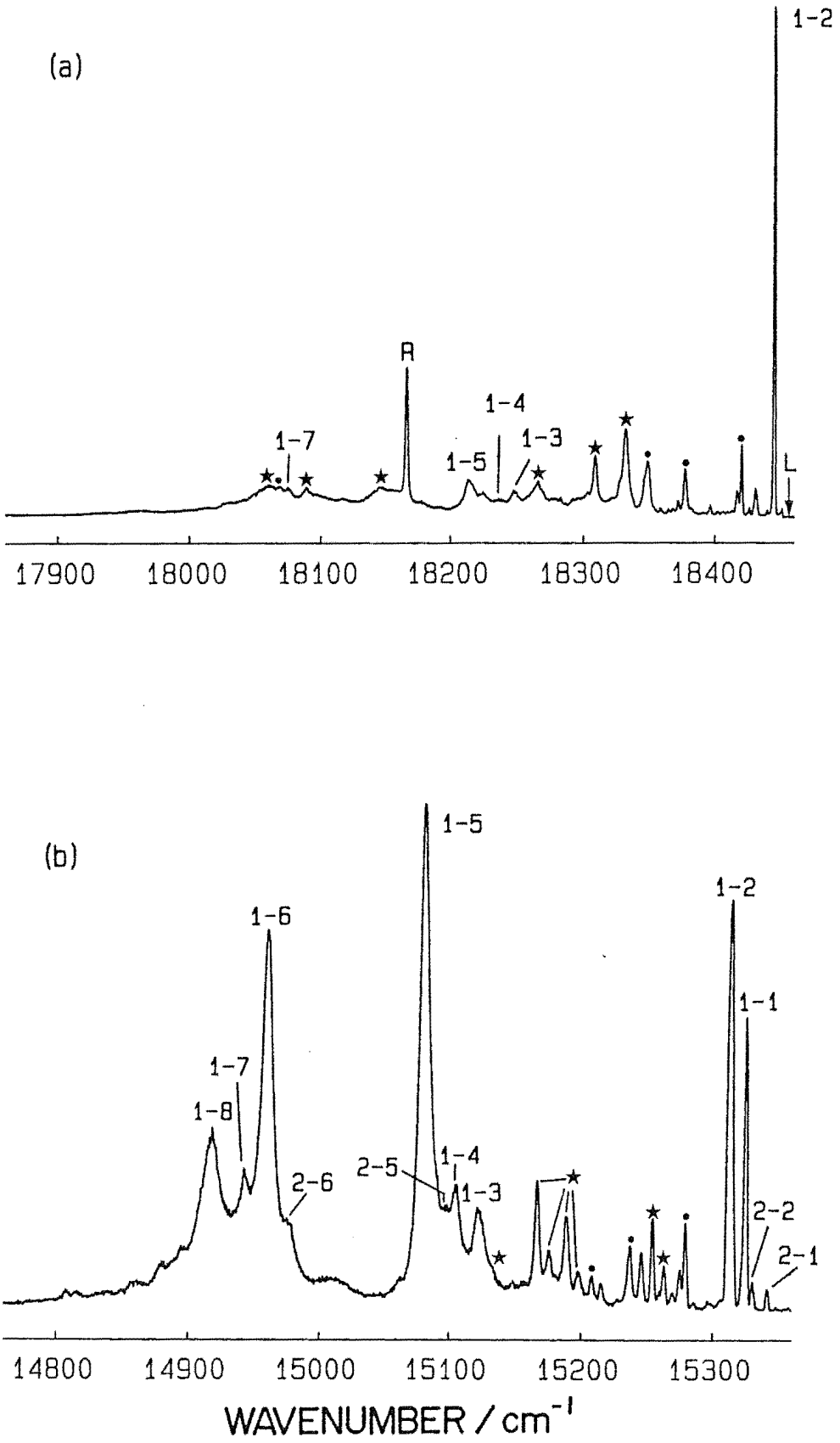

Figure 6.8 : 10K fluorescence for laser excitation of the $Z_1 \rightarrow E_1$ transition of the D6 site : (a) $^4S_{3/2} \rightarrow {}^4I_{15/2}$, and (b) $^4F_{9/2} \rightarrow {}^4I_{15/2}$. Transitions of the simultaneously excited S3 and S4 sites are identified by stars and dots respectively.

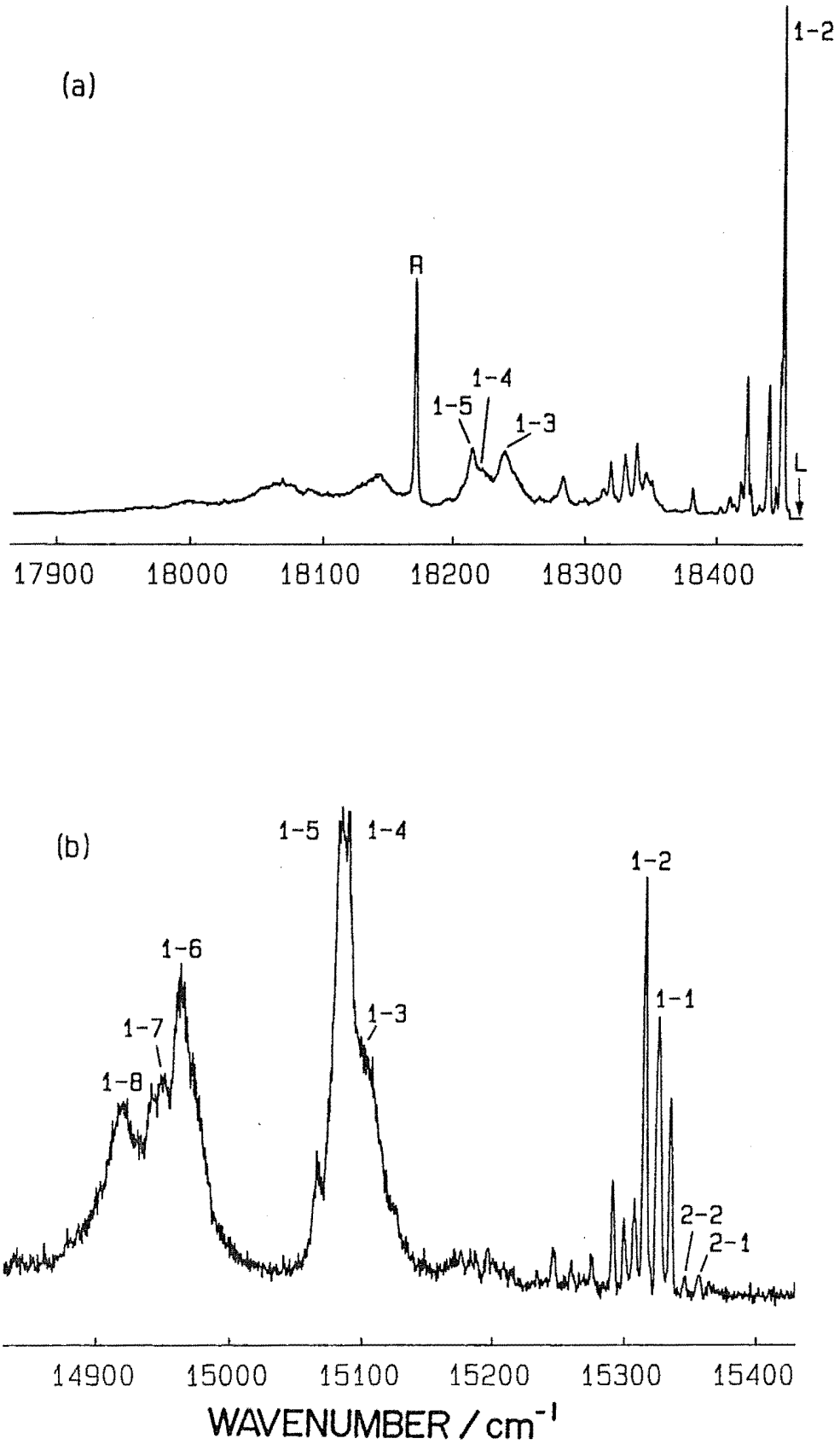

Figure 6.9 : 10K fluorescence for laser excitation of the $Z_1 \rightarrow E_1$ transition of the D7 site : (a) $^4S_{3/2} \rightarrow {}^4I_{15/2}$, and (b) $^4F_{9/2} \rightarrow {}^4I_{15/2}$.

levels derived were those common to both spectra. The S3 and S4 sites caused interference when pumping $Z_1 \rightarrow E_1$, and the S8 site was partially excited simultaneously with the $Z_1 \rightarrow E_2$ transition of the site.

The D7 site energy levels of the $^4I_{3/2}$ multiplet found by optical absorption were confirmed by laser excitation of the $Z_1 \rightarrow E_2$ transition. Levels of the $^4I_{15/2}$ and $^4F_{9/2}$ multiplets were also determined from the $^4S_{3/2} \rightarrow {}^4I_{15/2}$ and $^4F_{9/2} \rightarrow {}^4I_{15/2}$ spectra whilst pumping both the $Z_1 \rightarrow E_1$ and $Z_1 \rightarrow E_2$ transitions. With the latter excitation, simultaneous fluorescence from the S9 site occurred and so it was less useful than $Z_1 \rightarrow E_1$ excitation. No $^4I_{13/2}$ levels could be confirmed by other excitation. The $E \rightarrow Z$ and $D \rightarrow Z$ emission spectra for the site are given in Figure 6.9. As with the D6 site, this site did not exhibit fluorescence bleaching.

Attempts to selectively excite the D1 or D8 sites in several crystals were unsuccessful and transitions of the sites could not be resolved from the resultant emission of several fluoride ion sites. Similarly, the few remaining absorption transitions in the spectrum, including the broad feature 'a', were pumped but no distinct emission from these sites was obtained. A surprising result was that no fluorescence was observed while pumping the transition U5 at 18406.3 cm^{-1} despite the relatively small amount of background emission from other sites, suggesting a different site configuration to the D^- ion sites classified and a weaker emission intensity.

A thorough search was conducted for vibronic transitions for each of the D^- ion sites studied. The D3

and D4 sites, with their partially selectively excited $Z_1 \rightarrow E_1$ transitions, exhibited several lines in the expected vibronic region for both the $^4S_{3/2} \rightarrow {}^4I_{15/2}$ and $^4F_{9/2} \rightarrow {}^4I_{15/2}$ spectra. The vibronic intervals that could be assigned from these spectra are included in Table 6.2. The most distinct of these local modes is 'b' for the D4 site which was readily identified for parent transitions from both the $^4S_{3/2}$ and $^4F_{9/2}$ levels.

The local mode 'a' of the D4 site is only a tentative assignment, since vibronics from all three low-lying Z levels were not identified due to the presence of the $E_1 \rightarrow Z_1$ and $D_1 \rightarrow Z_1$ electronic transitions. The most convincing evidence for this vibronic interval is the intense line at 14826.5 cm^{-1} which is related to the site. Other features were present in the vibronic spectra of both sites, suggesting that further local modes were present, but they could not be matched to expected energy level spacings of the parent transitions. This is attributed both to overlapping lines and to smaller peaks being swamped by the background fluorescence level.

The D6 site exhibited several vibronic peaks, but as the site has only two low-lying ground state levels, correlation of peaks by the Z_1 to Z_2 energy level separation was less reliable than that for the D2 and D3 sites. Nevertheless, vibronic intevals of (434 ± 1) cm^{-1}, (459.5 ± 2) cm^{-1} and (505.5 ± 2) cm^{-1} can be tentatively assigned on this basis.

The remaining pumped deuteride ion sites had related features in the vibronic region that were mixed with other sites' fluorescence and a high background fluorescence

Table 6.2 : Wavenumbers and vibronic transitions of the D3 and D4 sites as measured in the 10K fluorescence spectra of deuterated SrF_2:0.05%Er^{3+} crystals.

Site	Local Mode	Wavenumber (± 0.5 cm^{-1})	Parent electronic transition	Vibronic interval (± 1.0 cm^{-1})
D3	a	17964.5	$E_1 \rightarrow Z_1$	451.0
		17944.5	$\rightarrow Z_2$	450.5
		17920.0	$\rightarrow Z_3$	449.5
	b	17827.0	$E_1 \rightarrow Z_1$	588.5
		17809.0	$\rightarrow Z_2$	586.0
		17786.0	$\rightarrow Z_3$	584.5
	c	17739.5	$E_1 \rightarrow Z_1$	676.0
		17719.0	$\rightarrow Z_2$	676.0
		17696.5	$\rightarrow Z_3$	674.0
D4	a	17977.0	$E_1 \rightarrow Z_1$	423.0
		17928.5	$\rightarrow Z_3$	421.0
		14826.5	$D_1 \rightarrow Z_1$	422.5
	b	17914.0	$E_1 \rightarrow Z_1$	486.0
		17896.5	$\rightarrow Z_2$	487.0
		17864.0	$\rightarrow Z_3$	485.5
		17615.5	$\rightarrow Z_4$	487.0
		17563.0	$\rightarrow Z_5$	485.0
		17517.0	$\rightarrow Z_6$	483.5
		14762.5	$D_1 \rightarrow Z_1$	486.5
		14744.0	$\rightarrow Z_2$	487.5
		14712.5	$\rightarrow Z_3$	486.0
	c	17833.5	$E_1 \rightarrow Z_1$	566.5
		17818.0	$\rightarrow Z_2$	565.5
		17784.0	$\rightarrow Z_3$	565.5
	d	17700.5	$E_1 \rightarrow Z_1$	699.5
		17686.0	$\rightarrow Z_2$	697.5
		17652.5	$\rightarrow Z_3$	697.0

level, so no positive identification of any vibronic intervals could be made. Nevertheless, the presence of such vibronic features is further confirmation of the D^- ion origin of these sites.

6.3 Site Classification and Discussion

Proposals regarding the nature of the D^- ion site configurations can be made on the basis of the results obtained by both absorption and l.s.e.

Since the site distributions remain unchanged for 0.05%Er^{3+} and 0.035%Er^{3+} crystals, all sites involve a single Er^{3+} ion consistent with that expected for the low dopant level. In any case, the thermal treatment during deuteration would reduce the presence of any Er^{3+} ion cluster sites (Moore and Wright 1981) making the observation of such sites at the intensity level of the D^- sites unlikely.

6.3.1 The D1 Site

This site is proposed to be a D^- ion analogue of the F^- ion J site which is considered to consist of an Er^{3+} ion charge compensated by an F^- interstitial ion in the next nearest neighbour position along the <111> crystal axis direction.

Evidence for the D1 site assignment is as follows :

(a) The site is the first to form for short deuteration durations consistent with having only a single D^- ion in the site.

(b) The crystal field levels of the $^4S_{3/2}$ and $^4F_{9/2}$ multiplets are closely similar to those of the J

site, being at slightly lower frequencies due to the expected covalency effects.

(c) The crystal field levels of the $^4I_{15/2}$ multiplet are very similar to those of the J site.

(d) The small Z_2 and Z_3 separation is indicative of only a small deviation from cubic site symmetry (Aizenberg *et al.* 1972) consistent with the relatively distant NNN charge compensation.

(e) The D^- to H^- isotope shifts for all $^4S_{3/2}$ and $^4F_{9/2}$ multiplet levels as determined from the absorption spectra are small (less than 1 cm^{-1}), as expected for the NNN hydrogenic ion charge compensation site.

The relative intensity of the D1 site to the J site was observed to increase almost linearly with the duration of deuteration. The D1:J site ratios of the $Z_1 \rightarrow D_1$ transition were 0.29, 0.75 and 1.22 for 16, 68 and 144 hour deuterations respectively. Unlike the proposed single D^- ion sites of $CaF_2:Er^{3+}$ (the C_{4V} and W sites) which decreased substantially with increasing deuteration duration, the D1 site intensity increased between 16 and 68 hours and decreased only very slightly between 68 hours and 144 hours of deuteration.

A D^- ion site of exact trigonal symmetry requires two infra-red local modes, but the only previous site categorised by infra-red spectroscopy [EFJ77] has rhombic symmetry and was found in crystals hydrogenated for short durations only. Infra-red spectroscopy of crystals with longer hydrogenation duration should determine a site

corresponding to D1 with only two local mode vibrations.

6.3.2 The D8 Site

The close similarity of the levels of this site to those of the D1 site is suggestive of a slightly perturbed site configuration. An obvious modification would be a site involving an additional D^- ion substituted for an F^- ion in the lattice. A definite configuration cannot be assigned with the present data and will require optimisation to a level such that l.s.e. can be used on the site.

6.3.3 Near Cubic Symmetry Site

The intense broad absorption features observed in both multiplets are assigned, by analogy with the $CaF_2:Er^{3+}$ system, to an Er^{3+} ion site of 'near cubic' symmetry. Like the α, β, γ sites of $CaF_2:Er^{3+}$, the enhanced intensity after deuteration is attributed to substitutional D^- ions near Er^{3+} ions having remote charge compensation removing exact inversion symmetry of the site, thereby relaxing the selection rules for electric dipole transitions. As it is centred almost symmetrically between the two $^4S_{3/2}$ levels of the D1 site (which is expected to have only a small perturbation from cubic symmetry), the position of the peak 'a' is consistent with a cubic symmetry centre. Unlike the $CaF_2:Er^{3+}$ system where the three distinct sites α, β and γ were distinguished, the relative intensity of the broad lines in the $^4I_{15/2} \rightarrow {}^4F_{9/2}$ absorption spectra did not vary with the duration of deuteration, so the lines e, f and g (Figure 6.4) are all attributed to a single site.

The appearance of the perturbed cubic centres in the optical spectrum after deuteration is reasonable since previous EPR studies (Antipin *et al.* 1967), (Brown *et al.* 1969b), have reported that a significant fraction of Er^{3+} ions in $SrF_2:Er^{3+}$ are in cubic symmetry centres.

6.3.4 Family A Sites

The D2, D3, D4 and D5 sites form a distinct category of sites and have been labelled Family A sites. There is a marked similarity between the energy levels and transition intensities for these sites and those of the Family A sites of the deuterated $CaF_2:Er^{3+}$ system.

Energy levels of the $^4I_{15/2}$ multiplet have the same pattern as the $CaF_2:Er^{3+}$ analogues, with three low-lying levels, one intermediate energy level and a group of three (Z_5,Z_6 and Z_7) at higher energy. The Z_8 level was difficult to determine for both systems.

Comparison of the spectra of these sites with those of the $CaF_2:Er^{3+}$ Family A sites shows that the $E_1 \rightarrow Z_4$ transition is weak, while $D_1 \rightarrow Z_4$ and $D_1 \rightarrow Z_6$ are relatively intense. The intensity pattern of the $D_1 \rightarrow Z_4$, Z_5, Z_6 and Z_7 transitions for the D3 and D4 sites (Figures 6.5(b) and 6.6(b)) is very similar to that for the R and J site. Absorption intensity patterns are also very similar, with very weak $Z_1 \rightarrow E_2$ and $Z_1 \rightarrow D_1$ transitions and intense $Z_1 \rightarrow E_1$ amd $Z_1 \rightarrow D_2$ transitions.

The other principal similarity of the sites of the family is that they all bleach upon excitation of the $Z_1 \rightarrow E_1$ transition. Reversible polarised bleaching (Chapter

Seven) was exhibited by the D2 site for the <100> geometry, similar to that of the R and J sites of $CaF_2:Er^{3+}$.

On the basis of the similarities to $CaF_2:Er^{3+}$ sites outlined above, the sites of the family are assigned configurations perturbed from the D^-(NN) C_{4V} symmetry site by additional D^- ions substituted for lattice F^- ions.

Several of the vibronic intervals that could be positively identified were of vibrational frequencies expected for a D^- ion in a substitutional lattice position. By scaling with the ratio of the D^- ion T_d site energies in CaF_2 and SrF_2, the intervals 'b' and 'c' of the D4 site correspond to equivalent CaF_2 vibronics of 525 cm^{-1} and 611 cm^{-1} which are very comparable to vibronic intervals of substitutional D^- ions in the R and J sites.

None of the major sites, D2 to D5, of the $SrF_2:Er^{3+}:D^-$ system can be assigned the configuration of the simple D^- C_{4V} site involving a single interstitial D^- ion such as that observed for $CaF_2:Er^{3+}$. Such a site would have a simple vibronic spectrum of two local mode vibronic intervals at approximately 660 cm^{-1} and 695 cm^{-1} if the pattern established for other rare-earth ion sites [EFJ77] is extrapolated, and should have no vibronic features at lower frequency. Although none of the vibronic spectra of the sites could be completely categorised, no site had such a simple spectrum. Some sites had unassigned features in this region but all had additional vibronic features, either assigned or partially obscured, at lower frequencies,indicative of nearby substitutional D^- ions.

The C_{4V} site, if it exists, is likely to be at the high energy end of the site sequence of the $^4F_{9/2}$ and $^4S_{3/2}$

multiplet levels since the covalency effect, causing a reduction in energy levels, is least for a single D^- ion site. Due to its appearance, albeit weakly, after a short duration of deuteration and its resemblance of several energy levels, the D5 site seemed the most likely site to be the analogue of the D^- C_{4V} site in $CaF_2:Er^{3+}$. This assignment was discounted, however, by both the vibronic spectrum and by the observation of fluorescence bleaching which was not expected for a simple C_{4V} configuration. The hydrogenic C_{4V} site has been identified for Er^{3+}, Pr^{3+} (Syme *et al.* 1984) and Nd^{3+} (Han, Private Communication) in both SrF_2 and CaF_2 and also for $CaF_2:Ho^{3+}$ (Paris 1986) and none of these sites exhibited any bleaching whatsoever.

No exact configurations were verified for these sites as none has a complete set of vibronic intervals determined to date. On the basis of its reversible bleaching characteristics and its relatively large intensity in the absorption spectra, the D2 site is tentatively assigned to the R site configuration of Figure 5.17(a). The remainder of Family A sites are proposed to be derived from C_{4V} symmetry by one or more substitutional D^- ions in various lattice positions.

6.3.5 Family B Sites

The two remaining sites classified in Table 6.1, D6 and D7, are closely similar to each other but distinctly different from the other D sites. Neither site exhibited fluorescence bleaching, and both sites had $Z_1 \rightarrow E_1$ and $Z_1 \rightarrow E_2$ transitions observed in the absorption spectra, but only very weak $^4I_{15/2} \rightarrow {}^4F_{9/2}$ transitions.

The energy levels and transition intensities for absorption and emission are very similar to those of the Family B sites in $CaF_2:Er^{3+}$. In the $SrF_2:Er^{3+}$ case, however, the absorption intensity of these sites relative to Family A sites is much less. The similarity with the $CaF_2:Er^{3+}$ sites is illustrated by comparison of the $^4F_{9/2} \rightarrow {}^4I_{15/2}$ emission spectrum for the D6 site (Figure 6.8(b)) with that of the $CaF_2:Er^{3+}$ N site (Figure 5.20).

As the D5 and D6 sites resemble the $CaF_2:Er^{3+}$ sites, which are derived from the F^- B site, similar model configurations are expected (Chapter Five) for them. Since its polaristion ratios support an exact trigonal symmetry for the F^- B site, this family of sites is expected to have basic trigonal symmetry. It is proposed that the D5 and D6 sites are perturbed from C_{3V} symmetry by additional D^- ions replacing F^- ions. The three vibronics proposed for the D6 site have a mean energy of 466 cm^{-1} which is consistent with a substitutional D^- ion rather than an interstitial one. As the expected vibronics of the more distant interstitial D^- ion are not clearly identified, a definite configuration cannot be assigned to either site.

6.4 Spectroscopy of Known Fluoride Ion Sites

The four known single Er^{3+} ion sites involving F^- ion charge compensation [KW77] were examined in more detail here than previously, since crystal field levels of the N sites have not been published and information available for the J site was found to be partially incorrect. The J site has been correlated [Ai73a] to the principal EPR site of trigonal symmetry, supposedly having interstitial F^- ion

charge compensation in the <111> direction from the Er^{3+} ion. No model has been previously presented for any of three N sites.

6.4.1 The J Site

Laser selective excitation of the site was possible for either $Z_1 \rightarrow E_1$ or $Z_1 \rightarrow E_2$ excitation, and the resultant spectra are included in Figure 6.10. The energy levels determined from the spectra are compared to the previously reported values in Table 6.3. This site is unique for the $CaF_2:Er^{3+}$ or $SrF_2:Er^{3+}$ systems in that it has broad intense emission features assigned to vibronic sidebands of the electronic transitions [Ai69], and these are labelled by an star in the spectra.

New aspects of the J site investigated in this study include :

(a) The Z_4 level has been identified from the $^4S_{3/2}$ emission spectrum.

(b) Several of the $^4I_{13/2}$ levels have been reassigned.

(c) Several emission transitions were found to be polarised.

Only one transition to the Z_4 level has been previously identified. Aizenberg *et al.* (1973a) reported assignment of the level by the $P_1 \rightarrow Z_4$ transition at 3162.6Å. It was found in this study that neither $D_1 \rightarrow Z_4$ nor $E_1 \rightarrow Z_4$ transitions appeared for $Z_1 \rightarrow E_1$ excitation, but if the $Z_1 \rightarrow E_2$ transition was selectively excited, then the $E_2 \rightarrow Z_4$ transition appeared weakly. This provided convenient verification of the previous value (Table 6.3).

Table 6.3 : Energy levels (in cm^{-1}) of the J,N1,N2 and N3 fluoride ion compensation sites as derived from the 10K fluorescence spectra of SrF_2:0.05%Er^{3+} crystals. Uncertainties are ± 0.5 cm^{-1} for the E,D and Z levels and ± 1.0 cm^{-1} for the Y levels, except where indicated.

	J		N1	N2	N3
	Previous* Assignment	Present Assignment			
E_2	18608	18608.1	18590.2	18593.3	-
E_1	18586	18586.0	18568.2	18550.0	18543.9
D_3	-	15490.2	-	-	-
D_2	15454	15456.0	-	-	-
D_1	15447	15449.1	15413.8	15405.8	15402.0
Y_7	6934	6884.2	6888.0	6819.3	6814.0
Y_6	6906	6876.7	6829.0	6814.1	6802.5
Y_5	6881	6870.2	6816.5	-	6775.5
Y_4	6851	-	6798.0	6778.1	6766.8
Y_3	6630	6631.6	6640.4	6653.3	6659.2
Y_2	6619	6619.8	6601.2	6591.7	6589.2
Y_1	6608	6609.8 ± 0.8	6590.0	6574.5	6570.8
Z_8	595	598.5	464.5	486	481.0
Z_7	556	558.5	440.5	407.0	397.0
Z_6	513	515.0	421.5	391.5	386.8
Z_5	494	496.0	401.5	369.5	354.4
Z_4	118	116.0	-	158.5	243.0
Z_3	88	89.0 ± 0.3	52.5	35.3 ± 0.3	32.7
Z_2	80	81.4 ± 0.3	46.3 ± 0.3	34.7 ± 0.3	29.0
Z_1	0	0	0	0	0

* Taken from Aizenberg *et al.* (1973a).

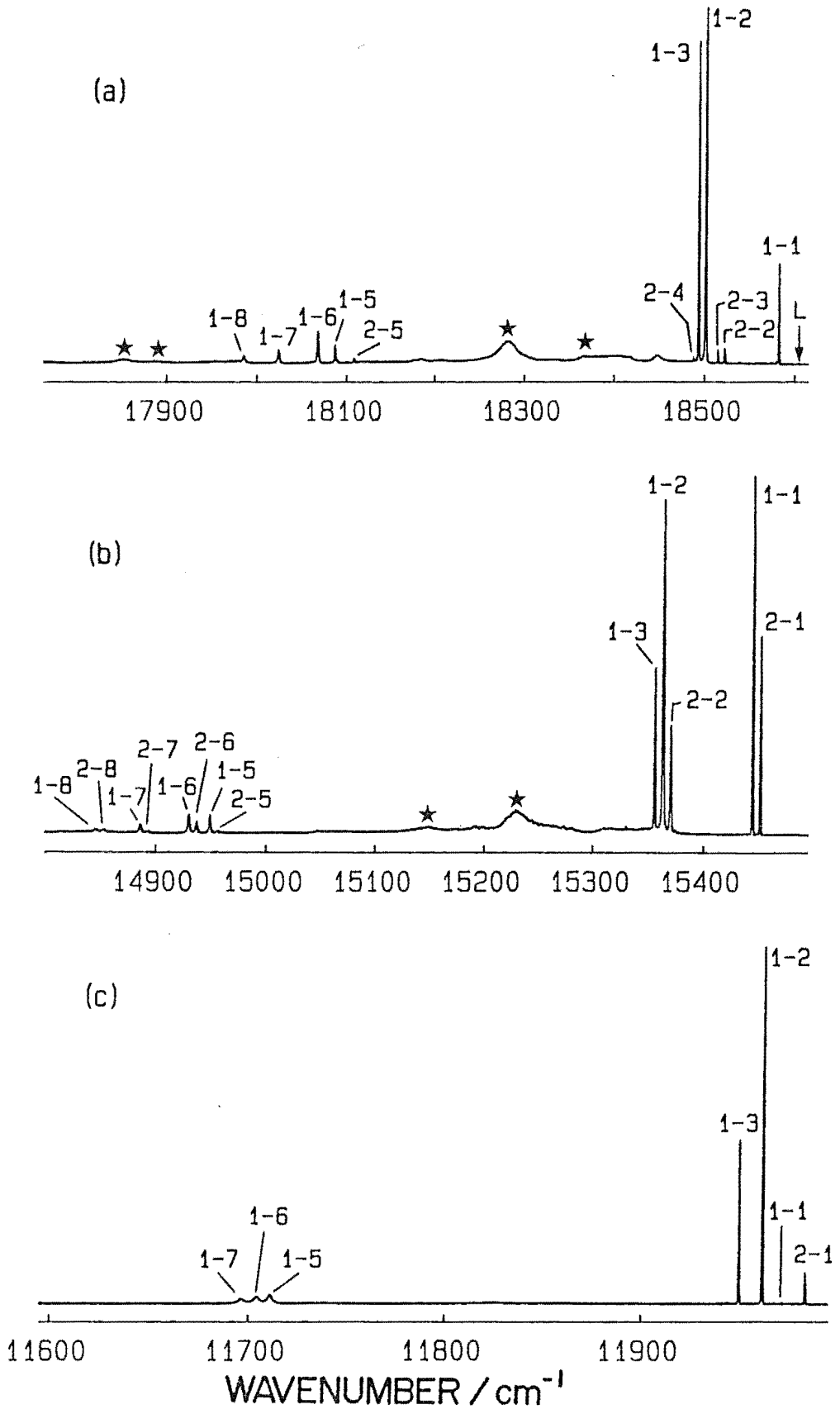

Figure 6.10 : 10K fluorescence for $Z_1 \rightarrow E_2$ laser excitation of the F^-J site : (a) $^4S_{3/2} \rightarrow {}^4I_{15/2}$, (b) $^4F_{9/2} \rightarrow {}^4I_{15/2}$, and (c) $^4S_{3/2} \rightarrow {}^4I_{13/2}$. Vibronic transitions associated with the site are identified by stars.

Emission to the $^4I_{13/2}$ multiplet showed three weak peaks attributed to Y_5, Y_6 and Y_7. The energies of these levels were not in agreement with the previous workers and replace their values. The assignment of the Y_1 level from the laser selective excitation spectrum is not trivial. Aizenberg *et al.* used the transitions from the P_1 and P_2 levels of the $^2P_{3/2}$ multiplet to identify the Y_1 level. Since they neither published spectra nor specifically discussed the assignment, it is assumed that the transitions are reasonably intense and that the assignment is reliable. Close examination of the E → Y spectrum of Figure 6.10(c) revealed a very small peak corresponding to the $E_1 \rightarrow Y_1$ transition and an even smaller one for $E_2 \rightarrow Y_1$ sufficient to provide confirmation of Aizenberg's assignment. The more intense features in this region of the spectrum are assigned to the $E_1 \rightarrow Y_2$ and $E_2 \rightarrow Y_2$ transitions.

The polarisation dependence of the site emission was found to be negligible for crystals of the <100> geometry as expected for the proposed trigonal symmetry. Transitions were, however, polarised in the <111> geometry, and the x(yy)z:x(yx)z polarisation ratios observed for $Z_1 \rightarrow E_1$ and $Z_1 \rightarrow E_2$ excitation are given in Table 6.4. The $E_2 \rightarrow Z_4$ fluorescence was too weak to give a reliable ratio.

An assignment of the energy level symmetry labels on the basis of the polarisation results was attempted, but none of the ratios observed coincided exactly with the predicted $\frac{3}{7}$ or $\frac{15}{11}$ ratios that would occur for the appropriate symmetry of the pumping transition levels. Comparison of Table 6.4 with Table 5.22 shows that the sequence of ratios is different to that of the B site of

TABLE 6.4 : Observed and predicted intensity ratios of polarised emission transitions of the F^-J site in <111> oriented SrF_2:0.05%Er^{3+} crystals. Predictions for two different proposals (a and b) of irrep symmetry assignment with laser excitation of both the $Z_1 \rightarrow E_1$ and $Z_1 \rightarrow E_2$ transitions are included. Experimental uncertainties are ±10%

Upper State	Proposed irrep label (a)	Proposed irrep label (b)	Lower State	Proposed irrep label (a)	Proposed irrep label (b)	Polarisation Ratio $Z_1 \rightarrow E_1$ excitation Expected (a)	Observed	Expected (b)	Polarisation Ratio $Z_1 \rightarrow E_2$ excitation Expected (a)	Observed	Expected (b)
E_2	Γ_4	$\Gamma_{5,6}$	Z_1	Γ_4	$\Gamma_{5,6}$	$\frac{3}{7} \rightarrow \frac{15}{11}$	0.80	$\frac{3}{7}$	Arb.	laser	3
			Z_2	Γ_4	Γ_4	"	1.04	$\frac{15}{11}$	"	0.88	$\frac{3}{7}$
			Z_3	Γ_4	Γ_4	"	1.13	$\frac{15}{11}$	"	0.81	$\frac{3}{7}$
E_1	$\Gamma_{5,6}$	Γ_4	Z_1	Γ_4	$\Gamma_{5,6}$	$\frac{15}{11}$	laser	$\frac{15}{11}$	$\frac{3}{7} \rightarrow \frac{15}{11}$	0.85	$\frac{3}{7}$
			Z_2	Γ_4	Γ_4	$\frac{15}{11}$	1.15	$\frac{3}{7} \rightarrow \frac{15}{11}$	"	0.82	$\frac{3}{7} \rightarrow 3$
			Z_3	Γ_4	Γ_4	$\frac{15}{11}$	1.22	"	"	0.82	"
			Z_4	$\Gamma_{5,6}$	$\Gamma_{5,6}$	$\frac{3}{7}$	-	$\frac{15}{11}$	$\frac{3}{7} \rightarrow 3$	-	$\frac{3}{7}$
			Z_5	$\Gamma_{5,6}$	Γ_4	$\frac{3}{7}$	0.923	$\frac{3}{7} \rightarrow \frac{15}{11}$	"	1.16	$\frac{3}{7} \rightarrow 3$
			Z_6	$\Gamma_{5,6}$	Γ_4	$\frac{3}{7}$	0.857	"	"	1.09	"
			Z_7	Γ_4	Γ_4	$\frac{15}{11}$	1.06	"	$\frac{3}{7} \rightarrow \frac{15}{11}$	1.12	"
			Z_8	Γ_4	$\Gamma_{5,6}$	$\frac{15}{11}$	1.16	$\frac{15}{11}$	"	0.82	$\frac{3}{7}$

trigonal symmetry. This implies a switching of several symmetry labels.

It is surmised that some depolarisation of the fluorescence may have occurred even in the best crystals grown here, and no commercially grown or oriented samples were available for comparison. Some depolarisation is not surprising since the crystals grown here were not as easily cleaved as the $CaF_2:Er^{3+}$ samples, and more scattering of the laser light was apparent. The reason for the difference between $CaF_2:Er^{3+}$ and $SrF_2:Er^{3+}$ is not obvious but could be due to a more gradual temperature gradient in the growth furnace at the higher temperature required to grow SrF_2, resulting in less well-defined orientation with localised regions of off-axis crystallisation.

If the limiting case for a significant depolarisation is considered where any ratio greater than unity is taken as $\frac{15}{11}$ and any ratio less than one is assumed to be as small as $\frac{3}{7}$, then two possible assignments are consistent with the data and the expected number of $\gamma_{5,6}$ levels. These are :

(a) $\gamma_{5,6}$: Z_4, Z_5, Z_6, E_1

γ_4: $Z_1, Z_2, Z_3, Z_7, Z_8, E_2$

and (b) $\gamma_{5,6}$: Z_1, Z_4, Z_8, E_2

γ_4: $Z_2, Z_3, Z_5, Z_6, Z_7, E_1$

All other combinations which would conserve the requirement of having three $\gamma_{5,6}$ symmetry wavefunctions were

discounted as they have at least two ratios that are the reverse of that required.

It has been proposed that the J site has only a small perturbation from cubic symmetry [Ai73a], so it seems likely that the Γ_7 groundstate wavefunction (Aizenberg *et al.* 1972) of the cubic site will transform to a γ_4 wavefunction groundstate for the C_{3V} site. This suggests that option (a) is the more likely of the two. In any case, as both options require $\gamma_{5,6}$ symmetry of the Z_4 level, that could not be confirmed in this study, a verification of exact trigonal symmetry for the J site could not be made.

If the true extent of depolarisation occurring is not as severe as required to allow option (a), then the site must have an off-axis distortion reducing the symmetry to less than C_{3V} and mixing the γ_4 and $\gamma_{5,6}$ wavefunctions. An optical Zeeman study of the site would determine an exact site symmetry and an ENDOR study would detect the nuclear moments of the neighbours and might indicate the presence of such a distortion. Polarisation studies with the highest quality oriented samples available would be helpful and should identify the symmetry of the Z_4 level. If this is not of the $\gamma_{5,6}$ type, then the site symmetry could not be purely C_{3V}. With the present data the exact symmetry cannot be determined.

6.4.2 The N Sites

Table 6.3 includes the energy levels determined by laser excitation of the N1, N2 and N3 sites and Figures 6.11 and 6.12 give the spectra of the N2 and N3 sites. Of these

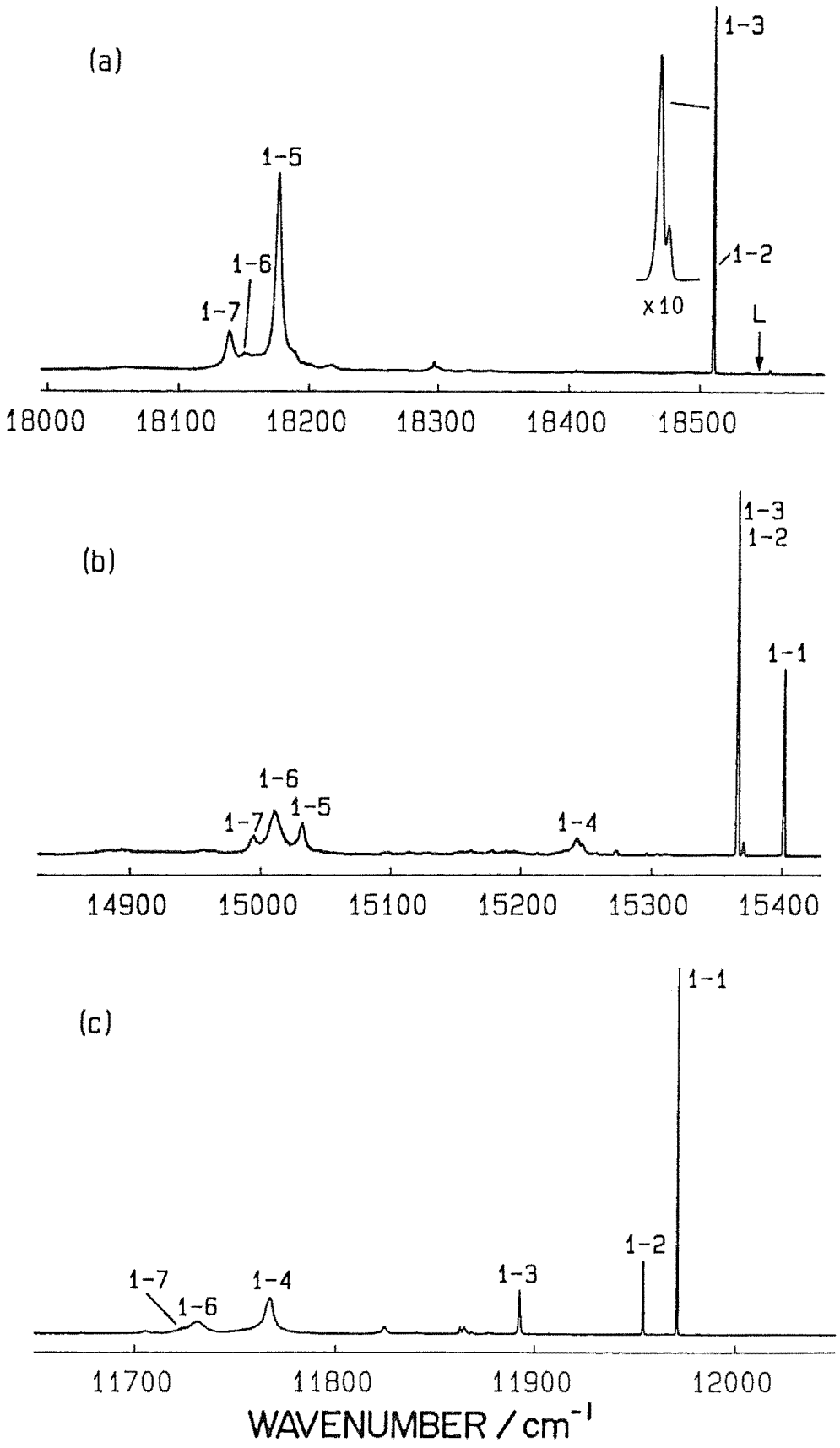

Figure 6.11 : 10K fluorescence for laser excitation of the $Z_1 \rightarrow E_1$ transition of the N2 site : (a) $^4S_{3/2} \rightarrow {}^4I_{15/2}$, (b) $^4F_{9/2} \rightarrow {}^4I_{15/2}$, and (c) $^4S_{3/2} \rightarrow {}^4I_{13/2}$.

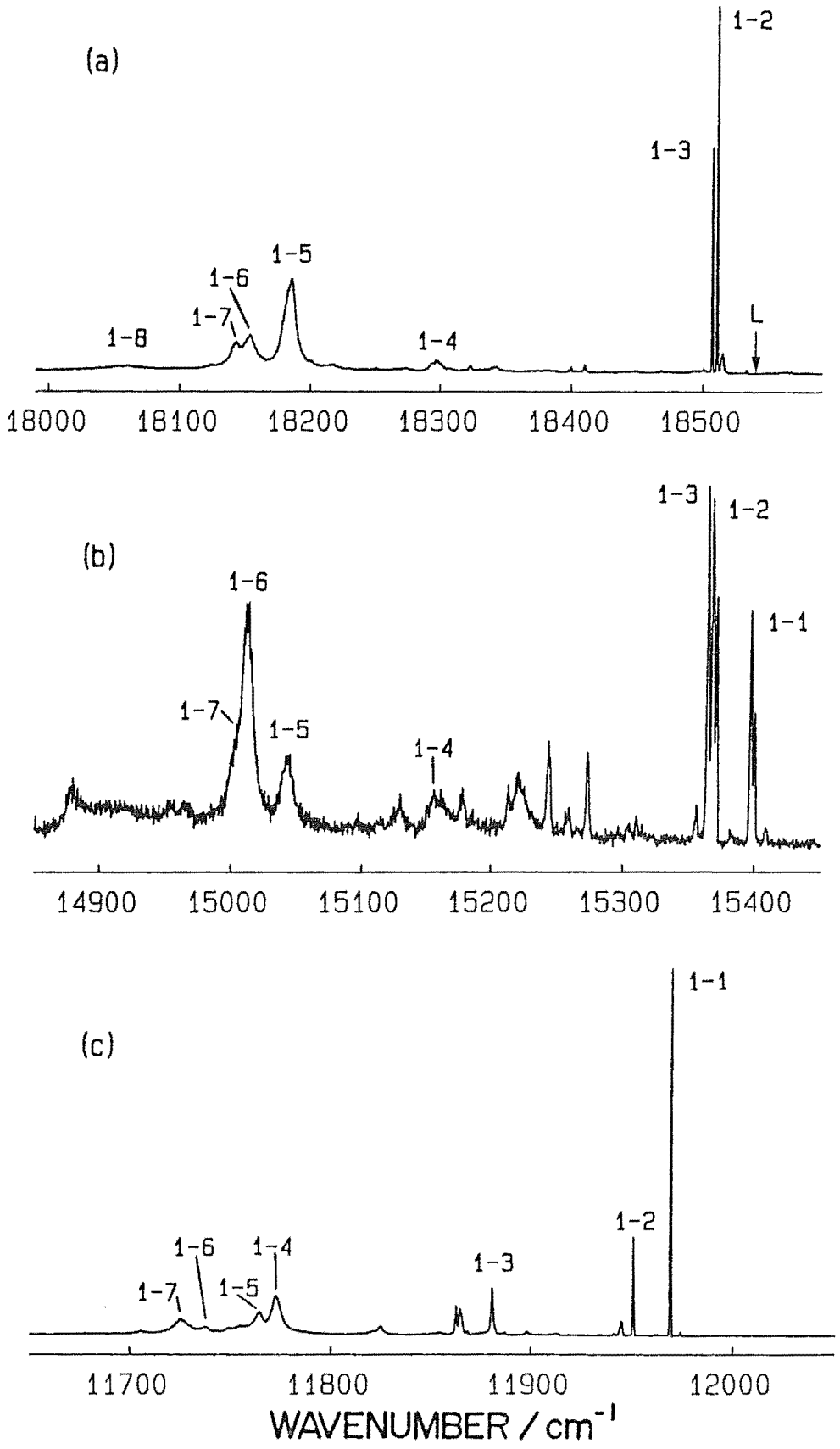

Figure 6.12 : 10K fluorescence for laser excitation of the $Z_1 \rightarrow E_1$ transition of the N3 site : (a) $^4S_{3/2} \rightarrow {}^4I_{15/2}$, (b) $^4F_{9/2} \rightarrow {}^4I_{15/2}$, and (c) $^4S_{3/2} \rightarrow {}^4I_{13/2}$.

sites, the N2 site was found to have the greatest intensity in all crystals.

All three sites had very similar energy levels and emission spectra and they closely resembled those of the F^-A site in $CaF_2:Er^{3+}$ [TW75]. Characteristic signatures of the sites include the weak $E_1 \rightarrow Z_4$ transition and the group of three low-lying ground state levels. In this study the Z_2 and Z_3 levels of the N2 site were found to be separated by 0.6 cm^{-1}. The previous report [KW77] did not resolve this structure and the close similarity to the N1 and N3 sites was not as obvious.

As all three sites maintain constant relative intensity to the J site for Er^{3+} concentrations as low as 0.0001% [KW77], there is no possibility that the sites involve more than one Er^{3+} ion. A site configuration for these sites has not previously been proposed and it is likely that one of the sites, probably N3, is the simple C_{4V} site with a nearest neighbour charge compensating F^- ion. It was shown by Brown *et al.*(1969b) using EPR that a tetragonal site exists for low Er^{3+} ion concentration that was weak compared to the trigonal site. The g values obtained support the presence of a site analogous to the $CaF_2:Er^{3+}$ F^- A site.

Both the N1 and N2 sites show a surprisingly small E_1, E_2 splitting of 22.3 cm^{-1} and 43.3 cm^{-1} respectively, compared to the 83.0 cm^{-1} splitting for the F^- A site (Freeth *et al.*1982), while the E_2 level of the N3 site is unknown. Since this splitting is primarily determined by the second degree crystal field term $B_0^2 C_0^{(2)}$, the expected reduction between CaF_2 and SrF_2 is only 83% as given by the cube of the ratio of lattice parameters. This corresponds

to an expected E_1,E_2 splitting of approximately 69 cm^{-1} for a C_{4V} site in SrF_2, making the N1 and N2 sites unlikely candidates.

The $Z_1 \rightarrow E_2$ absorption transition of the N3 site was too weak to detect with the laser. Such a small ratio of intensity of the $Z_1 \rightarrow E_2$ and $Z_1 \rightarrow E_1$ transitions is consistent with the $CaF_2:Er^{3+}$ C_{4V} symmetry sites. The crystal field levels also bear the closest resemblance to those of the F^- A site, so it is surmised that the N3 site is the most likely site to have C_{4V} symmetry and that the N1 and N2 sites are modifications of this.

6.5 Spectroscopy of New Non-hydrogenic Sites

The spectroscopy of the $H^-$and D^- ion sites in the $SrF_2:Er^{3+}$ system was more difficult than for the $CaF_2:Er^{3+}$ system since many sites with small absorption but relatively intense emission were present. The spectra and energy levels of some of these sites had to be resolved to enable the assignment of other lines in the spectrum to particular D^- ion sites. A total of nine sites labelled S1 to S9 were identified and the energy levels are summarised in Table 6.5. Most energy levels were determined from spectra recorded for vacuum cycled or hydrogenated crystals to distinguish from D^- ion site fluorescence.

These sites do not involve hydrogenic ion charge compensation since the fluorescence intensity and transition frequencies were identical for hydrogenated and deuterated crystals and no local mode vibronics of hydrogenic ions were observed. In all cases, however, the sites were enhanced

TABLE 6.5 : Energy levels (in cm^{-1}) of the new fluoride ion sites, S1 to S9, as derived from the 10K fluorescence spectra of SrF_2:0.05%Er^{3+} crystals. Uncertainties are ±0.5 cm^{-1} for the Z, D and E levels and 1.0 cm^{-1} for the Y levels except where indicated

	S1	S2	S3	S4	S5	S6	S7	S8†	S9
E_2	18529.9	18398.0	-	-	18425.0	18425.5	18571.0	18469.8	-
E_1	18430.3	18324.5	18457.5	18457.1	18361.0	18357.5	18454.0	18421.2	18410.0
D_3	15410.5	-	-	-	-	-	-	-	-
D_2	15332.0	15235.5	15324.0	-	-	-	15316.5	-	-
D_1	15301.3	15227.5	15316.0	15318.0	15236.5	15232.3	15309.5	15279.6	15259.2
Y_7	6813.5	6762.0	6796.5	-	6798.5	-	6807.0	6717.5	6855.5
Y_6	6742.0	6749.0	6770.5	-	6777.0	-	6757.0	6712.5	6764.5
Y_5	6709.5	6697.0	6756.0	6778.5*	6749.0	6737.0*	6697.0	6604.5	6688.5
Y_4	6683.0	6619.0	6708.5	6735.5*	6645.5	6655.5	6676.5	6571.5	6662.5
Y_3	6643.5	6565.5	6685.0	6611.0	6587.5	6588.0	6664.0	6556.0	6633.0
Y_2	6572.0	6541.0	6656.5	6582.0	6554.5	6549.0	6586.5	6553.5	6585.5
Y_1	6539.0±0.8	6512.0	6585.5	6567.0	6535.5	6525.5	6538.0	6533.5	6537.8±0.8
Z_8	436.5	358.0	393.5	422.0	421.5§	-	399.0	310.0	462.5
Z_7	314.0	341.0	365.5	394.5	397.0	-	348.5	300.0	350.0
Z_6	286.5	260.0	308.5	366.0	350.0	355*	295.5	293.5	272.0
Z_5	239.0	175.0	189.0	339.0	219.5	108.0	174.5	109.0	202.0
Z_4	199.5	98.5	146.5	107.4	93.3	81.0	150.0	105.0	140.8
Z_3	71.5	92.0	125.0	79.3	63.0	73.0	126.0	76.0	103.6
Z_2	36.5±0.4	17.0	59.0	35.9±0.4	25.7±0.4	25.3±0.4	61.5±0.4	8.8±0.4	65.3±0.4
Z_1	0	0	0	0	0	0	0	0	0

* Since other levels are missing for the multiplet, the label assignment is uncertain for these levels.

† The energy levels given for this site are those obtained from intense transitions. The following levels were also associated with the site : 115, 125, 151 and 327 cm^{-1} (Z levels) and 6642, 6651.5, 6665 and 6671 cm^{-1} (Y levels).

§ Transitions to this level have structure of unknown origin at 429.5 cm^{-1}.

and discrimination improved, to various extents, by heating the crystals with aluminium in either hydrogen or deuterium gas or under vacuum. The sites are likely to involve fluoride ion charge compensation.

Figures 6.13-6.17 present the spectra for some of the new sites and provide the basis for discrimination of D^- ion site emission and for future investigation of the charge compensation mechanism involved in these sites.

Although these sites are not of direct importance to the main emphasis of this study, the following aspects are of particular interest :

(a) The S1 and S2 sites have the greatest intensity of the sites for most crystals and were observed at intensities up to 5% of that observed for the F^- J site in crystals deuterated for 144 hours.

(b) The S3 and S4 sites have overlapping $Z_1 \rightarrow E_1$ transitions and were not able to be isolated completely. An optimisation of the relative intensity of each set of lines of a given site was possible by detuning the laser to the edge of the absorption lines, enabling the determination of most energy levels. The sites were always observed together and may form a single centre of weakly coupled Er^{3+} ions similar to the F1 and F2 sites of $CaF_2:Er^{3+}$.

(c) The S8 site appears to involve a clustered pair of Er^{3+} ions as it has more than J + ½ energy levels for the case of the $^4I_{15/2}$ and $^4I_{13/2}$ multiplets. One set of levels is associated with more intense transitions and these are included in Table 6.5.

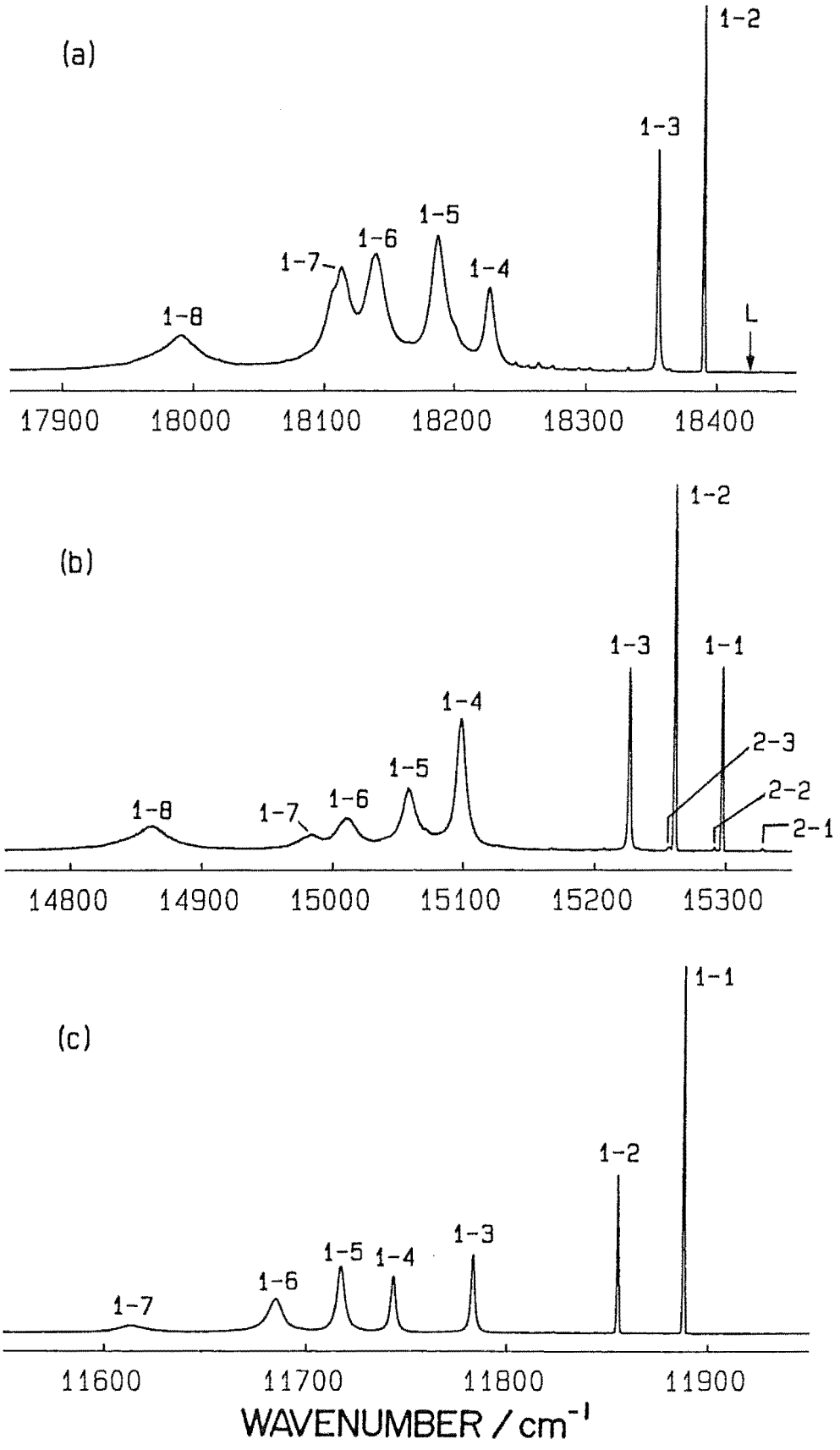

Figure 6.13 : 10K fluorescence for laser excitation of the $Z_1 \rightarrow E_1$ transition of the S1 site : (a) $^4S_{3/2} \rightarrow {}^4I_{15/2}$, (b) $^4F_{9/2} \rightarrow {}^4I_{15/2}$, and (c) $^4S_{3/2} \rightarrow {}^4I_{13/2}$.

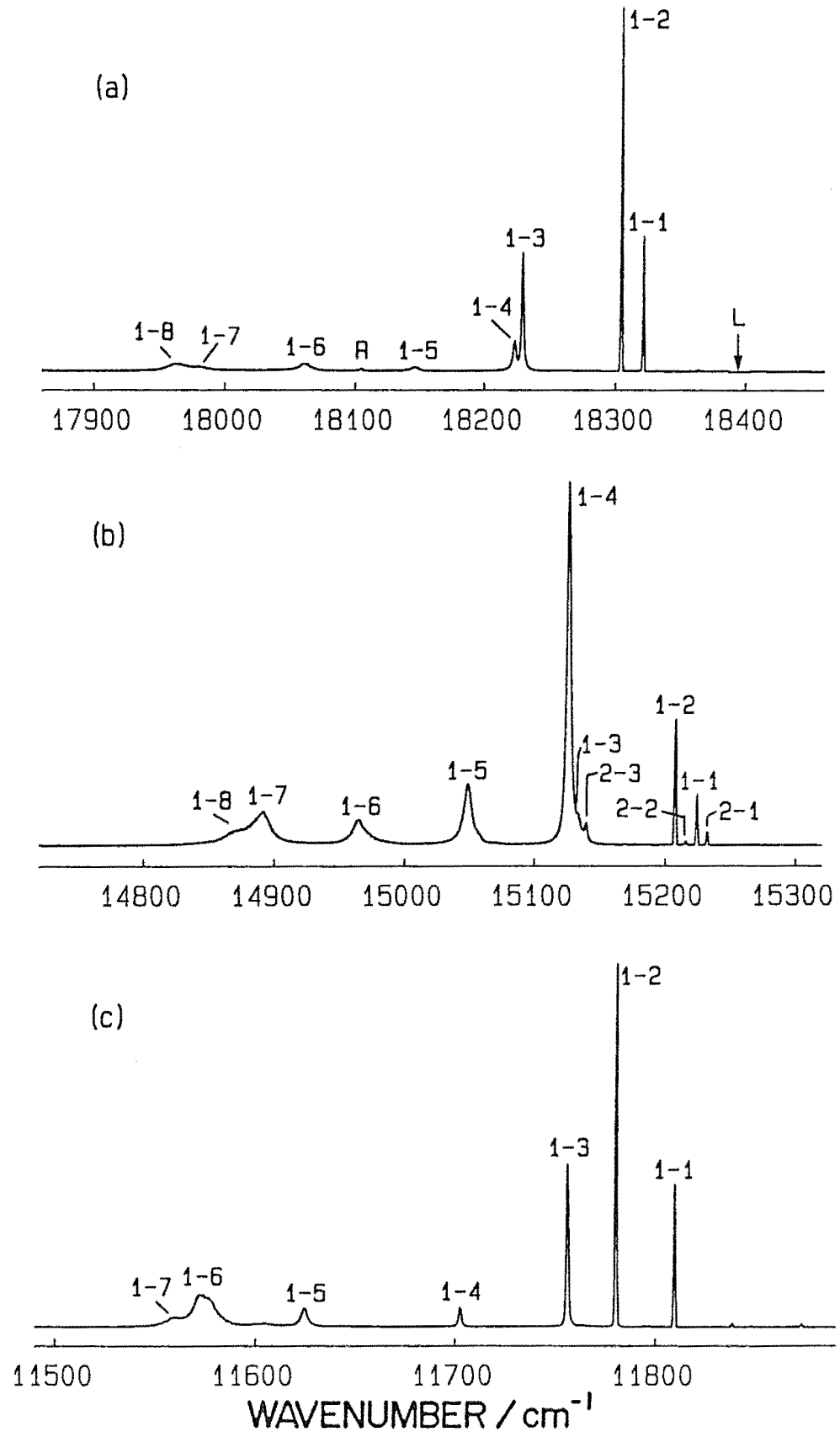

Figure 6.14 : 10K fluorescence for laser excitation of the $Z_1 \rightarrow E_2$ transition of the S2 site : (a) $^4S_{3/2} \rightarrow {}^4I_{15/2}$, (b) $^4F_{9/2} \rightarrow {}^4I_{15/2}$, and (c) $^4S_{3/2} \rightarrow {}^4I_{13/2}$.

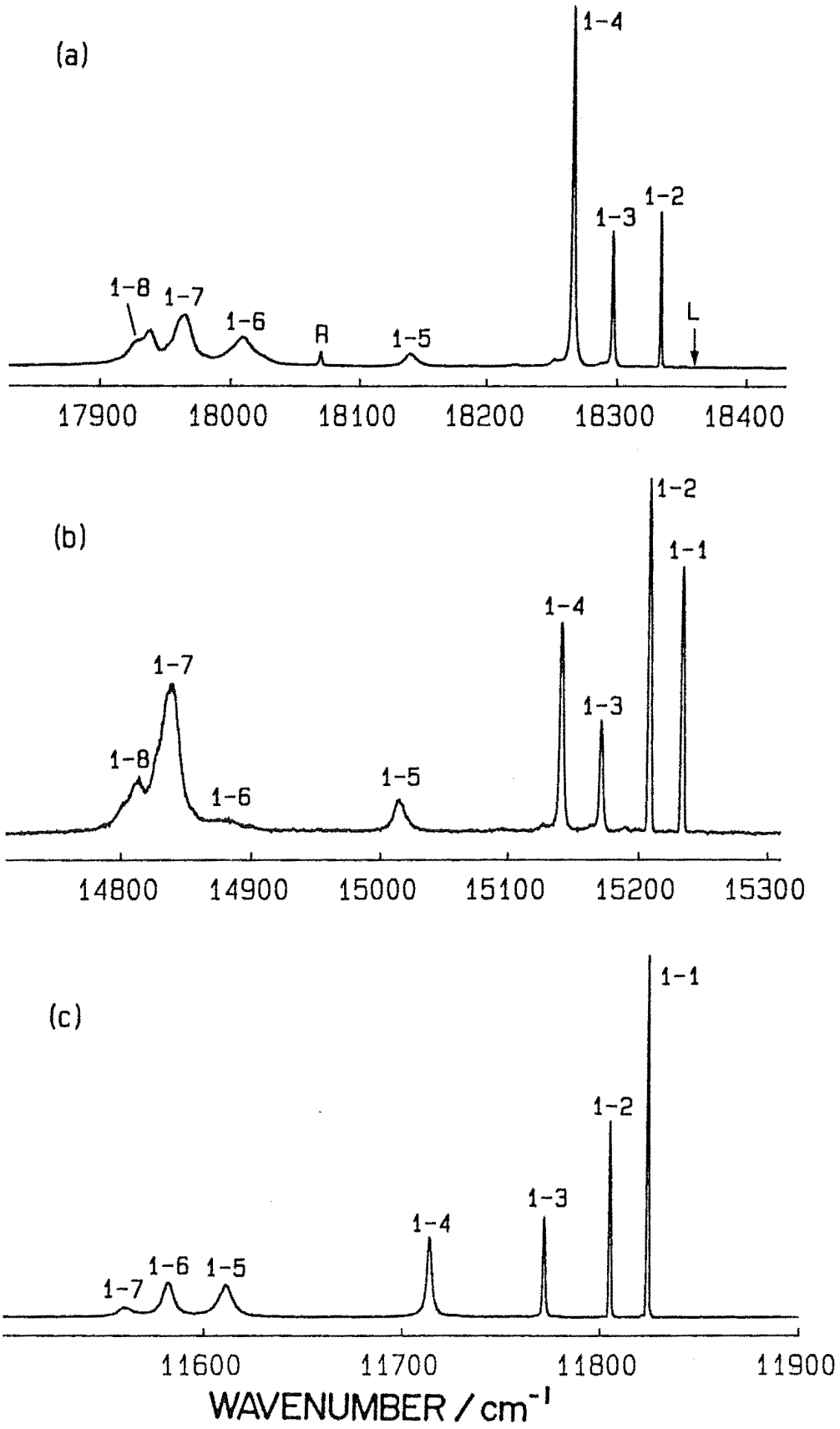

Figure 6.15 : 10K fluorescence for laser excitation of the $Z_1 \rightarrow E_1$ transition of the S5 site : (a) $^4S_{3/2} \rightarrow {}^4I_{15/2}$, (b) $^4F_{9/2} \rightarrow {}^4I_{15/2}$, and (c) $^4S_{3/2} \rightarrow {}^4I_{13/2}$.

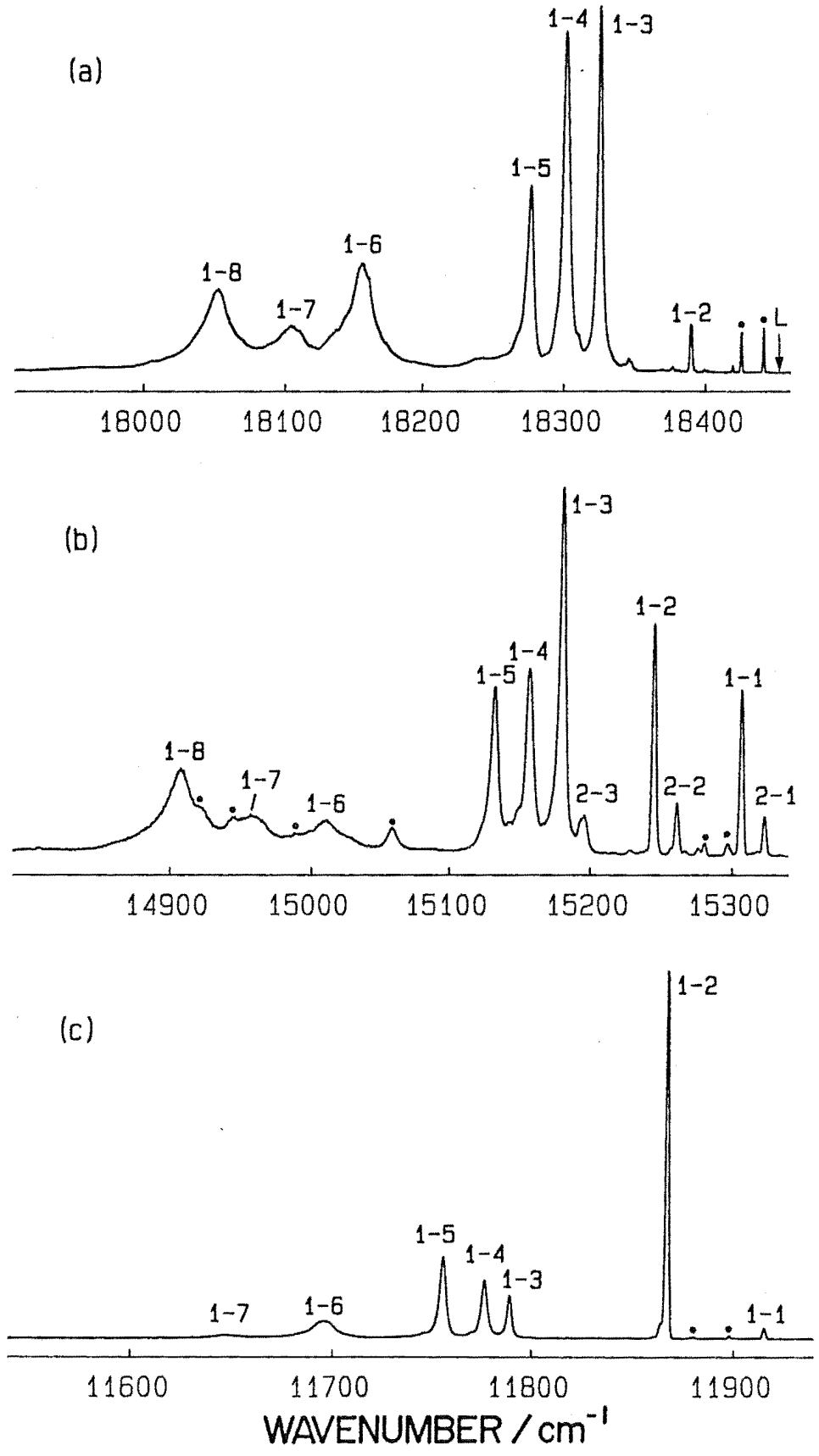

Figure 6.16 : 10K fluorescence for laser excitation of the $Z_1 \rightarrow E_1$ transition of the S7 site : (a) $^4S_{3/2} \rightarrow {}^4I_{15/2}$, (b) $^4F_{9/2} \rightarrow {}^4I_{15/2}$, and (c) $^4S_{3/2} \rightarrow {}^4I_{13/2}$.

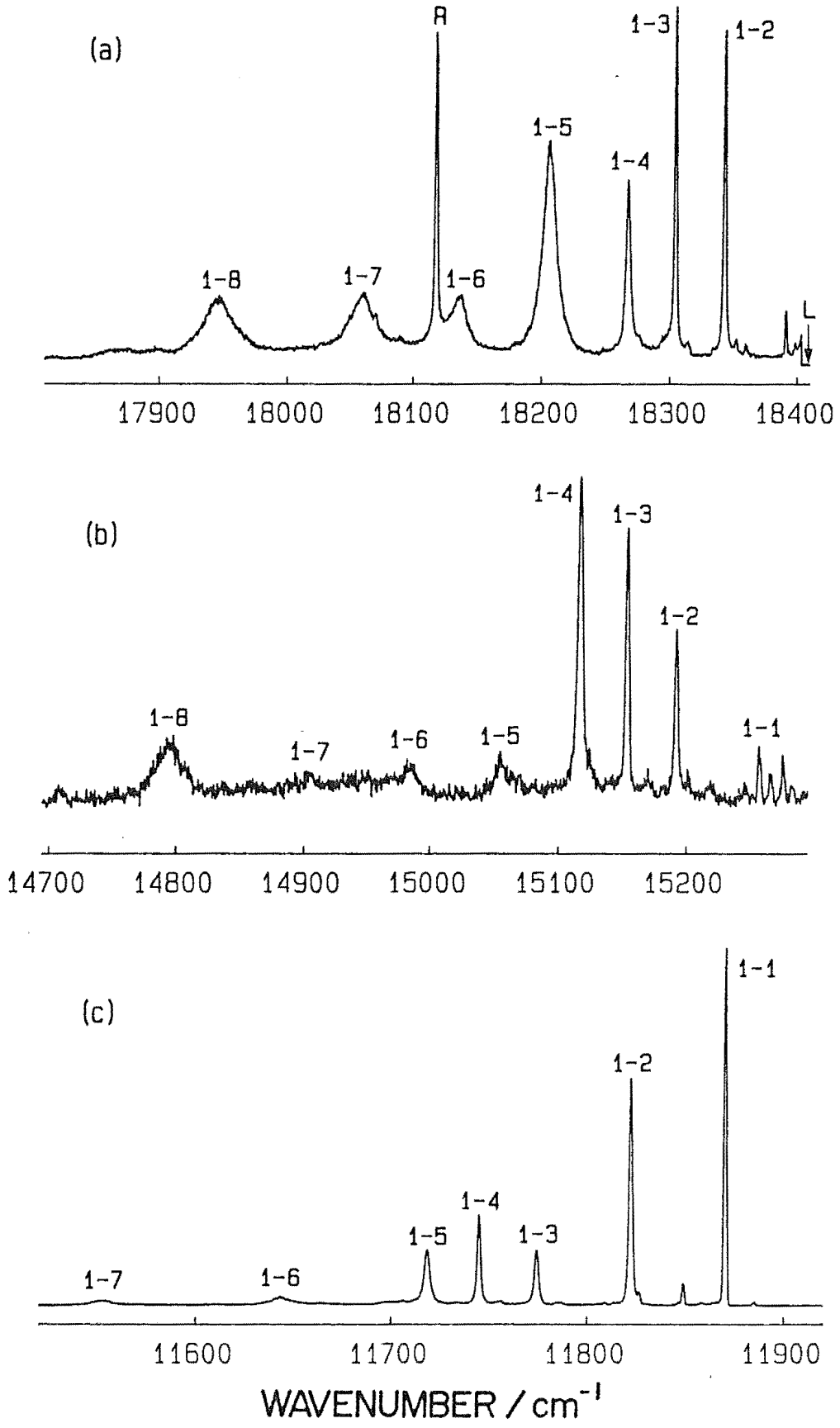

Figure 6.17 : 10K fluorescence spectra for laser excitation of the $Z_1 \rightarrow E_1$ transition of the S9 site : (a) $^4S_{3/2} \rightarrow {}^4I_{15/2}$, (b) $^4F_{9/2} \rightarrow {}^4I_{15/2}$, and (c) $^4S_{3/2} \rightarrow {}^4I_{13/2}$.

Additional levels are associated with much weaker transitions.

(d) The S9 site fluorescence from $^4S_{3/2} \rightarrow {}^4I_{13/2}$ is more intense relative to the $^4S_{3/2} \rightarrow {}^4I_{15/2}$ emission than any of the $CaF_2:Er^{3+}$ or $SrF_2:Er^{3+}$ sites previously reported, and transitions in the two spectra are of comparable intensity for $Z_1 \rightarrow E_1$ excitation. The $^4F_{9/2} \rightarrow {}^4I_{15/2}$ emission intensity is particularly weak.

(e) The principal D^- ion site, D2, has its $Z_1 \rightarrow E_1$ absorption transition overlapping with lines of the S5 and S6 sites, and all three site spectra often appear superposed.

The configurations of these sites were not able to be determined and techniques such as EPR and ionic thermocurrent measurements on vacuum cycled crystals may give an insight into the charge compensation mechanisms involved. Such studies would require correlation to specific optical sites by monitoring site distribution changes, as seen by both techniques, as a function of chemical treatment. As the H^- ion analogues of the D1 to D8 sites are only likely to be resolved by successful minimisation or elimination of several of these sites by chemical techniques, further investigations of such a nature would be productive.

6.6 Crystal Field Fitting at Trigonal Symmetry Sites

6.6.1 SrF_2 J Site

Computer programs were written to fit the data obtained

for the F^-J site to a C_{3V} symmetry crystal field Hamiltonian. One previous attempt at such a fit has been reported by Aizenberg *et al.* (1973b), but the Hamiltonian used assumed only small perturbation from cubic symmetry and used only an axial and two cubic parameters. The quality of fit obtained was not particularly good and was not well quantified. A reassignment of some of the crystal field levels should give a more reliable indication of the parameters and a new parameterisation will allow for some deviation from cubic symmetry about the Er^{3+} ion.

Since the polarisation information obtained in this study is insufficient to prove C_{3V} symmetry unambiguously, future work should be aimed at direct verification by such techniques as optical Zeeman studies. In the interim it is productive to determine whether the crystal field data can be satisfactorily fitted to a trigonal field, and to check that the resultant parameters are physically reasonable.

The following form of the Racah tensor expansion of the crystal field Hamiltonian was used :

$$
\begin{aligned}
V_{CF} = {} & b_0^2\, C_0^{(2)} + b_c^4\left[C_0^{(4)} + \sqrt{\tfrac{10}{7}}\left(C_3^{(4)} - C_{-3}^{(4)}\right)\right] \\
& + b_c^6\left[C_0^{(6)} - \tfrac{1}{4}\sqrt{\tfrac{35}{6}}\left(C_3^{(6)} - C_{-3}^{(6)}\right) + \tfrac{1}{8}\sqrt{\tfrac{77}{3}}\left(C_6^{(6)} + C_{-6}^{(6)}\right)\right. \\
& + b_{trig}^4\left[C_0^{(4)} - \tfrac{1}{2}\sqrt{\tfrac{7}{10}}\left(C_3^{(4)} - C_{-3}^{(4)}\right)\right] \\
& + b_{trig}^6\left[C_0^{(6)} + \tfrac{4}{7}\sqrt{\tfrac{10}{21}}\left(C_3^{(6)} - C_{-3}^{(6)}\right) - \tfrac{4}{7}\sqrt{\tfrac{11}{21}}\left(C_6^{(6)} + C_{-6}^{(6)}\right)\right] \\
& + \hat{b}_{trig}^6\left[\sqrt{\tfrac{11}{42}}\left(C_3^{(6)} - C_{-3}^{(6)}\right) + \sqrt{\tfrac{5}{21}}\left(C_6^{(6)} + C_{-6}^{(6)}\right)\right] \qquad (6.1)
\end{aligned}
$$

These tensor combinations for the JJ_z basis can be obtained from the conversion tables of Butler (1981) for the invariant scalers in the point group basis for the symmetry reduction $SO_3 \rightarrow O \rightarrow D_3 \rightarrow C_3$.

The Fortran routines used were based on the following method :

The possible combinations of wavefunctions in the $|JJ_z>$ basis for $J = \frac{15}{2}$ and $\frac{13}{2}$ form a 30 x 30 element symmetric matrix that can be stored in a 465 element array since only one half of the matrix is needed.

Initially these matrix elements are generated for each k,q value of the tensor combination multiplied by the appropriate coefficients of Equation 6.1. A file with the six matrices for each parameter plus one more matrix for the spin orbit interaction was created.

The parameter ζ was determined by the separation of the barycentres of the two multiplets which results from the non zero matrix element for diagonal terms of the spin orbit interaction. In this case the multiplet separation is 2.5ζ.

A single energy matrix can be generated by summing the seven products of parameter values with the appropriate array of matrix elements. Diagonalising the matrix gives the predicted energy levels as eigenvalues and wavefunctions as eigenfunctions. The recommended parameter changes are then calculated by standard least squares methods, and the energy matrix is recalculated using the new parameters. This iterative process is repeated until the deviation

between the predicted and observed energy levels is minimised.

These methods were used to fit the $^4I_{15/2}$ and $^4I_{13/2}$ multiplet data of Table 6.3. To minimise the number of parameters varied, the second degree axial parameter b_0^2 may be determined from the (22.1±0.3) cm^{-1} splitting of the two components E_1 and E_2 of the $^4S_{3/2}$ multiplet.

Dieke (1968) has given modified Stevens' operator equivalent factors of the crystal field multiplets that are multiplied by b_0^2 to give the crystal field splitting for $J = \frac{3}{2}$ multiplets.

This gives $b_0^2 = \frac{22.1cm^{-1}}{0.1159} = 190.7\ cm^{-1}$.

A verification is obtained by applying the appropriate factor, 0.2039, to the splitting of the $^2P_{3/2}$ multiplet determined by Aizenberg *et al.* (1973a) to be 38.0 cm^{-1} :

$$b_0^2 = \frac{38.0cm^{-1}}{0.2039} = 186.4\ cm^{-1} .$$

This agreement gives confidence that an average value for b_0^2 of 189 cm^{-1} could be used in the computer fitting.

Since the J site energy levels appear to be quite similar to the cubic site (Aizenberg *et al.* 1972) a preliminary attempt was made to fit the $^4I_{15/2}$ and $^4I_{13/2}$ data by using a Hamiltonian with only the axial, b_0^2, term and the two cubic parameters, b_c^4 and b_c^6, as follows :

$$H_{CF} = b_0^2 C_0^{(2)} + b_c^4 \left[C_0^{(4)} + \sqrt{\frac{10}{7}} \left(C_3^{(4)} - C_{-3}^{(4)} \right) \right] +$$

$$b_c^6 \left[C_0^{(6)} - \frac{1}{4} \sqrt{\frac{35}{6}} \left(C_3^{(6)} - C_{-3}^{(6)} \right) + \frac{1}{8} \sqrt{\frac{77}{3}} \left(C_6^{(6)} + C_{-6}^{(6)} \right) \right]$$

All three parameters and the spin orbit coupling factor were allowed to vary and were fitted by least squares to a standard deviation of energy levels of 10 cm^{-1} giving best fit parameters of :

$$b_0^2 = 184.7 \text{ cm}^{-1} \qquad b_c^4 = 1117.4 \text{ cm}^{-1} \qquad b_c^6 = 1005.5 \text{ cm}^{-1}$$
$$\text{and } \zeta = 2577.1 \text{ cm}^{-1} \quad .$$

It was apparent from the deviation of the fit that the trigonal terms should be included, so the C_{3V} crystal field Hamiltonian of equation 6.1 was used with B_0^2 being fixed at its expected value, and the remaining five crystal field parameters and spin orbit coupling factor being fitted by least squares deviation to the eight known $^4I_{15/2}$ and six $^4I_{13/2}$ crystal field levels. The cubic parameter values obtained above provided a useful starting point for the fit.

The fit obtained had a standard deviation for fourteen energy levels of 4.3 cm^{-1} and gave the following best fit parameters :

$b_0^2 = 189.0\ cm^{-1}$ $b_c^4 = 1113.0\ cm^{-1}$ $b_c^6 = 986.7\ cm^{-1}$

$b_{trig}^4 = -246.8\ cm^{-1}$ $b_{trig}^6 = 103.6\ cm^{-1}$ $\hat{b}_{trig}^6 = -280.4\ cm^{-1}$

and $\zeta = 2578.0\ cm^{-1}$.

The calculated crystal field levels are compared to the experimental values in Table 6.6.

The basis for assigning C_{3V} symmetry to the J site is the substantial intensity of the site in the optical spectrum compared to the dominance in the EPR spectrum of a site with trigonal symmetry [Br69b]. If the two sites are identical then the g values for the Z_1 level of the J site should be those determined by EPR :

$$g_{\|} = 6.163 \pm 0.005$$

and

$$g_{\perp} = 7.038 \pm 0.007$$

Analysis of the wavefunctions produced by the above crystal field fit, however, yielded g values for the Z_1 level of :

$$g_{\|} = 5.14$$

and

$$g_{\perp} = 7.46 \quad .$$

This result suggests further data were required to provide a more accurate indication of the true parameter values, the program was modified to include least squares fitting to the two g values. The data was weighted to the experimental uncertainties and the best fit obtained had a standard deviation of energy levels of 5.2 cm^{-1}. Analysis

Table 6.6 : Calculated and experimentally determined energy levels (in cm^{-1}) of the $^4I_{15/2}(Z)$ and $^4I_{13/2}(Y)$ multiplets of the $SrF_2:Er^{3+}$ J site. Calculated values are those obtained by a least squares fit of the experimental data to a C_{3V} symmetry Hamiltonian either with inclusion of g values † (fit (b)) or without (fit (a)).

State	Calculated (a)	Experimental	Calculated (b)	Wavefunction
Z_1	0	0	0	γ_4
Z_2	80.9	81.4 ± 0.3	81.6	γ_4
Z_3	85.1	89.0 ± 0.3	89.9	$\gamma_{5,6}$
Z_4	114.5	116.0 ± 0.5	111.3	γ_4
Z_5	498.7	496.0 "	502.9	$\gamma_{5,6}$
Z_6	510.7	515.0 "	507.2	γ_4
Z_7	562.5	558.0 "	562.2	γ_4
Z_8	599.0	598.0 ± 1.0	600.3	$\gamma_{5,6}$
Y_1	6606.2	6609.8 ± 1.0	6611.5	γ_4
Y_2	6623.1	6619.8 "	6624.3	$\gamma_{5,6}$
Y_3	6638.1	6631.6 "	6635.0	γ_4
Y_4	6845.4	not known	6845.5	γ_4
Y_5	6860.8	6870.2 ± 1.2	6856.9	$\gamma_{5,6}$
Y_6	6875.4	6876.5 ± 1.2	6874.8	γ_4
Y_7	6888.7	6884.2 ± 1.2	6889.8	γ_4
$g_{\parallel}$	5.141*	6.163 ± 0.005	6.135	
$g_{\perp}$	7.457*	7.038 ± 0.007	7.000	
Stnd.devtn. of energy levels	4.3		5.2	

* not included in this fit.
† g values of Brown *et al.* (1969b).

of the wavefunctions calculated gave the irrep symmetry labels included together with energy levels and g values in Table 6.6. The resultant best fit parameters obtained were the following :

$$b_0^2 = 189.0 \text{ cm}^{-1} \quad b_c^4 = 1097.7 \text{ cm}^{-1} \quad b_c^6 = 999.4 \text{ cm}^{-1}$$

$$b_{trig}^4 = -142.9 \text{ cm}^{-1} \quad b_{trig}^6 = 106.8 \text{ cm}^{-1} \quad \hat{b}_{trig}^6 = -222.8 \text{ cm}^{-1}$$

$$\text{and } \zeta = 2577.8 \text{ cm}^{-1} \quad .$$

Since this provided a much more accurate fit to the g values, these parameters are considered the most reliable obtained.

As very little trigonal field fitting for this type of site has previously been done, no comparisons can be made with the trigonal parameters obtained. It can be shown, however, that the second degree axial and both cubic parameters obtained are approximately those expected, and the fit obtained is therefore physically realistic.

The b_0^2 parameter is proportional to D^{-3} where D is the separation of the Er^{3+} ion and the interstitial F^- ion. If a point charge model is assumed then this value can be compared to the F^-A site value of $B_0^2 = 608 \text{ cm}^{-1}$ (Freeth *et al.* 1982). The NNN distance is $\sqrt{3}$ greater than the NN distance and the lattice constant of SrF_2 is 1.06 times that of CaF_2, therefore the ratio of separations in the J site and the CaF_2 C_{4V} site is 1.84. The estimated b_o^2 value of the J site would thus be approximately $(1.84)^{-3}\ B_0^2 \simeq 100$ cm^{-1}. The difference between this and the b_0^2 value

obtained is reasonable since the true separations are modified by lattice distortion about the Er^{3+} and F_I^- pair. Aizenberg *et al.* (1973a) obtained a very similar (converted) b_0^2 value of 178 cm^{-1} for their crystal field fit.

Appropriate factors for converting the tetragonal symmetry Hamiltonian cubic parameters, B^4 and B^6 (Equation 5.1), which use the z axis of quantization, to the trigonal symmetry Hamiltonian cubic parameters, b_c^4 and b_c^6, which use a <111> axis of quantization, can be derived and are shown by Hutchings (1964) to be $-\frac{2}{3}$ and $\frac{16}{9}$ for the fourth and sixth degree terms respectively. The values of $B^4 = -1744.5$ cm^{-1} and $B^6 = 447.78$ cm^{-1} given by Freeth *et al.* (1982) for the F^-A site of C_{4V} symmetry convert to $b^4 \simeq 1160$ cm^{-1} and $b^6 \simeq 800$ cm^{-1}. The cubic parameters obtained for the J site can therefore be considered physically realistic and indicative of a nearest-neighbour cube of eight F^- ions for both sites. Conversion of the results of Aizenberg *et al.* for their best fit, neglecting fourth and sixth degree trigonal terms, gives parameter values of $b_c^4 \simeq 1060$ cm^{-1} and $b_c^6 \simeq 960$ cm^{-1} which are comparable with the present results.

The trigonal terms b_{trig}^4, b_{trig}^6 and $\hat{b}_{trig}^6$ are relatively small compared to the cubic terms, indicating a small perturbation in the fourth and sixth degree from cubic symmetry. These values will provide a basis for comparison with other trigonal systems that could be fitted to the same Hamiltonian in the future.

6.6.2 CaF_2 B and G1 Sites

As a supplement to this work, the data obtained for two trigonal sites of $CaF_2:Er^{3+}$, the F^-B and $O^{2-}G1$, site were

fitted to the Hamiltonian of Equation 6.1.

The G1 site has been correlated to the site involving a single O^{2-} ion replacing an F^- ion on the corner of a cube about the Er^{3+} ion. EPR measurements of oxygenated crystals show a dominant trigonal symmetry site with $g_{\|}$ = 2.21 and $g_{\perp}$ = 8.84 (Ranon and Low 1963). The site was fitted both with and without these g values being specified,and the best fit energy levels having standard deviations of 4.1 cm^{-1} and 3.8 cm^{-1} are included in Table 6.7.

Best fit parameters for the site with specified g values were as follows, with the parameters for the fit without g values in brackets :

$$b_0^2 = 1285.0\ cm^{-1} \qquad b_c^4 = 1129.9(1120.2)cm^{-1}$$

$$b_c^6 = 859.3(863.1)cm^{-1}$$

$$b_{trig}^4 = 762.7(818.6)cm^{-1}$$

$$b_{trig}^6 = -148.5(-152.4)cm^{-1}$$

$$\hat{b}_{trig}^6 = 53.8(21.9)cm^{-1} \qquad \zeta = 2580.6(2580.2)cm^{-1}$$

The b_0^2 parameter was fixed by the large E_2, E_1 splitting of 149.0 cm^{-1}.

An indication of whether the parameters are reasonable can be gained by considering the proposed model configuration. Charge compensation is by an O^{2-} ion in a closer position to the rare-earth ion than a nearest-neighbour F^- interstitial ion, resulting in an

Table 6.7 : Calculated and experimentally determined energy levels (in cm^{-1}) of the $^4I_{15/2}(Z)$ and $^4I_{13/2}(Y)$ multiplets of the $CaF_2:Er^{3+}$ G1 site. Calculated values are those obtained by a least squares fit of the experimental data to a C_{3V} symmetry Hamiltonian either with inclusion of g values † (fit (b)) or without (fit (a)).

State	Calculated (a)	Experimental	Calculated (b)	Wavefunction
Z_1	0	0	0	γ_4
Z_2	49.8	50.3 ± 0.4	49.1	$\gamma_{5,6}$
Z_3	99.4	99.8 ± 0.4	97.9	γ_4
Z_4	195.9	199.0 ± 0.5	194.8	γ_4
Z_5	429.7	428.5 "	429.6	γ_4
Z_6	443.4	442.5 "	445.6	$\gamma_{5,6}$
Z_7	458.1	457.5 "	460.9	γ_4
Z_8	749.6	750.5 "	743.2	$\gamma_{5,6}$
Y_1	6585.4	6586.7 ± 0.8	6585.1	γ_4
Y_2	6607.2	6613.0 ± 1.0	6607.1	$\gamma_{5,6}$
Y_3	6693.3	6683.0 "	6692.2	γ_4
Y_4	6781.3	-	6784.5	γ_4
Y_5	6795.9	-	6798.2	$\gamma_{5,6}$
Y_6	6811.3	6814.5 ± 1.0	6812.8	γ_4
Y_7	7066.7	-	7064.0	γ_4
$g_{\parallel}$	2.232*	2.206 ± 0.007	2.226	
$g_{\perp}$	8.766*	8.843 ± 0.010	8.798	
Stnd.devtn. of energy levels	3.8		4.1	

* not included in this fit.
† g values of Ranon and Low (1963).

increase in the value of b_0^2 compared to the $F^- C_{4V}$ site. Since b_0^2 is proportional to $R \frac{q_1 q_2}{R^3}$ and the separation of the O^{2-} and Er^{3+} ion is for an undistorted lattice with point charges, a factor of $\frac{\sqrt{3}}{2}$ of that for the F^- C_{4V} site, then :

$$b_0^2 \simeq \frac{1}{(\sqrt{3}/2)^3} = 1.6 B_0^2 = 970 \text{ cm}^{-1}$$

where B_0^2 is that obtained for the C_{4V} site (Freeth *et al.*)

Alternatively, the b_0^2 value can be compared to that for the J site in SrF_2 obtained above. The distance D_{G1}, of the charge compensation by the O^{2-} ion is a factor of one half of the ratio of lattice constants smaller than that of the interstitial F^- ion of the J site, that is :

$$D_{G1} = \tfrac{1}{2}\left(\frac{5.45}{5.78}\right) D_J = 0.47 D_J \quad ,$$

giving $$b_0^2(G1) \simeq \frac{1}{(0.47)^3} b_0^2(J) \simeq 1800 \text{ cm}^{-1} \quad .$$

The value obtained of 1285 cm^{-1} is intermediate between these estimates and is reasonable since some relaxation of the lattice is expected (Corish *et al.* 1982) for the most stable configuration of ions, and hence the distances between ions are expected to be modified to some extent.

The value of the G1 site cubic parameters b_c^4 and b_c^6 is slightly modified from the F^-J site and the trigonal terms are greater. Conversion to the <111> axis of quantization gives $F^- C_{4V}$ site B^4 and B^6 values of $b_c^4 \simeq 1160$ cm^{-1} and

$b_c^6 \simeq 790\ cm^{-1}$. These values are not substantially changed for the G1 site, indicating that most of the F^- ions in the nearest-neighbour cube around the Er^{3+} ion are not affected. The increase of the b_{trig}^4, b_{trig}^6 and $\hat{b}_{trig}^6$ parameters compared to the J site is consistent with the additional charge on one corner of the cube and the different size of the O^{2-} ion causing more lattice distortion than the J site.

The crystal field levels of the B site, which was shown to be trigonal by polarisation results, were fitted both with and without the g values (as determined by EPR (Ranon and Low 1964)), and the levels from both fits are included in Table 6.8. The quality of the fit obtained was not as good as for the J site or G1 site fits with standard deviations of the energy levels of 8.8 cm^{-1} without g values, and 9.1 cm^{-1} including g values.

The best fit parameters with and without (in brackets) g values fitted were the following :

$$b_0^2 = 140.6\ cm^{-1}\quad b_c^4 = 112.1(82.8)cm^{-1}\quad b_c^6 = 581.6(581.0)cm^{-1}$$

$$b_{trig}^4 = -292.6(-76.7)cm^{-1}\quad b_{trig}^6 = -513.5(-530.7)cm^{-1}$$

$$\hat{b}_{trig}^6 = -300.1(-341.6)cm^{-1}\quad \zeta = 2593.4(2593.5)cm^{-1}$$

It should be noted that the g values used have not been unambiguously correlated to the B site but are used in this case simply because they are the values for the dominant trigonal CaF_2:Er^{3+} EPR site that has not yet been assigned to an optical site (Ranon and Low (1964)). The inclusion of the g values has a significant effect on the fourth degree

Table 6.8 : Calculated and experimentally determined energy levels (in cm^{-1}) of the $^4I_{15/2}(Z)$ and $^4I_{13/2}(Y)$ multiplets of the $CaF_2:Er^{3+}$ B site. Calculated values are those obtained by a least squares fit of the experimental data to a C_{3V} symmetry Hamiltonian either with inclusion of g values † (fit (b)) or without (fit (a)).

State	Calculated (a)	Experimental	Calculated (b)	Wavefunction
Z_1	0	0	0	γ_4
Z_2	38.5	43.5 ± 0.3	42.7	$\gamma_{5,6}$
Z_3	221.7	227.0 ± 0.5	224.8	γ_4
Z_4	242.0	261.0 ± 1.0	246.5	γ_4
Z_5	266.3	272.0 "	258.8	$\gamma_{5,6}$
Z_6	358.5	342.0 "	363.9	γ_4
Z_7	398.4	385.0 "	396.6	γ_4
Z_8	453.9	461.0 "	449.6	$\gamma_{5,6}$
Y_1	6628.6	6629.2 ± 0.8	6626.6	γ_4
Y_2	6693.7	6686.0 ± 1.0	6689.2	$\gamma_{5,6}$
Y_3	6721.2	6718.0 "	6726.3	γ_4
Y_4	6756.5	6754.0 "	6752.0	γ_4
Y_5	6767.7	6774.0 ± 1.5	6768.6	γ_4
Y_6	6775.1	6779.0 "	6784.7	$\gamma_{5,6}$
Y_7	6813.4	6816.0 "	6809.0	γ_4
$g_{\parallel}$	3.81*	3.30 ± 0.01	3.35	
$g_{\perp}$	8.28*	8.54 ± 0.02	8.49	
Stnd.devtn. of energy levels	8.8		9.1	

* not included in this fit.
† g values of Ranon and Low (1963).

terms, and until an accurate correlation of the two sites is performed, or the g values are determined by optical Zeeman measurements, it will not be clear which set of parameters is more reliable.

The pattern of symmetry labels of the wavefunctions predicted by the crystal field fit is identical to that determined by polarisation, giving confidence that the parameters are physically realistic despite the obvious differences, particularly of the cubic terms compared with those of the G1 and J sites.

The cubic parameters do not suggest an eight-fold F^- ion co-ordination for the Er^{3+} ion. Rather, a model involving vacancies, such as that recently proposed by Welsh (1985), may be more appropriate for the site. Since the NNN charge compensation mechanism has normally been assumed for this site, these results indicate that an ENDOR study, which would identify the nearest-neighbour ions, would be most productive. In any case, the actual configuration for the site must have the exact trigonal symmetry demonstrated by the polarisation results of Table 5.22.

CHAPTER SEVEN

BLEACHING PHENOMENA

7.1 Introduction

As mentioned in the two preceding chapters, there exist hydrogenic sites in both $CaF_2:Er^{3+}$ and $SrF_2:Er^{3+}$ that bleach upon laser selective excitation. That is, the fluorescence intensity monitored for a single transition is observed to decrease with time if an electronic transition of the site is excited by the laser. Moreover, for some sites in samples oriented in the <100> geometry, with linearly polarised laser light incident parallel to the [100] unit edge cell, the fluorescent level after bleaching with the laser polarised in the [001] direction can be substantially recovered by switching the laser polarisation to the [010] direction. This new phenomenon, discovered first for the R site in $CaF_2:Er^{3+}$, has been labelled 'reversible polarised bleaching' (Cockroft *et al.* 1987b). It is proposed that the effect is due to a form of photochemical holeburning involving preferential hydrogenic ion migration. Although the exact mechanism is not yet fully understood, the effect has generated preliminary interest as a potential mechanism for reversible optical memory storage. Further work on parallel systems has been undertaken (Macfarlane *et al.* 1987 (in press), Reeves, Han (Private Communication)), and high resolution optical measurements on the $CaF_2:Er^{3+}$ system are presently being made at another laboratory (Macfarlane (Private Communication)).

The purpose of this chapter is to outline the related observations for the $CaF_2:Er^{3+}$ and $SrF_2:Er^{3+}$ systems.

7.2 Background

It is useful to outline two areas of research that bear some relevance to this work: firstly, the reorientation effects of F^- or H^- ions in fluorite systems, as measured by established techniques; and secondly, the only other type of rare-earth centre in fluorites for which some photo-induced reorientation effects, albeit for electron-vacancy pairs only, have been observed.

7.2.1 Ion Reorientation Effects

High temperature mobility of ions in the fluorite structure crystals has been established with both the CaF_2 and SrF_2 systems being fast ion conductors (superionics) with transition temperatures of 1430K and 1400K respectively (Hayes and Stoneham 1985 and references therein). At these temperatures the thermal energy of the F^- ions is sufficient to overcome the potential barrier holding them in position,and application of an electric field will result in relatively high ionic conducting predominantly due to anion migration (Lidiard 1974). Catlow *et al.* (1977) have also investigated contributions due to cation migration.

When trivalent rare-earth ions RE^{3+} are present in the lattice, the additional interstitial F^- charge compensating ions that are present can migrate, if they have sufficient energy, to neighbouring interstitial positions about the RE^{3+} ion. This reorientation of the electric dipole formed by the RE^{3+} - F^- ion pair is generally thermally activated.

Two experimental techniques are well suited for measuring such reorientation.

In the ionic thermocurrent (I.T.C.)method the crystal is subjected to an electric field which aligns the RE^{3+}- F^- dipoles, and then cooled to low temperature. As the temperature is slowly raised, the current is monitored between the crystal surfaces. When a temperature is reached such that an anion has sufficient thermal energy for migration to a particular site configuration, a peak current is observed. From the temperatures and lineshapes of the peaks, the activation energy, E, and reciprocal frequency factor τ_o can be obtained, since a simple thermally activated reorientation such as for the Er^{3+}- F_I^- dipole formed by the NN charge compensated site in CaF_2 has a relaxation time given by

$$\tau(T) = \tau_o \, e^{E/kT} \qquad (7.1)$$

where E is the activation energy for a double well potential corresponding to neighbouring F_I^- ion positions. τ_o contains the terms independent of temperature

$$\tau_o = (w \, \nu_o)^{-1} e^{-\Delta S/k} \qquad (7.2)$$

with w being the number of possible jump paths, ν_o the vibrational frequency of the jumping species, ΔS the entropy of activation and k the Boltzmann constant. The form of the ITC peak, i, is described (Kitts and Crawford 1974) by

$$i(T) = \frac{AP_o}{\tau_o} e^{-E/kT} \exp\left(-\frac{1}{b\tau_o}\int_{T_o}^{T} E^{-E/kT'} dT'\right) \qquad (7.3)$$

where A is the crystal surface area, b is the heating rate and P_o is the initial polarisation :

$$P_o = p^2 \epsilon_p N/3kT_p \qquad (7.4)$$

with p the dipole moment, ϵ_p the polarising electric field, N the total dipole concentration and T_p the temperature of polarisation.

The complementary method of dielectric loss measurements derives the same parameters E and τ_o by measuring the rate at which the dipole polarisation can follow an oscillating electric field of frequency ω. Again, dipole relaxation times of the form given in equation 7.1 are assumed. The real and imaginary parts of the complex dielectric constant, ϵ' and ϵ'' respectively, are given by :

$$\epsilon' = \epsilon'_H + D/T(1+\omega^2\tau^2) \qquad (7.5)$$

$$\text{and} \quad \epsilon'' = D\omega\tau/T(1+\omega^2\tau^2) \qquad (7.6)$$

where ω is the frequency of the applied field, ϵ'_H is the high frequency limit of the dielectric constant and $D = Np^2/3\epsilon_o k$ is the dipole strength (Andeen *et al.*1977). The complex component ϵ'' can then be measured for various frequencies and temperatures determined such that $\omega\tau = 1$. The activation parameters, E and τ_o, can then be found for each peak by a best fit to the equation :

$$\ell n\omega = - E/kT - \ell n\tau_o \qquad (7.7)$$

The previous reports of dielectric loss and ITC measurements for the non hydrogenated $CaF_2:Er^{3+}$ and $SrF_2:Er^{3+}$ systems are summarised at the beginning of the two preceding chapters.

A previous attempt has been made to detect the dielectric loss peak for Gd^{3+}-H_I^- and Gd^{3+}-D_I^- dipole reorientation (Edgar and Welsh 1975). In both cases no peak was found.

Motivated by the reorientation effects observed for the hydrogenic sites in the present study, an attempt has been made at another laboratory (H.K. Welsh, Private Communication) to measure the dielectric loss peaks for hydrogenated $CaF_2:Er^{3+}$. The results to date are preliminary and cover only the region of the R_I peak due to the F^-NN ion reorientation. While more work is required to complete the study, it is apparent that the weakly hydrogenated system has a considerably wider F^- tetragonal peak than the parent crystals. This may be due either to an overlap of the Er^{3+}-H^- reorientation activation energy, or to the presence of H^- ions substituted into the F^- ion cubes around the Er^{3+}-F_I^- dipole for some of the tetragonal centres. As the hydrogenation duration is increased, the same behaviour was observed as for the optical spectra with the complete disappearance of the F^- ion tetragonal site relaxation peak. For a 68-hour hydrogenated crystal, two small peaks were detected in this same region with similar activation energies together with one additional absorption for high frequencies at lower temperatures. While these

results are preliminary, the two similar peaks are suggestive of relaxations for the R and J site since the H^- C_{4V} site is rather weak after such a long hydrogenation. Further work will be done and site correlation may be achieved by the known pattern of growth for the R site with time after hydrogenation.

One further technique for the analysis of dipole reorientation energies was reported by Edgar and Welsh (1975) for the hydrogenated $CaF_2:Gd^{3+}$ system. This utilised the EPR line broadening effect of the relaxation time associated with the anion hopping motion, and showed that the activation energies for the tetragonal Gd^{3+}- H_I^- and Gd^{3+}- D_I^- dipoles were very similar to that for Gd^{3+}- F_I^-, but the pre-exponential frequency factors are several times larger for the hydrogenic systems, consistent with higher vibrational frequencies. The EPR broadening technique is particularly useful since it directly identifies the symmetry of the species involved in reorientation.

Two principal mechanisms have been considered for the reorientation of the tetragonal dipole formed by RE^{3+}- F_I^- NN charge compensated pairs. Corish *et al.*(1982) have performed extensive computer simulations to determine the activation energies and relative likelihood of each of the mechanisms shown in Figure 7.1. The first is the direct jump of the anion through a cube edge in the [110] direction, and the second is the interstitialcy noncollinear (INC) mechanism, where a migrating interstitial anion displaces a lattice anion into a neighbouring interstitial site and occupies the site of the displaced ion. The direct jump was found, for pure CaF_2, to have a much higher

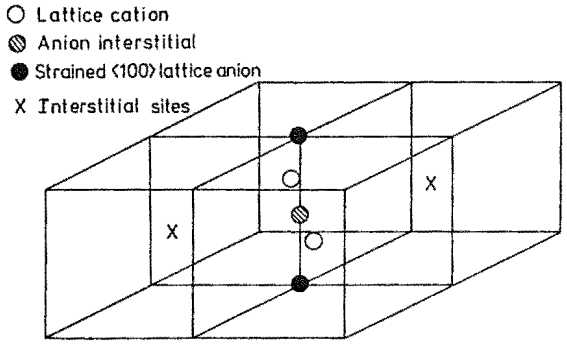

(a) Direct interstitial migration with no rare-earth ion involved (after Catlow (1976))

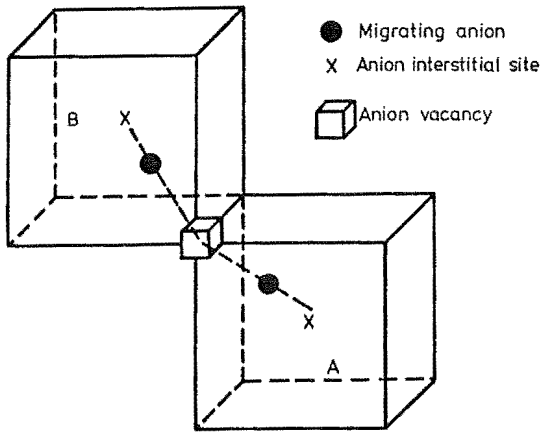

(b) Interstitialcy non-collinear (INC) mechanism (after Catlow *et al.* (1976))

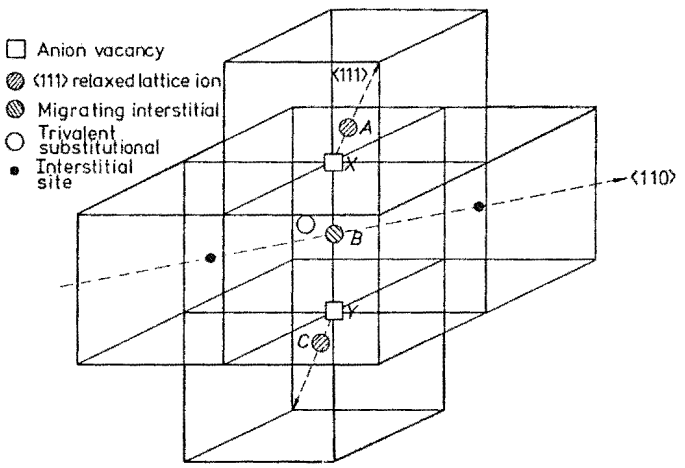

(c) Modified direct migration with lattice anion positions distorted by the RE^{3+} ion (after Catlow (1976))

Figure 7.1 : Mechanisms for F^- ion migration in fluorite lattices.

activation energy than the INC mechanism, suggesting it did not contribute significantly to processes such as fast ion conduction (Catlow *et al.* 1977).

When trivalent rare-earth ions are substituted for the lattice cations, a distortion of the lattice dependent on the dopant ionic radii occurs. Corish *et al.* (1982) have calculated that for the most stable site configuration, the lattice anions marked 'x' and 'y' in Figure 7.1(c) are relaxed in the <111> direction from their original lattice equilibrium positions. This relaxation aids the passage of the migrating anion by the direct route and reduces the activation energy for the process. However, for the case of F^- anions, the INC process is still predicted to be more probable although the activation energy difference between the two mechanisms is reduced. Corish *et al.* concluded that the INC mechanism is responsible for the R_I dielectric loss relaxation and ITC peak of the reorientating Re^{3+}-F_I^- NN charge compensating ion pair.

Another process which was predicted to be dominant for the trigonal symmetry sites with F^- ion NNN charge compensation was the relaxation to NN sites. The process NNN → NNN involves a double INC mechanism and was predicted to be energetically unfavourable.

7.2.2 Photochromic Centres

In addition to the hydrognic ion reorientation presented here, only one other type of RE^{3+} ion centre in the fluorite crystals exhibits any partial optically induced reorientation effect. These centres are known as the photochromic centres. The reorientation involves electrons

in vacancies and is apparently due to a different mechanism to the hydrogenic sites. These centres have several interesting properties and an excellent review has been given by Hayes (1974) which includes appropriate references for the material described below.

If CaF_2 crystals containing Y, La, Ce, Gd, Tb or Lu are exposed to ionizing radiation at room temperature, the optical absorption spectra of all crystals consists of four bands of a similar nature and the crystals are coloured (Staebler and Kiss 1967, 1969). If the crystals containing La, Ce, Gd or Tb are irradiated at room temperature with u.v. light (λ<400 nm), the absorption bands decrease and a new absorption grows in the visible region. This colour change is unstable and if left at room temperature for several days the crystals return to the original state. However, if the crystal is exposed to visible light, the colour is switched almost immediately and can be reversed again with u.v. light.

It was shown by EPR (Anderson and Sabisky 1971), optical (Staebler and Schnatterly 1971) techniques and ENDOR (Aldous and Baker 1976), that the sites have trigonal symmetry and involve an RE^{3+} ion surrounded by seven F^- ions in their usual cube positions and a fluoride vacancy in one cube corner, (Figure 7.2). This vacancy has two trapped electrons occupying a 1s type orbital providing charge compensation for the RE^{3+} ion. Exposure to the u.v. light can cause ionisation of one of the trapped electrons into the conduction band, and the subsequent trapping of this electron elsewhere in the crystal. In cases where the rare-earth ion is easily reduced, the electron can be

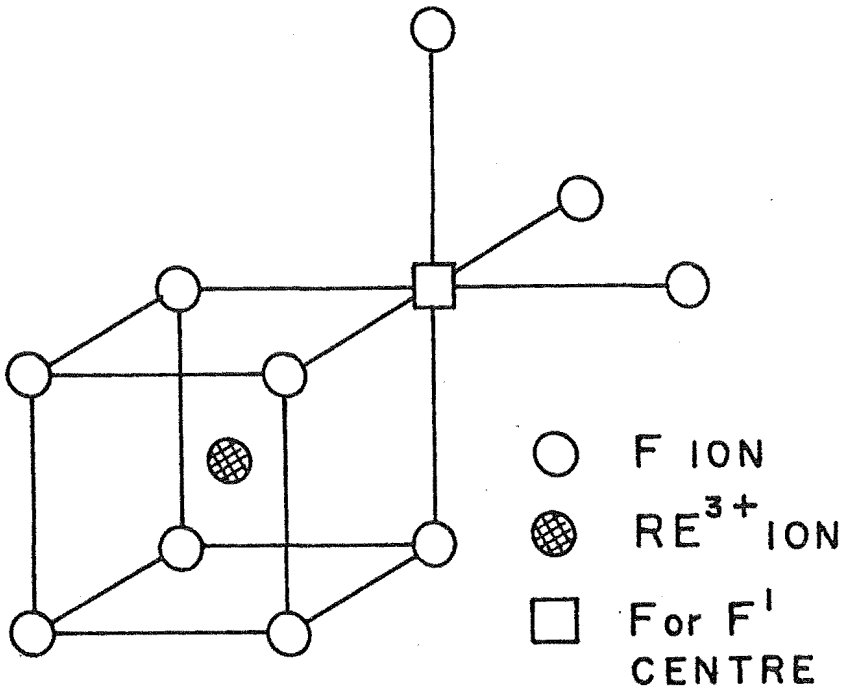

Figure 7.2 : Model of the photochromic centres in fluorite crystals (after Aldous and Baker 1976).

trapped by the rare-earth ion to form RE^{2+}. This RE^{2+} centre can give rise to absorption in the visible region and is the switched state of the photochromic. Optical excitation of the RE^{3+} ions can then reionise them to form the original site.

Since the site has trigonal symmetry, each of the bands has a preferential absorption for either π or σ polarised light. Staebler and Schnatterly (1971) found that bleaching with polarised light for several rare-earth/electron sites resulted in a preferential reorientation of some of the vacancy positions detected by polarised absorption measurements in the <111> crystal orientation. Absorption for polarisation in the <100> direction produced no reorientation of the centre, thus confirming trigonal symmetry. The mechanism for optically induced reorientation of the photochromic centres is different to that for the hydrogenic systems of this study since it is thermally activated and does not occur below about 200K (Hayes 1974).

7.3 Observations

7.3.1 Bleaching

The hydrogenic site bleaching was observed for the P, X, R, J and K sites in $CaF_2:Er^{3+}$ and the D2, D3, D4 and D5 sites in $SrF_2:Er^{3+}$. The P and X sites which are proposed to have an underlying trigonal symmetry modified by additional hydrogenic ions, are of less interest to this study as no reversibility for either site was observed in any orientation. The bleaching of these two sites may be due to hydrogenic ion migration to form another site, probably

of tetragonal symmetry, since, as explained in the preceding section, a double INC mechanism would be required for a NNN → NNN hydride ion reorientation which is less probable than a NNN → NN process.

All of the remaining sites were proposed, in the preceding chapters, to have site configurations comprising an Er^{3+} ion with hydrogenic ion NN charge compensation, and one or more additional substitutional hydrogenic ions in the lattice such as shown in Figure 5.17(a).

The bleaching experiments were generally performed with <100> oriented crystals and the laser linearly polarised in the directions y or z of Figure 7.3.

The general trends observed for the bleaching can be summarised as follows :

(a) The decay rates, form of time dependence and depth of bleaching varied between the sites.

(b) The rate of decay was faster and the extent of bleaching greater for the H^- ion sites compared to the D^- ion sites.

(c) The decay rate increased with increasing laser power.

(d) The absorption decreased simultaneously with the fluorescence.

(e) Bleaching rates were generally reduced for higher temperatures.

(f) The bleaching was persistent at 10K for at least two hours, the longest period tested.

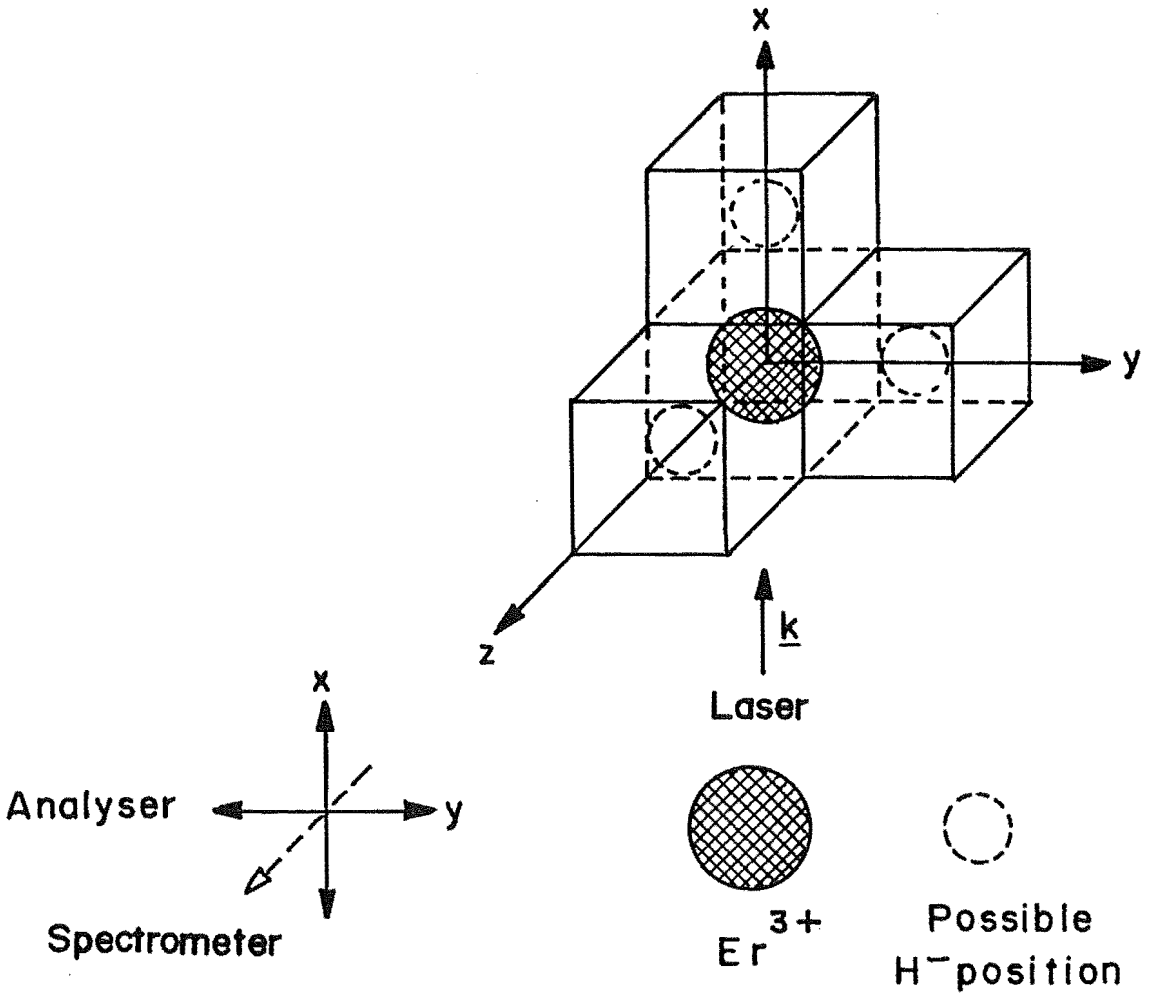

Figure 7.3 : Polarisation geometry used to study bleaching centres.

(g) Warming the crystal to 150K and recooling resulted in an almost completely restored fluorescence level.

Quantifying many of these observations proved difficult. Precise reproducibility for some measurements was not possible since only one measurement could be made for each part of a crystal, and any further information had to be obtained by moving the crystal to a fresh portion. This movement could only be done reliably a small number of times depending on sample size, and assumes perfectly uniform hydride ion site concentration in the samples. Reproducibility in the frequency domain was also difficult since the laser is normally tuned to a transition by monitoring the fluorescence level whilst altering the laser frequency. Since the fluorescence level rapidly decreased for resonance excitation, it was difficult to optimise the laser frequency by the normal method. For most of the $CaF_2:Er^{3+}$ sites the laser was tuned by inspection of the scattered image of the laser beam on a screen after passing through the sample, and observing the dip in intensity corresponding to peak absorption as the laser frequency hit resonance. Once the laser frequency was on resonance the sample was moved rapidly to a fresh portion and the fluorescence decay was recorded.

Figure 7.4 shows the normalised fluorescence intensity for the D^- ion R and J sites with a laser power of 15 mw at a temperature of 10K. The initial decay rate of the R site is faster than the J site but the decay depth is greater for the J site which continues to decay almost indefinitely. The time scale of the R site plot is expanded to show the

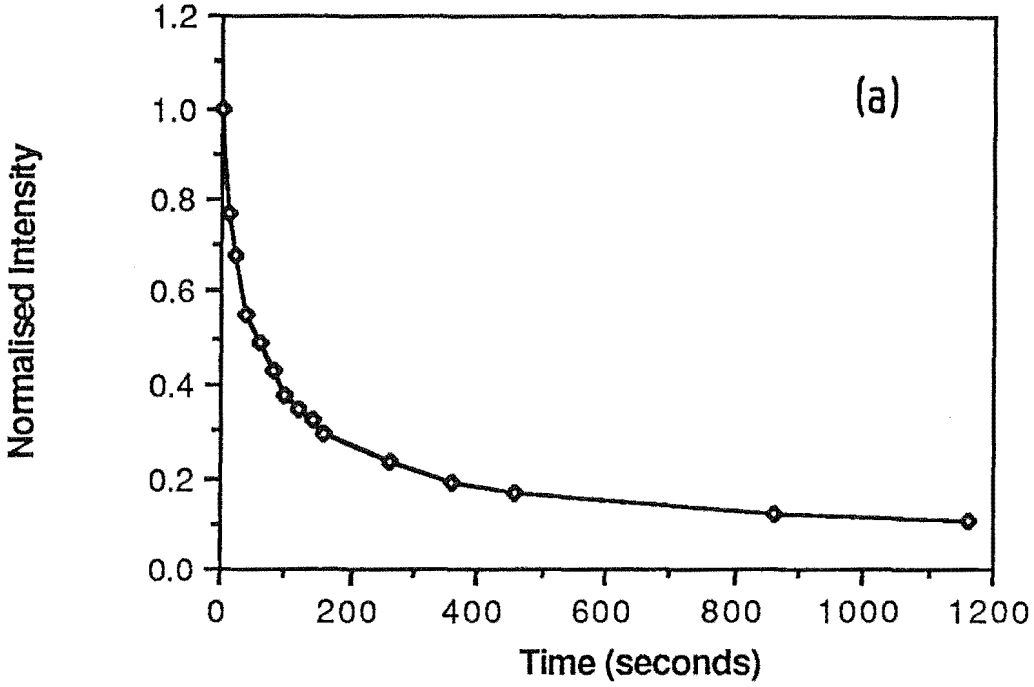

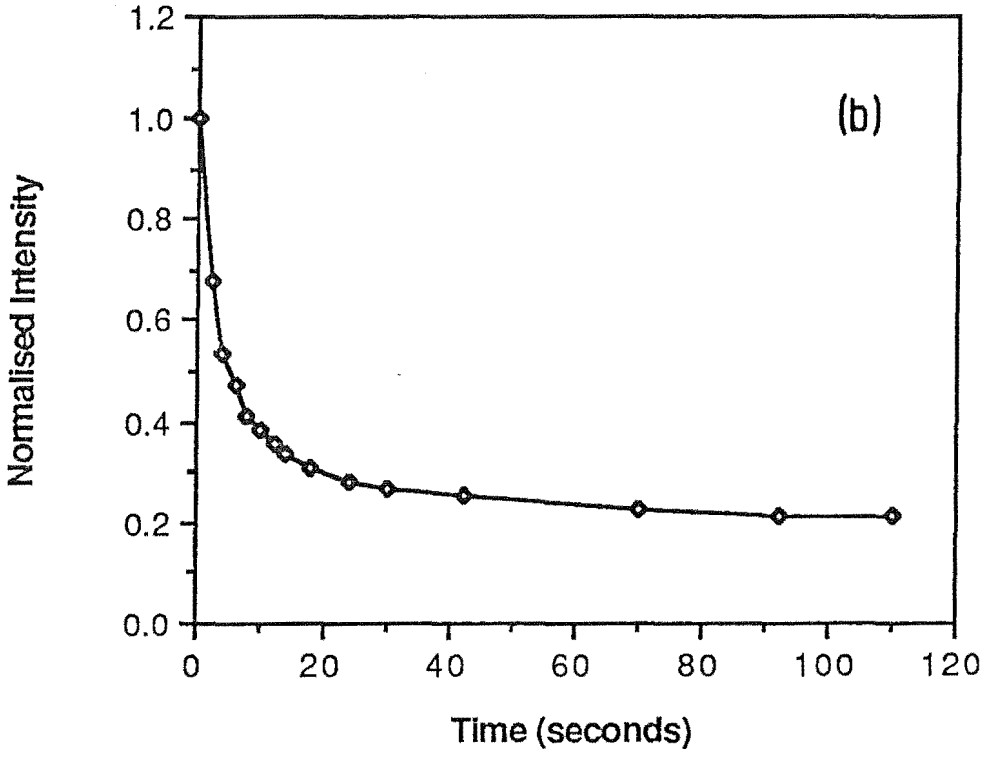

Figure 7.4 : Time dependence of the fluorescence decay monitoring $E_1 \rightarrow Z_3$ while pumping $Z_1 \rightarrow E_1$ with 18mW at 10K : (a) The D^-J site, and (b) the D^-R site.

initial decay more clearly, and after a time of about 140 seconds the fluorescence reaches an equilibrium value of about 0.205 on the normalised scale and does not decrease further.

The D^-K site bleaches in a similar manner to the D^-J site but the intensity was observed to decrease to a level of about 6% of its initial value. This extent of bleaching compares to a minimum level of 10% and 20% of initial levels observed for the D^-J and D^-R sites respectively. It should be noted, however, that these are the most extreme bleaching limits observed and that they varied between experiments. For instance, the R site was often observed to bleach to only 40% of its original level. This irreproducibility is attributed partly to the very rapid decay rate in the first few milliseconds that is damped by the electrometer-chart recorder time constant so that the initial peak recorded is not always the true maximum value, and partly to the problem of overlap with previously bleached regions.

The sites in CaF_2 were found to bleach more rapidly than the SrF_2 sites. The D2 site had a time dependence very similar to the R site but with 'half peak height' decay time about six times longer. The D3, D4 and D5 sites had time dependence more like the J than the R site but, again, the 'half peak height' times were about six times longer than for the J site.

The H^- ion analogues of each of these sites all had a 'decay to half peak height' time of less than 3 seconds. This was a factor of two faster than the D^-R site analogue, and a factor of approximately fifteen faster than the D^-J site analogue. The extent of bleaching was also increased

for the H^-R site with a final fluorescence level which was only 9% of its original value.

An attempt was made to determine the time dependence of the decay curves but it was found that each site had a differing dependence, with all, except the J site, apparently being a mixture of $\frac{1}{t}$ and exponential contributions. The D^-J site decay curve of Figure 7.5 is plotted as reciprocal intensity against time, assuming a steady state fluorescence level at infinite time of 6% of the initial. This gives an excellent linear fit indicating an $I \alpha \frac{1}{t}$ time dependence for the site. Because of the variety of time dependence encountered, it is not possible to define useful time constants for comparison of the sites. This variation of time dependence suggests that two or more mechanisms are responsible for the observed decays, except for the J site which is dominated by a single mechanism.

An example of the power dependence of the bleaching is given in Figure 7.6 which compares the decay curves with the D^-R site with incident laser power of 12 mW and 1.2 mW. The half peak height decay times are (3.8 ± 0.8) sec for 12 mW excitation and (17.5 ± 0.8) sec for 1.2 mW excitation; that is, a factor of 4.6 slower for a factor of ten change in power. It was not possible using the dye available for $^4I_{15/2} \rightarrow {}^4S_{3/2}$ excitation to cover a wide enough range of powers to determine satisfactorily the form of power dependence because of power and frequency instability at both high and low laser powers. The 1.2 mW plot was achieved by placing an attenuating filter in the path of the laser, and filters were not available for intermediate attenuation.

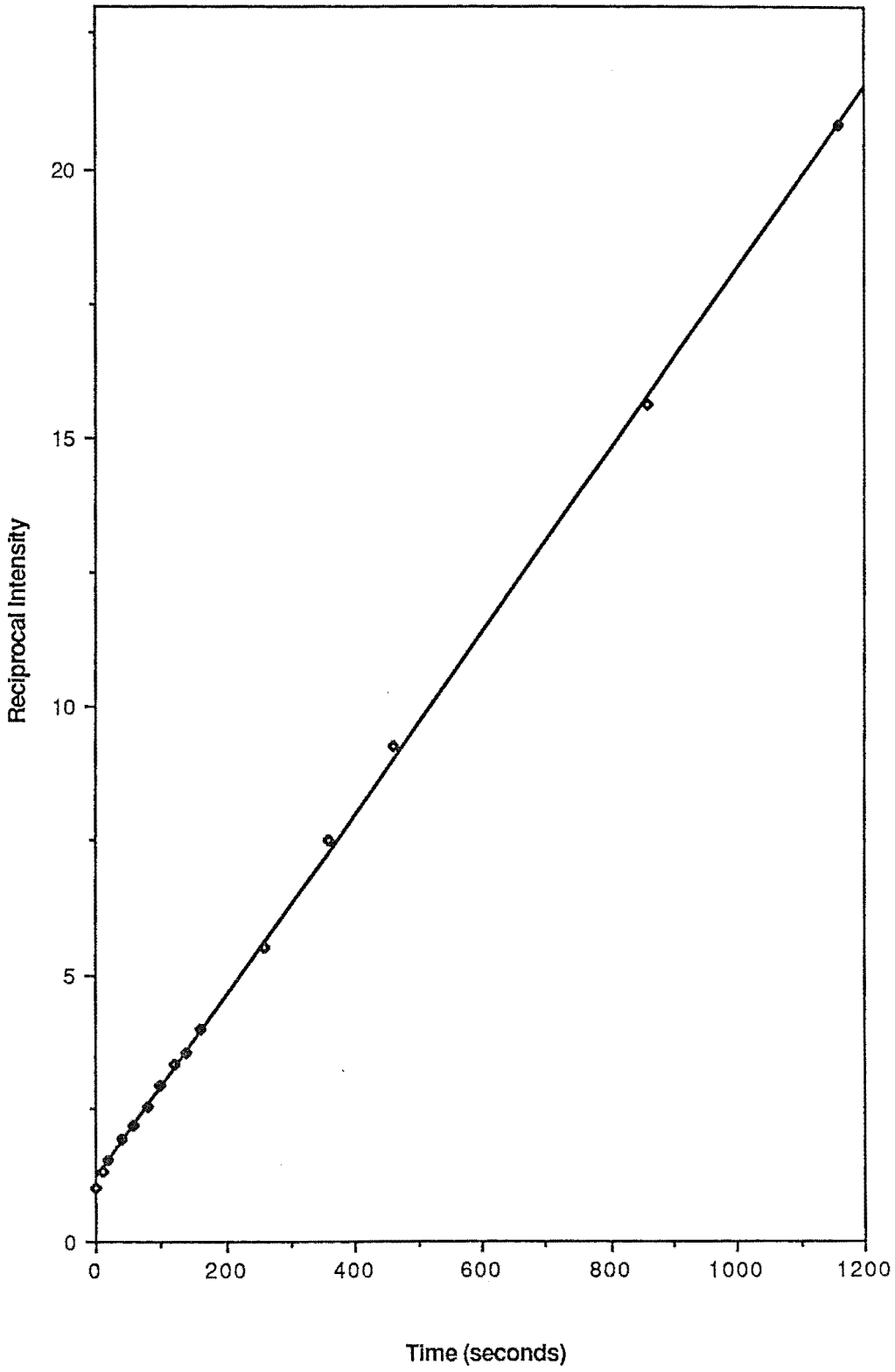

Figure 7.5 : Time variation of reciprocal intensity, assuming an asymptotic intensity of 0.06, for $Z_1 \rightarrow E_1$ excitation with 18mW of the D^-J site in CaF_2:0.05%Er^{3+}.

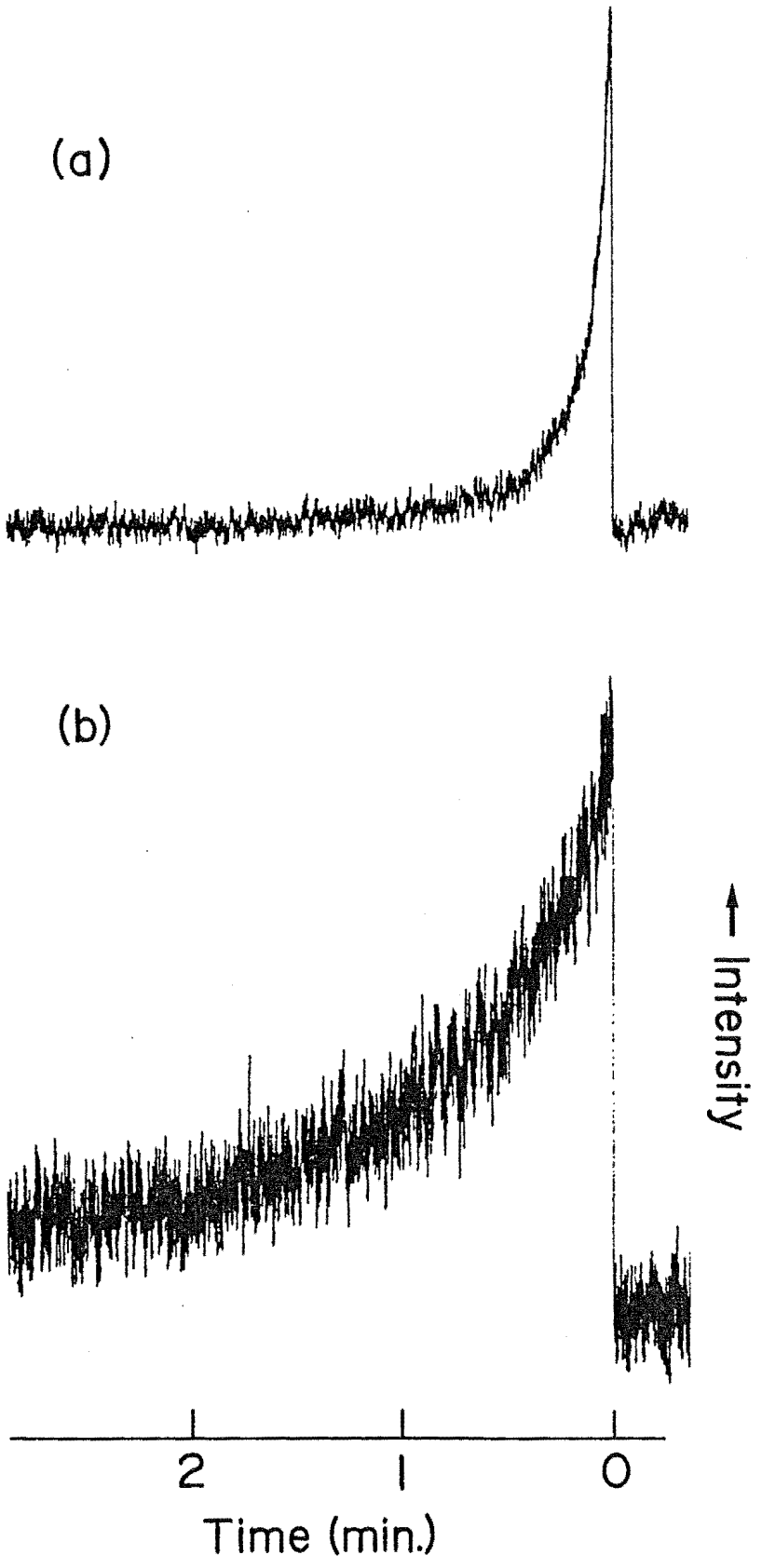

Figure 7.6 : Fluorescence decay curves for $Z_1 \rightarrow E_1$ laser excitation of the D^-R site at 10K : (a) for 12mW excitation, and (b) for 1.2mW excitation.

These bleaching phenomena have subsequently been found for analogous hydrogenic centres in both Nd^{3+} and Pr^{3+} centres in CaF_2 and SrF_2 (Reeves, Han, Private Communication)) and these are more appropriate for both temperature and power dependence studies since they are pumped by the more stable R6G dye which has a greater power range. Consolidated results of such investigations may give some indication of the limiting factors determining the bleaching rates.

The optical absorption of the pumping transition was measured by monitoring the intensity of the laser beam after passage through the crystal. In all cases the absorption was found to decrease simultaneously with the fluorescence at the same rate of decay. This was evidence that the number of absorbing centres in the sample was decreasing with time, suggesting a change in the site configuration. It is proposed that all of the bleaching observed is due to photo-induced migration of hydride ions in the site.

7.3.2 Reversible Polarised Bleaching

A small group of the bleaching sites, R, J, and D2, exhibit the phenomenon of reversible polarised bleaching described in the introduction. The D^-R site, since it has the best emission, was the most extensively investigated, and the fluorescence level for a sequence of laser polarisation changes is shown in Figure 7.7. The geometry co-ordinate system used is that shown in Figure 7.3. The site is excited by the $Z_1 \rightarrow E_1$ transition with the laser having a direction of propagation x and the spectrometer in direction z monitoring the $E_1 \rightarrow Z_2$ transition. Initially the laser

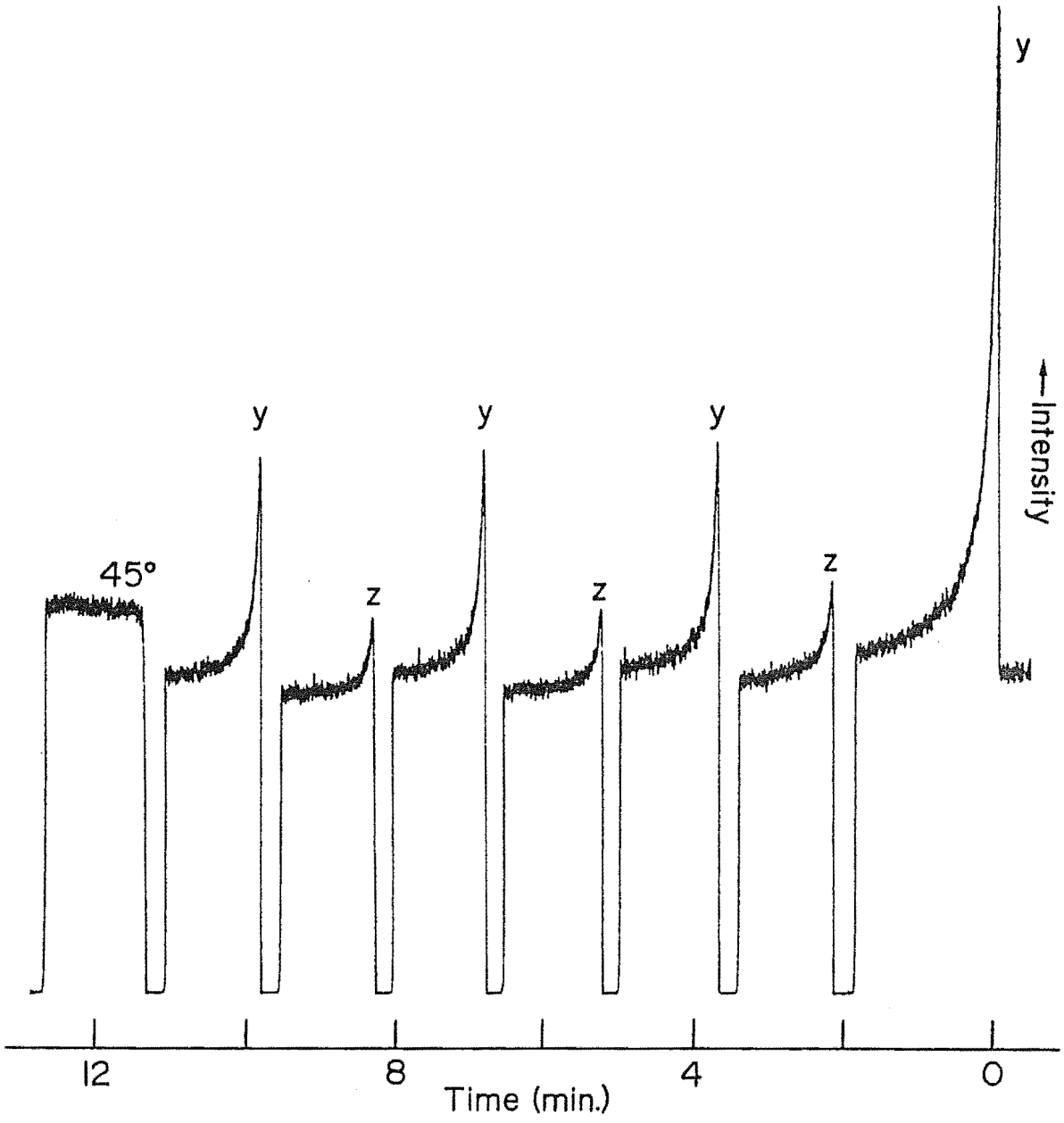

Figure 7.7 : Fluorescence intensity (monitoring $E_1 \rightarrow Z_2$) for reversible polarised bleaching at 10K of the D^-R site upon laser excitation of the $Z_1 \rightarrow E_1$ transition (18mW). The labels 'y', 'z', and '45°' indicate the polarisation of the laser and the detected fluorescence is scrambled using a Hanle wedge. The initial decay is in a fresh portion of crystal and the laser beam is blocked while changing polarisations.

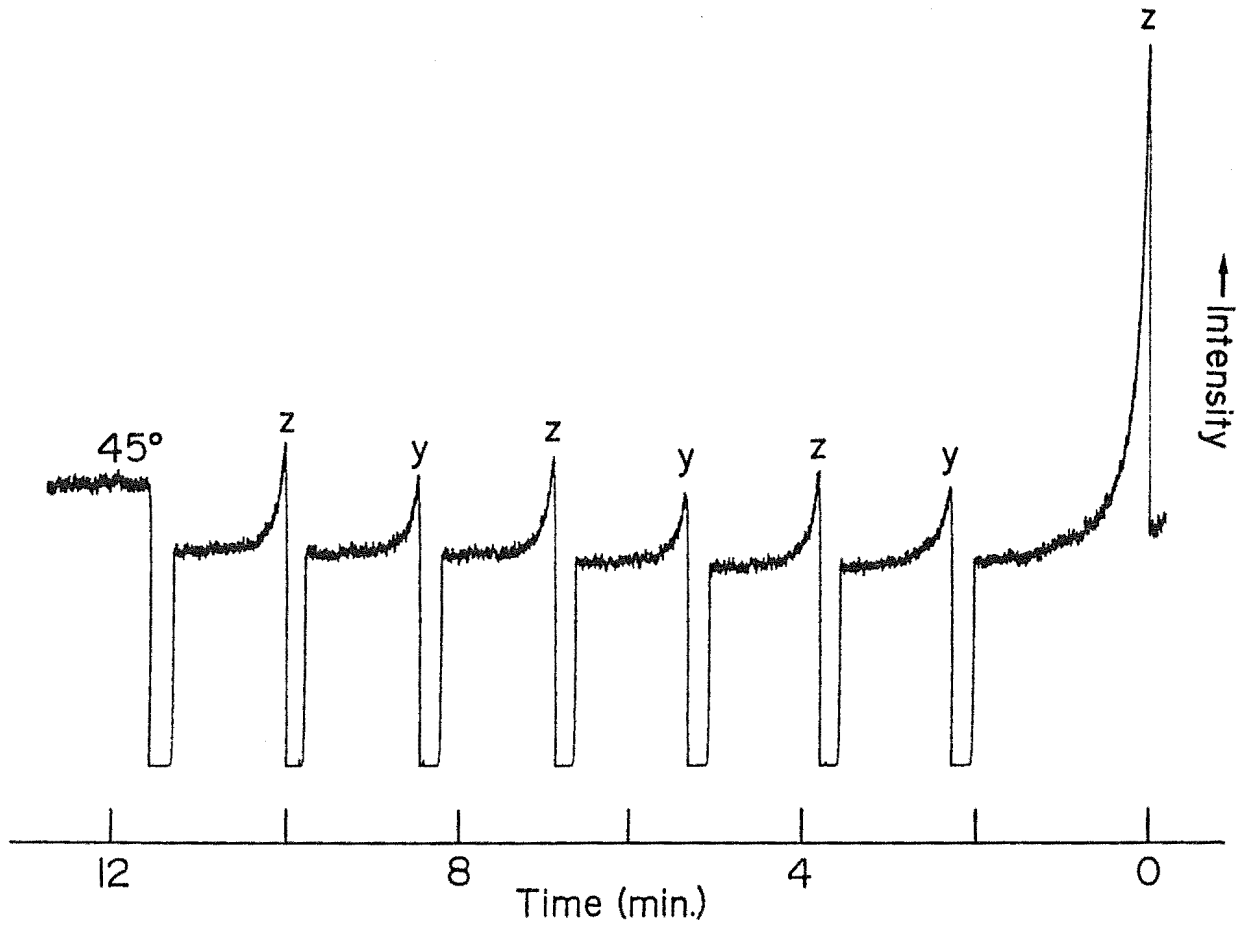

Figure 7.8 : Fluorescence intensity (monitoring $E_1 \rightarrow Z_3$) for reversible polarised bleaching of the D^-R site for laser excitation of the $Z_1 \rightarrow E_1$ transition at 10K.

polarisation is set in direction z and the fluorescence level is allowed to decrease. The polarisation is then switched to y and the fluorescence level recovers to about half of the original level. Successive switching of the direction of polarisation results in a fully recovered fluorescence level for each of the two polarisations. The assymmetry between the two input polarisations was reproducible and also occurred for the T^- ion analogue of the site. Figure 7.8 shows a similar sequence of polarisation switching for monitoring of the $E_1 \rightarrow Z_3$ transition and illustrates that the polarisation direction which has the greatest recoverable fluorescence level depends on the transition monitored. For each of these two transitions there is no loss associated with the recovery process except for the initial bleaching exposure, provided that this first exposure is of adequate duration to bleach to the equilibrium level. The other important feature of these observations is that if, after several switches, the polarisation is set to an angle midway between y and z henceforth referred to as 45^o, the fluorescence level is found to be constant at a higher level than the steady state level of either polarisation.

The J and D1 sites exhibit similar recoverable bleaching effects except that the decay time scale is longer, and if the initial bleach is not of adequate duration to reach an equilibrium level (several minutes), then successively switched recovery levels continue to decline until a steady level of fluorescence and consistent recovery is reached. A reversible bleaching pattern is shown for the J site decay in Figure 7.9.

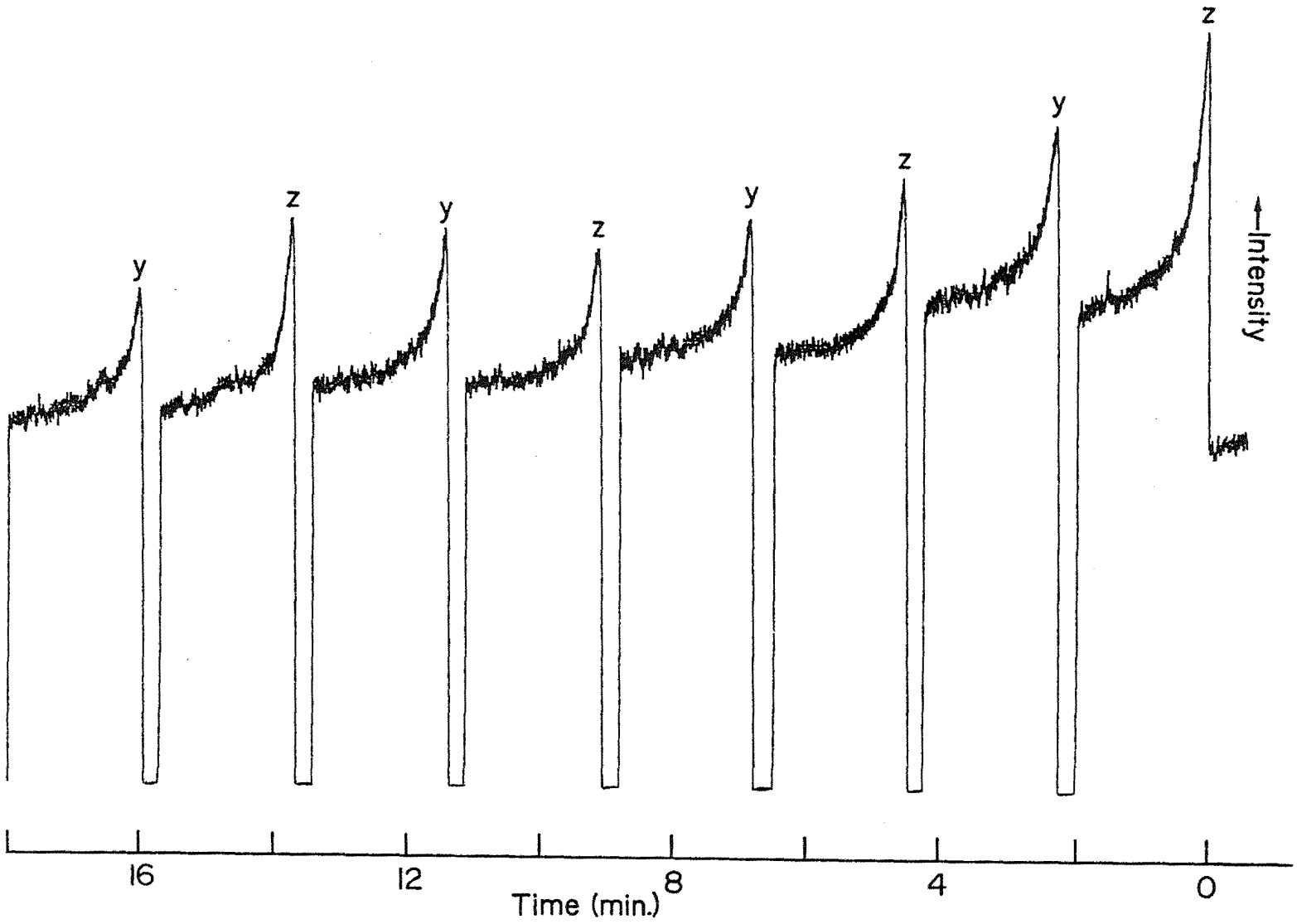

Figure 7.9 : Fluorescence intensity (monitoring $E_1 \rightarrow Z_3$) for reversible polarised bleaching of the D^-J site at 10K upon laser excitation of the $Z_1 \rightarrow E_1$ transition (17 mW).

Figure 7.10 shows a sequence of polarisation changes for the D^-K site, a non reversible site. It can be seen that the bleaching levels for each polarisation are almost independent and no recovery occurs for either polarisation on pumping the other.

The assymmetry of the fluorescence levels for the two laser polarisations for the R site was investigated further by placing a polarisation analyser in front of the spectrometer and monitoring the fluorescence level for each of the orthogonal directions, x and y, of Figure 7.3. Figures 7.11 and 7.12 illustrate the different behaviour of the two polarised components of the fluorescence. The reversible component of fluorescence, that is the fluorescence level restored above the steady state equilibrium level, is dramatically different for the two emission components comprising the $E_1 \rightarrow Z_2$ transition shown in Figure 7.7. For this transition there is the contribution to the reversible component due to emission polarised in the y direction if the site is excited with light in the z direction. The observed fluorescence for such excitation is purely polarised in the x direction. Such a well-defined polarisation ratio in these oriented crystals is consistent with the proposed axial symmetry for the site and the involvement of NN charge compensation in the <100> direction.

The bleaching of the T^- R site was considerably slower than that of the D^-R site and the site was also reversible with the same ratios of recovery for different polarisations. The only difference observed was that almost no unrecoverable loss of intensity occurred in the

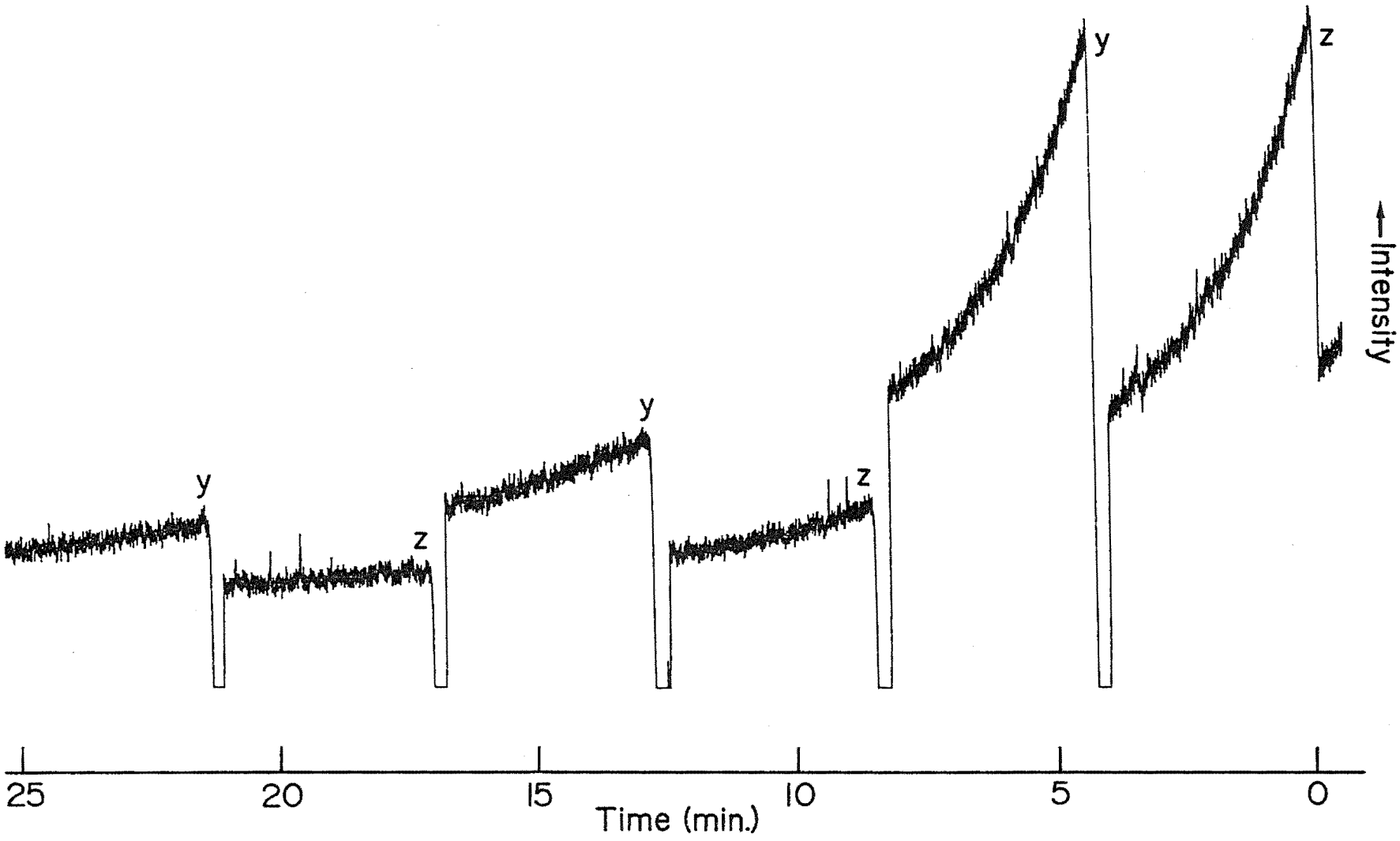

Figure 7.10 : Fluorescence intensity ($E_1 \rightarrow Z_3$ transition) for laser excitation of the $Z_1 \rightarrow E_1$ transition of the D^-K site at 10K. The bleaching is non-reversible.

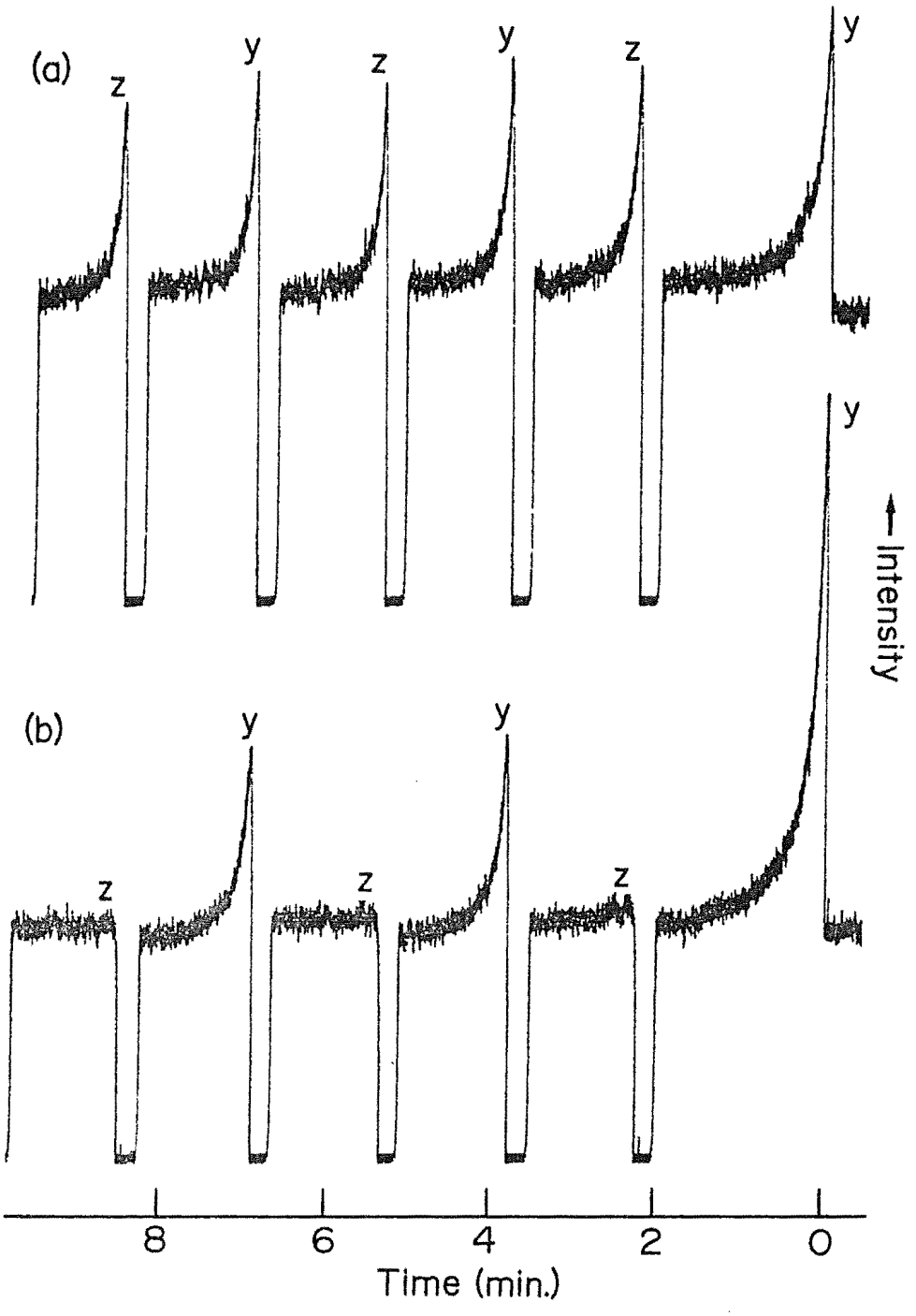

Figure 7.11 : Fluorescence intensity ($E_1 \rightarrow Z_2$ transition) of the D^-R site for $Z_1 \rightarrow E_1$ excitation at 10K : (a) monitoring emission polarised in the y direction, and (b) emission polarised in the z direction.

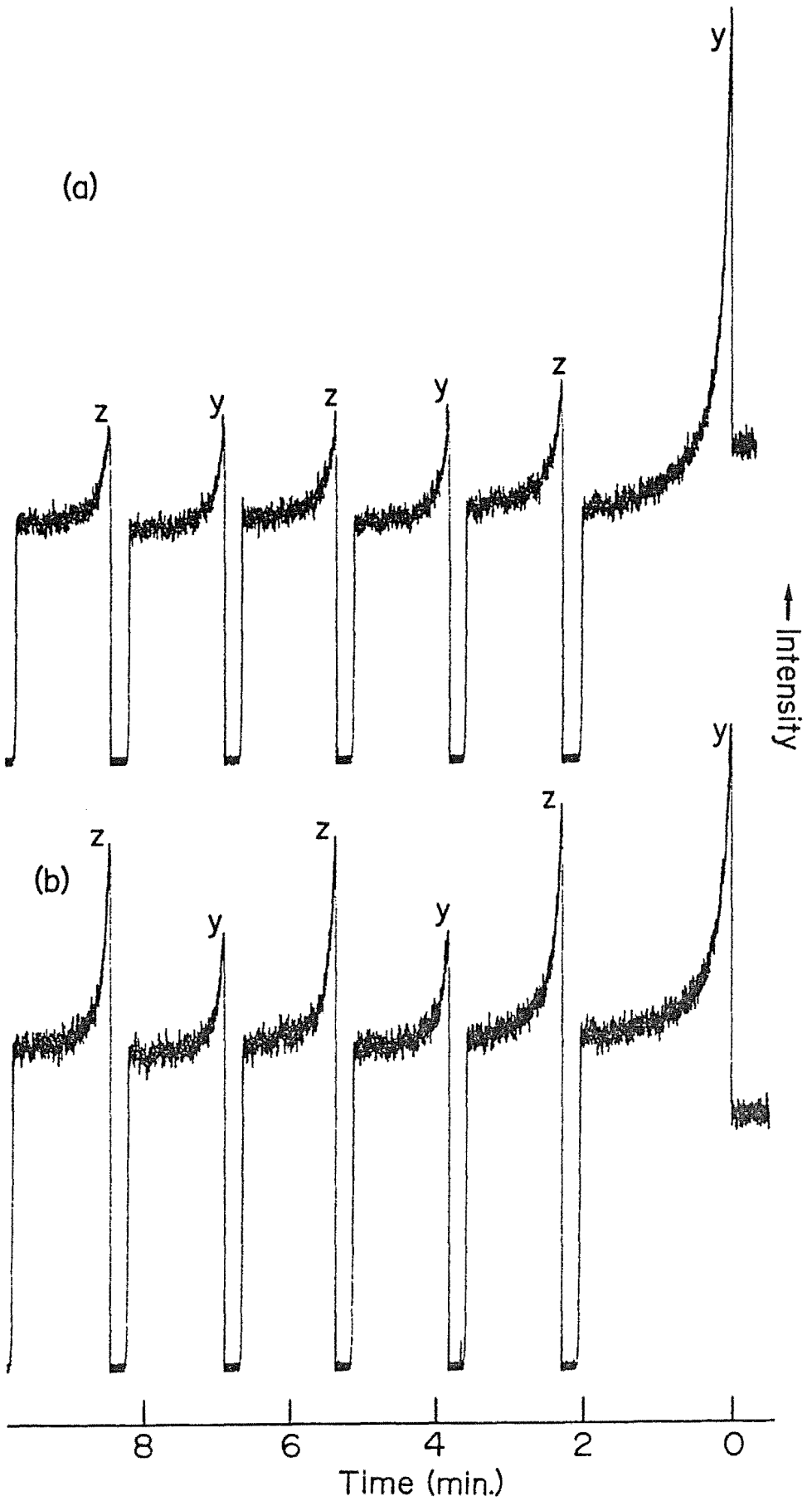

Figure 7.12 : Fluorescence intensity ($E_1 \rightarrow Z_3$ transition) of the D^-R site for $Z_1 \rightarrow E_1$ excitation at 10K : (a) monitoring emission polarised in the y direction, and (b) emission polarised in the z direction.

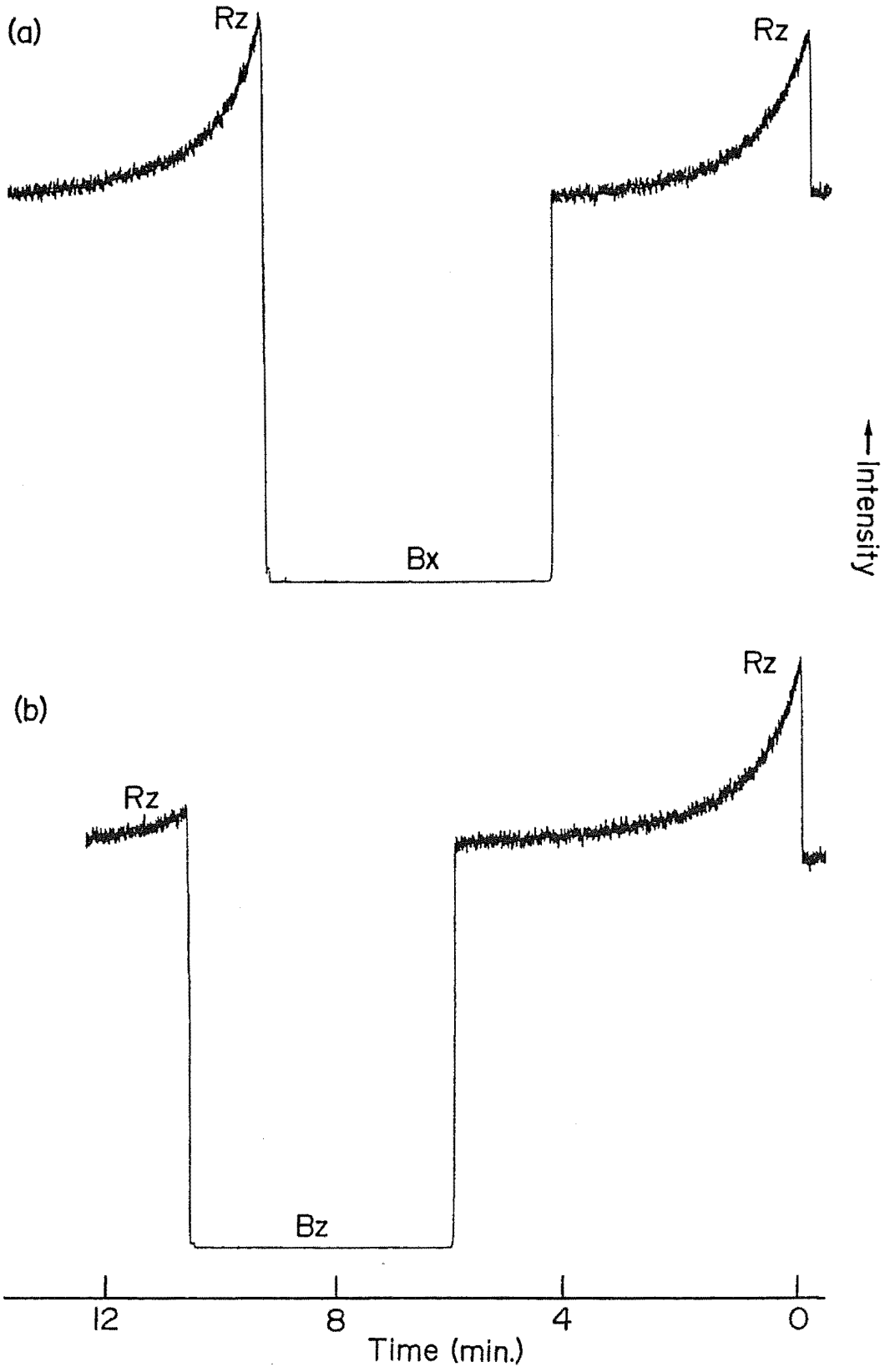

Figure 7.13 : Fluorescence intensity (monitoring $E_1 \rightarrow Z_3$) for laser excitation of the $Z_1 \rightarrow E_1$ transition of the T^-R site. Restoration of fluorescence is shown after a period of laser excitation of the $Z_1 \rightarrow E_2$ transition of the F^-B site using : (a) the opposite polarisation (full restoration), and (b) the same polarisation (only slight restoration).

initial bleach for the T^- site and recovery after the next bleaching was almost complete.

Using the D^- sites it was difficult to determine whether the effect of recovery was resonant or whether off resonance pumping would also restore the fluorescence level since the laser could not be returned to exactly the same position within the inhomogeneous linewidth of the bleaching site transition before further bleaching occurred. The T^-R site was used to check this, since the laser could be accurately retuned to the site after other excitation before significant bleaching could occur. It was found that off resonance excitation did not generally lead to any recovery. However, laser excitation of the F^-B site could be used to restore the site fluorescence subject to the same polarisation sequence used for direct excitation. That is, if the site is bleached with laser polarisation y and the F^-B site is pumped for three to five minutes with laser polarisation x, then the fluorescence for the R site measured with laser polarisation y is restored to its original level (Figure 7.13(a)). However, if the B site is pumped using the same polarisation as the initial R site bleach, then virtually no R site recovery occurs (Figure 7.13(b)). This R site restoration was maximised by tuning on the B site and was not observed for other sites in the crystal.

7.3.3 Frequency Domain Reversibility

In addition to the reversible polarised bleaching restoration, it was observed that the bleached R site fluorescence level could be partially restored by manually

tuning the laser, polarised in the 45^{o} direction, slightly higher or lower in frequency. The fluorescence level could then be cyclically restored by alternation of the laser frequency between two peaks separated by 0.5 ± 0.2 cm^{-1}. This effect was studied by scanning the laser frequency with a stepping motor whilst monitoring the broad band fluorescence in the region of the $E_1 \rightarrow Z_5$, Z_6 and Z_7 transitions. Figure 7.14 shows a sequence of three excitation scans. The first is before bleaching, while the second is after bleaching the $Z_1 \rightarrow E_1$ transition of the site. The central peaks for both $Z_1 \rightarrow E_1$ and $Z_2 \rightarrow E_1$ transition have split into two components with the lower frequency component having the greater intensity. Figure 14(c) is the same region scanned after bleaching with the laser tuned to the lower frequency component, and shows an increase in the higher frequency component with a corresponding decrease in the lower one. This sequence could be cyclically repeated and suggests the presence of two separate sites of very similar energy that are interconverted photochemically.

No other site in $CaF_2:Er^{3+}$, $SrF_2:Er^{3+}$, $CaF_2:Pr^{3+}$, $SrF_2:Pr^{3+}$(Reeves, Private Communication), $CaF_2:Nd^{3+}$ or $SrF_2:Nd^{3+}$ (Han, Private Communication) exhibits such a splitting into two components within the inhomogeneous linewidth of transitions. The $SrF_2:Pr^{3+}$ system does, however, have photoproduct sites with transitions at quite different wavelengths to the original excitation (Macfarlane *et al.* in press) and distinctly different site configurations. Analogous behaviour was looked for in the

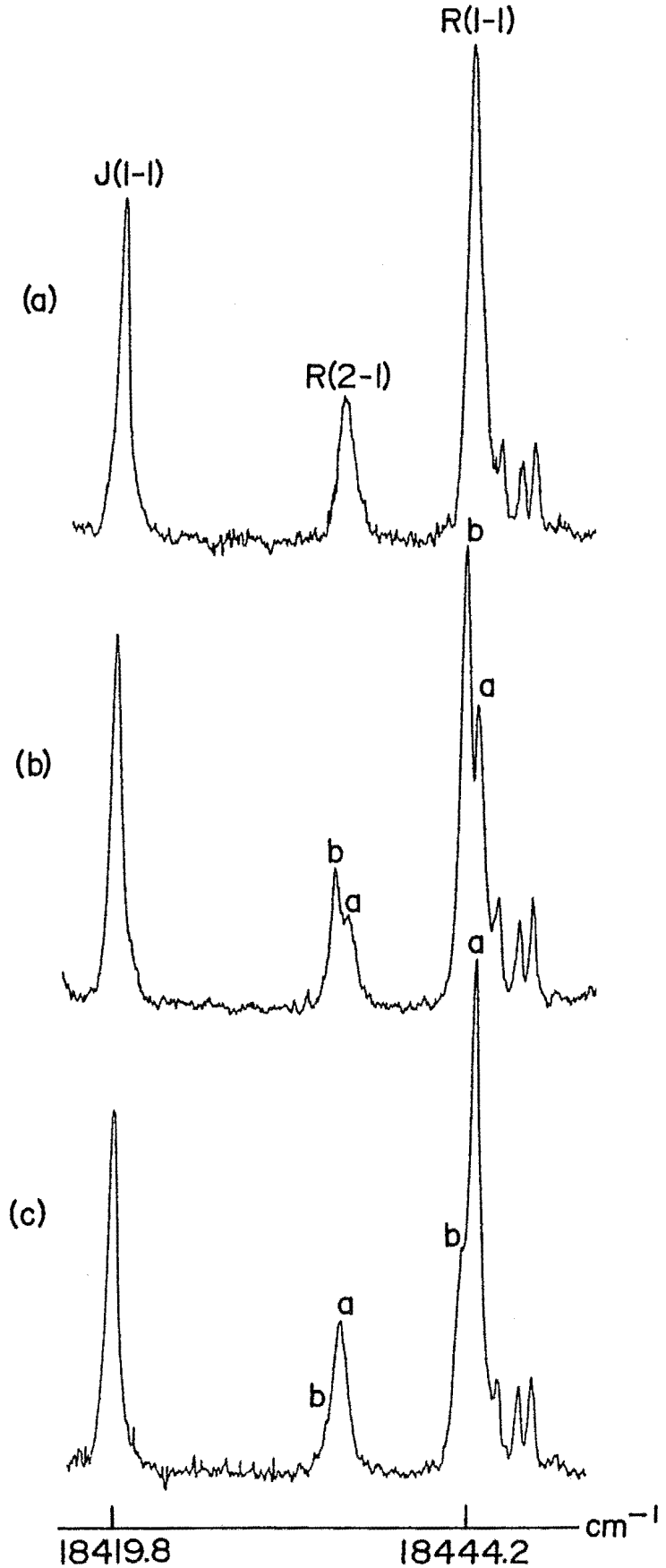

Figure 7.14 : 10K excitation spectra monitoring the $E_1 \rightarrow Z_5, Z_6$ and Z_7 transition region of the D^-R and J sites in a CaF_2:0.05%Er^{3+} crystal. (a) Scanning a fresh portion of crystal; (b) same crystal portion after bleaching with $Z_1 \rightarrow E_1$ excitation of the R site, (c) after bleaching component 'b' of the $Z_1 \rightarrow E_1$ transition of the R site.

nonreversible Er^{3+} ion sites but no such photoproduct sites were determined.

7.4 Discussion

No optically induced bleaching effects have been observed for any of the F^- ion charge compensated centres or for the hydrogenic C_{4V} site from which the bleaching sites discussed are derived. The vibronic evidence and isotope shifts (Chapters Five and Six) demonstrate that the bleaching sites have additional hydrogenic ions replacing fluoride ions in the lattice around these centres. It is proposed that the mechanism for bleaching is the change of site configuration resulting from the migration of hydrogenic ions activated by energy transfer from the optically excited Er^{3+} ions. Since the effect occurs for a number of sites in Er^{3+}, Pr^{3+} and Nd^{3+} doped crystals, the exact site configuration is obviously not critical.

7.4.1 Time Dependence

No obvious interpretation of the observed time dependence for the D^-J site has been found. An intensity proportional to reciprocal time is similar to that for bimolecular reaction rates observed, where the probability of formation of a molecule is proportional to the square of the concentration remaining. In the present case, if it is assumed that the fluorescence intensity is proportional to the number of absorbing centres so that the probability of conversion to another centre (either crystallographically inequivalent or an orthogonal reorientation) is constant, then the observed time dependence should be single

exponential decay. The reciprocal rate observed from the J site implies that the probability of conversion changes as the site population changes in the sample. Since the concentration of Er^{3+} sites is small and no other evidence of interaction between sites is observed, then such dependence is not expected. The decay of other sites with their apparent mixture of single exponentials and $\frac{1}{t}$ dependence was equally ambiguous and suggests that competing processes with different rates may be occurring .

7.4.2 Reorientation Models

The reversible polarised bleaching effects observed can be best explained with a model of reorientation of the hydride ion in <100> Er^{3+} - H^- ion pairs. The two processes for F^- ion reorientation discussed in the introduction to this chapter are also considered likely for this system. Figure 7.15 shows the reorientation of the proposed configuration of the D^-J site (Chapter Five) by the INC mechanism. Coupling by the electron-phonon interaction transfers electronic energy from the excited Er^{3+} ion to vibrational energy of the D^- ions associated with the site which may gain sufficient vibrational energy to assist the INC mechanism. There are two resultant dipole reorientations possible that are orthogonal to the original,and some redistribution of dipoles is expected. Changing the laser polarisation may excite a set of centres with different orientation and some restoration of the original site distribution is expected.

An alternative method of reorientation is the direct migration (Figure 7.1(a)) of an interstitial

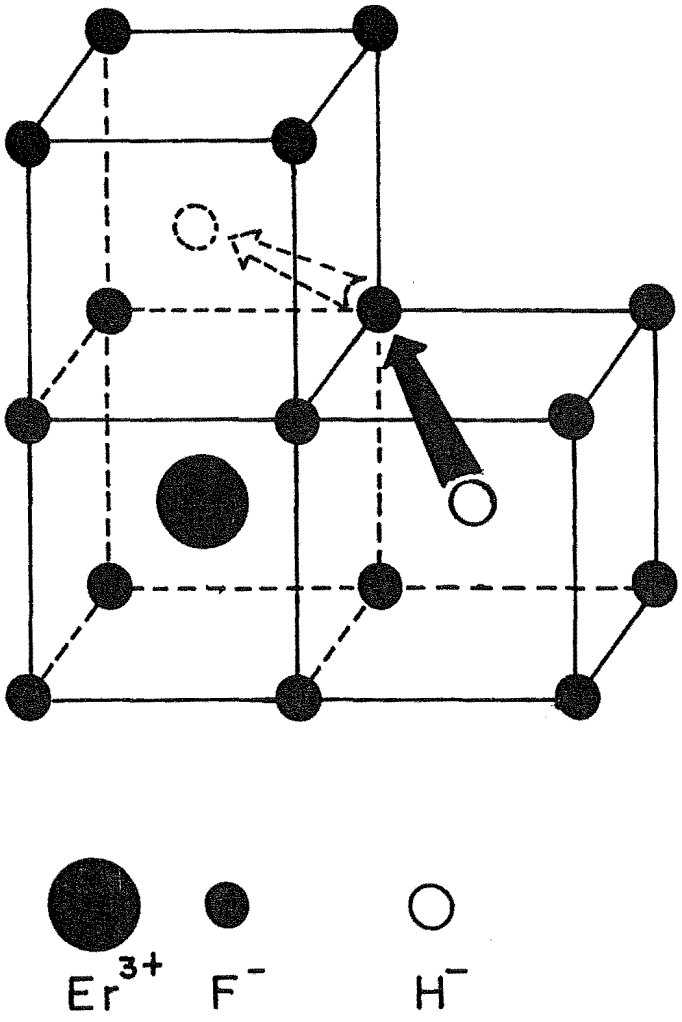

Figure 7.15 : A possible mechanism (INC) for reorientation of the hydrogenic J site in $CaF_2:Er^{3+}$ crystals.

hydrogenic ion along a <110> direction. The presence of substitutional hydrogenic ions adjacent to the Er^{3+} ion or the interstitial ion could cause ionic displacements favourable for direct transfer. This is consistent with the lack of bleaching for the simple single H^- ion C_{4V} sites of Er^{3+}, Nd^{3+}, Pr^{3+} and Ho^{3+}.

Distortion of the lattice due to hydrogenic substitutional ions has not yet been measured directly nor considered by computer simulation techniques, but was shown to be an important factor for the stability of D^- sites in the $SrF_2:Er^{3+}$ case described in Chapter Six. The absence of the simple D^- C_{4V} site and dominance, after long deuteration, of versions of the site modified by substitutional D^- ions, suggests favourable lattice distortion to allow interstitial D^- ion charge compensation. Such distortions in the general case may also affect the activation energies for the bleaching process observed for some sites. It is not known which of the two reorientation mechanisms is dominant.

7.4.3 Polarisation of Emission

Regardless of the exact mechanism for reorientation, it can be assumed that a particular centre may undergo reorientation only if it absorbs the incoming light.

The polarisation of the emission for the R site can be explained using the electric dipole selection rules for sites of C_{4V} symmetry. Full reversibility of fluorescence for laser polarisation switching is only consistent with the $Z_1 \rightarrow E_1$ transition having pure σ polarised absorption and no π component. That is, only centres that are orthogonal to

the $\underline{E}$ vector of laser light can absorb and be excited whilst those parallel are not excited. Such transition occurs between states of $\tau_6 \rightarrow \tau_7$ or $\tau_7 \rightarrow \tau_6$ symmetry (Table 4.1) so that Z_1 and E_1 wavefunctions must be of opposite symmetry.

The observed polarisation of Figure 7.11 is consistent with the $E_1 \rightarrow Z_2$ transition having σ emission only and no component of emission polarised parallel to the excited dipole. Thus the symmetry label of the Z_2 wavefunction must be the same as for Z_1 but opposite to E_1. This can be shown, with reference to Figure 7.11, as follows : The initial bleach is with the laser polarised in the y direction, such that centres aligned in the x and z directions only are excited and may reorientate, resulting in a preferential population increase of centres in the y direction and an equal depletion of the x and z centres. Since all emission of the excited centres is assumed to be perpendicular only (σ) to the axis of the centre, the polarising sheet analyser (Figure 7.3) aligned in the x direction will pass only emission from sites aligned in the z direction, while the analyser in the y direction will pass emission of sites aligned in both the x and z directions. This accounts for the greater intensity of the initial bleaching peak for the x(yy)z polarisation than for x(yx)z.

On switching the laser polaristion to the z direction, the y and x aligned centres now absorb the incident light with a greater initial population of y centres, due to the existing initial bleaching. The net effect of the new excitation is a preferential alignment of centres in the z direction and a depletion of y and x aligned centres to an equal, steady state population. As this redistribution occurs, the

observed σ emission from the y aligned centres (initially dominant) decays. For the x analyser direction, the σ emission from the y site is observed. For the y analyser direction the y site fluorescence is blocked and no restoration of fluorescence is observed.

If the laser polarisation is returned to the y alignment, the z centres have the dominant absorption, and the emission intensity is detected equally for the analyser in the x or y directions.

In summary, these predictions account for all of the observed restoration levels of Figure 7.11. The intensities of the reversible components for x(yx)z, x(zx)z and x(yy)z polarisations are equal, the recovered component of x(zy)z polarisation is zero and the loss of intensity between the initial and subsequent bleaches for x(yy)z polarisation is also consistent with the assignment.

Figure 7.12 shows the analogous behaviour observed by monitoring the $E_1 \rightarrow Z_3$ transition and can be used to verify that the Z_3 and E_1 levels have the same irrep label of wavefunction symmetry so that the transition has σ and π emission (Table 4.1). The absorption and repopulation effects are the same as the case discussed above since the $Z_1 \rightarrow E_1$ transition is still being pumped. Again, laser polarisation parallel to the y direction results in a net increase in population for the y aligned centres, and similarly, z polarisation gives preferential alignment in the z direction.

For the analyser in the x direction, π emission from the x aligned centres and σ emission from the z and y centres is detected, while for the y analyser direction, π

emission from the y centres and σ emission from the x and z centres is detected.

The x(yy)z, x(yx)z and x(zx)z components are therefore equal but the x(zy)z component is different since it involves π emission. The observed x(zy)z component is larger (Figure 7.12), proving that the π emission component is more intense than the σ component in this case. The initial bleach peak of Figure 7.12(a) is large since it comprises the π component of emission of centres aligned in the x direction before they are redistributed to the y and z directions.

When the Z_2 - E_1 transition was pumped by the laser, the intensity could not be repeatedly restored by polarisation switching, and the peak levels decreased with each cycle. This is expected since the Z_2 - E_1 transition does not have pure σ absorption but has both σ and π components. Some of the centres undergoing reorientation to the x axis direction cannot, therefore, be excited by π absorption and a net loss of centres to this alignment will occur.

7.4.4 R Site Transition Structure

The splitting of the R site into two components could not be studied precisely using the present system, due to the broad linewidth of the laser compared to the components. The observed splitting seems to be related to an effect observed by Dr R.M. Macfarlane of IBM Research Laboratories, San Jose. Motivated by the reversible bleaching effects observed here, he has undertaken preliminary high resolution measurements on the deuterated and tritiated $CaF_2:Er^{3+}$

system. The laser used had a linewidth of 1MHz and was scanned over the $Z_1 \rightarrow D_1$ transitions of several hydrogenic sites. Preliminary excitation results show that the $Z_1 \rightarrow D_1$ transitions of the R site, C_{4V} site and two other weak hydrogenic sites can be resolved into two lines of equal intensity.

This effect is new and seems exclusive to hydrogenic sites involving Er^{3+}. Application of a magnetic field did not increase the separation of the lines, suggesting that they are due to two distinct centres per site rather than to the lifting of the Kramers degeneracy by magnetic interaction. The separation of the components was 16.3 GHz and 11.5GHz and the component linewidths were 5GHz and 2GHz for the C_{4V} and R sites respectively.

The R site exhibited an effect at 1.7K similar to that observed here. Excitation of any frequency within the linewidth of one component burnt a hole and created an antihole in a corresponding position of the other component (Figure 7.16). If the laser was scanned repeatedly over the width of a component, the entire component could be bleached and its intensity transferred to the other component (Figure 7.17). Similarly, the second component could be bleached with a simultaneous increase in the first. The bleaching, however, was short-lived for excitation in this multiplet, typically lasting 10-20 seconds and did not occur above 4K. The relative intensity of the two components of other sites could not be changed by laser excitation.

Further results are required to understand this effect fully but it is consistent with each site having two

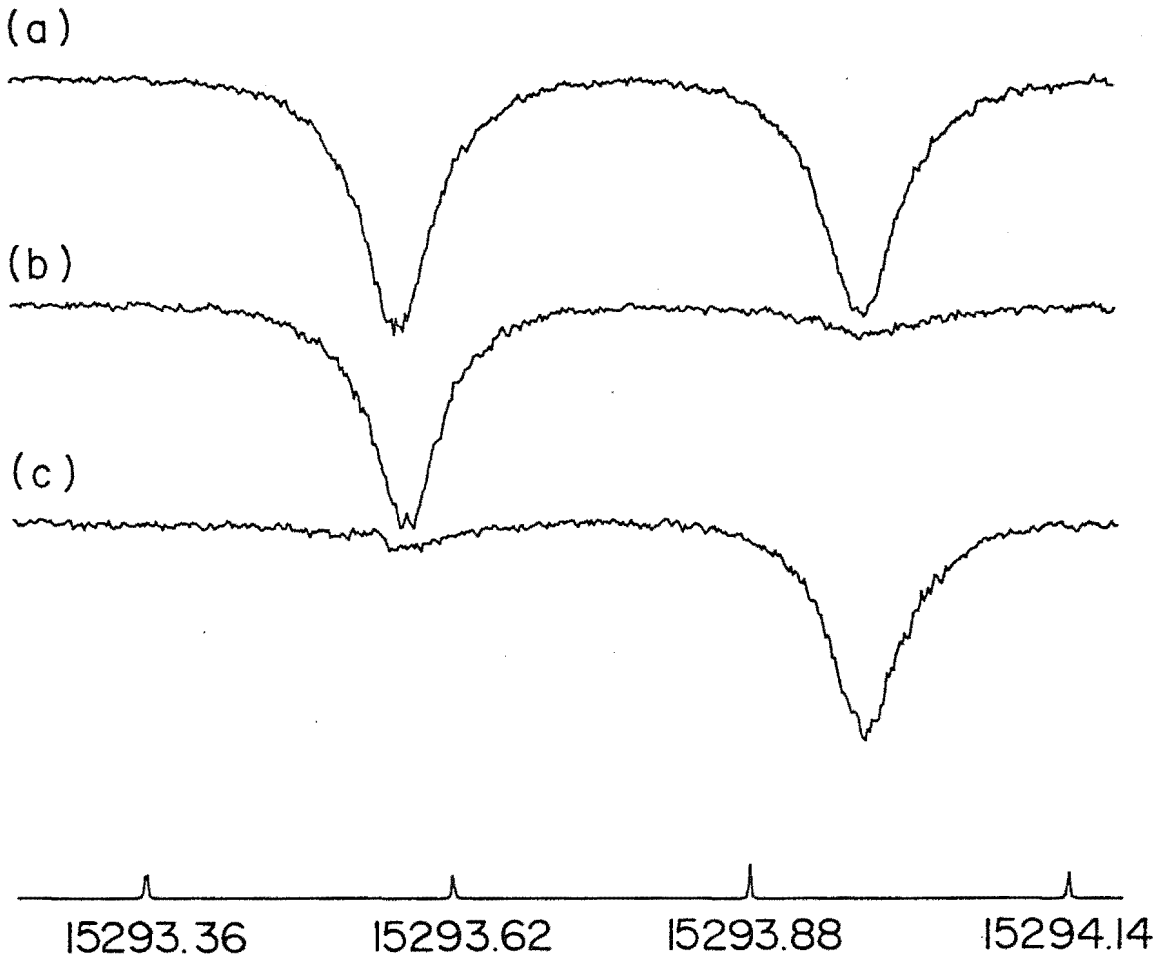

Figure 7.16 : Excitation spectra of the $Z_1 \rightarrow D_1$ transition of the D^- R site in $CaF_2:Er^{3+}$ at 1.7K using a laser with 1 MHz bandwidth; (a) before bleaching; (b) after burning the high frequency line, and (c) after burning the low frequency component in (b). Plot (a) is not to the same scale as (b) and (c). (Spectrum provided by R.M. Macfarlane).

slightly inequivalent stable interstitial hydrogenic ion positions within the same lattice cube. It is not obvious why the excitation of the $Z_1 \rightarrow E_1$ transition should change the intensity of the two components at 10K rather than the lower temperatures required for $Z_1 \rightarrow D_1$ excitations.

7.5 Summary

The purpose of this chapter has been to outline the observations of the bleaching and reversible polarisation bleaching found in this study. Reliable parameterisation of variables was found to be difficult using the available equipment, and a full explanation of some of the effects can not be given at this stage.

Analysis of the polarisation of the emission has provided answers to several previously unexplained effects. The complete reversibility of the R site, after the initial bleach, without loss to a third orientation, is due to an electronic absorption transition with no π component. The loss between the initial and second bleach can also be accounted for. A symmetry very close to C_{4V} is demonstrated for the reversible sites by their strict obedience of the electric dipole selection rules. Additional information such as the relative strength of π and σ emission may be obtained by studying the emission polarisation. Erbium ions in C_{4V} symmetry have no transitions of pure π absorption, but it is likely that rare-earth ions that do have may exhibit reversible polarised bleaching when pumping one transition (σ absorption only), and non-reversible behaviour when pumping another transition (π absorption only). Such polarised

emission work on other RE^{3+} ions may provide interesting results.

Since reversible polarisation bleaching is now a generally observed effect, a compilation of the information from studies of analogous rare-earth sites presently being undertaken, further study using high resolution techniques and the final results of the dielectric relaxation measurements (Welsh, Private Communication), should lead to a better understanding of the mechanisms involved. Regardless of specific mechanisms, however, the effect is likely to be studied further as it offers a useful insight into the dynamics of light ion migration and is of interest for the redistribution in population of oriented sites. Future calculations of energies of formation of hydrogenic sites are likely (Catlow, Private Communication) and may give an indication of the most probable reorientation mechanisms.

CHAPTER EIGHT

THE SPECTROSCOPY OF $CsCdBr_3:Er^{3+}$

8.1 Introduction

As a supplement to the spectroscopic study of hydrogenated rare-earth doped fluorite crystals, a preliminary investigation of the somewhat different system of $CsCdBr_3$ doped with Er^{3+} ions was undertaken.

No optical work has previously been reported for this system. Previous studies of different crystals (of general form $A^+M^{2+}X_3^-$) with this structure doped with trivalent ions have shown that one site, consisting of two dopant ions in close proximity, is predominantly formed (McPherson and Henling 1977). This type of system is relatively new, and the first report of RE^{3+} doping in AMX_3 hosts was for $CsCdBr_3:Gd^{3+}$ about one decade ago (Henling and McPherson 1977). The bulk of the subsequent work on related systems has used EPR spectroscopy or low resolution optical spectroscopy.

The purpose of this investigation was to determine the nature of Er^{3+} ion sites in $CsCdBr_3$, to test whether fluorescent levels were suitable for detection using the available apparatus and whether any form of energy transfer occurs for the sites observed. This chapter reports the results of the investigation together with an interpretation of the spectra obtained.

8.1.1 Crystal Structure

$CsCdBr_3$ is one of a number of AMX_3 crystals that form

in a hexagonal structure isomorphous to that of $CsNiCl_3$ (McPherson *et al.* 1980). The prominent feature of the structure is a system of infinite linear chains of face-sharing $(Cd^{2+}Br_6^-)^{4-}$ octahedra parallel to the crystallographic c axis. Charge neutrality in the crystal is provided by Cs^+ ions occupying positions between the chains (Figure 8.1).

Most of these compounds have a deviation from ideal octahedral geometry. The $(MX_6)^{4-}$ octahedra separations are elongated along the linear chains due to electrostatic repulsion between neighbouring M^{2+} ions within the chains (McPherson *et al.* 1980), giving a trigonal distortion along the c axis. Since the separation of adjacent M^{2+} ions is much smaller than the separation of the chains, the lattice has a distinct one-dimensional character along the chain axis.

The crystal has space group symmetry D_{6h}^4 with two formula units per unit cell, and Cd^{2+} ions in the chains occupy sites of trigonal, D_{3d} symmetry. McPherson *et al.* (1980) performed the structural analysis of $CsCdBr_3$.

8.1.2 Rare-earth Ions in $CsCdBr_3$

Trivalent ions of several metals, including the rare-earths, are normally incorporated as pairs into crystals of $CsCdBr_3$ (McPherson and McPherson 1981, Blasse *et al.* 1985, Berdowski *et al.* 1985, Barthem *et al.* 1985). Three Cd^{2+} ions in a linear chain can be replaced by two RE^{3+} ions on either side of a cation vacancy.

The point group symmetry of each independent RE^{3+} ion of the site is reduced to C_{3V} by the presence of the other.

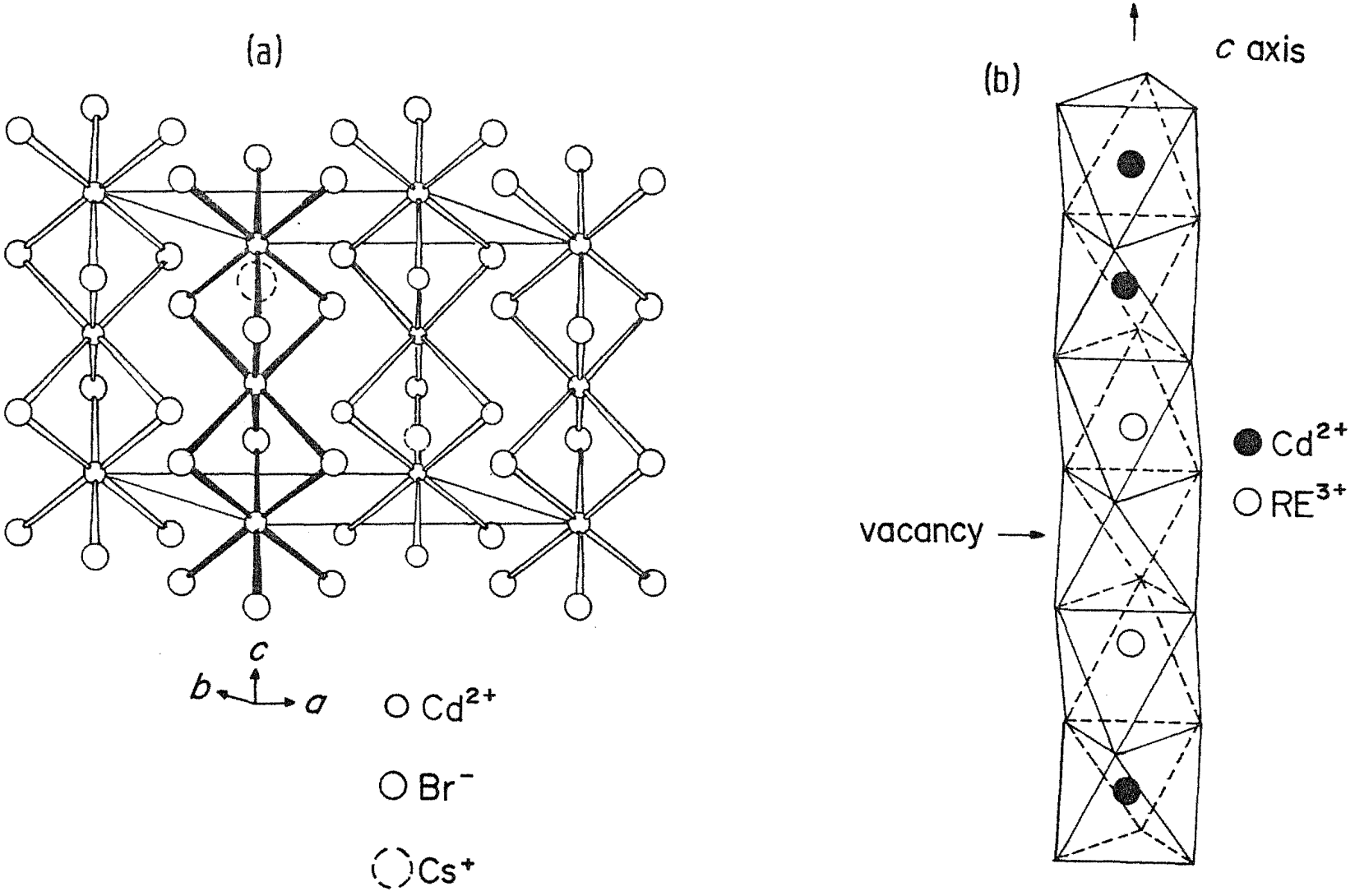

Figure 8.1 : (a) Structure of the $CsCdBr_3$ crystal lattice. (b) Configuration of the RE^{3+} ion pair site in $CsCdBr_3$.

If, however, there is strong interaction between the RE^{3+} ions, the states of the combined pair system, which has D_{3d} symmetry, would be appropriate.

Since crystals of this structure tend to cleave parallel to the c axis, they can be oriented and mounted with this axis contained in the plane of rotation of the magnetic field for EPR studies. Therefore, EPR is a convenient technique to investigate ion pairs in the chain, and was used for most of the initial work on such systems (McPherson *et al.* 1977).

Rare-earth doping of the $CsCdBr_3$ system has not been investigated as extensively as similar salts such as $CsMgI_3$ (McPherson and Tallut 1982) and $CsMgCl_3$ (McPherson and Martin 1984 and references therein). Other RE^{3+} dopants reported for $CsCdBr_3$ are Ce^{3+} (McPherson and McPherson 1981, Blasse *et al.* 1985), Tb^{3+} (Berdowski *et al.* 1985, Lammers and Blasse 1986) and Nd^{3+} (Barthem *et al.* 1985). If two rare-earth ion types are present, then heterogeneous pairs such as Ce^{3+} - Tm^{3+} are formed (McPherson and McPherson 1981).

It has been demonstrated that the ion pair sites formed are ideal for examination, by optical techniques, of energy transfer processes between the two ions, since they are relatively close (Barthem *et al.* 1985). Optical studies are simplified by the fact that about 90% of RE^{3+} ions present form in the pair site with well-defined symmetry.

The first of these optical studies was by broad band absorption and emission, and showed that if the 4f-5d transition of Ce^{3+} was excited with uv irradiation, then subsequent transfer of energy to the Tm^{3+} ion in the mixed

pair site resulted in emission at 14200 cm^{-1} from the Tm^{3+} ion. Energy transfer decreased when the crystal was warmed above 100K (McPherson and McPherson 1981).

The application of laser selective excitation provides more precise control in the excitation to specific crystal field levels. Berdowski *et al.* (1985) reported cross-relaxation between Tb^{3+} ions in pairs by exciting to the $^5D_3$ level and recording the decay curves of emission from $^5D_3$ and $^5D_4$. The cross-relaxation rate had a strong temperature dependence that was explained using phonon assisted processes. It was also shown that a small proportion of Tb^{3+} ions exist in single ion sites, but no model of charge compensation was proposed. More detailed luminescence spectra for Tb^{3+} ion sites were subsequently published (Lammers and Blasse 1986).

A brief report of a laser excitation study of the $CsCdBr_3:Nd^{3+}$ system by Barthem *et al.* (1985) illustrated that efficient upconversion and cross-relaxation occurred for pulsed excitation of $^4I_{9/2} \rightarrow {}^4G_{5/2}$ or $^4I_{9/2} \rightarrow {}^2H_{11/2}$ transitions. Excitation, monitoring both upconverted and direct fluorescence, showed that the weak transitions due to a site containing a single isolated Nd^{3+} ion could be distinguished from the dominant pair site, since only the latter exhibits efficient upconversion. It was found that the transition frequencies of pair sites and isolated ion sites were very similar since the crystal field is almost the same for both.

8.1.3 Erbium Ions in Similar Hosts

Trivalent erbium has been studied in other hosts of the

type AMX_3. In most of these cases the emphasis has been on energy transfer between the Er^{3+} and the divalent metal ions such as Er^{3+} - Mn^{2+} transfer in $RbMnF_3$ (Iverson and Sibley 1980), $RbMgF_3:Mn^{2+}:Er^{3+}$ (Sarder *et al.* 1982, Shinn *et al.* 1982), $CsMnBr_3$, $RbMnBr_3$ and $CsMnI_3$ (Talluto *et al.* 1984). The broadband absorption and emission spectra of Er^{3+} in $CsMgI_3$ have also been reported (McPherson and Talluto 1982). No laser selective excitation of Er^{3+} ions in this class of material has been reported.

8.2 Results

8.2.1 Outline

Unlike any previous study of this type of system, the present study utilises the upconversion process of the pair sites to give a comprehensive spectroscopic classification of the crystal-field levels, and uses higher resolution optical measurements than almost all relevant reported work.

Crystals with 0.3% and 0.7% Er^{3+} dopant levels were investigated by optical absorption and laser selective excitation, with all lines present being common to both concentrations. In most multiplets all transitions were assigned to a single, dominant site although in other multiplets some lines remain unassigned.

The crystallographic $\underline{c}$ axis of $CsCdBr_3$ is parallel to the intersection of two cleavage planes. Where possible,crystals were first cleaved in this manner and a parallel face for each of the two planes was then cleaved. In most cases the accurately oriented samples obtained were small and difficult to clamp to the crystal holder. These crystals were generally used only once because the thermal

cycling of the cryostat tended either to crack or dislodge them, resulting in shattering. Because the samples were also hygrosopic and surfaces became cloudy between experiments, a new sample was used for each run. For these reasons most of the laser selective excitation work is unpolarised since the largest samples available with a single good surface to reduce laser scatter were not, in general, fully oriented. The optical absorption measurements presented here are, however, polarised and were recorded using the best oriented sample available with a path length of 4 mm.

8.2.2 Optical Absorption Spectroscopy

The optical absorption spectra were recorded using white light incident perpendicular to the c axis of the sample. A polaroid sheet was used to select the component either parallel (π absorption) or perpendicular (σ absorption) to the c axis.

Transitions from the $^4I_{15/2}$ multiplet to the $^4F_{9/2}$, $^4S_{3/2}$, $^2H_{11/2}$, $^4F_{7/2}$, $^4F_{5/2}$, $^4F_{3/2}$, $^2H_{9/2}$ and $^4G_{11/2}$ multiplets were assigned and most were found to be polarised. The polarised absorption spectra for the first two multiplets at 12K are shown in Figures 8.2 and 8.3, and the assigned transitions are marked. Upper multiplet energy levels could be derived from these transitions while the Z_1, Z_2, Z_3, Z_4 and Z_5 energy levels of the $^4I_{15/2}$ multiplet were identified by temperature dependence up to 100K. Figure 8.4 shows the 40K spectra of the $^4I_{15/2} \rightarrow {}^4S_{3/2}$ transitions and illustrates that marked polarisation

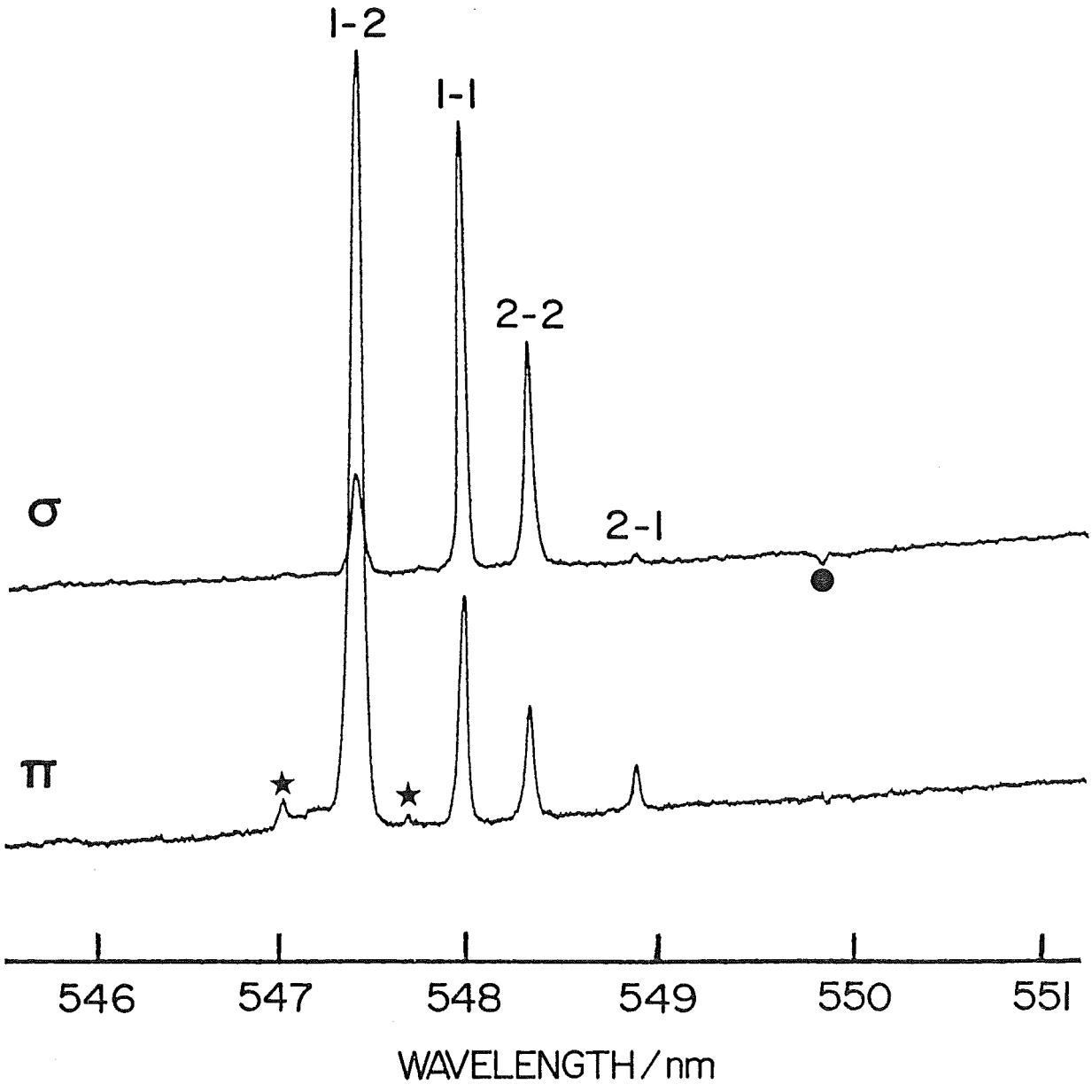

Figure 8.2 : $^4I_{15/2} \rightarrow {}^4S_{3/2}$ absorption spectra of a 4 mm thick $CsCdBr_3$:0.7%Er^{3+} crystal for both σ and π polarisation at 12K. Transitions of the Er^{3+} ion pair site are identified by numerical labels representing the lower and upper multiplet levels involved. The feature marked by a spot is $E_1 \rightarrow Z_3$emission of the site.

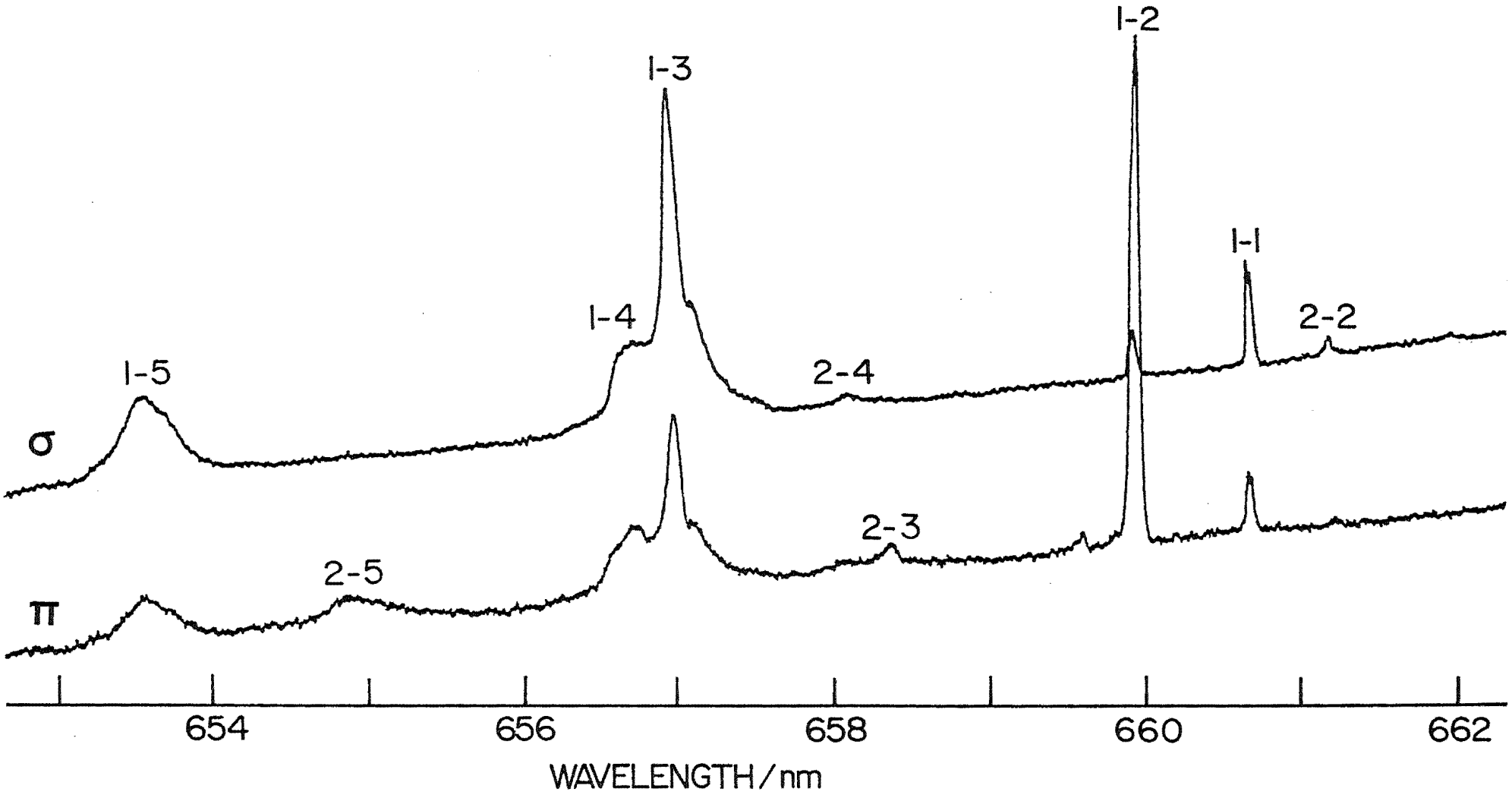

Figure 8.3 : $^4I_{15/2} \rightarrow {}^4F_{9/2}$ absorption spectra of a 4 mm thick $CsCdBr_3$:0.7%Er^{3+} crystal for both σ and π polarisations at 12K.

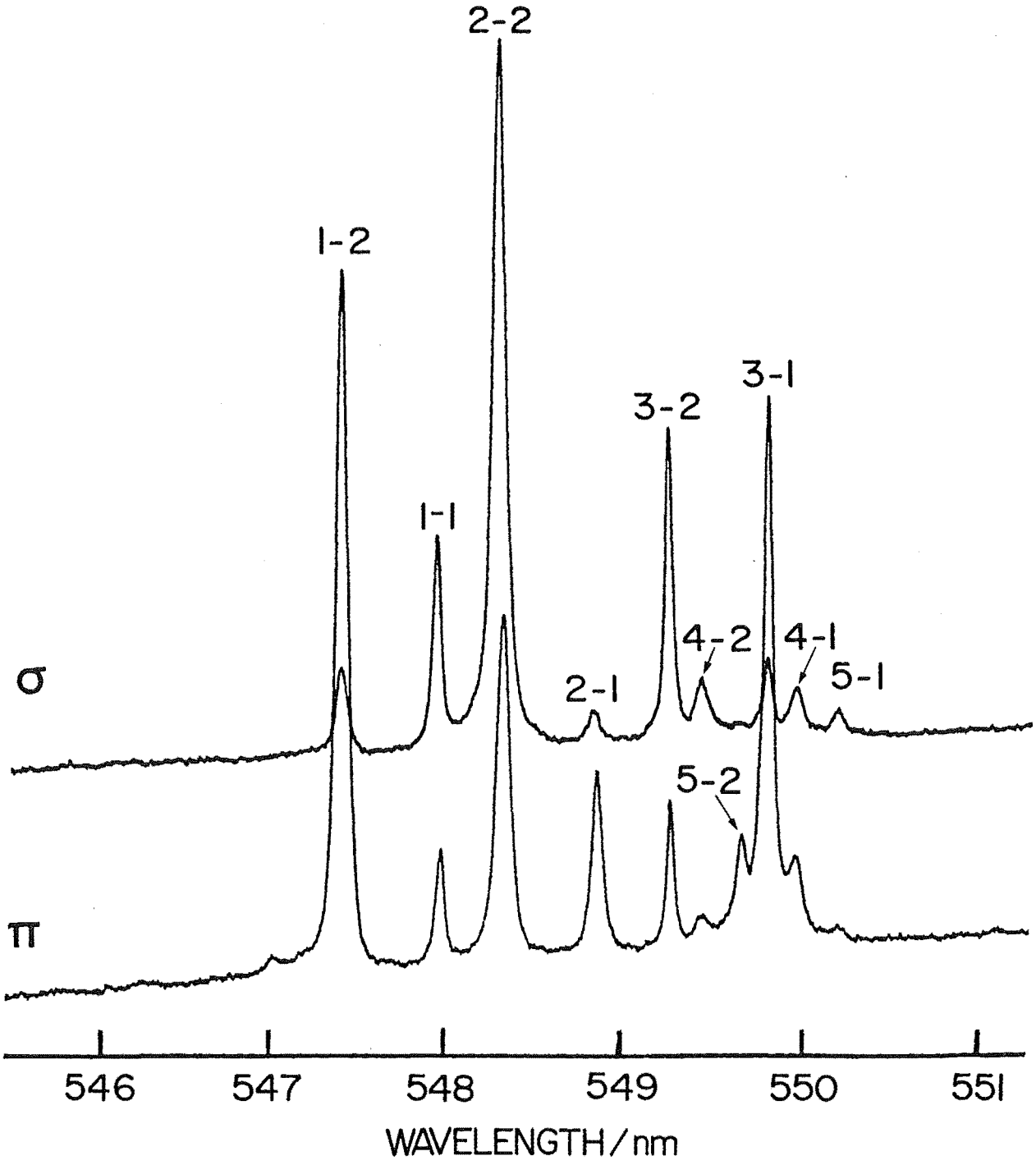

Figure 8.4 : $^4I_{15/2} \rightarrow {}^4S_{3/2}$ absorption spectra of a 4 mm thick $CsCdBr_3$:0.7%Er^{3+} crystal for both σ and π polarisation at 40K.

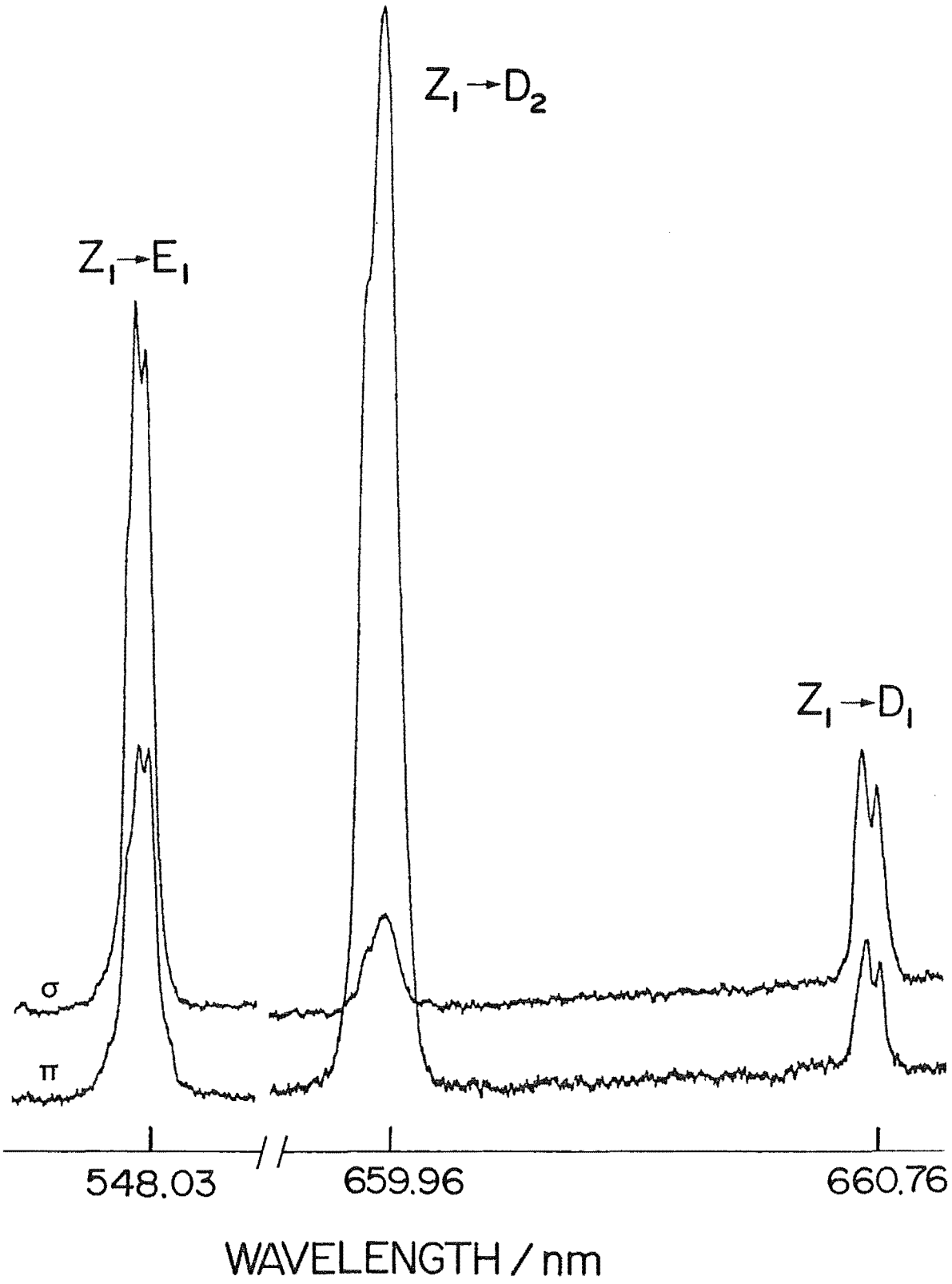

Figure 8.5 : Higher resolution optical absorption spectra of transitions of the Er^{3+} ion pair site in $CsCdBr_3$ for σ and π polarisations at 12K. The zero transmission level is offset beyond the page to enhance the structural features.

is also exhibited for several of the transitions from higher Z levels.

Table 8.1 summarises the σ and π intensities for each transition relative to the most intense transition listed for each of the multiplets.

Figure 8.5 illustrates an interesting phenomenon observed using narrower slits and an offset expansion for the recording of the spectra. The $Z_1 \rightarrow E_1$, $Z_1 \rightarrow D_1$ and $Z_1 \rightarrow D_2$ transitions were found to have a fine structure of two peaks separated by (0.5 ± 0.2) cm^{-1}. The relative intensity of these components was not found to vary markedly with polarisation although, like other transitions, the overall intensity of the line did. There was evidence of an additional very weak feature on both sides of the $Z_1 \rightarrow E_1$ transition. None of the other transitions was observed to exhibit the effect.

Certain other weak features were observed in some spectra. Figure 8.2 has two weak lines marked with a star that were strongly polarised. Several other multiplets, notably the $^4I_{15/2} \rightarrow {}^4F_{5/2}$ and the $^4I_{15/2} \rightarrow {}^2H_{11/2}$, have more transitions than are expected for their J_z value.

8.2.3 Laser Selective Excitation Spectroscopy

The laser selective excitation of the $Z_1 \rightarrow E_2$ transition at 18266 cm^{-1} resulted in a naked eye detectable "white light" fluorescence glow. Spectral examination of the fluorescence showed that it consisted of thirteen groups of transitions in the region 11000 cm^{-1} - 30000 cm^{-1} accessible with the available equipment, and indirect

TABLE 8.1 : Line widths, peak heights and intensity ratios of polarised absorption transitions for the Er^{3+} pair site of $CsCdBr_3$:0.7%Er^{3+}. The peak heights are relative to the maximum absorption for each of the multiplet spectra and have an uncertainty of ±0.5 unless specified. Data was recorded at 12K, unless otherwise indicated.

Upper Multiplet	Transition	Wavenumber	Linewidth (cm^{-1})	Relative Peak Height σ	Relative Peak Height π	Ratio $\frac{\sigma}{\pi}$
$^4S_{3/2}$*	$Z_1 \rightarrow E_1$	18247.1	1.8 ± 0.2	29.8	16.1	1.85 ± 0.09
	$Z_2 \rightarrow E_1$	18216.1	2.4 "	3.7	24.8	0.15 ± 0.02
	$Z_3 \rightarrow E_1$	18184.0	1.9 "	9.2	78.9	0.12 ± 0.01
	$Z_4 \rightarrow E_1$	18177.9	2.9 ± 0.3	5.5	10.6	0.52 ± 0.07
	$Z_5 \rightarrow E_1$	18170.5	2.4 ± 0.4	3.2	1.8	1.8 ± 0.8
	$Z_1 \rightarrow E_2$	18266.3	2.5 ± 0.2	11.5	100.0	0.120± 0.006
	$Z_2 \rightarrow E_2$	18235.3	2.9 "	100.0	47.7	2.10 ± 0.03
	$Z_3 \rightarrow E_2$	18203.4	1.8 "	44.0	20.6	2.14 ± 0.08
	$Z_4 \rightarrow E_2$	18197.1	2.4 ± 0.4	6.8	3.2	2.1 ± 0.5
	$Z_5 \rightarrow E_2$	18190.0	2.5 "	0.9	13.3	0.07 ± 0.04
$^4S_{3/2}$	$Z_1 \rightarrow E_1$	18247.1	1.6 ± 0.2	56.3	29.0	1.94 ± 0.05
	$Z_2 \rightarrow E_1$	18216.1	1.1 ± 0.3	0.8	5.5	0.15 ± 0.11
	$Z_1 \rightarrow E_2$	18266.3	2.3 ± 0.2	12.2	100.0	0.120± 0.006
	$Z_2 \rightarrow E_2$	18235.3	1.5 ± 0.3	28.2	13.9	2.03 ± 0.11
$^4F_{9/2}$	$Z_1 \rightarrow D_1$	15134.2	1.2 ± 0.2	10.5	19.8	0.53 ± 0.04
	$Z_1 \rightarrow D_2$	15152.5	1.5 ± 0.3	100.0	8.7	11.5 ± 0.7
	$Z_2 \rightarrow D_2$	15121.0	1.0 ± 0.2	1.5	2.9	0.52 ± 0.26
	$Z_1 \rightarrow D_3$	15218.0	2.9 "	65.7	34.3	1.92 ± 0.04
$^2H_{11/2}$	$Z_1 \rightarrow F_1$	18970.5	1.3 ± 0.3	3.8±0.3	14.2±0.3	0.27 ± 0.03
	$Z_2 \rightarrow F_1$	18939.5	1.2 "	0.86 "	3.8 "	0.23 ± 0.10
	$Z_1 \rightarrow F_2$	18976.0	1.7 ± 0.2	75.6 "	37.8 "	2.00 ± 0.02
	$Z_2 \rightarrow F_2$	18945.1	1.2 ± 0.3	1.0 "	0.5 "	2.0 ± 1.8
	$Z_1 \rightarrow F_3$	19016.5	2.0 ± 0.2	100.0 "	50.8 "	0.510± 0.005
$^4F_{7/2}$	$Z_1 \rightarrow G_1$	20341.5	2.4 ± 0.3	100.0±0.3	49.5±0.3	2.02 ± 0.02
	$Z_2 \rightarrow G_1$	20310.5	1.5 ± 0.4	1.7 "	1.0 "	1.7 ± 0.8
	$Z_1 \rightarrow G_2$	20386.0	3.8 ± 0.3	1.3 "	63.1 "	0.180± 0.006
	$Z_1 \rightarrow G_3$	20407.0	3.5 "	31.8 "	18.5 "	1.72 ± 0.04
$^4F_{5/2}$	$Z_1 \rightarrow H_1$	22014.8	2.0 ± 0.3	76.6	37.3	2.05 ± 0.04
	$Z_2 \rightarrow H_1$	21983.8	1.6 ± 0.4	5.7	2.9	2.0 ± 0.5
	$Z_1 \rightarrow H_2$	22017.1	2.3 "	24.6	100.0	0.250± 0.006
	$Z_2 \rightarrow H_2$	21986.1	1.3 "	7.4	13.9	0.53 ± 0.05
$^4F_{3/2}$	$Z_1 \rightarrow I_1$	22388.0	1.5 ± 0.4	5.7	2.6	2.2 ± 0.6
	$Z_1 \rightarrow I_2$	22411.0	2.1 ± 0.3	25.9	100.0	0.260± 0.006
	$Z_2 \rightarrow I_2$	22380.0	1.0 ± 0.4	1.6	2.6	0.62 ± 0.31
$^4G_{11/2}$	$Z_1 \rightarrow L_1$	26025.0	4.3 ± 0.4	100.0	57.2	1.75 ± 0.02
	$Z_2 \rightarrow L_1$	25994.0	4.1 "	13.9	35.0	0.40 ± 0.02
	$Z_1 \rightarrow L_2$	26032.0	5.7 "	33.9	85.6	0.400± 0.008
	$Z_2 \rightarrow L_2$	26001.0	3.8 "	77.2	43.9	1.76 ± 0.03

* Measured at 40K

evidence was found for at least one more set of lines.

Unpolarised spectra for the $^4S_{3/2}$, $^4F_{9/2}$, $^4I_{9/2}$, $^4G_{11/2}$, $^2H_{9/2}$, $^4F_{5/2}$, $^4F_{7/2}$ and $^2H_{11/2}$ multiplets to the $^4I_{15/2}$ multiplet, and $^4G_{9/2}$, $^4F_{5/2}$, $^4F_{7/2}$ and $^4S_{3/2}$ multiplets to the $^4I_{13/2}$ multiplet, all recorded for $Z_1 \rightarrow E_2$ excitation, are presented in Figure 8.6. The transitions in the spectra were all found to be reproducible by pumping the $Z_1 \rightarrow E_1$ or $Z_2 \rightarrow E_2$ transitions, and the extensive energy level scheme of Table 8.2 was completed with information from these fluorescence measurements. All transitions observed in these spectra can be assigned according to the energy level scheme.

Consistent with the behaviour of Er^{3+} ions in other hosts, the transitions for $^2H_{11/2} \rightarrow {}^4I_{15/2}$ fluorescence had weak intensity. This is due to rapid non-radiative decay to the nearby $^4S_{3/2}$ manifold. Of interest in the spectrum were absorption peaks in the underlying broadband fluorescence in this spectral region (Figure 8.6g).

Table 8.3 summarises the intensities of the maximum peak in each spectral region relative to the most intense fluorescence peak, the $E_1 \rightarrow Z_3$ transition, for 18mw excitation of the $Z_1 \rightarrow E_2$ transition.

Additional spectral lines observed in the 13800-14300 cm^{-1} region are unidentified, and the polarised spectra are given in Figure 8.7. Although the intensities of these lines are also optimised by tuning on the principal site fluorescence, the transition energies do not fit the pattern of any expected Er^{3+} multiplet. These lines were found to have the same relative intensity pattern when pumping the $Z_1 - E_2$ transition with π polarisation as the $Z_1 \rightarrow E_1$

Figure 8.6 : Unpolarised 12K fluorescence spectra for laser excitation of the $Z_1 \rightarrow E_2$ transition of the Er^{3+} ion pair site in a $CsCdBr_3$:0.7%Er^{3+} crystal.

(a) $^4S_{3/2} \rightarrow {}^4I_{13/2}$ (E → Y)

(b) $^4I_{9/2} \rightarrow {}^4I_{15/2}$ (B → Z)

(c) $^4F_{7/2} \rightarrow {}^4I_{13/2}$ (G → Y)

(d) $^4F_{9/2} \rightarrow {}^4I_{15/2}$ (D → Z)

(e) $^4F_{5/2} \rightarrow {}^4I_{13/2}$ (H → Y)

(f) $^4S_{3/2} \rightarrow {}^4I_{15/2}$ (E → Z)

(g) $^2H_{11/2} \rightarrow {}^4I_{15/2}$ (F → Z)

(h) $^4F_{5/2} \rightarrow {}^4I_{15/2}$ (H → Z)

(i) $^4F_{7/2} \rightarrow {}^4I_{15/2}$ (G → Z)

(j) $^2H_{9/2} \rightarrow {}^4I_{15/2}$ (K → Z)

(k) $^4G_{11/2} \rightarrow {}^4I_{15/2}$ (L → Z)

(l) $^4G_{9/2} \rightarrow {}^4I_{13/2}$ (T → Y)

Transitions are identified by a numerical label representing the appropriate upper and lower multiplet crystal field levels involved. The laser position is identified by "L" in Figure (f).

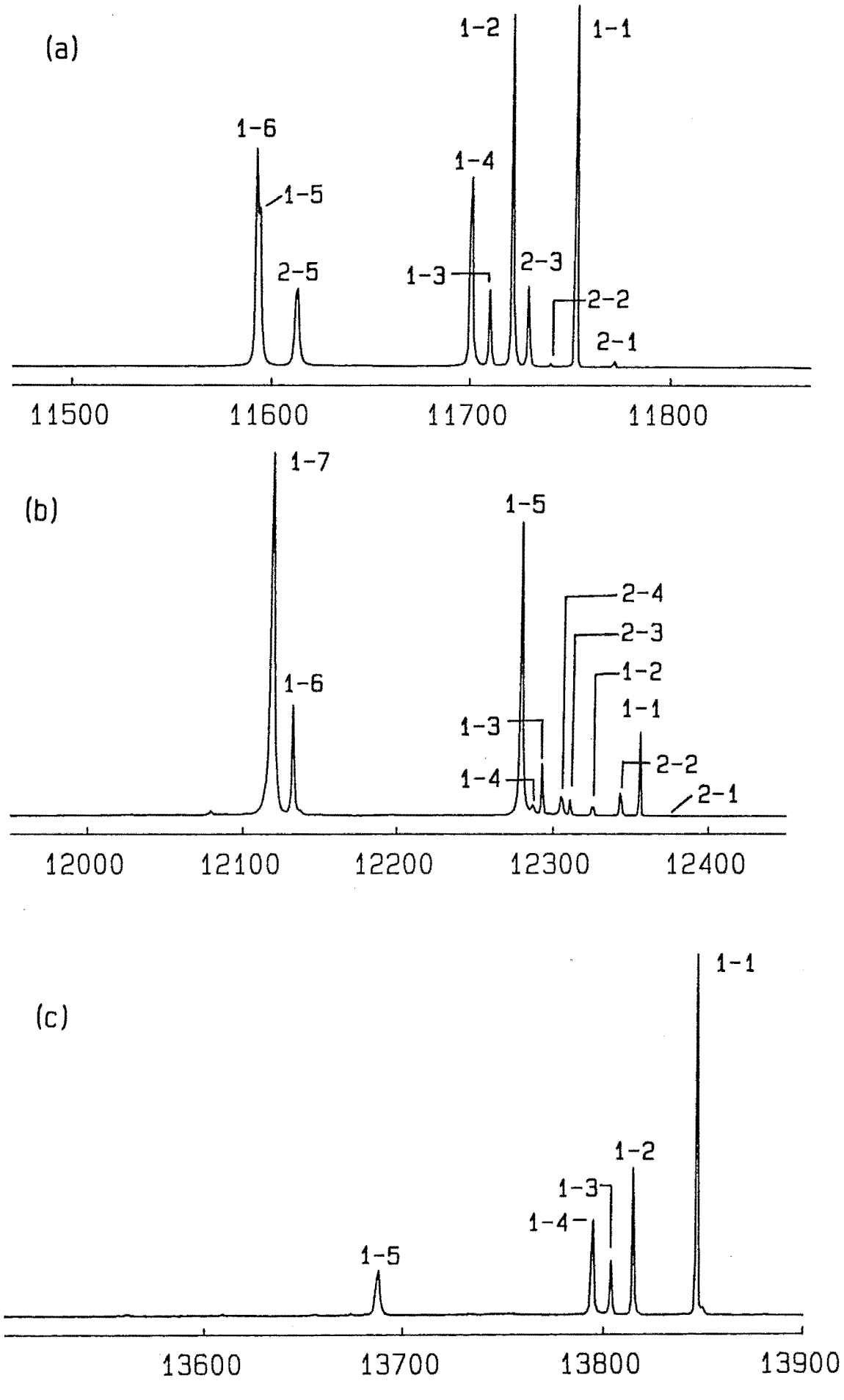
(a)
1-2
1-1
1-6
1-4
1-5
2-5
1-3
2-3
2-2
2-1
11500
11600
11700
11800
(b)
1-7
1-5
2-4
2-3
1-6
1-2
1-1
1-3
2-2
1-4
2-1
12000
12100
12200
12300
12400
(c)
1-1
1-2
1-3
1-4
1-5
13600
13700
13800
13900

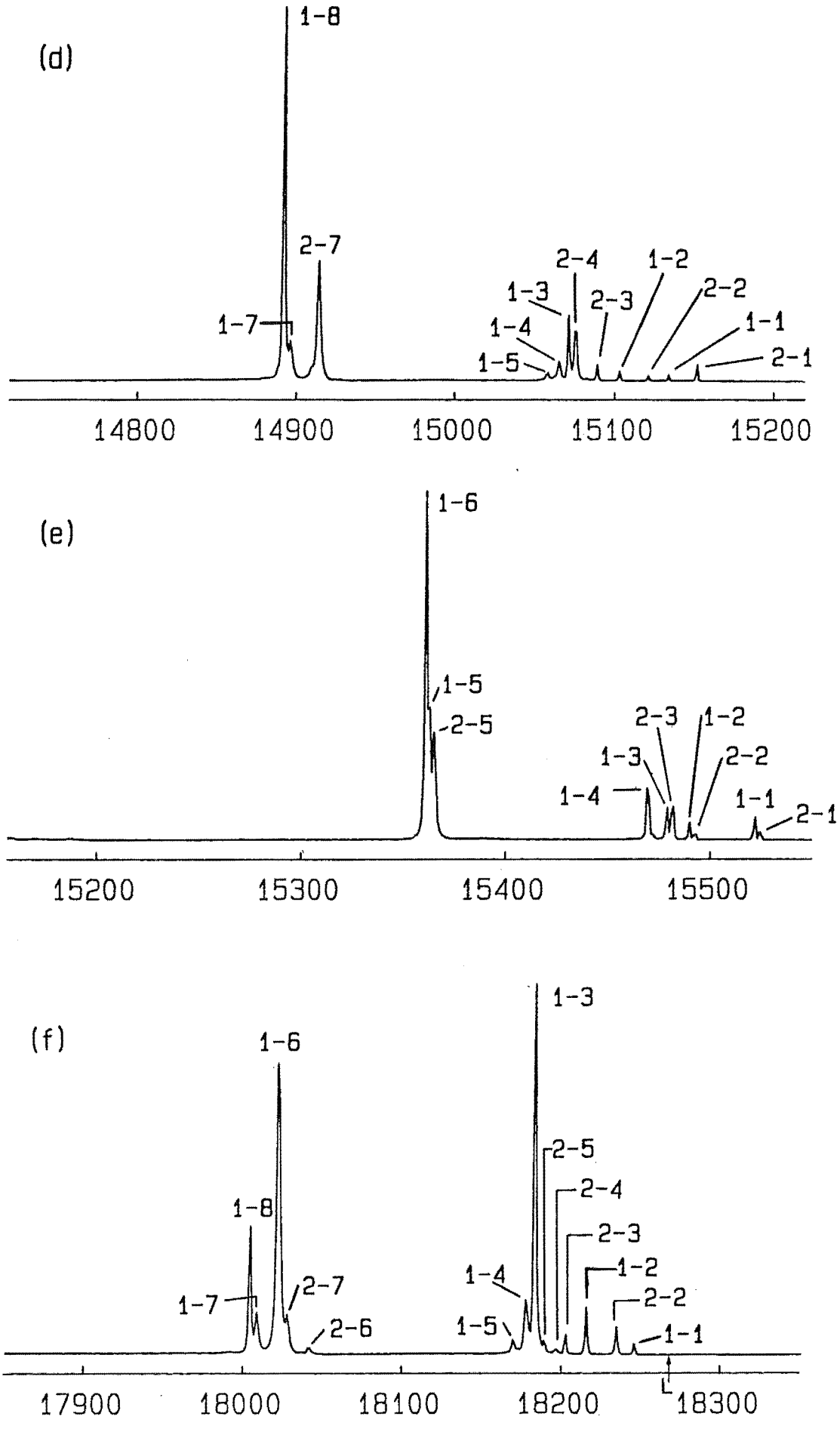
(d)
1-8
2-7
1-7
2-4
1-2
1-3
2-3
2-2
1-4
1-1
1-5
2-1
14800
14900
15000
15100
15200
(e)
1-6
1-5
2-5
2-3
1-2
1-3
2-2
1-4
1-1
2-1
15200
15300
15400
15500
(f)
1-3
1-6
2-5
1-8
2-4
2-3
1-2
1-4
2-7
1-7
2-2
2-6
1-5
1-1
17900
18000
18100
18200
18300

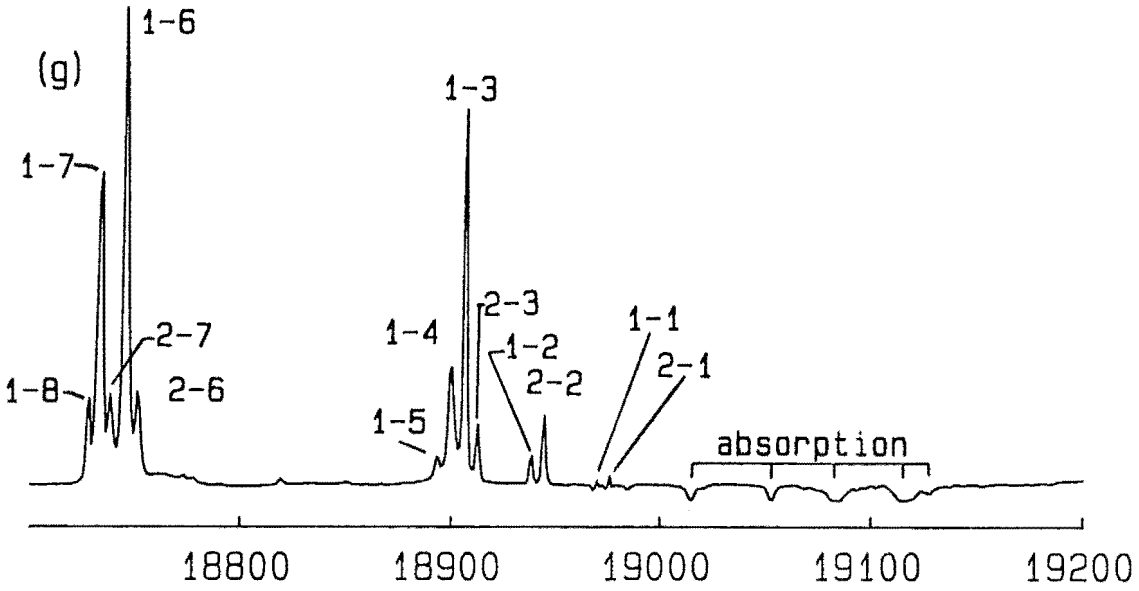
(g)
1-6
1-7
1-3
2-3
1-4
1-2
1-1
2-7
2-2
2-1
1-8
2-6
1-5
absorption
18800
18900
19000
19100
19200

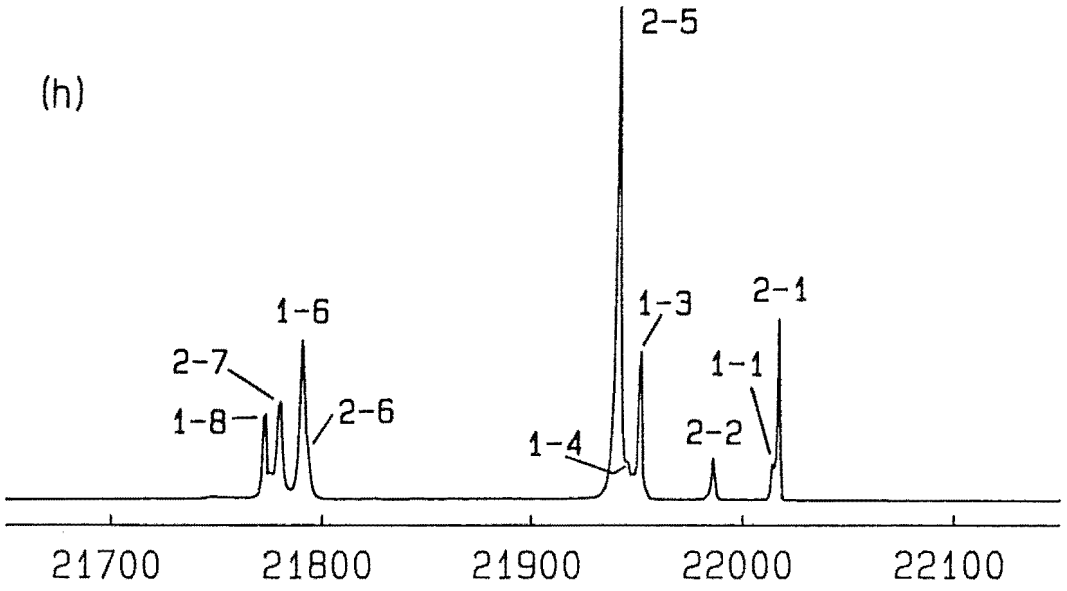
(h)
2-5
1-6
1-3
2-1
2-7
1-1
1-8
2-6
1-4
2-2
21700
21800
21900
22000
22100

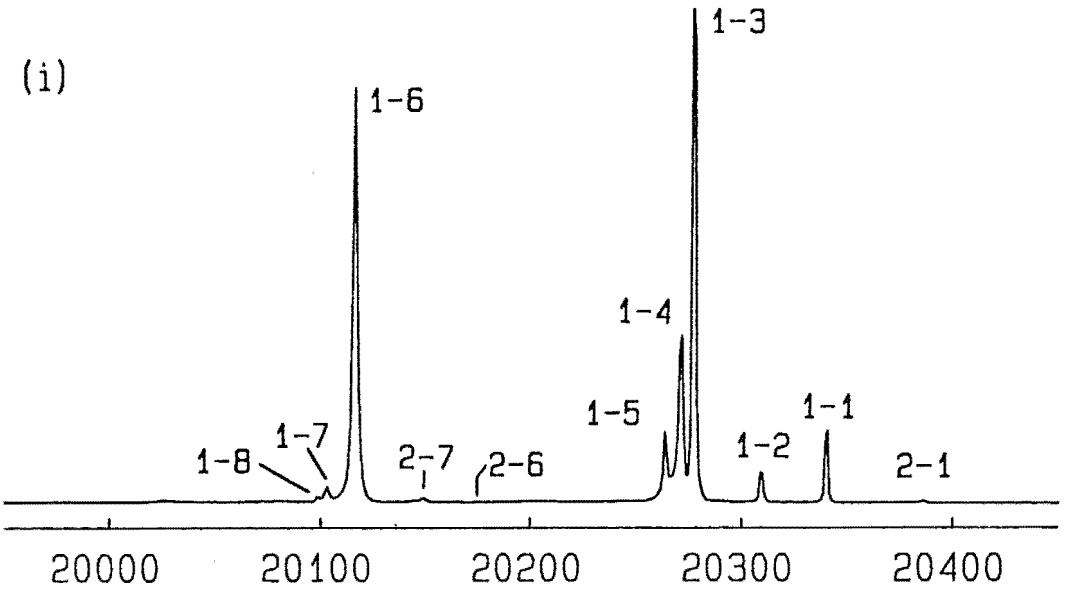
(i)
1-3
1-6
1-4
1-5
1-7
1-1
1-8
2-7
2-6
1-2
2-1
20000
20100
20200
20300
20400

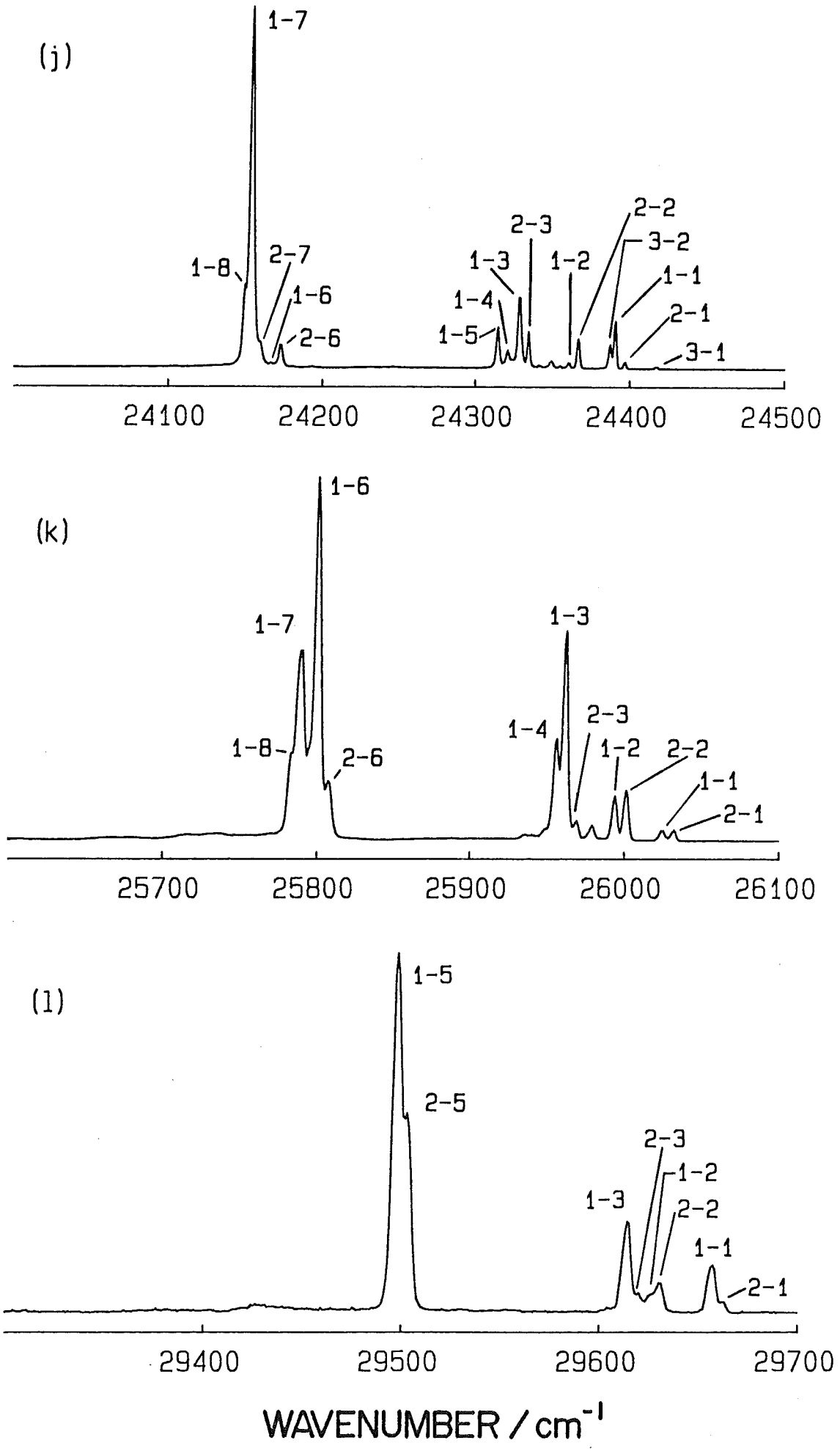
(j)
1-7
1-8
2-7
1-6
2-6
2-3
1-3
1-2
2-2
3-2
1-4
1-1
1-5
2-1
3-1
24100
24200
24300
24400
24500
(k)
1-6
1-7
1-3
1-8
2-6
1-4
2-3
1-2
2-2
1-1
2-1
25700
25800
25900
26000
26100
(l)
1-5
2-5
2-3
1-2
1-3
2-2
1-1
2-1
29400
29500
29600
29700
WAVENUMBER / cm-1

Table 8.2 : Energy levels (in cm^{-1}) for twelve multiplets of the pair site in $CsCdBr_3:Er^{3+}$ as determined by optical absorption and laser selective excitation of the $Z_1 \rightarrow E_2$ transition. Uncertainty is ± 0.5 cm^{-1}

Level Number	$^4I_{15/2}$ (E)	$^4I_{13/2}$ (Y)	$^4I_{9/2}$ (B)	$^4F_{9/2}$ (D)	$^4S_{3/2}$ (E)	$^2H_{11/2}$ (F)	$^4F_{7/2}$ (G)	$^4F_{5/2}$ (H)	$^4F_{3/2}$ (I)	$^2H_{9/2}$ (K)	$^4G_{11/2}$ (L)	$^4G_{9/2}$ (T)
1	0	6494.0	12356.5	15134.2	18247.1	18970.5	20341.5	22014.8	22388.0	24390.8	26025.0	36151.0
2	31.0	6526.0	12374.0	15152.5	18266.3	18976.0	20386.0	22017.1	22411.0	24397.1	26032.0	36155.0
3	63.0	6537.5		15218.0		19016.5	20407.0	22099.0		24417.4		
4	69.2	6546.0		15222.5		19084.0						
5	76.5	6653.5		15298.5		19117.0						
6	224.2	6655.5				19130.5						
7	237.4											
8	241.8											

Table 8.3 : Relative intensities of the peak transitions for each of the thirteen groups of fluorescence transitions observed for $Z_1 \longrightarrow E_2$ laser excitation of the Er^{3+} pair site in $CsCdBr_3$:0.7%Er^{3+} at 12K. Laser polarisation was at 45° to the axis and fluorescence was scrambled with a Hanle wedge. All intensities are scaled to give an $E_1 \longrightarrow Z_3$ value of 1000.

Transitions	Spectral region (cm^{-1})	Peak transition Energy ($\pm$ 0.5cm^{-1})	Assignment	Relative intensity
$^4G_{9/2} \longrightarrow {}^4I_{13/2}$	29700-29450	29497.5	$T_1 \longrightarrow Y_5$	0.00335
$^4G_{11/2} \longrightarrow {}^4I_{15/2}$	26050-25750	25800.0	$L_1 \longrightarrow Z_6$	0.234
$^2H_{9/2} \longrightarrow {}^4I_{15/2}$	24450-24100	24152.8	$K_1 \longrightarrow Z_7$	0.598
$^4F_{5/2} \longrightarrow {}^4I_{15/2}$	22050-21750	21941.0	$H_2 \longrightarrow Z_5$	0.947
$^4F_{7/2} \longrightarrow {}^4I_{15/2}$	20400-20100	20278.5	$G_1 \longrightarrow Z_3$	310
$^2H_{11/2} \longrightarrow {}^4I_{15/2}$	19200-18700	18746.5	$F_1 \longrightarrow Z_6$	0.170
$^4S_{3/2} \longrightarrow {}^4I_{15/2}$	18300-18000	18184.1	$E_1 \longrightarrow Z_3$	1000
$^4F_{5/2} \longrightarrow {}^4I_{13/2}$	15550-15350	15361.0	$H_1 \longrightarrow Y_5$	0.501
$^4F_{9/2} \longrightarrow {}^4I_{15/2}$	15200-14850	14892.2	$D_1 \longrightarrow Z_8$	20.5
Possibly Sm^{2+}	14300-14100	14218.0	unknown	0.0697
$^4F_{7/2} \longrightarrow {}^4I_{13/2}$	13900-13600	13847.0	$G_1 \longrightarrow Y_1$	0.214
$^4I_{9/2} \longrightarrow {}^4I_{15/2}$	12400-12100	12119.0	$B_1 \longrightarrow Z_7$	2.16
$^4S_{3/2} \longrightarrow {}^4I_{13/2}$	11800-11550	11753.0	$E_1 \longrightarrow Y_1$	5.75

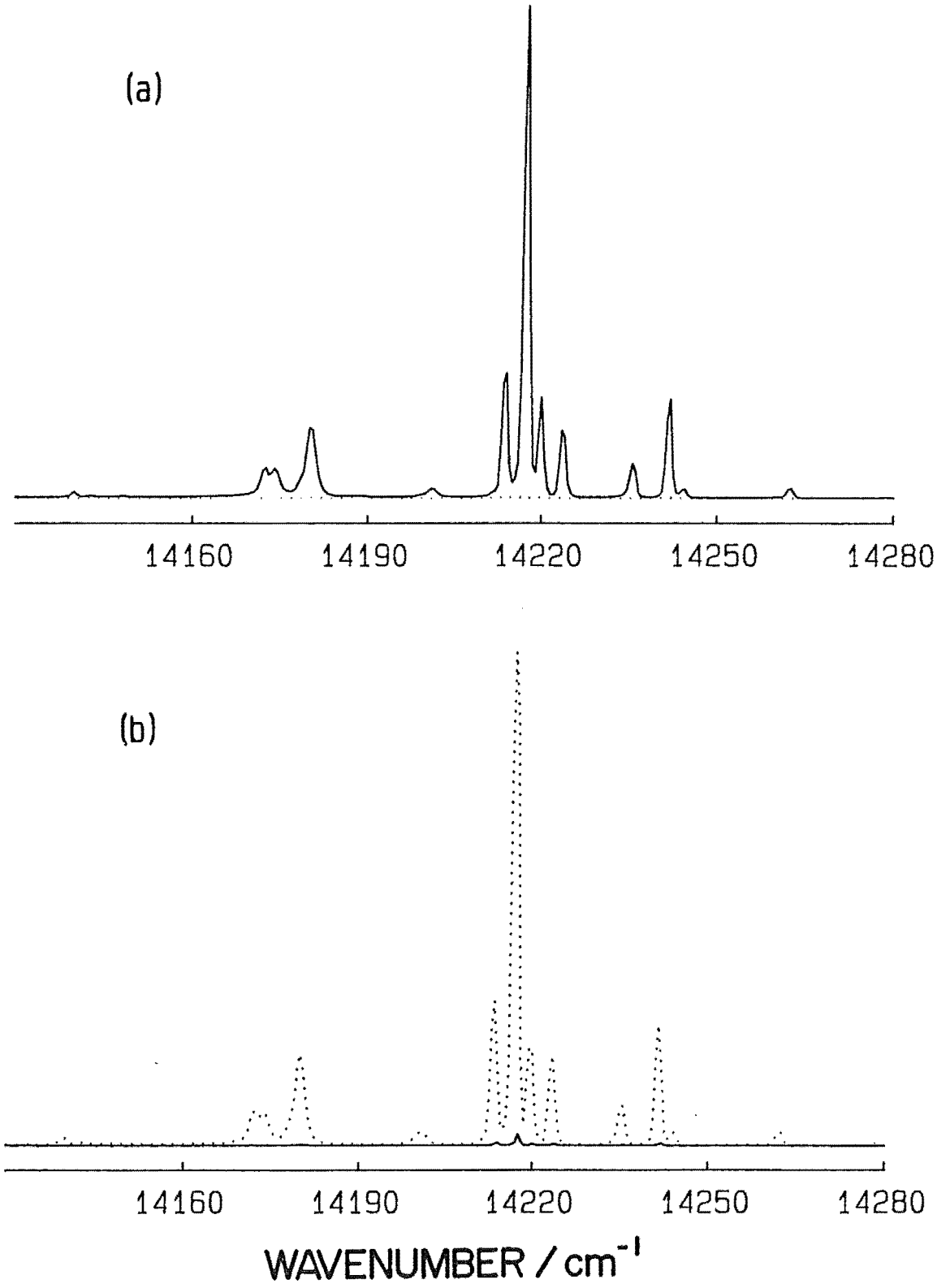

Figure 8.7 : Unassigned fluorescence transitions observed for laser excitation of the Er^{3+} ion pair site in $CsCdBr_3:Er^{3+}$ crystals at 12K: (a) for $Z_1 \rightarrow E_1$ excitation, and (b) for $Z_1 \rightarrow E_2$ excitation. The dotted and solid lines are for π and σ laser polarisations respectively with the fluorescence being scrambled by a Hanle wedge.

transition with σ polarisation. However, for excitation at either frequency with the opposite polarisation, the intensity of the emitting transitions was reduced to less than 2% of the original for all transitions.

Polarised emission spectra were recorded for the $^4S_{3/2} \rightarrow {}^4I_{15/2}$ transitions upon $Z_1 \rightarrow E_2$ excitation. The four polarisations : σ absorption with π emission ($\sigma\pi$), σ absorption with σ emission ($\sigma\sigma$), ($\pi\sigma$) and ($\pi\pi$) are shown in Figure 8.8. Figure 8.9 shows the two emission plots, one for σ absorption and one for π absorption with the fluorescence detected being π in both cases. The peak of the ($\sigma\pi$) plot has been scaled to equal the ($\pi\pi$) plot to illustrate that a separation of emission components for σ and π absorption occurs. All of the emission peaks after π absorption were found to be 0.3-0.5 cm^{-1} higher in frequency than the corresponding σ absorption excited fluorescence, and this small effect was verified by superposing six independent spectra of the same region having various combinations of absorption and emission polarisations.

8.2.4 Fluorescence Lifetime Measurements

The nitrogen pumped pulsed dye laser was used to determine fluorescence lifetimes of the $^4S_{3/2} \rightarrow {}^4I_{15/2}$, $^4F_{7/2} \rightarrow {}^4I_{15/2}$ and $^2H_{11/2} \rightarrow {}^4I_{15/2}$ multiplet transitions.

The lifetimes, at a temperature of 12K, determined by excitation of the $Z_1 \rightarrow E_1$, $Z_1 \rightarrow F_1$ and $Z_1 \rightarrow G_1$ transitions while monitoring the $E_1 \rightarrow Z_6$, $F_1 \rightarrow Z_6$ and $G_1 \rightarrow Z_6$ transitions respectively, were determined to be the following :

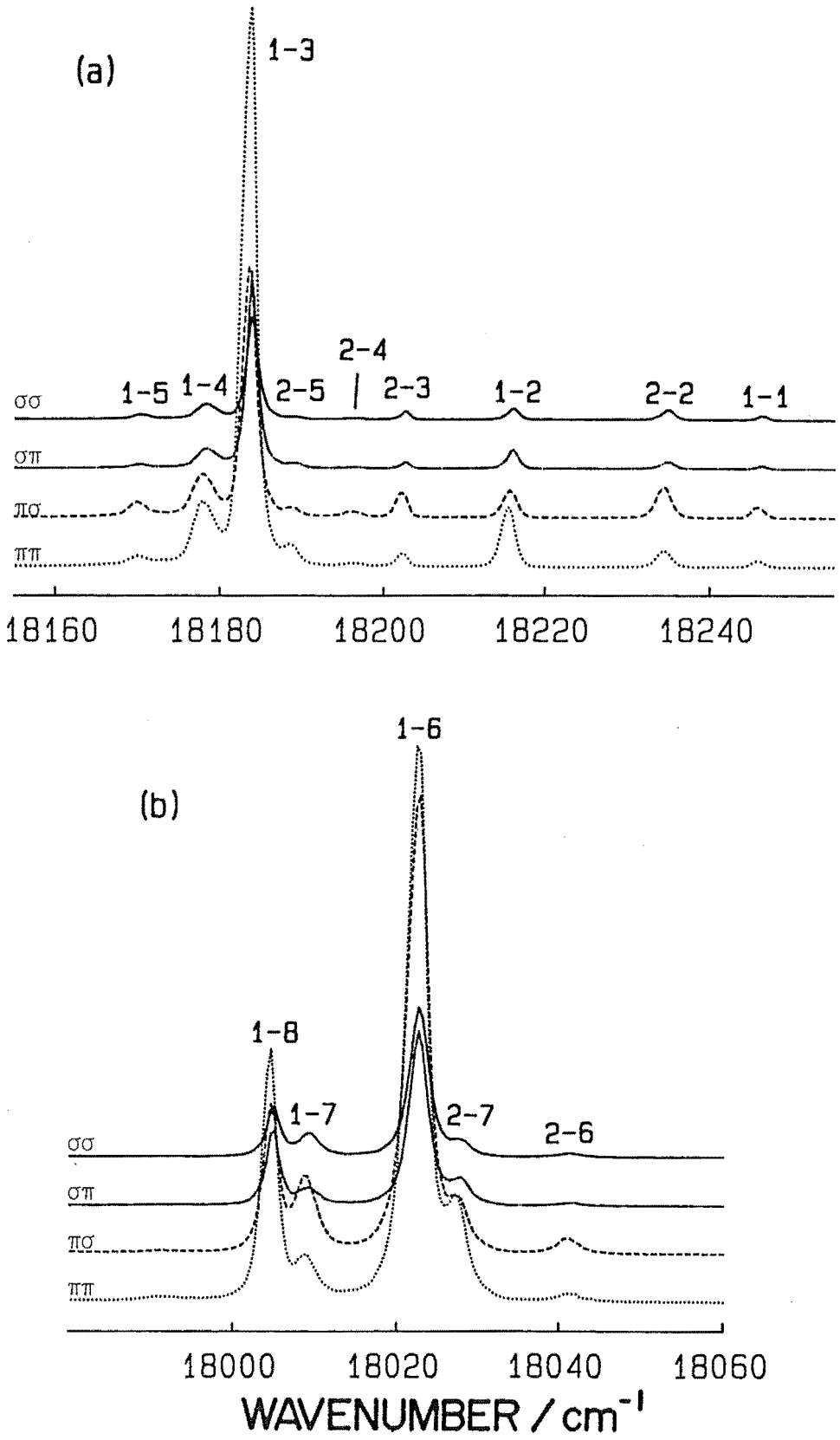

Figure 8.8 : $^4S_{3/2} \rightarrow {}^4I_{15/2}$ polarised fluorescence transitions for laser excitation of the $Z_1 \rightarrow E_2$ transition in $CsCdBr:Er^{3+}$ crystals at 12K.

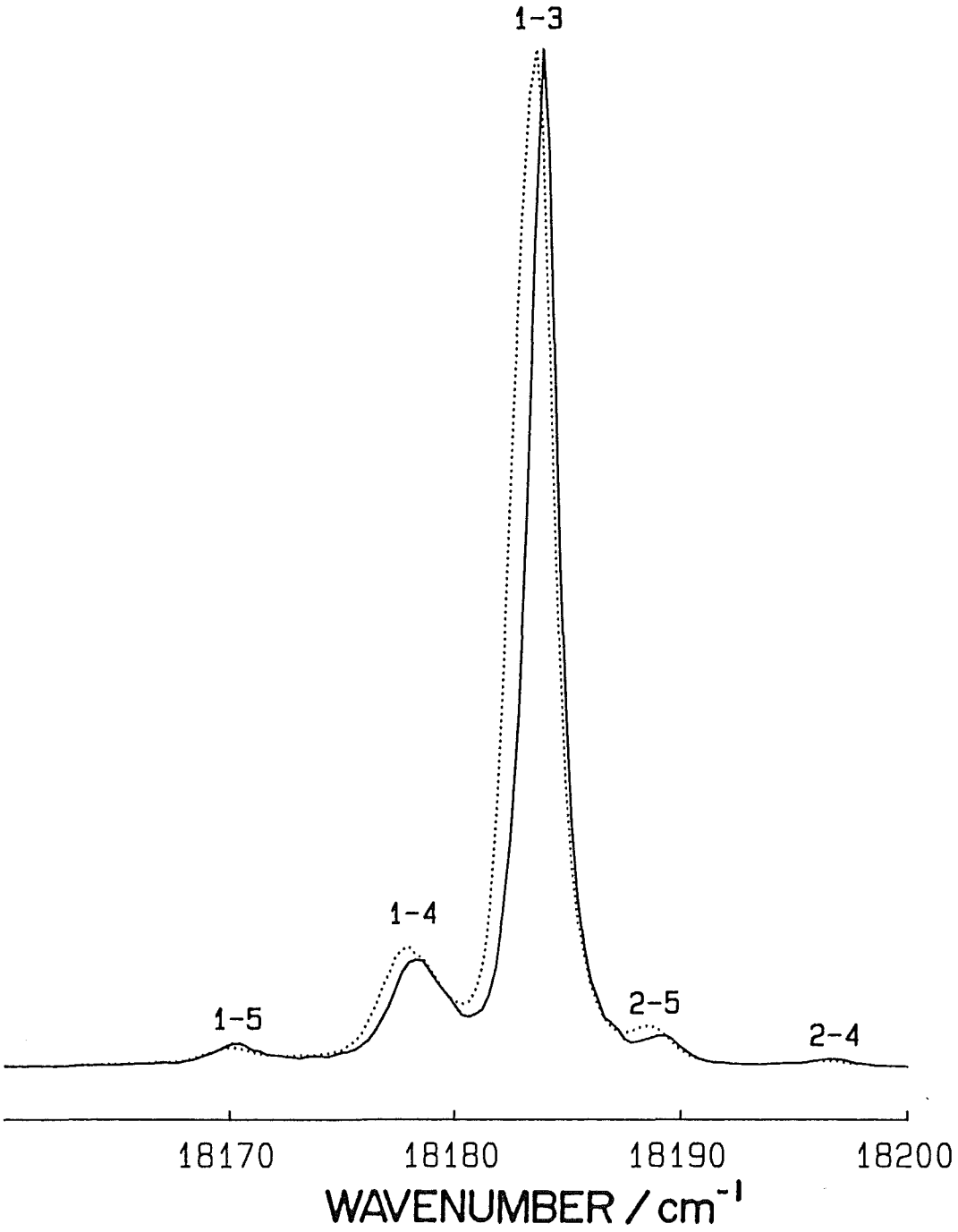

Figure 8.9 : 12K $^{+}S_{3/2} \rightarrow {}^{4}I_{15/2}$ fluorescence transitions for $Z_1 \rightarrow E_2$ excitation, scaled to give equal $E_1 \rightarrow Z_3$ intensities for π emission with both π(dotted line) or σ (solid line) absorption. An energy shift of 0.3 cm^{-1} is observed for most transitions.

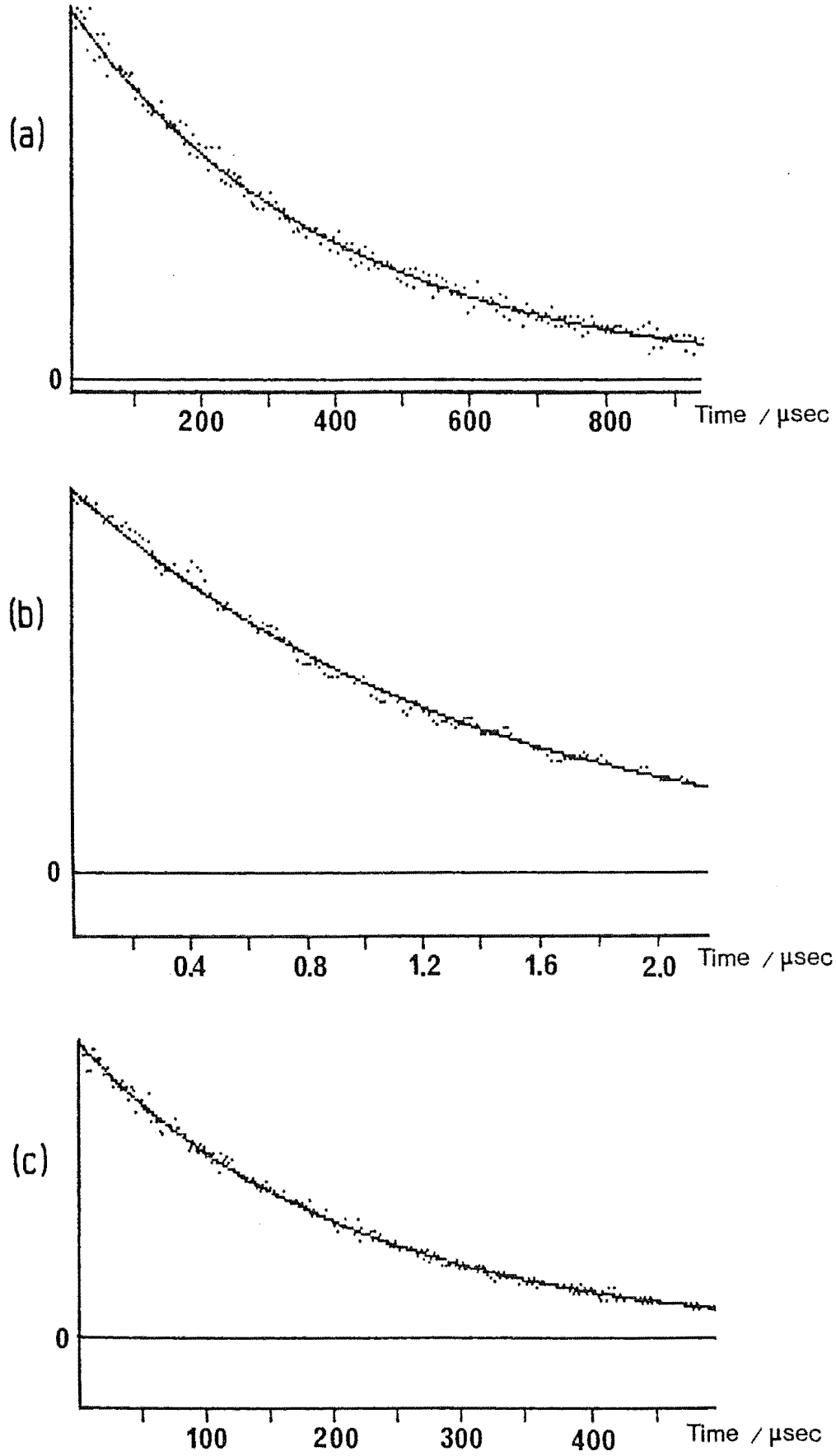

Figure 8.10 : Fluorescence time dependence of the Er^{3+} ion site in $CsCdBr_3$:0.7%Er^{3+} for : (a) the $^4S_{3/2}$ manifold (pump $Z_1 \rightarrow E_1$ monitor $E_1 \rightarrow Z_6$) (b) the $^2H_{11/2}$ manifold (pump $Z_1 \rightarrow F_1$, monitor $F_1 \rightarrow Z_6$), and (c) the $^4F_{7/2}$ manifold (pump $Z_1 \rightarrow G_1$, monitor $G_1 \rightarrow Z_6$). The solid curves are those fitted to give the lifetimes determined.

Table 8.4 Fluorescence lifetimes for direct excitation of three manifolds.

Manifold	Lifetime (μsec)
$^4S_{3/2}$	400 ± 10
$^2H_{11/2}$	1.40 ± 0.05
$^4F_{7/2}$	210 ± 6

Fluorescence curves for these excitations are given in Figure 8.10.

The upconverted fluorescence from the $^4F_{7/2}$ manifold for excitation of the $Z_1 \rightarrow E_1$ or $Z_1 \rightarrow E_2$ transitions was considerably weaker for pulsed excitation than for the cw excitation used for the rest of the spectroscopy. Attempts to determine the temporal dependence of this fluorescence were not successful.

8.3 Discussion

It is proposed that the principal site formed in these crystals is the Er^{3+} - vacancy - Er^{3+} site analogous to that of the $CsCdBr_3:Nd^{3+}$ system recently reported (Blasse *et al.* 1985). The efficient upconverted fluorescence observed for the site, with $^4F_{7/2} \rightarrow {}^4I_{15/2}$ fluorescence being nearly one third as intense as the directly pumped $^4S_{3/2} \rightarrow {}^4I_{15/2}$ fluorescence, is strong evidence for such a proposal.

A possible mechanism for the upconversion observed is the excitation of both ions in the pair followed by one ion transferring all of its energy co-operatively to the other which is then excited to the $^4G_{9/2}$ manifold at almost twice the excitation energy. Evidence for such a process is

provided by observation of the $^4G_{9/2} \rightarrow {}^4I_{13/2}$ transitions at ~ 29500 cm^{-1}, indicative of at least some ions being excited to the multiplet. The $^4G_{9/2} \rightarrow {}^4I_{15/2}$ transitions at ~ 36150 cm^{-1} are too high in frequency to be detected directly using the available equipment. A similar upconversion process was proposed by Tallant *et al.* (1976) for cluster sites in $CaF_2:Er^{3+}$, and an appropriate energy transfer scheme is shown in Figure 2.4.

The fine structure splitting observed in the optical absorption spectra for some transitions is attributed to the interaction between the two ions in the site to form slightly modified product wavefunctions with a lifting of the original degeneracy. This effect appears most clearly for the Z_1 level and was not observed to be greater than 0.5 cm^{-1} for any transition.

The observation of slight shifts in emission line frequencies in l.s.e. spectra dependent on laser polarisation seems to be new for this type of system, and is possibly a further manifestation of the wavefunction mixing. This particular effect should be investigated further in other systems since, for example, a magnetic exchange interaction between the ions would be expected to produce components distinguishable by polarisation. Such an interaction would vary with rare-earth dopant.

If each ion in the pair site had C_{3V} symmetry due to the axial field of the other, and if no exchange interaction between ions occurred, then the ratios of π to σ absorption should be very well defined and obey the C_{3V} group electric dipole selection rules of Table 4.2. In particular, each transition involving a $\tau_{5,6}$ wavefunction would have only one

non-zero component, σ or π, whereas $\gamma_4 \rightarrow \gamma_4$ transitions would be expected to have a variety of ratios. While most of the transitions were well polarised, no consistent assignment could be made since no absorption transitions for the site had a component that was absolutely zero. For C_{3V} symmetry, either the E_1 or E_2 level must be $\gamma_{5,6}$ so that transitions from this state to all ground states would have either a dominant σ or π component. While several transitions to both E_2 and E_1 had relatively large π components, none had a σ component that dominated by greater than a factor of 2.14 (Table 8.1). If this inconsistency was due entirely to depolarisation by scattering or misalignment of the sample, then there seems no reason why the σ components would be scrambled more than the π components. It therefore seems possible that the symmetry is reduced from C_{3V} by some previously unreported lattice distortion.

Some of the unassigned lines in the absorption spectra, for instance those marked by a star in Figure 8.2, had well-defined polarisation ratios. This is indicative of good crystal orientation and C_{3V} symmetry. It is proposed that some of these lines are due to a single Er^{3+} ion site in the chain with more remote charge compensation. The lines were generally weak, consistent with previous findings that 90% of RE^{3+} ions form in pairs (Blasse *et al.* 1985).

The strong polarisation dependence of the unassigned transitions around 14200 cm^{-1} indicates that strict electric dipole selection rules are obeyed. Since non-zero component of (laser) absorption is π for one Er^{3+} transition and σ for another, the energy must be absorbed by the Er^{3+}

ion and transferred to another ion. It is not obvious, however, why the absorption components are so well defined in this case, but not for the polarised Er^{3+} transitions (Figure 8.8) measured in the same crystal during the same experiment. One possible source of these lines is the 4f → 5d transitions of Sm^{2+} ions that may be present in trace quantities. Similar transitions in this spectral region were observed for $CaF_2:Er^{3+}$ (Chapter Five).

The fast lifetime observed for the $^2H_{11/2}$ manifold is consistent with a rapid non-radiative decay to the $^4S_{3/2}$ manifold located only 700 cm^{-1} lower in energy. Fluorescence from this level is not normally seen at all for Er^{3+} systems such as $CaF_2:Er^{3+}$ and $SrF_2:Er^{3+}$. The $^4S_{3/2}$ manifold lifetime of 400 μsec. is comparable to the 710 μsec. lifetime in $CaF_2:Er^{3+}$ [TW75], and faster than that expected for a single Er^{3+} ion site. This factor could be used in future studies to discriminate the single ion sites by scanning the laser and detecting the signal with variable boxcar delays.

An obvious difference between this system and the pair sites of $CaF_2:Er^{3+}$ is the lifetime of the $^4F_{7/2}$ manifold which is a factor of 1000 longer in the present case. This indicates that one of the cross-relaxation mechanisms involving this level is less active for these sites, and illustrates that non-radiative decay processes are very sensitive to a change in the inter-ion distance. The specific processes involved could be investigated further with information about other multiplets, using different dyes or dye lasers.

8.4 Summary

The primary aim of this study was achieved, with many spectroscopic energy levels being determined using the available equipment, for the dominant site, which was found to contain a pair of Er^{3+} ions.

This type of system shows promise for optical studies with a view to investigating the crystal field influence on the sites. Although this work is preliminary, it establishes the feasibility of studying many similar Er^{3+} systems with different host crystals. A particular advantage is that the inter-ion separation may be varied by changing hosts, thus changing the axial crystal field but maintaining the same underlying symmetry.

An obvious extension using the results of this work is to double-dope the crystals with other RE^{3+} ions to form heterogeneous pair sites. The Er^{3+} - Yb^{3+} system would almost certainly give interesting results, as most of the upconversion processes for energy transfer to the Er^{3+} ion involve the normally very fast non-radiative decay from the $^4F_{7/2}$ manifold (Wright 1976), a decay channel which is considerably less active in this system.

Single frequency dye laser excitation studies may be required to resolve accurately the components of the fine structure observed on certain transitions and to determine the form of interaction involved.

These results form the first reported extensive crystal field level determination of Re^{3+} pair centres in AMX_3 hosts using the efficient upconversion process resulting from

laser selective excitation, and further work of this nature is likely to be undertaken.

CHAPTER NINE

CONCLUSION

This dissertation has described the results of a laser selective excitation study of erbium ions in three host lattice systems.

The principal emphasis has been on the hdyrogenated $CaF_2:Er^{3+}$ system, with sixteen hydrogenic sites, including thirteen with nearby charge compensation and three with remote compensation, being studied. The range of sites and complexity of spectra is considerably greater than for the parent, non-hydrogenated system for this level of dopant concentration. Most of the new sites involve an interstitial hydrogenic ion providing charge compensation for the trivalent ion, and have additional hydrogenic ions substituting for regular fluoride ions in the lattice. The result of this substitution is a slight reduction of symmetry producing sites of similar crystal-field energy level patterns with the thirteen sites of nearby charge compensation, each being classified into one of two "families" of related sites. Measurement of the isotope shifts of electronic transition frequencies, resulting from the substitution of D^- or T^- ions for the H^- ions, together with the classification of vibronic transitions associated with the various vibrational modes of hydrogenic ions, has enabled assignment of specific configurations to several of the sites. Evidence was found in the optical absorption, laser excitation, and infra-red absorption studies for hybrid sites involving both H^- and D^- ions in appropriately

treated crystals.

It was found that the distribution of hydrogenic sites formed in a crystal can be controlled principally by variation of the duration of heating during the hydrogenation process. This site distribution was then observed to change as the crystals aged, with some sites increasing rapidly before reaching an equilibrium and then decreasing after a period of several months. These effects are worthy of a specific study and may provide an indication of the effect of the charge compensation requirement on the diffusion of hydride ions in the lattice.

The infra-red study of the hydrogenated $CaF_2:Er^{3+}$ system revealed local mode energies assigned to seven new hydrogenic sites, and also revealed several new, unassigned, modes. All local modes of the system, including those previously reported, were calibrated and summarised. This summary is likely to be of use for future infra-red laser excitation studies.

An optical study of the previously unreported deuterated $SrF_2:Er^{3+}$ system enabled the classification of eight new hydrogenic sites involving nearby charge compensation and an additional "near cubic" symmetry site. Selective excitation of these sites was found to be more difficult for this system than for the $CaF_2:Er^{3+}$ system, with the resultant fluorescence generally including transitions of underlying fluoride ion sites. Analysis of this fluorescence resulted in the classification of nine new fluoride ion sites.

A principal and surprising result of the $SrF_2:Er^{3+}$ study was the change in preferred D^- ion charge compensation

configuration with increasing duration of the deuteration treatment. Short deuterations produced an expected D^- ion analogue of the trigonal symmetry F^- J site having next nearest-neighbour charge compensation. As the duration of deuteration was increased, the sites with approximately tetragonal symmetry dominated the spectra, with a large increase relative to the trigonal site. An additional surprising feature of the system was the apparent absence of a simple, single D^- ion, C_{4V} symmetry site, despite the formation of related sites modified by additional substitutional D^- ions. Similar studies of other RE^{3+} ions, particularly those having similar radii, would be helpful to interpret this behaviour.

Reversible polarised bleaching, a new effect, was observed for hydrogenic sites in both $SrF_2:Er^{3+}$ and $CaF_2:Er^{3+}$ crystals of the <100> orientation. While this effect is not yet fully understood, it can be attributed to reorientation of (almost) tetragonal symmetry dipoles undergoing preferential migration of hydrogenic ions upon laser excitation of the Er^{3+} ion electronic transitions. Other rare-earth ion systems have recently been found to exhibit a similar effect (Cockroft *et al.* 1987b), and further study and consolidation of information may provide more answers. Preliminary high resolution laser studies by Macfarlane (Private Communication) indicate that such techniques may be better suited to the study of such systems. One appropriate experiment for the future would involve the application of a magnetic field with laser selective excitation of the Zeeman components of specific orientation. This would enable, by appropriate bleaching,

control of the relative populations of centres in each orientation. Alternatively, the application of an electric field would create a differential of barrier heights for reorientations either perpendicular or parallel to the field, enabling control of orientation processes.

Previous studies of similar systems have not reported the polarisation dependence of emission for oriented samples. It was shown, in Chapter Four, that polarised laser selective excitation could be used to identify site symmetry without the use of applied magnetic fields. Trigonal site symmetry can be conclusively determined by an absence of polarisation dependence for emission in <100> oriented samples, together with the observation of appropriate intensity ratios in <111> oriented samples. This was used to confirm trigonal symmetry for the F^- B site in $CaF_2:Er^{3+}$, the configuration of which has been the subject of recent literature debate (Welsh 1985). Polarisation dependence was also used to assign wavefunction symmetry labels and revealed an anomaly in the Z_5 irrep label of the F^- A site in $CaF_2:Er^{3+}$. Consideration of the polarisation of emission should be an integral part of all future laser selective studies on systems of this type.

Crystal field analysis of data for the tetragonal and trigonal symmetry sites of the $CaF_2:Er^{3+}$ and $SrF_2:Er^{3+}$ systems was undertaken. The hydrogenic C_{4V} parameters obtained update the previous attempts, using less experimental data (Edgar *et al.* 1979), and produced parameters more consistent with the fluoride ion analogue site (Freeth *et al.* 1982). Parameters obtained for the trigonal crystal field fitting of the F^- J site in

$SrF_2:Er^{3+}$ are consistent with the proposed model, having a complete nearest-neighbour shell of fluoride ions.
The F^- B site parameters, however, seem inconsistent with a complete nearest-neighbour shell. The experimental results presented here, for several sites, may form the basis for future theoretical considerations.

Spectroscopy of the $CsCdBr_3:Er^{3+}$ system utilised the efficient upconversion, upon laser excitation, of the dominant pair site present. The crystal field energy levels were relatively easily determined, and such studies of similar systems would provide a useful basis for consideration of both crystal field variation and energy exchange problems. Some optical transitions were split by an interaction in the system, and further work, probably requiring higher resolution lasers, should be undertaken to determine the origin of this splitting. It was found that these components could be partially selectively excited by varying the polarisation of the laser.

In summary, the laser selective excitation technique was found to be very powerful for the study of these Er^{3+} ion systems with a wide variety of information being obtained by its application. While further general optical spectroscopy of these systems is unlikely to produce significant advancement of the results presented here, it is clear that several specific aspects are worthy of further study. In particular, the application of very much higher resolution laser spectroscopy is likely to provide insight into several unanswered questions. The basis of information provided here would also be complemented by further study using techniques such as dielectric loss,

ITC, optical Zeeman spectroscopy, EPR and ENDOR. Hydrogenated systems, with additional effects observable due to dynamical interactions, are likely to be of particular interest for future experimental and theoretical consideration.

REFERENCES

Aizenberg I.B., Davydova M.D., Malkin B.Z., Smirnov A.I. and Stolov A.L., 1973a, *Sov. Phys. - Solid State*, **15**, 914, [Ai73a]

Aizenberg I.B., Davydova M.D. and Stolov A.L., 1973b, *Sov. Phys. - Solid State*, **14**, 2710

Aizenberg I.B., Livanova L.D., Saitkulov I.G. and Stolov A.L., 1969, *Sov. Phys. - Solid State*, **10**, 1595, [Ai69]

Aizenberg I.B., Malkin B.Z. and Stolov A.L., 1972, *Sov. Phys. - Solid State*, **13**, 2155 [Ai72]

Aldous R. and Baker J.M., 1976, *Phys. Lett.*, **57A**, 85

Andeen C.G., Fontanella J.F., Wintersgill M.C., Welcher P.J., Kimble R.J. and Matthews G.E., 1981, *J. Phys. C*, **14**, 3557

Andeen C., Hayden L.M. and Fontanella J., 1980, *Phys. Rev. B*, **21**, 794

Andeen C., Link D. and Fontanella J., 1977, *Phys. Rev. B*, **16**, 3762

Anderson C.H. and Sabisky E.S., 1971, *Phys. Rev. B*, **3**, 527

Antipin A.A., Kurkin I.N., Livanova L.D., Potvorova L.Z. and Ya. Shenkun L., 1967, *Sov. Phys. - Solid State*, **8**, 2130

Auzel F.E., 1973, *Proc. IEEE*, **61**, 758

Baker J.M., 1974, Rare-Earth and other impurity ions in non-cubic sites, Ch 6 in *Crystals of the Fluorite Structure*, ed. W. Hayes (Oxford : Clarendon Press)

Barthem, R.B., Buisson R., Vial J.C. and Chaminade J.P., 1985, *J. de Physique*, **C7**, 113

Becquerel J., 1908, *Phys. Z.*, **8**, 632

Berdowski P.A.M., Lammers M.J.J. and Blasse G., 1985, *J. Chem. Phys.*, **83**, 476

Bethe H., 1929, *Ann. Physik*, **3**, 133

Bethe H., 1930, *Z. Physik*, **60**. 218

Blasse G., Wolfert A. and McPherson G.L., 1985, *J. Solid State Chem.*, **57**, 396

Bloembergen N., 1959, *Phys. Rev. Lett.*, **2**, 84

Brown M.R. and Shand W.A., 1970, *Advanced Quantum Electronics*, ed. D.W. Goodwin (New York: Academic Press) .

Brown M.R., Thomas H., Whiting J.S.S. and Shand W.A., 1969a, *J. Chem. Phys.*, **50**, 881, [Br69a]

Brown M.R., Roots K.G., Williams J.M., Shand W.A., Groter C. and Kay H.F.,1969b, *J. Chem. Phys.*, **50**, 891, [Br69b]

Butler P.H., 1981, *Point Group Symmetry Applications Methods and Tables* (New York: Plenum)

Campbell J.A., University of Canterbury, Private Communication

Campbell J.A., Sievers A.J. and Jones G.D., 1982, *Bull. Am. Phys. Soc.*, **27**, 402

Catlow C.R.A., University of Keele, Private Communication

Catlow C.R.A., 1976, *J. Phys. C*, **9**, 1845

Catlow C.R.A., Chadwick A.V. and Corish J., 1983a, *Rad. Eff.*, **75**, 61

Catlow C.R.A., Chadwick A.V., Greaves G.N. and Moroney L.M., 1984, *Nature*, **312**, 601

Catlow C.R.A., Moroney L.M., Chadwick A.V. and Greaves G.N., 1983b, *Rad. Eff.*, **75**, 159

Catlow C.R.A., Moroney L.M., Chadwick A.V. and Greaves G.N., 1983c, *EXAFS and Near Edge Structures* (Berlin : Springer-Verlag), pp.200-202

Catlow C.R.A., Norgett M.J. and Ross T.A., 1977, *J. Phys. C*, **10**, 1627

Chambers D.N., 1971, *J. Phys. C*, **4**, 1977

Chambers D.N. and Newman R.C., 1969, *Phys. Stat. Sol.*, **35**, 685

Chambers D.N. and Newman R.C., 1971, *J. Phys. C.*, **4**, 1977

Cheetham A.K., Fender B.E. and Cooper M.J., 1971, *J. Phys. C*, **4**, 3107

Cockroft N.J., 1983, Honours III project report, University of Canterbury

Cockroft N.J., Thompson D., Jones G.D. and Syme R.W.G., 1987a, *J. Chem. Phys.*, **86**, 521

Cockroft N.J., Han T.P.J., Reeves R.J., Jones G.D. and Syme R.W.G. 1987b, *Optics Letters*, **12**, 36

Corish J., Catlow C.R.A., Jacobs P.W.M. and Ong S., 1982, *Phys. Rev. B*, **25**, 6425 [Co82]

Coulson C.A. and Sharma C.S., 1962, *Proc. Phys. Soc.* (London), **79**, 920

CRC *Handbook of Chemistry and Physics*, 1982, ed. R.C. Weast (Boca Raton Florida : CRC Press)

Denham P., Field G.R., Morse P.L. and Wilkinson G.R., 1970, *Proc. Roy. Soc.* (London), A317, 55

Dieke G.H., 1968, *Spectra and Energy Levels of Rare Earth Ions in Crystals* (New York : Wiley)

Dorenbos P. and den Hartog H.W., 1985, *Phys. Rev. B*,, 31, 3932

Edgar A., Freeth C.A. and Jones G.D., 1977, *Phys. Rev.* B, 15, 5023 [EFJ77]

Edgar A., Jones G.D. and Presland M.R., 1979, *J. Phys. C*, 12, 1569

Edgar A and Welsh H.K., 1975, *J. Phys. C.*, 8, L336

Elcombe M.M. and Pryor A.W., 1970, *J. Phys. C.*, 3, 492

Elliott R.J., Hayes W., Jones G.D., Macdonald H.F. and Sennett C.T., 1965, *Proc. Roy. Soc.* (London) A289, 1

Esterowitz L., Noonan J. and Bahler J., 1967, *Appl. Phys. Lett.*, 10, 126

Feofilov P.P. and Ovsyankin V.V., 1967, *Appl. Optics*, 6, 1828

Fontanella J.F., Jones D.L. and Andeen C.G., 1978, *Phys. Rev. B*, 18, 4454

Fontanella J., Treacy D.J. and Andeen C., 1980, *J. Chem. Phys.*, 72, 2235

Freeth C.A., 1980, Ph.D. Thesis, University of Canterbury

Freeth C.A., Jones G.D. and Syme R.W.G., 1982, *J. Phys. C*, 15, 5667 [Fr82]

Greenblatt M. and Banks E., 1977, *J. Electrochem. Soc.*, 124 409

Gustafson F.J., 1978, Ph.D. Thesis, University of Wisconsin, University Microfilms, Ann Arbor, Michigan

Gustafson F.J. and Wright J.C., 1977, *Anal. Chem.*, 49, 1680 [Gw77]

Hall J.C. and Schumacher R.T., 1962, *Phys. Rev.*, 127, 1892 [HS62]

Han T.P.J., University of Canterbury, Private Communication

Harrington J.A., Harley R.T. and Walker C.T., 1970, *Sol. State Com.*, 8, 407

Hayes W., 1974, *Crystals with the Fluorite Structure* (Oxford : Clarendon)

Hayes W and Stoneham A.M., 1985, *Defects and Defect Processes in Nonmetallic Solids* (New York : Wiley)

Henling L.M. and McPherson G.L., 1977, *Phys. Rev. B*, **16**, 4756

Hutchings M.T., 1964, *Solid State Physics*, **16** (New York: Academic), pp.227-73

Iverson M.V. and Sibley W.A., 1980, *Phys. Rev. B*, **21**, 2522

Jacobs I.T., Jones G.D., Zdansky K. and Satten R.A., 1971, *Phys. Rev. B*, **3**, 2888

Johnson L.F. and Guggenheim H.J., 1971, *Appl. Phys. Lett.*, **19**, 44

Johnston M.V. and Wright J.C., 1979, *Anal. Chem.*, **51**, 1774

Jones G.D., 1964, D. Phil. Thesis, University of Oxford

Jones G.D., 1979, *Aust. J. Phys.*, **32**, 629

Jones G.D., Pelid S., Rosenwaks S. and Yatsiv S., 1969, *Phys. Rev.*, **183**, 353

Jones G.D. and Satten R.A., 1966, *Phys. Rev.*, **147**, 566

Jones G.D., Yatsiv S., Peled S. and Rosenwaks S., 1968, *Localised Excitations in Solids*, ed. R.F. Wallis (New York : Plenum), p.512

Jouant J.P., Bissleux C. and Mary G., 1984, *J. Lumin.*, **29**, 261.

Judd B.R., 1963, *Operator Techniques in Atomic Spectroscopy* (New York : McGraw Hill)

Kitts E.L. and Crawford J.H., 1974, *Phys. Rev. B.*, **9**, 5264

Kramers H.A., 1930, *Proc. Amsterdam Acad.*, **33**, 959

Kurz, M.D. and Wright J.C., 1977, *J. Lumin.*, **15**, 169 [KW77]

Lammers M.J.J. and Blasse G., 1986, *Chem. Phys. Lett.*, **126**, 405

Latter R., 1955, *Phys. Rev.*, **99**, 510

Lenting B.P.M., Numan J.A.J., Bijvank E.J. and den Hartog H.W., 1976, *Phys. Rev. B*, **14**, 1811

Lezama A., Oria M. and de Araujo C.B., 1986, *Phys. Rev. B*, **33**, 4493

Lidiard A.B., 1974, "Kinetics and Thermodynamics at point defects", Ch 3 in *Crystals of the Fluorite Structure*, ed. W. Hayes (Oxford : Clarendon Press)

Macfarlane R.M., IBM Almaden Research Centre, Private Communication

Macfarlane R.M., Reeves R.J. and Jones G.D., Optics Letters, in press.

Maradudin A.A., Montroll E.W. and Weiss G.H. 1963, *Solid State Physics*, Suppl 3, ed. F. Seitz and D. Turnbull (New York : Academic Press)

Maradudin A.A. and Peretti J., 1967, *Phys. Rev.*, **161**, 852

Mayer M.G., 1941, *Phys. Rev.*, **60**, 184

McPherson A.M. and McPherson G.L., 1981, *Solid State Comm.*, **37**, 501

McPherson G.L. and Henling L.M., 1977, *Phys. Rev. B*, **16**, 1889

McPherson G.L. and Martin L.A., 1984, *J. Am. Chem. Soc.*, **106**, 6884

McPherson G.L., McPherson A.M. and Atwood J.L., 1980, *J. Phys. Chem. Solids*, **41**, 495

McPherson G.L. and Talluto K., 1982, *Solid State Comm.*, **43**, 331

Merz J.L. and Pershan P.S., 1967, *Phys. Rev.*, **162**, 217

Miller M.P., Tallant D.R., Gustafson F.J. and Wright J.C., 1977, *Anal. Chem.*, **49**, 1474

Miyakawa T. and Dexter D.L., 1970, *Phys. Rev. B*, **1**, 2691

Montroll E.W. and Potts R.B., 1955, *Phys. Rev.*, **100**, 525

Moore D.S., 1980, Ph.D. Thesis, University of Wisconsin, University Microfilms Ann Arbor, Michigan

Moore D.S. and Wright J.C., 1979, Chem. Phys. Lett., **66**, 173

Moore D.S. and Wright J.C., 1981, *J. Chem. Phys.*, **74**, 1626

Newman R.C., 1973, Infra-red Studies of Crystal Defects (London : Taylor and Francis Ltd.) [Ne73]

Newman R.C. and Woodward R.J., 1974, *J. Phys. C*, **7**, L432

Nielson C.W. and Koster G.F. 1964, Spectroscopic Coefficients for p^n, d^n and f^n Configurations (Cambridge, Mass. : MIT Press)

Paris M., 1986, Honours III project report, University of Canterbury

Ranon U. and Low W., 1963, *Phys. Rev.*, **132**, 1609

Rector C.W., Pandey B.C. and Moos H.W., 1966, *J. Chem. Phys.*, **45**, 171 [RPM66]

Reddy T.Rs., Davies E.R., Baker J.M., Chambers D.N., Newman R.C. and Ozbay B., 1971, *Phys. Lett.*, **9**, 17

Reeves R.J., University of Canterbury, Private Communication

Reid M.F., 1981, Ph.D. Thesis, University of Canterbury

Reid M.F. and Butler P.H., 1982, *J. Phys. C*, **15**, 4103

Riesberg L.A. and Weber M.J., 1976, "Relaxation Phenomenon in Rare Earth Luminescence", Ch 3 in *Progress in Optics XIV*, ed. E. Wolf (Amsterdam : North Holland)

Robson A.B., 1969, M.Sc. Thesis, University of Canterbury

Rotenberg M., Bivins R., Metropolis N and Wooten J.K., 1959, The 3-j and 6-j symbols (Cambridge, Mass. : MIT Press)

Sarder D.K., Shinn M.D. and Sibley W.A., 1982, *Phys. Rev. B*, **26**, 2382

Schaefer G., 1960, *J. Phys. Chem. Solids*, **12**, 233

Schlesinger M. and Drake G.W.F., 1976, *Can. J. Phys.*, **54**, 1699

Shinn M.D., Windscheif J.C., Sarder D.K. and Sibley W.A., 1982, *Phys. Rev. B*, **26**, 2371

Staebler D.L. and Kiss Z.J., 1967, *Bull. Am. Phys. Soc.*, **12**, 670

Staebler D.L. and Kiss Z.J., 1969, *Appl. Phys. Lett.*, **14**, 93

Staebler D.L. and Schnatterly S.E., 1971, *Phys. Rev. B*, **3**, 516

Stevens K.W.H., 1952, *Proc. Phys. Soc.* (London), **A65**, 209

Syme R.W.G., Reeves R.J. and Jones G.D., 1984, *J. Lumin.*, **31**, 248

Tallant D.R., Miller M.P. and Wright J.C., 1976, *J. Chem. Phys.*, **65**, 510

Tallant D.R., Moore D.S. and Wright J.C., 1977, *J. Chem. Phys*, **67**, 2897

Tallant D.R. and Wright J.C., 1975, *J. Chem. Phys.*, **63**, 2074 [TW75]

Talluto K.F., Trautmann V.F. and McPherson G.L., 1984, *Chem. Phys.*, **88**, 299

Thompson D., 1983, M.Sc. Thesis, University of Canterbury

Timans J.W.J. and den Hartog H.W., 1976, *Phys. stat. sol(b)*, 73, 283 [TI76]

van Vleck J.H., 1937, *J. Phys. Chem.*, 41, 67

Ward R.W. and Whippey P.W., 1974, *Can. J. Phys.*, 52, 1185

Welsh H.K., CSIRO Division of Applied Physics, Sydney, Australia, Private Communication

Welsh H.K., 1985, *J. Phys. C*, 18, 5637

Wietfeldt J.R., Moore D.S., Tissue B.M. and Wright J.C., 1986, *Phys. Rev. B*, 33, 5788

Wright J.C., 1976, "Upconversion and Excited State Energy Transfer in Rare-Earth Doped Material"s, Ch 4 in *Topics in Applied Physics* Vol. 15, ed. F.K. Fong (Berlin : Springer-Verlag) [Wr76]

Wybourne B.G., 1965, Spectroscopic Properties of Rare Earths (New York : Wiley) [Wy65]

Yatsiv S., Peled S., Rosenwaks S. and Jones G.D., 1967, *Optical Properties of Ions in Crystals*, ed. H.M. Crosswhite and H.W. Moos (New York : Interscience), p.409

Ziman J.M., 1972, *Principles of the Theory of Solids*, 2nd Ed. (Cambridge University Press)

APPENDIX I

Components of C_{4v} and C_{3v} Centres in the <111> Geometry

The determination of polarisation ratios for sites of C_{4v} and C_{3v} symmetry in the <111> oriented fluorite crystals presented in Chapter Four required the following calculation of the components of absorption and emission for each of the possible alignments of the sites with respect to the experimental geometry.

A1.1 C_{3v} Symmetry

The four possible alignments of the trigonal axis for the C_{3v} site are labelled A, B, C and D in Figure 4.3(b) where the plane of the page is the (1,1,1) plane. Centre A is directly out of the page and centres B, C and D are directed upwards from the page forming an angle of $\beta = \cos^{-1}(\frac{1}{3}) \simeq 70.53^{o}$ with the direction of centre A. Figure 4.3(c) shows an alternative projection of the centres looking parallel to the (1,1,1) plane.

The experiments use a right angle geometry with the laser incident in direction x which for the special case shown in Figure 4.3(b), is chosen to be the projection onto the (1,1,1) plane of the X axis of Figure 4.3(a). The y axis is one of the directions in which the laser may be polarised and is orthogonal to x and on the (1,1,1) plane. The other direction, z, in which the laser may be polarised, is chosen as the axis of alignment of centre A.

To solve for the general case of an arbitrary direction of laser incidence parallel to the (1,1,1) plane, the axis system can be rotated by an angle α about the z axis giving the x', y', z' co-ordinate frame where x' is the new

direction of laser propagation and z' (=z) is in the direction of the spectrometer which detects the fluorescence.

The Euler angle formulation for co-ordinate rotations, where the rotation about one axis followed by a rotation about one of the resultant axes can be represented by the matrix product of the two separate matrices, may be applied to this system.

The appropriate transformation matrix for a rotation by angle α about the z axis is

$$R_z(\alpha) = \begin{bmatrix} \cos\alpha & \sin\alpha & 0 \\ -\sin\alpha & \cos\alpha & 0 \\ 0 & 0 & 1 \end{bmatrix} \qquad \text{A1.1}$$

Similarly a rotation by angle β about the y axis has

$$R_y(\beta) = \begin{bmatrix} \cos\beta & 0 & -\sin\beta \\ 0 & 1 & 0 \\ \sin\beta & 0 & \cos\beta \end{bmatrix} \qquad \text{A1.2}$$

For the present case the new x', y', z' co-ordinates may be expressed in terms of the original x, y, z co-ordinates in the following way

$$\begin{bmatrix} x' \\ y' \\ z' \end{bmatrix} = \begin{bmatrix} \cos\alpha & \sin\alpha & 0 \\ -\sin\alpha & \cos\alpha & 0 \\ 0 & 0 & 1 \end{bmatrix} \begin{bmatrix} x \\ y \\ z \end{bmatrix} \qquad \text{A1.3}$$

This technique may be applied to find new co-ordinate axes for each possible centre with one axis being parallel to the centre and the other two orthogonal. The transformation matrix will relate these new co-ordinates to

the experimental co-ordinates giving the perpendicular and parallel components of each centre contributing to each of the experimental polarisations.

A new set of cartesian axes x_i'', y_i'', z_i'' can be defined for each of the three remaining centres (i = B, C, D), such that x_i'' and y_i'' lie in the (1,1,1) plane orthogonal to the z_i'' axis which is defined to be aligned with the trigonal symmetry axis of the ith centre.

The necessary transformation can be made by first rotating the x' and y' axes about the z' axis by the angle separating the x' axis (Figure 4.3(b)) from the projection onto the (1,1,1) plane of the trigonal axis of the ith centre. The resultant axis system is then rotated by an angle β about the new y_i'' axis to give a new z_i'' axis aligned with the trigonal axis of symmetry of the ith centre.

The appropriate angles of rotation about the z' are $(\frac{\pi}{3} - \alpha)$, $(\pi - \alpha)$ and $(\frac{5\pi}{3} - \alpha)$ for centres B, C and D respectively with the angle of rotation about the y" axis being β in all cases. (Refer to Figures 4.3(b) and (c))

Thus, for centre B:

$$\begin{bmatrix} x_B'' \\ y_B'' \\ z_B'' \end{bmatrix} = \begin{bmatrix} \cos\beta & 0 & -\sin\beta \\ 0 & 1 & 0 \\ \sin\beta & 0 & \cos\beta \end{bmatrix} \begin{bmatrix} \cos(\frac{\pi}{3} - \alpha) & \sin(\frac{\pi}{3} - \alpha) & 0 \\ -\sin(\frac{\pi}{3} - \alpha) & \cos(\frac{\pi}{3} - \alpha) & 0 \\ 0 & 0 & 1 \end{bmatrix} \begin{bmatrix} x' \\ y' \\ z' \end{bmatrix}$$

$$= \begin{bmatrix} \cos\beta\cos(\frac{\pi}{3} - \alpha) & \cos\beta\sin(\frac{\pi}{3} - \alpha) & -\sin\beta \\ -\sin(\frac{\pi}{3} - \alpha) & \cos(\frac{\pi}{3} - \alpha) & 0 \\ \sin\beta\cos(\frac{\pi}{3} - \alpha) & \sin\beta\sin(\frac{\pi}{3} - \alpha) & \cos\beta \end{bmatrix} \begin{bmatrix} x' \\ y' \\ z' \end{bmatrix}$$

Similarly, by substituting the appropriate angles and using the identities:

$$\cos(\pi-\alpha) = -\cos\alpha$$

$$\sin(\pi-\alpha) = \sin\alpha$$

$$\cos(\frac{5\pi}{3}-\alpha) = \cos(\frac{\pi}{3}+\alpha)$$

and $$\sin(\frac{5\pi}{3}-\alpha) = -\sin(\frac{\pi}{3}+\alpha)$$

the following transformations are obtained:

$$\begin{bmatrix} x''_C \\ y''_C \\ z''_C \end{bmatrix} = \begin{bmatrix} -\cos\beta\cos\alpha & \cos\beta\sin\alpha & -\sin\beta \\ -\sin\alpha & -\cos\alpha & 0 \\ -\sin\beta\cos\alpha & \sin\beta\sin\alpha & \cos\beta \end{bmatrix} \begin{bmatrix} x' \\ y' \\ z' \end{bmatrix}$$

and

$$\begin{bmatrix} x''_D \\ y''_D \\ z''_D \end{bmatrix} = \begin{bmatrix} \cos\beta\cos(\frac{\pi}{3}+\alpha) & -\cos\beta\sin(\frac{\pi}{3}+\alpha) & -\sin\beta \\ \sin(\frac{\pi}{3}+\alpha) & \cos(\frac{\pi}{3}+\alpha) & 0 \\ \sin\beta\cos(\frac{\pi}{3}+\alpha) & -\sin\beta\sin(\frac{\pi}{3}+\alpha) & \cos\beta \end{bmatrix} \begin{bmatrix} x' \\ y' \\ z' \end{bmatrix}$$

Inversion of these matrices gives the experimental geometry co-ordinates x', y' and z' as a function of the axes set for each centre alignment B, C and D. The appropriate transformations for all four centres are:

$$\begin{bmatrix} x' \\ y' \\ z' \end{bmatrix} = \begin{bmatrix} \cos\alpha & \sin\alpha & 0 \\ -\sin\alpha & \cos\alpha & 0 \\ 0 & 0 & 1 \end{bmatrix} \begin{bmatrix} x \\ y \\ z \end{bmatrix}$$

$$\begin{bmatrix} x' \\ y' \\ z' \end{bmatrix} = \begin{bmatrix} \cos\beta\cos(\frac{\pi}{3}-\alpha) & -\sin(\frac{\pi}{3}-\alpha) & \sin\beta\cos(\frac{\pi}{3}-\alpha) \\ \cos\beta\sin(\frac{\pi}{3}-\alpha) & \cos(\frac{\pi}{3}-\alpha) & \sin\beta\sin(\frac{\pi}{3}-\alpha) \\ -\sin\beta & 0 & \cos\beta \end{bmatrix} \begin{bmatrix} x''_B \\ y''_B \\ z''_B \end{bmatrix}$$

$$\begin{bmatrix} x' \\ y' \\ z' \end{bmatrix} = \begin{bmatrix} -\cos\beta\cos\alpha & -\sin\alpha & -\sin\beta\cos\alpha \\ \cos\beta\sin\alpha & -\cos\alpha & \sin\beta\sin\alpha \\ -\sin\beta & 0 & \cos\beta \end{bmatrix} \begin{bmatrix} x''_C \\ y''_C \\ z''_C \end{bmatrix}$$

$$\begin{bmatrix} x' \\ y' \\ z' \end{bmatrix} = \begin{bmatrix} \cos\beta\cos(\frac{\pi}{3}+\alpha) & \sin(\frac{\pi}{3}+\alpha) & \sin\beta\cos(\frac{\pi}{3}+\alpha) \\ -\cos\beta\sin(\frac{\pi}{3}+\alpha) & \cos(\frac{\pi}{3}+\alpha) & -\sin\beta\sin(\frac{\pi}{3}+\alpha) \\ -\sin\beta & 0 & \cos\beta \end{bmatrix} \begin{bmatrix} x''_D \\ y''_D \\ z''_D \end{bmatrix}$$

For the ith centre the π component of emission is that with $\underline{E}$ parallel to the z''_i axis, and the σ component is that with $\underline{E}$ along the x''_i or y''_i axes. The spectrometer detects light polarised in the x' or y' directions depending on the analyser position. Only σ polarised emission can be detected from centre A since the dipole is aligned in the direction of propagation of fluorescence. The other three centres have a mixture of σ and π polarised emission detected for the x' and y' analyser positions. These components can be obtained directly from the transformation matrices. With the analyser in the x' direction the total component 'seen' of centres B, C and D is

$$\sigma(x') = \cos\beta\cos(\tfrac{\pi}{3}-\alpha)(x''_B) - \sin(\tfrac{\pi}{3}-\alpha)(y''_B)$$
$$- \cos\beta\cos\alpha(x''_C) - \sin\alpha(y''_C)$$
$$+ \cos\beta\cos(\tfrac{\pi}{3}+\alpha)(x''_D) + \sin(\tfrac{\pi}{3}+\alpha)(y''_D)$$

The σ component of the B, C and D centres for the y' analyser direction is:

$$\sigma(y') = \cos\beta\sin(\tfrac{\pi}{3}-\alpha)(x''_B) + \cos(\tfrac{\pi}{3}-\alpha)(y''_B)$$
$$+ \cos\beta\sin\alpha(x''_C) - \cos\alpha(y''_C)$$
$$- \cos\beta\sin(\tfrac{\pi}{3}+\alpha)(x''_D) + \cos(\tfrac{\pi}{3}+\alpha)(y''_D)$$

The π component for x' analyser direction is:

$$\pi(x') = \sin\beta\cos(\tfrac{\pi}{3}-\alpha)(z''_B) - \sin\beta\cos\alpha(z''_C)$$
$$+ \sin\beta\cos(\tfrac{\pi}{3}+\alpha)(z''_D)$$

Finally the π component for y' analyser direction is:

$$\pi(y') = \sin\beta\sin(\tfrac{\pi}{3}-\alpha)(z''_B) + \sin\beta\sin\alpha(z''_C)$$
$$- \sin\beta\sin(\tfrac{\pi}{3}+\alpha)(z''_D) .$$

For the laser polarisation z' the π and σ components are

$$\pi(z') = \cos\beta(z''_B + z''_C + z''_D)$$

$$\sigma(z') = -\sin\beta(x''_B + x''_C + x''_D)$$

The various polarisation intensities are proportional to the product of the squares of the components for absorption and emission.

Each of the polarisations possible is considered for each centre separately and then added. In the notation used henceforth, $(\sigma)_a$ is defined as σ absorption, $(\sigma)_e$ as σ emission and so on. The product label $(\sigma\pi)$ is defined as σ absorption followed by π absorption, $(\pi\sigma)$ has the reverse order while $(\sigma\sigma)$ and $(\pi\pi)$ have absorption and emission both σ or both π respectively.

Consider the specific case of x'(z'x')z' polarisation (that is, z' laser polarisation and x' analyser polarisation at the spectrometer as shown in Figure 4.2):

Centre A has $1(\pi\sigma)$ unit intensity.

Centre B has the product intensity,

$$I_B = [\sin^2\beta(\sigma)_a + \cos^2\beta(\pi)_a] \times [(\cos^2\beta \cos^2(\tfrac{\pi}{3}-\alpha) + \sin^2(\tfrac{\pi}{3}-\alpha))(\sigma)_e + (\sin^2\beta \cos^2(\tfrac{\pi}{3}-\alpha))(\pi)_e]$$

where the first term in square brackets is the absorption term and the second term is the emission term. The substitutions $\cos^2\beta = \frac{1}{9}$ and $\sin^2\beta = \frac{8}{9}$ can be made to give:

$$I_B = [\tfrac{8}{9}(\sigma)_a + \tfrac{1}{9}(\pi)_a] \times [\tfrac{1}{9}(1 + 8\sin^2(\tfrac{\pi}{3}-\alpha)(\sigma)_e + \tfrac{8}{9}\cos^2(\tfrac{\pi}{3}-\alpha)(\pi)_e]$$

and multiplication gives:

$$I_B = \frac{8}{81}\,(1 + 8\sin^2(\tfrac{\pi}{3}-\alpha))(\sigma\sigma) + \frac{64}{81}\cos^2(\tfrac{\pi}{3}-\alpha)(\sigma\pi)$$

$$+ \frac{1}{81}\,(1 + 8\sin^2(\tfrac{\pi}{3}-\alpha))(\pi\sigma) + \frac{8}{81}\cos^2(\tfrac{\pi}{3}-\alpha)(\pi\pi)$$

Similar treatment for the C and D centres gives

$$I_C = \frac{8}{81}\,(1 + 8\sin^2\alpha)(\sigma\sigma) + \frac{64}{81}\cos^2\alpha\ (\sigma\pi)$$

$$+ \frac{1}{81}\,(1 + 8\sin^2\alpha)(\pi\sigma) + \frac{8}{81}\cos^2\alpha\ (\pi\pi)$$

and $$I_D = \frac{8}{81}\,(1 + 8\sin^2(\tfrac{\pi}{3}+\alpha))(\sigma\sigma) + \frac{64}{81}\cos^2(\tfrac{\pi}{3}+\alpha)(\sigma\pi)$$

$$+ \frac{1}{81}\,(1 + 8\sin^2(\tfrac{\pi}{3}+\alpha))(\pi\sigma) + \frac{8}{81}\cos^2(\tfrac{\pi}{3}+\alpha)(\pi\pi)$$

The total intensity is therefore the sum of contributions from all four centres:

$$x'(z'x')z' = \frac{8}{81}[3 + 8\{\sin^2(\tfrac{\pi}{3}-\alpha) + \sin^2\alpha + \sin^2(\tfrac{\pi}{3}+\alpha)\}](\sigma\sigma)$$

$$+ \frac{64}{81}\,[\cos^2(\tfrac{\pi}{3}-\alpha) + \cos^2\alpha + \cos^2(\tfrac{\pi}{3}+\alpha)](\sigma\pi)$$

$$+ [1 + \frac{1}{81}[3 + 8\{\sin^2(\tfrac{\pi}{3}-\alpha) + \sin^2\alpha + \sin^2(\tfrac{\pi}{3}+\alpha)\}]](\pi\sigma)$$

$$+ \frac{8}{81}\,[\cos^2(\tfrac{\pi}{3}-\alpha) + \cos^2\alpha + \cos^2(\tfrac{\pi}{3}+\alpha)](\pi\pi)$$

But $$\sin^2(\tfrac{\pi}{3}-\alpha) = [\sin\tfrac{\pi}{3}\cos\alpha + \cos\tfrac{\pi}{3}\sin\alpha]^2$$

$$= \frac{3}{4}\cos^2\alpha + \frac{1}{4}\sin^2\alpha + \sqrt{3}\cos\alpha\sin\alpha$$

and $$\sin^2(\tfrac{\pi}{3}+\alpha) = \frac{3}{4}\cos^2 + \frac{1}{4}\sin^2\alpha - \sqrt{3}\cos\alpha\sin\alpha$$

Thus,

$$\sin^2(\tfrac{\pi}{3}-\alpha)+\sin^2\alpha+\sin^2(\tfrac{\pi}{3}+\alpha)=\tfrac{3}{2}=\cos^2(\tfrac{\pi}{3}-\alpha)+\cos^2\alpha+\cos^2(\tfrac{\pi}{3}+\alpha)$$

so that

$$x'(z'x')z' = \frac{40}{27}(\sigma\sigma) + \frac{32}{27}(\sigma\pi) + \frac{32}{27}(\pi\sigma) + \frac{4}{27}(\pi\pi)$$

The x'(y'x')z' polarisation has

$$I_A = \sigma\sigma$$

$$I_B = \frac{1}{81}[9 + 64\cos^2(\tfrac{\pi}{3}-\alpha)\sin^2(\tfrac{\pi}{3}-\alpha)](\sigma\sigma)$$
$$+ \frac{8}{81}[\cos^2(\tfrac{\pi}{3}-\alpha) + 8\cos^4(\tfrac{\pi}{3}-\alpha)](\sigma\pi)$$
$$+ \frac{8}{81}[\sin^2(\tfrac{\pi}{3}-\alpha) + 8\sin^4(\tfrac{\pi}{3}-\alpha)](\pi\sigma)$$
$$+ \frac{64}{81}[\sin^2(\tfrac{\pi}{3}-\alpha)\cos^2(\tfrac{\pi}{3}-\alpha)](\pi\pi)$$

$$I_C = \frac{1}{81}[9 + 64\cos^2\alpha\sin^2\alpha](\sigma\sigma) + \frac{8}{81}[\cos^2\alpha + 8\cos^4\alpha](\sigma\pi)$$
$$+ \frac{8}{81}[\sin^2\alpha + 8\sin^4\alpha](\pi\sigma) + \frac{64}{81}[\sin^2\alpha\cos^2\alpha](\pi\pi)$$

$$I_D = \frac{1}{81}[9 + 64\cos^2(\tfrac{\pi}{3}+\alpha)\sin^2(\tfrac{\pi}{3}+\alpha)](\sigma\sigma)$$
$$+ \frac{8}{81}[\cos^2(\tfrac{\pi}{3}+\alpha) + 8\cos^4(\tfrac{\pi}{3}+\alpha)](\sigma\pi)$$
$$+ \frac{8}{81}[\sin^2(\tfrac{\pi}{3}+\alpha) + 8\sin^4(\tfrac{\pi}{3}+\alpha)](\pi\sigma)$$
$$+ \frac{64}{81}[\sin^2(\tfrac{\pi}{3}+\alpha)\cos^2(\tfrac{\pi}{3}+\alpha)](\pi\pi)$$

When added together the dependence on α is found to cancel, giving the following:

$$x'(y'x')z' = \frac{44}{27}(\sigma\sigma) + \frac{28}{27}(\sigma\pi) + \frac{28}{27}(\pi\sigma) + \frac{8}{27}(\pi\pi)$$

The x'(z'y')z' polarisation has the same result as x'(z'x')z' and the remaining polarisation was determined by the same method outlined above, to be

$$x'(y'y')z' = \frac{20}{9}(\sigma\sigma) + \frac{20}{27}(\sigma\pi) + \frac{20}{27}(\pi\sigma) + \frac{8}{9}(\pi\pi)$$

These polarisation components are summarised in Table 4.3 and used to predict polarisation ratios of transitions.

A1.2 C_{4v} Symmetry

The C_{4v} symmetry sites have similar geometry to the C_{3v} sites but have only three symmetry axes with none aligned along the axis of the trigonal A centre. The angle between the <111> axis and the C_{4v} axes is now $\beta' = \cos^{-1}(\frac{1}{\sqrt{3}}) = \sin^{-1}(\sqrt{\frac{2}{3}})$ and the results can be obtained by suitable substitution into the expressions derived for the C_{3v} sites.

For instance, the x'(z'x')z' polarisation has

$$I_B = [\sin^2\beta'(\sigma)_a + \cos^2\beta'(\pi)_a] \times [(\cos^2\beta'\cos^2(\tfrac{\pi}{3}-\alpha) + \sin^2(\tfrac{\pi}{3}-\alpha))(\sigma)_e + (\sin^2\beta'\cos^2(\tfrac{\pi}{3}-\alpha))(\pi)_e]$$

$$= [\tfrac{2}{3}(\sigma)_a + \tfrac{1}{3}(\pi)_a][\tfrac{1}{3}(1+2\sin^2(\tfrac{\pi}{3}-\alpha))(\sigma)_e + (\tfrac{1}{3}\cos^2(\tfrac{\pi}{3}-\alpha))(\pi)_e]$$

$$= \frac{2}{9}(1 + 2\sin^2(\tfrac{\pi}{3}-\alpha))(\sigma\sigma) + \frac{2}{9}(\cos^2(\tfrac{\pi}{3}-\alpha))(\sigma\pi) + \frac{1}{9}(1 + 2\sin^2(\tfrac{\pi}{3}-\alpha))(\pi\sigma) + \frac{1}{9}(\cos^2(\tfrac{\pi}{3}-\alpha))(\pi\pi)$$

Addition of the other two centres gives:

$$x'(z'x')z' = \frac{4}{3}(\sigma\sigma) + \frac{2}{3}(\sigma\pi) + \frac{2}{3}(\pi\sigma) + \frac{1}{3}(\pi\pi)$$

The remaining polarisations were calculated in a similar manner and are summarised in Table 4.3.

APPENDIX II

PUBICATIONS CO-AUTHORED

Principal papers (included in this Appendix) :

(a) "Site Selective Spectroscopy of Hydrogenic sites in $CaF_2:Er^{3+}$ crystals".
J. Chem Phys. 86 (15 January 1987) 521-544.

(b) "Reversible Polarised Bleaching in Hydrogenated Rare-Earth-Doped Fluorites".
Optics Letters 12 (January 1987) 36-38.

Others (not included) :

(c) "Spectroscopy with Lasers". G.D. Jones, N.J. Cockroft., T.P.J. Han, R.J. Reevees, and R.W.G. Syme *Proceedings of the Second Asia-Pacific Physics Conference, Bangalore 1986.* Ed. S. Chandrasekhar (Singapore: World Scientific) 648-655.

(d) "Laser Excited Luminescence of Hydrogenated $SrF_2:Er^{3+}$ crystals". N.J.Cockroft and G.D. Jones, submitted to *J. Luminescence* for publication in the Proceedings of the International Conference on Luminescence, August 1987.

(e) "Dynamical Processes Involving Local Modes for Rare-Earth Centres in CaF". R.J. Reeves, G.D. Jones, N.J. Cockroft, T.P.J. Han, and R.W.G. Syme, submitted to *J.Luminescence* for publication in the Proceedings of the Dynamical Processes in Crystals Conference, August 1987.

Site-selective spectroscopy of hydrogenic sites in $CaF_2:Er^{3+}$ crystals[a)]

N. J. Cockroft, D. Thompson, [b)] G. D. Jones, and R. W. G. Syme
Department of Physics, University of Canterbury, Christchurch, New Zealand

(Received 4 September; accepted 10 October 1986)

Laser selective excitation and optical absorption studies of hydrogenated CaF_2:0.05% Er^{3+} crystals have revealed 16 Er^{3+} ion sites involving H^- or D^- ion charge compensation. The relative occurrence of these sites can be controlled over a wide range by varying the duration of the hydrogenation treatment. The hydrogenic nature of these sites is established by the observation of local mode absorption lines in the infrared, Er^{3+} ion electronic line isotope shifts and associated local mode vibronic lines involving the H^- and D^- ions. Local mode infrared absorption frequencies of four sites are reported for most rare-earth ions. Five new Er^{3+}–F^- sites were identified in the laser selective excitation study. For ⟨100⟩ and ⟨111⟩ oriented crystals the fluorescence spectra of several of the sites exhibit well-defined polarization which determines their Er^{3+} ion site symmetries. Symmetry confirmations are also established for the two previously reported single Er^{3+} ion sites involving fluoride ion compensation. Eleven of the hydrogenic sites reported here are classified into two families, each derived from a single Er^{3+} ion site of the parent crystal, while three others are attributed to sites of nearly cubic Er^{3+} ion symmetry. Detailed spectroscopic results for these sites are presented, together with a crystal-field analysis for the C_{4v} symmetry sites and some model assignments.

I. INTRODUCTION

The $CaF_2:Er^{3+}$ system was the first to be extensively studied by the laser selective excitation technique and was shown to have various erbium ion charge compensation sites.[1] This work formed the basis of a wide range of subsequent studies of the properties of the sites and processes occurring in the system.

Hydrogenation of CaF_2 crystals can introduce a relatively high concentration of negative hydride ions into the crystal lattice, and the crystals then show infrared absorption due to localized modes of the hydride ions.[2] Similar results are obtained with deuterium and tritium isotopes and, in general, the terms "hydrogenation", "hydrogenic", and "H^-" will be taken to cover all three isotopes, with H^-, D^-, or T^- used, where necessary, to specify ions of a particular isotopic species. In crystals containing trivalent erbium ions, the hydride ions can serve as charge compensators for the erbium ions giving rise to a variety of hydrogenic sites.[3] Such multisite systems are well suited to investigation by laser selective excitation, which can resolve transitions from different sites present and yield energy level schemes for the Er^{3+} $4f^{11}$ configuration for each site excited.

Features of the hydrogenated $CaF_2:Er^{3+}$ system, additional to those shared with the previously investigated $CaF_2:Er^{3+}$, include:

(a) Additional sites. The substitution of a hydrogenic ion for an F^- ion, either substitutionally at a fluoride ion lattice site or interstitially gives a rich distribution of lower symmetry hydrogenic sites, arising from relatively few fluoride ion compensated Er^{3+} sites (henceforth referred to as F^- sites). These new sites are of interest both as specific modifications of well-established F^- sites of known configuration and as sets of sites of similar structure.

(b) Local modes. The hydrogenic ion local modes provide, through infrared absorption, hydrogenic ion site symmetries while associated local mode vibronic lines, determined by laser selective excitation, correlate these with Er^{3+} ion sites.

(c) Electron-local mode phonon interaction effects. Er^{3+} ion electronic transitions have slightly different frequencies for equivalent H^- and D^- sites,[3] a consequence of electron-local mode phonon interaction effects where the greater amplitude of vibration of a H^- ion compared to a D^- ion gives a net shift in electronic level energies. Mixed H^-:D^- crystals can be used to distinguish single hydrogenic ion sites from multihydrogenic ion sites, with additional sets of transitions expected in the multihydrogenic ion case.

(d) Site distributions. Both H^- and D^- ions are more mobile than F^- ions.[4] As shown by the evolution of some sites with time, significant migration of H^- and D^- ions occurs in the calcium fluoride lattice even at room temperature.[5] The diffusion and migration of ions between sites can be usefully studied by monitoring the growth and decay of hydrogenic varieties of various sites.

This paper reports on the application of laser selective excitation, infrared absorption and optical absorption techniques to the study of the hydrogenated CaF_2:0.05% Er^{3+} system.

Infrared absorption measurements were used to determine and classify the hydride ion local modes into distinct groups corresponding to different hydrogenic charge compensation arrangements for most members of the rare-earth series. The number of transitions for a given arrangement gives an indication of the H^- ion site symmetry.[6] Four hydrogenic sites, additional to those already reported were found.

[a)] Work done in partial fulfillment of the requirements for the Ph.D. and M.Sc. dissertations of N. J. Cockroft and D. Thompson, respectively.

[b)] Present address: Laboratory of Atomic and Solid State Physics, Clark Hall, Cornell University, Ithaca, NY 14853.

 0021-9606/87/020521-24$02.10

The hydrogenic erbium sites, established through the optical absorption studies, were selectively excited with a cw dye laser by pumping the appropriate transition to the $(4f^{11})^4S_{3/2}$ multiplet of erbium. The resulting fluorescence yielded crystal-field levels of the $^4F_{9/2}$, $^4I_{15/2}$, and $^4I_{13/2}$ multiplets, together with local mode vibronic data.

During the course of this laser selective excitation study, crystal-field levels of five new sites attributed to fluoride ion compensation were also determined.

II. EXPERIMENTAL TECHNIQUES

For the infrared absorption measurements, calcium fluoride crystals containing 0.05% molar concentrations of rare earths were purchased either from the Hebrew University of Jerusalem, Israel or, more recently, Optovac Inc. Most of the optical absorption and laser selective excitation measurements were carried out on CaF_2:0.05% Er^{3+} crystals from Optovac Inc. or grown here.

Hydrogen, deuterium, or tritium was introduced into the crystals by the method of Hall and Schumacher[7,8] in which the crystals are heated in contact with molten aluminum in a hydrogen atmosphere at 860 °C for periods ranging from 4 to 68 h.

An alternative method was attempted to achieve a different site distribution by using calcium metal instead of aluminum in a two stage process. The first stage involved additive coloration of the crystals by heating them with calcium metal for 1 h at 870 °C in an argon atmosphere, followed by quenching in liquid nitrogen. The deeply colored crystals were then heated at 860 °C in hydrogen for 10 to 68 h. As this alternative method did not yield significantly different site distributions from the aluminum method it was only used occasionally.

The infrared absorption spectra were all recorded at 85 K using a Beckman IR12 infrared spectrophotometer equipped with a conduction type Dewar.

The optical absorption spectra were recorded photoelectrically on a Spex model 1700 0.75 m monochromator using a EMI 9558QA photomultiplier. Spectra were recorded at temperatures down to 10 K using a Cryosystem LTS22.1 closed cycle conducting type cryostat, and at 2 K with the crystals immersed in superfluid helium.

For the laser excited fluorescence spectra, all measured at 10 K, a Spectra Physics model 375 dye laser pumped by a Spectra Physics 171 argon ion laser was used for excitation, and a Spex 1403 double monochromator equipped with a RCA 31034A photomultiplier to record the fluorescence spectra under computer control. Photon counting techniques were used to give the high sensitivity needed for weak fluorescence lines. A rhodamine 590/640 mixture and coumarin 540 dyes were appropriate for laser excitation of the $^4F_{9/2}$ and $^4S_{3/2}$ multiplets of erbium, respectively. Typical laser powers of 15–40 mW were used for both multiplets. A birefringent tuning element for the dye laser gave a spectral line width of about 1 cm^{-1}.

Polarization spectra were recorded using a Spectra Physics polarization rotator to determine the laser polarization direction, and conventional polaroid sheet as an analyzer. A polarization scrambler equalized the spectrometer response for different polarizations.

For polarized bleaching studies, the laser excited fluorescence was monitored as a function of time by the Spex 1403 double monochromator with Keithley 180B electrometer output to a chart recorder. When required, simultaneous recording of the laser absorption by the crystal was obtained using a 931A photomultiplier sampling the transmitted laser beam, with its signal recorded on a second channel of the chart recorder.

All reported wave numbers are as measured in air.

III. INFRARED MEASUREMENTS

For each rare-earth dopant, infrared measurements were made on a range of crystals hydrogenated for periods from 4 to 24 h. Crystal thicknesses of 1–2 mm were appropriate for crystals containing 0.05% rare-earth ions. The time since hydrogenation varied up to 14 years, with the latest crystals being hydrogenated at 850 °C and quenched in liquid air. The older crystals comprised a variety of both rapidly quenched and slowly annealed crystals and their different thermal histories and times since hydrogenation resulted in widely varying spectra.

Hydrogenated crystals singly doped with the rare earths in their trivalent state, were examined from 800 to 1400 cm^{-1}. Typical spectra for crystals having similar hydrogenation treatment are shown in Fig. 1. Such spectra have been studied previously, but in less detail. Of the lines whose fre-

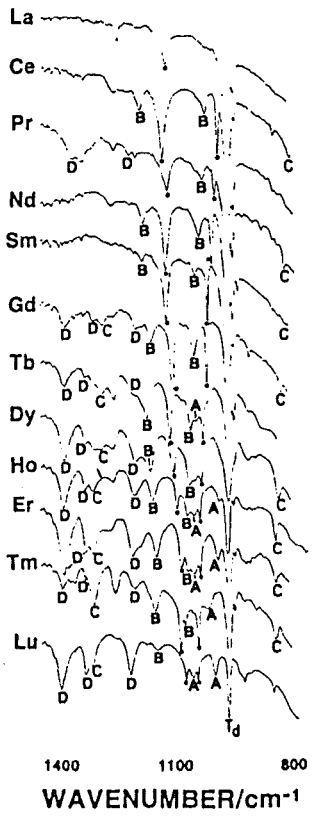

FIG. 1. Infrared absorption spectra at 85 K of hydrogenated calcium fluoride crystals containing 0.05% of trivalent rare-earth ions. A, B, C, and D identify four new H^- sites and the H^- C_{4v} site.

quencies are independent of the rare-earth ion present, the strongest is the well-established 965 cm^{-1} line also observed in hydrogenated calcium fluoride and attributed[2] to hydride ions in regular fluoride ion sites of tetrahedral (T_d) symmetry in the calcium fluoride lattice. Another line, with frequency independent of the rare-earth ion, has a frequency of 1312 cm^{-1} at 77 K and is assigned[4] to an interstitial hydride ion in an empty fluoride cell remote from the rare-earth ion.

Two strong lines having frequencies varying with the rare-earth ion present have been assigned[4] to charge compensating hydride ions occupying an interstitial site, of tetragonal (C_{4v}) symmetry, adjacent to the rare-earth ion. The lower frequency line was identified[9] as the doubly degenerate (X,Y) hydride local mode vibration and the higher frequency line as the singly degenerate (Z) hydride local mode vibration.

By studying many crystals with differing distributions of hydride local mode lines, the absorption lines of four new hydride ion sites, arbitrarily labeled A, B, C, D, were identified and their frequencies are listed in Table I. These four sites, along with the C_{4v}, cubic interstitial, and T_d sites, account for all the principal lines above 950 cm^{-1}. Additional local mode lines below 950 cm^{-1} did not show sufficient correlations to be assigned to these or other possible sites.

Attempts were made to correlate the A, B, C, and D sites with the erbium sites observed optically by comparing the intensities of the infrared local mode lines with those of electronic lines of erbium for a series of crystals. Such correlations are not straightforward because it is possible to have crystals with a rich infrared spectrum and few Er^{3+} optical lines and vice versa. The one correlation definitely established by such intensity comparisons is that between the infrared lines of the B site and the optical absorption lines[3] of the R site.

No deuterium local mode frequencies were determined in this infrared absorption study, because this would require crystal samples sufficiently thin to give transmission to below 650 cm^{-1} and such thin crystals would reveal lines of the principal sites only.[9]

A direct correlation between infrared sites and erbium optical sites can be established through matching of the infrared local mode frequencies with local mode vibronic frequency intervals, determined from the laser selective excitation spectra reported later in this paper. The frequency coincidences are not expected to be exact because the infrared local mode frequencies are recorded at 77 K, while the vibronic intervals are determined from 10 K spectra. Furthermore, when vibronic intervals are determined only for deuterated crystals the corresponding hydrogen local mode vibronic intervals have to be inferred using the reduced mass factor[2] of 1.38. Such comparisons gave good frequency agreement for the infrared B site and the optical R site.

This correlation of sites through vibronic intervals can provide assignments of some of the additional local mode lines observed in the region below 950 cm^{-1}.

The vibronic spectra of some of the optical sites show more than three local mode vibronic lines indicating these sites involve more than one hydride ion near the erbium ion with some of these local mode lines in the region below 950 cm^{-1}.

While the details regarding the vibronic spectra will be presented later the inferred infrared local mode assignments are included in the following discussion of the four sites identified by infrared absorption.

Site A. This site is present in the latter part of the rare-earth series in crystals hydrogenated 14 years ago, and it shows two infrared absorption lines (Fig. 1). Observation of the corresponding absorption lines in the early part of the series is hindered by the intense absorption centered at 965 cm^{-1} arising from the substitutional hydride ion.[2]

There are several optical sites with vibronic lines of similar local mode vibronic intervals, but none of these are close enough in frequency agreement with the A site infrared lines for any correlation to be established.

Site B. The two absorption lines of site B occur throughout the rare-earth series (Table I). They were first reported by Robson[10] who found that the alternatives of quenching the crystals at 200 °C min^{-1} or annealing them at 40 °C h^{-1} after hydrogenation produced no observable difference in the intensity of the lines of this B site, relative to those of the well-established C_{4v} site. In freshly hydrogenated crystals, the lines of the B site are very weak, but they grow with time,

TABLE I. Infrared absorption lines observed at 80 K in hydrogenated crystals of calcium fluoride containing 0.05% of rare-earth ions. The lines listed are classified as belonging to four distinct sites A, B, C, and D.

	Line positions (± 3 cm^{-1})								
Rare earth	Site A		Site B		Site C		Site D		
La			1015	1177					
Ce			1022	1190	807				
Pr			1023	1175			1215	1333	1382
Nd		1019	1031	1175	816		1218		
Sm			1043	1180	817				
Gd			1048	1161	824	1287	1198	1337	1383
Tb	983	1045	1058	1173		1290	1205	1335	1387
Dy			1058	1163	833	1291	1197	1332	1388
Ho	985	1050	1068	1158	842	1315	1207	1333	1390
Er	991	1050	1069	1149	843	1316	1208	1331	1390
Tm	1017		1075	1149	846		1203	1331	1390
Lu	998	1055		1147	848	1325	1218	1333	1395

at the expense of the C_{4v} site lines, being pronounced after a few days.

The similar variation with rare earth of these two lines with those of the C_{4v} site suggests that the B site is a modification of the C_{4v} site.

Combined infrared absorption and optical absorption studies for a series of 12 different erbium crystals give a good quantitative correlation of intensities between erbium R site optical absorption lines and B site infrared lines. The local mode vibronic data for this optical R site confirm this correlation and identify additional lines of the B site.

Site C. Only two absorption lines of this site have been observed (Table I) and it is predominant only in the latter part of the rare-earth series.

While the observation of only two lines appears to indicate a site of axial symmetry, an alternative assignment comes from the observation of the similar variation with rare earth of the C site lines and the lines of a low symmetry site found in strontium fluoride.[11] This site was postulated to have a fluoride ion in the nearest interstitial site in a ⟨111⟩ direction, together with the hydride ion substituting for one of the regular fluoride ions surrounding this interstitial fluoride ion. The C site is assigned as the calcium fluoride analog of this site and the third frequency expected to be in the 822 cm^{-1} region where several unidentified lines are present.

Site D. This site has three lines which increase in intensity along the rare-earth series (Fig. 1). The identification of the two higher energy lines, in the early part of the series, is less certain due to their low intensity and to the presence of some atmospheric water vapor lines in the spectrum. The average energy of the three lines of this site is 1310 cm^{-1} which is close to the frequency, 1312 cm^{-1}, of the isolated interstitial hydride ion.[4] This suggests that it is a rare-earth ion modification of that site and such sites are observed in the optical absorption spectrum.

IV. OPTICAL ABSORPTION SPECTRA

A. Optical spectra before hydrogenation

The lines of the optical absorption spectra of CaF_2:Er^{3+} crystals associated with F^- sites have been assigned, in several studies,[1,12–14] to the following sites:

(a) a site having cubic Er^{3+} ion symmetry,[12,13]

(b) a tetragonal (C_{4v}) symmetry site[14] (the A site) in which the charge compensating F^- ion is in the nearest-neighbor interstitial position, i.e., in a ⟨100⟩ direction from the Er^{3+} ion,

(c) a trigonal (C_{3v}) symmetry site (the B site) in which the charge compensating ion is in the next-nearest interstitial position, i.e., in a ⟨111⟩ direction from the Er^{3+} ion,

(d) two sites (C and C′) involving two Er^{3+} ions, and

(e) 15 other sites divisible into two families of 11 (D_{1a}–D_{1k}) and 4 (D_{2a}–D_{2d}) sites involving clusters of Er^{3+} ions.

CaF_2:Er^{3+} crystals fired in oxygen have different sets of absorption lines due to oxygen charge compensation sites.[15,16]

For 10 mm thicknesses of both the CaF_2:0.01% Er^{3+} and CaF_2:0.05% Er^{3+} crystals studied in this work, lines of only the A, B, and, to a lesser extent, C sites are apparent in the absorption spectra.

B. Optical absorption spectra after hydrogenation

The observed spectra vary markedly with the duration of the hydrogenation treatment. For hydrogenations of up to 16 h, several new lines appear, in addition to those of the F^- sites already present. For longer hydrogenation periods, the spectra become more complex with many new hydrogenic site lines appearing while the original F^- site lines have vanishing intensity. Details of these spectra are presented below.

The previous work[3] studied weakly hydrogentated crystals and reported the presence of two hydrogenic sites labeled C_{4v} and R. Correlations between the intensities of optical absorption lines and EPR lines established the C_{4v} site as having Er^{3+} ions in sites of tetragonal symmetry with a charge compensating H^- ion in the nearest-neighbor interstitial position. The R site was tentatively assigned to an Er^{3+} ion site having rhombic symmetry.

Sites involving D^- ions have very similar electronic transitions to those involving H^- ions. The small isotope shift has been discussed in some detail for the C_{4v} site.[3] Both the H^- and D^- sites were investigated by optical absorption. As the laser selective excitation studies were principally on the deuterated crystals, the absorption spectra shown are for such crystals with the hydrogenated crystals having closely similar spectra.

In the work here, we report a total of 16 hydrogenic sites, which can be conveniently divided into two classes: 13 sites involving nearby H^- ions and three sites of near-cubic Er^{3+} ion symmetry.

C. Hydrogenic sites involving nearby H^- ion charge compensation

Initial investigations of the crystals hydrogenated for 12 h revealed three hydrogenic sites for which three low-lying ground multiplet levels Z_1, Z_2, and Z_3 were appreciably populated at 77 K. These sites, in descending order of absorption intensity, are the previously reported C_{4v} and R sites,[3] and a new site arbitrarily labeled J.

The assignment of absorption lines to a specific site was done by comparing the spectra of many different crystals and determining which lines maintained a constant intensity relative to each other at a given crystal temperature. The energies of thermally populated crystal-field levels (Z_2 and Z_3) of the $^4I_{15/2}(Z)$ ground multiplet for a given site at temperatures between 10 and 100 K were used to identify other lines of the site since these must also occur in groups with the same Z_1, Z_2, Z_3 spacing, the lines originating from the Z_2 and Z_3 levels having vanishing intensity at the lowest temperatures.

The energy levels for the $^4I_{15/2}$, $^4F_{9/2}$, $^4S_{3/2}$, $^2H_{11/2}$, $^4F_{7/2}$, and $^4F_{5/2}$ multiplets as derived from absorption are reported for these sites in Table II. The lines of the $^4F_{3/2}$ multiplet were too broad to be assigned.

TABLE II. Energies (in cm^{-1}, ± 0.5 unless otherwise indicated) of crystal-field levels of several Er^{3+} ion multiplets for the C_{4v}, R, and J sites, as derived from the 10 K absorption spectra of weakly hydrogenated CaF_2: 0.05% Er^{3+} crystals.

	C_{4v}	R	J
$^4F_{3/2}$	22 336.9 ± 0.8	22 296.0 ± 0.8 22 258.6 ± 0.8	22 285.0 ± 1.2
$^4F_{7/2}$	20 772.6 ± 0.7 20 631.5 ± 0.7	20 760.4 ± 0.7 20 602.0 ± 0.7	
$^2H_{11/2}$	19 446.3 19 345.1 19 254.4 19 235.3 ± 0.8 19 225.7	19 339.2 ± 1.2 19 309.6 ± 1.0 19 238.8 ± 0.8 19 230.2 19 178.2	19 215.5 19 158.4 ± 0.8 19 135.6 ± 0.8
$^4S_{3/2}$	18 480.5	18 444.2	18 418.4
$^4F_{9/2}$	15 393.1 15 333.9 ± 0.8	15 379.2 15 297.5 ± 0.8	15 369.7 15 271.5 ± 0.8
$^4I_{15/2}$	25.8 ± 0.4 4.5 ± 0.3 0	35.4 ± 0.4 8.6 ± 0.3 0	44.0 11.3 ± 0.3 0

The absorption transitions to the $^4S_{3/2}$ multiplet were the simplest to analyze as only two crystal-field levels (E_1 and E_2) occur for each site present. Detailed study of the $^4I_{15/2} \rightarrow {}^4S_{3/2}$ absorption revealed lines of ten additional sites arbitrarily labeled K,M,P,L,T,N,S,V,X, and W (Fig. 2). For most of these sites, identification of lines was confirmed by observation of transitions arising from the thermally populated Z_2 level of the ground multiplet. In addition, transitions from Z_3 were identified for the K and M sites. Corresponding lines from most of these sites were also identified in the $^4I_{15/2} \rightarrow {}^4F_{9/2}$ absorption (Fig. 3). The crystal-field levels attributed to these new H^- sites are listed in Table III. The standard notation of a letter with a numerical subscript is used to label the levels of the various multiplets.

Hydrogen–deuterium isotope shifts were studied for absorption transitions to the $^4S_{3/2}$ multiplet. These shifts were determined to greater accuracy by measuring the absorption spectra of hydrogenated and deuterated crystals placed in series and are given in Table IV. The observation of such shifts confirms the hydrogenic nature of these sites and the magnitude of the shifts indicates nearby H^- charge compensation for these sites.

D. Hydrogenic sites of near cubic symmetry

In addition to the new sites classified above, one additional absorption feature appears for both the $^4S_{3/2}$ and $^4F_{9/2}$ multiplets. After a long hydrogenation treatment, the 2K $^4I_{15/2} \rightarrow {}^4S_{3/2}$ multiplet absorption spectrum has a broad line at 18 607.4 cm^{-1} with side structure at 18 611.5, 18 603.9, and 18 595.3 cm^{-1} [identified by a,b,c,d, respectively, in Fig. 2(b)]. Likewise the 2K $^4I_{15/2} \rightarrow {}^4F_{9/2}$ multiplet spectrum has three sets of lines labeled α (15 576.6, 15 534.8, and 15 485.1 cm^{-1}), β (15 572.9, 15 538.1, and 15 471.4 cm^{-1}), and γ (15 563.8 and 15 439.9 cm^{-1}) in Fig. 3(b). The principal peak in the $^4S_{3/2}$ multiplet spectrum is thought to be a hydrogenic equivalent of the line identified[12,13] as due to an Er^{3+} ion in a cubic symmetry site with remote charge compensation. Transitions for purely cubic crystals are expected to be very weak because electric dipole transitions are forbidden for sites having inversion symmetry. The observation of lines of such sites with enhanced intensity after hydrogenation is attributed to the effect of additional remote substitutional H^- (or D^-) ions. The lowering of the Er^{3+} ion site symmetry from exact cubic symmetry gives nonzero electric dipole transition intensities and, through the random distribution of these extra ions, broad lines.

The separate sites α,β,γ of Fig. 3 were distinguished through the change in their relative occurrence with duration of the hydrogenation treatment. The α lines appear first, then the β, finally the γ. Similar behavior could not be confirmed for the $^4S_{3/2}$ multiplet spectrum features because of overlap with A,B, and C F^- site lines. Further weak structure in Fig. 3(b) has not been assigned.

Since the EPR results[3] show that a significant proportion of cubic Er^{3+} sites are present in the crystal, the appear-

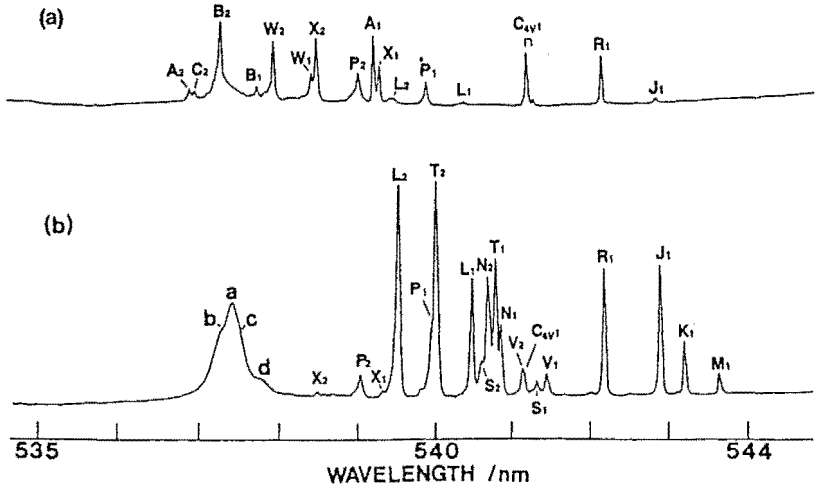

FIG. 2. $^4I_{15/2} \rightarrow {}^4S_{3/2}$ (E) absorption spectra for 10 mm thick crystals of deuterated CaF_2:0.05% Er^{3+} at 2 K: (a) 16 h deuteration, (b) 68 h deuteration. The various hydrogenic site transtions are identified by their site label and the particular upper multiplet crystal-field level involved. Structure associated with near cubic H^- sites is identified by a, b, c, and d.

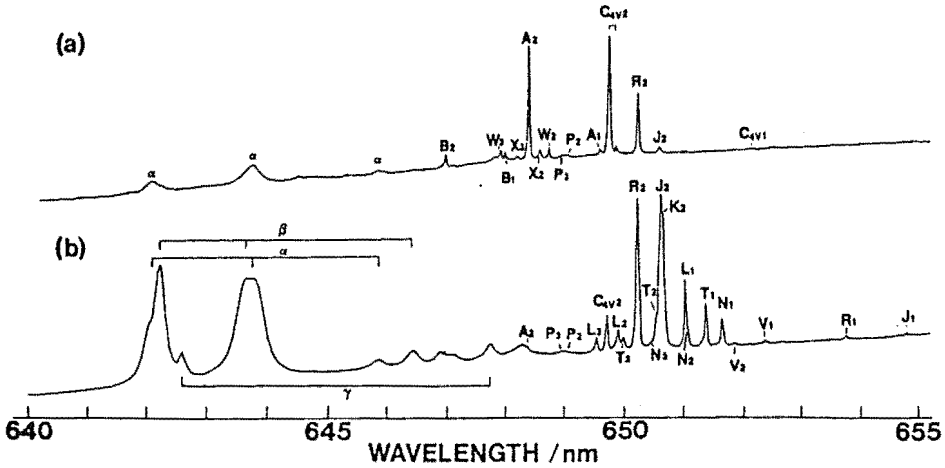

FIG. 3. $^4I_{15/2} \rightarrow {}^4F_{9/2}$ (D) absorption spectra for 10 mm thick crystals of deuterated CaF_2:0.05% Er^{3+} at 2 K: (a) 16 h deuteration, (b) 68 h deuteration. The various hydrogenic site transitions are identified by their site label and, where assigned, the particular upper multiplet crystal-field level involved.

ance of associated lines in the optical spectrum, through perturbations, is reasonable.

As the transitions observed are too broad to assign unambiguously any excited ground-state multiplet transitions in the higher temperature absorption spectra, their correspondence to the cubic site of CaF_2:Er^{3+} could not be confirmed.

E. Hydrogenic site distributions

1. Duration of hydrogenation

This plays a key role in determining site distributions and it is possible to produce almost any desired site distribution solely through control of the time the crystal is hydrogenated. New sites are observed to grow at the expense of existing ones and this feature aids in the assignment of lines to specific sites. Most of the crystals were hydrogenated for periods of 16, 36, or 68 h at a temperature of 860 °C, then quenched to room temperature. Alternative hydrogenation temperatures between 800 and 900 °C had only a slight effect on the total amount of hydrogen introduced with the site distributions essentially the same as for 860 °C. More rapid quenching of the crystal using liquid nitrogen gave very similar spectra and, as it often caused cracking of the crystal, was not adopted.

Figures 2 and 3 illustrate the differences between a 16 and a 68 h deuteration. After 16 h deuteration the spectrum reveals lines of the fluoride A and B sites, the lines of the deuteride C_{4v}, P, W, and X sites, weaker lines of the R and L sites, and very weak lines of the J site. After 68 h deuteration the spectrum shows strong lines due to the deuteride T, L, J, and R sites, less intense lines of the K, N, S, and V sites, weak lines of the deuteride P, M, and C_{4v} sites but only traces of lines of the fluoride A, B, or C sites and the deuteride X or W sites. Intermediate deuteration periods of 30 and 50 h produce intermediate site distributions. Broken 68 h deuteration treatments of three successive 20 h deuterations separated by 4 h cooling periods produce lines of both 16 and 50 h deuterations.

TABLE III. Energies (in cm^{-1}, ± 0.4 unless otherwise indicated) of three Er^{3+} ion multiplets for ten new hydrogenic sites, as derived from the 10 K absorption spectra of hydrogenated or deuterated CaF_2:0.05% Er^{3+} crystals. The D^- site energies are in parentheses.

		K	M	P	L	T	N	S	V	X	W
	E_2	...	...	18 548.8 (51.3)	18 532.0 (5.0)	18 515.0 (8.2)	18 491.0 (5.3)	18 493.5 (8.1)	18 475.2 (9.7)	18 568.5 (70.2)	18 589.5 (90.2)
$^4S_{3/2}$	E_1	18 407.2 (9.3)	18 391.2 (4.2)	18 518.4 (20.1)	18 499.1 (502.3)	18 488.9 (92.0)	18 485.8 (9.5)	18 469.6 (73.4)	18 464.0 (9.2)	18 541.1 (1.5)	18 572.9 (2.7)
	D_2	...	...	15 409.4 (10.4)	15 395.3 (6.3)	15 383.6 (5.7)	15 372.4 ± 0.8 (4.8)	...	...	15 428.3 ± 0.8 (9.7)	15 436.6 ± 0.6 (7.1)
	D_1	15 368.5 (70.0)	...	15 405.9 (7.9)	15 385.0 (7.5)	15 371.0 ± 0.8 (2.9)	15 356.6 (60.0)	15 333.9 ± 0.8 (6.5)	15 338.4 (42.5)	15 418.6 (9.7)	15 415.7 ± 0.6 (15.7)
$^4F_{9/2}$	D_1	15 260.3 ± 0.6 (1.0)	...	...	15 358.8 (60.8)	15 350.7 (3.1)	15 343.9 (6.8)	15 320.1 ± 0.8 (2.8)	15 326.5 (30.5)	(15 391)[a]	...
	Z_4	55.8 (57.0)	60.3 (60.6)	...	...	...	...	...	...	...	...
$^4I_{13/2}$	Z_3	20.0 ± 0.3 (20.9)	33.0 ± 0.3 (32.1)	21.7 ± 0.3 (20.8)	23.5 ± 0.3 (22.5)	24.5 (25.5)	27.2 ± 0.3 (26.2)	...	29.7 (30.6)	29.8 (29.3)	...
	Z_1	0	0	0	0	0	0	0	0	0	0

[a] Identified by laser selective excitation, but not seen in absorption.

TABLE IV. Electronic line isotope shifts (in cm^{-1}, ± 0.3) of D^- sites relative to H^- sites determined from the 10 K absorption spectrum of hydrogenated and deuterated CaF_2: 0.05% Er^{3+} crystals placed in series.

	P	L	T	N	S	V	W	X	C_{4v}	R	J	K	M
E_2	2.5	3.1	3.7	3.9	4.2	4.7	0.7	1.8	a	a	...	...	...
E_1	1.8	3.0	3.0	4.3	4.5	5.4	−0.2	0.5	−1.8	0	1.4	2.1	3.0

[a]Obscured by F^- site lines.

2. Time evolution of observed site distributions

It is observed that steady state site distributions were not reached until several weeks after hydrogenation. Some sites are observed to grow at the expense of others. Such effects indicate appreciable preferential migration of H^- ions between sites in the crystals even at room temperature. The most dramatic change is for the R site which doubles its intensity in the first two months, thereafter increasing only slightly. Other sites that increase with time are the P and X sites, while the W site decreases.

Storage of the crystals at elevated temperatures accelerates these site distribution changes. After a week, crystals maintained at 500 K attain site distributions typical of several month old crystals.

3. Er^{3+} ion concentration

Crystals of 0.01% Er^{3+} concentration deuterated under identical conditions to 0.05% Er^{3+} crystals have indistinguishable optical absorption.

4. Hydrogenation treatments using calcium metal

Hydrogenation treatments involving a two-step process using calcium metal instead of aluminum were found to give comparable site distributions, but the total hydrogen concentration (as determined from infrared absorption measurements of the tetrahedral site line at 965 cm^{-1}) was increased up to four times. Nevertheless, this modified treatment was not adopted since it produces very brittle crystals, with absorption by residual color centers produced in the first stage of the hydrogenation process.

5. Effect of oxygen treatment

A crystal of CaF_2:0.05% Er^{3+} was heated in oxygen in the presence of aluminum to assess the effect of possible trace oxygen entering the crystals. This crystal was found to contain principally the G1 site[16] due to oxygen charge compensation. This crystal, together with another crystal cleaved from the same boule, was then hydrogenated in the usual way for 40 h. The two crystals were found to have indistinguishable spectra, apart from the G1 site present in the previously oxygenated crystal. It is concluded that none of the reported hydrogenic sites are due to inadvertent oxygen contamination or to combined oxygen–hydrogen charge compensation sites.

F. Discussion and preliminary site classification

The presence of the 13 distinctly different hydrogenic sites (Tables II and III) contrasts with the existence of only two main F^- sites in the parent crystals. During the hydrogenation process the crystals are heated to temperatures (1133 K) known to be sufficient to dissociate almost all Er^{3+} ion cluster sites.[17,18] This, together with absence of concentration dependence of sites between the 0.01% Er^{3+} and 0.05% Er^{3+} crystals, confirms that we can discount the occurrence of cluster sites involving multiple Er^{3+} ions in these hydrogenated crystals.

The large number of observed hydrogenic sites arises through the many inequivalent positions an additional H^- ion can occupy relative to an Er^{3+}-charge compensating ion pair. The F^- A and B sites of the parent crystals are two simple Er^{3+}–F^- charge compensation arrangements and the primary effect of any hydrogenation treatment is to produce hydrogen analogs of these arrangements.

The hydrogenic analog of the F^- A site is the hydrogenic C_{4v} site.[3] The series of sites R, J, K, and M have several common features:

(a) They have absorption transitions at frequencies below those of the hydrogenic C_{4v} site and these occur in the sequence R, J, K, and M.

(b) They have similar energy level schemes. The Z_1–E_1, Z_1–Z_2, and Z_2–Z_3 energy level separations show systematic trends along the series C_{4v}, R, J, K, and M (Tables II and III).

(c) There are similar intensity patterns for corresponding absorption transitions for the different sites (Figs. 2 and 3).

It is, therefore, proposed that these sites R, J, K, and M are modifications of the hydrogenic C_{4v} site. The determination of likely configurations for each site needs consideration of both the isotope shift data, and the results of laser selective excitation studies in following sections.

The other set of sites characterized by marked resemblences are the P, L, T, N, S, and V set. The common features include:

(a) The absorption lines of the sites occur at higher frequencies than those of the C_{4v}, R, J, K, and M set (Figs. 2 and 3).

(b) The sites have similar energy level patterns (Table III), which differ significantly from those for the C_{4v}, R, J, K, and M family. The Z_3 levels for these sites are not observed because, as will be shown by laser selective excitation, they all lie at sufficiently high energies above their Z_1 levels to be depopulated even at 100 K.

(c) The sites show similar absorption line intensity patterns. Both the $Z_1 \rightarrow E_1$ and $Z_1 \rightarrow E_2$ absorption transitions are apparent with the latter more intense in contrast to the situation found for the R, J, K, M family

where the $Z_1 \rightarrow E_2$ transition is not observed (Fig. 2).

It is proposed that these sites are modifications of the hydrogenic analog of the F^-B site. The simple hydrogenic analog of the F^-B site is not yet conclusively established. On the basis of its simultaneous occurrence with the F^-A and B sites and the hydrogenic C_{4v} site in briefly hydrogenated crystal, the P site is identified as the most likely candidate for the postulated ⟨111⟩ oriented Er^{3+}–H^- ion pair. Again, consideration of both the isotope shift data and laser excitation results is needed for any postulated configurations for the L, T, N, S, and V sites.

The remaining sites X and W do not show sufficient resemblence to either of the above sets of sites for any assignment to be made.

The two families of sites exhibit similar behavior in the variation of individual site concentrations, with duration of hydrogenation treatment. For one family, the F^-A site is first replaced by the hydrogenic C_{4v} site, followed by the sequential growth of the R, J, K, and M sites. Likewise, for the other family, the P site appears first at the expense of the F^- B site, followed by successive appearance of lines of the L, T, N, S, and V sites. After 68 h hydrogenation, the dominant sites for each set are the J and T sites, respectively.

G. Isotope shifts of mixed hydrogen–deuterium crystals

Crystals that have been treated in a 1:1 mixture of hydrogen and deuterium are expected to show two sets of absorption lines: one from the H^- sites and the other from the corresponding D^- sites. This was found for the hydrogenic C_{4v} site.[3] Crystals hydrogenated in a 1:1 mixture of hydrogen and deuterium for 68 h have broader absorption lines for the L, T, N, S, V, J, and K sites indicative of the presence of mixed H^-/D^- varieties of these sites. The existence of these additional absorptions suggest that all these sites involve two hydrogenic ions in their configuration. This hypothesis is confirmed by an analysis of the vibronic spectra of these sites by laser selective excitation presented below.

V. LASER SELECTIVE EXCITATION SPECTRA

In laser selective excitation a tunable dye laser is used selectively to excite a particular absorption transition and the resulting fluorescence is monitored.[1] If the absorption line pumped is sufficiently well isolated from others, only one type of site is excited and the resulting fluorescence arises solely from this site.

There are a number of ways in which the excitation energy is dispersed. The basic fluorescence spectrum arises from radiative transitions of individual erbium ions to lower multiplets. Alternatively the decay to a lower multiplet can be a nonradiative process involving the excitation of a number of lattice phonons.

When more than one erbium ion is involved in a site then further decay mechanisms are available. One possibility is energy transfer upconversion. If the ions are crystallographically equivalent both may be excited and one ion may then transfer some of its energy to another leaving the second in a state of higher energy than can be excited directly by the laser. A second decay mechanism is pair relaxation. When the ions are inequivalent only one of them may be excited, and it can then lose energy by exciting another ion in the site while dropping to a lower multiplet. In both of these processes energy conservation may involve creation or annihilation of lattice phonons.

In the hydrogenated crystals, the hydrogenic sites have the additional possibility of decay mechanisms involving H^- and D^- local mode phonons. Transitions involving the simultaneous emission of a photon and a local mode phonon can occur, giving rise to vibronic transitions at lower energies than the zero phonon parent electronic transition.

In general the hydrogenic sites have energy levels lower than the corresponding levels of the analogous fluoride sites. Fluorescence spectra from the various hydrogenic sites were obtained by pumping appropriate $^4I_{15/2} \rightarrow {}^4S_{3/2}$ transitions, usually $Z_1 \rightarrow E_1$. Several of the sites could also be pumped cleanly using the $Z_1 \rightarrow E_2$ transition, while for others, their fluorescence was swamped by more intense fluorescence from fluoride sites having sufficient absorption at the same laser wavelength to be simultaneously excited. In such cases pumping the $Z_2 \rightarrow E_1$ transitions provided an alternative verification since the Z_2 level is partially populated at 10 K.

Although the absorption lines of the F^- sites in 68 h hydrogenated crystals have become too weak to be observed, laser selective excitation still yields F^- site emission lines at about 1% of parent crystal intensity, sufficient to cause discrimination difficulties between D^- and F^- sites having coincident energy levels at the laser pump wavelength. Laser excitation studies pumping transitions to the $^4F_{9/2}$ multiplet were hampered by such underlying excitation of F^- sites present. The $Z_1 \rightarrow D_1$ transitions for the hydrogenic sites have energies below the range of the red dye used, while interfering F^- sites precluded clean pumping of $Z_1 \rightarrow D_2$ transitions. The emission from this multiplet was, therefore, also obtained by pumping the $^4S_{3/2}$ multiplet.

As a consequence of nonradiative processes involving hydrogenic ions, both the H^- and D^- sites have weaker fluorescence than the F^- sites by factors of typically 10^4 and 10^3, respectively. The weakness of H^- relative to D^- site fluorescence is a result of higher local mode phonon frequencies for the H^- sites giving nonradiative decay channels involving fewer phonons than for D^- sites. This situation also gives rise to shorter fluorescence lifetimes.[19] Because of this strong influence of local mode phonon decay channels on the fluorescence intensities of hydrogenic sites the deuterated crystals were preferentially studied. For some of the sites the H^- site emission was undetectable, while the corresponding D^- site emission was readily observed.

A. Polarized fluorescence spectra

For particular high symmetry sites, if polarized laser light is incident along a crystal symmetry direction, some orientations of these rare-earth ion sites are preferentially excited giving rise to a polarized fluorescence spectrum. As such polarization effects can be of assistance in identification of site symmetry and crystal-field energy levels, the polarization intensity ratios expected for both tetragonal (C_{4v}) and trigonal (C_{3v}) symmetry are now derived.

With plane-polarized laser light incident along one of

the ⟨100⟩ directions of the calcium fluoride host crystal the fluorescence observed in another ⟨100⟩ direction is found in general to be partially polarized for C_{4v} sites (Fig. 4). Here the polarization geometry is specified by $x(ab)z$, where x is the direction of the incident laser beam, z the direction of propagation of the fluorescence, $a(=y$ or $z)$ the plane of polarization (E vector) of the laser light and $b(=x$ or $y)$ the polarization of the fluorescence. The selection rules for electric dipole transitions for Er^{3+} ions in a C_{4v} symmetry are given by

C_{4v}	γ_6	γ_7
γ_6	$\pi\sigma$	σ
γ_7	σ	$\pi\sigma$

Here π or σ polarization correspond to the E vector of the light parallel or perpendicular, respectively, to the z axis of the C_{4v} group.

The fourfold (z) axis of the C_{4v} site (as determined by the orientation of the charge compensating ion) can be aligned along the [100], [010], or [001] crystal axes. Inspection of the above selection rules shows that for transitions between γ_6 and γ_7 electronic levels two of the three sets of C_{4v} site orientations contribute to the diagonal $x(yy)z$ polarization fluorescence, whereas only one set of C_{4v} sites contributes in each of the other three polarization geometries. Thus for pump transitions from the $Z_2(\gamma_6)$ first excited level to γ_7 levels and subsequent fluorescent decay to γ_6 levels, a 2:1 intensity ratio is predicted for $x(yy)z$:$x(yx)z$ polarization, assuming equal population of the three C_{4v} site orientations. Where either of the two transitions (absorption or emission) is γ_6 to γ_6 or γ_7 to γ_7, any observed polarization is a consequence of the absorption and emission probabilities of specific transitions involved for the different polarization geometries. Thus any departure from 2:1 intensity ratio between $x(yy)z$ and $x(yx)z$ polarization would confirm the involvement of a γ_6 to γ_6 or γ_7 to γ_7 transition, whereas the observation of a 2:1 intensity ratio would be consistent with γ_6 to γ_7 transitions.

For Er^{3+} ions in a C_{3v} symmetry the electric dipole selection rules are given by

C_{3v}	γ_4	$\gamma_{5,6}$
γ_4	$\pi\sigma$	σ
$\gamma_{5,6}$	σ	π

where π and σ polarizations are now defined with respect to the threefold (z') axis of the C_{3v} group. The four possible orientations for the trigonal z' axis are equally inclined to each ⟨100⟩ direction of the host crystal and the fluorescence intensities for trigonal sites should be independent of polarization in the ⟨100⟩ experimental geometry used to study the C_{4v} sites. However, by using a crystal cut and oriented so that the fluorescence is observed in a ⟨111⟩ direction, it is possible to confirm the identification of the trigonal site symmetry from polarization results.

The analysis is more complicated than for C_{4v} sites in the ⟨100⟩ geometry as the four possible z' axis orientations are not orthogonal and σ, π polarizations are not clearly separated for all trigonal sites simultaneously. The expected polarization intensity ratios $x'(y'y')z'$:$x'(y'x')z'$ and $x'(y'x')z'$:$x'(z'x')z'$ for a ⟨111⟩-oriented crystal, assuming equal population of the four trigonal site orientations, are listed in Table V. These results are independent of the direction (x') of the laser beam within the selected ⟨111⟩ plane and the results for $x'(z'y')z'$ polarization are the same as for $x'(z'x')z'$. Where the polarization ratios are listed as arbitrary, or a range of possible values is indicated, the actual

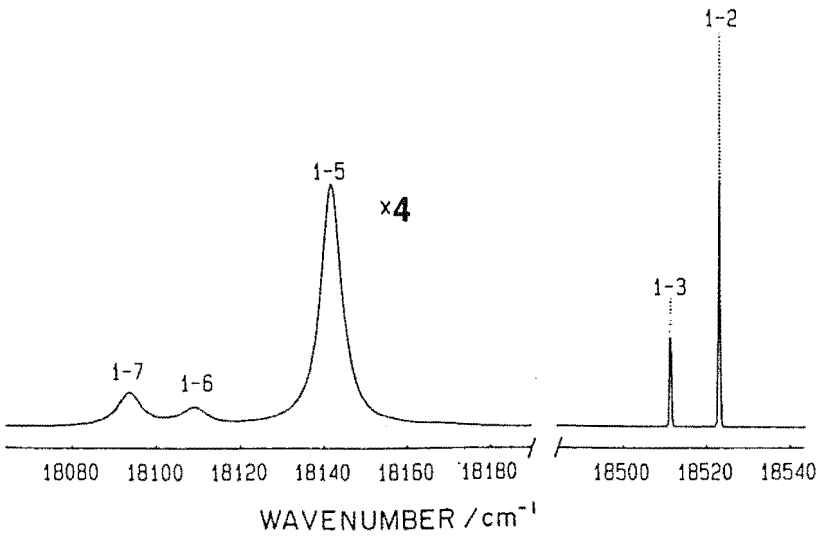

FIG. 4. 10 K polarized $(x(yx)z$—$,x(yy)z\cdots)^4S_{3/2}\rightarrow{}^4I_{15/2}$ fluorescence for laser excitation of the $Z_1\rightarrow E_1$ transition of the F^- C_{4v} site. Transitions are identified by the numerical subscripts for the upper and lower energy level labels.

TABLE V. Predicted polarization intensity ratios for trigonal (C_{3v}) and tetragonal (C_{4v}) sites in a ⟨111⟩-oriented crystal.

Pump transition	Decay transition	Polarization ratios $\frac{x'(y'y')z'}{x'(y'x')z'}$	Polarization ratios $\frac{x'(y'x')z'}{x'(z'x')z'}$
C_{3v} sites			
$\gamma_4 \rightarrow \gamma_4$	$\gamma_4 \rightarrow \gamma_4$	Arbitrary	Arbitrary
	$\gamma_4 \leftrightarrow \gamma_{5,6}$	$\frac{1}{4} \rightarrow \frac{4}{11}$	$\frac{1}{4} \rightarrow \frac{4}{11}$
	$\gamma_{5,6} \rightarrow \gamma_{5,6}$	$\frac{1}{4} \rightarrow 3$	$\frac{1}{4} \rightarrow 2$
$\gamma_4 \leftrightarrow \gamma_{5,6}$	$\gamma_4 \rightarrow \gamma_4$	$\frac{1}{4} \rightarrow \frac{4}{11}$	$\frac{1}{4} \rightarrow \frac{4}{11}$
	$\gamma_4 \leftrightarrow \gamma_{5,6}$	$\frac{4}{11}$	$\frac{4}{11}$
	$\gamma_{5,6} \rightarrow \gamma_{5,6}$	$\frac{1}{4}$	$\frac{1}{4}$
$\gamma_{5,6} \rightarrow \gamma_{5,6}$	$\gamma_4 \rightarrow \gamma_4$	$\frac{1}{4} \rightarrow 3$	$\frac{1}{4} \rightarrow 2$
	$\gamma_4 \leftrightarrow \gamma_{5,6}$	$\frac{1}{4}$	$\frac{1}{4}$
	$\gamma_{5,6} \rightarrow \gamma_{5,6}$	3	2
C_{4v} sites			
$\gamma_6 \rightarrow \gamma_6$, $\gamma_7 \rightarrow \gamma_7$	$\gamma_6 \rightarrow \gamma_6$, $\gamma_7 \rightarrow \gamma_7$	Arbitrary	Arbitrary
	$\gamma_6 \leftrightarrow \gamma_7$	$\frac{1}{3} \rightarrow \frac{3}{1}$	$\frac{1}{3} \rightarrow \frac{3}{1}$
$\gamma_6 \leftrightarrow \gamma_7$	$\gamma_6 \rightarrow \gamma_6$, $\gamma_7 \rightarrow \gamma_7$	$\frac{3}{1}$	$\frac{3}{1}$
	$\gamma_6 \leftrightarrow \gamma_7$	$\frac{1}{3} \rightarrow \frac{3}{1}$	$\frac{1}{3} \rightarrow \frac{3}{1}$

observed ratios will be determined by absorption and emission probabilities rather than the experimental geometry. An additional complication with the ⟨111⟩-orientation geometry is that the tetragonal (C_{4v}) sites will, in general, also show some polarization. Although the three possible tetragonal axis orientations are equally inclined to a ⟨111⟩ direction, they will not be equally inclined to the laser beam. The expected polarization intensity ratios for C_{4v} sites in this orientation are also listed in Table V.

Comparison of polarization behavior for the two different crystal orientations (⟨100⟩ or ⟨111⟩) has enabled firm identification of any trigonal or tetragonal character for the various sites studied.

B. Description of the laser selective excitation spectra of hydrogenic sites

Table VI gives the energy levels determined for eight D^- sites while Table VII gives energy levels for five new F^- sites discovered during the course of this work. The results for each set of sites will now be discussed in turn.

1. The C_{4v} site

The H^- C_{4v} site shows fluorescence at 15 K, while the D^- and T^- C_{4v} sites also give fluorescence at 85 K. The H^- and D^- C_{4v} site fluorescence lines are factors of 8000 and 2000 weaker than their F^- C_{4v} counterparts at 10 K.

Fluorescence was recorded for the $^4S_{3/2}$ to $^4I_{15/2}$, $^4F_{9/2}$ to $^4I_{15/2}$, and $^4S_{3/2}$ to $^4I_{13/2}$ transitions. Figure 5 shows typical spectra for the D^- C_{4v} site. From the spectra, eight levels of the $^4I_{15/2}$ multiplet are identified. For $Z_1 \rightarrow E_1$ excitation, fluorescence transitions are observed from the E_1 level to the Z_2, Z_3, Z_5, Z_7 levels. With careful examination an additional very weak transition was observed to the Z_8 level. For the same excitation, the dominant $^4F_{9/2}$ to $^4I_{15/2}$ transitions are $D_1 \rightarrow Z_4$ and $D_1 \rightarrow Z_6$ in close analogy to the situation for the F^- C_{4v} site[20] and these transitions determine the energies of the Z_4 and Z_6 levels. These results also show that the strongest $Z \rightarrow D$ transition observed in the absorption spectrum [Fig. 3(a)] is to the D_2 level and there is a D_1 level at lower energy. Again this is a close correspondence with the F^- C_{4v} site.[20] All seven levels of the $^4I_{13/2}$ multiplet were also identified by transitions from the E_1 level. The E_2 level of the D^- C_{4v} site was located coincident with the E_2 level of the F^- B

TABLE VI. Energy levels (in cm^{-1}) of eight D^- sites derived from the 10 K fluorescence spectra of deuterated CaF_2: 0.05% Er^{3+} crystals.

	C_{4v}	R	J	K	L	T	N	V
E_2	18 613.6 ± 0.8	18 590.9 ± 1.0	···	···	18 535.0 ± 0.4	18 518.2 ± 0.4	18 495.3 ± 0.4	18 479.7 ± 0.8
E_1	18 478.7 ± 0.4	18 444.2 ± 0.4	18 419.8 ± 0.4	18 409.3 ± 0.4	18 502.3 ± 0.4	18 492.0 ± 0.4	18 489.5 ± 0.4	18 469.2 ± 0.8
D_3	···	···	···	···	15 396.3 ± 0.4	15 385.7 ± 0.4	15 374.8 ± 0.4	15 362.0 ± 0.4
D_2	15 392.4 ± 0.4	15 380.0 ± 0.4	15 370.7 ± 0.4	15 370.0 ± 0.8	15 387.5 ± 0.4	15 372.9 ± 0.4	15 360.0 ± 0.4	15 342.5 ± 0.4
D_1	15 331.8 ± 0.4	15 297.5 ± 0.4	15 272.0 ± 0.4	15 261.0 ± 1.0	15 360.8 ± 0.4	15 353.1 ± 0.4	15 346.8 ± 0.4	15 330.5 ± 0.4
Y_7	6 894.8 ± 1.2	6 935.3 ± 1.2	6 965.3 ± 1.2	···	6 837.5 ± 1.2	6 851.1 ± 1.2	6 850.5 ± 1.2	6 844.5 ± 1.2
Y_6	6 824.0 ± 1.0	6 849.0 ± 1.2	6 861.8 ± 1.2	···	6 817.1 ± 1.2	6 818.1 ± 1.2	6 817.0 ± 1.2	6 813.5 ± 1.2
Y_5	6 800.6 ± 1.2	6 806.7 ± 1.0	6 826.3 ± 1.0	···	6 797.8 ± 1.0	6 802.6 ± 1.0	6 810.8 ± 1.0	6 807.5 ± 1.0
Y_4	6 795.8 ± 1.0	6 795.9 ± 1.0	6 798.3 ± 1.0	···	6 794.3 ± 0.8	6 792.1 ± 0.8	6 788.3 ± 0.8	6 776.5 ± 0.8
Y_3	6 709.4 ± 0.8	6 723.3 ± 0.8	6 731.3 ± 0.8	···	6 727.0 ± 1.2	6 730.6 ± 1.2	6 733.7 ± 1.2	6 730.5 ± 1.2
Y_2	6 596.6 ± 0.8	6 605.1 ± 0.8	6 611.8 ± 0.8	···	6 701.5 ± 0.8	6 709.6 ± 0.8	6 708.9 ± 0.8	6 701.5 ± 0.8
Y_1	6 561.2 ± 0.8	6 563.4 ± 0.8	6 566.3 ± 0.8	···	6 634.3 ± 0.8	6 635.1 ± 0.8	6 635.8 ± 0.8	6 633.5 ± 0.8
Z_8	583.5 ± 2.0	642.0 ± 2.0	678.0 ± 2.0	···	516.2 ± 1.5	510.5 ± 1.5	509.3 ± 1.5	503.0 ± 1.5
Z_7	424.1 ± 0.7	454.9 ± 0.8	466.0 ± 1.2	471.0 ± 1.2	467.3 ± 1.0	464.5 ± 1.0	462.5 ± 1.0	469.0 ± 1.0
Z_6	422.0 ± 1.0	426.3 ± 0.8	449.5 ± 0.8	461.5 ± 0.8	437.2 ± 0.8	436.4 ± 0.8	439.4 ± 0.8	434.0 ± 0.8
Z_5	374.4 ± 0.7	373.4 ± 0.8	377.5 ± 0.8	401.0 ± 0.8	305.1 ± 0.8	306.0 ± 0.8	301.7 ± 0.8	307.5 ± 0.8
Z_4	281.4 ± 1.0	308.8 ± 0.8	326.0 ± 0.8	342.0 ± 1.0	290.1 ± 0.8	298.0 ± 0.8	289.6 ± 0.8	289.0 ± 0.8
Z_3	25.0 ± 0.3	35.7 ± 0.4	44.9 ± 0.4	57.0 ± 0.5	283.8 ± 0.5	278.6 ± 0.5	272.7 ± 0.5	258.0 ± 0.5
Z_2	2.9 ± 0.3	9.1 ± 0.3	12.1 ± 0.3	20.9 ± 0.3	22.5 ± 0.3	25.5 ± 0.4	26.2 ± 0.3	30.6 ± 0.3
Z_1	0	0	0	0	0	0	0	0

TABLE VII. Energy levels (in cm^{-1}) of the F1 to F5 sites as derived from the 10 K fluorescence spectra of CaF_2: 0.05% Er^{3+} crystals.

	F1	F2	F3	F4	F5
E_2	18 604.0 ± 0.5	18 605.5 ± 0.5	18 537.6 ± 0.5	18 528.9 ± 0.5	18 503.3 ± 0.5
E_1	18 585.1 ± 0.5	18 579.5 ± 0.5	18 484.2 ± 0.5	18 487.5 ± 0.5	18 469.8 ± 0.5
D_3	15 455.0 ± 0.5	...	...	...	...
D_2	15 441.0 ± 0.5	15 463.5 ± 0.5	15 397.2 ± 0.5	15 389.5 ± 0.5	...
D_1	15 431.4 ± 0.5	15 432.0 ± 0.5	15 373.2 ± 0.5	15 362.5 ± 0.5	15 334.5 ± 0.5
Y_7	6 840.0 ± 1.5	...	6 920.5 ± 1.5	6 891.9 ± 1.5	6 842.0 ± 1.5
Y_6	6 806.0 ± 1.5	6 891.0 ± 1.5	6 870.5 ± 1.5	6 874.7 ± 1.5	6 821.0 ± 1.5
Y_5	6 777.0 ± 1.0	6 880.0 ± 1.0	6 861.0 ± 1.0	6 833.2 ± 1.0	6 804.0 ± 1.2
Y_4	6 734.5 ± 1.0	6 867.0 ± 1.0	6 849.0 ± 1.0	6 820.9 ± 1.0	6 784.5 ± 1.0
Y_3	6 695.5 ± 1.0	6 674.5 ± 1.0	6 627.5 ± 1.0	6 631.7 ± 1.0	6 629.5 ± 1.0
Y_2	6 677.5 ± 1.0	6 626.0 ± 1.0	6 614.2 ± 1.0	6 608.8 ± 1.0	6 600.0 ± 1.0
Y_1	6 624.0 ± 1.0	6 621.5 ± 1.0	6 612.0 ± 1.0	6 596.8 ± 1.0	6 582.5 ± 1.0
Z_8	438.5 ± 1.0	618.0 ± 1.0	617.2 ± 1.0	554.5 ± 1.0	492.0 ± 1.0
Z_7	409.0 ± 1.0	560.0 ± 1.0	530.0 ± 1.0	524.7 ± 1.0	452.5 ± 1.0
Z_6	379.0 ± 1.0	521.2 ± 1.0	501.2 ± 1.0	476.0 ± 1.0	432.0 ± 1.0
Z_5	258.5 ± 1.0	499.5 ± 1.0	489.0 ± 1.0	453.3 ± 1.0	405.0 ± 1.0
Z_4	243.0 ± 1.0	115.5 ± 1.0	111.0 ± 1.0	116.7 ± 1.0	122.5 ± 1.0
Z_3	201.5 ± 1.0	92.0 ± 0.8	81.2 ± 0.8	82.1 ± 0.8	94.0 ± 0.8
Z_2	38.0 ± 0.4	69.2 ± 0.4	69.5 ± 0.4	59.0 ± 0.4	45.5 ± 0.5
Z_1	0	0	0	0	0

site and amends the previous assignment[3] based on optical absorption.

Polarization of the C_{4v} site fluorescence (Fig. 4) including observation of the predicted 2:1 intensity ratio for appropriate transitions, is consistent with the site symmetry and confirms the identification of several of the crystal-field energy levels. The observed intensity patterns for the H^- and D^- C_{4v} sites follow that of the corresponding F^- C_{4v} site which is given here for comparison since previous studies[1,20] do not report any polarization results. The polarization data for all observed transitions which are included in Table VIII would provide a basis for Judd–Ofelt[21,22] intensity calculations as done for the unpolarized C_{4v} site results.[23]

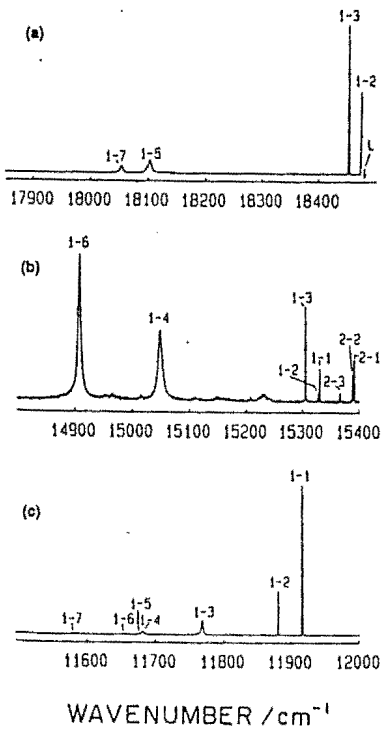

FIG. 5. 10 K fluorescence for laser excitation of the $Z_1 \rightarrow E_1$ transition of the D^- C_{4v} site: (a) ${}^4S_{3/2} \rightarrow {}^4I_{15/2}$, (b) ${}^4F_{9/2} \rightarrow {}^4I_{15/2}$, and (c) ${}^4S_{3/2} \rightarrow {}^4I_{13/2}$. Transitions are identified by the numerical subscripts for the upper and lower energy level labels. L identifies the laser excitation position.

Hydrogen and deuterium local mode vibronics were also observed in the selectively excited fluorescence spectra (Fig. 6). In the H^- spectra, there are two vibronic lines associated with each electronic line, having energy separations from their parent electronic transitions closely matching the two local mode energies[3] observed in the infrared. The spectra show analogous D^- vibronic lines whose energy separations from their parent electronic transition are a factor of 1.380 ± 0.007 less than those of H^-, consistent with the reduced mass ratio.[2]

All the observed vibronic lines are identified in Fig. 6 by both the terminating electronic level and by the (X,Y) or Z local mode phonon involved in the transition from the upper electronic level. The complete vibronic data, including polarization, are presented in Table IX together with the intensities of the observed vibronic lines relative to their corresponding electronic parent lines. The $E_1 \rightarrow Z_4(X,Y)$ vibronic is noteworthy in being clearly present, whereas the $E_1 \rightarrow Z_4(Z)$ vibronic is absent, consistent with the absence of the parent $E_1 \rightarrow Z_4$ electronic transition from the $E \rightarrow Z$ fluorescence spectrum of Fig. 5(a). The appearance of the $E_1 \rightarrow Z_4(X,Y)$ vibronic gives an additional determination of the Z_4 electronic level, confirms the identification of the Z_4 level from the $D_1 \rightarrow Z_4$ spectrum and is in agreement with the (X,Y) and Z assignment of the two local modes.

The crystal-field levels of the ${}^4I_{15/2}$ and ${}^4I_{13/2}$ multiplets were analyzed using the same C_{4v} crystal-field Hamiltonian

TABLE VIII. Wave numbers, linewidths, and relative intensities within each multiplet (± 10% between the two polarizations for a given transition) of 10 K fluorescence transitions of the F^-, H^-, and D^- C_{4v} sites measured in CaF_2: 0.05% Er^{3+} crystals.

Excitation	Transition	Wave number (cm^{-1})	Linewidth (cm^{-1}) (± 10%)	Relative intensity (± 15%) $x(yx)z$	$x(yy)z$
Laser tuned to F^-	$E_1 \rightarrow Z_2\gamma_6$	18 523.3 ± 0.4	1.0	0.40	0.65
C_{4v} site	$\rightarrow Z_3\gamma_7$	18 511.6 ± 0.4	1.0	0.15	0.23
$Z_1\gamma_7 \rightarrow E_1\gamma_7$ at	$\rightarrow Z_4\gamma_6$	...			
18 544.3 cm^{-1}	$\rightarrow Z_5\gamma_7$	18 140.5 ± 0.7	6.0	1.00	0.16
	$\rightarrow Z_6\gamma_6$	18 107.8 ± 0.7	7.0	0.090	0.14
	$\rightarrow Z_7\gamma_7$	18 092.5 ± 0.7	6.5	0.14	0.19
	$\rightarrow Z_8\gamma_6$	...			
	$D_2\gamma_7 \rightarrow Z_1$	15 424.5 ± 0.4	0.8	0.0006	0.000 5
	$\rightarrow Z_2$	15 403.5 ± 0.4	0.8	0.0012	0.002 1
	$\rightarrow Z_3$	15 391.3 ± 0.4	0.6	0.0004	0.000 6
	$D_1\gamma_6 \rightarrow Z_1$	15 396.0 ± 0.4	0.8	0.0039	0.006 3
	$\rightarrow Z_2$	15 375.0 ± 0.4	0.6	0.025	0.007 3
	$\rightarrow Z_3$	15 363.5 ± 0.4	0.6	0.017	0.029
	$\rightarrow Z_4$	15 165.0 ± 0.8	10.0	0.12	0.19
	$\rightarrow Z_5$	14 991.0 ± 0.8	obscured	...	...
	$\rightarrow Z_6$	14 959.5 ± 1.0	8.0	1.00	0.18
	$\rightarrow Z_7$	...			
	$\rightarrow Z_8$	...			
	$E_1 \rightarrow Y_1\gamma_6$	11 970.6 ± 0.6	0.4	0.61	1.00
	$\rightarrow Y_2\gamma_7$	11 940.8 ± 0.6	0.4	0.23	0.18
	$\rightarrow Y_3\gamma_7$	11 845.5 ± 0.6	1.7	0.23	0.28
	$\rightarrow Y_4\gamma_7$ / $\rightarrow Y_5\gamma_6$	11 727.8 ± 0.7	5.4	0.80	0.22
	$\rightarrow Y_6\gamma_6$	11 701.3 ± 0.8	8.5	0.085	0.064
	$\rightarrow Y_7\gamma_7$	11 665.6 ± 0.8	7.0	0.18	0.14
Laser tuned to F^-	$D_2 \rightarrow Z_2$	15 403.5 ± 0.4	0.8	0.0046	0.003 2
C_{4v} site $Z_1 \rightarrow D_2$ at	$\rightarrow Z_3$	15 391.3 ± 0.4	0.6	0.0012	0.000 83
15 424.5 cm^{-1}	$D_1 \rightarrow Z_1$	15 396.0 ± 0.4	0.8	0.0077	0.005 4
	$\rightarrow Z_2$	15 375.0 ± 0.4	0.6	0.022	0.033
	$\rightarrow Z_3$	15 363.5 ± 0.4	0.6	0.028	0.019
	$\rightarrow Z_4$	15 165.0 ± 0.8	10.0	0.18	0.13
	$\rightarrow Z_5$	14 991.0 ± 0.8	obscured	...	...
	$\rightarrow Z_6$	14 959.5 ± 1.0	8.0	0.55	1.00
	$\rightarrow Z_7$	...			
	$\rightarrow Z_8$	...			
	$E_1 \rightarrow Z_1$	18 544.3 ± 0.4	0.8	0.59	0.47
	$\rightarrow Z_2$	18 523.3 ± 0.4	1.0	1.00	0.79
	$\rightarrow Z_3$	18 511.6 ± 0.4	1.0	0.40	0.33
	$\rightarrow Z_4$	...			
	$\rightarrow Z_5$	18 140.5 ± 0.7	6.0	0.27	0.45
	$\rightarrow Z_6$	18 107.8 ± 0.7	7.0	0.047	0.039
	$\rightarrow Z_7$	18 092.5 ± 0.7	6.5	0.076	0.07
	$\rightarrow Z_8$	...			
Laser tuned to F^-	$E_1 \rightarrow Z_1$	18 544.3 ± 0.4	1.0	0.17	0.26
C_{4v} site $Z_1 \rightarrow E_2\gamma_6$	$\rightarrow Z_2$	18 523.3 ± 0.4	1.0	0.32	0.59
at 18 628.9 cm^{-1}	$\rightarrow Z_3$	18 511.6 ± 0.4	1.0	0.13	0.22
	$\rightarrow Z_4$	...			
	$\rightarrow Z_5$	18 140.5 ± 0.7	6.0	1.00	0.11
	$\rightarrow Z_6$	18 107.8 ± 0.7	7.0	0.091	0.15
	$\rightarrow Z_7$	18 092.5 ± 0.7	6.5	0.14	0.20
	$\rightarrow Z_8$	...			
Laser tuned to	$E_1 \rightarrow Z_2\gamma_6$	18 476.0 ± 0.4	0.8	0.38	0.55
H^- C_{4v} site	$\rightarrow Z_3\gamma_7$	18 454.7 ± 0.4	0.8	0.90	0.63
$Z_1\gamma_7 \rightarrow E_1\gamma_7$ at	$\rightarrow Z_4\gamma_6$	...			
18 480.2 cm^{-1}	$\rightarrow Z_5\gamma_7$	18 104.0 ± 0.7	7.5 ± 1.0	1.00	0.45
	$\rightarrow Z_6\gamma_6$	...			
	$\rightarrow Z_7\gamma_7$	18 054.5 ± 0.7	7.0	0.30	0.40
	$\rightarrow Z_8\gamma_6$	...			

TABLE VIII (*continued*).

Excitation	Transition	Wave number (cm^{-1})	Linewidth (cm^{-1}) (±10%)	Relative intensity (±15%) $x(yx)z$	Relative intensity (±15%) $x(yy)z$
Laser tuned to D^- C_{4v} site $Z_1 \rightarrow E_1$ at 18 478.7 cm^{-1}	$E_1 \rightarrow Z_2$	18 475.8 ± 0.4	1.2	0.39	0.53
	$\rightarrow Z_3$	18 453.7 ± 0.4	1.2	1.00	0.60
	$\rightarrow Z_4$	...			
	$\rightarrow Z_5$	18 104.3 ± 0.7	7.5 ± 1.0	0.64	0.34
	$\rightarrow Z_6$	...			
	$\rightarrow Z_7$	18 054.6 ± 0.7	6.0	0.18	0.27
	$\rightarrow Z_8$	17 895.7 ± 1.0	10.0 ± 2.0	very weak	
	$D_3\gamma_7 \rightarrow Z_1$	15 392.4 ± 0.4	2.4	0.053	0.033
	$\rightarrow Z_2$	15 389.3 ± 0.4	1.8	0.017	0.024
	$\rightarrow Z_3$	15 367.4 ± 0.4	1.2	0.0075	0.007 2
	$D_1\gamma_6 \rightarrow Z_1$	15 331.8 ± 0.4	1.8	0.023	0.028
	$\rightarrow Z_2$	15 329.0 ± 0.4	1.8	0.011	0.011
	$\rightarrow Z_3$	15 306.7 ± 0.4	2.9	0.11	0.14
	$\rightarrow Z_4$	15 050.4 ± 0.8	9.4	0.43	0.57
	$\rightarrow Z_5$	...			
	$\rightarrow Z_6$	14 909.8 ± 0.8	6.5	1.00	0.45
	$\rightarrow Z_7$	...			
	$\rightarrow Z_8$	...			
	$E_1 \rightarrow Y_1\gamma_6$	11 917.5 ± 0.6	0.8	0.74	1.00
	$\rightarrow Y_2\gamma_7$	11 882.1 ± 0.6	1.2	0.51	0.31
	$\rightarrow Y_3\gamma_7$	11 769.3 ± 0.6	2.0	0.22	0.24
	$\rightarrow Y_4\gamma_7$	11 682.9 ± 0.8	2.8	0.14	0.078
	$\rightarrow Y_5\gamma_6$	11 678.1 ± 1.0	2.0	very weak	
	$\rightarrow Y_6\gamma_6$	11 654.7 ± 1.0	2.0	0.01	0.01
	$\rightarrow Y_7\gamma_7$	11 583.9 ± 1.0	6.0	0.045	0.045
Laser tuned to D^- C_{4v} site $Z_2 \rightarrow E_1$ at 18 475.8 cm^{-1}	$E_1 \rightarrow Z_1$	18 478.7 ± 0.4	1.0	0.37	0.51
	$\rightarrow Z_2$	laser			
	$\rightarrow Z_3$	18 453.7 ± 0.4	1.0	1.00	0.35
	$\rightarrow Z_4$	...			
	$\rightarrow Z_5$	18 104.3 ± 0.7	7.0	0.66	0.042
	$\rightarrow Z_6$	...			
	$\rightarrow Z_7$	18 054.6 ± 0.7	6.0	0.14	0.23
	$\rightarrow Z_8$	...			
	$E_1 \rightarrow Y_1$	11 917.5 ± 0.6	0.8	0.59	1.00
	$\rightarrow Y_2$	11 882.1 ± 0.6	1.2	0.51	0.15
	$\rightarrow Y_3$	11 769.3 ± 0.6	2.2	0.15	0.26
	$\rightarrow Y_4$	11 682.9 ± 0.8	3.0	0.12	0.022
	$\rightarrow Y_5$	11 678.1 ± 1.0	2.2	very weak	
	$\rightarrow Y_6$	11 654.7 ± 1.0	2.2	0.011	0.008 3
	$\rightarrow Y_7$	11 583.9 ± 1.0	6.0	0.060	0.045

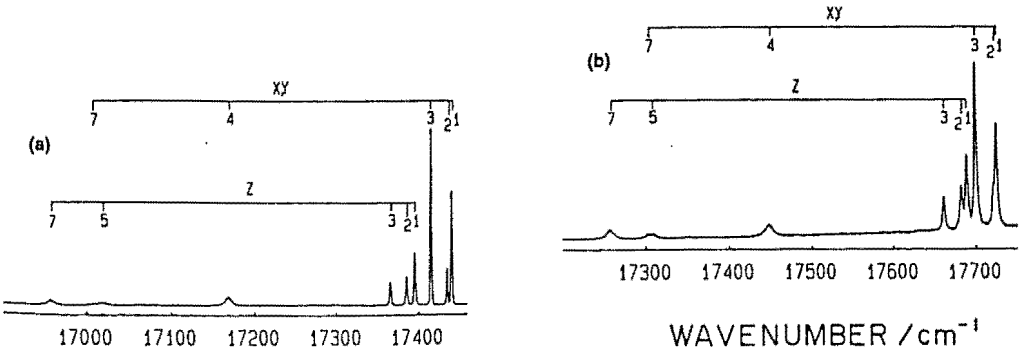

FIG. 6. 10 K fluorescence ($^4S_{3/2} \rightarrow {}^4I_{15/2}$) vibronics for $Z_1 \rightarrow E_1$ excitation: (a) the H^- C_{4v} site, and (b) the D^- C_{4v} site. All transitions are from E_1 and are labeled by the terminal Z level and the particular local mode [(X, Y) or Z] involved.

TABLE IX. Spectral data for the local mode vibronic fluorescence transitions of the H^- and D^- C_{4v} sites in CaF_2: 0.05% Er^{3+} crystals at 10 K.

		Deuterium local mode vibronics						Hydrogen local mode vibronics					
Parent electronic transition	Associated local mode	Wave number (cm^{-1})	Vibronic interval (cm^{-1})	Linewidth (cm^{-1}) ($\pm 10\%$)[a]	Relative intensity ($\pm 15\%$)[a] $x(yx)z$	$x(yy)z$	Intensity ratio[b] ($\times 10^{-3}$) ($\pm 20\%$)	Wave number (cm^{-1})	Vibronic interval (cm^{-1})	Linewidth (cm^{-1}) ($\pm 10\%$)	Relative intensity ($\pm 15\%$)[b] $x(yx)z$	$x(yy)z$	Intensity ratio[b] ($\times 10^{-3}$) ($\pm 20\%$)
$E_1 \rightarrow Z_1$	X,Y	17 728.1 ± 0.4	750.6 ± 0.5	2.1	0.73	0.52	Laser	17 443.2 ± 0.4	1037.3 ± 0.5	1.8	0.77	0.44	Laser
	Z	17 692.3 ± 0.4	786.4 ± 0.5	2.6	0.52	0.71	Laser	17 397.7 ± 0.4	1082.8 ± 0.5	2.4	0.36	0.37	Laser
$\rightarrow Z_2$	X,Y	17 724.5 ± 0.4	751.3 ± 0.5	2.2	0.40	0.28	5.5	17 437.2 ± 0.4	1038.8 ± 0.5	1.2	0.17	0.074	7.1
	Z	17 685.4 ± 0.4	790.4 ± 0.5	3.0	0.43	0.48	5.5	17 387.5 ± 0.4	1088.5 ± 0.5	2.4	0.20	0.22	6.7
$\rightarrow Z_3$	X,Y	17 703.1 ± 0.4	750.6 ± 0.5	2.1	0.93	1.00	9.1	17 417.6 ± 0.4	1037.1 ± 0.5	1.8	1.00	0.97	14.3
	Z	17 664.5 ± 0.4	789.2 ± 0.5	2.6	0.30	0.32	3.0	17 368.2 ± 0.4	1086.5 ± 0.5	2.4	0.19	0.15	3.0
$\rightarrow Z_4$	X,Y	17 451.3 ± 0.5	746.0 ± 0.8	9.4	0.23	0.32	...	17 170.1 ± 0.6	1031.3 ± 0.9	8.8	0.18	0.26	...
$\rightarrow Z_5$	Z	17 311.0 ± 0.8	793.3 ± 1.1	10.0 ± 2.0	0.17 ± 0.06	0.11 ± 0.04	1.2 ± 0.3	17 018.6 ± 0.8	1085.4 ± 1.1	12.0 ± 2.0	0.10 ± 0.03	0.073 ± 0.02	1.4 ± 0.4
$\rightarrow Z_7$	X,Y	17 306.0 ± 0.8	748.6 ± 1.1	10.0 ± 2.0	0.14 ± 0.05	0.095 ± 0.03	3.3 ± 0.8	17 010.1 ± 0.8	1044.4 ± 1.1	9.6 ± 2.0	0.069 ± 0.02	0.053 ± 0.02	2.9 ± 1.0
	Z	17 260.1 ± 0.5	794.5 ± 0.8	7.7	0.15	0.023	4.0	16 959.1 ± 0.6	1095.4 ± 0.9	9.6 ± 1.5	0.10 ± 0.03	0.14 ± 0.04	5.8

[a] ($\pm 10\%$) between each polarization for a given transition.
[b] Relative to the corresponding parent electronic line.

and intermediate coupling wave functions used in the analysis of the F^-C_{4v} site. The crystal-field parameters were determined from a least-squares fit of 15 measured levels of the ^4I manifold and the measured magnetic splitting factors for the two lowest crystal-field levels.[20] The best parameter values, giving a standard deviation energy level fit of 1.9 cm^{-1}, are listed in Table X, together with the orbital angular momentum reduction factors. The predicted Z_1 and Z_2 g values are in close agreement with those observed.[3]

Because of the observation of additional crystal-field levels, the crystal-field parameters for the hydrogenic C_{4v} site differ significantly from those reported earlier[3] and the observation made previously that the cubic field is substantially smaller for the hydrogenic C_{4v} site than the F^- C_{4v} site is no longer supported. To make a valid comparison of the crystal-field parameters between the H^-, D^-, and F^- C_{4v} sites it is appropriate to express the crystal-field Hamiltonian as a sum of tensor operators transforming as the identity irrep of the C_{4v} group. The required five C_{4v} scalars lead to the following group symmetrical decomposition of the crystal-field Hamiltonian[24]:

$$H_{CF} = X^{2+2+0+00}\sqrt{5}U^{2+2+0+00} + X^{4+0+0+00}\sqrt{9}U^{4+0+0+00} + X^{4+2+0+00}\sqrt{9}U^{4+2+0+00} + X^{6+0+0+00}\sqrt{13}U^{6+0+0+00} + X^{6+2+0+00}\sqrt{13}U^{6+2+0+00},$$

where the X^{kl0+00} are crystal-field parameters associated with the unit tensor operators U^{kl0+00} and the labels refer to the O_3, O_h, D_{4h}, C_{4v} and C_4 groups, respectively. These crystal-field parameters[24] have modified values (in cm^{-1}) for the H^-, D^-, and F^- C_{4v} sites of

$X^{2+2+0+00} = 510,\ 518\ (372),$ $X^{4+0+0+00} = -480,\ -477\ (-577),$

$X^{4+2+0+00} = 286,\ 289\ (238),$ $X^{6+0+0+00} = 495,\ 493\ (506),$

$X^{6+2+0+00} = -207,\ -208\ (-153),$

TABLE X. Calculated and experimentally determined energy levels of the $^4I_{13/2}(Y)$ and $^4I_{15/2}(Z)$ multiplets of the H^- and D^- C_{4v} sites in CaF_2:0.05% Er^{3+} crystals at 10 K. The g values for the two lowest crystal-field levels and the crystal-field Hamiltonian parameters (in cm^{-1}) are included.

	H^- C_{4v} site energy (cm^{-1})		D^- C_{4v} site energy (cm^{-1})	
State	Calculated	Observed	Calculated	Observed
Y_7	6896.1	6893.3 ± 1.5	6897.3	6894.8 ± 1.2
Y_6	6824.7	6823.3 ± 1.2	6824.2	6824.0 ± 1.0
Y_5	6799.3	6802.1 ± 1.5	6798.8	6800.6 ± 1.2
Y_4	6798.8	6796.1 ± 1.0	6798.5	6795.8 ± 1.0
Y_3	6709.9	6708.9 ± 0.8	6710.3	6709.4 ± 0.8
Y_2	6593.7	6596.9 ± 0.8	6593.6	6596.6 ± 0.8
Y_1	6560.2	6562.1 ± 0.8	6559.7	6561.2 ± 0.8
Z_8	590.1	...	590.0	583.5 ± 2.0
Z_7	426.3	426.5 ± 0.8	424.9	424.1 ± 0.7
Z_6	426.0	423.0 ± 1.5	423.9	422.0 ± 1.0
Z_5	373.9	376.5 ± 0.8	372.2	374.4 ± 0.7
Z_4	277.2	279.1 ± 1.0	281.4	281.4 ± 1.0
Z_3	26.0	25.8 ± 0.3	25.1	25.0 ± 0.3
Z_2	4.4	4.5 ± 0.3	2.8	2.9 ± 0.3
Z_1	0	0	0	0
$Z_1g_\parallel$	7.469	7.465 ± 0.005	7.339	7.335 ± 0.005
$Z_2g_\parallel$	1.682	1.683 ± 0.001	1.682	1.683 ± 0.001
$Z_1g_\perp$	6.30	6.10 ± 0.05	6.34	6.10 ± 0.05
$Z_2g_\perp$	9.08	9.09 ± 0.01	9.08	9.09 ± 0.01
ζ	2363.0		2363.3	
k_s	0.9778		0.9859	
k_s	0.9850		0.9876	
B_0^2	834.9		847.5	
B_0^4	1180.0		1189.6	
B_0^6	623.7		628.2	
B^4	−1663.0		−1663.4	
B^6	416.0		413.7	

where the F^- parameters are in parentheses. The cubic parameters $X^{k0+0+\infty}$ are now similar, consistent with the intuitively simple model of an Er^{3+} ion having a substantially unchanged immediate environment of eight F^- ions. The 37% increase in the tetragonal symmetry parameter $X^{2+2+0+\infty}$ follows the trend found for other rare-earth ions.[25] These revised H^- C_{4v} site parameter values have relevance for superposition model[24] and other[26] calculations relating them to the corresponding F^- C_{4v} site values. Revised conclusions for erbium may be necessary.

2. The R, J, K, M sites

The laser selective excitation results reported here support the classification of these sites as a related family.

H^-, D^-, and T^- varieties of the R site all show fluorescence at 15 K with the H^- site having the weakest emission. D^- varieties of the J and K sites were also found, while attempts to detect fluorescence from the M site were unsuccessful. Representative fluorescence spectra are presented in Fig. 7, while Table VI lists the derived energy levels.

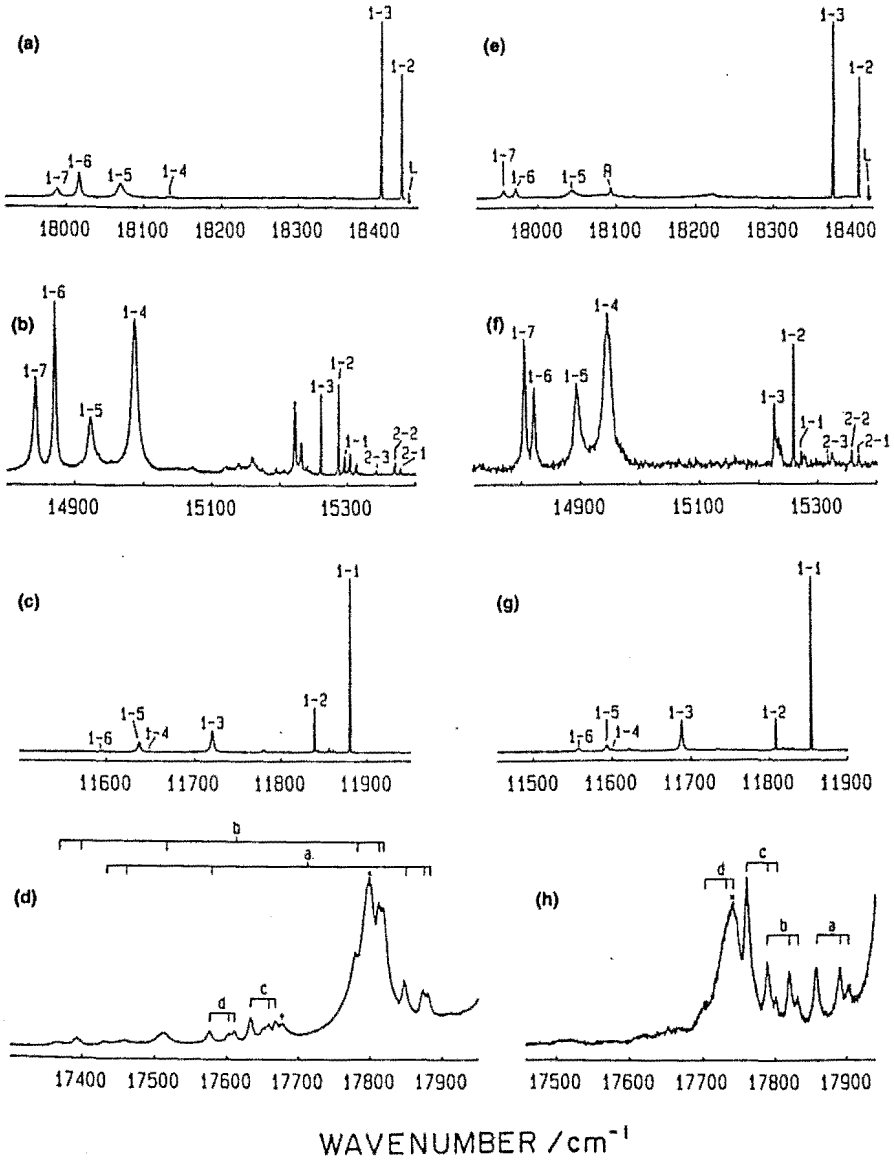

FIG. 7. 10 K fluorescence of the D^- R site [(a)–(d)] and the D^- J site [(e)–(h)] for $Z_1 \rightarrow E_1$ excitation: (a), (e) $^4S_{3/2} \rightarrow {}^4I_{15/2}$, (b), (f) $^4F_{9/2} \rightarrow {}^4I_{15/2}$, (c), (g) $^4S_{3/2} \rightarrow {}^4I_{13/2}$, (d), (h) $^4S_{3/2} \rightarrow {}^4I_{13/2}$ vibronics. In each case labels a, b, c, d identify groups of transitions from E_1 with the same vibronic interval. × identifies the $E_1 \rightarrow Z_4$ electronic transition. † identifies a possible additional vibronic interval. L identifies the laser excitation position. R identifies the first order Raman scattering line.

The R, J, K sites all show selective bleaching. Monitoring individual fluorescent lines of the D^- sites reveals intensity decreases by factors of up to 5, 10, and 15 for the R, J, K sites, respectively, after 3–5 min, with most of this decrease occurring in the first 20 s for the R and K sites and a more gradual decrease for the J site.

Simultaneous monitoring of the laser light transmitted through the crystal shows that the crystal absorption decreases by up to 70% over the same period. In all cases, the H^- sites show more rapid bleaching than the corresponding D^- sites. Moving the laser beam to a different segment of the crystal or slightly altering the laser frequency within the absorption profile restores the initial fluorescence intensity, which again rapidly decreases. Once a particular segment of the crystal has been bleached the change is observed to persist at 15 K for 2h, the longest period tested. Recovery of the original fluorescence intensity is achieved by thermal cycling of the crystals to room temperature.

For ⟨100⟩ oriented crystals, by suitable sequential pumping with the laser polarized in the two possible ⟨100⟩ directions, bleaching and successive recovery of R site fluorescence could be accomplished. Subsequent pumping of the R site with the laser polarized in a ⟨110⟩ direction gave a stable intermediate level of fluorescence. Similar effects were observed for the J and K sites with the measurements being less precise, because of the weaker fluorescence of these sites.

These bleaching effects caused some experimental difficulties in the determination of energy levels for these sites. As the fluorescence intensity decreases while the spectrum is scanned, the relative intensities of lines are affected and weak features like vibronic lines become difficult to record.

The fluorescence spectra of the R, J, and K sites have the following common features:

(a) Corresponding transitions have similar relative intensities to those of the C_{4v} sites. For example, the $E_1 \rightarrow Z_4$ and $E_1 \rightarrow Z_6$ fluorescence transitions are weak, while the corresponding $D_1 \rightarrow Z_4$ and $D_1 \rightarrow Z_6$ transitions are relatively intense.

(b) The energy level patterns for all the sites show systematic trends along the series C_{4v}, R, J, and K (Table VI).

(c) The fluorescence lines of the J and K sites show sufficient polarization in the ⟨100⟩ geometry to indicate an approximate tetragonal symmetry derived from the C_{4v} site. There was no detectable polarization dependence for the ⟨111⟩ oriented crystals or for the R site in either orientation. These polarization dependences are for the decreased intensity fluorescence lines obtained after the sites have been bleached for several minutes and a relatively stable level of fluorescence reached.

Local mode vibronic spectra were measured for the R and J sites and representative spectra are presented in Fig. 7. The vibronic spectra for both the H^- and D^- R sites and the D^-J site have lines corresponding to more than three distinct local mode vibronic intervals indicating that more than one H^- or D^- ion is present for these sites. Table XI presents the vibronic analysis. Two of the R site vibronic lines correlate with the deuterium analogs of the two local mode lines of the infrared B site, consistent with the correlation of the R site with the infrared B site.

Only tentative assignments of the R,J,K, and M sites can be attempted on the present data. These sites are related to the C_{4v} site and are low symmetry modifications of it. The R site is believed to be one of the several rhombic symmetry sites observed by EPR.[3] A possible rhombic site for CaF_2:Er^{3+} is shown in Fig. 8(a). Such a model has an H^- ion in a substitutional site adjacent to the Er^{3+} ion, and this

TABLE XI. Wave numbers and vibronic transitions of the R and J sites as measured in the 10 K fluorescence spectra of hydrogenated CaF_2: 0.05% Er^{3+} crystals.

		D^- R site		H^- R site			D^- J site	
Parent electronic transition	Local mode	Wave number (± 0.5 cm^{-1})	Vibronic interval (± 1.0 cm^{-1})	Wave number (± 0.5 cm^{-1})	Vibronic interval (± 1.0 cm^{-1})	Local mode	Wave number (± 0.5 cm^{-1})	Vibronic interval (± 1.0 cm^{-1})
$E_1 \rightarrow Z_1$	R_a	17 884.0	560.0	17 681.0	763.0	J_a	17 902.5	517.5
$\rightarrow Z_2$		17 876.5	558.5	17 673.0	762.5		17 890.5	517.0
$\rightarrow Z_3$		17 850.0	558.5	17 648.0	761.0		17 858.5	516.5
$\rightarrow Z_6$		17 462.0	556.0					
$\rightarrow Z_7$		17 434.0	555.5					
$E_1 \rightarrow Z_1$	R_b	17 821.0	623.0	17 598.5	845.5	J_b	17 832.0	588.0
$\rightarrow Z_2$		17 815.0	620.0	17 591.0	844.5		17 821.0	586.5
$\rightarrow Z_3$		17 783.0	625.5	17 565.0	844.0		17 791.0	584.0
$\rightarrow Z_4$		17 514.5	621.0					
$\rightarrow Z_6$		17 396.0	622.0					
$\rightarrow Z_7$		17 367.5	622.0					
$E_1 \rightarrow Z_1$	R_c	17 671.0	773.0	17 374.0	1070.0	J_c	17 801.5	618.5
$\rightarrow Z_2$		17 661.5	773.5	17 365.0	1070.5		17 790.5	617.0
$\rightarrow Z_3$		17 636.0	772.5	17 338.0	1071.0		17 762.0	613.0
$E_1 \rightarrow Z_1$	R_d	17 613.5	830.5	17 298.0	1146.0	J_d	17 742.0 $\pm$ 1.5	678.0 $\pm$ 2.0
$\rightarrow Z_2$		17 605.5	829.5	17 290.0	1145.5		17 732.0 $\pm$ 1.0	675.5 $\pm$ 1.5
$\rightarrow Z_3$		17 578.0	830.5	17 260.0	1149.0		17 700.0 $\pm$ 1.0	675.0 $\pm$ 1.5

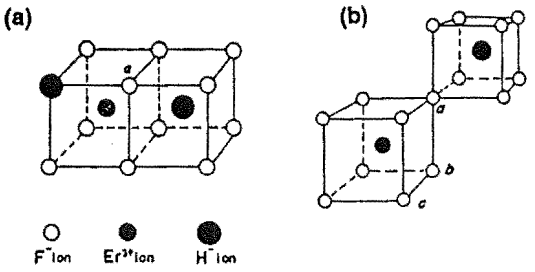

FIG. 8. (a) Model for the R site. A proposed model for the J site is that having the substitutional H^- ion at position *a*. (b) Model for the P site. Proposed models for the T, L, N sites have additional substitutional H^- ions at *a*, *b*, or *c*.

H^- ion has local mode vibrations derived from the well-established T_d site H^- line[2] at 965 cm^{-1}. The additional interstitial H^- charge compensating ion has local mode vibrations related to those of the C_{4v} site. This model of two H^- ions is, therefore, expected to have two sets of three H^- local mode lines, with those of the H^- ion closer to the Er^{3+} ion giving the stronger vibronics. The main features of this model account qualitatively for the observed features of the R site vibronics. The four local mode vibronic intervals are assigned as follows: the two lower energy vibronic intervals R_a and R_b are attributed to a substitutional hydrogenic ion replacing one of the eight F^- ions around an Er^{3+} ion and having approximate trigonal (C_{3v}) symmetry; the other two vibronic intervals R_c and R_d are attributed to the nearest-neighbour interstitial hydrogenic ion. There is evidence that the lower vibronic interval for the interstitial hydrogenic ion corresponds to the doubly degenerate vibrational mode as there is a possible additional vibronic interval [with line marked by † in Figure 7(d)] of 1057 cm^{-1} for H^- and 763 cm^{-1} for D^-, indicating a small splitting of this mode. The remaining broad intense line at 17 814 cm^{-1} for H^- and 17 802 cm^{-1} for D^- is assigned as the $E_1 \rightarrow Z_8$ electronic transition (Fig. 7). This tentative model accounts for all the observed lines.

The J site shows a spectrum with fewer lines. In analogy to the case of the R site, the broad intense line at 17 742 cm^{-1} for D^- is assigned as the $E_1 \rightarrow Z_8$ transition. This has superposed on it the Z_1,Z_2,Z_3 structure of a local mode vibronic interval, J_d, at 678.0 cm^{-1}. There are also three well-defined local mode vibronic progressions J_a, J_b, and J_c (Table XI), which are again assigned to a substitutional D^- ion adjacent to the Er^{3+} ion.

For all the sites R,J,K, and M it is proposed that there is a substitutional hydrogenic ion located at one of several possible inequivalent positions relative to the Er^{3+}–interstitial hydrogenic ion pair of the C_{4v} site and these different possible configurations give rise to this closely related family of sites. Because of the observation of three distinct local mode frequencies for the substitutional hydrogenic ion, the J site is proposed to have this substitutional ion at position *a* of Fig. 8(a).

With the limited vibronic data available from the weak J site fluorescence and the absence of any vibronic data for either the K or M sites it is difficult to make any more detailed model proposals.

All the sites show reversible bleaching effects which are not apparent for the C_{4v} site, the prototype site for this family. It is envisaged the presence of the second hydrogenic ion allows the interstitial hydrogenic ion to migrate between equivalent, orthogonal orientations for the two different laser polarizations. As there are three equivalent ⟨100⟩ directions, it is expected that the fluorescence will show decrease and recovery levels appropriate to the fraction of the sites undergoing reversible changes.

3. The P,L,T,N,S,V sites

The laser selective excitation results reported here supported the classification of these sites as another family. As the fluorescence of these sites lies in the same spectral region as several F^- sites, discrimination against F^- sites was more difficult than was the case for the R,J,K,... sites. These discrimination difficulties led to accidental pumping and identification of five new F^- sites, which are described later.

The P site shows bleaching effects similar to those found for the R,J, and K sites, but without the reversible bleaching behavior shown by these. Laser excitation of the D^- P site verified the energy levels assigned by optical absorption (Table III) but the bleaching, together with simultaneous F^- site fluorescence, precluded determination of additional electronic lines and the local mode vibronic spectrum.

Fluorescence of the D^- varieties of the L,T, and N sites was recorded for the $^4F_{9/2}$ to $^4I_{15/2}$, $^4S_{3/2}$ to $^4I_{13/2}$, and $^4I_{15/2}$ transitions for both $Z_1 \rightarrow E_1$ and $Z_1 \rightarrow E_2$ excitation, each excitation giving closely similar spectra. However, as the N site has close E_1 and E_2 levels it differed in having superposed fluorescence from E_2 as well as E_1 in the spectrum. Similar excitation yielded a less complete spectrum for the V site, with significant masking by F^- site fluorescence, while the S site spectrum could not be measured at all.

Attempts to pump the H^- varieties of these sites were largely unsuccessful, in part because the H^- sites fluoresced even more weakly relative to their corresponding D^- sites than did the H^- C_{4v} site relative to the D^- C_{4v} site.

The fluorescence spectra of these D^- sites are similar (Fig. 9) and show marked resemblences to that of the F^- B site[1] in both energy level pattern and in relative intensities of corresponding transitions. Most of the $^4I_{15/2}$ crystal-field levels of Table VI were derived from fluorescence transitions from the $^4F_{9/2}$ multiplet because these were generally more prominent and less obscured by competing F^- site transitions than those from the $^4S_{3/2}$ multiplet. The spectra also show an additional transition between the assigned transitions to the Z_7 and Z_8 levels and additional broad structure near the transition to the Z_3 level (Fig. 9). These additional features are attributed to lattice phonon structure at 495.0, 487.5, and 481.5 cm^{-1} for the L,T,N sites, respectively, and near 250 cm^{-1} for all three sites. These frequencies correlate with the known longitudinal and transverse optical phonon frequencies of CaF_2.[27-29] For the spectrometer sensitivity used, the first order Raman scattering line of the CaF_2 host lattice at low temperature[30] frequently appeared as a single sharp line at 327 cm^{-1} from the laser pump frequency.

For all but the L and V sites, there is a complete absence

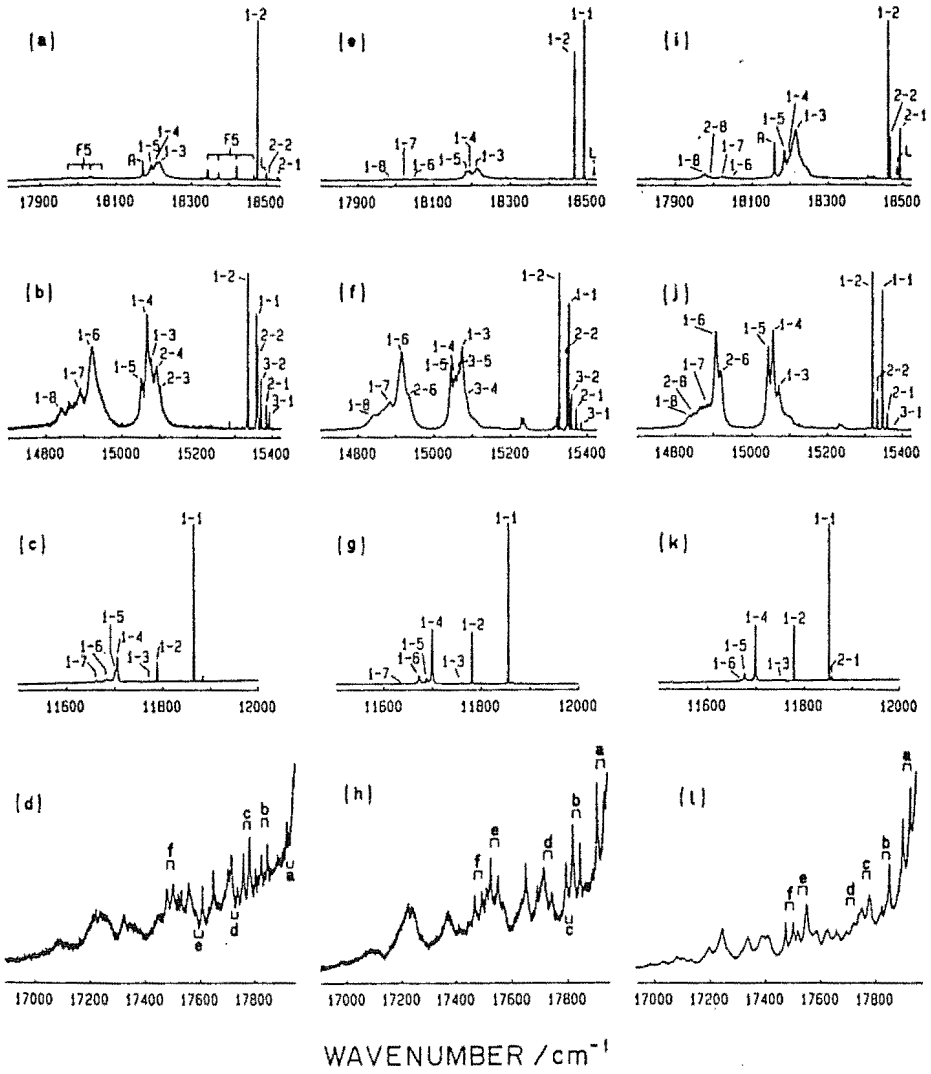

FIG. 9. 10 K fluorescence of the D^- L site [(a)–(d)], the D^- T site [(e)–(h)] and the D^- N site [(i)–(l)] for excitation of the $Z_1 \rightarrow E_1$ [(a)–(d)], [(f)–(k)] or $Z_1 \rightarrow E_2$ [(e) and (l)]: (a), (e), (i) $^4S_{3/2} \rightarrow {}^4I_{15/2}$, (b), (f), (j) $^4F_{9/2} \rightarrow {}^4I_{15/2}$, (c), (g), (k) $^4S_{3/2} \rightarrow {}^4I_{13/2}$, (d), (h), (l) $^4S_{3/2} \rightarrow {}^4I_{15/2}$ vibronics.

of fluorescence polarization for the ⟨100⟩ geometry, while partial polarization of all sites is apparent for the ⟨111⟩ geometry, consistent with an underlying trigonal symmetry structure for these sites. The extent of ⟨111⟩ polarization observed varies with the site, being marked for the P and T sites, significant for the L site and slight for the N and V sites.

Local mode vibronic spectra for the D^- varieties of the L,T,N sites are shown in Fig. 9 while Table XII gives the vibronic analysis. Broad unassigned vibronic features are present and are variously attributed to second order lattice phonon structure and to local mode vibronics associated with higher electronic Z levels. The L,T,N sites all show six distinct local mode vibronic intervals indicating more than one D^- ion is present in each of these sites, consistent with the increased linewidth of transitions observed in the absorption studies of mixed crystals. Figure 10 shows the fluorescence spectra obtained for several laser pump frequencies within the broad absorption line profile for the $Z_1 \rightarrow E_2$ transition of the T site in a 1:1 mixed H^-/D^- crystal. Similar results are obtained for the L site. It is found that as the laser is tuned from the pure D^- site absorption frequency towards the H^- site value, fluorescence transitions of progressively shifted frequency are obtained, due to excitation of mixed H^-/D^- sites of varying local site configuration.

The relative stability of cubic sites of rare-earth ions increases along the rare-earth series.[31] EPR measurements show that rare-earth ions in the earlier part of the series have predominantly C_{4v} type sites while rare-earth ions in the latter part possess a greater variety of sites, including those of trigonal symmetry and those derived from cubic sites.

TABLE XII. Wave numbers and vibronic intervals of local mode vibronic transitions of the D^- L, T, and N sites as measured in the 10 K fluorescence spectrum of deuterated CaF_2: 0.05% Er^{3+} crystals.

		L site		T site		N site		N site	
Local mode	Terminating level	Wave number from E_1 level ($\pm 0.5\ cm^{-1}$)	Vibronic interval ($\pm 1.0\ cm^{-1}$)	Wave number from E_1 level ($\pm 0.5\ cm^{-1}$)	Vibronic interval ($\pm 1.0\ cm^{-1}$)	Wave number from E_1 level ($\pm 0.5\ cm^{-1}$)	Vibronic interval ($\pm 1.0\ cm^{-1}$)	Wave number from E_2 level ($\pm 0.5\ cm^{-1}$)	Vibronic interval ($\pm 1.0\ cm^{-1}$)
a	Z_1	17 947.0	555.5	17 936.5	555.5	17 925.5	564.5	17 933.0	562.5
	Z_2	17 925.0	555.0	17 910.5	556.0	17 897.5	564.5	17 906.5	563.0
b	Z_1	17 852.0	650.5	17 848.0	644.0	17 844.5 ± 1.0	645.0 ± 1.5	17 856.0	639.5
	Z_2	17 830.0	650.0	17 822.5	644.0	17 818.5	645.0	17 830.0	639.5
c	Z_1	17 787.5	715.0	17 822.5	669.5	17 777.0 ± 1.0	712.5 ± 1.5	17 782.0 ± 1.0	713.5 ± 1.5
	Z_2	17 764.5	715.5	17 796.0	670.0	17 749.0 ± 1.0	714.5 ± 1.5	17 755.0	714.5
d	Z_1	17 741.5	761.0	17 745.0	747.0	17 721.0	768.5	17 727.0 ± 1.0	768.5 ± 1.5
	Z_2	17 719.0	761.0	17 718.0 ± 1.0	748.5 ± 1.5	obscured	···	17 698.5 ± 1.0	771.0 ± 1.5
e	Z_1	17 613.0	889.5	17 553.5	938.5	17 547.5 ± 1.0	942.0 ± 1.5	17 553.5	942.0
	Z_2	17 589.5 ± 1.0	890.5 ± 1.5	17 527.5	939.0	17 519.5	944.0	17 533.5 ± 1.0	946.0 ± 1.5
f	Z_1	17 505.5	997.0	17 494.5	997.5	17 500.0	988.5	17 506.5	989.0
	Z_2	17 483.0	997.0	17 469.0	997.5	17 471.5	992.0	17 479.5	990.0

Similar behavior is found here for the optical spectra. Many more hydrogenic sites are found for the Er^{3+} system, as compared to Pr^{3+} [19] and Nd^{3+} [32] where the C_{4v} site is dominant and the others are derived from the C_{4v} site and have lower energies than it.

The observation of an EPR site of trigonal symmetry in 12 h hydrogenated crystals[3] suggests that an H^- analog of the F^- B site is present, i.e., a site in which an Er^{3+} ion is charged compensated by an H^- ion located in a next-nearest-interstitial position. The most likely candidate for such a trigonal symmetry H^- site is the P site since it appears in weakly hydrogenated crystals, is the first member of this family of sites to be produced in any hydrogenation treatment, and has marked ⟨111⟩ polarization, after bleaching, consistent with trigonal symmetry. An alternative F^- B site model[33] would not obviously give hydrogenic varieties having the required trigonal symmetry.

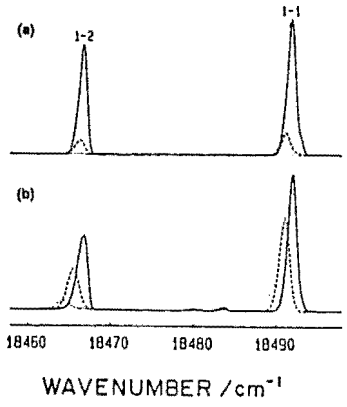

FIG. 10. Comparison of 10 K fluorescence ($^4S_{3/2} \rightarrow {}^4I_{15/2}$) for the T site for three closely spaced laser frequencies within the $Z_1 \rightarrow E_2$ absorption profile in a CaF_2:0.05% Er^{3+} crystal: (a) deuterated for 68 h, (b) treated for 68 h in a 1:1 mixture of hydrogen and deuterium.

With this assignment, the L,T,N,S, and V sites are all proposed to be modifications of the P site having additional hydrogenic ions migrating to substitutional positions near the Er^{3+}–hydrogenic ion pair. This is in analogy to the development of the R,J,K, and M sites from the C_{4v} site.

The observation of six vibronic intervals (Table XII) supports this model. The three lower vibronic intervals centered around 640 cm^{-1} are attributed to a substitutional D^- ion and are derived from the T_d site frequency of 694 cm^{-1}. The three other vibronic intervals are assigned to an interstitial D^- ion in a ⟨111⟩ direction from the Er^{3+} ion [Figure 8(b)]. Similar low symmetry sites involving an F^- interstitial ion have been proposed for hydrogenic sites in hydrogenated strontium fluoride crystals containing rare-earth ions from the latter part of the rare-earth series.[11]

There are several possible positions for the substitutional hydrogenic ion relative to the proposed P site configuration, and both the isotope shifts and the polarization behavior give some guide to possible site configurations. The L,T,N,S, and V sites all possess large isotope shifts consistent with substitutional hydrogenic ions as nearest neighbors to the Er^{3+} ion.

As the T site bears a strong resemblence to the P site in having significant ⟨111⟩ polarization, it is a good candidate for a ⟨111⟩ site with an additional substitutional hydrogenic ion in position *a* of the modified P site configuration [Fig. 8(b)]. The existence of six vibronic lines (Table XII) would require a displacement of one or the H^- ions off axis. The L and N sites have closely similar vibronic intervals, with the L site showing both ⟨111⟩ and ⟨100⟩ polarization and the N site weak ⟨111⟩ polarization. Possible L and N site configu-

rations have the substitutional hydrogenic ion at positions *b* or *c*. The isotope shifts are consistent with these choices. The S and V sites are expected to have similar configurations to the L,T, and N sites, but there is insufficient vibronic data on them for any substitutional hydrogenic ion positions to be proposed.

4. Other hydrogenic sites

The near cubic symmetry and W sites, identified by optical absorption have weak fluorescence which could not be clearly distinguished from swamping F^- site fluorescence simultaneously excited when the laser was tuned to pump absorption transitions. The levels of the D^- X site listed in Table III were confirmed by fluorescence measurements, which also determined the D_1 level to be at 15 391 cm^{-1}. The X site also exhibited bleaching.

C. Fluoride ion sites

During the course of this study measurements were also carried out on the various F^- sites present. These were partially to supplement previous work, such as the polarization data for the C_{4v} site, and partially to determine energy levels of sites that were giving discrimination problems in locating specific hydrogenic site lines. Other aspects, such as upconversion of single Er^{3+} ion sites, appeared and are also discussed in this section.

1. F1–F5 sites

Five further sites were identified in the laser excitation study. They have a fluorescence intensity of between 1% and 10% of that for the well-established F^- sites yet show no distinct lines in their absorption spectra. Because of this high fluorescence efficiency they are attributed to additional F^- sites.

Of the five sites, labeled F1 to F5, two (F1 and F2) appear in the parent crystals (as received from Optovac) while the remainder appear in crystals thermally cycled to 860 °C with aluminum either in vacuum or as part of the hydrogenation treatment. Representative spectra are presented in Figs. 11 and 12, while Table VII gives the derived energy levels. There is difficulty in assigning some of the $E \rightarrow Y$ transitions for the F1 and F2 sites as simultaneous excitation of both sites is unavoidable, F2 being weaker than F1.

The F1 and F2 sites show coupled behavior. Pumping one yields emission of the other, even though their energy levels are distinct. Likewise, both show efficient upconversion; pumping either gives strong upconversion spectra of both. The F1 site has no polarization in either ⟨100⟩ or ⟨111⟩ geometries; the F2 site has well-defined ⟨100⟩ polarization, but no ⟨111⟩; the F3 has distinct trigonal symmetry ⟨111⟩ polarization, but no detectable ⟨100⟩; the F4 site has distinct ⟨111⟩ and slight ⟨100⟩ polarization, and the F5 site

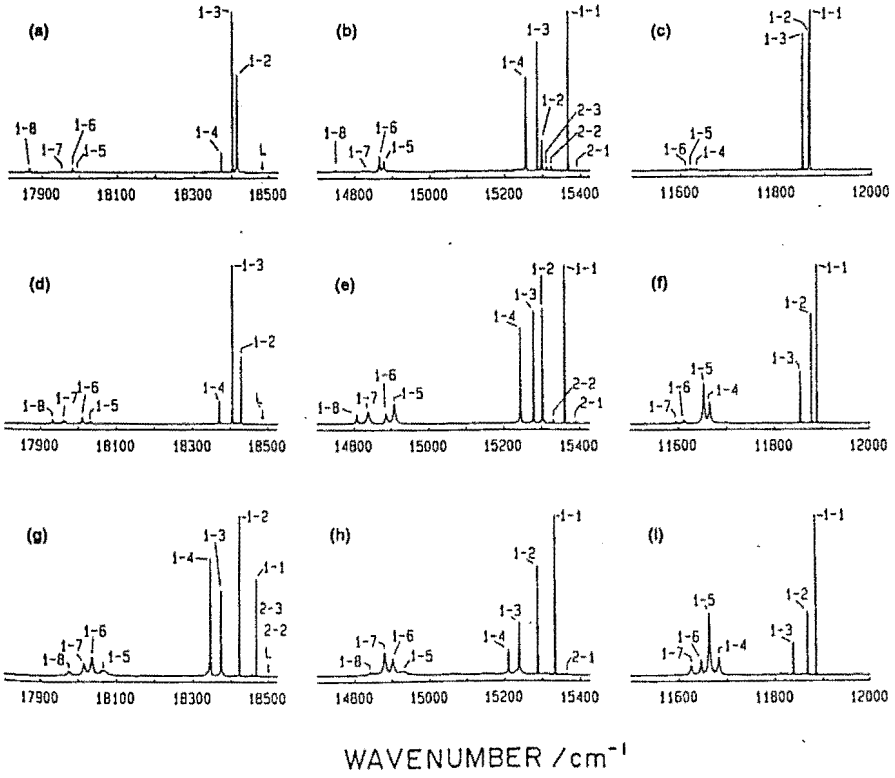

FIG. 11. 10 K fluorescence spectra of the F3 site [(a)–(c)], the F4 site [(d)–(f)], and the F5 site [(g)–(i)]: (a), (d), (g) $^4S_{3/2} \rightarrow {}^4I_{13/2}$, for $Z_1 \rightarrow E_1$ excitation. (b), (e), (h) $^4F_{9/2} \rightarrow {}^4I_{15/2}$, for $Z_1 \rightarrow E_1$ excitation. (c), (f), (i) $^4S_{3/2} \rightarrow {}^4I_{13/2}$, for $Z_1 \rightarrow E_2$ excitation. L identifies the laser excitation position.

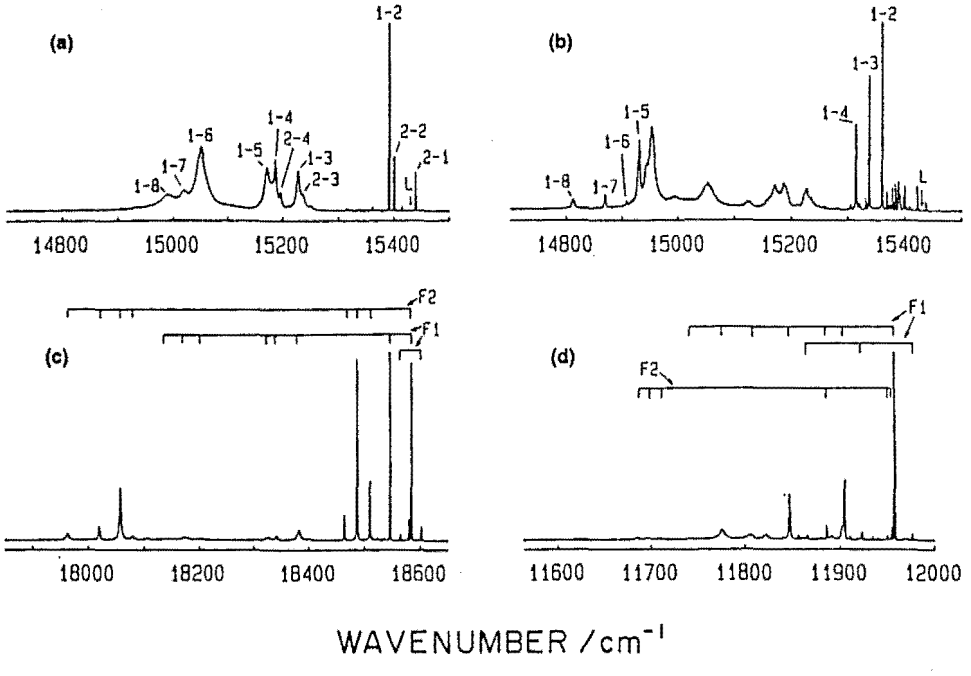

FIG. 12. 10 K fluorescence spectra of the F1 and F2 sites: (a) $^4F_{9/2} \rightarrow {}^4I_{15/2}$, for $Z_1 \rightarrow D_1$ excitation of F1 site. (b) $^4F_{9/2} \rightarrow {}^4I_{15/2}$, for $Z_1 \rightarrow D_1$ excitation of F2 site. (c) $^4S_{3/2} \rightarrow {}^4I_{15/2}$, upconversion, $Z_1 \rightarrow D_1$ excitation of F1 site. (d) $^4S_{3/2} \rightarrow {}^4I_{13/2}$, for $Z_1 \rightarrow E_2$ excitation of F1 site. In (c) and (d), transitions from $^4S_{3/2}$ are labeled by F1 and F2 as appropriate.

has both ⟨100⟩ and ⟨111⟩ polarization. The F1 site has an energy level scheme like that of the F^- B site and the P,L,T,N,S,V family of D^- sites. The F2 to F5 sites are a group with closely similar energy level patterns, different from all other sites reported to date in CaF_2, but resembling those of the J site[34] in SrF_2:Er^{3+} and the L site[35] in BaF_2:Er^{3+}. All these sites have similar energy level patterns to that of the cubic site.[12,13] For the F1 and F2 sites a possible configuration is the juxtaposition of F^- C_{4v} and F^- C_{3v} sites in a pair arrangement, which would account for most of the observations. The F3, F4, and F5 sites involve a single Er^{3+} ion. They have $J + \frac{1}{2}$ energy levels for each multiplet, appear at low Er^{3+} ion concentration and no evidence of upconversion was found. These sites may be examples of the various site configurations $1|2_1$, $1|2_2$, etc.[36] predicted to be at least marginally stable in CaF_2. Such sites would be formed by the F^- A or B sites trapping an additional F^- interstitial ion. On the other hand, the effect of aluminum in scavenging F^- ions could produce sites involving lattice vacancies.

2. Polarization of the F^- B and C sites and the oxygen charge compensation G1 site

The B and G1 sites have a complete absence of polarization of their fluorescence lines for the ⟨100⟩ polarization geometry and pronounced polarization for the ⟨111⟩ geometry, consistent with the trigonal symmetry described for both these sites.[14,16]

The F^- C site showed no polarization in the ⟨111⟩ geometry and only a slight ⟨100⟩ polarization, supporting several proposed low symmetry Er^{3+} ion pair models.[37]

3. Upconversion spectra of the F^- C_{4v} site

Fluorescence is observed from the F^- C_{4v} site $^4S_{3/2}$ multiplet on laser excitation of transitions to the $^4F_{9/2}$ multiplet. The intensities of these upconversion transitions are a factor of 10^5 less than the same transitions for direct excitation into the $^4S_{3/2}$ multiplet. For upconversion into the $^4S_{3/2}$ multiplet the measured polarization ratios, $x(yy)z$:$x(yx)z$, of the fluorescence transitions $E_1 \rightarrow Z_2$, $E_1 \rightarrow Z_3$, and $E_1 \rightarrow Z_5$ are 0.79, 0.80, and 1.7, respectively, while the polarization data of Table VIII yield corresponding ratios of 1.6, 1.5, and 0.16 for direct excitation of these transitions.

Since the F^- C_{4v} site is accepted as being a single Er^{3+} ion site the upconversion mechanism involved is postulated to be the successive absorption of two photons by a single Er^{3+} ion rather than the cooperative two Er^{3+} ion excitation process proposed for dimer site upconversion.[1] The single ion stepwise excitation process[38,39] requires an appreciable lifetime for the intermediate state involved in the upconversion process. Accidental coincidences of $^4F_{9/2}$ multiplet lines of the D^- C_{4v} site with F^- site lines precluded observation of upconversion spectra of the D^- C_{4v} site. An alternative proposal is the intercluster mechanism reported for CaF_2:Pr^{3+}.[40] Measurements of the fluorescence lifetimes of various upconversion spectral lines for several rare-earth ion systems would help identify the upconversion mechanism operating.

4. Other emission spectra

Strong fluorescence characterized by a sharp line at 14 110 cm^{-1} and vibronic side structure was obtained by

pumping the hydrogenated, deuterated and parent crystals in the 18 410 to 18 530 cm^{-1} region at 15 K. No distinct optical absorption transitions occur near 14 000 cm^{-1}. The origin of this fluorescence is attributed to trace quantities of samarium in the crystals, both as grown here and in those purchased from Optovac Inc. During the hydrogenation treatment, the aluminum caused reduction of any Sm^{3+} to Sm^{2+} and the appearance of the Sm^{2+} lines.[41,42]

The tritiated calcium fluoride crystals containing erbium become green colored with time due to the formation of color centers created by the internal irradiation of the crystals through the β decay of the tritium. At 15 K, these crystals show fluorescence bands from 17 300 to 17 800 cm^{-1} with a strong sharp line at 17 675 cm^{-1}. This fluorescence is observed only with the tritiated crystals and is attributed to color centers.

VI. DISCUSSION AND CONCLUSIONS

The $CaF_2:Er^{3+}$ system has previously been extensively studied by laser selective excitation.[1,16,17,20] Supplementation of such studies by utilizing polarization can determine site symmetries of relatively high symmetry sites. For ⟨100⟩ oriented crystals, tetragonal symmetry sites have well-polarized fluorescence lines. Trigonal symmetry sites have fluorescence lines with no polarization in this geometry, but do show polarization for ⟨111⟩ oriented crystals.

Application of the laser selective excitation technique to the investigation of hydrogenated $CaF_2:Er^{3+}$ crystals has revealed a great variety of new sites, involving one or more hydrogenic ions. For Er^{3+} ion concentrations of 0.05% or less, 16 new sites involving single Er^{3+} ions were observed, with model configurations proposed for most of these.

The site distributions proved to be dependent on the duration of the hydrogenation treatment which can be chosen to obtain almost any desired distribution.

The hydrogenated $CaF_2:Er^{3+}$ system has proved to have several aspects worthy of further study:

(a) The F^-, H^-, D^- series of C_{4v} sites is an excellent group for crystal-field[3], superposition model[24] and intensity[23] calculations. In all of these, the effect of the different charge compensating ion can be quantitatively examined.

(b) The H^- and D^- local modes play a significant role in determining fluorescence lifetimes, which are found to be markedly sensitive to the charge compensating ion present.[4,19]

(c) Absorption lines of other multiplets accessible to dye laser excitation can be assigned to specific sites by scanning the laser while monitoring well-established fluorescence transitions of these sites and several $^2H_{11/2}$ multiplet lines have been so confirmed.

(d) Upconversion is a relatively weak process for the single Er^{3+} ion F^- C_{4v} site observed here, but gives a method of determining higher crystal-field levels. The corresponding D^- C_{4v} site is known to show upconversion for other rare-earth systems studied[43] but could not be distinguished for the erbium case because of pump line overlap. Upconversion excitation spectra obtained by scanning the laser while monitoring appropriate fluorescence transitions would yield two photon excitation spectra, differing in intensity and polarization from the more usual one-photon excitation spectra described earlier.

(e) The wide variety of hydrogenic sites produced, both in basic symmetry type and in families of closely related species, makes a promising set for crystal-field calculations, following those already carried out for the C_{4v} sites.[24] For such calculations, both rotational Zeeman[14,44] and correlated EPR and optical studies[11] are needed to determine exact Er^{3+} ion site symmetries and to establish more definite models than those already proposed. These model determinations have relevance to models of dipole cluster activation energies already carried out for various F^- sites in CaF_2.[36,45]

(f) Tritium varieties of the C_{4v} and R sites have been briefly studied and are noteworthy in having fluoresaence at 77 K. Tritiated crystals have difficulties for experimental study in that color centers are produced by β decay of the tritium and the crystals produced to date show the simultaneous presence of the corresponding H^- sites. Nevertheless the T^- centers should provide useful supplementary results consistent with the trends observed in going from H^- to D^- and H^- to F^-.

(g) Ultraviolet irradiation at 77 K produces new sites stable below room temperature and these have characteristic electronic and vibronic spectra.[9,46] With the hydrogenated $CaF_2:Er^{3+}$ spectra now largely classified, such studies should reveal various new sites whose lack of stability precludes their formation in crystals stored at room temperature and above.

(h) The present studies have classified 16 H^- sites for the 0.05% Er^{3+} ion concentration crystals. Measurement of higher concentration crystals[47] should reveal Er^{3+} ion cluster sites with both Er^{3+} ions and H^- ions in arrangements analogous to the many D1 and D2 sites reported for the parent system.[1] Superstructure arrangements[48] should appear at the higher Er^{3+} ion concentrations, resulting in hydrogenic modifications of the high concentration limit site similar to the D2(a) site, but having even broader optical lines.

(i) The defect equilibria among sites have been detailed[17] for the F^- sites in $CaF_2:Er^{3+}$. Analogous studies would be appropriate for the H^- and D^- sites, with the expectation of more varied behavior and effects extending to lower crystal temperatures.

(j) Dielectric loss [37,48–52] and ionic thermal current methods[53–55] are powerful techniques for determining activation energies of various sites. Their application to corresponding H^- and D^- sites should give similar activation energies, while the greater mobility of H^- and D^- ions relative to F^- should yield more marked temporal behavior.

(k) Carbon dioxide laser saturation studies[56] on the infrared absorption lines of H^- ions have been done for the H^- C_{4v} sites of several rare earths in CaF_2. Of those studies, erbium was the only one showing any saturation effects and this appears to be associated with the relatively low (4.5 cm^{-1}) energy separation of the Z_1 and Z_2 crystal-field levels in erbium. With the R, J, and K sites of erbium having similar Z_1 and Z_2 energy level separations and with the R site known to have the infrared local mode lines of the B site in the carbon dioxide laser range, further carbon dioxide laser

saturation measurements would be useful to verify any correlation between observed saturation and Er^{3+} energy level structure, and determine any role the Er^{3+} energy levels play in the saturation process.

(1) The selective bleaching observed for several sites is a form of photochemical holeburning, which has considerable promise for investigating migration of ions between different positions in the lattice and the formation of different end product sites. The reversible bleaching exhibited by the R and J sites is of interest for the creation of oriented species for further spectroscopic study. Neither laser selective bleaching nor polarization reversible selective bleaching have been observed for any F^- ion sites and both appear to be unique to H^- and D^- sites. These phenomena are attributed to the relative mobility of H^- and D^- ions compared to F^- ions, and are observed for several rare-earth ions in both CaF_2 and SrF_2, for which results will be presented elsewhere.[57]

In summary, the hydrogenated $CaF_2:Er^{3+}$ system has proved as productive of interesting phenomena in laser spectroscopy studies as the parent system, and has the potential to continue to do so in the future.

ACKNOWLEDGMENTS

This research was supported by the New Zealand University Grants Committee through Research Grants. Two of us (NJC, DT) acknowledge support from N.Z.U.G.C. Postgraduate and Commonwealth Scholarships, respectively. We thank R. A. Ritchie, T. Rowe, and W. G. Smith for technical assistance.

[1]D. R. Tallant and J. C. Wright, J. Chem. Phys. 63, 2074 (1975).
[2]R. J. Elliott, W. Hayes, G. D. Jones, H. F. Macdonald, and C. T. Sennett, Proc. R. Soc. London 289, 1 (1965).
[3]A. Edgar, G. D. Jones, and M. R. Presland, J. Phys. C 12, 1569 (1979).
[4]G. D. Jones, S. Peled, S. Rosenwaks, and S. Yatsiv, Phys. Rev. 183, 353 (1968).
[5]S. Yatsiv, S. Peled, S. Rosenwaks, and G. D. Jones, *Optical Properties of Ions in Crystals* (Interscience, New York, 1967), p. 409.
[6]R. C. Newman, *Infrared Studies of Crystal Defects* (Taylor and Francis, London, 1973).
[7]J. C. Hall and R. T. Schumacher, Phys. Rev. 127, 1892 (1962).
[8]B. Welber, J. Chem. Phys. 43, 3015 (1965).
[9]I. T. Jacobs, G. D. Jones, K. Zdansky, and R. A. Satten, Phys. Rev. B 3, 2888 (1971).
[10]A. B. Robson, M.Sc. thesis, University of Canterbury, 1969.
[11]A. Edgar, C. A. Freeth, and G. D. Jones, Phys. Rev. B 15, 5023 (1977).
[12]D. S. Moore, Ph.D. thesis, University of Wisconsin, 1980, University Microfilms, Ann Arbor, Mich.
[13]I. B. Aizenberg, B. Z. Malkin, and A. L. Stolov, Sov. Phys. Solid State 13, 2155 (1972).
[14]C. W. Rector, B. C. Pandey, and H. W. Moos, J. Chem. Phys. 45, 171 (1966).
[15]F. J. Gustafson and J. C. Wright, Anal. Chem. 51, 1762 (1979).
[16]F. J. Gustafson, Ph.D. thesis, University of Wisconsin, 1978, University Microfilms, Ann Arbor, Mich.
[17]D. S. Moore and J. C. Wright, J. Chem. Phys. 74, 1626 (1981).
[18]D. S. Moore and J. C. Wright, Chem. Phys. Lett. 66, 173 (1979).
[19]R. W. G. Syme, R. J. Reeves, and G. D. Jones, J. Lumin. 31, 248 (1984).
[20]C. A. Freeth, G. D. Jones, and R. W. G. Syme, J. Phys. C 15, 5667 (1982).
[21]B. R. Judd, Phys. Rev. 127, 750 (1962).
[22]G. S. Ofelt, J. Chem. Phys. 37, 511 (1962).
[23]M. F. Reid, Ph.D. thesis, University of Canterbury, 1981.
[24]M. F. Reid and P. H. Butler, J. Phys. C 15, 4103 (1982).
[25]C. A. Freeth and G. D. Jones, J. Phys. C 15, 6833 (1982).
[26]K. Lesniak, J. Phys. C 19, 2721 (1986).
[27]M. M. Elcombe and A. W. Pryor, J. Phys. C 3, 492 (1970).
[28]R. W. Ward and P. W. Whippey, Can. J. Phys. 52, 1185 (1974).
[29]M. Schlesinger and G. W. F. Drake, Can. J. Phys. 54, 1699 (1976).
[30]P. Denham, G. R. Field, P. L. Morse, and G. R. Wilkinson, Proc. R. Soc. London Ser. A 317, 55 (1970).
[31]M. J. Weber and R. W. Bierig, Phys. Rev. A 134, 1492 (1964).
[32]T. P. J. Han (private communication).
[33]H. K. Welsh, J. Phys. C 18, 5637 (1985).
[34]I. B. Aizenberg, M. P. Davydova, B. Z. Malkin, A. I. Smirnov, and A. L. Stolov, Sov. Phys. Solid State 15, 914 (1973).
[35]M. P. Miller and J. C. Wright, J. Chem. Phys. 68, 1548 (1978).
[36]J. Corish, C. R. A. Catlow, P. W. M. Jacobs, and S. Ong, Phys. Rev. B 25, 6425 (1982).
[37]C. G. Andeen, J. J. Fontanella, M. C. Wintersgill, P. J. Welcher, R. J. Kimble Jr., and G. E. Matthews, Jr., J. Phys. C 14, 3557 (1981).
[38]N. Bloembergen, Phys. Rev. Lett. 2, 84 (1959).
[39]J. P. Jouart, C. Bissleux, and G. Mary, J. Lumin. 29, 261 (1984).
[40]A. Lezama, M. Oria, and C. B. de Araujo, Phys. Rev. B 33, 4493 (1986).
[41]D. L. Wood and W. Kaiser, Phys. Rev. 126, 2079 (1962).
[42]P. P. Feofilov and A. A. Kaplyanskii, Opt. Spectrosc. 12, 272 (1962).
[43]G. D. Jones, N. J. Cockroft, T. P. J. Han, R. J. Reeves, and R. W. G. Syme, Proceedings of the Second Asia–Pacific Physics Conference, Bangalore, 1986 (in press).
[44]A. F. Leung, J. Phys. C 6, 2234 (1973).
[45]I. J. Ashburner and R. C. Newman, J. Phys. C 5, L283 (1972).
[46]C. R. A. Catlow, J. Phys. C 9, 1845 (1976).
[47]I. B. Aizenberg, M. S. Orlov, and A. L. Stolov, Sov. Phys. Solid State 15, 1240 (1973).
[48]C. R. A. Catlow, A. V. Chadwick, G. N. Greaves, and L. M. Moroner, Nature 312, 601 (1984).
[49]A. Edgar and H. K. Welsh, J. Phys. C 8, L336 (1975).
[50]J. Fontanella and C. Andeen, J. Phys. C 9, 1055 (1976).
[51]C. Andeen, D. Link, and J. Fontanella, Phys. Rev. B 16, 3762 (1977).
[52]A. Edgar and H. K. Welsh, J. Phys. C 12, 703 (1979).
[53]E. L. Kitts and J. H. Crawford, Jr., Phys. Rev. B 9, 5264 (1974).
[54]B. P. M. Lenting, J. A. J. Numan, E. J. Bijvank, and H. W. den Hartog, Phys. Rev. B 14, 1811 (1976).
[55]Z. C. Nauta-Leeffers and H. W. den Hartog, Phys. Rev. B 19, 4162 (1979).
[56]J. A. Campbell, A. J. Sievers, and G. D. Jones, Bull. Am. Phys. Soc. 27, 402 (1982).
[57]N. J. Cockroft, T. P. J. Han, R. J. Reeves, G. D. Jones, and R. W. G. Syme, Opt. Lett. (in press).

Reversible polarized bleaching in hydrogenated rare-earth-doped fluorites

N. J. Cockroft, T. P. J. Han, R. J. Reeves, G. D. Jones, and R. W. G. Syme

Department of Physics, University of Canterbury, Christchurch, New Zealand

Received August 11, 1986; accepted October 15, 1986

By using site-selective laser spectroscopy, several sites in hydrogenated and deuterated rare-earth-doped fluorite crystals have been found to exhibit reversible bleaching. The site orientations can be switched between orthogonal directions by corresponding changes in the laser polarization. Such effects are a form of photochemical hole burning and are attributed to laser-induced migration of H^- or D^- ions between equivalent interstitial positions adjacent to the rare-earth ion.

An unusual phenomenon of reversible polarized bleaching has been observed for some hydrogenic sites in calcium and strontium fluorides containing 0.05% rare-earth ions. Previous studies of the hydrogenated and deuterated crystals reveal the existence of several low-symmetry sites derived from the hydrogenic C_{4v} site.[1] Recent laser-selective-excitation studies have shown that these sites (both H^- and D^- varieties) differ in the placement, relative to a ⟨100⟩ oriented RE^{3+}–H^- ion charge-compensation pair, of a second H^- ion substituting for an adjacent lattice F^- ion. Detailed spectroscopy of these sites will be presented elsewhere.

Many of these sites exhibit bleaching when studied by laser-selective excitation using a Spectra-Physics 375 tunable dye laser. On pumping appropriate rare-earth electronic transitions, with laser powers in the range 10 to 100 mW, the intensity of various fluorescence lines are observed to decrease by factors of up to 15 in times ranging from 10 sec to 5 min. Illuminating a different segment of the crystal restores the initial fluorescence level, which again rapidly decreases. Slightly shifting the laser frequency within the absorption contour gives a similar pattern of fluorescence response. Simultaneous monitoring of the transmitted laser light shows decreases in the absorption of up to 70% over the same period. This decreased absorption has been observed to persist at 15 K for 2 h, the longest period tested. Both H and D isotopes show the effect, and in all cases studied the H^- sites give a more rapid fluorescence decrease than the corresponding D^- sites.

Some of these bleachable sites exhibit a new phenomenon of reversible polarized bleaching. This effect is clearest for ⟨100⟩ oriented crystals with the laser light incident parallel to, say, the [100] unit cell edge. After bleaching with the laser polarized in the [001] direction, fluorescence could be substantially restored by switching the laser polarization to the [010] direction. Moreover, by suitable sequential pumping with the laser polarized in these two directions, an apparently indefinite sequence of bleaching and successive recovery of the fluorescence could be accomplished. Recovery levels of 95% or more are found for several sites after many cycles of successive bleaching [Fig. 1(a)]. Corresponding effects are seen in the transmission of the laser light. Subsequent pumping of the site with the laser polarized in the [011] direction gives a relatively stable intermediate level of fluorescence. Table 1 summarizes the number of bleachable centers found to date. Neither the hydrogenic C_{4v} site, from which nearly all these sites are derived, nor any of the fluoride ion charge-compensation sites studied have been observed to show this effect. Preliminary time-dependence studies of the bleaching rates reveal a mixture of single-exponential decay and two-body $1/t$ decay behavior,[2] depending on the site studied.

Temperature-dependence studies of the previously reported C_s site[3] in SrF_2:Pr^{3+} show bleaching times increasing with temperature until no bleaching effects are observed at a crystal temperature of 100 K. Preliminary studies of the same site at 2 K using a single-mode dye laser revealed a hole of width 800 MHz burned into the absorption contour, characteristic of photochemical hole burning.

The bleaching characteristics vary for different absorption lines of a given site. For a particular site in SrF_2:Nd^{3+}:D^- two of the three absorption transitions to the $^4G_{5/2}$ multiplet (at 17 026.3 and 17 153.5 cm^{-1} in vacuum) gave distinctly different fluorescence-decrease rates. Excitation of the third absorption transition (at 17 164.2 cm^{-1}) gave no sign of bleaching but removed any asymmetry induced by previous pumping of either of the two other transitions.

These reversible bleaching observations can be understood on a model of reorientation of ⟨100⟩ RE^{3+}–H^- ion pairs. The exact configuration of the sites showing reversible bleaching cannot be of critical significance, as a number of sites display the effect. A possible site configuration, derived from the well-established hydrogenic C_{4v} site, is presented in Fig. 2, which also shows a proposed reorientation mechanism.[4,5] Selective excitation with appropriately polarized laser light could result in the substitutional H^- ion's migrating to an adjacent empty interstitial posi-

0146-9592/87/010036-03$2.00/0

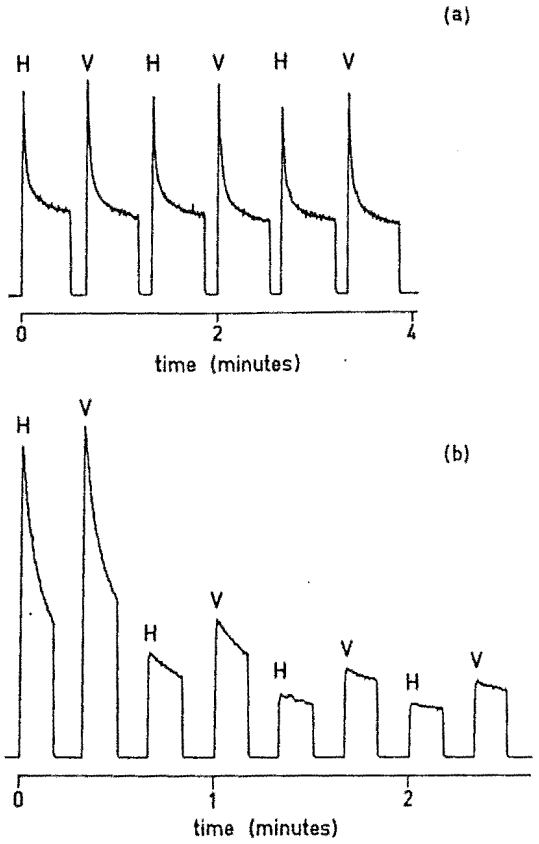

Fig. 1. Fluorescence intensity as a function of time for a sequence of laser excitations for two possible polarization directions, $V[001]$ and $H[010]$, of (a) the 16 612.8-cm^{-1} transition in a ⟨100⟩ oriented SrF_2:0.05% Pr^{3+}:D^- crystal showing bleaching and successive recovery of fluorescence and (b) the 16 667.0-cm^{-1} transition in a ⟨100⟩ oriented SrF_2:0.05%Pr^{3+}:D^- crystal showing independent bleaching of the different site orientations.

tion. The charge-compensating ion of this pair then occupies the vacated substitutional position, resulting in a preferential reorientation of the RE^{3+} H^- pair into the two directions at 90° to the original alignment. An alternative mechanism of direct interstitial H^- ion migration along a ⟨110⟩ direction could equally well be invoked.[4] The presence of the substitutional H^- ion adjacent to the RE^{3+} ion could permit ion displacements favorable for direct transfer of the interstitial H^- ion, whereas the simple H^- C_{4v} site shows no reorientation under the same excitation conditions.

Subsequent laser excitation of the reoriented RE^{3+}–H^- ion pair causes a return to the original alignment. As there are three equivalent ⟨100⟩ directions and only two laser-polarization directions, there is a preferential excitation of some site orientations. The extent of preferential orientation and recovery depends on the relative absorption coefficients of the transition being excited for laser light parallel (π type) and perpendicular (σ type) to the site's principal symmetry axis. The clearest polarization results are expected for Pr^{3+} ions, for which π- and σ-type transitions can be separately excited, whereas the odd-electron systems studied (Nd^{3+} and Er^{3+}) have either σ or mixed $\sigma\pi$ transitions. Nevertheless, all three ions show pronounced reversible bleaching and recovery effects.

The varied behavior of the previously mentioned SrF_2:Nd^{3+} site can be understood if the absorption transition yielding no bleaching effects has an isotropic absorption cross section whereas the other two are of predominantly σ type.

For the sites that do not exhibit the reversible phenomenon [Fig. 1(b)] there is no preferential reorientation of the RE^{3+}–H^- pairs, and the differently oriented pairs bleach independently. For these sites the H^- migration creates a new center with its absorption transition out of resonance with the laser. An example of site interconversion is seen to exist between two different sites in SrF_2:Nd^{3+}:H^-; there the bleaching of one site by laser irradiation at 17 085 cm^{-1} can be removed by subsequent irradiation of the absorption line at 17 096 cm^{-1} of the second closely related site and vice versa.

Table 1. Number of Bleachable Centers Established to Date in Hydrogenated Rare-Earth-Doped Fluorite Crystals[a]

Crystal	Number of Bleachable Centers	Number Showing Reversible Behavior
CaF_2:Pr^{3+}	3	2
SrF_2:Pr^{3+}	4	2
CaF_2:Nd^{3+}	1	–
SrF_2:Nd^{3+}	2	1
CaF_2:Er^{3+}	4	3

[a] Equivalent H^- and D^- varieties are not counted separately.

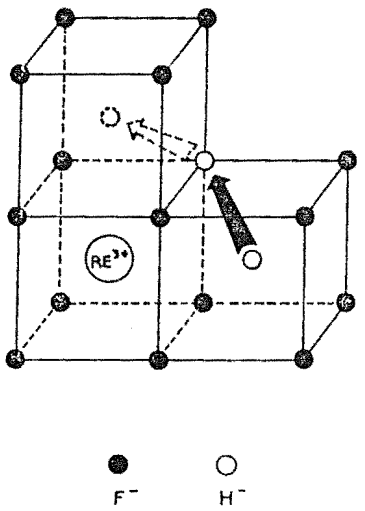

Fig. 2. A possible configuration for sites exhibiting reversible polarized bleaching. The arrows indicate one mechanism giving centers reoriented at 90° to the original alignment.

The fastest possible rate of fluorescence decay will be determined by the time for the incident light flux to bleach all the absorbing centers of a given site. For the laser powers used, the fastest decay rates of the order of 1 sec observed here approach this limit. The rate of fluorescence decrease will depend also on the various diffusion processes and paths involved, with H^- sites reorienting more rapidly than the corresponding D^- ones because of the greater mobility of H^- ions.

This phenomenon of reversible bleaching is under more detailed study, as it offers a useful insight into the dynamics of light ion migration, is of interest for the redistribution in population of oriented sites, and could have application in the optical storage and retrieval of information.

This research was supported by research grants from the University Grants Committee (UGC) of New Zealand. N. J. Cockroft and R. J. Reeves acknowledge support by UGC postgraduate scholarships. We thank Ross Ritchie, Terry Rowe, and Wayne Smith for technical assistance and the Australian National University for access to equipment for the high-resolution measurements.

References

1. A. Edgar, G. D. Jones, and M. R. Presland, J. Phys. C 12, 1569 (1979).
2. B. Welber, J. Chem. Phys. 43, 3015 (1965).
3. R. W. G. Syme, R. J. Reeves, G. D. Jones, J. Lumin. 31, 248 (1984).
4. C. R. A. Catlow, J. Phys. C 9, 1845 (1976).
5. Z. C. Nauta-Leeffers and H. W. den Hartog, Phys. Rev. B 19, 4162 (1979).